ESCR ESTI JOINT MEETING 2023

OCTOBER 26-28
BERLIN, GERMANY

ONLINE ABSTRACT SYLLABUS

ESTI ABSTRACTS

Abstracts appear as submitted to the system and have not been checked for correctness and completeness.

EUROPEAN SOCIETY OF CARDIOVASCULAR RADIOLOGY

www.escr.org | www.myesti.org

ESTI EUROPEAN SOCIETY OF THORACIC IMAGING

A-365

Additional targeted question on pre-existing statin therapy on participant health questionnaire prior to chest CT significantly reduces referral rate for further cardiovascular risk assessment in participants undergoing lung cancer screening

R. Jamal[1], A. Oo[2], J. Dunbar[2], G. Adam[2], S. Lam[2], K. Johnson[2], K. Vedwan[2], E. Woo[3], S. Harden[2], C. Peebles[2], A. Abbas[2], J. Shambrook[2]

[1]University Hospital Southampton NHS Foundation Trust, UHS Foundation Scheme, Southampton, United Kingdom, [2]University Hospital Southampton NHS Foundation Trust, Department of Radiology, Southampton, United Kingdom, [3]University Hospital Southampton NHS Foundation Trust, Department of Thoracic Surgery, Southampton, United Kingdom

Purpose/Objectives

The Targeted Lung Health Check (TLHC) programme was introduced in 10 pilot regions within the UK in 2020 with the aim of detecting lung cancer early in a high-risk population. Low-dose CT (LDCT) is performed in participants with a high risk of lung cancer. Coronary artery calcification (CAC) is a common incidental finding on screening LDCT and as an indicator of coronary atherosclerotic disease it is potentially important as a cardiovascular risk stratification tool in asymptomatic patients.

In our TLHC programme, participants with significant coronary calcium on screening LDCT have an automated letter sent to their primary care physician. This recommends review of their patients' cardiovascular risk factors and consideration of statin therapy. The volume of new coronary risk assessment referrals is potentially a significant burden to primary healthcare services.

We evaluated the use of a targeted pre-screening question on pre-existing statin therapy prior to lung cancer screening CT to assess if this would reduce the burden of primary care coronary risk assessment referral in our population.

Methods & Materials

People aged 55-74-years who are current/ former smokers were invited for LDCT if found to be high risk for lung cancer via a screening questionnaire within our TLHC. All participants who had a screening LDCT between August 2020 and January 2023 were included. All participants were asked an additional (off protocol) question whether the patient was already on statin therapy.

All LDCT studies were evaluated for presence of CAC using a standard scoring system published in 2020. All participants with moderate/severe CAC were advised to have further coronary disease risk assessments with their primary care physician to consider statin therapy unless they had told us that they were already taking statins in their pre-scan questionnaire.

Results

In total, 4899 participants underwent LDCT and 1580 participants (32%) demonstrated moderate or severe coronary artery calcification. Of these 1580 participants, 1083 (69%) were already taking statin therapy at the time of their scan. For these individuals, no further primary care recommendation was made. Therefore, our intervention reduced coronary risk referrals to primary care services by 69% within our TLHC programme.

Conclusion

Adding a targeted pre-screening question on statin therapy significantly reduced the number of referrals for primary care coronary risk assessment in our TLHC population. If incorporated as routine practice, this intervention has the potential to significantly reduce the cost and primary care resource burden of cardiovascular incidental findings identified within national lung cancer screening pathways.

References:

[1] Williams MC, Abbas A, Tirr E, Alam S et al, (2020), Reporting incidental coronary, aortic valve and cardiac calcification on non-gated thoracic computed tomography, a consensus statement from the BSCI/BSCCT and BSTI, Br J Radiol, 94(1117):20200894

[2] Jonas DE, Reuland DS, Reddy SM, et al., (2021), Screening for Lung Cancer with Low-Dose Computed Tomography: Updated Evidence Report and Systematic Review for the US Preventive Services Task Force, JAMA, 971-987, 325(10)

[3] Olufunmilayo H. Obisesan, Albert D. Osei, S.M. Iftekhar Uddin, et al., (2021), An Update on Coronary Artery Calcium Interpretation at Chest and Cardiac CT, Radiology: Cardiothoracic Imaging, 25;3(1):e200484

[4] Stewart J, Manmathan G, Wilkinson P., (2017), Primary prevention of cardiovascular disease: A review of contemporary guidance and literature, JRSM Cardiovasc Dis., 1;6:2048004016687211

[5] Graby J, Soto-Hernaez J, Murphy D et al., (2023), Coronary artery calcification on routine CT has prognostic and treatment implications for all ages, Clinical Radiology, S0009-9260(23)00074-0

A-428

Angiography-MRI in the evaluation of Thoracic Outlet Syndrome

M. Ragusi, D. Gandola, C. Maino, C. Talei Franzesi, T. P. Giandola, R. Corso, D. Ippolito
IRCCS San Gerardo, Monza, Italy

Purpose/Objectives

To evaluate the diagnostic performance of an Angiographic-MRI (MRA) protocol in the study of Thoracic Outlet Syndrome

Methods & Materials

From September 2019 to March 2022, a total of 20 patients underwent angio-MRI to investigate vascular TOS. Protocol sequences includes Balanced Fast Field Echo M2D, Turbo Spin Echo T1 weighted, high-resolution TSE T1 weighted, HR DIXON T2 weighted, contrast-enhanced MRA (CE- MRA), pre and post-contrast T1-weighted High Resolution Isotropic Volume Examination.
Baseline sequences were performed with the arms in adduction, CE-MRA sequences were performed both with arms in adduction and abduction, with injection of contrast media repeated for each arms' position (Gadobutrol 1.0mol/L; 5 + 5 ml). The total acquisition time is about 20 minutes.

Results

Sixteen patients showed unilateral TOS (n=16, 80%), with the left side more frequently involved (n=10, 64.5%) than the right one (n=6, 45.5%). Thirteen patients showed venous compression (vTOS) (65%), 3 patients arterial TOS (aTOS) (15%), only in one case an overlap between vTOS-aTOS (5%) was reported.
Eight patients showed compression with the arm in abduction (50%), 8 with the arm both in adduction and abduction (50%).
In two cases TOS was caused by an osseus abnormalities following surgery (10%), in 2 cases (10%) only an osseus abnormalities, and in one case exclusively surgery (5%).
In 6 patients (30%) vTOS was associated with thrombosis. Twenty percent of TOS were caused by muscle hypertrophy or wrong insertion.
Five out of sixteen case involved the scalene triangle (31%), 8/16 the costo-clavicular space (50%) and 3/16 patients the subacromial-pectoralis space (19%). In 4/20 patients vascular TOS was not identified (20%).

Conclusion

Angio-MRI protocol with CE-MRA sequence with arms in adduction and abduction allows to identify the presence of vascular TOS, along with the identification of the intrinsic and extrinsic abnormalities causing pathology.
The proposed protocol is extremely effective in identifying vascular TOS, resulting in a valuable integration to clinical data for understanding the pathology and to guide the correct management.

A-253

Artificial intelligence analysis of chest radiographs to triage patients with acute thoracic symptoms in an emergency department

E. J. Hwang, J. M. Goo, J. Nam, C. M. Park
Seoul National University Hospital, Department of Radiology, Seoul, Republic of Korea (South Korea)

Purpose/Objectives

To evaluate whether an artificial intelligence (AI) tool for automated analysis of chest radiographs (CRs) can help triage patients who visit an emergency department (ED) with acute thoracic symptoms

Methods & Materials

This secondary analysis of a prospective randomized clinical trial included patients who visited the ED of a tertiary referral institution with symptoms suggesting acute thoracic diseases (fever, dyspnea, chest pain, hemoptysis, cough, chilling sense, or sputum) and underwent CRs. An AI tool that can automatically detect pulmonary nodules, consolidation, and pneumothorax in a CR was applied to the initial CRs obtained in the ED. We evaluated whether the AI analysis can predict the composite outcome of 1) hospitalization, 2) transfer to other institutions hospitalization, 3) revisiting ED within 30 days, and 4) death due to any cardiopulmonary diseases. The area under the receiver operating characteristic curve (AUC) was used to compare the predictive performance of the AI analysis with that of initial triage results based on the physical examination. Sensitivities and specificities of the AI analysis were also evaluated at various thresholds for comparison with the interpretation of CRs by duty trainee radiologists in ED.

Results

A total of 3,576 patients (mean age 64 years; 1,966 male; diagnosis of any acute cardiopulmonary disease in 1,519 participants) were included. Composite events occurred in 1,148 (32.1%) patients (hospitalization, transfer, revisit, and death in 757, 314, 64, and 13 patients, respectively). The AI analysis showed higher performance than the initial triage result (AUC, 0.800 vs. 0.611; $P<0.001$) for the prediction of the outcome. At sensitivities of 99%, 95%, and 90% for the identification of patients with the composite event, the AI analysis showed specificities of 8.1%, 28.6%, and 47.3%, respectively, to defer low-risk or non-cardiopulmonary disease patients from immediate further evaluation. At the same sensitivity as the radiologists' interpretation (62.9%), the AI analysis exhibited similar specificity to the radiologists' interpretation (81.0% vs. 83.0%).

Conclusion

Automated analyses of CRs using an AI tool may help triage patients with acute thoracic symptoms in the ED by identifying high-risk cardiopulmonary disease patients and precluding low-risk or non-cardiovascular disease patients from immediate further evaluation.

A-409

Assessment of lobar and segmental bronchi instability with time-resolved low dose 4DCT of the whole chest and correlation with pulmonary function tests in COPD

A. Bischoff[1,2,3], P. Trauth[1,2,3], O. Weinheimer[1,2,3], H.-U. Kauczor[1,2,3], F. C. Trudzinski[2,4], F. Trinkmann[2,4], F. J. F. Herth[2,4], C. P. Heußel[1,2,3], M. O. Wielpütz[1,2,3]

[1]University Hospital of Heidelberg, Diagnostic and Interventional Radiology, Subdivision of Pulmonary Imaging, Heidelberg, Germany, [2]German Center for Lung Research (DZL), Translational Lung Research Center Heidelberg (TLRC), Heidelberg, Germany, [3]Thoraxklinik Heidelberg at the University Hospital of Heidelberg, Diagnostic and Interventional Radiology with Nuclear Medicine, Heidelberg, Germany, [4]Thoraxklinik Heidelberg at the University Hospital of Heidelberg, Pneumology and Critical Care Medicine, Heidelberg, Germany

Purpose/Objectives

Chronic obstructive pulmonary disease (COPD) can be associated with airway collapsibility due to chronic inflammatory processes and subsequent cartilage malacia[1]. While airway collapsibility of the trachea can be investigated with bronchoscopy, the assessment of dynamic airway changes of peripheral bronchi is mostly unknown. Time resolved 4DCT of the whole chest was established for quantification of tracheal collapsibility[2][3]. The aim of this study is to objectively quantify the collapsibility of peripheral airways down to the 5th generation by time-resolved 4DCT of the whole chest and to correlate dynamic changes with clinical data and pulmonary function tests (PFT).

Methods & Materials

Low-dose 4DCT of the whole chest was performed in 46 freely breathing patients with clinically suspected airway instability. 30 had COPD GOLD III-IV. The respiratory cycle was divided into 5%-wide steps resulting in 21 3D datasets per patient

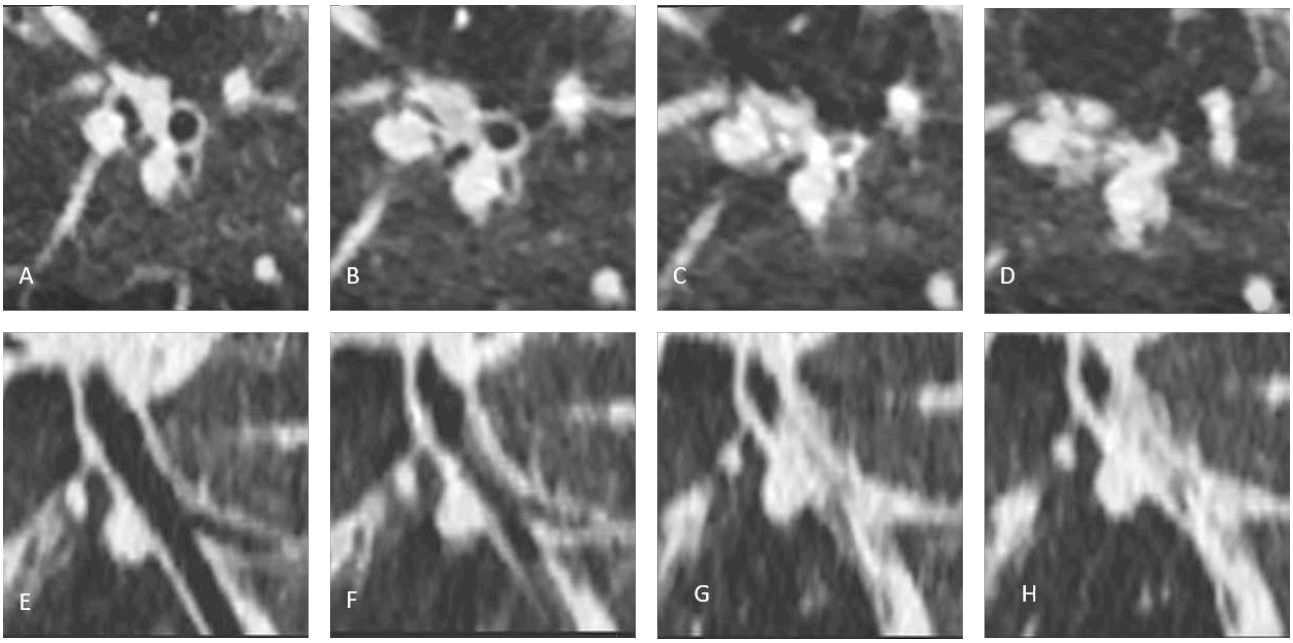

4DCT imaging of peripheral bronchi with significant collapse at early expiration in axial (upper row) and sagittal orientation (lower row).

. The bronchial tree was semi-automatically segmented on the dataset in every patient. Changes in volume (pBV) of the airway segments from the 3rd to 5th generation (lobar, segmental and first subsegmental bronchi) were objectified with in-house software. Correlations between airway changes and clinical data (GOLD stage), quantitative data of additional inspiratory CT (emphysema index, EI%), and spirometry (FEV_1%) were investigated using Spearman correlation coefficient and multiple linear regression.

Results

A significant change in pBV was found in 23 patients. Patients with COPD showed significantly higher collapsibility of pBV than the control group (mean reduction of pBV(%): 50% vs. 36%; $P<0.05$). In COPD, changes in pBV were found earlier in the respiratory cycle (timepoint 20% vs. 40%) and with faster collapse during expiration

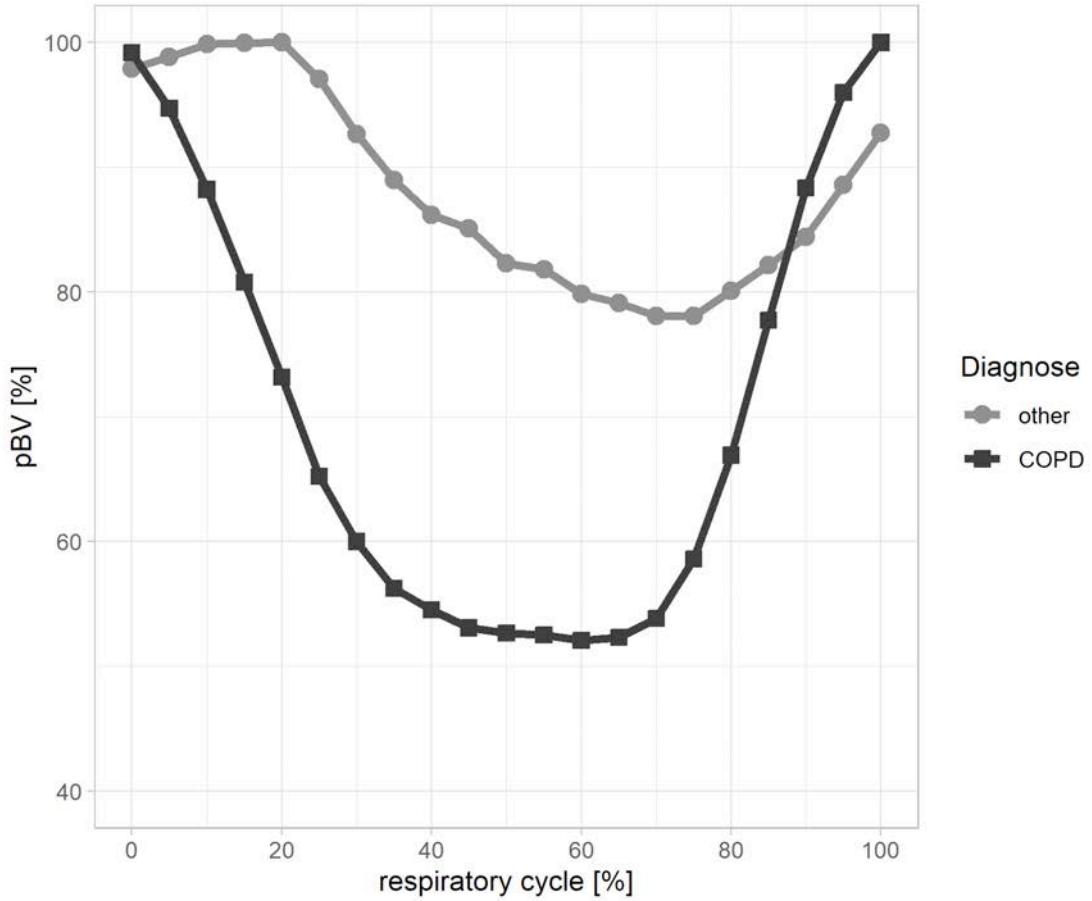

Quantification of pBV (%) along the respiratory cycle in 4DCT of COPD patients and control group.

. EI% correlated with change in pBV (r=0.69; P<0.01). FEV_1% correlated inversely with pBV (r=-0.58; P<0.01). On note, significant collapsibility of the trachea did not predict instability of the more peripheral airways (P>0.5).

Conclusion

4DCT of the whole chest provides a non-invasive method for detecting respiratory dynamics of central and peripheral airways by using objective software quantification. The correlation with PFT indicates a relevant influence of peripheral airway dynamics of disease severity in COPD patients. Further, collapsibility of central airways seems to be independent of peripheral airway dynamics.

References:

[1] Murgu SD, Colt HG, (2006), Tracheobronchomalacia and excessive dynamic airway collapse, Respirology, 388-406, 4, https://doi.org/10.1111/j.1440-1843.2006.00862.x

[2] Boiselle PM, Michaud G, Roberts DH, Loring SH, Womble HM, Millett ME, O'Donnell CR, (2012), Dynamic expiratory tracheal collapse in COPD: correlation with clinical and physiologic parameters, Chest, 1539-1544, 142, https://doi.org/10.1378/chest.12-0299

[3] Wielpütz MO, Eberhardt R, Puderbach M, Weinheimer O, Kauczor HU, Heussel CP, (2014), Simultaneous assessment of airway instability and respiratory dynamics with low-dose 4D-CT in chronic obstructive pulmonary disease: a technical note, Respiration, 294-300, 87, https://doi.org/10.1159/000357448

A-722

Automatic Detection and Categorization of Lung Cancer on 18F-PET/CT through Retina U-Net and Anatomical Region Segmentation

A. Sauter[1], P. Jäger[2], S. Yang[3], G. Sommer[4], J. Bremerich[3], K. Maier-Hein[2], T. Weikert[3]
[1]Kantonsspital Baden, Baden, Switzerland, [2]German Cancer Research Center, Division of Medical Image Computing, Heidelberg, Germany, [3]University Hospital Basel, Basel, Switzerland, [4]Hirslanden Klinik St. Anna, Luzern, Switzerland

Purpose/Objectives
The purpose of this study was to develop and evaluate the performance of a Retina U-Net algorithm for the detection of primary lung tumors and associated metastases of all stages on FDG-PET/CT.
Methods & Materials
The study utilized a dataset of 364 FDG-PET/CT scans from patients with histologically confirmed lung cancer, encompassing tumors of all stages. All lung tumors, lymphatic metastases, and distant metastases were manually segmented as 3D volumes using whole-body PET/CT series. The data was split into a training (n=216), validation (n=74), and internal test data set (n=74). The detection performance for all lesion types at multiple classifier thresholds was evaluated, and false-positive-findings-per-case (FP/c) was calculated. Detected lesions were assigned to categories T, N, or M using an automated anatomical region segmentation, and the reasons for false positives were visually assessed and analyzed.
Results
The results of the study showed that the sensitivity for T lesions was 86.2% (95% CI: 77.2-92.7) at an FP/c of 2.0 on the internal test set. The anatomical correlate to most false positives was the physiological activity of bone marrow (16.8%). TNM categorization based on the anatomical region approach was correct in 94.3% of lesions. Performance on the external test set confirmed the good performance of the algorithm, with an overall detection rate of 88.8% (95% CI: 82.5-93.5%) and FP/c of 2.7.
Conclusion
In conclusion, the Retina U-Net algorithm demonstrated promising results for tumor detection tasks on PET/CT scans, and could be useful as a reading assistance tool in this field. The study also revealed that false positives have anatomical correlates that could guide further algorithm improvements. The code for the algorithm is publicly available.

A-166

Changes in Tumor-to-Blood Ratio as a prognostic marker for progression-free survival and overall survival in neuroendocrine tumor patients undergoing peptide receptor radionuclide therapy.

O. J. Pettersson[1], M. Weber[2], R. Seifert[2], R. Seifert[2], B. Schaarschmidt[3], W. Fendler[2], B. Schaarschmidt[3], W. Fendler[2], C. Rischpler[2], H. Lahner[4], K. Herrmann[2], A. Sundin[1]

[1]Uppsala University, Department of Surgical Sciences, Uppsala, Sweden, [2]Department of Nuclear Medicine, University of Duisburg-Essen and German Cancer Consortium (DKTK)-University Hospital Essen, Essen, Germany., Department of Nuclear Medicine, Essen, Germany, [3]Institute of Diagnostic and Interventional Radiology and Neuroradiology, University Hospital Essen, Essen, Germany, Essen, Germany, [4]Department of Endocrinology and Metabolism, Division of Laboratory Research University of Duisburg-Essen and German Cancer Consortium (DKTK)-University Hospital Essen, Essen, Germany, Essen, Germany

Purpose/Objectives

To calculate Tumor-to-Blood Ratio (TBR) on ^{68}Ga-DOTATOC-PET/CT in neuroendorcrine tumor (NET) patients undergoing peptide receptor radionuclide therapy (PRRT) with ^{177}Lu-DOTATATE and relate changes in TBR to progression-free survival (PFS) and overall survival (OS).

The authors OJ Pettersson and M Weber contributed equally.

Methods & Materials

The institutional database of the University Clinic Essen was screened for NET patients who had undergone least two cycles of PRRT with ^{177}Lu-DOTATOC and ^{68}Ga-DOTATOC-PET/CT for baseline and follow-up imaging.

The ^{68}Ga-DOTATOC-PET/CT examinations were read by two independent readers (Weber, M., Pettersson O.J.), blinded for all clinical and imaging information except the type disease and the type of examination.

Boa_Image_Frame Uptake Values (SUV) in the reference organs, namely the blood in the left ventricle and in the aorta, the kidney and the spleen were recorded as SUV_{mean} and SUV_{max}.

The ratios between the SUV_{max} of the tumor and the SUV_{mean} of the left ventricle for TBR were calculated. Due to a high inter-reader variability when the aorta was used as reference organ in a prior exploratory study, the blood pool of the aorta was dismissed as reference. In other words, only the blood in the left ventricle was used as reference for the TBR recordings.

Changes in TBR from baseline to follow-up were tested for correlation with PFS and OS. PFS was defined as the interval from the start of PRRT until clinical, radiological or an interdisciplinary tumor board decision of progressive disease, or until the death of the patient. OS was defined as the interval from initiation of therapy until the last follow-up or death.

Results

Out of 438 screened patients, 262 NET patients had undergone at least two cycles of PRRT with ^{177}Lu-DOTATATE and/or ^{90}Y-DOTATOC. The present study focused on 139 patients that had undergone PRRT with ^{177}Lu-DOTATATE.

NET patients without progressive disease on first imaging after baseline and an increasing TBR between baseline and follow-up had a shorter PFS, both in the univariate (HR 2.13 [95%CI 1.18-3.85]; p=0.01, n=94) and in the multivariable (HR=3.29 [95%CI 1.62-6.68]; p<0.01, n=94) analyses.

Moreover, the lung or the thymus as location of the primary tumor was associated with a shorter PFS (HR 14.2 [95%CI 1.96-102.7]; p=0.01, n=94).

Increasing TBR from baseline to follow-up was associated with shorter OS both in the univariate (HR 1.87 [95%CI 1.22-2.86]; p<0.01, n=139) and in the multivariable (HR 1.94[95%CI 1.13-3.32]; p=0.02, n=139) analyses.

Conclusion

Increasing TBR in NET patients undergoing PRRT with ^{177}Lu-DOTATATE was in the present cohort associated with shorter PFS and OS. Moreover, the lung or the thymus as location of the primary tumor was associated with shorter PFS.

A-161

Chest contrast-enhanced computed tomography assessment of ESC/ERS pulmonary hypertension clinical classification: a study of reliability.

L. Cereser[1], G. Zussino[1], C. Montanaro[1], C. Cicciò[2], R. Girometti[1], C. Zuiani[1]
[1]Institute of Radiology, Department of Medicine, University of Udine, Udine, Italy, [2]Department of Diagnostic Imaging and Interventional Radiology, IRCCS Sacro Cuore Don Calabria Hospital, Negrar (VR), Italy

Purpose/Objectives

Pulmonary hypertension (PH) is a multifaceted disease with different etiologies and clinical presentation. The European Society of Cardiology (ESC) and the European Respiratory Society (ERS) recently released a joint update on PH classification, including recommendations on the use of imaging techniques [01]. While chest contrast-enhanced computed tomography (CECT) plays a pivotal role in this setting [02] [03], there is limited information on its reliability in classifying PH. In this light, we aimed to assess the inter-reader agreement in the classification of PH on CECT.

Methods & Materials

The study retrospectively included 60 consecutive patients diagnosed with PH who underwent chest 64-row multidetector CECT between 2014-2022 at our University Hospital. In the case of multiple examinations, the one nearest to the time of PH diagnosis was selected. Two readers experienced in thoracic imaging, i.e., reader 1 (R1) and reader 2 (R2), independently reviewed all the CECT scans. Readers reported any abnormality among diffuse lung diseases (fibrosis and emphysema), heart abnormalities (including left chambers dilatation/wall thickening, coronary calcifications, and valvular abnormalities), vascular signs of chronic thromboembolism, and esophageal dilatation. Based on such findings, they were asked to classify each PH case into groups 1-5 according to the 2022 ESC/ERS guidelines [01]. Using unweighted Cohen's kappa (k) statistic with 95% confidence intervals (CI), we evaluated the agreement between R1 and R2 in detecting CECT abnormalities and defining PH groups. The k coefficients were interpreted according to Landis and Koch [04].

Results

Table 1 reports the prevalence values of CECT abnormalities with corresponding inter-reader agreement results.

Chest CECT findings	Readers		Inter-reader agreement k (95%CI) [4]	
	R1 N (%)	R2 N (%)		
Lung [1]	17 (28.3)	15 (25)	0.77 (0.59-0.94)	Substantial
Heart [2]	22 (36.7)	22 (36.7)	0.33 (0.09-0.57)	Fair
Pulmonary vessels [3]	11 (18.3)	7 (11.7)	0.69 (0.46-0.92)	Substantial
Esophageal dilatation	11 (18.3)	10 (16.7)	0.69 (0.46-0.92)	Substantial

Notes:
CECT, contrast-enhanced computed tomography; R1, reader 1; R2, reader 2; k, kappa value; CI, confidence interval
[1] Fibrosis and/or emphysema
[2] At least two of the following three findings: left chambers dilatation/wall thickening, coronary calcifications, and valvular abnormalities
[3] Vascular signs of chronic thromboembolism
[4] Kappa values interpretation was according to Landis and Koch (Biometrics, 1977)

Prevalence values of CECT abnormalities with corresponding inter-reader agreement results

The inter-reader agreement was substantial for most CECT findings (k ranging 0.69-0.77), except for heart abnormalities (fair agreement, k=0.33 [0.09-0.57]). The inter-reader agreement for defining PH groups was almost perfect (k=0.81 [95%CI 0.70-0.93]). Figure 1 resumes the results via radial charts.

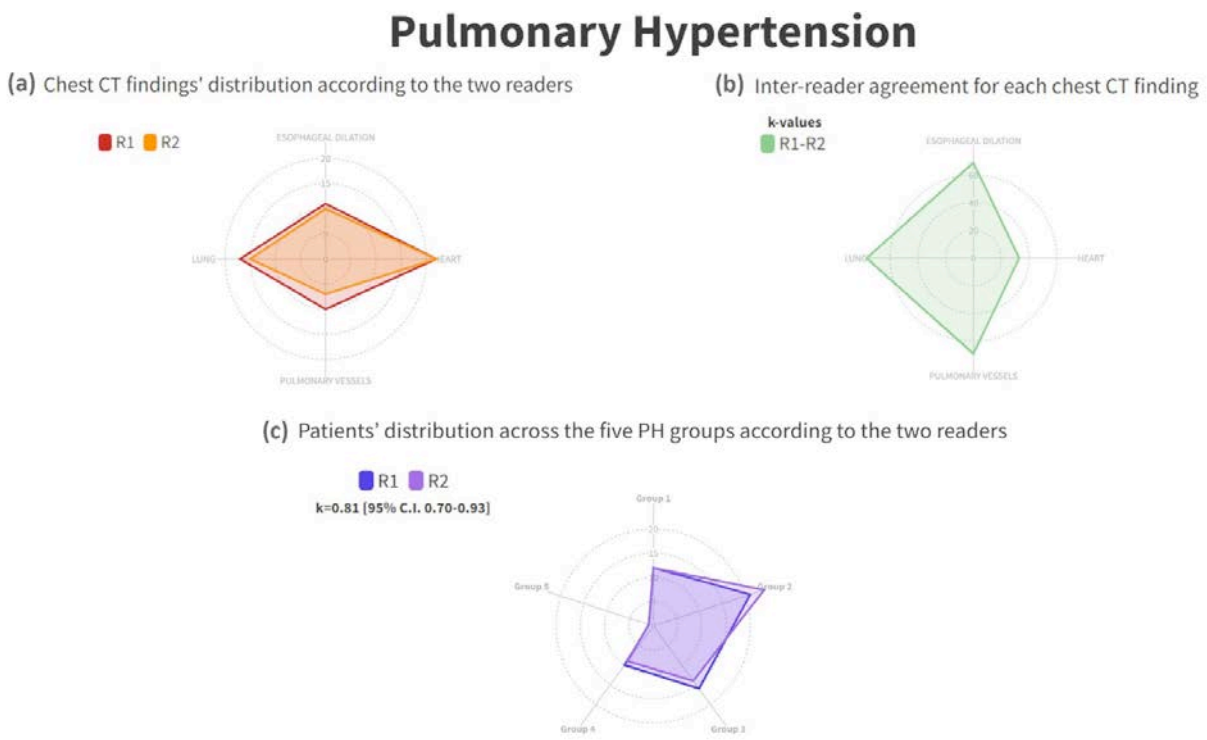

Radar charts illustrate: (a) the chest CT findings' distribution according to the two readers (R1 and R2), (b) the inter-reader agreement for each CT finding, and (c) the patients' distribution across the five pulmonary hypertension (PH) groups according to R1 and R2.

Figure 2 illustrates PH groups' example cases from the series.

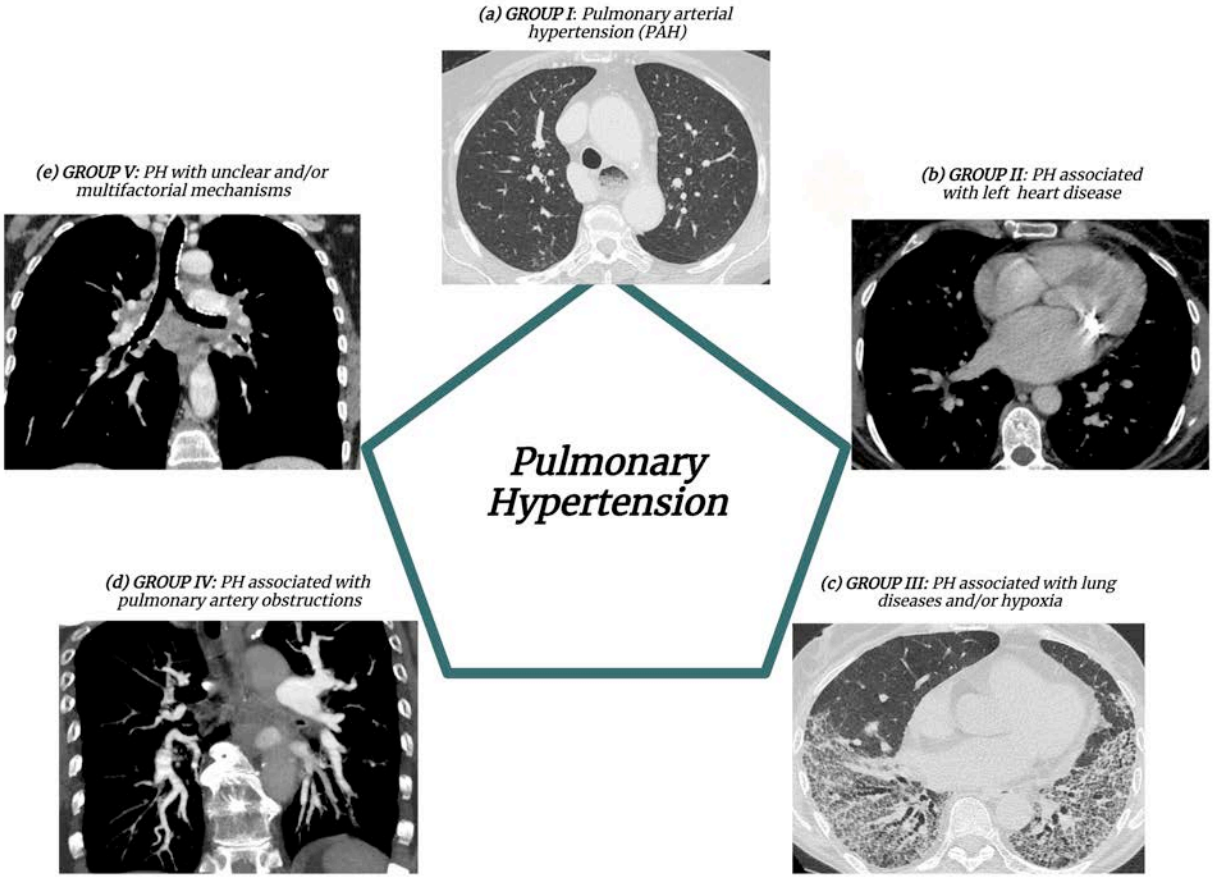

Typical group-specific pulmonary hypertension (PH) signs: (a) esophageal dilatation with no lung abnormalities; (b) left atrium dilatation and mitral valve calcifications; (c) extensive lung fibrosis; (d) signs of chronic thromboembolic pulmonary disease; (e) multiple mediastinal enlarged lymph nodes in sarcoidosis.

Conclusion
Despite poor reliability in assessing heart abnormalities, the inter-reader agreement in classifying PH was high when experienced radiologists interpreted CECT. Our results suggest that radiology-based multidisciplinary decision making in the setting of PH can be done on a reliable basis.

References:

[01] Humbert M, Kovacs G, Hoeper MM, et al, (2022), 2022 ESC/ERS Guidelines for the diagnosis and treatment of pulmonary hypertension, Eur Heart J, 43:3618-3731
[02] Foley RW, Kaneria N, Ross RVM, et al, (2021), Computed tomography appearances of the lung parenchyma in pulmonary hypertension., Br J Radiol, 94(1117):20200830
[03] Remy-Jardin M, Ryerson CJ, Schiebler ML, et al, (2021), Imaging of pulmonary hypertension in adults: a position paper from the Fleischner Society, Eur Respir J, 57(1):2004455
[04] Landis JR, Koch GG, (1977), The measurement of observer agreement for categorical data, Biometrics, 33:159-174

A-446

Chest CT radiomics' diagnostic role in differentiating tumorlet and granulomas: a pilot study

S. Nardacci, D. Caruso, D. De Santis, M. Zerunian, F. Palmeri, B. Masci, A. Del Gaudio, F. Pucciarelli, D. Valanzuolo, A. Laghi
Sapienza - University of Rome, Department of Medical Surgical Sciences and Translational Medicine - Radiology Unit - Sant'Andrea University Hospital, Rome, Italy

Purpose/Objectives

Pulmonary carcinoid tumorlets (TL) are rare benign incidental findings at pathological examination, they arise from hyperplastic neuroendocrine cells originating from bronchial and bronchiolar mucosa, measuring ≤ 5 mm[1]. TL can also arise from diffuse idiopathic pulmonary neuroendocrine cell hyperplasia (DIPNECH)[2].

TL are round or ovoid-shaped nodules, usually multiple, either solid or ground-glass[1][3].

Differentiating TL from other entities, such as granulomas, only on the basis of CT features, may be challenging; therefore, the aim of this study is to identify CT radiomics features of both TL and granulomas and to evaluate the potential role of radiomics in differentiating them.

Methods & Materials

Ninety patients with pathological diagnosis of granulomas or TL and pre-surgical chest CT, were retrospectively enrolled from 2013 to 2021.

Exclusion criteria were negative chest CT, lung nodules <2mm, previous surgical resections, and significant chest CT motion artefacts.

Two radiologists, in consensus, performed volumetric lung segmentation on each CT scan by using the open-source software 3D Slicer; radiomics features were extracted from CT datasets and results were compared with pathology. Performances of chest CT radiomics features in differentiating TL from granulomas was tested by Receiver operating characteristic (ROC) curves and the areas under the curve (AUCs), calculating sensitivity and specificity.

Results

From an initial population of 90 patients, 35 patients (39%) were excluded; hence, the final population consisted of 55 patients (F:M=38:17); 32 patients (58%) diagnosed with TL and 23 patients (42%) diagnosed with granulomas.

A total of 107 radiomics feature were extracted. Significant differences were found in 16 of them: 3 Shape, 1 First Order, 2 Grey Level Co-occurrence Matrix (GLCM), 2 Gray Level Dependence Matrix (GLDM), 4 Grey-Level Run Length Matrix (GLRLM), and 4 Gray Level Size Zone Matrix (GLSZM), all with P <0.05.

In particular, Long Run High Gray Level Emphasis (GLRLM feature) showed the best performances in discriminating TL from granulomas (AUC: 0.896; sensitivity: 92.3%; and specificity: 76.5%) along with Flatness (Shape feature), characterized by an AUC:0.903, sensitivity of 76.9%, and specificity of 100%; all P<0.001(Figure 1).

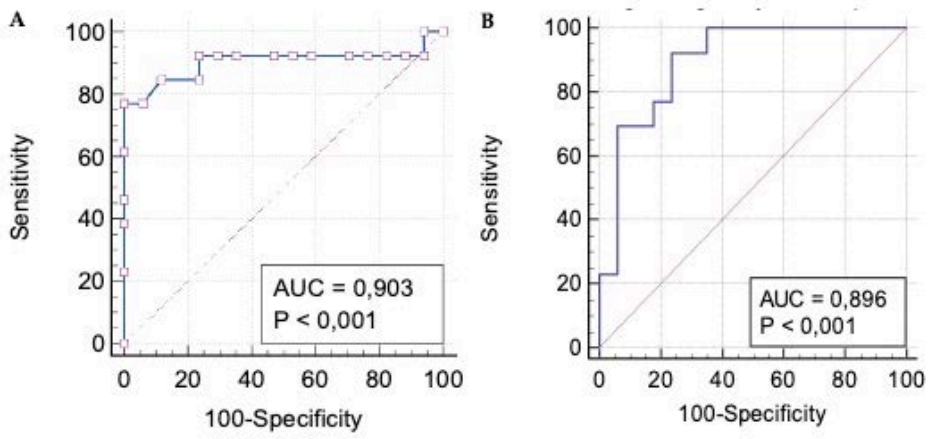

ROC curves used to test the performance of radiomics features in discriminating tumorlets from granulomas, show the best two AUCs:A) Flatness showed an AUC of 0.903, sensibility of 76.9%, and specificity of 100%,(P < 0.001);B); Long Run High Gray Level Emphasis demonstrated an AUC of 0.896,sensibility of 92.3%,and specificity of 76.5%(P < 0.001).

.

Conclusion

Radiomics may play a role as non-invasive imaging tool in differentiating TL from granulomas, identifying precancerous lesions at an early stage.

References:

[1] Rossi G, Cavazza A, Spagnolo P, Sverzellati N, Longo L, Jukna A, Montanari G, Carbonelli C, Vincenzi G, Bogina G, Franco R, Tiseo M, Cottin V, Colby TV., (2016), Diffuse idiopathic pulmonary neuroendocrine cell hyperplasia syndrome., Eur Respir J., doi:10.1183/13993003.01954-2015
[2] Koo CW, Baliff JP, Torigian DA, Litzky LA, Gefter WB, Akers SR., (2010), Spectrum of pulmonary neuroendocrine cell proliferation: diffuse idiopathic pulmonary neuroendocrine cell hyperplasia, tumorlet, and carcinoids., AJR Am J Roentgenol, doi: 10.2214/AJR.09.3811.
[3] Ginsberg MS, Akin O, Berger DM, Zakowski MF, Panicek DM., (2004), Pulmonary tumorlets: CT findings., AJR Am J Roentgenol., doi: 10.2214/ajr.183.2.1830293.

A-612

Computed Tomographic Phenotypes in Pulmonary Sarcoidosis — Results of a Multinational Delphi Study

N. Sivarasan[1], S. Desai[2], A. Wells[3]
[1]Department of Radiology, Guy's and St Thomas' Hospital, Stoneleigh, United Kingdom, [2]Department of Radiology, Royal Brompton Hospital, London, United Kingdom, [3]Interstitial Lung Disease Unit, Royal Brompton Hospital, London, United Kingdom

Purpose/Objectives

In contrast with computed tomographic (CT) appearances, histopathological findings— and, specifically, non-caseating granulomas — do not explain the major variability in clinical features, physiology and outcome in pulmonary sarcoidosis. We aimed to establish, by multinational consensus, agreement on CT/morphological phenotypes in sarcoidosis.

Methods & Materials

Thematic interviews were conducted with Core Expert Panel members (chest physicians, n=6 and thoracic radiologists, n=6; all with established research experience in sarcoidosis and/or interstitial lung diseases). This yielded 34 Delphi statements, which were presented to participants, evaluating the spectrum of possible CT phenotypes but also potential relationships between specific CT features, lung function tests, clinical features and outcome. Delphi participants were members of the i) Core Expert Panel, ii) Fleischner Society (FS) and/or The World Association of Sarcoidosis and Other Granulomatous Disorders (WASOG), and iii) up to 3 nominess from each of the FS and WASOG members. In two Delphi rounds participants responded employing a standard 5-point Likert scale (strongly agree, agree, neutral/unsure, disagree and strongly disagree). An *a priori* threshold of ≥70% agreement (strongly agree or agree) or ≥70% disagreement (strongly disagree or disagree) was considered consensus. Statements with >30% but <70% agreement in Round 1 were amended as necessary for clarity and entered in Round 2 whereas statements with <=30% agreement in Round 1 were excluded.

Results

Of 174 invitees, 146 (84%; M=82. Physicians, n=98, radiologists, n=48; mean duration in practice, 21±10 years), originating from 28 countries (UK/Europe=39%; USA=25%), completed the Delphi. After Round 1, 13/34 (38%) statements reached ≥70% consensus agreement (including a statement on the utility of 'baseline' CT in patients with evidence of interstitial disease: 138/146 [94%]) and ≥70% consensus disagreement on 3/34 (9%). There was unequivocal agreement on the statements that i) there are distinct CT phenotypes in sarcoidosis (142/146 [97%]) and ii) CT features are broadly categorised as fibrotic or non-fibrotic (121/146 [83%]). On completion of Round 2, consensus was reached on seven CT phenotypes categorised as non-fibrotic (nodular patterns, n=3; consolidation, n=1):

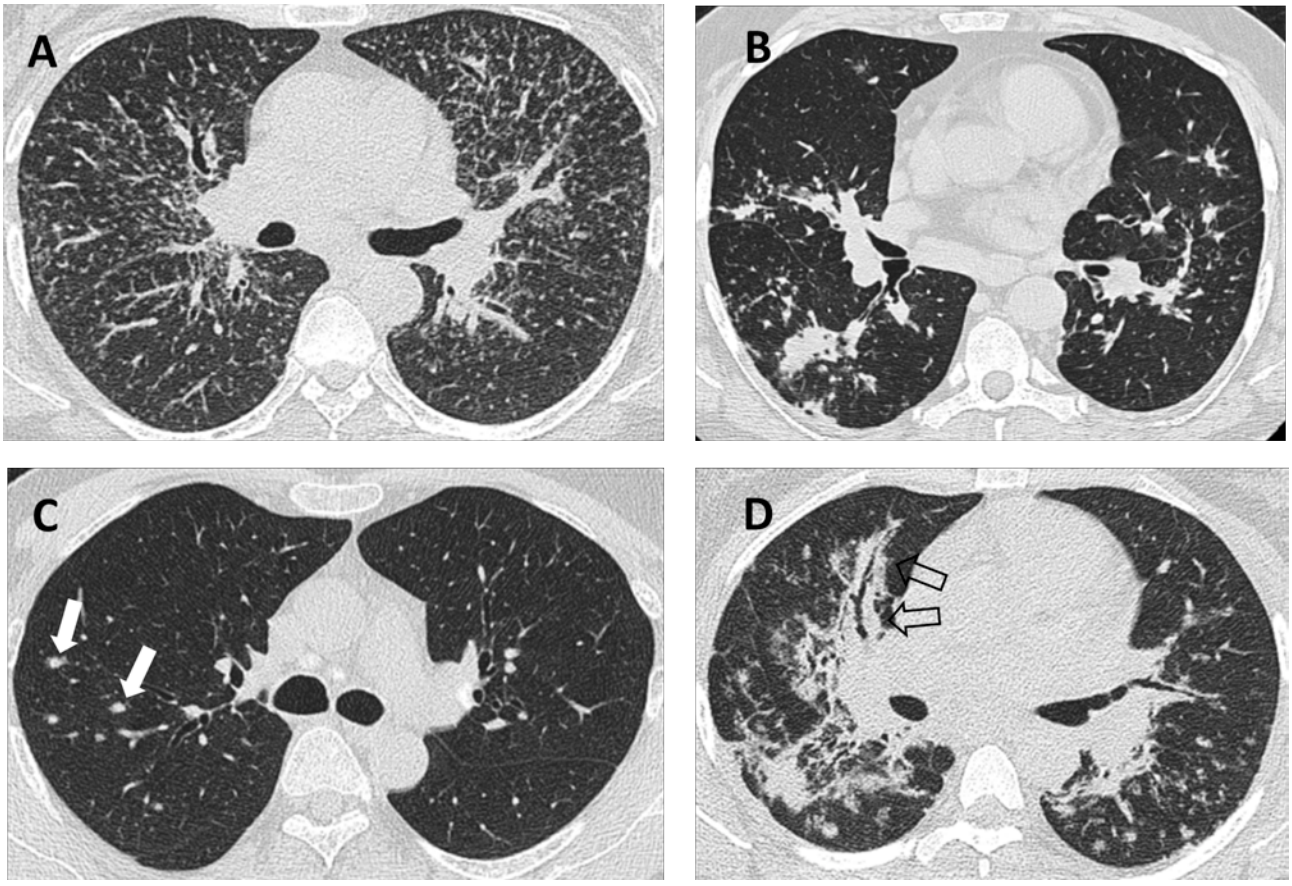

HRCT images showing four phenotypes — considered non-fibrotic — reaching Delphi consensus. A) HRCT showing innumerable peri-bronchovascular, peri-fissural and sub-pleural micronodules; B) multiple larger peri-bronchovascular nodules; some of the larger nodules have smaller surrounding micronodules (the 'galaxy sign'); C) HRCT showing scattered larg
and fibrotic (n=3; bronchocentric fibrosis with or without cavitation and a mimic of progressive massive fibrosis):

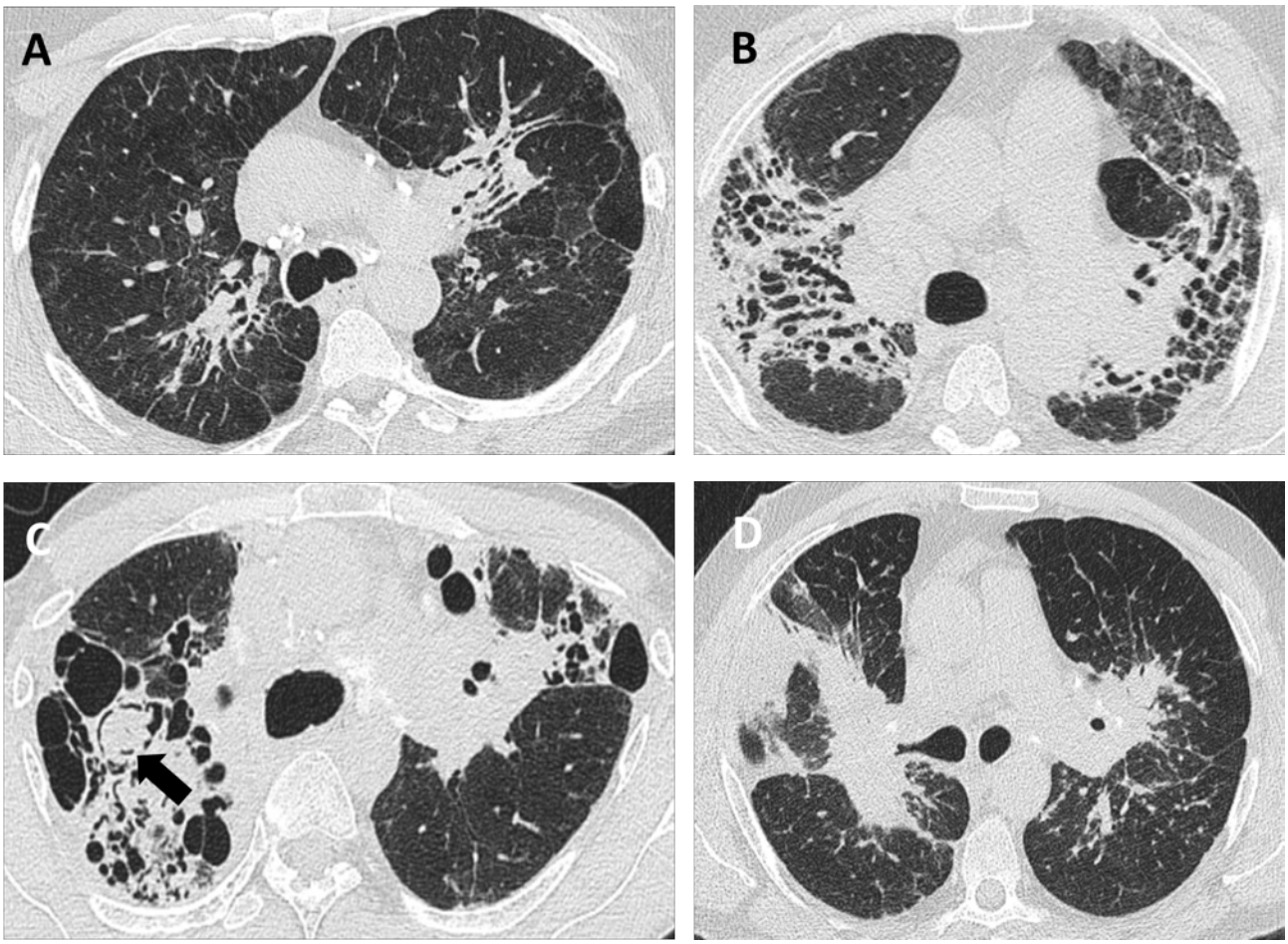

HRCT images showing three phenotypes — considered fibrotic — reaching Delphi consensus. A/B) HRCT images showing bilateral bronchocentric reticulation C) Upper lobe fibrocavitary disease. NB There is a mycetoma in one of the right upper lobe cavities (arrow) and D) dense, bilateral bronchocentric ‘masses’ giving an appearance of progressive massive

Conclusion

Experts overwhelmingly recommend ‘baseline’ CT in sarcoidosis patients with evidence of parenchymal disease and agree that there are distinct fibrotic or non-fibrotic CT phenotypes. These findings have the potential to anchor future research and stimulate the development of a new morphological classification in sarcoidosis.

A-510

Computed Tomography chracterization of lung abnormalities in Granulomatous and Lymphocytic Interstitial Lung Disease of Common Variable Immunodeficiency

N. Landini[1], M. P. Bondioni[2], C. Milito[1], R. Scarpa[3], F. Cinetto[3], C. Catalano[1], V. Panebianco[1]
[1]Sapienza University, policlinico Umberto I, Rome, Italy, [2]ASST-Spedali Civili di Brescia, Brescia, Italy, [3]University of Padova, Padova, Italy

Purpose/Objectives
Granulomatous Lymphocytic Interstitial Lung Disease (GL-ILD) is a possible complication of Common Variable ImmunoDeficiency (CVID) that may manifest with several lung abnormalities, leading to poorer prognosis. We aimed to investigate computed tomography (CT) findings of GL-ILD in CVID, also in comparison with lung abnormalities of non-GL-ILD CVID patients, in order to provide elements that may be helpful in GL-ILD diagnosis.
Methods & Materials
We retrospectively searched the electronic archives of four Referral Centers for Primary Immunodeficiencies (Rome, Padua, Milan and Brescia), from 2018 to 2021, to identify the first CT scans performed at time GL-ILD diagnosis in CVID patients, as well as the same number of CVID patients without GL-ILD, matched for sex and age. Exclusion criteria were: therapy for GL-ILD, clinical suspicion of superimposed infection or lymphoma. Two radiologist, in consensus, assessed CT findings in upper, lower field and whole lungs, describing also if the disease was prevalent in upper or lower fields, or diffuse. CT findings were: bronchiectasis, bronchial wall thickening, mucous plugs, tree in bud, mosaic perfusion, small nodules (≤10 mm), big nodules, consolidations, ground glass opacities (GGO), reticulations, fibrotic ILD, areas of cavitation/necrosis and parenchymal bands. Small nodules were described as centrilobular, perilymphatic or randomly distributed. Nodules were considered as multiple if >3. The presence of enlarged lymphnodes (axis brevis >10 mm), pleural or pericardial effusion was also noted. Fisher exact test was adopted to compare upper and lower fields abnormalities in GL-ILD patients, as well as to compare CT findings between GL-ILD and non GL-ILD subjects. For each abnormality, Odds Ratios (OR) for GL-ILD were computed.
Results
38 GL-ILD subjects (23 females, median age 50 years) and 38 matched controls were identified. Most common GL-ILD CT findings in GL-ILD (>50% patients) were: bronchiectasis, multiple non-perilymphatic small nodules, GGO, consolidations, bands and enlarged mediastinal lymphnodes. The disease was usually predominant in lower fields (92%). Bronchiectasis, GGO, reticulations, fibrosis and bands were significantly more frequent in lower fields (p-value<0.05). Considering whole lungs analysis, small nodules (≤10 mm), consolidations, reticulations and fibrosis had an OR>10 (p-value<0.05) in identifying GL-ILD versus non GL-ILD patients.
Conclusion
GL-ILD patients usually have a lower field predominant disease, mainly characterized by bronchiectasis, non-perilymphatic nodules, GGO, consolidations, bands and enlarged mediastinal lymphnodes. Small nodules, consolidations, reticulations and fibrosis are highly suggestive of GL-ILD in CVID.

A-663

Critical vs non-critical triage of chest X-rays based on a comprehensive AI model – validation on a ground-truthed, real-world dataset

C. Tang[1,2], C. Jones[1,3], M. Milne[1], N. Ektas[1], H. McHugh[1,4]
[1]Annalise.ai, Sydney, Australia, [2]Gosford Hospital, Gosford, Australia, [3]I-MED Radiology Network, Brisbane, Australia, [4]Harrison.ai, Sydney, Australia

Purpose/Objectives
Artificial intelligence has the potential to augment clinical workflow and improve patient outcomes and radiologist productivity through worklist triage. This retrospective study assessed the performance of a comprehensive AI model, capable of detecting 124 findings on chest radiographs (CXR), for differentiating CXR cases with critical or time-sensitive findings that were considered to require immediate or urgent reporting.
Methods & Materials
The predictions of the AI model (Annalise Enterprise CXR) were post-processed into a single output score aiming to maximise differentiation of critical from non-critical cases. Nine of the AI model's 124 findings were categorised as critical, based on the need for immediate triage to prevent significant patient morbidity and mortality. Consultant radiologists blinded to the model outputs ground-truthed a dataset of 3080 CXR cases, comprising 533 critical and 2547 non-critical studies that were mutually exclusive from the model training data at the patient level. Thresholds were calculated at 90%, 95% and 99% sensitivity based on model training data and performance on the testing data was reported at these thresholds.
Results
Post-processed model outputs to differentiate cases with critical findings achieved an overall AUC of 0.97. The model achieved a specificity of 0.90, 0.84 and 0.68 at the 90%, 95% and 99% sensitivity thresholds, respectively. At a threshold to achieve 99% sensitivity, 44% of cases were predicted positive, with a positive predictive value (PPV) and a negative predictive value (NPV) of 0.39 and 1.00, respectively, and eight false negatives (FN). At the 95% sensitivity threshold, the model achieved the following – 29% cases positive, PPV: 0.56, NPV: 0.99, and FN: 25. Results at the 90% sensitivity threshold were 24% cases positive, PPV: 0.66, NPV: 0.98, and FN: 45.
Conclusion
Processing the outputs of a comprehensive CXR AI model into a single score to distinguish critical from non-critical cases was shown to be highly accurate compared to ground truth labels. This internal validation produced metrics suggesting viability as a critical finding triage tool, which could be further evaluated in future prospective studies.

A-385

CT Radiomics-guided EGFR Mutation Targeting Therapy in Non-Small Cell Lung Cancer

M. Chen[1], Y. Han[2], K. Linton-Reid[1], P. Viola[2], A. Mani[2], H. Lu[1], M. Bahket[2], E. Aboagye[1], S. Copley[1]
[1]Imperial College London, Surgery and Cancer, London, United Kingdom, [2]Imperial College Healthcare NHS Trust, London, United Kingdom

Purpose/Objectives

Newer generation tyrosine kinase inhibitors (TKI) are becoming more effective against cancers exhibiting certain driver mutations[1]. Epidermal growth factor receptor (EGFR) mutation is the most common treatment target in non-small cell lung cancer (NSCLC) [2]. Treatment decision is currently guided by tissue sampling and genetic testing, an invasive process limited by patient tolerance, procedural complications, costs, tumour heterogeneity and mutation evolution. Radiomic features are quantitative metrics derived from imaging data and can non-invasively capture important disease information in cancer [3][4]. Prior works have developed radiomics-based models to predict for single driver mutations in NSCLC[5]. Co-mutation status, such as concomitant EGFR and BRAF mutations, is associated with increased treatment resistance[6]. Exclusive EGFR positivity, where all other main driver mutations are negative, forms a favourable treatment situation, which has not yet been addressed adequately in the radiomics literature. Our study objective is to develop a radiomics-based model to predict for such mutational status.

Methods & Materials

This ethically approved retrospective study comprises 304 patients with NSCLC (age (mean + SD): 68.0 ± 13.2, male:female [M:F] = 174:130) who underwent CT scans and tissue sampling with genetic testing at our multi-centre institution between February 2012 and July 2018. An independent cohort of 51 patients (Age: 69.5 ± 8.1 M:F = 35:16) from the Cancer Imaging Archive was included for external validation. We computed radiomic features (n=1,998) from multi-region tumoural segmentations performed by a thoracic radiologist with 9 years of experience.

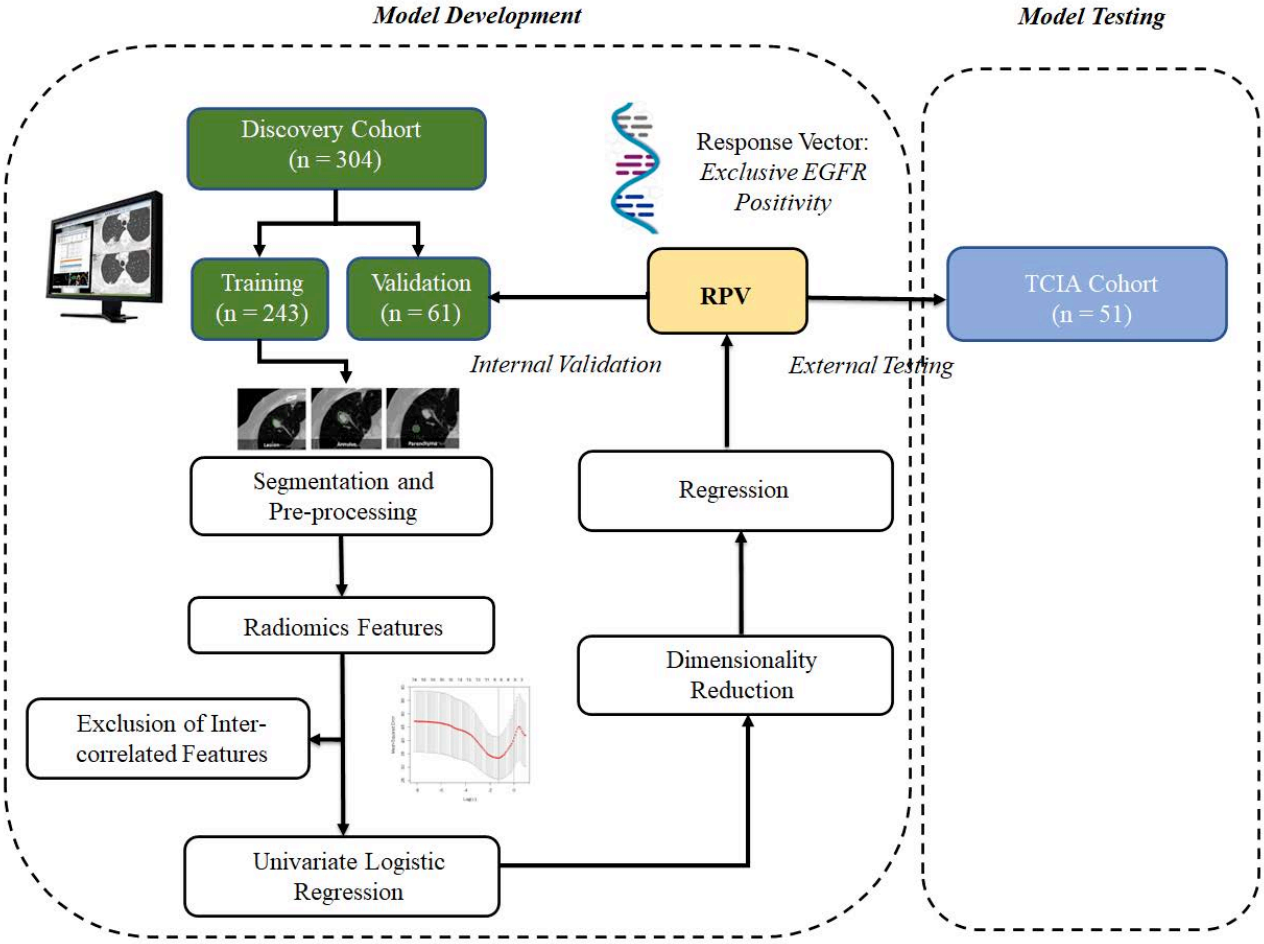

Model development pipeline

Taking exclusive EGFR positivity (BRAF, NRAF, KRAS, PIK3Ca and ALK-1 negative) as the response vector, we developed a composite radiomics predictive vector (RPV) using the best performing dimensionality reduction and regression methods.

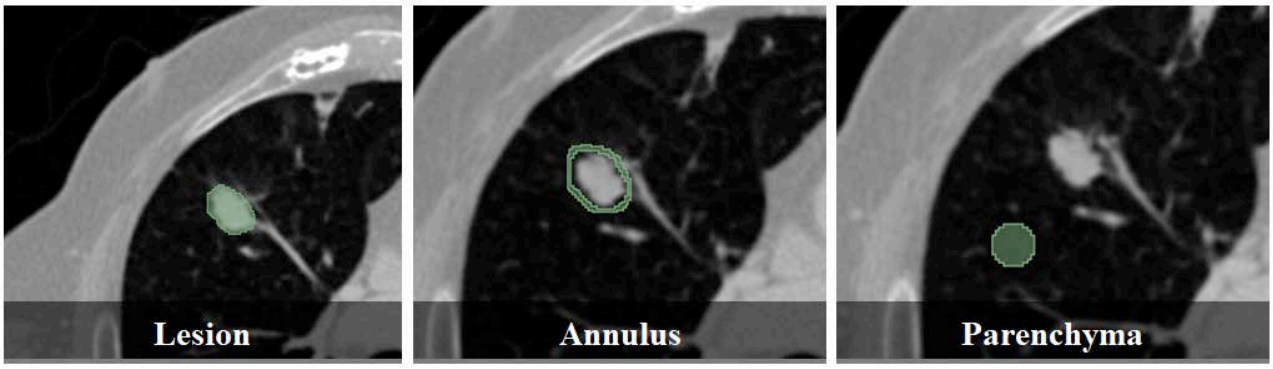

Multi-regional segmentation approach: main tumour, peri-lesional annulus and a representative lung parenchyma were delineated. This was validated in the independent testing cohort, as assessed by predictive accuracy.

Results

K-nearest neighbours and Spearman were identified as the best performing dimensionality reduction and regression methods, respectively. A composite 9-feature RPV predicted exclusive EGFR positivity to an accuracy of 0.89, 95% CI: 0.78–0.95 and 0.75, 95% CI: 0.60-0.86 in the internal and external testing sets, respectively.

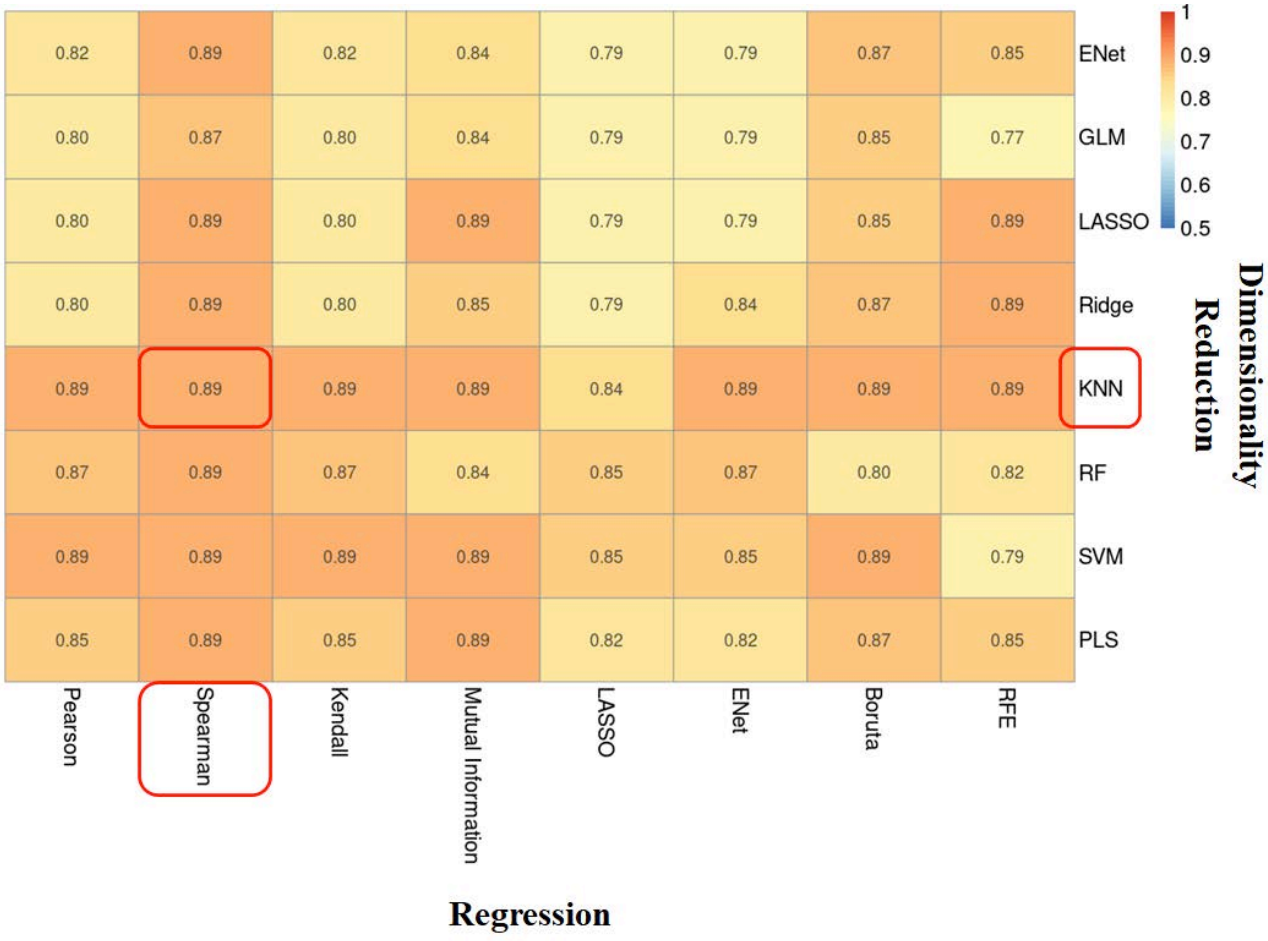

Best performing model development based on predictive accuracy. Note the K-nearest neighbour (KNN) and Spearman were the best performing dimensionality reduction and regression methods.

The component features were extracted from all three regions of interests, with most (n = 5) from the peri-lesional area; consistent with usual distribution of oncogenetic cells driving tumour growth.

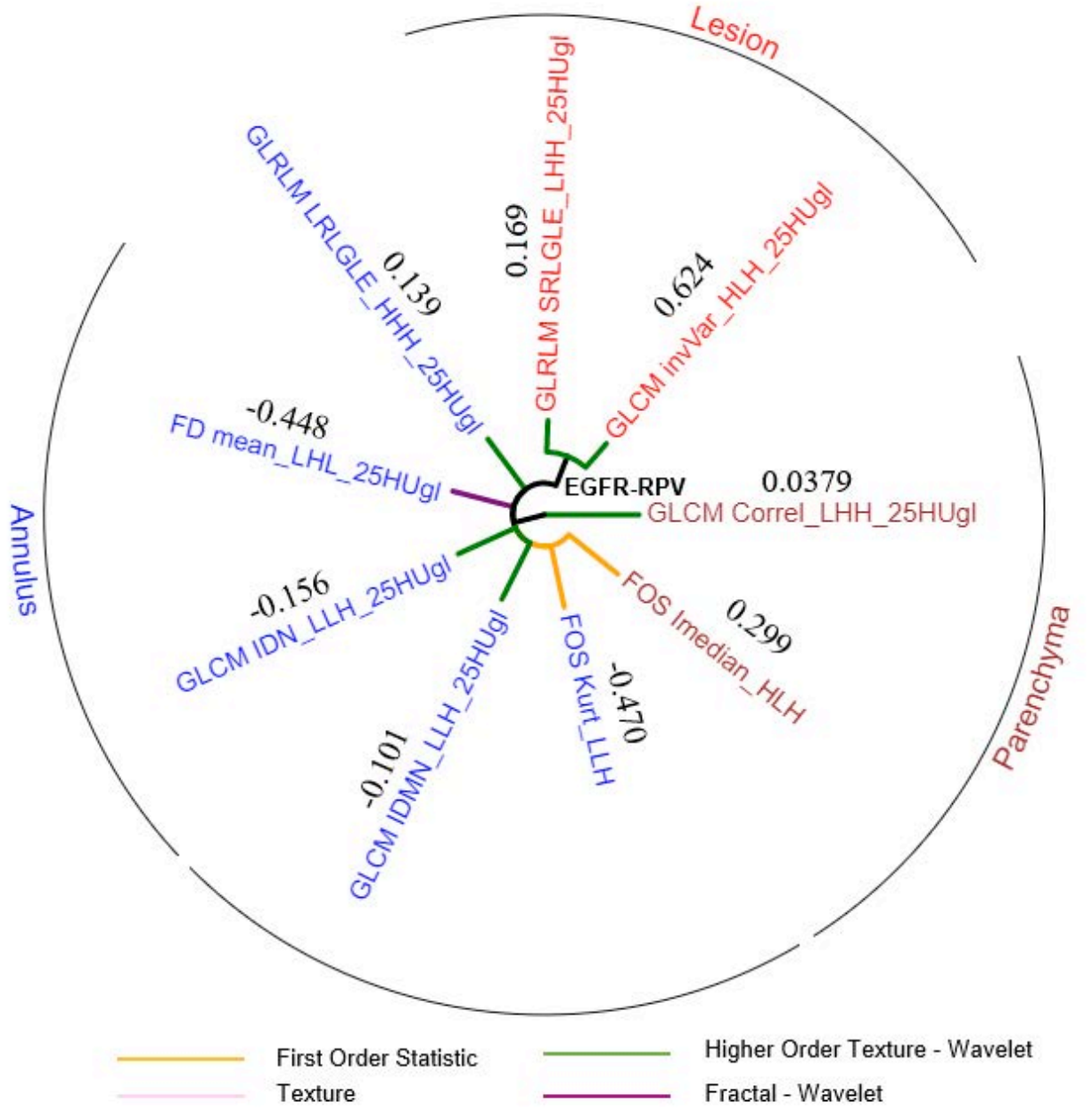

Component features of RPV. Note most features are from the perilesional annulus region; a finding consistent with the usual distribution of oncogenetic cells driving tumour growth.

Conclusion

A CT radiomics-based signature can facilitate personalised medicine by guiding treatment decisions for EGFR mutation targeting therapy in NSCLC.

References:

[1] Steuer CE, Khuri FR, Ramalingam SS., (2015), The next generation of epidermal growth factor receptor tyrosine kinase inhibitors in the treatment of lung cancer, Cancer, E1–E6

[2] Rothschild SI. , (2015), Targeted Therapies in Non-Small Cell Lung Cancer—Beyond EGFR and ALK, Cancers , 930-949

[3] Lambin P, Rios-Velazquez E, Leijenaar R, Carvalho S, van Stiphout RG, Granton P, Zegers CM, Gillies R, Boellard R, Dekker A, Aerts HJ., (2012), Radiomics: extracting more information from medical images using advanced feature analysis, Eur. J. Cancer , 441–446, 48

[4] Chen M, Lu H, Copley SJ, Han Y, Logan A, Viola P, Cortellini A, Pinato DJ, Power D, Aboagye EO , (2023), A novel radiogenomics biomarker for predicting treatment response and pneumotoxicity from programmed cell death protein or ligand-1 inhibition immunotherapy in NSCLC, Journal of Thoracic Oncology, S1556-0864(23)00096-5

[5] Jia TY, Xiong JF, Li XY, Yu W, Xu ZY, Cai XW, Ma JC, Ren YC, Larsson R, Zhang J, Zhao J, Fu XL., (2019), Identifying EGFR mutations in lung adenocarcinoma by noninvasive imaging using radiomics features and random forest modeling, European Radiology, 4742–4750, 29

[6] Peng P, Lv G, Hu J, Wang K, Lv J, Guo G., (2021), Co-mutations of epidermal growth factor receptor and BRAF in Chinese non-small cell lung cancer patients, Ann. Transl. Med, 1321–1321, 9

A-419

CT-based diaphragm analysis to evaluate the diaphragm configuration with increasing COPD severity

J. T. Bakker[1,2], J. E. Hartman[1,2], K. Klooster[1,2], D. A. Lynch[3], M. C. van der Molen[1,2], J.-P. Charbonnier[4], M. Tsiaousis[4], R. Vliegenthart[5], D.-J. Slebos[1,2]

[1]University Medical Center Groningen, Department of Pulmonary Diseases, Groningen, The Netherlands, [2]University Medical Center Groningen, Groningen Research Institute for Asthma and COPD, Groningen, The Netherlands, [3]National Jewish Health, Department of Radiology, Denver, Colorado, United States of America, [4]Thirona, Nijmegen, The Netherlands, [5]University Medical Center Groningen, Department of Radiology, Groningen, The Netherlands

Purpose/Objectives

Individuals with severe COPD often experience hyperinflation, a condition where air becomes trapped in the lungs, leading to changes in diaphragm configuration, specifically flattening. This is thought to be a key factor in the functional decline of these individuals. Current hyperinflation assessments primarily focus on lung volume measurements. Although, analyzing changes in diaphragm configuration may provide more valuable information. However, the extent to which the diaphragm configuration change contributes to lung function impairment is not well understood. CT scans are frequently utilized to evaluate the emphysema status of individuals with COPD, and these scans may also provide information about the diaphragm. However, accurately delineating the diaphragm can be difficult. For diaphragm configuration extraction, a viable alternative to delineation is using the intersection of the lungs and diaphragm. The goal of this study is to develop a CT-based tool for analyzing the diaphragm configuration by extraction of the lung-diaphragm intersection and investigating the relationship of the diaphragm configuration with pulmonary function in individuals with COPD.

Methods & Materials

This study uses a CT-based diaphragm quantification tool which derives the diaphragm configuration from the diaphragm-lung intersection in three steps: 1) identification of the pulmonary lobes using an AI-based lung quantification analysis platform (LungQ, Thirona, Nijmegen, The Netherlands), 2) extracting a 3D-shape map of the identified lung-diaphragm intersection (figure 1A), and 3) calculating the diaphragm index (ratio of identified diaphragm surface area / projected surface area)[1]. Inspiratory CT scans were obtained from the complete first phase of the multi-center COPDGene study (n=9567) and used to evaluate the relation between the automatically extracted diaphragm index and FEV_1%-predicted, GOLD stages, and CT quantified emphysema (LAA<-950; low attenuation regions below -950HU) (Figure 1).

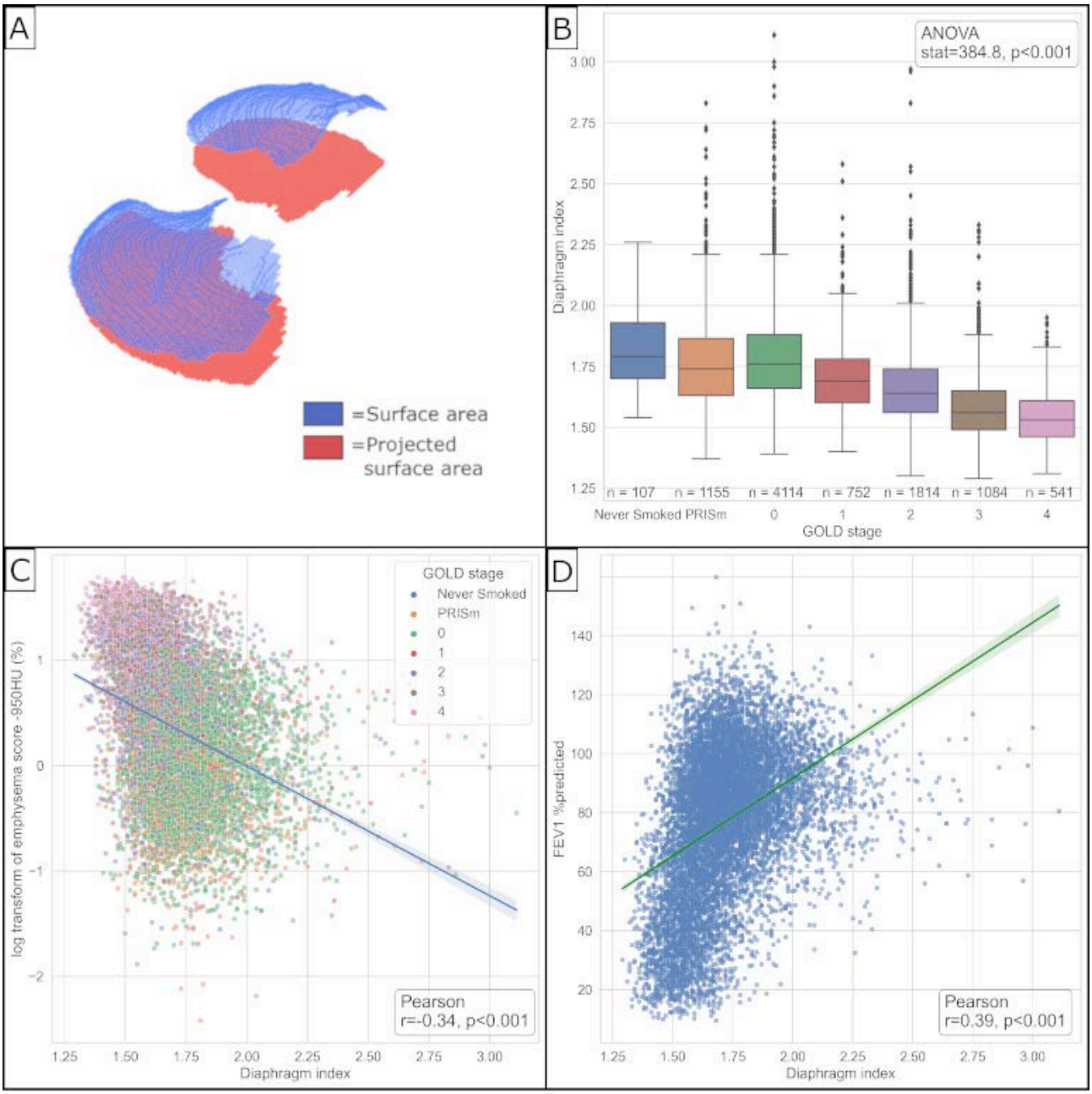

Figure 1. [A] 3D rendering of a diaphragm segmentation, the surface area is marked in blue and the projected surface area is marked in red. [B] Boxplot of the diaphragm index versus GOLD stages. A post-hoc Tukey's test determined that most groups had significantly different means ($p<0.001$). [C] Emphysema destruction score (percentage at -950HU) versus diaphragm index, the GOLD stages are included in color with legend. [D] FEV1 %predicted versus diaphragm index.

Results

We found a significant association between the diaphragm index and emphysema (figure 1C) and between the diaphragm index and FEV_1 %-predicted (figure 1D). We found significant differences in diaphragm index between GOLD stages (Figure 1B).

Conclusion

We developed an automatic CT-based diaphragm quantification analysis, which is able to demonstrate significant differences in diaphragm configuration relative to pulmonary function in COPD.

References:

[1] Chang Y, Bae J, Kim N, Park JY, Lee SM, Seo JB, (2016), Three-dimensional quadratic modeling and quantitative evaluation of the diaphragm on a volumetric CT scan in patients with chronic obstructive pulmonary disease, Wiley, Medical Physics, 4273-4282, 7

A-369

CT-derived small and peel pulmonary vessel blood volume measurements as potential imaging biomarkers for the diagnosis of PAH and CTEPH

D. Alkhanfar[1,2,3], S. Alabed[1,3], K. Dwivedi[1,3,4], L. Abdulaal[1], Y. Shahin[1,3], C. Johns[1,3], P. Garg[4], A. R. Thompson[1,4], A. M. Rothman[1,4], A. Hameed[4], A. Charalampopoulos[4], J. M. Wild[1,2], R. Condliffe[4], D. G. Kiely[2,4], A. J. Swift[1,2,3]

[1]University of Sheffield, IICD / Academic Unit of Radiology, Sheffield, United Kingdom, [2]University of Sheffield, INSIGNEO, Institute for In Silico Medicine, Sheffield, United Kingdom, [3]Sheffield Teaching Hospitals, Department of Clinical Radiology, Sheffield, United Kingdom, [4]Sheffield Teaching Hospitals NHS Foundation Trust, Sheffield Pulmonary Vascular Disease Unit, Royal Hallamshire Hospital, Sheffield, United Kingdom

Purpose/Objectives

The purpose of this study was to investigate the differences in pulmonary vascular tree structures between control patients, patients with pulmonary arterial hypertension (PAH) and those with chronic thromboembolic pulmonary hypertension (CTEPH) using computed tomography (CT) pulmonary vessel analysis.

Methods & Materials

This retrospective study included control and patients diagnosed with either PAH or CTEPH who had undergone CT and right heart catheter (RHC) within the same day. The CT pulmonary vessel software was used to extract and segment the pulmonary vascular trees into central <0.8, 1.2 and 1.6 ml/m2 small pulmonary vessel volumes (SPVVs), peripheral 15, 30 and 45 mm peel pulmonary vessel volumes (PPVVs) and total lung and vessel volumes. RHC measurements were taken to diagnose patients and calculate the pulmonary vascular resistance (PVR) and pulmonary function testing (PFTs) to calculate the transfer factor for carbon monoxide (TLCO). Statistical analyses were performed to determine any significant differences between the three groups.

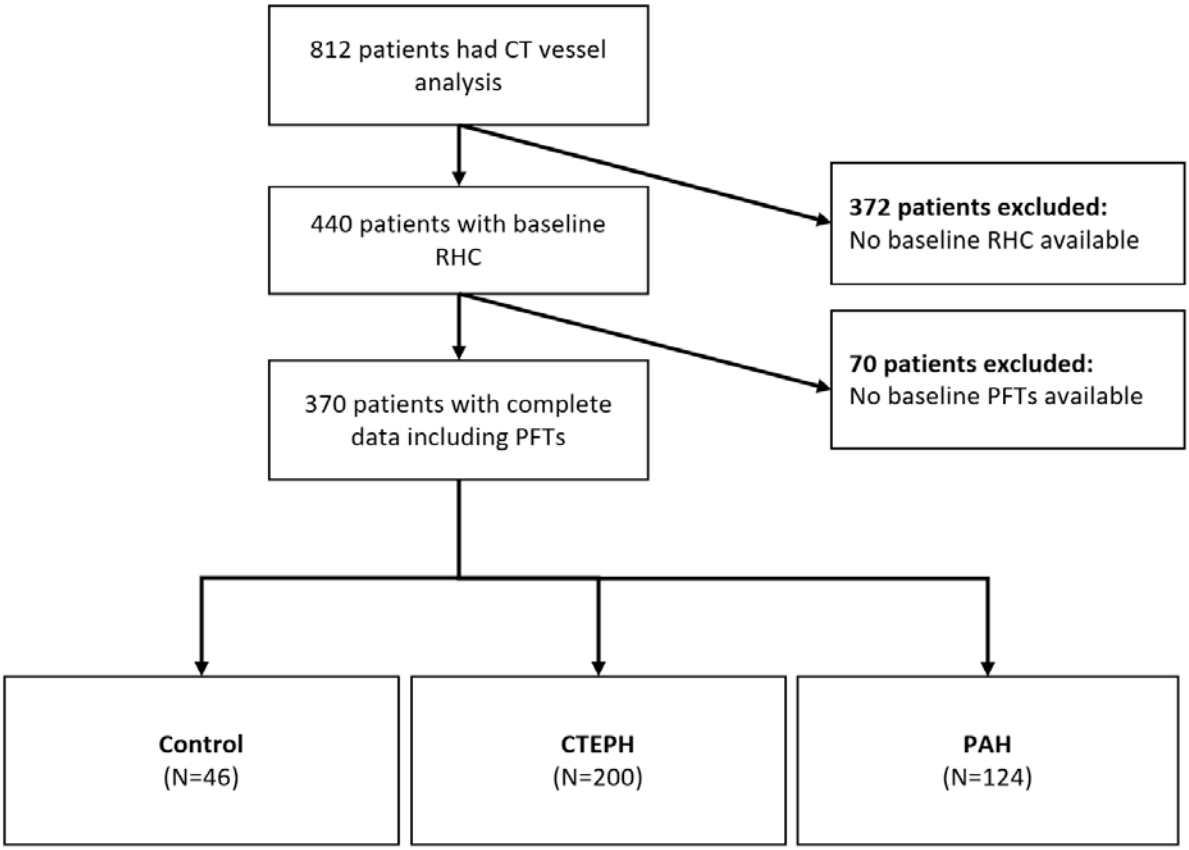

Study flow chart demonstrating the inclusion criteria and groups of patients included in the study.

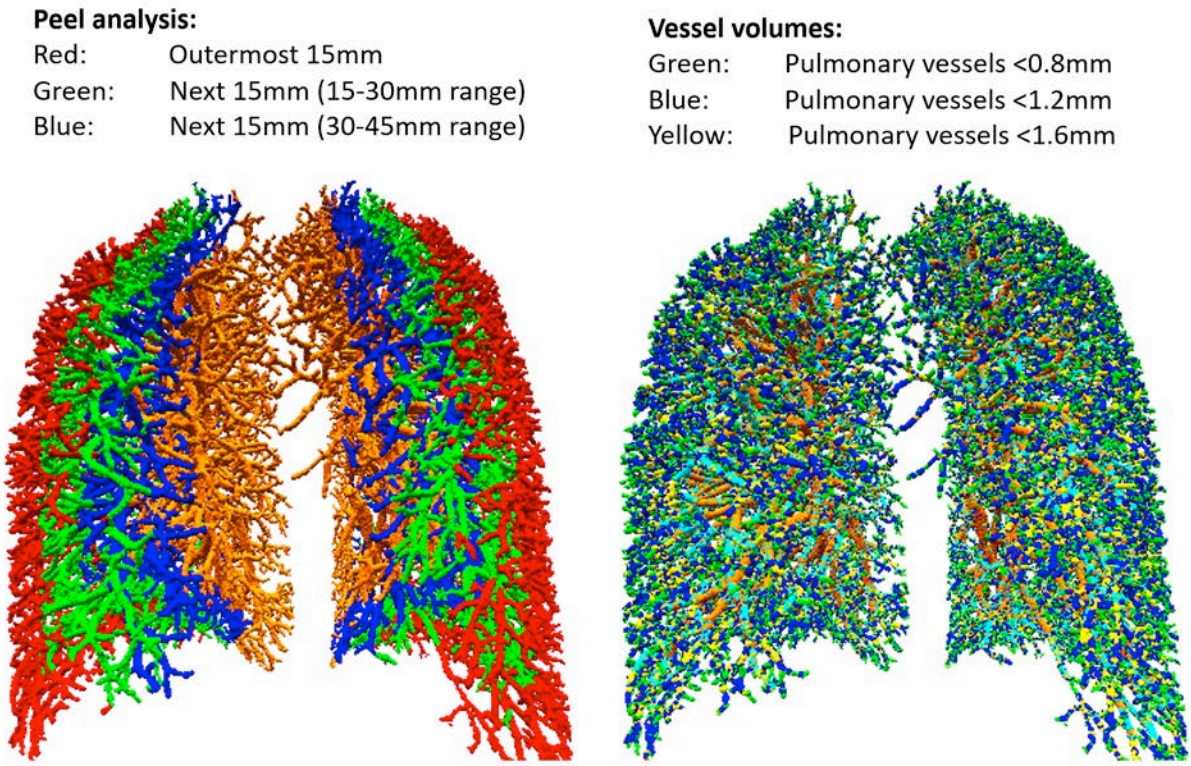

Vascular masks for peel pulmonary vessels (left) show peel vessels at 15-mm (red), 30-mm (green), and 45-mm (dark blue) depths from pleural surface. Small pulmonary vessels (right) with a diameter of 0.4 mm (red), 0.8 mm (green), 1.2 mm (dark blue), 1.6 mm (yellow), and 2 mm (cyan). The light brown colour represents large proximal vessels.

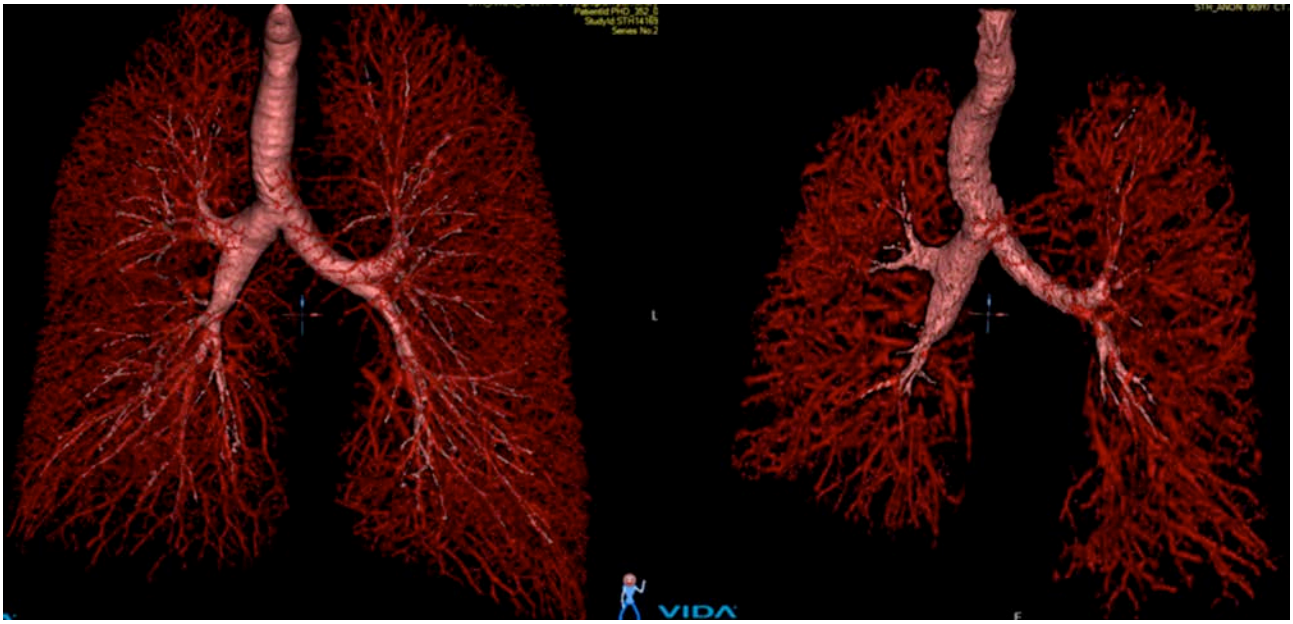

Pulmonary vessel masks. A visual comparison of an example of a patient with CTEPH (Right) and a control patient with no pulmonary vascular disease (Left).

Results

This study found that control (46 patients), PAH (124 patients) and CTEPH (200 patients) can be distinguished by their different peripheral vessel volume percentages. CTEPH had significantly lower PPVVs and vessel volume index, and significantly higher SPVVs and lung volumes than both control and PAH (all $p<0.05$). SPVVs had a significant positive correlation with haemodynamics and both SPVVs and PPVVs had a significant negative correlation with TLCO in CTEPH, but such correlations were not evident in PAH. At Kaplan-Meier analysis, in patients with segmental/subsegmental CTEPH, loss of small pulmonary arteries predicted mortality; log rank chi square was 5.54 and $p=0.01$ for SPVV <0.8mm, 4.35 and $p=0.03$ for SPVV <1.2mm and 5.04 and $p=0.02$ for SPVV <1.6mm. Small vessel changes did not predict mortality in PAH or in central/lobar CTEPH.

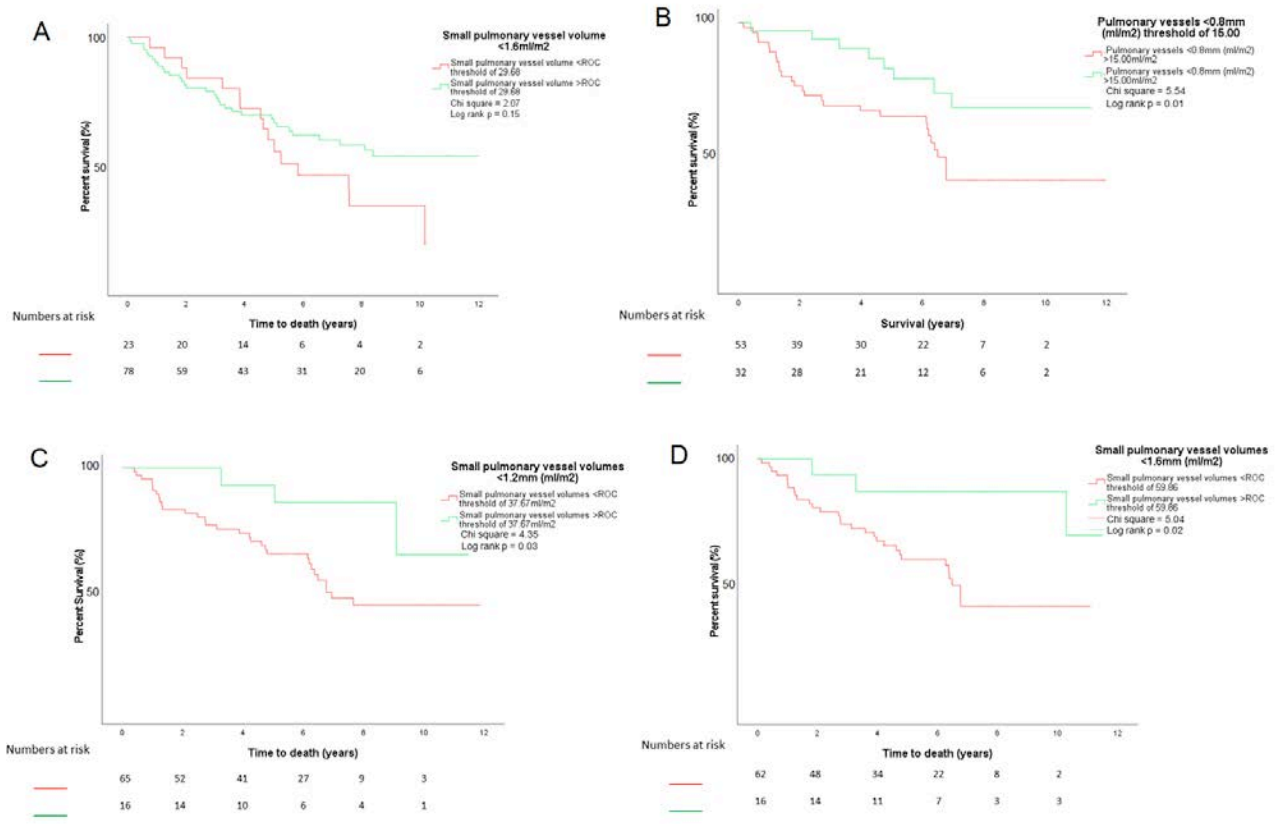

Kaplan-Meier plot showing patients with greater and lesser small vessel volumes than the receiver operating characteristic (ROC) curve thresholds. A) refers to SPVVs <1.6mm in patients with lobar/central CTEPH; B), C) and D) refer to SPVVs <0.8, 1.2 and 1.6mm respectively in patients with segmental/subsegmental CTEPH.

Conclusion

PAH and CTEPH can be differentiated based on automatic measurements of pulmonary blood vessels and CT can potentially be used to support the diagnosis and differentiate between the two conditions.

A-517

CT-guided percutaneous wire localization of pulmonary nodules: the influence of the shape of the wire on complications and outcome.

Y. J. Markenstein[1], F. T. H. Bodewes[1], B. I. Hiddinga[2], W. Timens[3], C. van de Wauwer[4], M. E. Erasmus[4], T. R. G. Stams[1], T. Velleman[1], M. D. Dorrius[1], G. J. de Jonge[1]

[1]University Medical Center Groningen, Medical Imaging Center, Groningen, The Netherlands, [2]University Medical Center Groningen, Lung disease and tuberculosis, Groningen, The Netherlands, [3]University Medical Center Groningen, Pathology and Medical Biology, Groningen, The Netherlands, [4]University Medical Center Groningen, Cardiology & Thorax Surgery, Groningen, The Netherlands

Purpose/Objectives

Resection of small pulmonary nodules can be facilitated by CT-guided percutaneous wire localization of the nodule prior to Video-Assisted Thoracic Surgery (VATS), and is associated with high diagnostic accuracy and therapeutic efficacy. The aim of this study was to compare the incidence of complications and outcome between two different wire systems.

Methods & Materials

We included 78 consecutive patients who underwent CT-guided wire localization in the period August 2019 - March 2023. In 39 patients, a Somatex Duo System wire was used (fish hook shaped wire) and in the other 39 patients a Somatex Lung Marker System was used (spirally shaped wire). The incidence of complications and outcome was compared between both groups in terms of minor and major complications (minor: small pneumothorax, mild parenchymal hemorrhage or minor hemoptysis, major: drain placement for large pneumothorax, hemothorax, air embolism or longer hospital stay), representativeness of the histological diagnosis, and duration of procedures (CT and operation room (OR) time). Statistical analyses were performed using SPSS software, including the chi-squared for the nominal variables and a Manova test for the ratio variables.

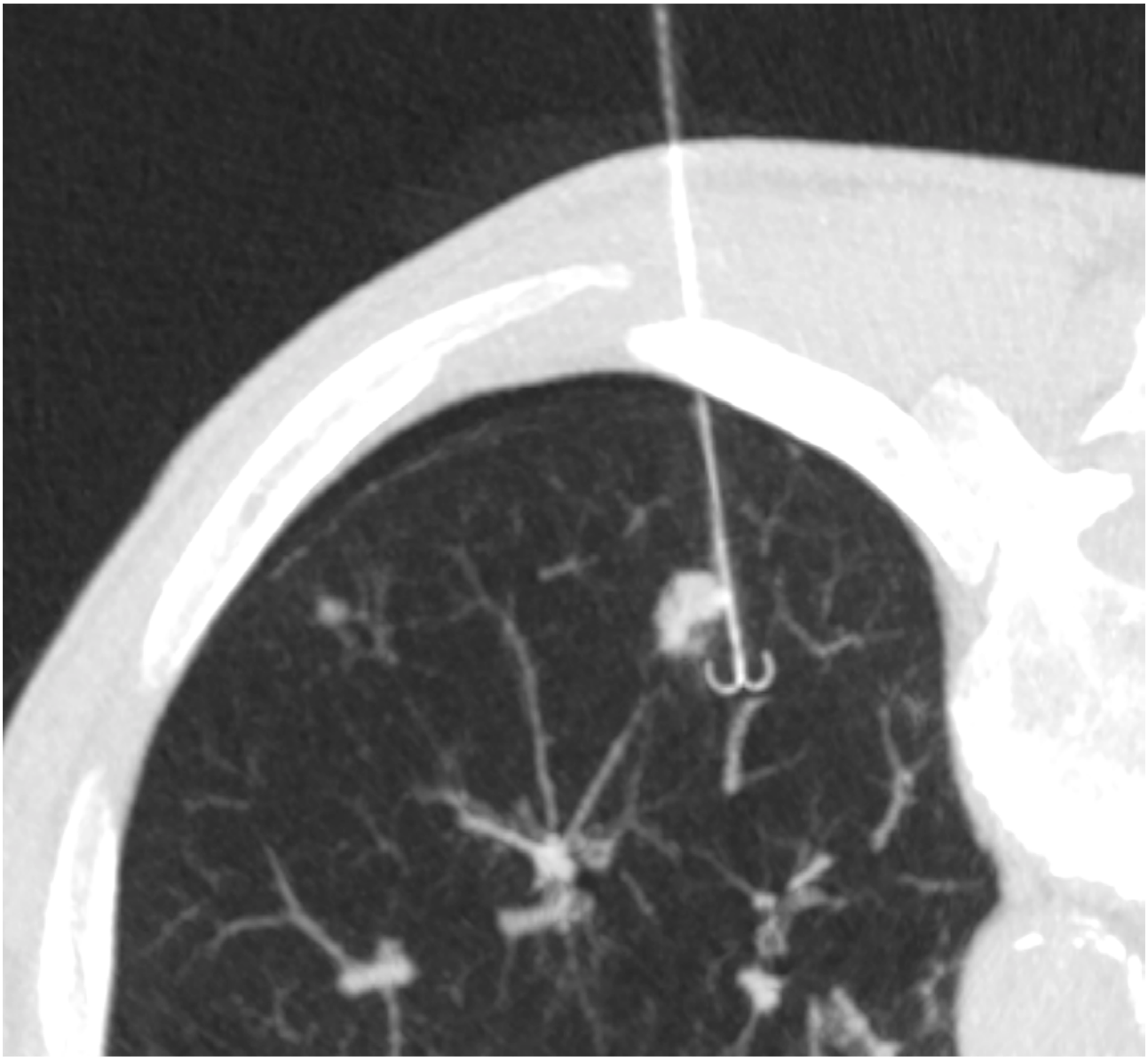

Fish hook shaped wire

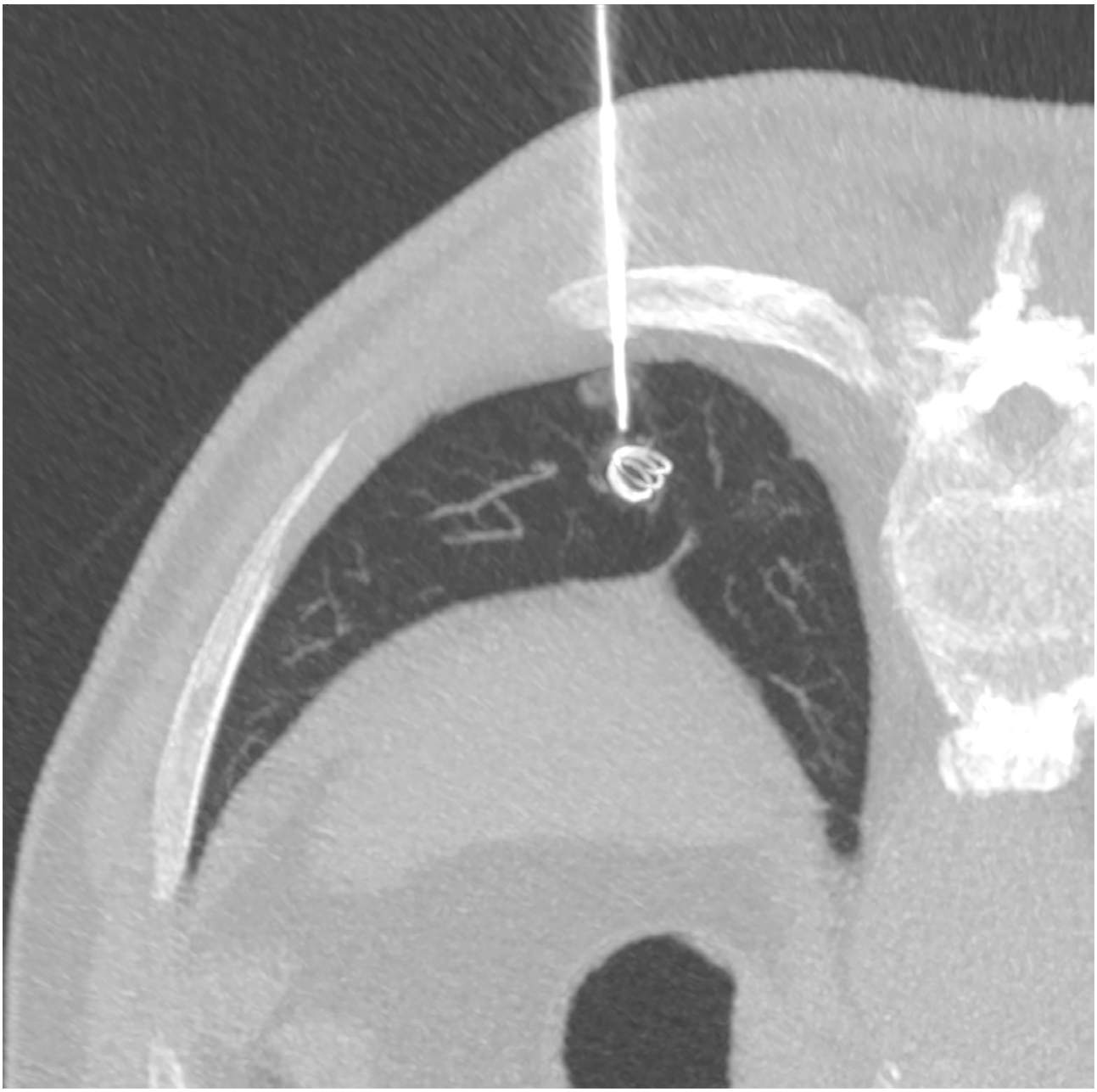

Spirally shaped wire

Results

There was no statistical difference in CT and OR time between the two groups (fish hook wire localization: 30,8 ± 11,1 min; OR-time: 69,3 ± 41,0 min, spiral wire localization: 30,7 ± 9,8, OR-time: 66,4 ± 27,25). Also, the incidence of minor (fish hook wire: 74%; spiral wire: 56%) and major (for both wires 3%) complications during CT-guided percutaneous wire localization was not considered significantly different. The spiral wire had a superficial / pleural location in 5 patients, but this did not affect the surgical outcome. During VATS, there were no significant differences found between the incidence of complications: in 11 (hookwire: 6; spiral wire: 5) cases the wire was dislodged and there were 4 cases reported in which a bleeding occurred during VATS (hookwire:2; spiral wire:2). No significant difference was found for representativeness of resection between the hookwire (37/39) and the spiral wire (39/39).

Conclusion

In this study, no statistically significant differences were found between the two types of localization wires in terms of complications and outcome. However, more experience with the usage of the newly introduced spiral wire might influence and improve the outcome, and future studies including greater sample sizes will provide more clarification regarding the optimal wire localization kit.

A-439

Deep learning automated quantification of lung disease in pulmonary hypertension on CT pulmonary angiography with external validation

K. Dwivedi[1], M. Sharkey[2], S. Alabed[1], A. Swift[1]
[1]University of Sheffield, Sheffield, United Kingdom, [2]Sheffield Teaching Hospitals NHS Trust, Sheffield, United Kingdom

Purpose/Objectives
Lung disease assessment in precapillary pulmonary hypertension (PH) is essential for appropriate patient management. All patients undergo Computational Tomography (CT) imaging routinely as part of the ERS/ESC guidelines diagnostic algorithm. This study aims to develop an artificial intelligence (AI) deep learning model for lung texture classification in CT Pulmonary Angiography (CTPA), and evaluate its correlation with clinical assessment methods.

Methods & Materials
In this retrospective study with external validation, 122 patients with pre-capillary PH were used to train (n=83), validate (n=17) and test (n=10 internal test, n=12 external test) a patch based DenseNet-121 classification model. 'Normal', 'Ground glass', 'Ground glass with reticulation', 'Honeycombing', and 'Emphysema' were classified as per the Fleishner Society glossary of terms. Ground truth classes were segmented by two radiologists with patches extracted from the labelled regions. Proportion of lung volume for each texture was calculated by classifying patches throughout the entire lung volume to generate a coarse texture classification mapping throughout the lung parenchyma. AI output was assessed against diffusing capacity of carbon monoxide (DLCO) and specialist radiologist reported disease severity.

Results
Micro-average AUCs for the validation, internal test, and external test were 0.92, 0.95, and 0.94, respectively. The model had consistent performance across parenchymal textures, demonstrated strong correlation (R = 0.63 for normal lung) with diffusing capacity of carbon monoxide (DLCO). 'None', 'mild', 'moderate' and 'severe' emphysema scored by radiologists corresponded to 1(0,9) %, 4(2,14)%, 31(21,51)%, and 69(33,77)% as quantified by the deep learning learning model; there was a significant ($p<0.001$) difference between groups.

Characteristic	Full Cohort N = 122[1]	Dataset groups				
		training, N = 83[1]	validation, N = 17[1]	internal test, N = 10[1]	external test, N = 12[1]	p-value[2]
Age at diagnosis, years	68 (60, 75)	68 (60, 75)	66 (61, 75)	67 (54, 78)	69 (65, 73)	>0.9
Sex, female	58 (49%)	37 (46%)	10 (59%)	5 (50%)	6 (50%)	0.8
Body Mass Index	27.2 (23.8, 31.8)	27.4 (23.8, 30.8)	27.6 (25.0, 32.6)	25.7 (23.6, 27.1)	25.9 (21.9, 33.3)	0.4
WHO Function class						0.9
2	10 (8.5%)	7 (8.8%)	1 (6.2%)	1 (11%)	1 (8.3%)	
3	58 (50%)	42 (52%)	8 (50%)	4 (44%)	4 (33%)	
4	49 (42%)	31 (39%)	7 (44%)	4 (44%)	7 (58%)	
FVC, percent predicted	78 (65, 103)	80 (65, 104)	78 (67, 105)	67 (58, 110)	73 (63, 74)	0.7
FEV1, percent predicted	69 (53, 85)	70 (56, 85)	67 (48, 89)	73 (51, 76)	64 (51, 80)	>0.9
FEV1 / FVC ratio	73 (59, 81)	72 (58, 81)	66 (56, 78)	73 (63, 79)	77 (67, 84)	0.5
DLCO, percent predicted	26 (18, 37)	27 (18, 42)	23 (19, 27)	25 (22, 27)	27 (17, 31)	0.3
mPAP, mm Hg	46 (35, 54)	45 (34, 56)	47 (40, 56)	39 (28, 48)	46 (41, 50)	0.3
CT scanner manufacturer						**<0.001**
GE	107 (90%)	80 (100%)	17 (100%)	9 (90%)	1 (8.3%)	
Siemens	6 (5.0%)	0 (0%)	0 (0%)	0 (0%)	6 (50%)	
Canon	6 (5.0%)	0 (0%)	0 (0%)	1 (10%)	5 (42%)	
Normal lung	43 (20, 63)	46 (30, 70)	26 (19, 62)	25 (15, 42)	34 (17, 53)	0.058
Ground glass (GG)	5 (1, 13)	4 (1, 10)	5 (2, 20)	10 (2, 19)	7 (4, 11)	0.3
Ground glass with reticulation (GGR)	6 (1, 24)	4 (0, 17)	14 (2, 26)	23 (3, 36)	7 (2, 30)	0.11
Honeycombing	2 (1, 7)	2 (1, 6)	2 (1, 13)	4 (2, 10)	5 (2, 9)	0.2
Emphysema	10 (1, 33)	15 (1, 32)	8 (2, 26)	13 (0, 46)	1 (0, 12)	0.4
Fibrosis	11 (2, 32)	6 (1, 26)	18 (3, 42)	30 (8, 41)	10 (6, 40)	0.10

[1] Median (IQR); n (%)

[2] Kruskal-Wallis rank sum test; Fisher's exact test

Table 1: Patient characteristics for the full cohort, training, validation, internal and external test datasets.

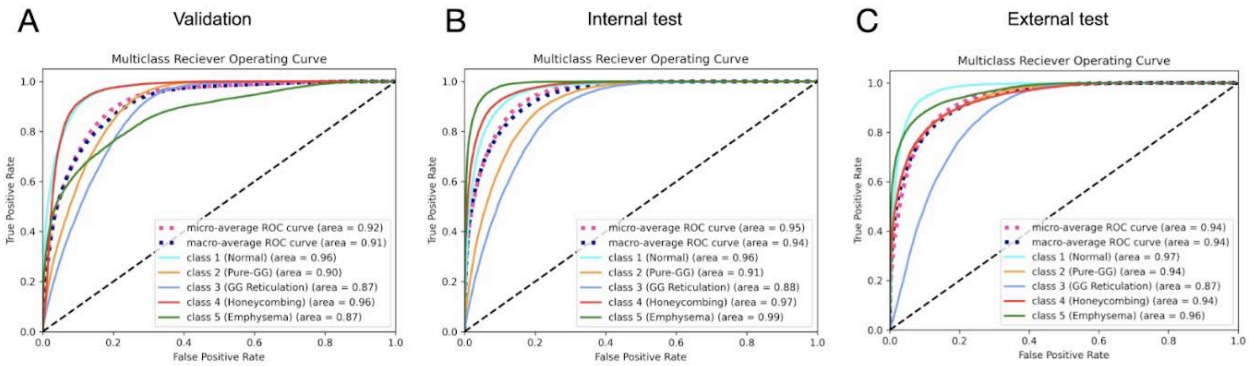

Multiclass Receiver Operating Curve for validation (A), internal test (B) and external test (C) datasets of the hypertuned model

Conclusion

The deep learning classification model demonstrates excellent performance on external validation. The clinical utility of its output has been demonstrated. This objective, repeatable measure of disease severity can aid in patient management in adjunct to radiological reporting.

A-574

Dual-source dual-energy CTPA in obese patients with reduced contrast media volume: image quality and virtual monoenergetic reconstructions (VMI+).

P. Seitz, T. Schönfeld, C. D. Krieghoff, C. Lücke, M. Gutberlet, R. F. Gohmann
Leipzig Heart Center, Diagnostic and Interventional Radiology, Leipzig, Germany

Purpose/Objectives

To investigate the feasibility and objective image quality of dual-energy CT pulmonary angiography (DE-CTPA) with reduced contrast in unselected, obese patients compared with standard protocol (Std.) CT pulmonary angiography in single-energy mode on the same second-generation dual-source CT.

Methods & Materials

86 patients were included (inclusion criteria: Suspected pulmonary artery embolism (LAE), DE-CTPA or Std., BMI >25 kg/m2, and age >18 y). We retrospectively analyzed the contrast-to-noise ratio (CNR), as well as patient -characteristics. Asynchronous virtual monoenergetic reconstructions (VMI+) were compared in DE-CTPA in 49 patients versus Std. in 37 patients. The studies were performed at 80kV/Sn 140 kV in DE-CTPA and 100-120 kV in Std. Contrast volume was 25 ml and 50 ml in DE-CTPA-Group and Str. group respectively. Flow rate was 4ml/s in both groups. VMI+ reconstructions were performed for 40 keV and 80 keV. Signal/intensity Contrast (in Hounsfield units), Contrast-to-noise ratio (CNR), Signal-to-noise-ratio was determined in all pulmonary arteries down to the segmental level.

Results

Median BMI for DE-CTPA group (35.3 [32.5 - 38.2]) and Std. group (30.6 [28.7- 34.3]) differed significantly (*p<0.001*). The other patient characteristics showed no significant differences. Especially LAE detection rate did not differ significantly.

For VMI+ reconstruction at 40keV, median total CNR was 25.2 [12.4- 42.0], and 11.90 [6.8 - 22.4] for 80keV, respectively, and 10.31 [8.8- 12.5] for Std.

CNR at 40keV was significantly higher than in the Std. group (*p< 0.0001*), and at 80kV showed no significant difference from Std. (*p=0,61*) and .

For VMI+ reconstruction at 40keV, median total SNR was 11.9 [9.2- 16.3], and 12.10 [9.6 - 15.2] for 80kV, respectively, and 10.70 [9.6 - 13.5] for Std.

SNR at 40kV (*p=0,32*) and at 80keV (*p= 0,24*) showed no significant difference to Std. .

Comparison of objective image quality is depicted in **Table 1**.

Conclusion

DE-CTPA allows a significant reduction in the amount of KM in obese patients without significantly affecting the LAE detection rate. Using VMI+ reconstruction, better objective image quality can be achieved even in obese patients compared to Std.

	Dual-Energy CTPA						**Standard CTPA**	
	VMI+ 40 keV			*VMI+ 80 keV*				
	MW/Median		p-Wert	MW/Median		p-Wert	MW/Median	
Signal intensity/Contrast (HU)	681,6	[569,3 - 820,0]	< 0,0001	199,6	[168,4 - 242,4]	< 0,0001	354	[311,5 - 459,9]
Noise	55,3	[50,6 - 60,4]	< 0,0001	16,5	± 2,5	< 0,0001	33,8	± 4,3
Signal-to-noise-ratio	11,9	[9,2 - 16,3]	0,32	12,1	[9,6 - 15,2]	0,24	10,7	[9,6 - 13,5]
Contrast-to-noise-ratio	25,2	[12,4 - 42,0]	< 0,0001	11,9	[6,8 - 22,4]	0,61	10,3	[8,8 - 12,5]

Table 1: Comparison of objective Image Quality for Dual Energy CTPA dual-energy CT pulmonary angiography (CTPA) and Boa_Image_Frame CTPA; HU=Hounsfield Units; VMI+=Asynchronous virtual monoenergetic reconstructions

A-143

Elexacaftor/Tezacaftor/Ivacaftor Improves Bronchial Artery Dilatation Detected by Magnetic Resonance Imaging in Patients with Cystic Fibrosis

L. Wucherpfennig[1,2,3], S. M. F. Triphan[1,2,3], W. Sabine[4], H.-U. Kauczor[1,2,3], C. P. Heussel[1,2,3], O. Sommerburg[2,5], M. Stahl[6,7,8], M. A. Mall[6,7,8], M. Eichinger[1,2,3], M. O. Wielpütz[1,2,3]

[1]University Hospital Heidelberg, Department of Diagnostic and Interventional Radiology, Heidelberg, Germany, [2]Translational Lung Research Center Heidelberg (TLRC), German Center for Lung Research (DZL), Heidelberg, Germany, [3]Thoraxklinik at University Hospital Heidelberg, Department of Diagnostic and Interventional Radiology with Nuclear Medicine, Heidelberg, Germany, [4]Thoraxklinik at University Hospital Heidelberg, Department of Pulmonology and Respiratory Medicine, Cystic Fibrosis Center, Heidelberg, Germany, [5]University Hospital Heidelberg, Department of Translational Pulmonology and Division of Pediatric Pulmonology and Allergy and Cystic Fibrosis Center, Heidelberg, Germany, [6]Charité - Universitätsmedizin Berlin, corporate member of Freie Universität Berlin and Humboldt-Universität zu Berlin, Department of Pediatric Respiratory Medicine, Immunology and Critical Care Medicine, Berlin, Germany, [7]German Center for Lung Research (DZL), associated partner site, Berlin, Germany, [8]Charité - Universitätsmedizin Berlin, Berlin Institute of Health at Charité, Berlin, Germany

Purpose/Objectives

We recently demonstrated that magnetic resonance imaging (MRI) detects improvements in mucus plugging and bronchial wall thickening, but not lung perfusion in patients with cystic fibrosis (CF) treated with elexacaftor/tezacaftor/ivacaftor (ETI). It remains unclear, whether bronchial artery dilatation (BAD), a key feature of advanced lung disease, indicates irreversibility of perfusion abnormalities and whether BAD could be reversed in CF patients treated with ETI.

Methods & Materials

59 adults with CF underwent longitudinal chest MRI including MR angiography (MRA) twice, 35 CF patients (mean age 31±7y) before (MRI1) and after (MRI2) at least one month (mean duration 8±4mon) on ETI therapy and 24 control CF patients (mean age 31±7y) without ETI. MRI was assessed using the validated chest MRI score, and presence and total lumen area of BAD were assessed with commercial software.

Results

The MRI global score was stable in the control group from MRI1 to MRI 2 (mean difference: 1.1±3.4, P=0.054), but was reduced in the ETI group (-10.1±4.2, P<0.001). In the control as well as in the ETI group, BAD was present in almost all patients at baseline (95% and 94%, respectively) which did not change at MRI2. The BAD total lumen area did not change in the control group from MRI1 to MRI2 (mean difference: 1.0±3.0mm^2, P=0.099), but decreased in the ETI group (-6.6±5.8mm^2, P<0.001). This decrease correlated with improvements in the MRI global score (r=0.540, P<0.001).

Conclusion

Our data show that BAD may be partially reversible under ETI therapy in adult CF patients with established disease.

A-431

Estimating nodule size on Digital Chest Tomosynthesis – comparison of area and diameter measurements.

M. Oliveira Diniz[1,2], M. Khalil[1], E. Fagman[1,2], J. Vikgren[1,2], A. Svalkvist[3,4], M. Båth[3,4], Å. A. Johnsson[1,2]
[1]Institute of Clinical Sciences, Sahlgrenska Academy, University of Gothenburg, Department of Radiology, Gothenburg, Sweden, [2]Region Västra Götaland, Sahlgrenska University Hospital, Department of Radiology, Gothenburg, Sweden, [3]Institute of Clinical Sciences, The Sahlgrenska Academy, University of Gothenburg, Department of Radiation Physics, Gothenburg, Sweden, [4]Region Västra Götaland, Sahlgrenska University Hospital, Department of Medical Physics and Biomedical Engineering, Gothenburg, Sweden

Purpose/Objectives

To assess pulmonary nodule volume estimates based on area and mean diameter on digital tomosynthesis (DTS) of the chest in comparison to computed tomography (CT) as well as inter- and intraobserver agreement for the measurements.

Methods & Materials

Twenty four cases from the Swedish CArdioPulmonary bioImage Study [1][2] with solid pulmonary nodules examined with DTS and CT on the same day were evaluated in random order by 5 radiologists. One radiologist measured the nodules twice. The image viewer ViewDEX [3][4] was used for image visualization and data collection. Measurements were performed on coronal DTS and CT images. Additionally, a coronal maximum intensity series, a transaxial CT series and Computer Aided Detection (CAD) results were presented to the radiologists to aid detection of the nodule in DTS, figure 1. The observers were instructed to select the largest solid nodule based on CAD volume, draw the boundary area of the nodule with a freehand region of interest tool and thereafter draw the longest and its perpendicular diameter according to Fleischner guidelines [5]. All measurements on DTS were performed prior to the measurements on CT. Agreement was assessed according to Bland-Altman. The measurements of the observers were used to create an average observer regarding area and mean diameter of the nodules and volumes of spheres were calculated based on these estimates.

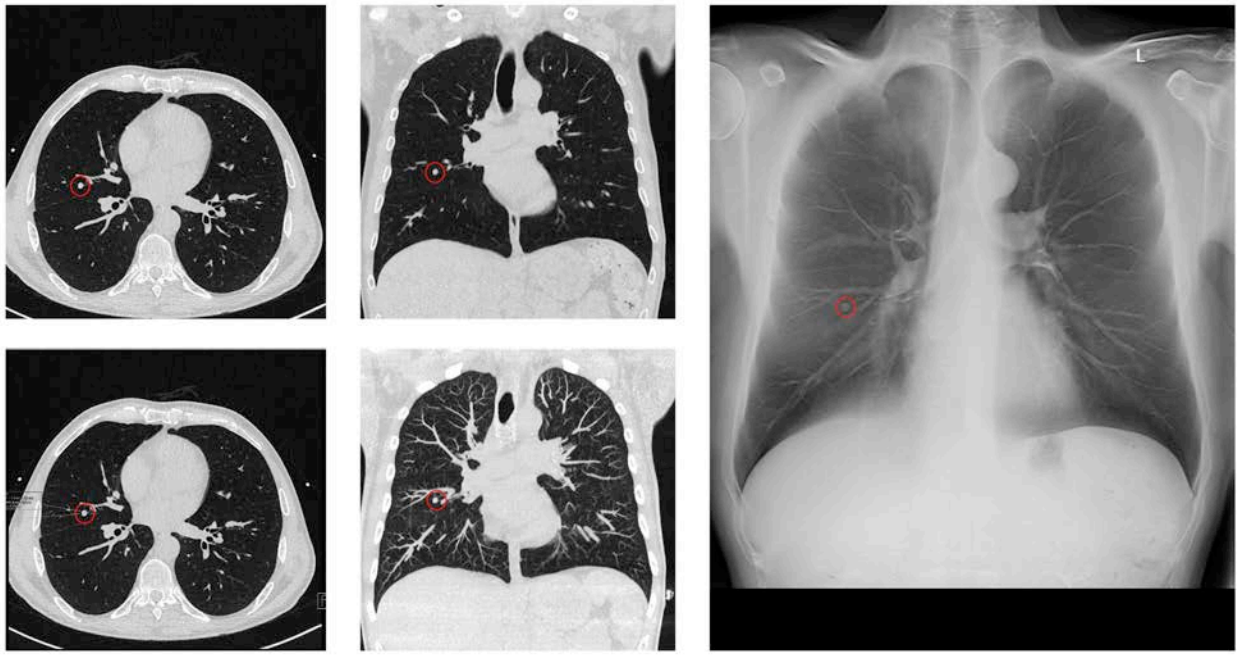

Figure 1.

Results

A total of 21 nodules were measured by all observers in both DTS and CT. The nodule volumes based on CT area ranged from 33 to 294 mm^3.The mean relative difference [with Limits of Agreement] between CT and DTS volumes for the average observer was 7.8 [-50.1;65.8]% and 14.5 [-50.1;80.0]% based on area and mean diameter, respectively. The mean relative difference between volume based on area and mean diameter on DTS was 5.2 [-27.7;38.2]% and the corresponding results for CT was -12.2 [-45.7;21.4]%. When comparing the individual observers regarding area and mean diameter measurements on DTS, mean difference ranged from -2.7 [-15.5;10.2]mm^2 to -6.4 [-38.7;26.2]mm^2 and from 0.3 [-1.4;2.1]mm to -1.5 [-5.1;2.0]mm, respectively. The corresponding results from CT ranged from 0.6 [-9.3;10.6]mm^2 to -1.0 [-15.3;13.4]mm^2 and from 0.1 [-1.0;1.3]mm to -0.5 [-2.4;1.4]mm, respectively. The intraobserver mean difference regarding area on DTS and CT was -0.3 [-15.0;15.6]mm^2 and 1.2 [-3.9;6.3]mm^2 and the corresponding results regarding mean diameter was -0.1 [-2.3;2.1]mm and 0.2 [-0.6;1.0]mm respectively.

Conclusion

The agreement between DTS and CT derived volume estimates based on nodule area were improved in comparison to volume estimates based on mean diameter. Measurement variability was greater in DTS compared to CT.

References:

[1] Bergström G, Berglund G, Blomberg A, Brandberg J, Engström G, Engvall J, Eriksson M, de Faire U, Flinck A, Hansson MG, Hedblad B, Hjelmgren O, Janson C, Jernberg T, Johnsson Å, Johansson L, Lind L, Löfdahl CG, Melander O, Östgren CJ, Persson A, Persson M, Sandström A, Schmidt C, Söderberg S, Sundström J, Toren K, Waldenström A, Wedel H, Vikgren J, Fagerberg B, Rosengren A. The Swedish CArdioPulmonary BioImage Study: objectives and design. J Intern Med. 2015 Dec;278(6):645-59. doi: 10.1111/joim.1
[2] Torén K, Olin AC, Lindberg A, Vikgren J, Schiöler L, Brandberg J, Johnsson Å, Engström G, Persson HL, Sköld M, Hedner J, Lindberg E, Malinovschi A, Piitulainen E, Wollmer P, Rosengren A, Janson C, Blomberg A, Bergström G. Vital capacity and COPD: the Swedish CArdioPulmonary bioImage Study (SCAPIS). Int J Chron Obstruct Pulmon Dis. 2016 May 2;11:927-33. doi: 10.2147/COPD.S104644. PMID: 27194908; PMCID: PMC4859418.
[3] Svalkvist A, Svensson S, Hagberg T, Båth M. VIEWDEX 3.0-RECENT DEVELOPMENT OF A SOFTWARE APPLICATION FACILITATING ASSESSMENT OF IMAGE QUALITY AND OBSERVER PERFORMANCE. Radiat Prot Dosimetry. 2021 Oct 12;195(3-4):372-377. doi: 10.1093/rpd/ncab014. PMID: 33683321; PMCID: PMC8507463.
[4] Svalkvist A, Svensson S, Håkansson M, Båth M, Månsson LG. VIEWDEX: A STATUS REPORT. Radiat Prot Dosimetry. 2016 Jun;169(1-4):38-45. doi: 10.1093/rpd/ncv543. Epub 2016 Jan 27. PMID: 26822421.
[5] MacMahon H, Naidich DP, Goo JM, Lee KS, Leung ANC, Mayo JR, Mehta AC, Ohno Y, Powell CA, Prokop M, Rubin GD, Schaefer-Prokop CM, Travis WD, Van Schil PE, Bankier AA. Guidelines for Management of Incidental Pulmonary Nodules Detected on CT Images: From the Fleischner Society 2017. Radiology. 2017 Jul;284(1):228-243. doi: 10.1148/radiol.2017161659. Epub 2017 Feb 23. PMID: 28240562.

A-584

Feasibility of AI-based automated reading for LungRADS categories assignment: a preliminary analysis.

V. I. Gallone[1], C. Zilioli[1], P. Favia[1], R. Mura[1], L. Leo[2], D. M. Cavalieri[1], D. Tesse[2], R. E. Ledda[1], G. Milanese[1], N. Sverzellati[1], M. Silva[1]
[1]University of Parma, Department of Medicine and Surgery, Parma, Italy, [2]University of Parma, Parma, Italy

Purpose/Objectives
To compare human and automated artificial intelligence (AI)-driven evaluation of chest ultra-low dose computed tomography (ULDCT) for categorization by LungRADS 1.1 system.
Methods & Materials
500 subjects enrolled in a lung cancer screening trial, named “Prospective Evaluation Of Preventive Lung HEalth (PEOPLHE)” underwent baseline chest ULDCT between September 2021 and March 2022. Prospective reading was performed by expert thoracic radiologist supported by computer-aided detection (CAD) (MM.Oncology, syngo.via, Siemens Healthineers) that served as second reader, ULDCT outcome was classified according to LungRADS 1.1. All 500 ULDCT scans were retrospectively evaluated by an AI-driven CAD (AVIEW LCS platform, Coreline soft) to obtain an automated LungRADS categorization, without human interaction.
The dominant nodule served as reference for comparison between human and automated readings. ULDCT results were compared across the full range of single LungRADS categories and then grouped into negative (categories 1 and 2, which share the same management) and positive (categories ≥3). Descriptive statistics were calculated and agreement was tested by K statistics.
Results
Prospective reading classified 203/500 (40.6%) LungRADS category 1, 235/500 (47%) category 2, 39/500 (7.8%) category 3, 18/500 (3.6%) category 4A, 2/500 (0.4%) category 4B and 3/500 (0.6%) category 4X, whereas AI software classified 152/500 (30.4%) category 1, 263/500 (52.6%) category 2, 49/500 (9.8%) category 3, 29/500 (5.8%) category 4A and 7/500 (1.4%) category 4B. The agreement on the single LungRADS category was 0.514 [95% CI 0.451-0.577] and accuracy 0.656 [95% CI 0.612-0.698]. 40/500 (8%) prospectively negative ULDCT were classified as positive by AI, while 17/500 (3.4%) prospectively positive were classified as negative by AI (1/17 was diagnosed mediastinal mass): agreement 0.547 [95% CI 0.444-0.650], accuracy 0.886 [95% CI 0.855-0.912], sensitivity 0.726 [95% CI 0.590-0.824] and specificity 0.909 [95% CI 0.878-0.944]. AI detected all 4 LC presenting as lung nodule, whereas it missed a LC showing as mediastinal mass.
Conclusion
AI showed moderate agreement, we observed a tendency to overestimation with consequent increased recall. According to our preliminary results, we suggest that AI-driven software can be used as supporting tool in ULDCT-based lung cancer screening for detection of parenchymal nodules, whilst mediastinal reading should always be checked visually.

A-546

Fibrosing variant of organizing pneumonia in recipients of hematopoietic stem cell transplantation: CT findings

J. I. Jung, K. S. Beck
Seoul St. Mary's Hospital, College of Medicine, The Catholic University of Korea, Radiology, Seoul, Republic of Korea (South Korea)

Purpose/Objectives

To evaluate the serial changes of CT features in allogenic hematopoietic stem cell transplantation (HSCT) recipients who showed progressive fibrosis on follow-up CT images.

Methods & Materials

We retrospectively reviewed 926 patients who underwent allogeneic HSCT at our hospital between 2010 and 2013. We then identified 21 patients (19 male and 2 female; mean age at transplant 39 years) who showed features of progressive fibrosis, as defined as presence of non-resolving or recurrent parenchymal abnormalities with traction bronchiectasis and progressively decreasing lung volume, on serial follow-up chest CT scans. We visually assessed the extent and distribution of lung abnormalities on baseline CTs that first showed signs of abnormality and last available CTs. Medical records of the patients were also searched for relevant clinical data, including types of stem cell transplantation, conditioning regimen, underlying hematological disorder, and presence of acute or chronic graft-versus-host disease (GVHD).

Results

21 patients with progressive fibrosis appeared as GGO (19/21, 90.5%), consolidation (14/21, 66.7%), and reticular or linear opacities (6/21, 28.6%), with a peribronchovascular (21/21, 100.0%) or peripheral (15/21, 71.4%) distribution, upper lung predominance (21/21, 100.0%), and mild traction bronchiectasis (mean score 1.2) on CTs when abnormalities were first noted (at median follow-up period of 19 months). This later showed progression with decreased lung volume and an increased extent and severity of traction bronchiectasis (mean score 2.4), GGO, consolidation, reticulation, and sometimes with honeycombing or bullae/cysts (5/21, 23.8%) on last follow-up CT scans (at median follow-up period, 47 months). 14 of 21 patients (66.7%) had acute GVHD and all of the patients had chronic GVHD. 12 patients died (57.1%) during follow-up. The patients were predominantly male (19/21), which showed significant difference (p=0.010) with those who did not develop this disease.

Conclusion

This study highlights the existence of fibrosing variant of organizing pneumonia in post-allogeneic HSCT patients and provides new insights into the radiologic characteristics of this disease.

A-271

Fully-automated Quantification of Functional Small Airway Disease on In- and Expiratory Chest CT Data Sets using Deep Learning

M. Pradella[1], S. Yang[1], M. Tamm[2], J. Halter[3], D. Stolz[2,4], K. Hostettler[2], D. Winkel[1]
[1]University Hospital Basel, Department of Radiology, Basel, Switzerland, [2]University Hospital Basel, Clinic of Respiratory Medicine, Basel, Switzerland, [3]University Hospital Basel, Department of Hematology, Basel, Switzerland, [4]University of Freiburg, Clinic of Respiratory Medicine and Faculty of Medicine, Freiburg, Germany

Purpose/Objectives

A number of diseases are associated with functional Small Airway Disease (fSAD) such as obliterative bronchiolitis, hypersensitivity pneumonitis or connective tissue diseases. Multiple studies have promoted the usefulness of in- and expiratory CT for assessment of fSAD [REF01][REF02]. However, this assessment is time-consuming, requires dedicated software solutions and readers' experience [REF02][REF03]. In this study, we aimed to investigate whether fSAD can be quantified fully-automatic using an in-house built, previously evaluated, deep learning (DL) based lung segmentation tool [REF04].

Methods & Materials

We retrospectively included chest CTs with in- and expiratory acquisitions from our PACS including the radiology reports. fSAD was defined as the difference of percentages of lung parenchyma <-950 HU on the inspiratory CT scan subtracted from lung parenchyma below -856 HU on expiratory CT scan [REF01][REF02].

Conventional assessment was performed using a dedicated software (Syngo.Via, Siemens Healthineers) which comprises a built-in lung segmentation. Respective fractions of involved parenchyma per acquisition were measured semi-manually and fSAD was calculated ($fSAD_{man}$). Cardiothoracic radiologists included them in their respective radiology reports.

The fully-automatic assessment comprises automatic segmentation of lungs on in- and expiratory CT scans using a previously established DL tool [REF04]. All required measurements and calculations were automated resulting in a fully-automatic report of fSAD ($fSAD_{auto}$).

We compared the two methods using Pearson correlation and Bland-Altman plots, including difference of means (bias). Furthermore, we defined relevant fSAD as >20% of lung involvement and evaluated fSAD classification by both methods.

Results

We included 105 CT exams from 95 patients in this study (mean age; 55.2±9.6 years, 38% female).

The mean lung volumes for inspiration and expiration were 5671±1426 mL and 2821±829 mL, respectively. An example cases is shown in Figure 1

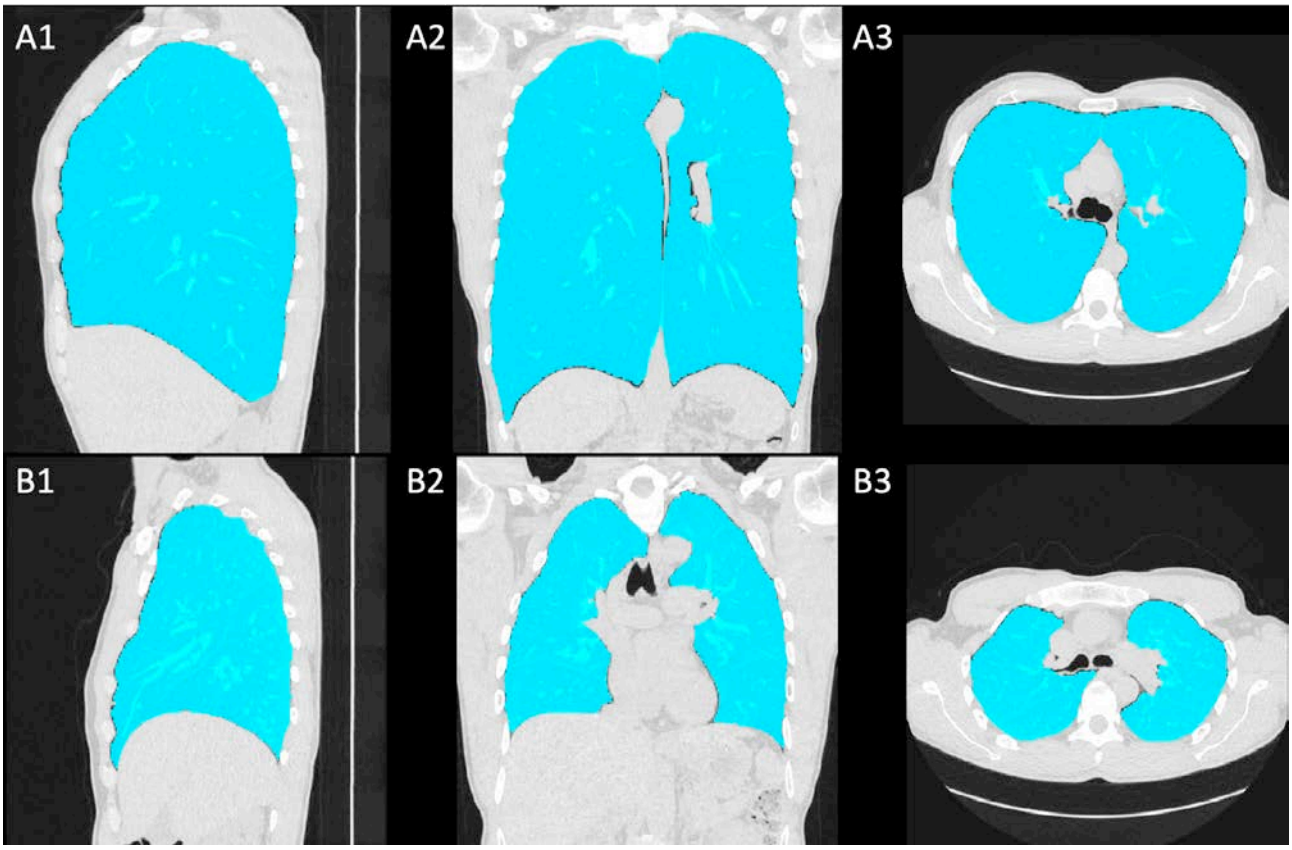

Example case of our DL-based lung segmentation tool on inspiratory (A1-3) and expiratory (B1-3) CT data set in sagittal, coronal and axial orientation.

.

Assessments of $fSAD_{auto}$ and $fSAD_{man.}$ showed excellent correlation between methods (r=1.0, p<0.001;

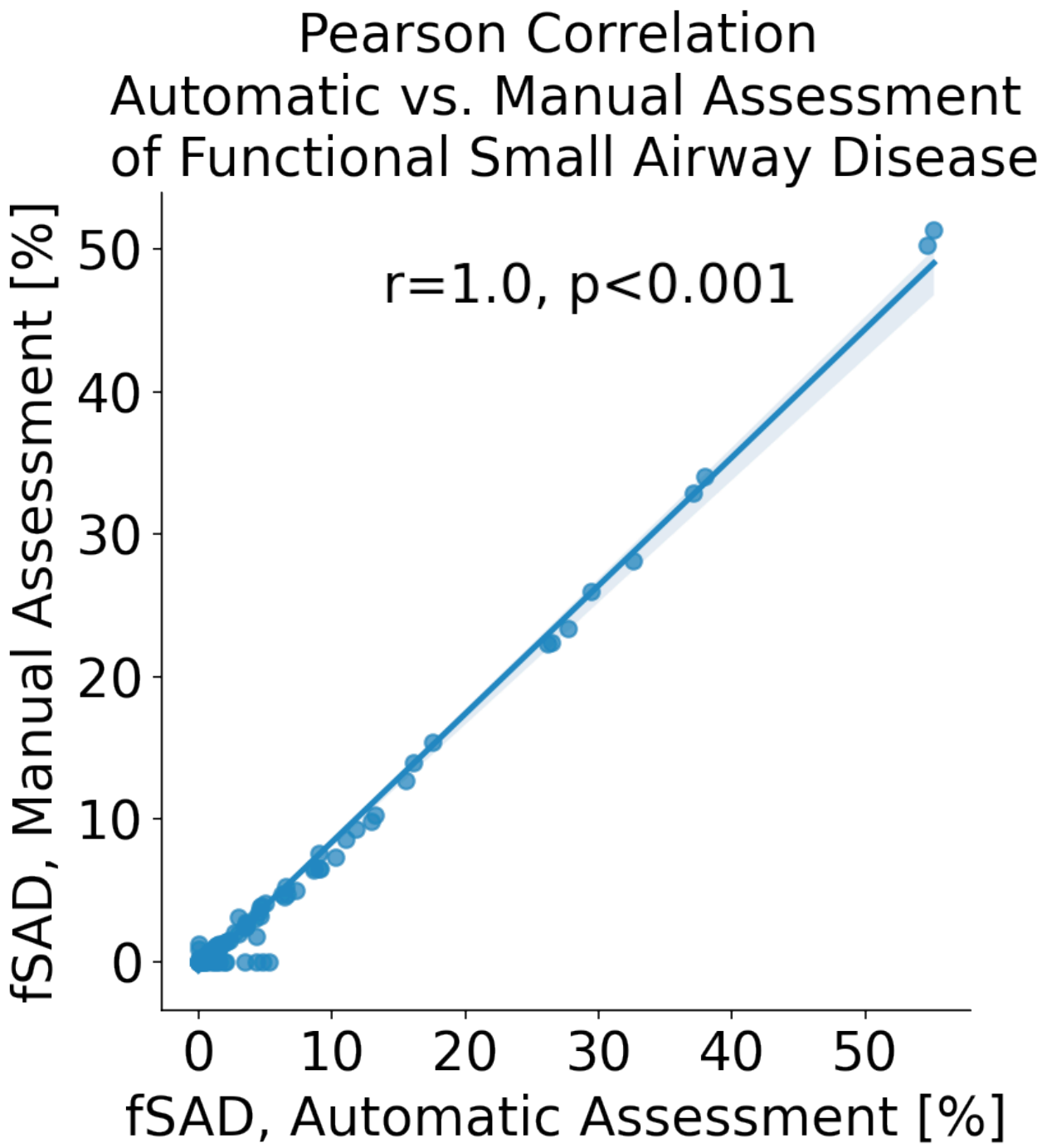

Pearson correlation between both methods showed excellent agreement (r=1.0, p<0.001).
). Furthermore, Bland-Altman plots revealed small bias of -1.2% with narrow limits of agreement (-4.0% - 1.5%,

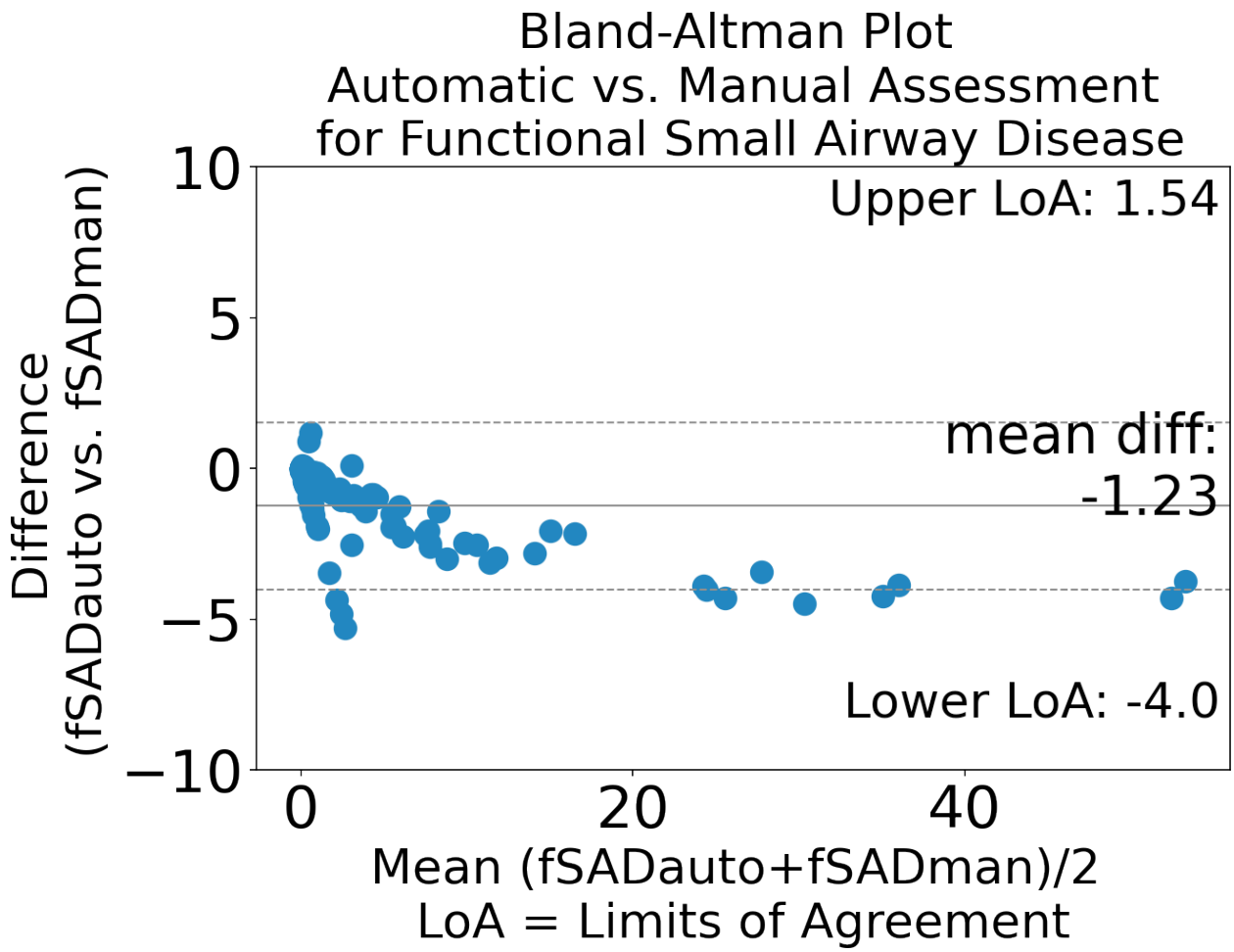

Bland-Altman Plots revealed small mean difference of -1.2 % with narrow limits of agreement between methods.
). A total of nine cases (9/105 (8.6%)) presented with relevant $fSAD_{man}$; those were all correctly classified using the $fSAD_{auto}$ workflow.

Conclusion

Our fully automatic assessment for fSAD assessment showed excellent agreement with the routinely used conventional assessment. While we only had a small number of cases with relevant fSAD in our cohort, which requires further investigation, our results suggest usefulness in daily radiology practice.

References:

[REF01] Galban CJ, (2012), Computed tomography-based biomarker provides unique signature for diagnosis of COPD phenotypes and disease progression., Nat Med

[REF02] Galban CJ, (2014), arametric Response Mapping as an Indicator of Bronchiolitis Obliterans Syndrome after Hematopoietic Stem Cell Transplantation. Biol Blood Marrow Transplant , Biol Blood Marrow Transplant

[REF03] Hasenstab KA, (2021), Automated CT Staging of Chronic Obstructive Pulmonary Disease Severity for Predicting Disease Progression and Mortality with a Deep Learning Convolutional Neural Network, Radiology: Cardiothoracic Imaging

[REF04] Anastasopoulos C, (2020), Development and clinical implementation of tailored image analysis tools for COVID-19 in the midst of the pandemic: The synergetic effect of an open, clinically embedded software development platform and machine learning, Eur J Radiol

A-322

High-pitch CT pulmonary angiography (CTPA) with ultra-low contrast medium volume for the detection of pulmonary embolism: a comparison with standard CTPA

R. Gohmann[1], T. Schönfeld[1], P. Seitz[1], C. Krieghoff[1], M. Gutberlet[1,2]
[1]Heart Center Leipzig at University of Leipzig, Department of Diagnostic and Interventional Radiology, Leipzig, Germany, [2]Heart Center Leipzig at University of Leipzig, Leipzig, Germany

Purpose/Objectives
To investigate the feasibility and image quality of high-pitch CT pulmonary angiography (CTPA) with reduced iodine volume and tube current in unselected normal weight patients.
Methods & Materials
In total, 81 consecutive patients undergoing CTPA for suspected pulmonary arterial embolism were retrospectively included: 41 in high-pitch mode with 20 ml of contrast medium (CM); and 40 with normal pitch and 50 ml of CM (**Table 1**). Subjective image quality was assessed and rated on a three-point scale. For objective image quality, attenuation and noise values were measured in all pulmonary arteries from the trunk to segmental level. Signal-to-noise ratio (SNR) and contrast-to-noise ratio (CNR) were calculated. Radiation dose estimations were recorded.
Results
There were no statistically significant differences in patient and scan demographics between high-pitch and standard CTPA (**Table 2**). Subjective image quality was rated good to excellent in over 90 percent of all exams with no significant group differences (p=0.32) (**Figure 1**). Median contrast opacification was lower in high-pitch CTPA (283.18 [216.06-368.67] HU, 386.81 [320.57-526.12] HU; p=0.0001). CNR reached a minimum of eight in all segmented arteries, but was lower in high-pitch CTPA (8.79 [5.82-12.42], 11.01 [9.19-17.90]; p=0.005). Median effective dose of high-pitch CTPA was lower (1.04 [0.72-1.27] mSv/mGy*cm; 1.49 [1.07-2.05] mSv/mGy*cm; p<0.0001).
Conclusion
High-pitch CTPA using ultra-low contrast volume (20 ml) rendered diagnostic images for the detection of pulmonary arterial embolism in most instances. Compared to standard CTPA, the high-pitch CTPA exams with drastically reduced contrast medium volume had also concomitantly reduced radiation exposure. However, image quality of high-pitch CTPA varied according to patient predisposition.

Table 1. Scan protocols and image reconstruction

	High-pitch CTPA	Standard CTPA
Automatic tube voltage selection	yes	yes
Tube voltage range [kV]	70-100	70-120
Automatic tube current modulation	CARE Dose 4D*	CARE Dose 4D*
Tube current [ref. mAs]	200	100
Tube potential [ref. kV]	70	120
Pitch	3.2	1.2
Rotation time [sec]	0.285	0.285
Table speed [mm/sec]	431	161
Contrast medium volume [ml]	20	50
Contrast medium injection rate [ml/sec]	4.0	4.0
Saline chaser volume [ml]	40	40
Saline chaser injection rate [ml/sec]	4.0	4.0
Kernel	I31f/4	I31f/3
Section thickness [mm]	0.75	0.75
Increment [mm]	0.7	0.7
Iterative reconstruction algorithm	ADMIRE	ADMIRE

Technical parameters of applied protocols. ADMIRE = Advanced Modeled Iterative Reconstruction (Siemens Healthineers, Erlangen, Germany).

Table 1. Scan protocols and image reconstruction

Table 2. Patient / scan demographics and image findings

		High-pitch CTPA	Standard CTPA	*p*-value
		n=41	n=40	
Age [years]		72.9 (64.0-81.8)	78.5 ± (69.1-81.9)	0.50
Weight [kg]		73.9 ± 17.5	80.2 ± 12.9	0.09
Height [cm]		168.9 ± 10.0	171.4 ± 8.2	0.30
BMI [kg/m²]		25.5 ± 4.8	27.3 ± 4.0	0.09
Females		17 (41.5)	14 (35.0)	0.55
Tube potential [kV]				
	70	2 (4.9)	0 (0)	
	80	12 (29.3)	18 (45.0)	0.63
	100	27 (65.9)	20 (50.0)	
	120	0 (0)	2 (5.0)	
PE detected		8 (19.5)	9 (22.5)	0.74

Patient baseline characteristics at time of hospital stay. Numbers are mean ± standard deviation, median (interquartile range) or count and (percentage). CTPA = computed tomography pulmonary angiography, BMI = body mass index, PE = pulmonary embolism.

Table 2. Patient / scan demographics and image findings

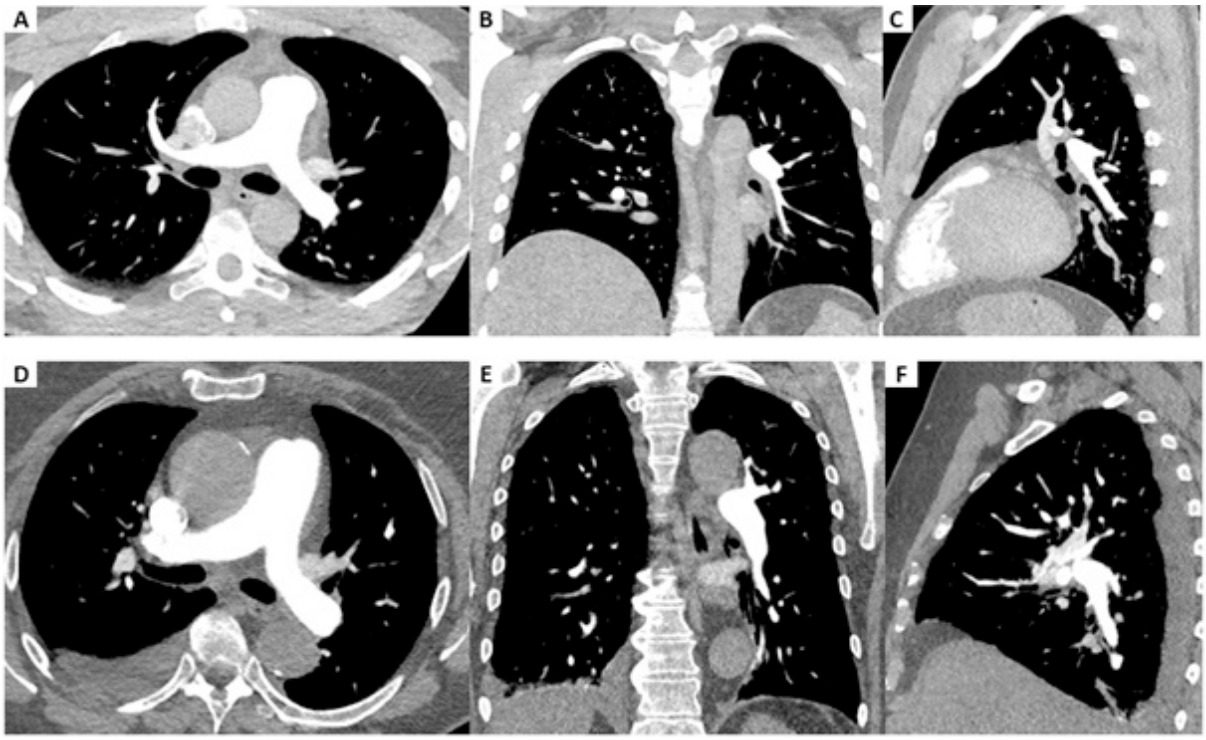

High-pitch CTPA (A-C) at 100 kVp (BMI: 29) and standard CTPA at 100 kVp (BMI: 30) in axial (A, D), coronal (B, E) and sagittal (C, F) view. Subjective and objective image quality were excellent for both studies (mean opacification of the pulmonary arteries: 375±27HU; 441±37HU). Radiation dose for high-pitch CTPA was lower (89.6 vs 135.0 mGy*cm).

A-368

Interobserver Agreement in Radiologists' Assessment of Chest CT in Interstitial Lung Disease: a systematic review and meta-analysis

L. Delaney, S. Alabed, M. Salehi, M. Goodlad, E. Checkley, H. Shah, A. Giri, A. Swift, K. Dwivedi
University of Sheffield, Department of Infection, Immunity & Cardiovascular Disease, Sheffield, United Kingdom

Purpose/Objectives
HRCT plays a central role in the investigation of patients with interstitial lung disease (ILD), and has important implications for disease prognostication and management. Previous work has demonstrated that there can be variation between expert chest radiologists when identifying diseases and disease patterns on HRCT, as well as disagreement when using standardised disease classification systems, such as the ATS/ERS/JRS/ALAT criteria for idiopathic pulmonary fibrosis (IPF).
The aim of this study was, therefore, to perform a meta-analysis of the interobserver agreement of reporting of thoracic CT scans in patients with ILD.
Methods & Materials
The protocol for the review was registered with PROSPERO (CRD42022361803). Relevant papers were identified via a search of EMBASE, MEDLINE and Cochrane up to September 2022. Studies were considered eligible for inclusion if they calculated the kappa value for interobserver agreement of the reporting of contrast or non-contrast chest CT scans between expert chest radiologists. Included studies were divided into two broad groups; those calculating the interobserver agreement of the 2011 or 2018 ATS/ERS/JRS/ALAT criteria for IPF, and those calculating the interobserver agreement for recognition of specific CT features of ILD. Quality assessment was performed using a modified version of the QUADAS-2 risk of bias tool. Pooled kappa values were calculated using a random effects model. Kappa values were interpreted using the Landis and Koch classification.
Results
15 papers (a total of 7123 scans) were selected for inclusion in the analysis. One study was found to be at high risk of selection bias. Concerning the ATS/ERS/JRS/ALAT guidelines for diagnosis of IPF, there was an overall interobserver agreement of 0.60 [0.52-0.68]. The 2011 guidelines had a kappa value of 0.55 [0.44-0.66], while the 2018 guidelines had a kappa value of 0.65 [0.54-0.77]. There was no significant difference in interobserver agreement between the 2011 and 2018 guidelines ($p = 0.2$).
The overall kappa value for agreement on presence or absence of specific features on HRCT was 0.56 [0.49-0.62]. Sub-group analysis demonstrated an agreement of 0.58 [0.49-0.66] for honeycombing, 0.51 [0.37-0.65] for ground glass opacification, 0.59 [0.34-0.83] for reticulation and 0.56 [033-0.78] for traction bronchiectasis, with no significant difference between subgroups ($p = 0.87$).
Conclusion
Our meta-analysis has demonstrated substantial agreement between chest radiologists when using the ATS/ERS/JRS/ALAT guidelines to assess for IPF on chest CT, and moderate agreement between expert chest radiologists in the recognition of individual disease features on CT scans. These findings have implications for the use of CT in diagnosis and prognostication of ILD.

References:

[1] Landis, J.R. and Koch, G.G, (1977), The Measurement of Observer Agreement for Categorical Data, Biometrics, 159-174, 33(1), https://doi.org/10.2307/2529310
[2] Raghu, G. et al, (2018), Diagnosis of Idiopathic Pulmonary Fibrosis. An Official ATS/ERS/JRS/ALAT Clinical Practice Guideline, American Journal of Respiratory and Critical Care Medicine, e44–e68, 198(5), https://doi.org/10.1164/rccm.201807-1255ST

A-655

Large Language Model Mortality Prediction: Outperforming Manual Labelling in Analysing CTPA Reports

S. Alabed[1,2,3,4], M. Sharkey[1], C. Johns[1,5], H. Beresford[5], M. Salehi[6], K. Dwivedi[1], P. Metherall[5], A. Swift[1,2,3]
[1]University of Sheffield, Infection, Immunity & Cardiovascular Disease, Sheffield, United Kingdom, [2]NIHR Sheffield Biomedical Research Centre, Sheffield, United Kingdom, [3]INSIGNEO, Institute for Insilico Medicine, Sheffield, United Kingdom, [4]Sheffield Teaching Hospitals, Clinical Radiology, Sheffield, United Kingdom, [5]Sheffield Teaching Hospitals, Sheffield, United Kingdom, [6]University of Sheffield, Sheffield, United Kingdom

Purpose/Objectives
CT pulmonary angiography (CTPA) serves as a powerful prognostic tool, and with the advent of Large Language Models (LLMs), natural language processing has taken a giant leap in efficiently extracting textual features and generating meaningful weightings. This cutting-edge study delves into the capabilities of LLMs to predict mortality from CTPA reports, while benchmarking their performance against manual feature extraction.
Methods & Materials
All CTPA reports from the Sheffield 3D lab between 2009-2018 were included, 80% were designated for training, with the remaining 20% reserved for testing. Expert radiologists manually labelled reports for pre-specified features like pulmonary embolism (PE), right heart strain, and pulmonary diseases such as interstitial lung disease, infection, and oedema. The PubMed Bidirectional Encoder Representations from Transformers (BERT) LLM was employed to tokenise the CTPA reports and autonomously extract features [PubMedBERT]. Both the manually labelled and tokenised data were assessed using ROC curves, Cox regression analysis, and Kaplan-Meier survival curves to estimate overall mortality in the testing dataset.
Results
A total of 20,073 patients (mean age 62±18 years, 59% female) formed the training dataset and 5,019 patients (mean age 62±18 years, 60% female) were included in the testing dataset. The complete dataset reported PE in 13% of cases and right heart strain in 8%. Consolidation was present in 38% of cases, emphysema in 17%, fibrosis in 7%, heart failure in 7%, nodule-or-mass in 24% and effusion in 25%. The ROC curves demonstrated an AUC of 0.67 for manually labelled features, while BERT risk features achieved a higher AUC of 0.77 ($p = 0.001$) for predicting overall mortality. Kaplan-Meier curves showed significantly lower survival probability in patients with BERT-identified risk features than those without BERT-risk features.
Conclusion
LLMs demonstrate a superior ability to predict mortality based on radiology reports compared to manually labelled features. This finding has the potential to aid radiologists in concentrating on key features when reporting, ultimately enhancing the effectiveness of their reports. Future research should focus on exploring the specific features identified by LLMs and examining the impact of radiology-specific LLMs to enhance accuracy further.

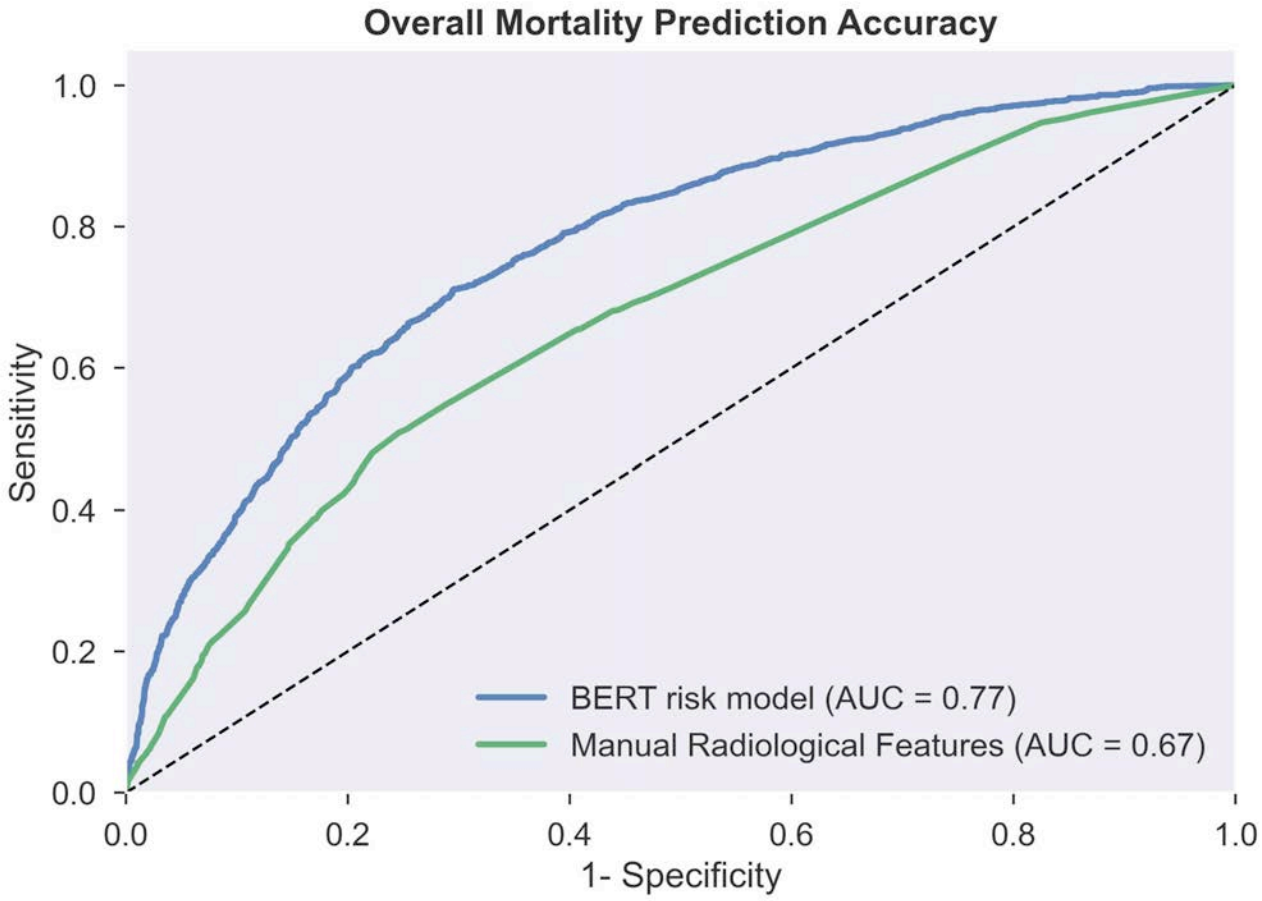

Figure 1: Receiver Operating Characteristic (ROC) Curve comparing the accuracy of PubMed Bert to Manual classification of risk

features in CTPA reports to predict mortality.

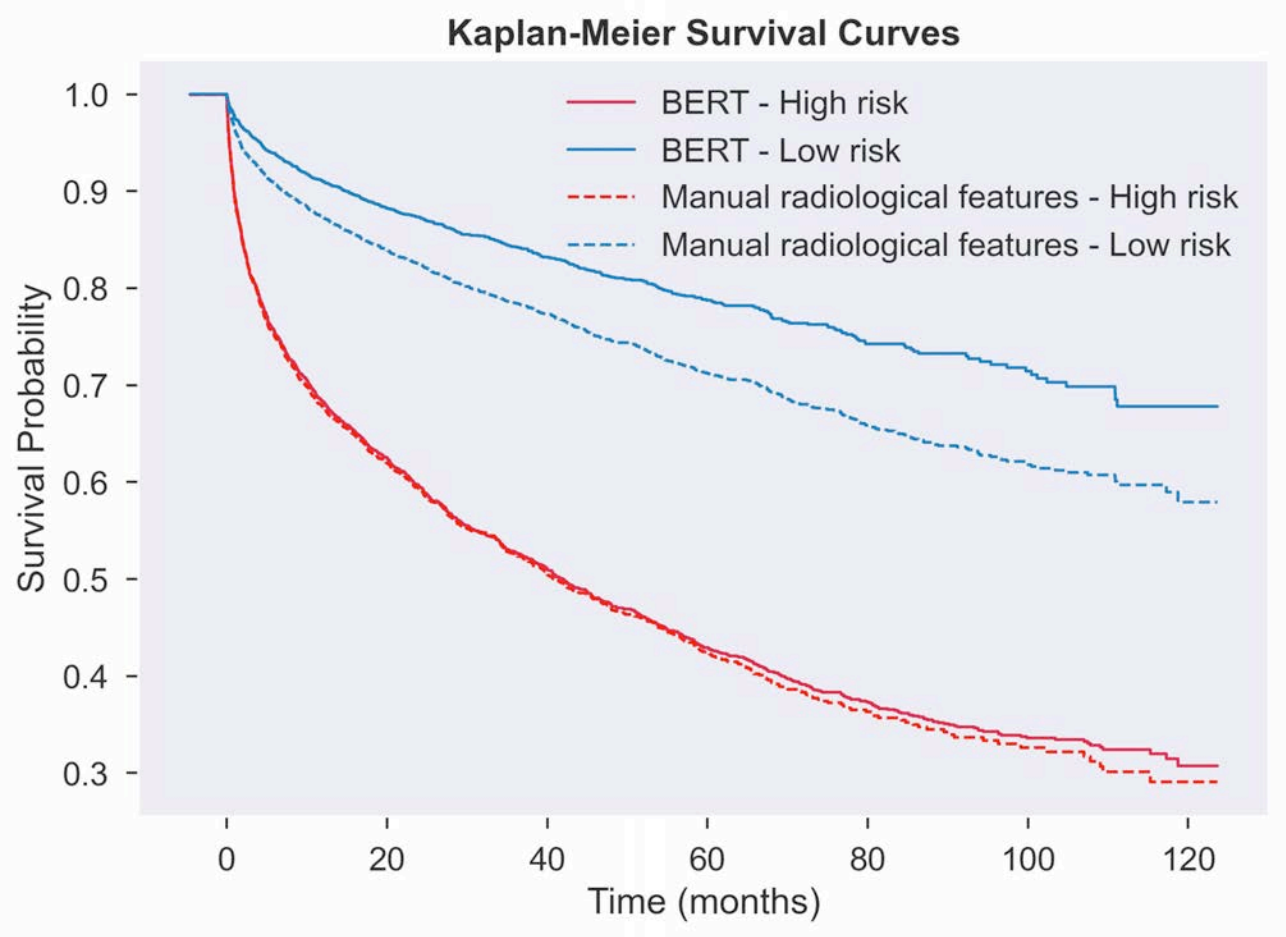

Kaplan-Meier survival curves comparing the BERT model to manual feature extraction from CTPA reports. The BERT model demonstrates a better separation between high and low-risk groups, highlighting its potential for improved risk stratification.

References:

[PubMedBERT] Gu, Y., Tinn, R., Cheng, H., Lucas, M., Usuyama, N., Liu, X., Naumann, T., Gao, J. & Poon, H., , (2020), Domain-Specific Language Model Pretraining for Biomedical Natural Language Processing. , arXiv preprint , arXiv:2007.15779., https://arxiv.org/abs/2007.15779, 2023-04-13

A-350

Low-dose computed tomography lung cancer screening integrated with smoking cessation: preliminary results of an Italian multicenter pilot study in view of an HTA.

G. Picozzi[1], E. Cavigli[2], D. Cozzi[2], C. Moroni[2], A. Bindi[2], S. Luvarà[2], A. Deliperi[3], C. Romei[3], L. Carrozzi[3], Z. Falaschi[1], D. Ghio[4], P. Gollini[5], S. Anglesio[5], I. Orlandi[6], M. Bartolucci[6], V. Miele[2], M. Mascalchi[2], G. Gorini[1]
[1]ISPRO Firenze, Florence, Italy, [2]Careggi, Florence, Italy, [3]AOU Pisa, Pisa, Italy, [4]HSR Milano, Milano, Italy, [5]Ospedale S. Giovanni Bosco, Torino, Italy, [6]Prato Hospital, Prato, Italy

Purpose/Objectives
Lung cancer (LC) screening trials with low-dose computed tomography (LDCT) is effective in reducing LC mortality. In order to develop a population-based LDCT screening in Italy, in view of an health technology assessment (HTA), this multicenter pilot study funded by the Italian Health Ministry aims to perform two annual LDCT rounds in combination with smoking cessation (SC), to 1.200 current and former heavy smokers aged 55-75 years, with a smoking history of ≥30 pack-years, in Tuscany (Florence, Pisa, Massa), Lombardy (Milan), and Piedmont (Turin) Region of Italy.
Methods & Materials
Participants are recruited using different strategies: general practitioners (GPs), smoking cessation centres (SCCs), online participation requests. Study recruiters fix LDCT appointments, administer brief SC advice, show the study SC website, and refer interested smokers to SCCs. In all but one centre, double reading of LDCT was performed, with at least one reading supported by a CAD System. Negative LDCT will be re-screened after one year, while positive scans are managed according to ACR Lung-RADS1.1. Coronary artery calcifications (CACs) and actionable incidental findings are reported.
Results
Up to February 2023, 476 participants have been recruited and 406 LDCT have been performed. Current smokers were the majority of participants (N= 410; 86.1%) and 136 (33.2%) were referred to SCCs. 47(11.6%) LDCT were positive. 22 subjects (46.8%) have been scheduled for a 6-month LDCT follow-up, 8 (17.0%) for a 3-month LDCT, 8 (17.0%) a 1-month LDCT, whereas 9 LDCT (19.1%) showed suspicious lung nodules requiring immediate referral to further assessments. Moderate/severe CACs were observed in 30.5% of LDCT.
Conclusion
This pilot study showed that each centre developed or optimized context-specific strategies to overcome local barriers and constraints, to perform LDCT scans and related further assessments and to provide SC at SCCs in the recruitment areas. A population-based LC screening program with LDCT integrated with SC seems to be feasible and well accepted by smoking participants.

A-658

Lung cancer screening reporting - a qualitative survey.

T. L. Lim[1], I. Das[2], J. C. L. Rodrigues[3], S. Hare[3], A. Tavare[3], G. Robinson[3]
[1]Kettering General Hospital NHS Foundation Trust, Kettering, United Kingdom, [2]Glenfield Hospital, University Hospitals of Leicester NHS Trust, Department of Radiology, Leicester, United Kingdom, [3]Heart&Lung Health, London, United Kingdom

Purpose/Objectives

Lung cancer screening (LCS) is currently being piloted in the UK through NHS Targeted Lung Heath Checks[1]. Heart & Lung Health(HLH) is a tele-radiology company and the largest independent provider of NHS targeted Lung Health Checks in the UK [2]. The complexity of thoracic CT requires a meticulous approach to reporting to ensure both cancers are correctly identified, and significant incidental findings are not missed. We conducted a qualitative assessment of how radiologists report LCS scans, to help understand if workflows could be optimized to improve user experience and minimize radiological errors.

Methods & Materials

Data was collected through a Google Forms optional questionnaire sent to all UK radiologists reporting LCS CT through the HLH network. The reporting platform is a cloud-based solution (CIMAR) with Veye Lung Nodules for nodule detection. The questionnaire focused on the routine practice of radiologists, including reporting sequence, number of different windows and planes reviewed, use of functionalities such as automated scrolling, maximum intensity projection (MIP), AI nodule detection, and the merit of creating an automated visual video checklist, incorporating all necessary slices, planes and windows prior to final verification.

Results

44 radiologists from the HLH reporting network responded to the survey. 95.5% of reporters routinely reviewed at least three windows (lung, mediastinum and bone) prior to verification, with 27.3% routinely reviewing at least one further additional window. 93.2% of reporters reviewed at least axial and sagittal planes in all cases, with 34.1% routinely reviewing the coronal plane. 88.6% used manual scrolling only. 77.3% of reporters routinely used the MIP functionality to aid nodule detection. 93.2% of reporters found AI nodule detection functionality helpful in their reporting workflow. 84.1% reporters found their normal sequence was to review the AI detected nodules first, followed by a manual review. 61.4% of reporters were unsure if the implementation of a video checklist would be helpful.

Conclusion

Most respondents reviewed ≥3 windows and ≥2 planes prior to verification, demonstrating significant time spent reviewing important incidental pathology, in additional to lung cancer. Most respondents agree that AI nodule detection is helpful by saving time in identifying nodules. Reviewing AI detected nodules was the preferred first line approach for most, confirming trust in AI-aided nodule detection as an initial review. Workflows designed for LCS should be optimized to aid radiologists, by ensuring all important windows, planes and functionalities are included.

References:

[1] Evaluation of the Targeted Lung Health Check programme, https://www.england.nhs.uk/contact-us/privacy-notice/how-we-use-your-information/our-services/evaluation-of-the-targeted-lung-health-check-programme/, 2023-04-14, NHS England
[2] Heart Lung Health, London, https://heartlunghealth.com/, 2023-04-14, Heart Lung Health

A-498

Magnetic Resonance Imaging Detects Delayed Perfusion Inside Perfusion Defects in Patients with Cystic Fibrosis

P. Leutz-Schmidt[1], J. Grolig[2], D.-E. Optazaite[2], O. Sommerburg[2], M. Eichinger[2], S. Wege[2], S. Y. Graeber[3], M. Puderbach[4], J.-P. Schenk[1], A. Alrajab[2], H.-U. Kauczor[2], M. Stahl[3], M. Mall[3], A. Koeppe[5], B. Nestler[5], S. Triphan[1], M. O. Wielpütz[1]
[1]Heidelberg University Hospital, Diagnostic and Interventional Radiology, Heidelberg, Germany, [2]Heidelberg University Hospital, Heidelberg, Germany, [3]Charité Universitätsmedizin Berlin, Berlin, Germany, [4]Hufeland Klinikum Bad Langensalza, Bad Langensalza, Germany, [5]Karslruhe Institute of Technology, Karlsruhe, Germany

Purpose/Objectives

Dynamic Contrast Enhanced Perfusion MRI (DCE-MRI) detects pulmonary perfusion abnormalities in patients with cystic fibrosis (CF) already from preschool age [1]. Little is known about the alterations of bronchial arterial inflow from the systemic circulation [2]. We hypothesized that in perfusion defect areas a delayed perfusion from bronchial arteries may be observed.

Methods & Materials

Morpho-functional MRI incl. DCE-MRI from 50 patients with CF (mean age 14.8±5.3y, range 6-29y) were included. The lung was segmented on a coronal 3D T1-weighted gradient echo sequence and registered onto DCE-MRI. An automatically placed ROI in the pulmonary artery was used to calculate the arterial input function (AIF), which was then used to quantify pulmonary blood flow (PBF) and mean transit time (MTT). Perfusion defects were classified using Otsu's method for clustering the R(t) maps at the time of maximum contrast enhancement in the entire lung, and were quantified as defects in percent (QDP) [3],[4]. Perfusion delay maps were calculated by upsampling the AIF and subtraction images in the time domain using cubic interpolation and calculating the cross-correlation between the interpolated subtraction image and a moving window of the edge-padded AIF. For each voxel the maximum correlation and its timepoint was determined to assess perfusion delay. Quantitative perfusion parameters were compared in areas with normal perfusion vs. perfusion defects according to defect classification.

Results

A representative perfusion defect map and its corresponding perfusion delay map are shown in *Figure 1*

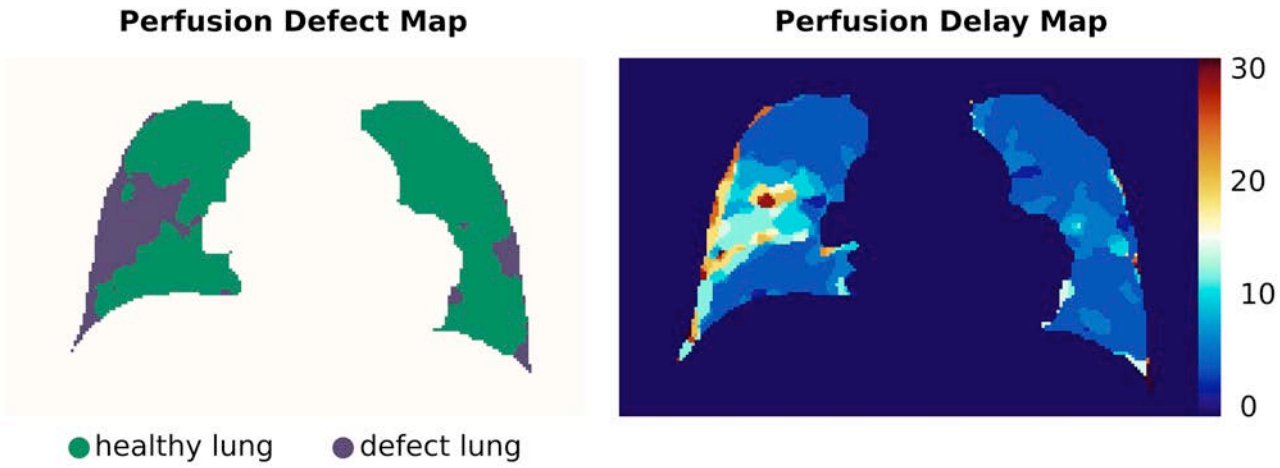

Figure 1: Perfusion defect map (left) and perfusion delay map (right) of a 14-year-old CF patient. Healthy areas show similar small perfusion delays, whereas defect areas show a heterogenous delayed perfusion.

. As can be seen the perfusion in the healthy areas occurs mostly at the same time, whereas delayed perfusion is visible in the defect areas. Histograms for each quantitative perfusion parameter and patient were calculated and a median histogram was generated for each value by averaging all histograms per quantitative perfusion parameter. Mean QDP was 26.4±20.8%. Mean PBF was 176.6±72.9 ml/100ml*min in normal, and 64.5±25.6 ml/100ml*min in perfusion defect areas ($p<0.001$). Corresponding MTT was 5.6±1.7s in normal and 7.4±2.4s in defect areas ($p<0.001$). Average median arterial delay was 3.4±0.7s in normal and 7.1±4.0s in perfusion defects ($p<0.01$), and the mean arterial correlation was 0.89±0.08 and 0.69±0.16 ($p<0.001$), respectively. *Figure 2* shows histograms for MTT, arterial delay and arterial correlation.

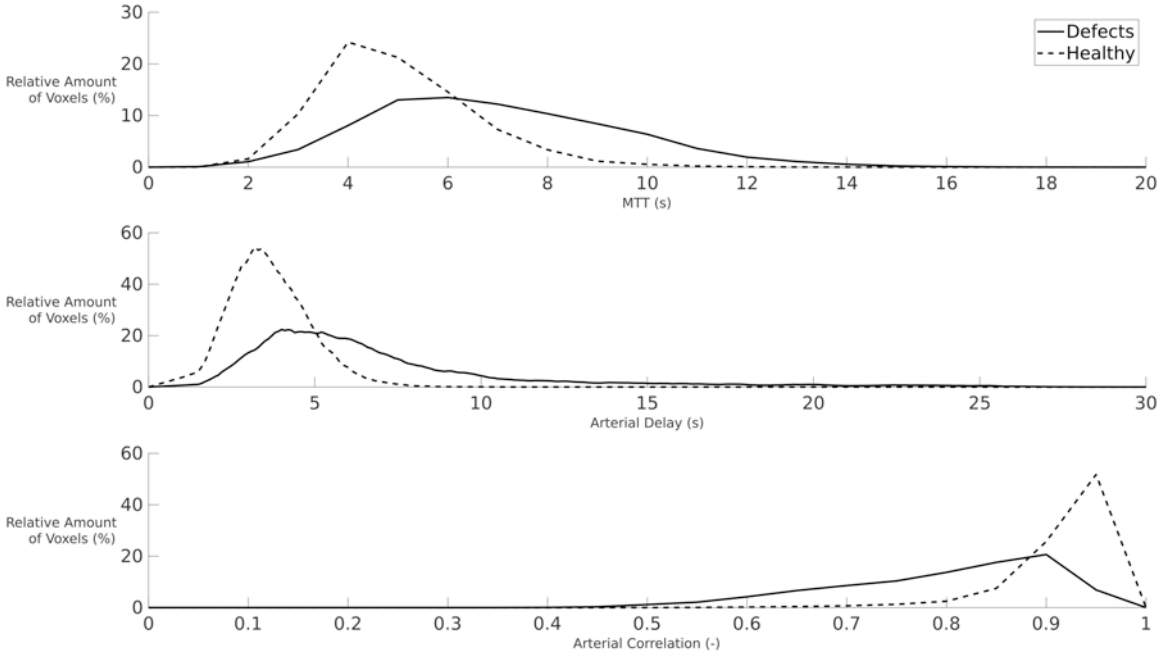

Figure 2: Median histograms for MTT, arterial delay and arterial correlation. The x-axis shows the quantitative perfusion parameters, while the y-axis shows the percent of voxels belonging to each bin. All three histograms of the defect areas are wider and have a smaller peak compared to their respective normal counterparts

Conclusion

Lung areas with perfusion defects in the pulmonary arterial phase show delayed perfusion in the systemic arterial phase in patients with CF, likely through bronchial arteries. Further studies may investigate the correlation of delayed perfusion with bronchial artery dilatation in advanced CF.

References:

[1] Wielpütz MO, Puderbach M, Kopp-Schneider A, Stahl M, Fritzsching E, Sommerburg O, Ley S, Sumkauskaite M, Biederer J, Kauczor HU, Eichinger M, Mall MA., (2014), Magnetic resonance imaging detects changes in structure and perfusion, and response to therapy in early cystic fibrosis lung disease., Am J Respir Crit Care Med, 956-965, 189

[2] Leutz-Schmidt P, Optazaite D-E, Sommerburg O, Eichinger M, Wege S, Steinke E, Graeber SY, Puderbach MU, Schenk J-P, Alrajab A, Triphan SMF, Kauczor H-U, Stahl M, Mall MA, Wielpütz MO, (2023), Magnetic resonance imaging detects onset and association with lung disease severity of bronchial artery dilatation in cystic fibrosis, ERJ Open Res, 9

[3] Schiwek M, Triphan SMF, Biederer J, Weinheimer O, Eichinger M, Vogelmeier CF, Jorres RA, Kauczor HU, Heussel CP, Konietzke P, von Stackelberg O, Risse F, Jobst BJ, Wielpütz MO, (2022), Quantification of pulmonary perfusion abnormalities using DCE-MRI in COPD: comparison with quantitative CT and pulmonary function, Eur Radiol, 1879-1890, 32

[4] Ter-Karapetyan A, Triphan SMF, Jobst BJ, Anjorin AF, Ley-Zaporozhan J, Ley S, Sedlaczek O, Biederer J, Kauczor HU, Jakob PM, Wielputz MO, (2018), Towards quantitative perfusion MRI of the lung in COPD: The problem of short-term repeatability, PLOS One, e0208587, 13

A-144

MRI T2-WI parameters correlate with CT and lung function tests in interstitial lung disease

C. A. Ruano[1,2], O. Fernandes[1,2], A. Borba[1], M. Grafino[2], A. Bernardo[2], M. F. Moraes-Fontes[3], T. Bilhim[4], K. Irion[5]
[1]Hospital de Santa Marta, Centro Hospitalar Lisboa Central, Lisbon, Portugal, [2]Hospital da Luz Lisboa, Lisbon, Portugal, [3]Champalimaud Foundation, Lisbon, Portugal, [4]Hospital Curry Cabral, Centro Hospitalar Lisboa Central, Lisbon, Portugal, [5]University of Florida, Gainesville, United States of America

Purpose/Objectives

To assess the correlation between T2-weighted (T2-W) MRI parameters with CT and lung function tests (LFT) in patients with interstitial lung disease (ILD).

Methods & Materials

T2-W images of 25 patients with ILD were acquired in a 1.5 T scanner, with axial respiratory-gated fat-saturated PROPELLER (periodically rotated overlapping parallel lines with enhanced reconstruction) sequence. Segmentation with delineation of the full extent of ILD was performed using an open-source software application, ITK-SNAP 3.8.0[1], with 6 additional small ROIs placed in the paraspinal muscles and normal lung.

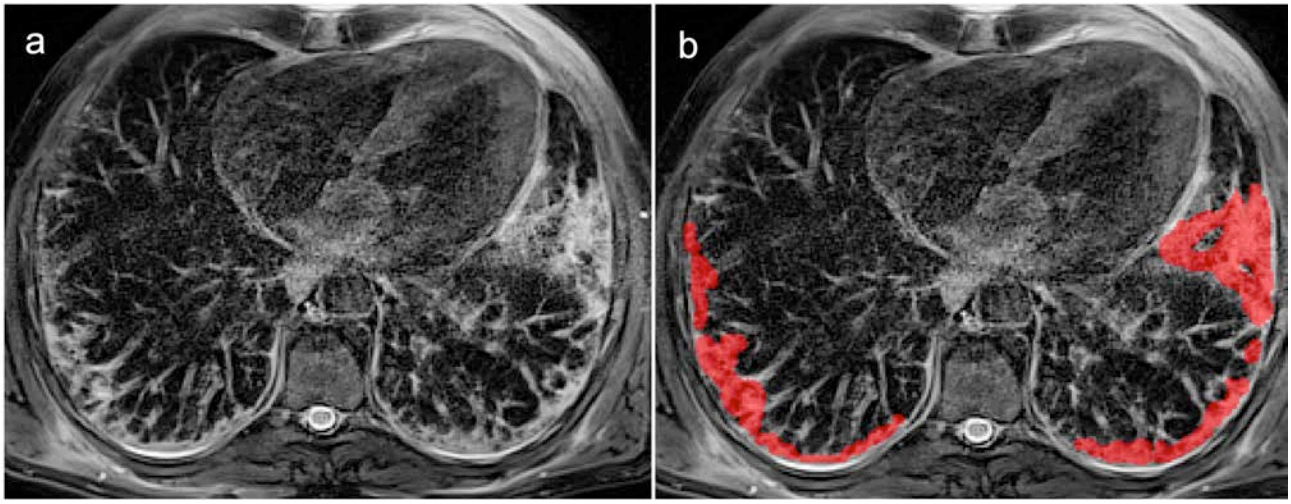

Axial fat-saturated T2-weighted images showing an example of segmentation (b) of interstitial lung disease, which presents as peripheral areas of high signal intensity (a). Normal lung has homogenous low signal intensity.

Signal intensity values were extracted by a dedicated software[2]. The total volume of segmented ILD was recorded, as well as two ratios, SI_{ILD}/SI_{muscle} and SI_{ILD}/SI_{lung} (ratios between the signal intensity of ILD and that of the paraspinal muscles[3] and normal lung, respectively).

CT images were evaluated with a visual semiquantitative scoring system [n=25, which determined an inflammation score (corresponding to the sum of ground-glass opacities (GGO) and GGO with reticulation scores), fibrosis score (sum of reticular and honeycombing scores) and total ILD score (sum of the previous scores)][4], and quantitatively with an automatic software, Imbio lung texture analysis [n=23, that determined the extent of GGO, reticulation, honeycombing and hyperlucent areas, as a percentage of individual lobe or total lung involvement; pulmonary vessel volume (PVV) was also calculated and corresponded to the volume of pulmonary arteries and veins as a percentage of lung volume][5].

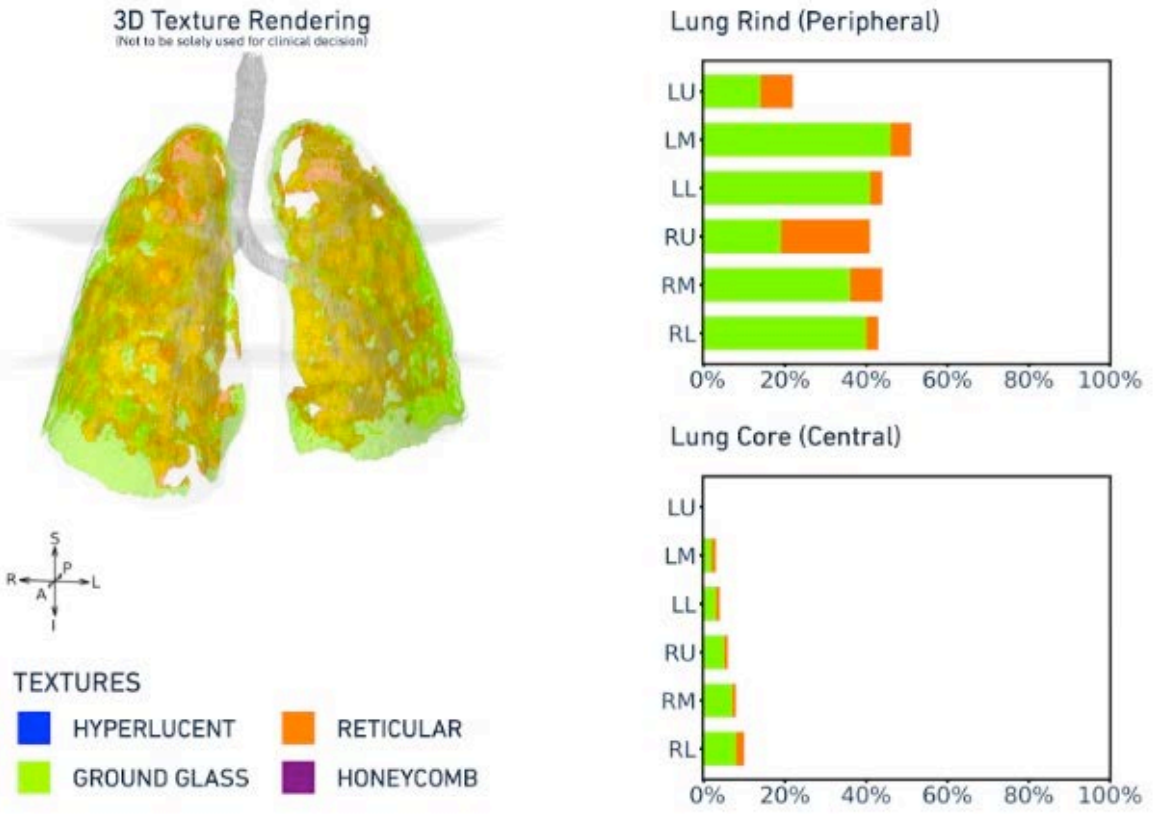

SUMMARY	Vol. (L)	Hyperlucent	Ground Glass	Reticular	Honeycombing	PVV (cm^3)
TOTAL LUNG:	3.5 L	0 %	18 %	4 %	0 %	118
Left Lung:	1.7 L	0 %	17 %	3 %	0 %	54
Left Upper LU		0 %	7 %	5 %	0 %	8
Left Middle LM		0 %	17 %	2 %	0 %	33
Left Lower LL		0 %	26 %	2 %	0 %	12
Right Lung:	1.8 L	0 %	19 %	5 %	0 %	64
Right Upper RU		0 %	12 %	12 %	0 %	10
Right Middle RM		0 %	16 %	4 %	0 %	33
Right Lower RL		0 %	27 %	3 %	0 %	20

Example of a summary report of the texture-based automatic quantification of interstitial lung disease, showing detailed quantification of each abnormality as a percentage of total lung (or lobe) volume.

MRI parameters were correlated with CT and LFT [forced vital capacity (FVC) and diffusing capacity of the lung for carbon monoxide (DLCO)].

Results

A significant positive correlation was seen between MRI ILD volume and the CT semiquantitative inflammation ($p<0.001$) and total ILD scores ($p<0.01$), as well as with additional quantitative CT parameters (% GGO, % total ILD and PVV; $p<0.001$). MRI SI_{ILD}/SI_{muscle} ratio was positively correlated with CT % reticulation and PVV ($p<0.01$); SI_{ILD}/SI_{lung} ratio was also positively correlated with % reticulation ($p<0.05$). A significant negative correlation was seen between MRI SI_{ILD}/SI_{muscle} ratio and volume of ILD with both FVC and DLCO ($p<0.05$).

MRI ILD volume had a slightly stronger negative correlation with FVC and DLCO (PCC=-0.516, $p<0.01$; PCC=-0.669, $p<0.001$; respectively) in comparison with CT quantification of total ILD, by semi-quantitative (PCC=-0.5006, $p<0.05$; PCC=-0.6359, $p<0.001$) or automatic analysis (PCC=-0.441, $p<0.05$; PCC=-0.572, $p<0.01$).

		Quantitative CT (n=23)				Lung function	
T2-WI data (n=25)		% Reticulation	% GGO	% total ILD	PVV	FVC	DLCO
SIILD/SImuscle	PCC / p	0.5370 / 0.008	0.2018 / 0.356	0.2732 / 0.207	0.542 / 0.0075	-0.495 / 0.012	-0.564 / 0.004
Volume of	PCC / p	0.046 /	0.749 /	0.751 /	0.668 /	-0.516 /	-0.669 /

ILD		0.833	0.0000	0.0000	0.0005	0.0083	0.0003
SIILD/SIlung	PCC / p	0.470 / 0.023	0.361 / 0.091	0.423 / 0.045	0.124 / 0.573	-0.195 / 0.350	0.078 / 0.716
Quantitative CT (n=23)							
% Reticulation	PCC / p	-	-	-	-	0.087 / 0.692	0.129 / 0.556
% GGO	PCC / p	-	-	-	-	-0.455 / 0.029	-0.593 / 0.003
% total ILD	PCC / p	-	-	-	-	-0.441 / 0.035	-0.572 / 0.004
PVV	PCC / p	-	-	-	-	-0.107 / 0.628	-0.294 / 0.174

Correlation of T2-WI data with automatic quantitative CT analysis and lung function (FVC and DLCO); correlation of automatic quantitative CT analysis with lung function (FVC and DLCO). PCC, Pearson correlation coefficient.

Conclusion

MRI parameters parallel ILD extension in CT and correlate inversely with lung function.

References:

[1] Yushkevich PA, Piven J, Hazlett HC, et al, (2006), User-guided 3D active contour segmentation of anatomical structures: Significantly improved efficiency and reliability, Neuroimage, 1116–28, 31(3)

[2] Constantino CS, Oliveira FPM, Silva M, et al, (2021), Are lesion features reproducible between 18F-FDG PET/CT images when acquired on analog or digital PET/CT scanners? , Eur Radiol, 3071–9, 31(5)

[3] Lutterbey G, Grohé C, Gieseke J, et al, (2007), . Initial experience with lung-MRI at 3.0 T: Comparison with CT and clinical data in the evaluation of interstitial lung disease activity, Eur J Radiol, 256–61, 61(2)

[4] Ooi GC, Mok MY, Tsang KWT, et al, (2003), Interstitial lung disease in systemic sclerosis an HRCT-clinical correlative study, Acta radiol, 258–64, 44

[5] Jacob J, Bartholmai BJ, Rajagopalan S, et al, (2016), Automated quantitative computed tomography versus visual computed tomography scoring in idiopathic pulmonary fibrosis validation against pulmonary function, J Thorac Imaging, 304–11, 31(5)

A-215

Non-contrast-Enhanced Functional Lung MRI to evaluate treatment response of ABPA in CF patients

I. Benlala[1], R. Klaar[2], T. Gaass[2], F. Laurent[1], G. Dournes[1], J. Dinkel[2]
[1]Bordeaux University Hospital, Pessac, France, [2]LMU Klinikum, Radiologie, Munich, Germany

Purpose/Objectives
To evaluate whether Fourier decomposition (FD) functional lung MRI can detect the response to treatment of allergic bronchopulmonary aspergillosis (ABPA) in cystic fibrosis (CF) patients.
Methods & Materials
Twelve CF patients were included in this retrospective longitudinal study. Inclusion criteria were: diagnosis of CF proven by sweat chloride and/or genetic testing, age older than 6 years, diagnosis of ABPA established by multidisciplinary sessions according to the CFFC criteria. All patients underwent lung MRI with 2D balanced steady-state free precession (bSSFP) sequence with Fourier decomposition (FD) at 1.5T scanner before and after treatment of ABPA. Total IgE and anti–A fumigatus specific IgE levels were measured before and after treatment as well as pulmonary function tests. Clinical and radiological improvement and/or a drop of at least 25% of total IgE were considered as positive response to ABPA treatments. Ventilation weighted (V) and perfusion weighted (Q) maps were obtained after FD processing of the 2D coronal bSSFP time resolved images before and after treatment of ABPA. Defects extent was assessed on the functional maps using a visual semi quantitative score. Mean and coefficient of variation (cv) of the ventilation signal intensity (VSI) and the perfusion signal intensity (QSI) were calculated. Measurements were performed independently by two readers and averaged. The reproducibility of the measurements was also assessed. Comparisons of medians were assessed using paired Wilcoxon test. Reproducibility was assessed using the intraclass correlation coefficient (ICC). Correlations were assessed using Spearman test. A p value <0.05 was considered as significant.
Results
Defects extent on both V and Q maps showed a significant reduction after ABPA treatment ($p<0.01$). VSI_mean was significantly increased after treatment ($p<0.01$). Visual analyses reproducibility showed an ICC >0.93. ICC of the quantitative measurements was almost perfect (>0.99). VSI_cv and QSI_cv variations correlated inversely with the variation of obstructive parameters of PFTs (rho = -0.68, p=0.01).
Conclusion
Non-contrast enhanced FD lung MRI appears to be able to reproducibly assessresponse to treatment of ABPA in CF patients and correlates with PFTs' obstructive parameters.

A-561

Pectoral muscle Indices Are Associated with Obstructive Sleep Apnea Severity

S. İcten[1], B. Arpinar Yigitbas[1], Z. N. Tekin[2], H. İ. Uzun[1], E. Ertan Yazar[1]
[1]Istanbul Medeniyet University Goztepe Prof Dr Suleyman Yalcin City Hospital, Chest Diseases, Istanbul, Turkey, [2]Istanbul Medeniyet University Goztepe Prof Dr Suleyman Yalcin City Hospital, Radiology, Istanbul, Turkey

Purpose/Objectives

Sarcopenia in sleep medicine has not yet been fully investigated in literature [1]. This study aims to identify sarcopenia in obstructive sleep apnea (OSA) patients using chest computed tomography (CT). Secondary endpoints are to assess sarcopenia by gender and OSA severity.

Methods & Materials

Patients who underwent polysomnography with a suspicion of OSA at a single tertiary sleep center between 2020 and 2023 were screened for chest CT. Patients whose chest CT was taken within the last 1 year were included in the study. Patients with cancer, muscle disease, surgery or trauma at the pectoral muscle level, and metabolic disease that may cause sarcopenia were excluded. Laboratory-based polysomnographic variables and anthropometric measurements were recorded. Severity of OSA was evaluated by apnea hypopnea index (AHI). Mild OSA was defined as AHI 5 to 15, moderate OSA as AHI 16 to 30, and severe OSA as AHI>30. Pectoralis muscle area (PMA) was measured retrospectively on a single axial slice of the chest CT scan above the aortic arc by a board-certifed radiologist with 15 years of experience. CT images were processed using 3D Slicer software and automated thresholding was performed to only include the pixels between – 29 and + 150 HU to prevent overestimation of muscle cross sectional area

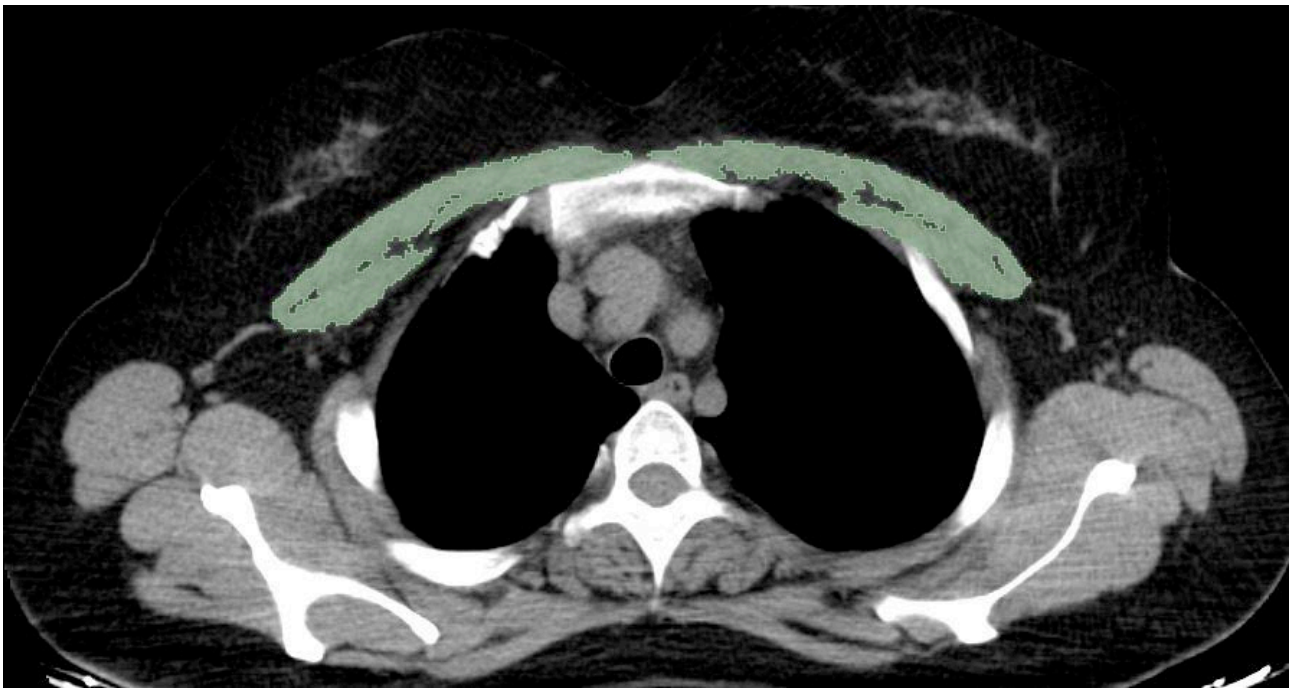

Pectoralis muscle segmentation on a single axial slice of the chest CT scan performed with 3D-Slicer

.

Results

A total of 97 patients (64 men) were included to the study, of whom 32 (33%)
had mild and 65 (67%) moderate- severe OSA. Considering the muscle mass differences between genders, evaluation was made by splitting the data between genders. Moderate-severe male OSA patient group had high body mass index (BMI), epworth score, AHI, oxygen desaturation index (ODI) and lower PMA/BMI ratio and PMA/Neck circumference(NC) ratio

Male	Mild OSA (AHI <15) N= 19	Moderate-Severe OSA (AHI >15) N=45	p value
PMA mm2, mean (SD)	5222.355 (1661.689)	4655.202 (1474.872)	0.181
PMA/Height2	1804.472 (579.959)	1581.933 (511.520)	0.132
PMA/BMI	179.874 (60.471)	138.726 (45.101)	0.004
PMA/NC2	3.31 (1.12)	2.56 (0.79)	0.010
Female	Mild OSA (AHI <15) N= 19	Moderate-Severe OSA (AHI >15) N=45	
PMA mm2	3020.491 (980.065)	4294.186 (1634.603)	0.017
PMA/Height2	1238.442 (426.339)	1780.453 (739.348)	0.023
PMA/BMI	82.097 (32.327)	106.047 (31.354)	0.042
PMA/NC2	2.13 (0.63)	2.58 (1.03)	0.175

Comparison of thorax CT measurements between OSA severity regarding gender. OSA: obstructive sleep apnea, AHI: Apnea hypopnea index, PMA: Pectoral muscle Area BMI: Body mass index NC2: Neck circumference squared

. Moderate – severe female patient group had higher epworth score, AHI, ODI, PMA/Height^2 and PMA/BMI ratio. Compared to men, women had lower PMA/BMI ratio (150.942 ± 53.145, 96.612 ± 22.419 respectively, p<0.001)

	Male N=64	Female N=33	p value
PMA mm2	4823.575 (1541.540)	3792.427 (1531.693)	0.002
PMA/Height2	1647.999 (537.907)	1566.933 (681.952)	0.523
PMA/BMI	150.942 (53.145)	96.612 (22.419)	<0.001
PMA/NC2	2.77 (0.95)	2.40 (0.90)	0.079

Comparison For Pectoral Muscle Indices Regarding Gender. OSA: obstructive sleep apnea, AHI: Apnea hypopnea index, PMA: Pectoral muscle Area BMI: Body mass index NC2: Neck circumference squared

. In multivariate logistic regression analysis revealed that odds ratio (OR) for PMA/BMI in moderate-severe male patients were 0.986 (p:0.033) and OR for PMA/ Height^2 ratio in moderate – severe female patients were 1.002 (p:0.037)

Model for Males

	B	Sig.	OR	95% CI Lower	95% CI Upper
EPWORTH	.107	.011	1.113	1.025	1.209
PMA/BMI	-.014	.033	.986	.974	.999
Constant	1.406	.251	4.081		

Model for females

	B	Sig.	OR	95% CI Lower	95% CI Upper
PMA/Height^2	.002	.077	1.002	1.000	1.004
EPWORTH	.149	.037	1.161	1.009	1.335
Constant	-4.498	.018	.011		

Logistic regression analysis for factors affecting moderate-severe OSA by gender

.

Conclusion

Present study showed that pectoralis muscle indices such as PMA/ Height^2 and PMA/BMI can be associated with severity of OSA. Gender differences stands out among PMA[2]. Lower muscle mass indices had an increased risk of moderate-severe OSA independent of age.

References:

[1] Szlejf C, Suemoto CK, Drager LF, Griep RH, Fonseca MJM, Diniz MFHS, Lotufo PA, Benseãor IM, Association of sleep disturbances with sarcopenia and its defining components: the ELSA-Brasil study, https://pubmed.ncbi.nlm.nih.gov/34878063/

[2] Moreno-Tamayo K, Manrique-Espinoza B, Guerrero-Zúñiga S, Ramírez-García E, Sánchez-García S, Sex Differences in the Association Between Risk of Obstructive Sleep Apnea, Insomnia, and Frailty in Older Adults, https://pubmed.ncbi.nlm.nih.gov/34456596/

A-200

Phenotyping of airway disease and emphysema in COPD patients with MRI in comparison to same-day CT: Results from a prospective multi-centre cohort trial

S. Nauck[1], M. Pohl[2], B. Jobst[1], C. Melzig[1], H. Meredig[3], O. Weinheimer[1], S. Triphan[1], O. von Stackelberg[1], C. P. Heußel[4], M. O. Wielpütz[1], H.-U. Kauczor[1], J. Biederer[1], S. Nauck[1,5]

[1]University Hospital Heidelberg, Diagnostic and Interventional Radiology, Heidelberg, Germany, [2]University Hospital Heidelberg, Institute of Medical Biometry, Heidelberg, Germany, [3]University Hospital Heidelberg, Neuroradiology, Heidelberg, Germany, [4]Thoraxklinik at the University of Heidelberg, Diagnostic and Interventional Radiology with Nuclear Medicine, Heidelberg, Germany, [5]Universitätsklinikum Heidelberg, Heidelberg, Germany

Purpose/Objectives

Chronic obstructive pulmonary disease (COPD) is a disease with high socio-economic burden worldwide. Therapy decision depends on disease manifestation in the lung, which may predominate as airway-type or emphysema-type. These “phenotypes” and other features of COPD can be differentiated using CT. Since MRI has been suggested as a radiation-free complement to CT [1], this prospective multi-centre study was launched to evaluate concordance between morpho-functional MRI and CT for the detection of key findings and differentiation of COPD phenotypes.

Methods & Materials

599 participants with COPD from 15 sites in Germany prospectively underwent same-day mopho-functional chest MRI and paired inspiratory-expiratory CT. Two readers systematically scored bronchial wall thickening, bronchiectasis, centrilobular nodules, air trapping and lung parenchyma defects in each lung lobe (usually scores 0-2 for absence, < 50% and ≥ 50%) and COPD phenotype, and a third reader acted as adjudicator establishing consensus. Sum scores were calculated and intermodality and interreader agreement were assessed using Cohen’s kappa (im-κ and ir-κ).

Results

Concordance of MRI and CT for phenotyping of COPD was substantial (im-κ = 0.63). Airway/emphysema/mixed COPD phenotypes were assigned in 347, 218 and 34/599 cases on CT (MRI: 370, 218 and 10/583 cases).

Mean sum scores on CT for bronchiectasis and bronchial wall thickening were 2.2/12 and 6/12 (MRI score for bronchiectasis/bronchial wall thickening 4.5/12; im-κ = 0.04 - 0.3). Expiratory right/left bronchial collapse was observed in 62 and 57/599 on CT (51 and 47/583 on MRI), respectively (im-κ = 0.49 - 0.52). Mean sum scores for markers of small airway disease on CT were 0.34/12, 0.37/12 and 0.9/12 for centrilobular nodules, mosaic attenuation and air-trapping (MRI: 0.15/12, 0.94/12, 7.6/11 and 1.3/12 for centrilobular nodules/peripheral mucus retention, air-trapping, perfusion deficits and parenchymal defects; im-κ 0.1-0.41). Mean CT emphysema score was 5.8/24 (lung defect score on MRI 1.3/12; im-κ = 0.18-0.26). Ir-κ was generally higher on CT and for features with high im-κ.

CT	MRI	Cohen's κ						Accuracy					
		RLL	RML	RUL	LUL	Ling.	LLL	RLL	RML	RUL	LUL	Ling.	LLL
Bronchiectasis	Bronchiectasis / Wall thickening	0.07	0.09	0.04	0.06	0.1	0.06	0.45	0.46	0.44	0.48	0.49	0.41
Wall thickening	Bronchiectasis / Wall thickening	0.3	0.14	0.24	0.25	0.17	0.31	0.75	0.65	0.65	0.64	0.6	0.77
Bronchial collapse	Bronchial collapse	0.29	0.11	0.07	0.33	0.1	0.23	0.9	0.95	0.96	0.99	0.97	0.86
Centrilobular nodules	Centrilob. nod. / Peripheral mucus	0.41	0.25	0.22	0.21	0.09	0.39	0.95	0.95	0.95	0.96	0.96	0.94
Air trapping	Air trapping	0.4	0.32	0.36	0.37	0.38	0.37	0.78	0.94	0.94	0.95	0.95	0.76
Emphysema	Parenchymal defects	0.18	0.26	0.23	0.2	0.21	0.2	0.54	0.59	0.54	0.53	0.57	0.55

Key	≤ 0.1	0.11 - 0.2	0.21 - 0.3	0.3 <	≤ 0.5	0.51 - 0.7	0.71 - 0.9	0.9 <

RLL: Right lower lobe
RML: Right middle lobe
RUL: Right upper lobe
LUL: Left upper lobe
Ling.: Lingula
LLL: Left lower lobe

Table 1. Intermodality concordance via Cohen's κ and accuracy of CT- and MRI-features on a lobar basis.

Conclusion

In a multi-centre setting, MRI and CT show a substantial concordance for phenotyping of COPD with variable intermodality and interreader concordance for diagnostic key features.These data indicate that MRI may be feasible as a radiation-free morphologic and functional imaging modality for COPD in scientific and clinical settings.

References:

[1] Jürgen Biederer, (2023), MR imaging of the airways, The British Institube of Radiology, The British Journal of Radiology, https://www.birpublications.org/doi/10.1259/bjr.20220630, 2023-03-24

A-140

Potential of ultra-high-resolution and 1024-pixel image matrix in photon-counting detector CT for the assessment of interstitial lung disease in patients with systemic sclerosis

L. Jungblut[1], T. Sartoretti[1], A. Landsmann[1], D. Nakhostin[1], T. El-Rabadi[2], V. Mergen[2], S. Jordan[1], C. M. Mihai[1], O. Distler[1], T. Frauenfelder[2], K. Martini[2]

[1]University Hospital Zurich, Department of Rheumatology, University Hospital Zurich, University of Zurich, Zurich, Switzerland, Zürich, Switzerland, [2]University Hospital Zurich, Institute of Diagnostic and Interventional Radiology, University Hospital Zurich, University of Zurich, Zurich, Switzerland, Zürich, Switzerland

Purpose/Objectives

To evaluate the potential of ultra-high-resolution (UHR) and 1024-matrix in photon-counting-detector CT (PCD-CT) in the assessment of interstitial-lung-disease (ILD) in patients with systemic-sclerosis (SSc).

Methods & Materials

In this IRB-approved study, patients with SSc referred for ILD-CT screening on a first-generation PCD-CT were included. Scans were acquired in the UHR mode at 100kVp at an image quality (IQ) level of 15 with a matrix-size of 512x512 and 1024x1024; each reconstructed at a slice-thickness of 1.5 and 0.2mm. Image noise was measured in the trachea. Subjective image quality (overall image quality, sharpness, noise) as well as ILD changes (ground-glass opacities and coarse reticulations) were assessed by two independent readers on a five-point Likert-scale.

Results

66 patients (mean age 57 years; 52 female) were retrospectively included. Mean CTDIvol was 0.69±0.18mGy. Interreader agreement for subjective image quality ranged from fair to almost perfect (Krippendorff-Alpha:0.258-0.862). Overall image quality was rated best at 1.5mm/1024 matrix images (reader 1:4(4.4), reader 2:5(4.5)). Image sharpness was superior in the 0.2mm images (p<0.001, median: 5(5.5) for both readers at both matrix sizes.

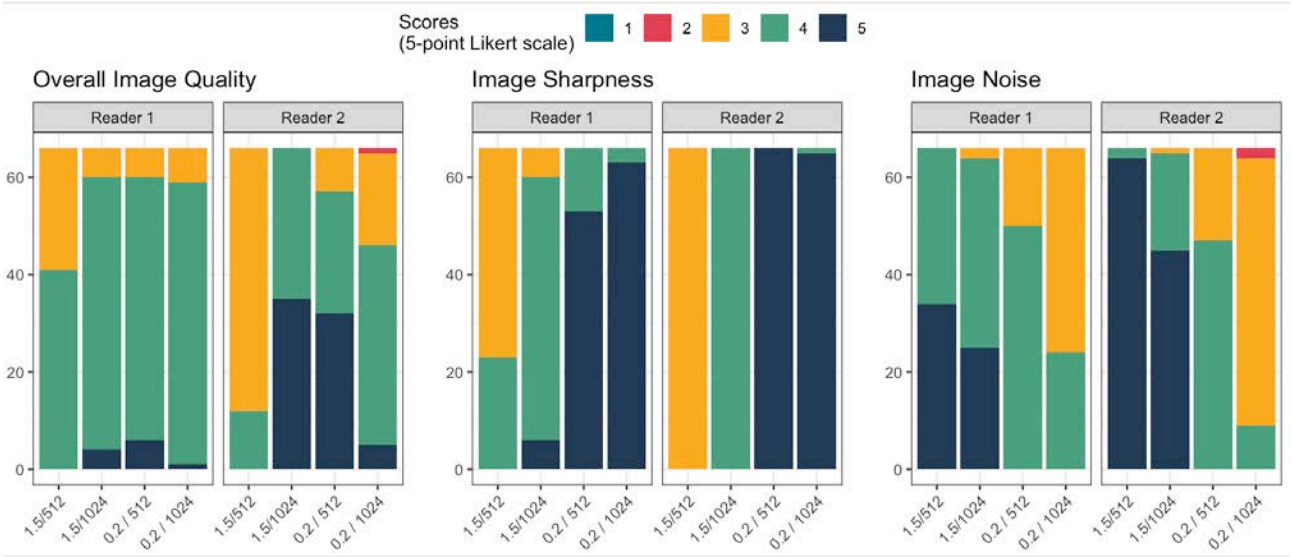

Results from qualitative image analysis

For the evaluation of ILD-typical changes 0.2mm slices significantly outperformed (p<0.001) images with 1.5mm slice thickness while there was no significant difference between the matrix sizes (p=0.037 for ground-glass opacities and p=0.066 for coarse reticulations).

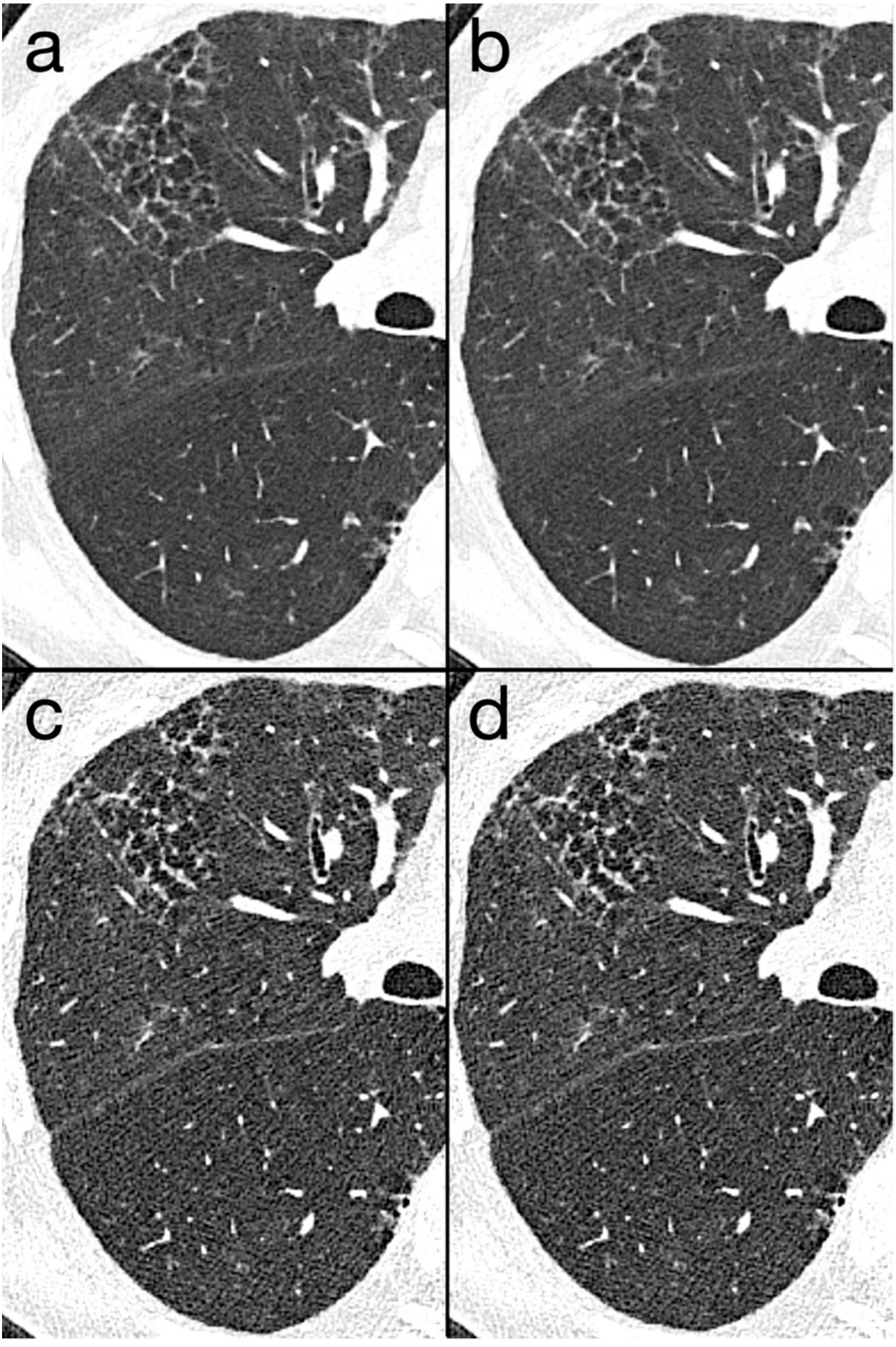
a
b
c
d

Chest computed tomography (CT) of a 42y female patient with reticulations consistent with ILD in axial plane. (a) 1.5 mm/512 reconstruction, (b) 1.5 mm/1024 reconstruction, (c) 0.2 mm/512 reconstruction, (d) 0.2 mm/1024 reconstruction.

Conclusion

Image sharpness as well as visibility of subtle ground glass opacities and coarse reticulations were rated superior in UHR mode compared to standard reconstructions. 1024 matrix-size may be beneficial in the evaluation of coarse reticulations.

A-646

Pre-interventional AI-supported automated lung parenchyma quantificationpredicts post-interventional complications in CT-guided lung biopsies

L. Müller[1], M. Halfmann[1], T. Jorg[1], G. Langs[2], M. Pieler[2], A. Makropoulos[2], P. Mildenberger[1]
[1]University Medical Center Mainz, Department of Radiology, Mainz, Germany, [2]Contextflow, Vienna, Austria

Purpose/Objectives
CT-guided biopsy of intrapulmonary lesions is a common procedure in the management of possibly malignant lung nodules. While previous studies have agreed upon risk factors for typical post-interventional complications such as pneumothorax, few have presented quantifiable cut-offs in order to identify patients at greater risk for complications. The aim of this study was therefore to apply an AI-algorithm to quantify lung parenchyma features in pre-interventional scans in order to predict post-interventional pneumothorax.
Methods & Materials
A total of 142 consecutive patients (73 female, 51 %) who had previously underwent biopsy in our institution between January 2021 and September 2022 were retrospectively identified from our database. An AI-based algorithm (contextflow, Vienna, Austria) subsequently analyzed specific lung patterns in both the planning and the immediate post-interventional scan and quantified lung volumes, and pathological patterns such as pleural effusion, mosaic perfusion patterns or emphysema. Logistic regression analyses were used to predict post-interventional pneumothorax.
Results
Patients undergoing biopsies had a mean age of 66 ± 11 years and peri-interventional pneumothorax was present in 57 (40 %) of cases. A median number of 3 (IQR 3-4) specimens were obtained during the biopsy and median needle thickness was 20 Gauge (IQR 18-20). Neither of both parameters showed could predict post-interventional pneumothorax (p=0.82 and p=0.18, respectively). However, greater amount of pre-interventional consolidations (p=0.03) and smaller lesion size (p=0.04) were predictors for post-interventional pneumothorax.
Conclusion
In patients undergoing lung biopsies, AI-supported automated quantification of lung parenchyma patterns helped identifying patients at greater risk of post-interventional pneumothorax. This may allow for development of risk stratification models and thereby support pre-interventional decision-making in the future.

A-666

Preliminary results analysis demonstrating the rate type and management of incidental findings (IF) referred to the East Surrey Hospital (ESH) Lung Screening Review Meeting (SRM) from the Crawley Target Lung Health Check (TLHC)

M. Hartley[1], C. Dodds[2], S. Bax[3], K. Nimako[3], C. O'Driscoll[4], V. Stewart[5], R. Ahmed[6], A. Villanueva[7]
[1]East Surrey Hospital. SURREY AND SUSSEX HEALTHCARE NHS TRUST, Radiology ST1, Redhill, United Kingdom, [2]East Surrey Hospital. SASH Trust, Radiology ST2, Redhill, United Kingdom, [3]East Surrey Hospital. Redhill, SURREY AND SUSSEX HEALTHCARE NHS TRUST, Respiratory Consultant, Redhill, United Kingdom, [4]East Surrey Hospital. Redhill, SURREY AND SUSSEX HEALTHCARE NHS TRUST, Lead Administrator, Redhill, United Kingdom, [5]Surrey and Sussex Cancer Alliance, Programme Manager, Guildford, United Kingdom, [6]East Surrey Hospital. Redhill, SURREY AND SUSSEX HEALTHCARE NHS TRUST., Consultant Radiologist, Redhill, United Kingdom, [7]East Surrey Hospital. SURREY AND SUSSEX HEALTHCARE NHS TRUST, Consultant Radiologist, Redhill, United Kingdom

Purpose/Objectives

The TLHC, led locally by Surrey and Sussex Cancer Alliance (SSCA), is an NHS England programme designed to identify early stage lung cancer in populations with smoking and lung cancer prevalence. ESH SRM covers Crawley TLHC, which has the 4th highest smoking and lung cancer prevalence within Surrey and Sussex (England). High risk patients undergo a low dose CT Chest, and if suspicious lung nodules or significant IF are detected can be referred to the ESH SRM (1).

As minor IF are common on TLHCs and can cause unneeded investigations and participant anxiety (1), TLHC's adhere to strict protocols for clinically insignificant findings, and have a target referral rate <15% (2,3). This includes nodules requiring non-LDCT work-up (<7%) and referral for significant IF (<8%).

The **aims** of this work are:

1. To determine the referral rate to SRM from Crawley TLHC
2. To report the percentage and type of IF referred to the SRM
3. To know the number of participants with IF that were referred to primary care to specialist clinics and moved to a cancer pathway from SRM
4. To discover the proportion of IF that were resolved within the SRM

Methods & Materials

The SSCA TLHC follows the published standard protocol and quality assurance standards prepared for the TLHC Programme by the Lung Clinical Expert Advisory Group (1,2).

Of 1380 invited people from Crawley to the SSCA TLHC, 1148 (83%) were screened. 1061 (92%) of these underwent a low-dose CT scan between 1/7/22 and 1/1/23 and were included in the data.

All patients suspicious lung nodules and significant IF reviewed at the SRM had their outcomes collected from the Sommerset Cancer Registry and registered in a spreadsheet including reason for referral to SRM, type of incidental findings, and management of outcome.

Results

119/1061 participants were referred to the ESH SRM (11.2%). 41/1061 (3.8%) were referred for suspicious lung nodules , 64 (6%) for significant IF, and 14 for IF and lung nodules (1.3%).

Of the 78/1061 patients with IF (7,4%), the most frequent finding was a dilated ascending aorta (Table 1).

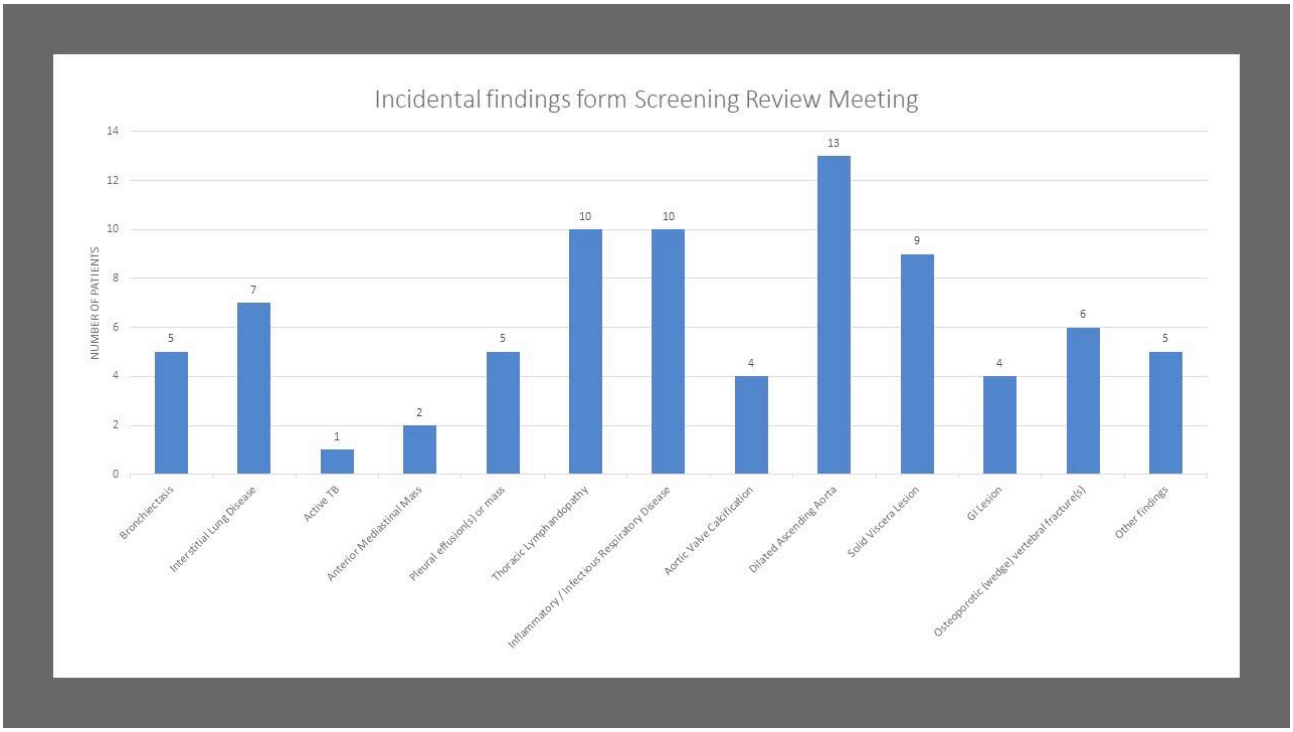

Table 1. Type of significant incidental findings of 78 participants referred from Crawley Target Lung Health Check to East Surrey Hospital Screening Review Meeting. 3 patients had 2 types of incidental findings.

1 participant (1.3%) was referred to their GP, 43 (55%) were referred to specialist clinics and 10 (13%) were moved to a cancer pathway. 32 (41%) participants with IF at ESH SRM were resolved within the SRM. 8 patients had two referrals.

Conclusion

The referral rate to ESH RM from Crawley TLH was 11.2% (target <15%), whilst the referral rate of IF was 7.4% (target <8%). Of those with IF, 1 participant was referred to GP, 43 (55%) were referred to specialist clinics and 32 (41%) moved to cancer pathway. 41% of referrals to the ESH SRM due to IF were resolved within the SRM.

References:

[1] NHS England. , (2022), Targeted screening for lung cancer with low radiation dose computed tomography. Standard protocol prepared for the Targeted Lung Health Checks Programme by the Lung Clinical Expert Advisory Group. , NHS England, Publication reference: PR1646.

[2] NHS England. , (2022), Targeted screening for lung cancer with low radiation dose computed tomography. Quality assurance standards prepared for the Targeted Lung Health Checks programme Prepared with guidance from the Lung Clinical Expert Advisory Group. , NHS England

[3] British Society of Thoracic Imaging and The Royal College of Radiologists. , (2020), Considerations to ensure optimum roll-out of targeted lung cancer screening over the next five years. London, The Royal College of Radiologists, Ref No.RCR (20)1.

A-276

Quantitative CT Evaluation of Lung Vessels in Systemic Sclerosis-related Pulmonary Hypertension

C. Marrocchio, S. Schirò, C. Zilioli, L. Leo, N. Sverzellati
University of Parma, Department of Medicine and Surgery, Unit of Radiological Sciences, Parma, Italy

Purpose/Objectives

Pulmonary hypertension (PH) is a relatively frequent complication of systemic sclerosis (SSc) with significant prognostic implications[1]. The etiopathogenesis is complex and involves multiple mechanisms, including pulmonary arterial hypertension, left-sided heart disease, interstitial lung disease (ILD), and pulmonary veno-occlusive disease[2]. Recent studies have utilized automated software to perform quantitative analyses on lung vessels and reported initial evidence in SSc, correlating quantitative vessel parameters with ILD features[3][4]. Moreover, quantitative analysis showed different patterns of vascular involvement in different PH subtypes[5]. However, no study has investigated the potential role of quantitative CT in patients with SSc and PH.

This study aims to use quantitative CT to characterize the vascular alterations in patients with SSc and to identify specific disease phenotypes in patients with SSc-related PH.

Methods & Materials

This is a multicenter retrospective study including patients with a diagnosis of SSc who had a chest CT suitable for quantitative analysis from 2007 to 2022. SSc patients were stratified into having or not having PH based on echocardiography/right heart catheterization. A matched control population with no underlying connective-tissue disease and a CT showing no significant abnormalities was identified. Radiological images were analyzed using a commercially available quantification software (Aview, Coreline Soft, Seoul, Republic of Korea). Three radiologists reviewed the images in consensus to manually correct the vessel segmentation and to assess for any associated relevant abnormalities. Groups were compared using the Mann-Whitney test.

Results

Preliminary results included 26 patients who met the inclusion criteria (F:22, M:4, mean age: 62.6 ± 9.7 years). Eighteen patients had SSc, of whom 9 had ILD and 10 had PH; 8 were normal controls, not significantly different for age and demographics.

Patients with SSc had a mean number of lung vessels of 1313.7 ± 600.8, significantly lower than normal controls (2060.3 ± 604.5, p=0.009). The SSc group had also significantly lower number of vessels under 5 mm2 (p=0.005) and lower aggregate vessel volume for vessels less than 5mm2 normalized to the total blood volume (p=0.04). The mean diameter of lung vessels was increased in the SSc group (2.1 ± 0.3 mm vs 1.7 ± 0.2 mm, p=0.0003).

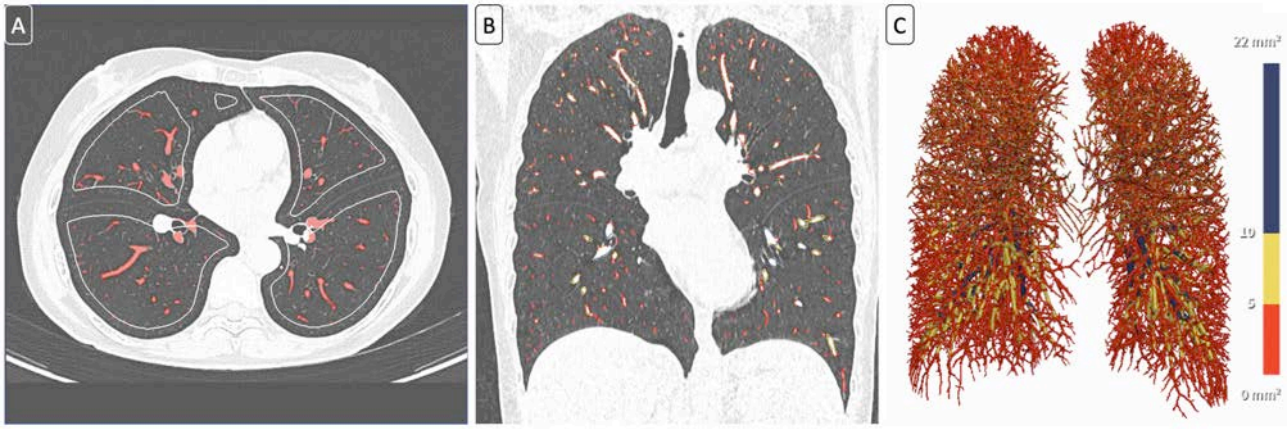

Patient with no underlying connective tissue disease. (A) Automatic software segmentation of lung vessels (red) on chest CT, with lobar masks isodistant from the lung pleura (white outline); (B, C) Coronal view and 3D reconstruction of the automatic vessel segmentation, with color coding according to the vessel area (mm2, legend in C)

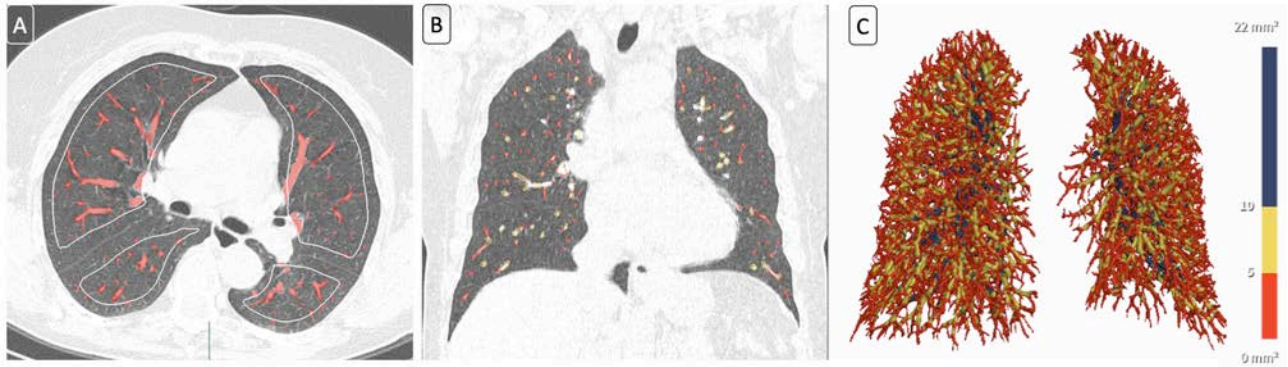

Patient with systemic sclerosis and no pulmonary hypertension. (A) Automatic software segmentation of lung vessels (red) on chest CT, with lobar masks isodistant from the lung pleura (white outline); (B, C) Coronal view and 3D reconstruction of the automatic vessel segmentation, with color coding according to the vessel area (mm2, legend in C)

When comparing SSc patients having and not having PH, the total surface area of lung vessels was significantly lower in patients with SSc and PH (p=0.02).

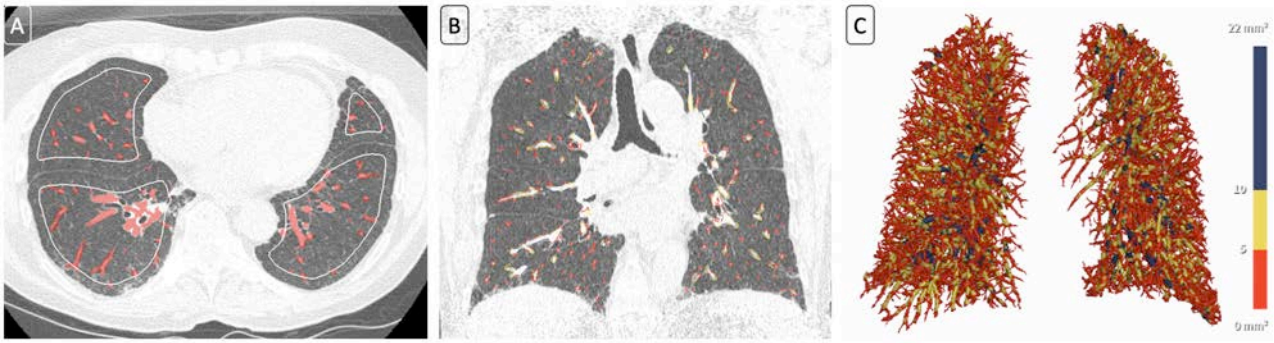

Patient with systemic sclerosis and pulmonary hypertension. (A) Automatic software segmentation of lung vessels (red) on chest CT, with lobar masks isodistant from the lung pleura (white outline); (B, C) Coronal view and 3D reconstruction of the automatic vessel segmentation, with color coding according to the vessel area (mm2, legend in C).

Conclusion

Our preliminary results show that patient with SSc, and specifically patients with PH, have pulmonary vessels changes that can be detected at quantitative analysis.

References:

[1] Anji Xiong, Qingting Liu, Jiaxun Zhong, Yuzi Cao, Qilang Xiang, Ziyi Hu, Shifeng Zhou, Zhuoyao Song, Huini Chen, Yan Zhang, Hongxu Cui, Shiquan Shuai, (2022), Increased risk of mortality in systemic sclerosis-associated pulmonary hypertension: a systemic review and meta-analysis, Advances in Rheumatology

[2] David Launay, Vincent Sobansky, Eric Hachulla, Marc Humbert, (2017), Pulmonary hypertension in systemic sclerosis: different phenotypes, European Respiratory Review, 145

[3] Joseph Jacob, Brian J Bartholmai, Srinivasan Rajagopalan, Maria Kokosi, Arjun Nair, Ronald Karwoski, Simon L F Walsh, Athol U Wells, David M Hansell, (2017), Mortality prediction in idiopathic pulmonary fibrosis: evaluation of computer-based CT analysis with conventional severity measures, European Respiratory Journal

[4] Cosimo Bruni, Mariaelena Occhipinti, Michael Pienn, Gianna Camiciottoli, Maurizio Bartolucci, Silvia Laura Bosello, Christian Payer, Zoltán Bálint, Anna Rita Larici, Alessandra Tottoli, Lorenzo Tofani, Enrico De Lorenzis, Gemma Lepri, Silvia Bellando-Randone, Amelia Spinella, Dilia Giuggioli, Francesco Masini, Giovanna Cuomo, Federico Lavorini, Stefano Colagrande, Horst Olschewski, Marco Matucci-Cerinic, (2022), Lung vascular changes as biomarkers of severity in systemic sclerosis-associated interstitial lung disease, Rheumatology

[5] Yousef Shahin, Samer Alabed, Dheyaa Alkhanfar, Juerg Tschirren, Alex M K Rothman, Robin Condliffe, James M Wild, David G Kiely, Andrew J Swift, (2022), Quantitative CT Evaluation of Small Pulmonary Vessels Has Functional and Prognostic Value in Pulmonary Hypertension, Radiology

A-307

Quantitative Functional Computed Tomography Assessment of GvHD-related Bronchiolitis Obliterans: Identification of Relevant Parameters and Correlation with Lung Function Tests

D. Winkel[1], J. Bremerich[1], M. Segeroth[1], M. Tamm[2], J. Halter[3], K. Hostettler[2], M. Pradella[1]
[1]University Hospital Basel, Clinic of Radiology & Nuclear Medicine, Basel, Switzerland, [2]University Hospital Basel, Clinic of Respiratory Medicine and Pulmonary Cell Research, Basel, Switzerland, [3]University Hospital Basel, Department of Hematology, Basel, Switzerland

Purpose/Objectives

To identify and evaluate CT-derived imaging parameters in patients with suspected bronchiolitis obliterans (BO) and to compare these parameters with established spirometry-derived parameters. Those parameters could help to identify patients-at-risk and guide appropriate treatment.

Methods & Materials

We included a total number of 60 patients treated with allogeneic hematopoietic cell transplantation (HCT) and suspected BO referred to functional CT imaging in inspiration and expiration[Ref1][Ref2] as well as spirometry testing within a time frame of ± 1 week in the study. Both lungs and lung lobes were automatically segmented using an AI-supported workflow (CT Pulmo 3D, syngo.via VB40A, Siemens Healthineers). Spirometry/bodyplethysmography-derived parameters were (among others): Forced Expiratory volume in the first second (FEV1), Tiffeneau-Index (FEV1/FVC max), residual volume (RV), total lung capacity (TLC). CT-derived parameters were both volumetric (total lung volume in inspiration and expiration, TLV_CTins, TLV_CTexp) and lung-density driven (mean lung density (MLD), low attenuation volume (LAV, defined as lung parenchyma <-950HU on the inspiratory CT scan and lung parenchyma below -856HU on expiratory CT scan), as well as the LAV difference (LAV_diff)). Values were compared using spearman correlation coefficients and correlation plots. Prediction of an obstruction in spirometric testing was performed using optimal cut-off point analyses using a Tiffeneau-Index < 0.7 as the threshold.

Results

We found a very strong correlation between inspiration parameters (TLV_CTinsp, TLC, r = 0.87, p < 0.001) and strong correlation between expiration parameters (TLV_CTexp, RV, r = 0.75, p < 0.001) volumes of both tests. The LAV difference correlated strongly with the FEV1/FVC (r = -0.62, p < 0.001), but not with the FEV1 (r = 0.11, p = 0.38)

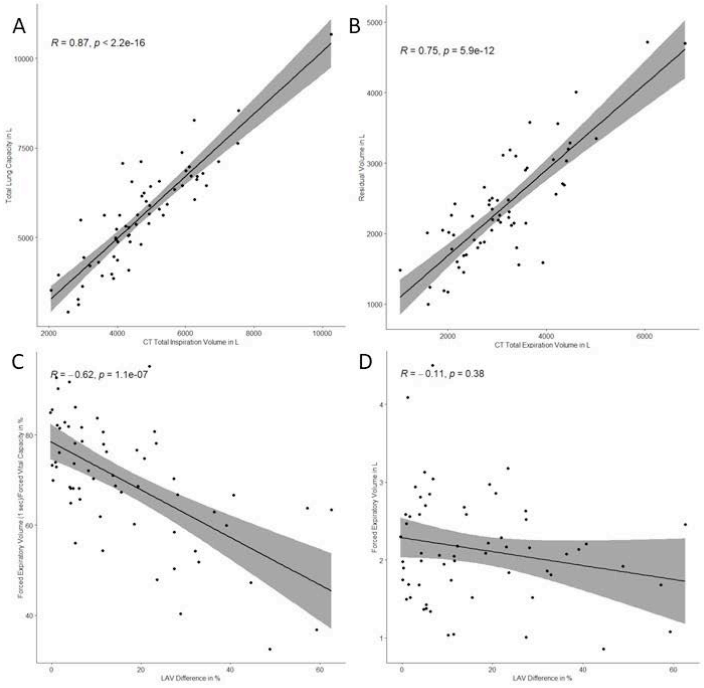

Figure showing spearman correlation plots of TLC and CT_TLVins (A), RV and CT_TLVexp (B), Tiffenau and LAV difference (C) and FEV1 and LAV difference (D).

. A LAV difference of 23.6% was best suited to predict relevant obstruction in spirometry (defined as FEV1/FVC > 0.7) with an area under the curve (AUC) of 0.79 (Accuracy: 75%, Sensitivity: 52%, Specificity: 97%)

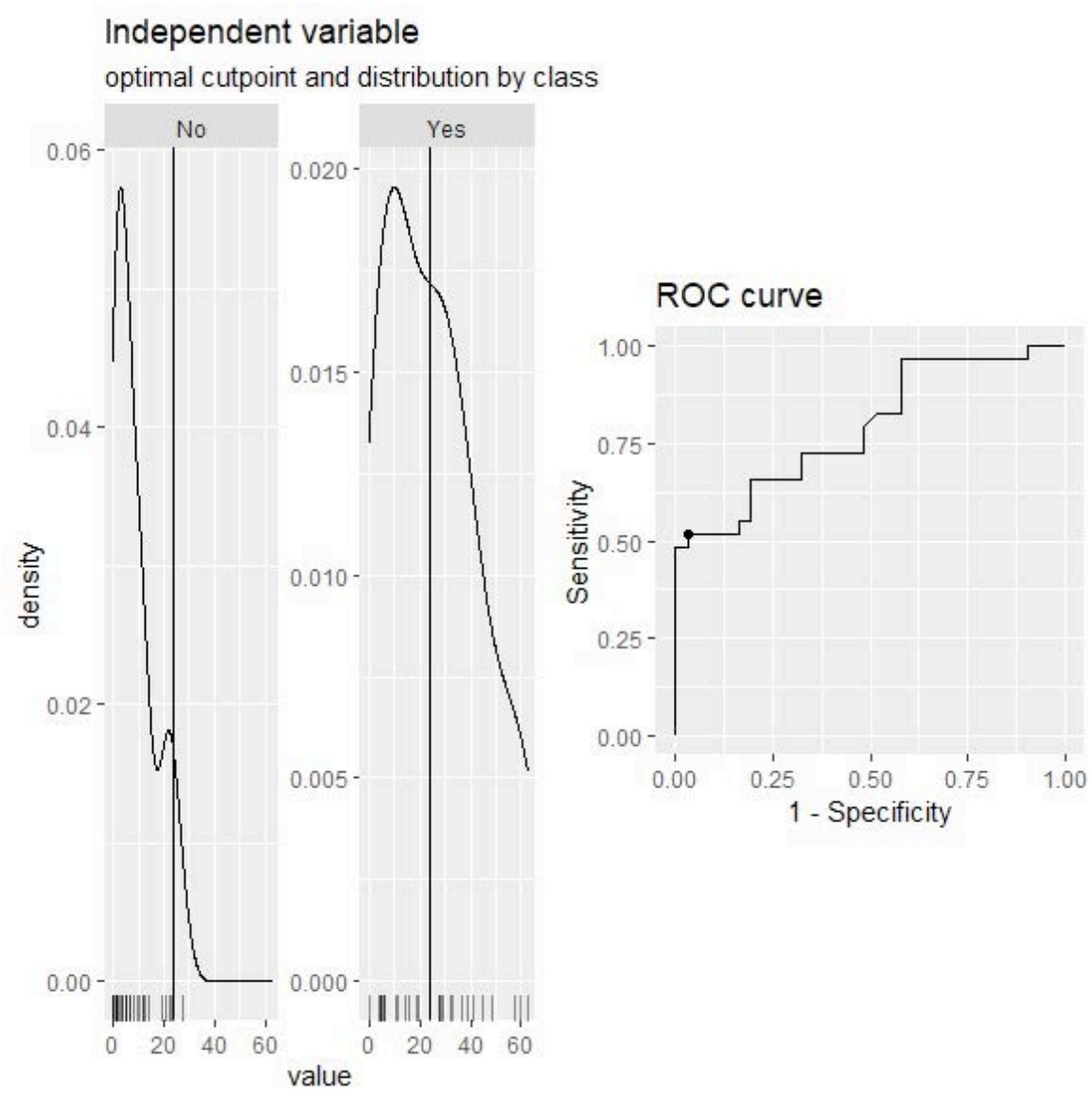

Figure demonstrating results of optimal cut-off value analyses using cutpointr (Version 1.1.2) in RStudio (RStudio Team (2020). RStudio: Integrated Development for R. RStudio, PBC, Boston, MA URL http://www.rstudio.com/) using an obstruction defined as a Tiffeneau-Index < 0.7 as the outcome parameter and LAV_diff as the predictor.

.

Conclusion

In patients with suspected BO, volumetric analyses from CT imaging and lung function testing showed overall a high correlation. LAV difference derived from functional CT imaging correlates best with the Tiffeneau index, but not with the FEV1. A cut-off value of LAV difference = 23.6% is best suited to predict obstruction in patients with suspected BO. At this cut-off value, functional CT imaging is especially suitable to identify patients without BO with a specificity of 97%.

References:

[Ref1] Galbán CJ, Boes JL, Bule M et al., (2014), Parametric Response Mapping as an Indicator of Bronchiolitis Obliterans Syndrome after Hematopoietic Stem Cell Transplantation, Biol Blood Marrow Transplant , 1592-1598, 20

[Ref2] Galban CJ, Han MK, Boes JL et al., (2012), Computed tomography-based biomarker provides unique signature for diagnosis of COPD phenotypes and disease progression, Nat Med , 1711-5, 18

A-172

Reference values for prevalence of solid lung nodules in an unselected general Western population

J. Cai[1], M. Vonder[1], G. J. Pelgrim[2], M. Rook[3], G. Kramer[3], H. J. Groen[4], G. H. de Bock[1], R. Vliegenthart[2]
[1]University Medical Center Groningen, Department of Epidemiology, Groningen, The Netherlands, [2]University Medical Center Groningen, Department of Radiology, Groningen, The Netherlands, [3]Martini Hospital Groningen, Department of Radiology, Groningen, The Netherlands, [4]University Medical Center Groningen, Department of Pulmonology, Groningen, The Netherlands

Purpose/Objectives
Most of the data on the prevalence of lung nodules originate from lung cancer screening studies in high-risk populations, the prevalence in the general population is largely unknown. The aim of this study was to establish reference values for the prevalence of lung nodules by age and sex in an unselected Western general population.

< quillbot-extension-portal >< quillbot-extension-portal ></quillbot-extension-portal>
Methods & Materials
ImaLife (Imaging in Lifelines) is a substudy of the population-based Lifelines cohort. Participants (≥45 years old) underwent low-dose chest computed tomography using a third-generation dual-source CT. The presence of solid lung nodules was registered by trained readers, and semi-automatic volumetric measurements were performed to determine the size of nodules. The prevalence of lung nodules (≥30 mm^3) and clinically relevant lung nodules (≥100mm^3) by age (5-years categories) and sex were presented.

< quillbot-extension-portal >< quillbot-extension-portal ></quillbot-extension-portal>
Results
In total, 12,075 participants (55.9% women; median age 60.1 years; 13.5% current smokers) were included. Overall, lung nodules and clinically relevant lung nodules were present in 41.9% (5,054/12,075) and 11.4% (1,377/12,075) of individuals. The prevalence of lung nodules increased with age, from 38.8% in men aged 45-50 years, to 60.4% in men ≥80 years. Corresponding percentages in women were 27.7% and 53.3%. The prevalence of clinically relevant nodules was 14.2% in men and 9.2% in women, with prevalence ranging from 9.1% to 24.4% in men and 4.1% to 15.1% in women as age increased. Men had a higher prevalence of nodules than women across all age categories, irrespective of nodule size.

< quillbot-extension-portal >< quillbot-extension-portal ></quillbot-extension-portal>
Conclusion
In this study, the prevalence and size of lung nodules in an unselected general Western population was determined. Results indicate that lung nodules are common in the Western general population and that clinically relevant lung nodules constitute a non-negligible part.
< quillbot-extension-portal >< quillbot-extension-portal ></quillbot-extension-portal>

A-702

Relationship between Right and Left Ventricle Function in Subjects Free of Cardiovascular Diseases

R. von Krüchten[1], R. Lorbeer[2], S. Rospleszcz[3], A. Peters[3], S. Karrasch[3], H. Schulz[4], F. Bamberg[1], C. Schlett[1], B. Mujaj[1]
[1]University Medical Center Freiburg, Freiburg, Germany, [2]Ludwig-Maximilians-University Hospital, Department of Radiology, Munich, Germany, [3]Helmholtz Zentrum München - German Research Center for Environmental Health, Institute of Epidemiology, Neuherberg, Germany, [4]German Center for Diabetes Research (DZD), Neuherberg, Germany

Purpose/Objectives
Right (RV) and left ventricular (LV) volumetric measurements by cardiac magnetic resonance imaging (MRI) are established parameters used to assess systolic and diastolic function), and the degree to which MRI-derived lung volumes impact LV function remains unclear. The aim was to investigate the relationship between RV and LV function in the KORA-MRI study through lung volumes.
Methods & Materials
In the KORA-MRI cohort study, 361 subjects underwent a whole-body 3T MRI scan. Cardiac functional parameters were measured from a cine-steady-state free precession sequence using cvi42. Lung volumes were derived semi-automatically using an in-house algorithm. Linear regression analyses assessed the relationships between RV and LV function adjusted for age, sex, cardiovascular risk factors, and lung volumes.
Results
Among 361 subjects (mean age 56.1±9.1 years; 43% women), RV end-diastolic volume was positively associated with LV end-diastolic (β=28.1, p=<0.001), end-systolic (β=11.0, p=<0.001), and stroke volume (β=17.0, p=<0.001), and inversely with ejection fraction (β=-1.4, p=0.001). RV end-systole was positively associated with LV end-diastolic (β=21.2, p=<0.001), end-systolic (β=11.5, p=<0.001), stroke volume (β=9.7, p=<0.001), and inversely with ejection fraction (β=-3.3, p=<0.001). When adjusting for lung volumes, the association between RV and LV did not attenuate, and no effect modification was observed. Interestingly, despite their different lung volumes in women and men, we did not observe any gender difference in the association between RV and LV parameters.
Conclusion
MRI-derived RV and LV volumetric parameters were strongly associated in subjects free of cardiovascular diseases, supporting the conception that RV function is crucial for LV function, independent of lung volumes.

A-367

Retrospective identification of low-risk individuals eligible for biennial lung cancer screening using PanCan-based and deep learning-based risk thresholds

N. Antonissen[1], K. Venkadesh[1], H. Piggelen-Gietema[2], R. Vliegenthart[3], Z. Saghir[4], M. Silva[5], G. Milanese[5], U. Pastorino[6], E. Scholten[1], M. Prokop[1], C. Schaefer-Prokop[7], C. Jacobs[1]

[1]Radboud University Medical Center, Medical Imaging, Nijmegen, The Netherlands, [2]Maastricht University Medical Center, Radiology, Maastricht, The Netherlands, [3]University Medical Center Groningen, Radiology, Groningen, The Netherlands, [4]University of Copenhagen (UCPH), Faculty of Health and Medical Sciences, Copenhagen, Denmark, [5]University Hospital of Parma, Department of Medicine and Surgery, Parma, Italy, [6]IRCCS Istituto Nazionale dei Tumori Foundation, Thoracic Surgery, Milan, Italy, [7]Meander Medical Center, Radiology, Amesfoort, The Netherlands

Purpose/Objectives

Current nodule management protocols for managing negative screening results have varying follow-up intervals; LungRADS recommends a 1-year screening interval for all negative screens (category 1/2), while the International Lung Screen Trial (ILST) protocol recommends a 1-year interval for participants with indeterminate nodules (PanCan score 1.5% - 6%) and 2-year interval for participants with no or very low risk nodules (PanCan score <1.5%). In this study, we retrospectively evaluated the use of PanCan and DL-based malignancy thresholds to identify individuals eligible for biennial screening, aiming to reduce screening-related harms and enhancing cost-effectiveness without causing potential delay of cancer diagnosis.

Methods & Materials

All baseline CT-scans from the Danish Lung Cancer Screening Trial (DLCST) and Multicentric Italian Lung Detection (MILD) were pooled and linked to a lung cancer diagnosis within 2 years, resulting in 4.157 non-cancer and 53 cancer cases. PanCan1a and DL-based malignancy risk scores were calculated for all screen-annotated nodules. For cases with no screen-annotated nodules, the risk score for participants was set as 0%. For both risk calculators, we used a nodule-risk cut-off of < 1.5% to identify low-risk participants for biennial follow-up, based on the ILST protocol. We computed the number of low-risk participants eligible for biennial screening for all included baseline scans (n=4.210) using the risk dominant nodule per scan and calculated the number of cancer cases in the biennial group.

Results

The DL-based and PanCan-based risk threshold < 1.5% identified 3.729 and 3.720 individuals, respectively, meeting the criteria for biennial screening. This would result in a reduction of 88.6% and 88.4% of the scans in the second screening round, respectively. The group referred for biennial screening included 14 and 16 cancers with DL and PanCan-based risk scores <1.5%, respectively. Most of the cancer cases (n=13), had no nodule annotated at baseline CT, leading to a 0% risk score at baseline. Retrospectively 4 of the 13 cancers were visible in the baseline scan, yet primarily not annotated by the screening radiologist.

Conclusion

Risk threshold-based identification of low-risk subjects for biennial screening largely reduces the number of 1-year follow-up scans. DL and PanCan for risk assessment performed very similarly, indicating the potential of DL for readily available risk assessment of baseline scans. A risk threshold of < 1.5%, as implemented in the ILST protocol, leads to delayed diagnosis of cancers either primarily missed during baseline or developing as interval cancers. More research is needed to study the type of cancers with delayed diagnosis and whether such delay leads to diagnostic stage shift.

A-693

Serial chest-CT up to more than 30 months after COVID-19 pneumonia: perilobular pattern as predictor of long-term pulmonary sequelae.

A. Poerio[1], F. Ciccarese[2], E. Carlicchi[3], M. Milandri[1], M. Pasquali[1], M. Morsiani[1], M. Zompatori[4]
[1]Ospedale Santa Maria della Scaletta - AUSL Imola, Radiology Unit, Imola, Italy, [2]IRCCS Azienda Ospedaliero-Universitaria di Bologna, Department of Radiology, Bologna, Italy, [3]Niguarda Hospital, Department of Radiology, Milano, Italy, [4]Villa Erbosa Hospital - San Donato Medical Group, Department of Radiology, Bologna, Italy

Purpose/Objectives
To assess the incidence and the evolution over time of residual fibrotic-like interstitial changes after COVID-19 pneumonia, in order to understand if there are any radiologic or clinical features that may predict the development of irreversible lung abnormalities, in particular pulmonary fibrosis.
Methods & Materials
We conducted a retrospective review of serial chest-CT obtained at least sixteen months and up to more than thirty months after disease onset in patients treated and dismissed for COVID-19 pneumonia. We evaluated the presence and extent of interstitial thickening, reticulations, fibrotic consolidations, traction bronchiectasis and honeycombing, and analyzed their stability or changes compared to CTs performed in the previous months; then we investigated the differences in clinical and radiological data between patients with and without CT signs suggestive of pulmonary fibrosis at long-term follow-up. When available, respiratory follow-up (PFTs and DLCO) data were included in the analysis. Patients with previous diagnosis of any type of fibrotic lung disease were excluded from the study.
Results
A total of 62 patients were included in the study (mean age: 67 years +-14 [SD]; 26 women [42%]). 21 out 62 patients (34%) showed residual fibrotic-like interstitial changes at the long-term follow-up, with a mean delay between baseline CT and last follow-up of 612 days (range: 474-981 days). Persistent fibrotic-like abnormalities were observed more frequently in patients with longer hospital stay (p: 0.002), ICU admission (p: 0.01) and/or need of ventilatory support (p: 0.0009) but can be found also in patients with mild form of disease and that never needed intensive care. We also found a strong association between the “perilobular pattern” detected at CT performed at hospital admission and the development of persistent fibrotic-like abnormalities (p: 0.007).
Conclusion
Fibrotic-like interstitial changes that can be detected after COVID-19 pneumonia show a morphological evolution over time compatible with a "fibrosing organizing pneumonia” and it may be possible to early identify patients most at risk of developing irreversible lung abnormalities through the recognition of specific CT signs, such as the perilobular pattern.

A-473

The Impact of Vaccination on the Severity of COVID-19 Pneumonia: Effectiveness of mRNA and Adenovirus Vector Vaccines and Comparison Between Vaccinated and Unvaccinated Patients

A. Onori, S. Vicini, L. De Pace, D. Bellini, M. Rengo, I. Carbone
Sapienza Università di Roma, Roma, Italy

Purpose/Objectives

The purpose of our study was to evaluate and compare the severity of COVID-19 pneumonia on chest CT imaging in unvaccinated and vaccinated COVID-19 individuals, along with the impact of different types of vaccines.

Methods & Materials

Retrospective observational study on COVID-19 positive patients with respiratory symptoms, and chest CT to evaluate lung involvement. Unvaccinated and vaccinated patients were included. Each CT exam was interpreted by 3 radiologists with the attribution of a score from 0 to 5 for each lobe (for a maximum value of 25) based on the percentage of parenchymal involvement according to Chang et al. Morphological patterns of lung involvement were also evaluated. Scores and characteristics were compared between vaccinated and unvaccinated patients and mRNA and Adenovirus Vector Vaccines.

Results

467 patients were analyzed, including 216 unvaccinated and 251 vaccinated (167 mRNA vaccine; 84 adenovirus vaccine). Unvaccinated patients showed a median CT score of 10/25 compared to the median score of 5/25 in the vaccinated (3/25 mRNA vaccine; 6/25 adenovirus vaccine) ($P < 0.05$). Considering a value >= 15 of the score as a cut-off, a diagnostic accuracy with AUC of 0.98, sensitivity of 100% and specificity of 93%, wa obtained in predicting admission to intensive care unit (ICU). Logistic regression analysis identified complete vaccination as a protective factor with respect to a score >= 15 (OR = 15.2).

Conclusion

Complete vaccination was found to be a protective factor in preventing the onset of severe COVID-19 pneumonia at imaging.

A-338

The use of pleural vents for iatrogenic pneumothorax secondary to percutaneous lung biopsy

P. Eneje[1], P. Shah[1], A. Syed[1], S. Lok[1], N. Sharma[2], M. Hajhosseiny[1], S. Buckingham[1]
[1]East and North Hertfordshire Trusts, Stevenage, United Kingdom, [2]Maidstone and Tunbridge Wells NHS trust, Tunbridge Wells, United Kingdom

Purpose/Objectives
There is a move to perform CT lung biopsies in an ambulatory setting to decrease cost and hospital acquired infection. Traditionally iatrogenic pneumothorax following image-guided lung biopsy required large bore pleural drain and hospital admission. More recently, Heimlich valves have been used in the ambulatory setting[1]. We describe initiating an ambulatory service using pleural vents as the primary pleural drainage device. We describe setting up the service, required training, and discuss the effectiveness of the device, with special considerations including dealing with pain management, and scenarios in which the patient should be more closely followed up.

Methods & Materials
A retrospective analysis of 199 patients, over a 3 year period, who underwent a percutaneous CT guided lung biopsy at our centre. There were no exclusion criteria. We recorded details including location of the lesion and its size, degree of emphysema, pulmonary fissure transgression, and number of samples taken. Subsequently we recorded details of when and how the pleural vent was inserted, the number of days it was in place, and any complications of the insertion.

Results
Of the 199 patients, 25 (12.5%) had a sizable or symptomatic pneumothorax requiring intervention. 24 patients were managed with a pleural vent, with 1 patient managed with a Heimlich valve chest drain. Of the patients managed with a pleural vent, 6 patients (25%) required admission, and 2 patients (8%) required subsequent chest drains due to ongoing complications.

Conclusion
The use of pleural vents has been shown to be an effective method in managing patients with an iatrogenic pneumothorax following image guided lung biopsies. They allow the ambulation of patients, obviating the need for inpatient management, with very good patient tolerance and safety, and low overall complication rates.

References:

[1] S S Hare, Ambulatory percutaneous lung biopsy with early discharge and Heimlich valve management of iatrogenic pneumothorax: more for less , Thorax

A-405

Automated CT quantification of interstitial lung abnormality according to the Fleischner Society in patients with resectable lung cancer: Prognostic significance

Y. Ahn, S. M. Lee, S. Choi, J. Choe, K.-H. Do, J. B. Seo
Asan Medical Center, Cardiothoracic Surgery,, Seoul, Republic of Korea (South Korea)

Objectives
To assess the prognostic significance of automatically quantified interstitial lung abnormality (ILA) according to the definition by the Fleischner Society in patients with resectable non–small cell lung cancer (NSCLC).
Methods & Materials
Patients who underwent lobectomy or pneumonectomy for NSCLC between January 2015 and December 2019 were retrospectively included. Preoperative CT scans were analyzed using the commercially available deep-learning-based automated quantification software for ILA. According to quantified results and the definition by the Fleischner Society and multidisciplinary discussion, patients were divided into normal, ILA, and interstitial lung disease (ILD) groups.
Results
Of the 1524 patients, 87 (5.7%) and 20 (1.3%) patients had ILA and ILD, respectively. Both ILA (HR, 1.81; 95% CI:1.25–2.61; P=.002) and ILD (HR, 5.26; 95% CI:2.99–9.24; P<.001) groups had poor recurrence-free survival (RFS). Overall survival (OS) decreased (HR 2.13 [95% CI: 1.27–3.58; P=.004] for ILA group and 7.20 [95% CI: 3.80–13.62, P<.001] for ILD group) as the disease severity increased. Both quantified fibrotic and non-fibrotic ILA components were associated with poor RFS (HR, 1.57; 95% CI: 1.12–2.21; P=.009 and HR, 1,11; 95% CI: 1.01–1.23; P=.03) and OS (HR, 1.59; 95% CI: 1.06–2.37; P=.02 and HR, 1.17; 95% CI: 1.03–1.33; and P=.01) in normal and ILA groups.
Conclusion
The automated CT quantification of ILA based on the definition by the Fleischner Society predicts outcomes of patients with resectable lung cancer based on the disease category and quantified fibrotic and non-fibrotic ILA components.

A-146

Clinical efficacy of ultra-low dose thoracoabdominal aorta computed tomography using tin-filter in patients with aortic disease: assessment of image quality and radiation dose

H. Kwon[1], J. H. Kim[2]
[1]Chung nam national university hospital, radiology, Daejeon, Republic of Korea (South Korea), [2]Chungnam National University Hospital, Radiology, Daejeon, Republic of Korea (South Korea)

Objectives
Computed tomography (CT) is currently the most common diagnostic imaging method for evaluating aortic disease. In thoracoabdominal aorta CT, radiation exposure is considered an important issue because patients may require repeated near whole-body imaging to evaluate entire aorta. Recently tin-filtered CT has been shown to be beneficial in reducing radiation exposure. We investigated the clinical feasibility of a tin-filtered 100 kV protocol for the diagnostic use, compared with standard thoracoabdominal aorta CT at 100 kV in patients with aortic disease. We assessed the image quality, radiation dose, and interobserver agreement.
Methods & Materials
We retrospectively reviewed 100 consecutive patients who underwent thoracoabdominal aorta CT for evaluating aortic disease. Fifty patients were examined with a dedicated tin-filtered 100 kV protocol CT. The other 50 patients were examined with a standard 100 kV protocol on a same scanner without tin-filter. Two readers independently evaluated image quality subjectively and objectively, and the interobserver agreement was also assessed. CT dose index volume (CTDIvol) and dose-length product (DLP) were recorded to compare radiation exposure. We classified segmentation of superior mesenteric artery and assessed the visuality of the segment of SMA respectively: proximal SMA (<1cm, S1), distal SMA (S2), proximal SMA branches (<1cm, S3), and distal SMA branches (S4).
Results
All CT scans showed diagnostic image quality for evaluating aortic disease. The tin-filtered 100 kV protocol showed sufficient image quality for diagnostic use, especially aortic disease; however, overall image quality and distal branch delineation from the tin-filtered 100 kV protocol were significantly lower than from the standard protocol. Interobserver agreement was moderate to almost perfect (k=0.57–1.00), except liver in tin-filtered image (k=0.30). Both signal-to-noise ratio and contrast-to-noise ratio in the IVC and aorta showed a significant difference (P<0.05). The tin-filtered 100 kV protocol showed a significant reduction in radiation dose compared to the standard protocol: CTDIvol, 12.09 *vs.* 35.47 mGy (P<0.001); and DLP, 398 *vs.* 1760.94 mGy*cm (P<0.001). The visuality of the segment of SMA on standard protocol demonstrated good result without significant difference compared with dedicated tin-filtered protocol.
Conclusion
Dedicated ultra-low dose thoracoabdominal CT using tin-filter can allow a significant reduction in radiation dose while maintaining sufficient diagnostic image quality.

A-293

Comparison of clinical and imaging features of SARS-CoV2 Omicron variant sublineages

J. E. Lee[1], Y.-H. Kim[1], J. Y. Lee[1], W. G. Jeong[2], Y. J. Jeong[3]
[1]Chonnam National University Hospital, Radiology, Gwangju, Republic of Korea (South Korea), [2]Chonnam National University Hwasun Hospital, Radiology, Hwasun, Republic of Korea (South Korea), [3]Pusan National University Yangsan Hospital, Radiology, Pusan, Republic of Korea (South Korea)

Objectives
To compare the adjusted risks of clinically severe disease and radiologically severe pneumonia of the Omicron BA.1/BA.2 and BA.5 subvariants in hospitalized patients.
Methods & Materials
In this multicenter retrospective cohort study, we analyzed the data of patients hospitalized and isolated for COVID-19 in the Republic of Korea between January 17 and December 5, 2022. The dominant periods of Omicron BA.1/BA.2 and BA.5 were determined to be January 17 to June 20, 2022, and July 4 to December 5, 2022, respectively. Clinical outcomes including risks of high-flow oxygen supplementation, mechanical ventilation, and death, and imaging pneumonia outcomes based on chest radiography and CT was compared among predominant subvariants using multivariable analyses stratified by the vaccination status.
Results
Of 1916 confirmed patients with COVID-19 (mean age, 72 years ± 16; 1019 men [53%]), 1269 were registered during the Omicron BA.1/BA.2 subvariant dominant period and 647 during the Omicron BA.5 subvariant dominant period. The BA.5 prevalence was associated with lower risks of high-flow O_2 requirement (OR 0.75, 95% CI: 0.57, 0.99, $P = .04$), mechanical ventilation (OR 0.49, 95% CI: 0.34, 0.72, $P < .001$]), and death (OR 0.47, 95% CI: 0.33, 0.68, $P < .001$) than the BA.1/BA.2 prevalence. The BA.5 prevalence was associated with lower risk of severe pneumonia on chest radiographs (OR 0.68, 95% CI: 0.53, 0.88, $P = .004$) and higher risk of atypical pattern pneumonia on CT images (OR 1.81, 95% CI: 1.26, 2.58, $P = .001$) than the BA.1/BA.2 prevalence.
Conclusion
The Omicron BA.5 subvariant was associated with lower clinical and pneumonia severity than the Omicron BA.1/BA.2 subvariants, even after adjusting for confounders, including vaccination status.

A-245

CT texture analysis of mediastinal lymphadenopathy on screening low dose CT for lung cancer

K. E. Shin, J. S. Park, J. W. Lee
SoonChunHyang University Bucheon Hospital, Radiology, Bucheon, Gyeonggi-do, Republic of Korea (South Korea)

Objectives

To compare differences between malignant and benign mediastinal lymphadenopathy on screening low dose CTs using texture analysis

Methods & Materials

This retrospective study enrolled 625 heavy smokers (with a history of at least 30 pack-years) aged between 54 and 74 who visited a single tertiary hospital from 2017 to 2020 for a low dose CT screening. Among the 625 subjects, 59 of them showed to have one or more enlarged (9mm or larger) isolated lymph node(s) in the mediastinum. The 59 patients (with a mean age of 61±4 and a male proportion of 99.1%) underwent an endobronchial ultrasound (EBUS)-guided transbronchial needle aspiration to check the pathology of 82 enlarged lymph nodes; 73 were confirmed as benign and 9 were malignant. These lymph nodes were reviewed on the low dose CT scans to analyze 3D textures by drawing the region of interest (ROI) using a commercially available software. The texture analysis values were compared using the Mann-Whitney test and a receiver operating characteristic (ROC) curve was plotted.

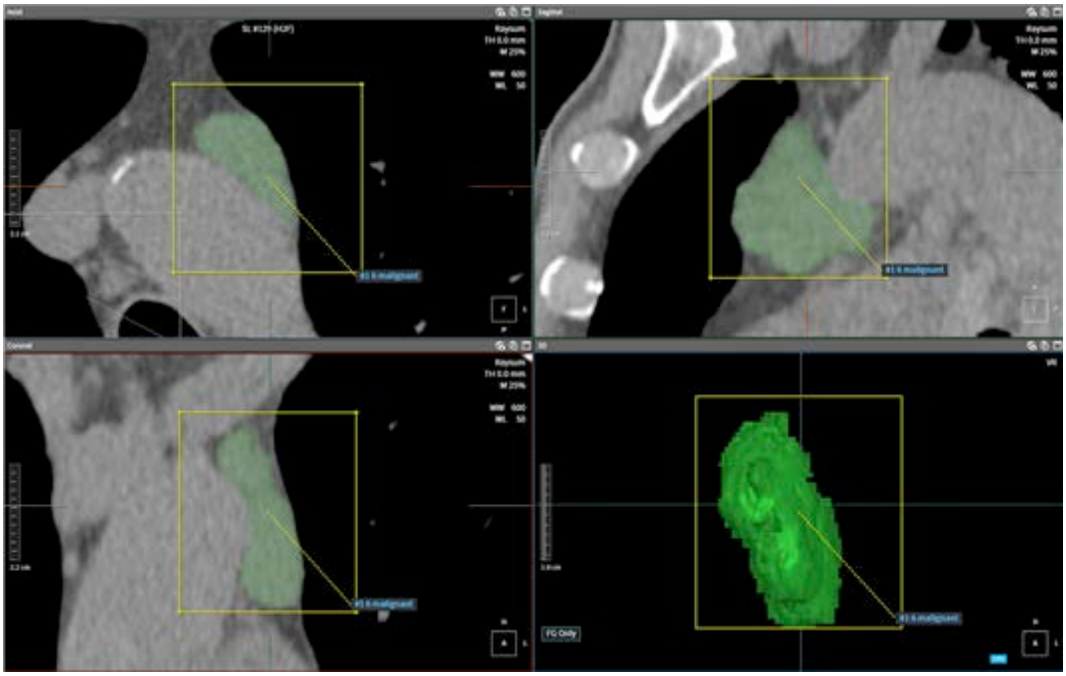

Segmentation of mediastinal lymph nodes for 3D texture analysis

Results

The texture analysis showed 70 out of a total 98 features to have significant characteristics in differentiating benign from malignant lymph nodes. Among them, gray-level cooccurrence metrices (GLCM) entropy, homogeneity values, and grey-level run length matrix with short run low gray emphasis (GLRLM_SRLGE) were identified to have the biggest differences between the two groups. The ROC curve of the 3D texture analysis showed high diagnostic accuracy; 100% sensitivity, 92% specificity, 0.988 area under the curve.

Conclusion

Texture analysis shows promising results as a tool to analyze malignancy probability of enlarged lymph nodes on screening low dose CTs.

A-735

Deep Learning-based Augmented Contrast Enhancement and De-noising Algorithms for CT Pulmonary Angiography: Improved Vascular Opacification and Diagnosis of Pulmonary Emboli.

E.-s. Cho[1], T. H. Kim[1], C. K. Ahn[2], J. M. Shin[3], J.-H. Kim[4,5,6]
[1]Gangnam Severance Hospital, Yonsei University College of Medicine, Radiology, Seoul, Republic of Korea (South Korea), [2]ClariPi AI Medical Imaging Solutions, Seoul, Republic of Korea (South Korea), [3]Incheon St. Mary's Hospital, Catholic University College of Medicine, Radiology, Incheon, Republic of Korea (South Korea), [4]Seoul National University Hospital, Radiology, Seoul, Republic of Korea (South Korea), [5]Graduate School of Convergence Science and Technology, Seoul National University, Department of Transdisciplinary Studies, Seoul, Republic of Korea (South Korea), [6]Seoul National University, Advanced Institutes of Convergence Technology, Seoul, Republic of Korea (South Korea)

Objectives
To investigate the impact of deep learning-based augmented contrast enhancement (DL-ACE) and deep learning-based de-noising (DL-DN) algorithms on image quality and diagnostic accuracy of pulmonary emboli (PE) at CT pulmonary angiography (CTPA).
Methods & Materials
This retrospective study included 1097 conventional CTPA scans. Commercial DL-ACE (ClariACE, ClariPi) and DL-DN (ClariCT.AI, ClariPi) algorithms were applied to conventional CTPA to increase vascular enhancement and decrease image noise, respectively. DL-ACE was developed based on the U-net architecture to predict vascular and parenchymal contrast enhancement by being trained with conventional CT angiography images obtained with dual-energy CT and paired virtual non-contrast (VNC) and iodine component images. By combining the VNC component image with a weight adjusted iodine component image, the CT angiography images with iodine-contrast boosting by 50% were generated. DL-DN was designed to predict possible image noise generated by low radiation from standard-dose CT images, and the denoised images were acquired by subtracting predicted noise from the original images.
The performance of CTPA using DL-ACE and DL-DN was compared with that of conventional CTPA based on the vascular attenuation value and contrast-to-noise ratio (CNR) of pulmonary arteries, CNR of measurable PE, image noise, subjective image quality, and diagnostic accuracy for detecting PE.
Results
DL-ACE significantly increased the attenuation value of the pulmonary arteries from 524.8 ± 185.6 HU to 772.0 ± 279.4 ($p < 0.001$), while DL-DN significantly decreased the image noise from 11.8 ± 2.1 to 5.0 ± 0.9 ($p < 0.001$). The CNRs of pulmonary arteries and PE were also significantly improved from 41.0 ± 12.4 and 40.4 ± 16.6 to 145.6 ± 45.3 and 139.2 ± 56.8 when DL-ACE and DL-DN were used, respectively. Subjective vascular enhancement and image noise were significantly better on CTPA using DL-ACE and DL-DN ($p < 0.001$). PE were present in 418 studies (38.1%). DL-ACE and DL-DN showed additional 6 segmental PE and 13 subsegmental PE, increasing the diagnostic accuracy for detecting PE.

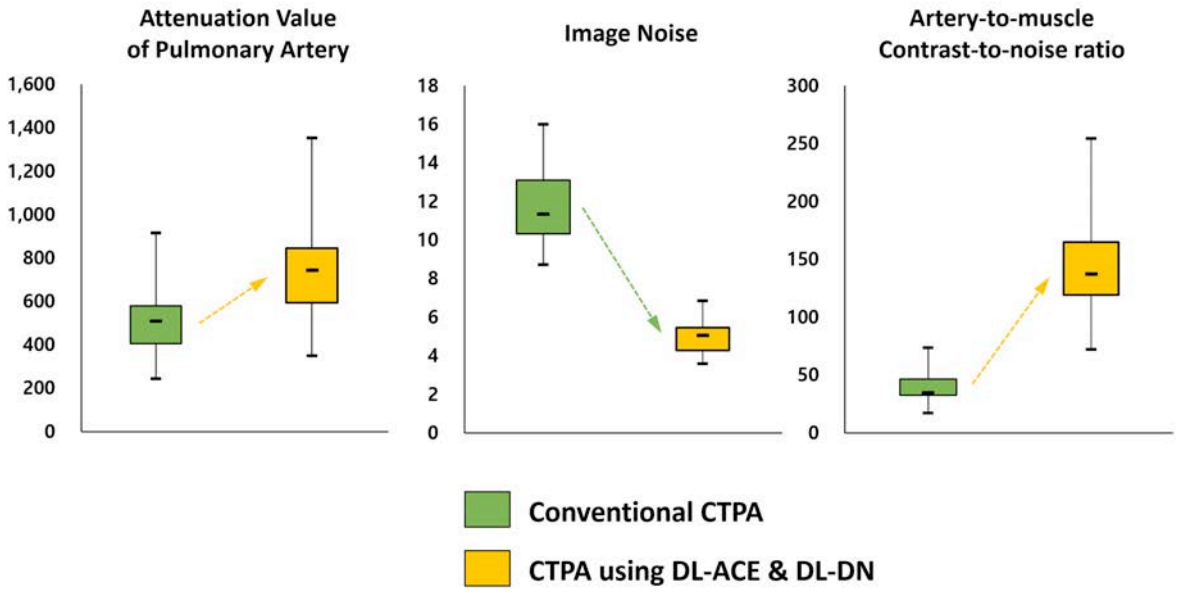

Comparison of the attenuation value of pulmonary arteries, image noise, and pulmonary artery-to-muscle contrast-to-noise ratio (CNR) between conventional CT pulmonary angiography (CTPA) and CTPA using DL-ACE and DL-DN

Conclusion
DL-ACE and DL-DN algorithms can improve the attenuation value and CNR of pulmonary arteries and image quality, and show an incremental benefit for detecting pulmonary emboli in CT pulmonary angiography.

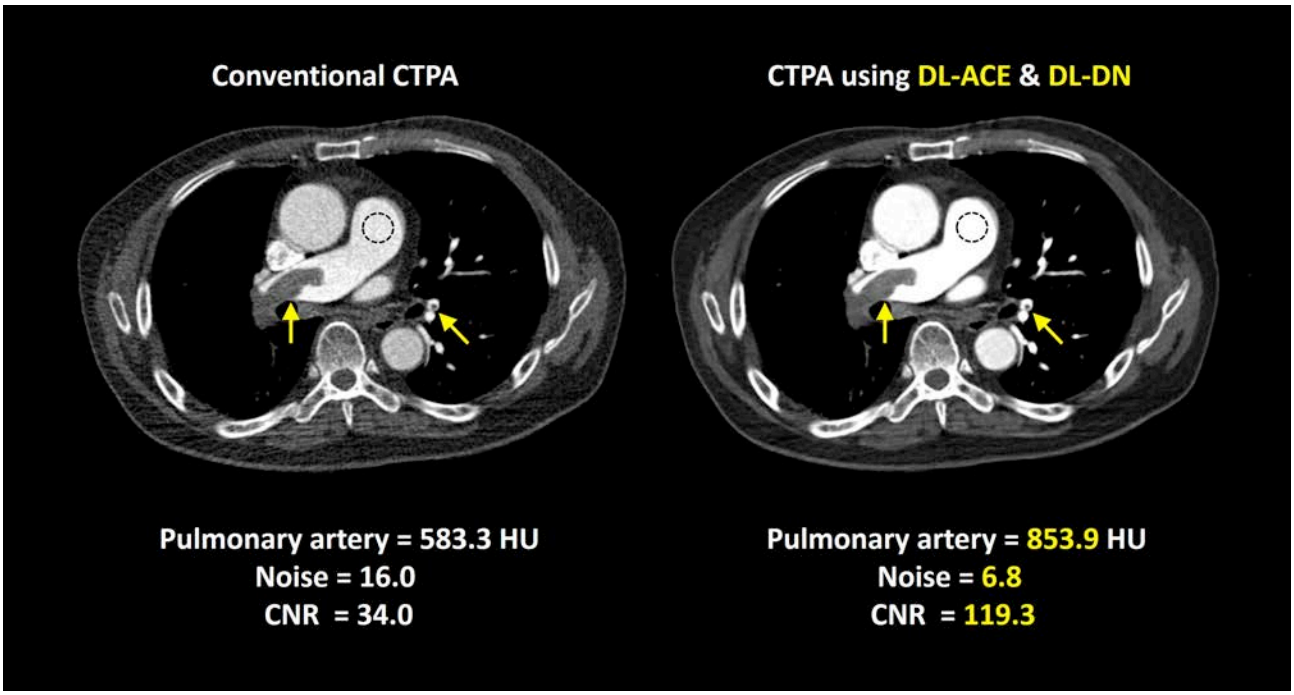

A 78 year-old-male with pulmonary emboli (arrows) in the both pulmonary arteries.

A-321

Delayed diagnosis of distant metastases in non-small cell lung cancer patients who underwent surgery: incidence and survival outcomes

S. Park, J. Choe, S. M. Lee, J. B. Seo, S. Choi
Asan Medical Center, Seoul, Republic of Korea (South Korea)

Objectives

In clinical practice, diagnosing distant metastasis on preoperative exams for non-small cell lung cancer (NSCLC) can be challenging, leading some patients with uncertain metastasis but otherwise early stage to undergo surgery. Limited data exist on surgical outcomes in patients with delayed diagnosis of distant metastasis after surgery. We aimed to analyze metastases which were diagnosed after surgery and the survival outcome of delayed diagnosis of distant metastasis in patients with NSCLC who underwent surgery.

Methods & Materials

Consecutive patients who underwent lobectomy or pneumonectomy for NSCLC between June 2010 and December 2017 were included and presence of distant metastasis before surgery was evaluated through a retrospective review of preoperative and postoperative imaging, surgical records, and medical records. Overall survival (OS) of patients with metastasis (stage IV disease) were compared with patients with stage IIIA and IIIB diseases, using Kaplan-Meier analyses and log-rank test. Cox proportional hazards model was applied by using propensity score-based matching (PSM) to evaluate prognostic impact of delayed diagnosis of distant metastasis with adjusting the differences in confounding variables between patients with and without metastasis. As a subgroup analysis, prognostic factors in patients with distant metastasis were investigated by using Cox proportional hazards model.

Results

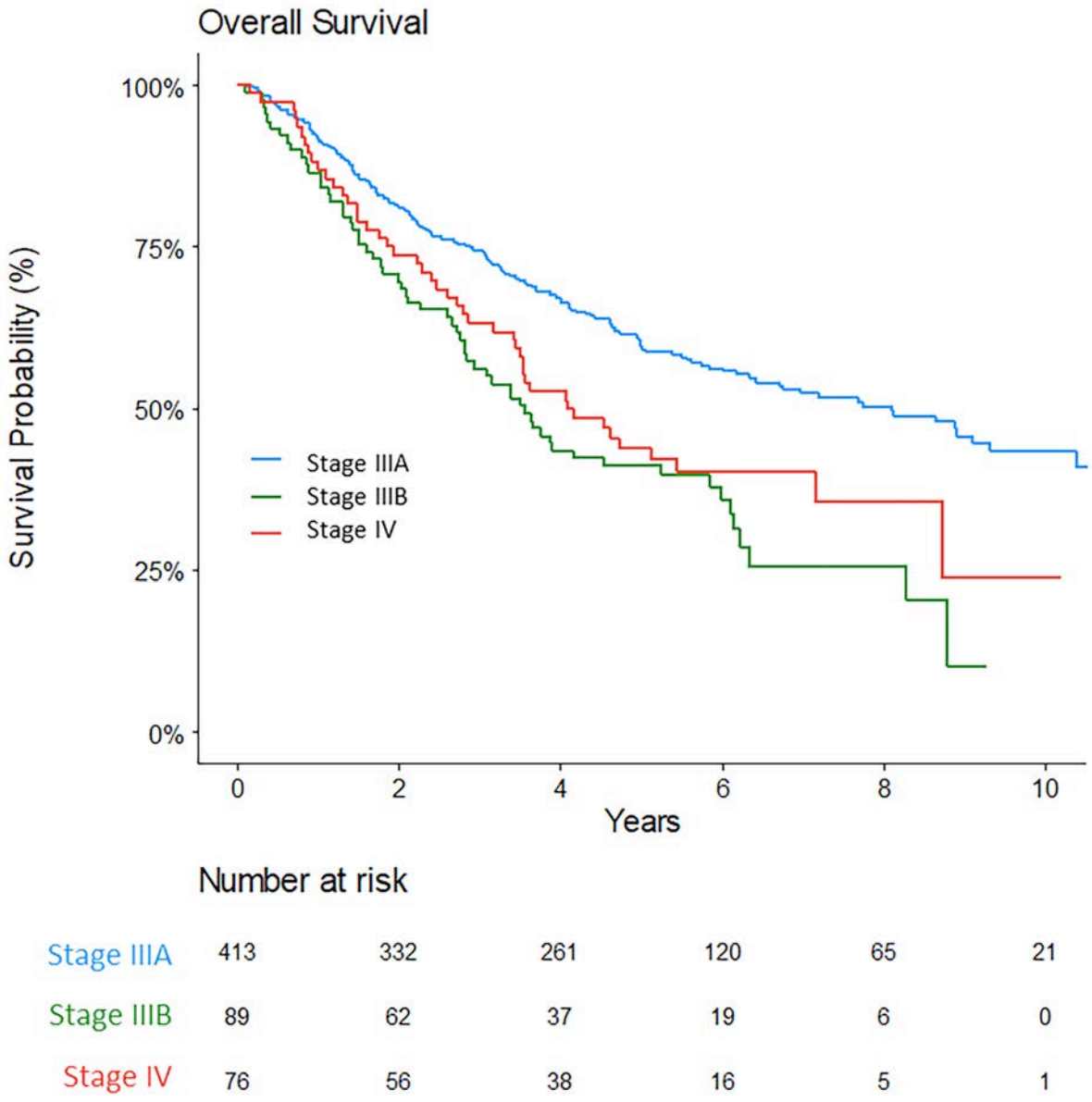

Kaplan-Meier OS curves of patients with postoperatively confirmed distant metastasis (stage IV) treated with surgery in comparison to patients with stage IIIA and stage IIIB diseases.

	Total numbers (M1/M0)	Hazard ratio (95% confidence interval)	P value
Before propensity score matching	76/2943	3.85 (2.85–5.19)	<0.001
After propensity score matching	75/286	1.87 (1.32–2.65)	<0.001

Prognostic impact of delayed diagnosis of distant metastasis on overall survival before and after propensity score matching

Out of 3019 patients (mean age, 63 years ± 10 [SD]; 1755 men), the rate of delayed diagnosis of distant metastasis after surgery was 2.5% (76/3019). Most common metastasis site was contralateral lung (26/76 [34.2%]), followed by pleura (17/76 [22.4%]), bone (15/76 [19.7%]), liver (5/76 [6.6%]), brain (4/76 [5.3%]), and others (9/76 [11.8%]). The median OS was 4.1 year for patients with stage IV disease, which was significantly worse than patients in stage IIIA (median OS, 8.2 year; $P < 0.001$), but similar to those in stage IIIB (median OS, 3.6 year; $P = 0.451$). After PSM, the prognostic impact of distant metastasis was significant after adjusting other clinical and pathological covariables including pT and pN categories (hazard ratio, 1.87; $P < 0.001$). Among the patients with distant metastasis, squamous cell carcinoma subtype was the only risk factor for worse prognosis (hazard ratio, 2.93; $P = 0.003$).

Conclusion

In patients with NSCLC who underwent surgery for curative treatment, the rate of delayed diagnosis of distant metastasis was 2.5% and the survival outcome was comparable to that of stage IIIB, which was slightly worse than expected for the pathological T and N categories and clinical characteristics.

A-434

Detection of Incidental Pulmonary Emboli in Conventional Chest CT: Application of Deep Learning-based Augmented Contrast Enhancement and De-noising Algorithms

E.-s. Cho[1], T. H. Kim[1], C. K. Ahn[2], J. M. Shin[3], J.-H. Kim[4,5,6]
[1]Gangnam Severance Hospital, Yonsei University College of Medicine, Radiology, Seoul, Republic of Korea (South Korea), [2]ClariPi AI Medical Imaging Solutions, Seoul, Republic of Korea (South Korea), [3]Incheon St. Mary's Hospital, Catholic University College of Medicine, Radiology, Incheon, Republic of Korea (South Korea), [4]Seoul National University Hospital, Radiology, Seoul, Republic of Korea (South Korea), [5]Graduate School of Convergence Science and Technology, Seoul National University, Department of Transdisciplinary Studies, Seoul, Republic of Korea (South Korea), [6]Seoul National University, Advanced Institutes of Convergence Technology, Seoul, Republic of Korea (South Korea)

Objectives
To investigate the feasibility of using deep learning-based augmented contrast enhancement (DL-ACE) and deep learning-based de-noising (DL-DN) algorithms to diagnose incidental pulmonary emboli (PE) in routine chest CT.
Methods & Materials
This retrospective study included 1387 conventional contrast-enhanced chest CT. Commercial DL-ACE (ClariACE, ClariPi) and DL-DN (ClariCT.AI, ClariPi) algorithms were applied to conventional CT images to increase vascular enhancement and decrease image noise, respectively.
DL-ACE was developed based on the U-net architecture to predict vascular and parenchymal contrast enhancement by being trained with post-contrast CT images obtained with dual-energy CT and paired virtual non-contrast (VNC) and iodine component images. By combining the VNC component image with a weight adjusted iodine component image, the post-contrast CT images with iodine-contrast boosting by 50% were generated. DL-DN was designed to predict possible image noise generated by low radiation from standard-dose images, and the denoised images were acquired by subtracting predicted noise from the original images.
The performance of CT images using DL-ACE and DL-DN was compared with that of conventional CT images based on the vascular attenuation value and contrast-to-noise ratio (CNR) of pulmonary arteries, CNR of measurable PE, image noise, subjective image quality, and diagnostic accuracy for detecting PE.
Results
DL-ACE significantly increased the attenuation value of the pulmonary arteries from 222.5 ± 52.0 HU to 313.8 ± 78.5 ($p < 0.001$), while DL-DN significantly decreased the image noise from 9.2 ± 2.0 to 3.8 ± 0.8 ($p < 0.001$). The CNRs of pulmonary arteries and PE were also significantly improved from 20.9 ± 8.4 and 21.5 ± 9.1 to 170.1 ± 88.7 and 73.0 ± 30.4 when DL-ACE and DL-DN were used, respectively. Subjective vascular enhancement and image noise were significantly better on CT images using DL-ACE and DL-DN ($p < 0.001$). Incidental PE were present in 87 studies (6.3%). DL-ACE and DL-DN showed 8 additional PE, increasing the diagnostic accuracy for detecting PE.

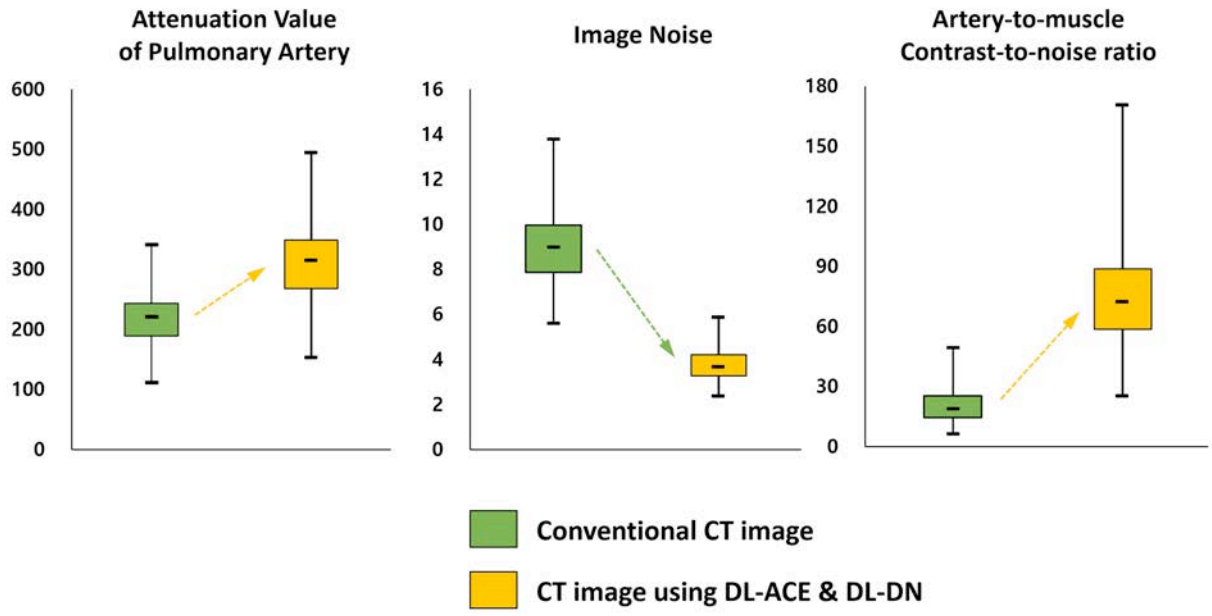

Comparison of the attenuation value of pulmonary arteries, image noise, and pulmonary artery-to-muscle CNR between conventional CT images and CT images using DL-ACE and DL-DN

Conclusion
DL-ACE and DL-DN algorithms can improve the attenuation value and CNR of pulmonary arteries and image quality, and show an incremental benefit for detecting incidental pulmonary emboli in conventional chest CT images.

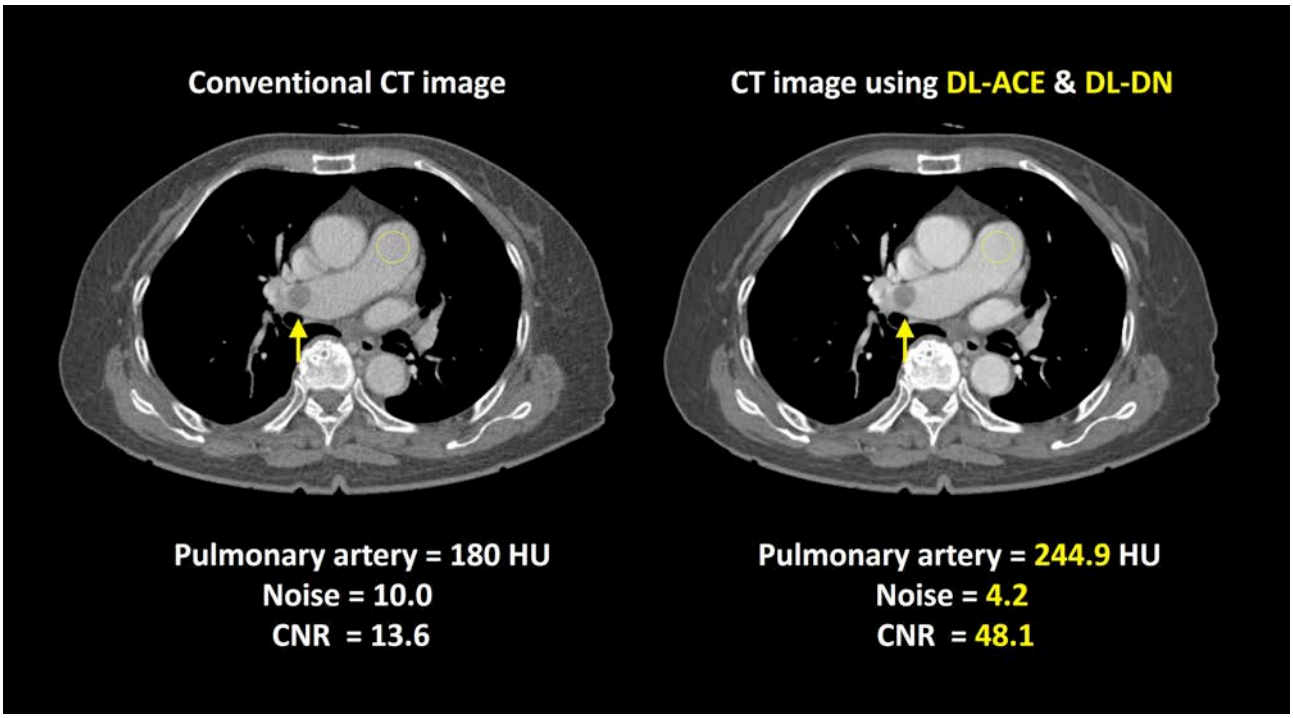

A 72 year-old-female with pulmonary embolism in the right pulmonary artery.

A-412

Diagnosing sensitive scoliosis on the chest radiographs with semi-supervised generative adversarial network (GAN)

S. Paik[1], W. Lee[2], N. Kim[3]
[1]Korean teleradiology reading center, Seoul, Republic of Korea (South Korea), [2]KTRC, Radiology, Seoul, Republic of Korea (South Korea), [3]Seoul Asan medical center, Seoul, Republic of Korea (South Korea)

Objectives
To develop and validate a deep learning-based screening tool for early diagnosis of scoliosis in adolescent's chest radiographs with semi-supervised generative adversarial network (GAN).
Methods & Materials
The dataset was constructed by aggregating data collected from two independent centers (Hanyang University Seoul Hospital, HUSH and Asan Medical Center, AMC). A semi-supervised learning framework with GAN was used to develop and validate screening tool for diagnosing scoliosis on chest PA radiographs of men and women in HUSH and AMC. Our proposed method uses training GAN with mild to severe scoliosis only in semi-supervised manner as an upstream task to learn scoliosis representations, and a downstream task to perform simple classification to differentiate normal and scoliosis sensitively. The sensitivity test on the classifier model was performed depending on the number of labeled training samples.
Results
The internal validation performance of the classifier with 512 patients (normal 256 and scoliosis 256) was 0.856 area under the receiver operating characteristic curve (AUROC), 0.958 negative predictive value (NPV), 0.950 sensitivity (SEN), and 0.285 specificity (SPE) when the threshold value of probability output of our model was 0.05.
Conclusion
Our deep learning-based AI software in semi-supervised manner achieved excellent performance in diagnosing scoliosis on the chest PA radiographs of young individuals, which could lead to a screening tool with high NPV and sensitivity and reduce the burden on radiologists for diagnosing scoliosis in the health screening chest radiographs.

A-243

Diagnostic accuracy and safety of CT-guided percutaneous core needle biopsy of lung for detecting malignancy in patients with chronic obstructive pulmonary disease

S. You, J. W. Park, Y. N. Kim, S. H. An, J. S. Sun
Ajou Universitiy School of Medicine, Pulmonology, Suwon, Republic of Korea (South Korea)

Objectives
This study aimed to evaluate the diagnostic accuracy and safety of CT-guided percutaneous core needle biopsy (PCNB) for the diagnosis of malignancy in patients with chronic obstructive pulmonary disease (COPD).
Methods & Materials
This study included 1,075 patients (840 patients without COPD and 235 patients with COPD) who underwent CT-guided PCNB from March 2017 to March 2022. The diagnostic accuracy, sensitivity, specificity and complication rates were analyzed in non-COPD group and COPD group. In subgroup analysis, the diagnostic accuracy and complication rate according to COPD stage were compared. The risk factors for complication were analyzed through univariable and multivariable regression analysis.
Results
The sensitivity, specificity and diagnostic accuracy in non-COPD group were 91.8% (655/713), 88.2% (112/127), and 91.3% (767/840) respectively. The sensitivity, specificity and diagnostic accuracy in COPD group were 94.3% (197/209), 88.5% (23/26), and 93.6% (220/235) respectively. There was no significant difference in diagnostic accuracy between two groups (p=0.211). The overall complication rate in non-COPD group and COPD group were 27.7% (233/840) and 29.4% (69/235), respectively. Pneumothorax incidence in non-COPD group and COPD group were 24.2% (203/840) and 23.8% (56/235), respectively. Diagnostic accuracy and complication rate were not associated with COPD stage (p=0.854, p=0.770). The procedure time (OR, 1.12; 95% CI, 1.054–1.1868; p <0.001) was an independent risk factor for complication in COPD patients.
Conclusion
CT-guided PCNB has demonstrated a reasonable diagnostic accuracy for detecting malignancy and an acceptable complication rate in COPD patients.

A-228

Effect of Interstitial Lung Abnormality on Concurrent Chemoradiotherapy-treated Stage III Non-small Cell Lung Cancer Patients

W. G. Jeong[1,2], Y.-H. Kim[2]
[1]Chonnam National university Hwasun Hospital, Hwasun-gun, Jeollanam-do, Republic of Korea (South Korea), [2]Chonnam National University Medical School, Radiology, Gwangju, Republic of Korea (South Korea)

Objectives
Pre-treatment interstitial lung abnormality (ILA) is associated with post-cancer treatment adverse events and high mortality rate in lung cancer patients. This study aimed to assess whether ILA affects the survival and development of symptomatic radiation pneumonitis (RP) in unresectable stage III non-small cell lung cancer (NSCLC) patients who had undergone definitive concurrent chemoradiotherapy (CCRT).
Methods & Materials
Data of stage III NSCLC patients who underwent definitive CCRT between January 2010 and November 2017 were retrospectively collected. Univariate and multivariate regression analyses were performed to evaluate the risk factors for symptomatic RP. The association between pretreatment ILA and survival was assessed using Kaplan– Meier analysis with log-rank test and Cox proportional hazards regression.
Results
This study included 201 patients (188 men) of a mean age of 64.7±7.3 years. Pre-treatment ILA and fibrotic ILA were observed in 21.9% and 12.9% of the patients, respectively. Symptomatic RP (grade ≥2) occurred in 13.5% of the patients. Fibrotic ILA was a significant risk factor for grade ≥2 RP and grade ≥3 RP ($p=0.004$ and 0.033, respectively). The survival rate was significantly poorer in patients with fibrotic ILA than in those without ILA. Cox proportional hazards regression revealed that fibrotic ILA was an independent risk factor for mortality ($p<0.001$).
Conclusion
Pre-treatment fibrotic ILA is significantly associated with symptomatic RP and poor survival in unresectable stage III NSCLC patients who have undergone definitive CCRT. CCRT should be cautiously performed in patients presenting pre-treatment fibrotic ILA to prevent adverse outcomes.

A-287

18G automated gun biopsy without coaxial introducter versus 20G semi-automated gun biopsy with coaxial introducter for subpleural lung biopsy

C. Park
Soonchunhyang University Cheonan Hospital, Radiology, Cheoan-si, Republic of Korea (South Korea)

Objectives
The purpose of this study was to compare safety and efficacy of 18G automated gun biopsy without coaxial introducter versus 20G semi-automated gun biopsy with coaxial introducter for subpleural lung biopsy.
Methods & Materials
Among 304 image-guided thoracic biopsies obtained at our institution in 2 years, 60 were subpleural lesions (39 men, 21 women; mean age, 67 years). Of those, 13 were performed using 18G automated gun biopsy without coaxial introducter (7 men, 6 women; mean age, 72) and 47 were performed by 20G semi-automated gun biopsy with coaxial introducter (32 men, 15 women; mean age, 67). Biopsy gun type, sample, number, sample adequacy, final pathologic results, complications (during biopsy & after biopsy), procedural time, lesion diameter were recorded. Chi-squared test, Fisher exact and t tests were used for statistical analysis.
Results
18G automated gun biopsy without coaxial introducter wan associated fewer complications (during the biopsy, 0%) than 20G semi-automated gun biopsy with coaxial introducter (25.5%, p = 0.042). Mean procedure times (±SD) were shorter with 18G automated biopsy (8.6 ± 2min) than 20G semi-automated biopsy (13.2 ± 2min; p<0.01). Sample adequacy was not differentiated between two groups. Complications after biopsy was not differentiated between two groups (18G automated gun biopsy ; pneumothorax 46.2%, hemoptysis 0%, 20G semi-automated gun biopsy ; pneumothorax 46.8%, hemoptysis 6.4% p=0.600).
Conclusion
By performing the biopsy with 18G automated gun biopsy without coaxial introducter did not puncture the pleura before sampling the tissue, so it can prevent the development of pneumothorax during the biopsy for subpleural lesion.

A-564

Chest Findings on Dorsal Spine Magnetic Resonance Imaging: Is it just about the spine or is there something more?

T. Chandra, A. Jain
Hamdard Institute of Medical Sciences and Research (HIMSR), Radiodiagnosis, New Delhi, India

Purpose

Magnetic resonance imaging(MRI) spine, especially for the dorsal spine, provides a unique opportunity to get a glimpse of the lung parenchyma, posterior mediastinum, and posterior pleura, previously explored for incidental findings[1]. High soft tissue resolution provided by MRI may be helpful in detecting and characterizing any incidental/coexistent thoracic findings.

Methods & Materials

A retrospective study in which 30 MR scans of the dorsal spine performed at our institute were included, from august 2022 to march 2023. T2 weighted(usually non-Fat Suppressed) axial and coronal images(part routine acquisition protocol) were used to evaluate the pulmonary findings. The patient demographics(including sex, age, and indication for the scan) were noted. A preliminary etiological diagnosis was made and imaging findings in the chest were recorded including mediastinal lesions, lung parenchymal changes like consolidation, nodules, bands, and pleural effusions. Normal variants were also recorded.

Results

Our sample included 16/30 men and 14/30 women, with ages ranging from 12 years to 70 years, with a mean age of ~ 36.83 years. All patients presented with backache, out of these ~36.6%(11/30) were diagnosed with infectious etiology- tuberculosis involving the vertebral column with a presumptive diagnosis of the same. Trauma(including falls) was the underlying reason for imaging for only 2 patients.

Only 2 patients presented with lung parenchymal changes which were identifiable on the MR images.

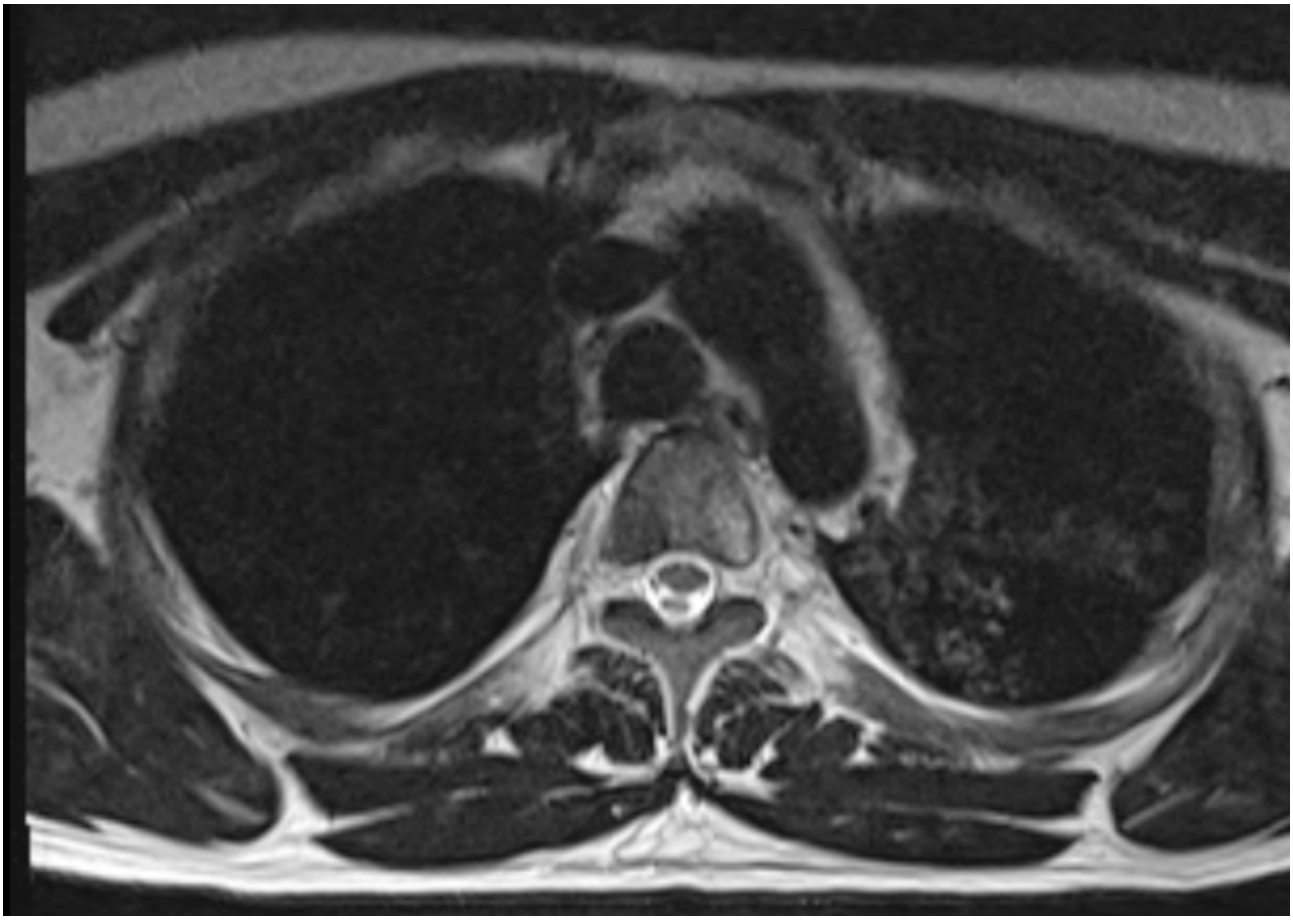

Fig.1 shows a T2 Non Fat-sat axial section of the thorax of a 26 year old man showing fibro-parenchymal changes in the left upper lobe and marrow signal intensity abnormality in the left half of the visualised dorsal vertebra consistent with infective etiology..

Five patients demonstrated pleural effusion- 4/5 had unilateral pleural effusion (3 right, 1 left) and a single case of bilateral pleural effusion was observed.

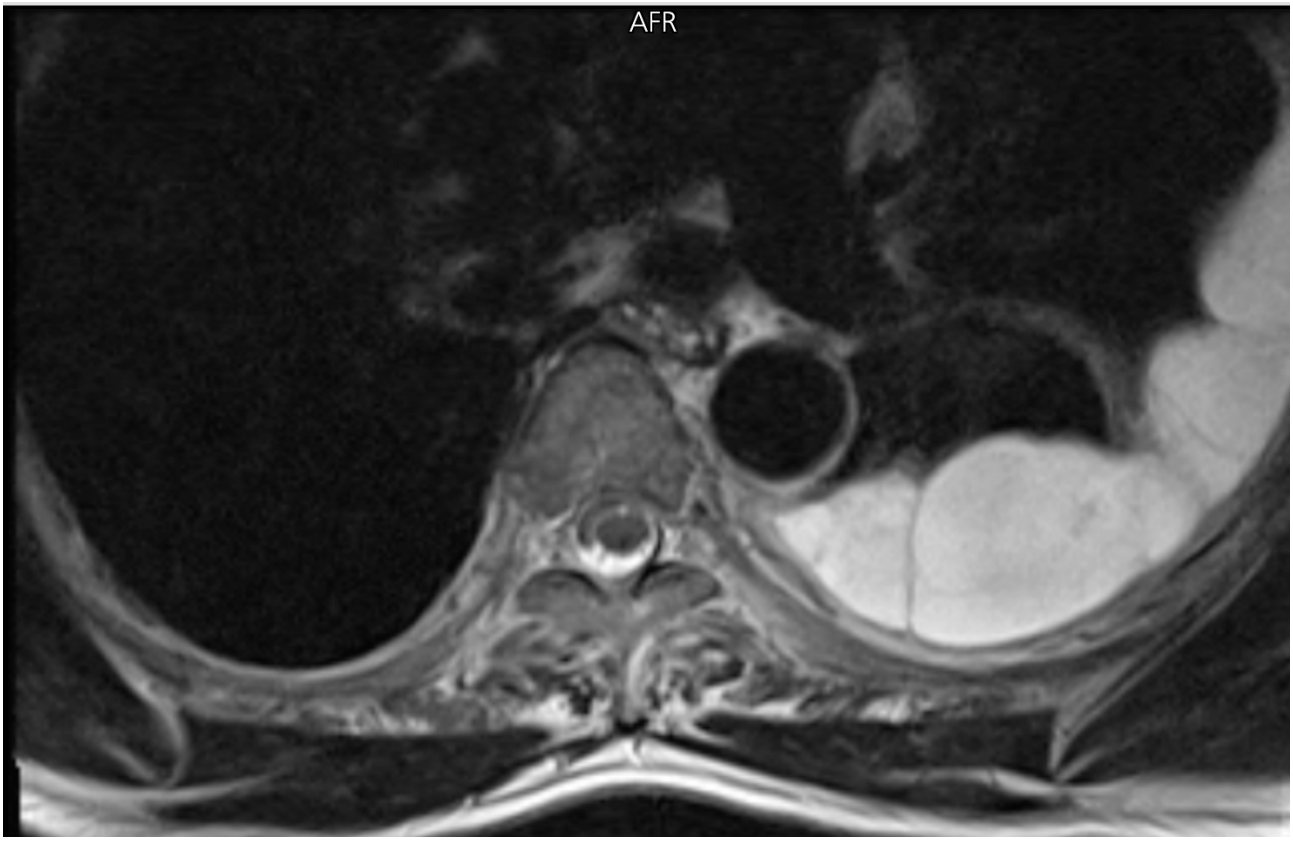

Fig.2 shows a T2 Non Fat-sat axial section of the thorax of a 40 year old lady with back ache since 1 year demonstrating left sided moderate loculated pleural effusion with multiple septa consistent with infective etiology..

All the cases of parenchymal changes as well as unilateral pleural effusions were associated with infectious etiology. Significant abdominal visceral pathologies were noted in two separate patients-subcapsular liver lesion and multiple small simple bilateral renal cortical cysts. Normal variants in form of an accessory azygous fissure and tortuous course of descending thoracic aorta were observed in one patient each. In the visualized mediastinum, a single case of hiatus hernia and two patients with retroperitoneal simple cysts were observed with benign imaging features in two different patients. An enlarged subcarinal node was noted in a patient with an otherwise normal scan.

Conclusion

Suspected infectious spondylodiscitis, is a relatively common indication for imaging of the dorsal vertebral region and hence in endemic regions, the role of MR spine imaging is beyond the assessment of just the spine. Future imaging protocols, if tailored with this background may allow us to glance at a contiguous extension or dissemination of the disease to/from the lung, mediastinum, or pleura before it's too late.

References:

[1] Mogahid M. A. Zidan,Ikhlas A. Hassan, Abdelrahaman M. Elnour, Mustafa Z. Mahmoud, Mohammed A. Alghamdi, Mohammed Salih,Mona Elhaj,5 and Wadah M. Ali, (2019), Incidental Extraspinal Findings in the Thoracic Spine during Magnetic Resonance Imaging of Intervertebral Discs, Scientific Scholar, Journal of Clinical Imaging Science, 37, V9, 10.25259/JCIS_50_2019, 2019-07-12

A-575

The added value of carotid ultrasound for cardiovascular risk stratification in a lung cancer screening population.

R. Mura[1], P. Favia[1], C. Zilioli[1], V. I. Gallone[1], S. Schirò[1], L. Leo[2], A. Priore[3], R. Multinu[1], R. E. Ledda[1], M. Silva[1], N. Sverzellati[1], G. Milanese[1]
[1]University of Parma, Department of Medicine and Surgery, Parma, Italy, [2]University of Parma, Parma, Italy, [3]AOU Parma, Diagnostic Department, Parma, Italy

Purpose/Objectives
to evaluate whether the use of carotid doppler ultrasound (CDU) could enrich cardiovascular (CV) profile-risk in a lung cancer screening (LCS) population.
Methods & Materials
159 high-risk volunteers from a low dose computed tomography (LDCT)-based LCS were enrolled (current and former smokers with a smoking history of at least 15-20 pack/years, aged 50–75). CDU were performed between October 2022 and April 2023, to evaluate both presence of atherosclerotic plaques and degree of carotid stenosis.
Subjects with focal carotid stenosis ≥50% were considered having a “high grade” stenosis; correlation between CV risk factors (body mass index BMI, smoking status, dyslipidemia) and carotid stenosis was evaluated.
We also compared data obtained by CDU with those by chest LDCT: LDCT scans were retrospectively analyzed by an artificial intelligence-driven computer-aided detection (CAD) software (AVIEW LCS platform, Coreline soft) to quantify emphysema and coronary calcification (CAC), by 3-mm thick slice (1.5mm increment) by Sa36 kernel.
Emphysema severity was stratified in 6 groups based on extent (i.e., 0%; <5%; 5-25%; 25-50%; 50-75%; >75%), while CAC was classified in 4 categories, according to Agatston score (A0, A1, A2 and A3).
Results
73/159 (46%) screenees were female; median age was 63. CDU identified 105 (66%) volunteers with intima-media plaques.
10 (6,3%; 4 females; 6 males) showed high grade carotid stenosis, among whom CAC score A1 in 6/10 (60%) and A3 in 4/10 (40%); none had a previous history of CV events or stroke.
The extent of emphysema was 5-25% in 3/10 (30%), <5% in 4/10 (40%), while 3/10 (30%) showed no emphysema.4/10 (40%) had a BMI of 18-25, 5/10 (50%) 25-30 and 1/10 (10%) 30-35 (grade 1 obesity).
Among the 149 subjects without high grade carotid stenosis, CAC was A0 in 42/149 (28,2%), A1 in 80/149 (53,7%), A2 in 13/149 (8,7%), and A3 in 10/149 (6,7%). 4/149 (2,7%) had previous undergone coronary stenting (CAC not feasible).
No significant correlations were observed between carotid stenosis and dyslipidemia or smoking status in overall population.
Subjects with high grade carotid stenosis showed higher degree of CAC than those with low grade or no carotid stenosis.
Conclusion
CDU could complement cardiovascular risk stratification in subjects without CAC but with signs of carotid arteries atherosclerosis (60% A1 among those with high grade carotid stenosis), representing a valid supportive tool to better stratify LCS participants at high-risk of CV events.

A-421

A 10-year retrospective evaluation of the impact of multidisciplinary discussions in the diagnosis and management of interstitial lung diseases

C. A. D'Amore[1], F. Volpi[1], L. Tavanti[2], F. Pistelli[3], G. Alì[4], G. Guglielmi[5], A. Della Rossa[6], F. Falaschi[7], A. De Liperi[7], E. Neri[1], C. Romei[7]
[1]Academic Radiology, University of Pisa, Department of Translational Research, Pisa, Italy, [2]Pulmonary Unit, Pisa University Hospital, Cardiothoracic and Vascular Department, Pisa, Italy, [3]Department of Surgical, Medical and Molecular Pathology and Critical Care, University of Pisa, Pisa, Italy, [4]Unit of Pathological Anatomy, Pisa University Hospital, Pisa, Italy, [5]Occupational Health Department, Pisa University Hospital, Pisa, Italy, [6]Rheumatology Unit, Pisa University Hospital, Pisa, Italy, [7]2nd Radiology Unit, Pisa University Hospital, Department of Radiology, Pisa, Italy

Purpose
The aim of this study was to evaluate the 10-year experience of the multidisciplinary discussion (MDD) at the Pisa University Hospital in the diagnosis and management of interstitial lung diseases (ILDs).
Methods & Materials
A single center retrospective observational study was conducted at the Pisa University Hospital. All patients who were referred to the multidisciplinary group from its creation in 2012 until August 2022 were included.
Results
A total of 1240 patients were evaluated. At baseline assessment, 772 common multidisciplinary diagnoses were obtained, while a definite diagnosis was not acquired in 458 cases. Idiopathic pulmonary fibrosis (IPF), non-specific interstitial pneumonia (NSIP) and smoking related ILDs were the more common multidisciplinary diagnosis. The histological evaluation was not routinely performed and it was made only in 9% of cases, giving a contribution to the diagnosis in 75% of cases. Patients with at least 1-year follow-up (n=1048) were re-discussed by the multidisciplinary group to confirm, modify or assess a diagnosis. A revision of common diagnosis was made: 61% of initial diagnosis were accepted, while 36% of diagnosis couldn’t be confirmed due to missing follow-up exams or visits. Eighteen diagnoses were indeed modified (3%).
Generally, those who only received a “diagnostic hypothesis” were changed into “revised diagnoses” in 57% of the cases, while 15% of cases were left as hypothesis after revision.
Conclusion
ILDs are an heterogenous group of diseases that may change over time from a clinical, functional and radiological point of view. A multidisciplinary approach for a long-term evaluation of ILDs is important to obtain a diagnosis and assess the appropriate management.

A-196

A prediction model for pulmonary embolism from clinical and chest X-ray data

C. B. Monti[1], E. Giambersio[1], M. Zanardo[1], D. Capra[1], F. Secchi[1,2], F. Sardanelli[1,2]
[1]University of Milan, Milano, Italy, [2]IRCCS Policlinico San Donato, San Donato Milanese, Milano, Italy

Purpose/Objectives

Pulmonary embolism (PE) is a common cause for emergency imaging referrals. The main imaging studies that patients with suspected PE usually undergo are represented by chest X-ray (CXR) and computed tomography (CT). The aim of our study was to build a machine learning model to identify patients with PE from CXR.

Methods & Materials

We retrospectively included all adult patients who had undergone CXR and CT within one day of each other at our institution. For each patient we recorded age and sex, clinical variables such as D-dimer, a personal history of cancer, deep vein thrombosis, tachycardia and presence of dyspnea or cough, and imaging variables, namely Westermark sign, Fleischner sign, Hampton hump, and presence of pleural effusion. We subsequently divided our population with an 85:15 split into training and testing datasets and trained a classificator (XGBoost) with 5-fold cross-validation on our training dataset to predict the presence of PE.

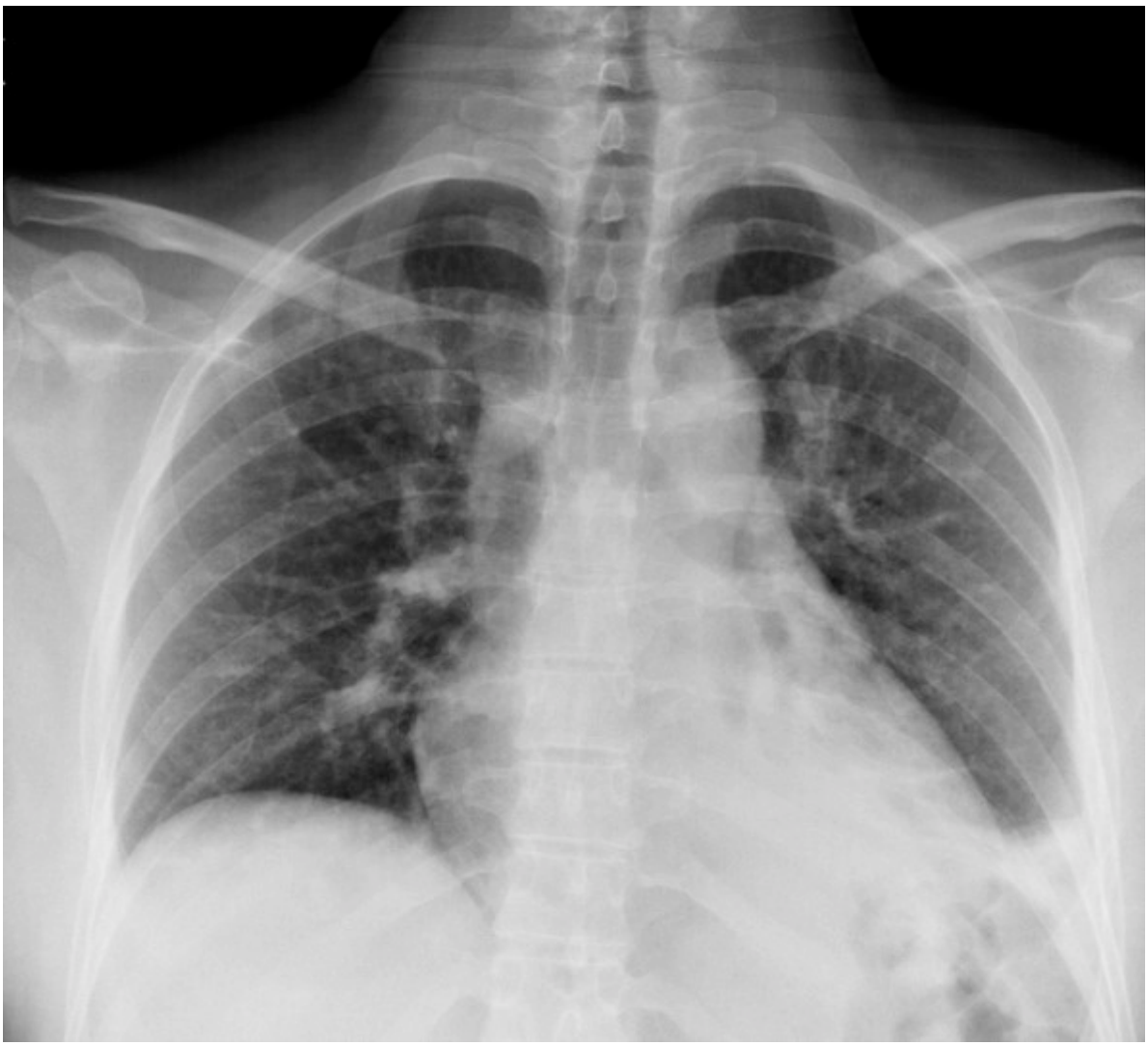

X-ray of a 64-year-old female patient with pulmonary embolism, with pleural effusion and positive Fleischner sign

Results

Our study population counted 255 patients, 150 (59%) of whom males, with a median age of 75 years (interquartile range, IQR, 61–83 years). Overall, 80 (31%) patients had PE. Median D-dimer was 3.19 (IQR 1.54–8.08), 52 (20%) patients had a history of cancer, 16 (6%) presented with deep vein thrombosis, 42 (16%) with tachycardia, 150 (59%) with dyspnea and 48 (19%) with cough. Westermark sign was positive in 2 (1%) patients, Fleischer sign in 25 (10%) patients, 4 (2%) presented with Hampton hump and 95 (37%) with pleural effusion. The accuracy for our classificator on the testing set was 85%, with 67% sensitivity and 93% specificity and an area under the curve of 0.92.

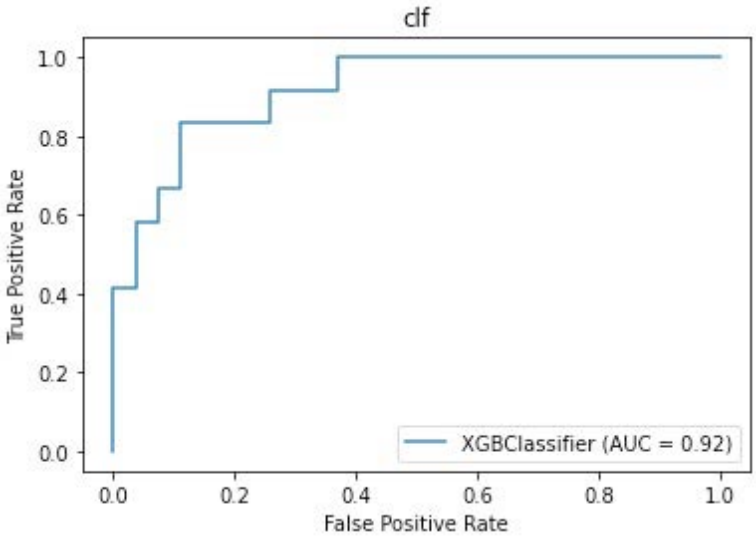

ROC curve from the classification of X-ray images

Conclusion

A model using clinical data and information from CXR predicts the presence of pulmonary embolism with substantial accuracy.

A-348

Acute exacerbation pattern as the presenting manifestation of idiopathic pulmonary fibrosis: frequency, CT characteristics and survival analysis.

J. Arenas-Jiménez[1,2,3], I. Gayá García-Manso[2,4], E. García-Garrigós[1,2,3], M. Sirera-Matilla[1,2], E. Nofuentes-Pérez[2,4], R. García-Sevila[2,4]
[1]Hospital General Universitario Dr. Balmis de Alicante, Radiology, Alicante, Spain, [2]Instituto de Investigación Sanitaria y Biomédica de Alicante (ISABIAL), Alicante, Spain, [3]Universidad Miguel Hernández, Departamento de Patología y Cirugía, Elche, Spain, [4]Hospital General Universitario de Alicante, Pneumology, Alicante, Spain

Purpose

Diagnosis of idiopathic pulmonary fibrosis (IPF) presenting as acute exacerbation (AE) requires the identification of both clinically significant respiratory deterioration (typically developing within less than 1 month) and the recognition of a characteristic CT pattern of bilateral ground-glass opacification and fibrotic changes[1]. Our purpose was to analyse the frequency, CT characteristics and prognosis of patients exhibiting a pattern of AE as the initial manifestation of IPF.

Methods & Materials

This retrospective study included 146 patients with IPF diagnosed in a tertiary hospital. Informed consent was waived by the hospital IRB. The number of patients first diagnosed of IPF with a clinical picture and CT consistent with AE, their clinical and radiological characteristics and survival analysis were recorded. CT pattern of AE was defined as bilateral ground-glass opacification appearing in areas of otherwise normal lung together with fibrotic changes consisting of basal predominance reticulation and lung distortion with traction bronchiectasis and honeycombing[1]. Diagnosis was made by a multidisciplinary team. In non-diagnostic radiological patterns, a histological usual interstitial pneumonia pattern diagnosis was confirmed by biopsy. CT was classified as diffuse, multifocal and peripheral[2], and the number of lung zones involved were registered according to Fleischner society division[3]. Survival time and the cause of death were registered.

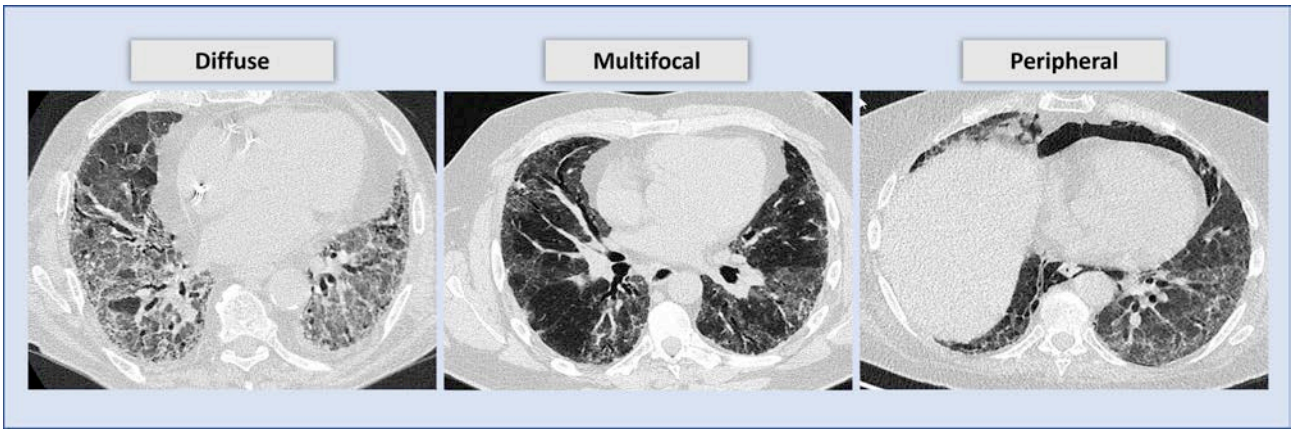

Classification of CT according to the distribution of ground-glass opacities

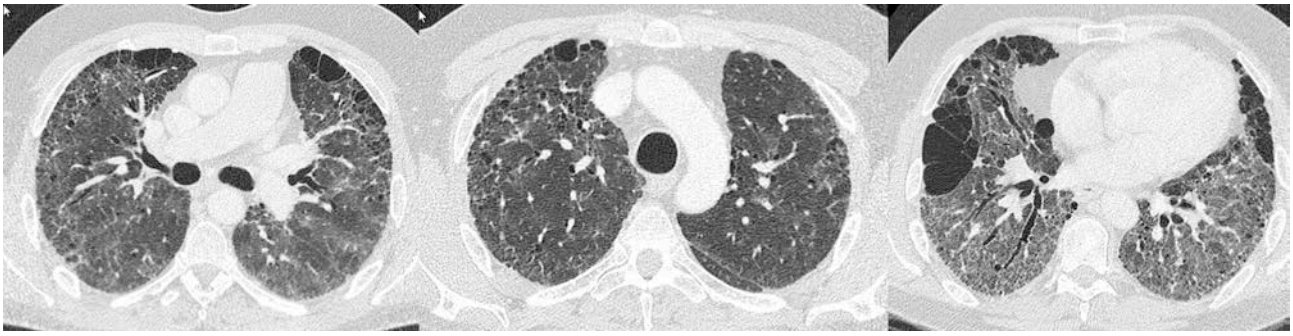

Fifty-six year-old smoker with 2 months onset of respiratory deterioration. Emphysema, traction bronchiectasis and diffuse ground-glass opacities are seen. Histological diagnosis was diffuse alveolar damage superimposed on usual interstitial pneumonia pattern.

Results

Twelve patients (8.2%) presented an AE pattern at the initial scan. Clinically, patients experienced respiratory deterioration for 3 days to 2 months (median 1 week) before admission. In only 2 cases a respiratory infection was recognized as a trigger. There was a seasonal variation with most cases (10 out of 12) occurring from January to May. Two patients were diagnosed by lung biopsies. Radiological distribution was diffuse in 7, multifocal in 3 and peripheral in 2. It affected all the 6 lung zones in all patients except in 2, involving 3 and 4 zones, respectively. Patients presenting with AE had lower DLCO and higher disease extension at CT ($p<0.001$). AE was a significant predictor of poor survival with higher mortality in those patients ($p<0.001$) with all patients except one dying within the first 2 years of follow-up (median 6 months, interquartile range 2.1-22 months). Six patients died of AE, 3 of them during the first admission and the other in subsequent episodes of AE. Only one patient died for non-respiratory cause and he showed peripheral pattern[4][5][6].

	Acute exacerbation	No acute exacerbation	p value

	pattern (n=12)	(n=134)	
Age at diagnosis, years	73.5 ± 13.9	71.0 ± 10.3	0.427
Male sex (%)	8 (66.7)	102 (76.1)	0.467
Ever smoked (%)	7 (58.3)	90 (67.2)	0.535
Duration of symptoms until diagnosis, months (IQR)	3.0 (2.0-12.0)	6.0 (2.0-12.0)	0.398
Survival time (months) (IQR)	6.0 (2.1-22.0)	46.0 (25.2-65.7)	0.001
FVC, %	64.2 ± 18.8	76.2 ± 20.7	0.095
DLCO, %	41.3 ± 2.5	53.1 ± 20.7	0.000
TLC, %	72.5 ± 2.1	72.7 ± 21.3	0.990
Global Extent (%)	75.0 (70.0-78.8)	60.0 (40.0-70.0)	0.000

Table 1. Comparison of the baseline characteristics between patients with IPF presenting with acute exacerbation as the initial manifestation and with other presentations.

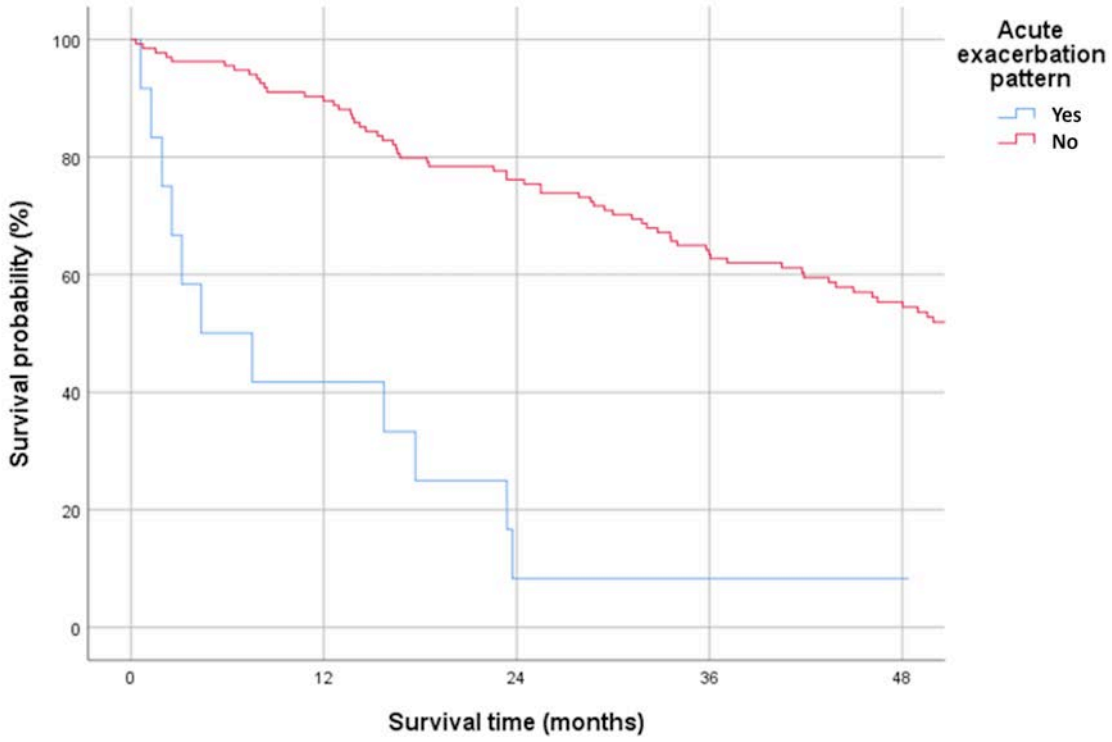

Kaplan Meier curve comparing survival between patients with acute exacerbation as the initial presentation of IPF and those with other presentations

Conclusion

AE is not rare as the presenting pattern in patients diagnosed of IPF and it carries a dismal prognosis. Radiologist should be aware of the characteristic pattern of AE in IPF since it determines a shorter survival.

References:

[1] Collard HR, et al., (2016), Acute exacerbation of idiopathic pulmonary fibrosis. An international work-ing group report., ATS journals, Am J Respir Crit Care Med , 265-275, 194, https://doi.org/10.1164/rccm.201604-0801CI

[2] Akira M, et al, (2008), Computed tomography findings in acute exacerbation of idiopathic pulmonary fibrosis., ATS journals, Am J Respir Crit Care Med , 372-8, 178, https://doi.org/10.1164/rccm.200709-1365OC

[3] Hatabu H, et al., (2020), Interstitial lung abnormalities detected incidentally on CT: a Position Paper from the Fleischner Society. , The Lancet, Lancet Respir Med, 726-737, 8, https://doi.org/10.1016/S2213-2600(20)30168-5

[4] Song JW, et al., (2011), Acute exacerbation of idiopathic pulmonary fibrosis: incidence, risk factors and outcome., ERS publications, Eur Respir J, 356-63, 37, https://doi.org/10.1183/09031936.00159709

[5] Enokida K, et al., (2023), Combination of computed tomography imaging pattern and severity of respiratory failure as factors associated with prognosis for acute exacerbation of idiopathic chronic fibrosing interstitial pneumonia. , PLoS ONE, e0279878, 18, https://doi.org/10.1371/journal.pone.027987

[6] Suzuki A, et al. , (2020), Acute exacerbations of fibrotic interstitial lung diseases. , Respirology, 525-34, 25, https://doi.org/10.1111/resp.13682

A-267

Analysis of pulmonary trauma sequelae on shock room CT examinations: frequency and extent of contusions compared with lacerations and their impact on patient outcome

M. Koßbiehl[1], L. Linderich[1], N. Sollmann[1], S. A. Schmidt[1], K. Schütze[2], M. Graeßner[3], D. Kildal[4], A. Beck[5], M. Beer[1], D. Vogele[1], C. Kloth[1]

[1]University Hospital Ulm, Department for Diagnostic and Interventional Radiology, Ulm, Germany, [2]Ulm University Medical Center, Department of Trauma-, Hand-, and Reconstructive Surgery, Ulm, Germany, [3]Ulm University Medical Center, Department of Anesthesiology, Ulm, Germany, [4]Spitalzentrum Oberwallis, Radiologie, Visp, Switzerland, [5]Ulm University Medical Center, Institute of Pathology, Ulm, Germany

Purpose

This study aimed to analyse the frequency and extent of lung contusions compared with lacerations in relation to trauma mechanism, outcome, and need for intensive care in polytrauma patients with CT examinations.

Methods & Materials

This single-center retrospective analysis consecutively included 355 patients (253 male, 71.2 %, mean age 46.33 ± 23.18 years) with CT datasets of polytrauma from 12/2015 to 06/2021, who had identified lung damage resulting from trauma. All lung CT examinations were read by two radiologists with 10 and 5 years of experience in thoracic imaging. All CT datasets were evaluated according to their quality (perfect-good-moderate-inadequate). Lung contusions and laceration were evaluated separately for all 5 lung lobes and were graduated into 25 % steps in their extent (0-20 points, 0-4 points for each lobe).

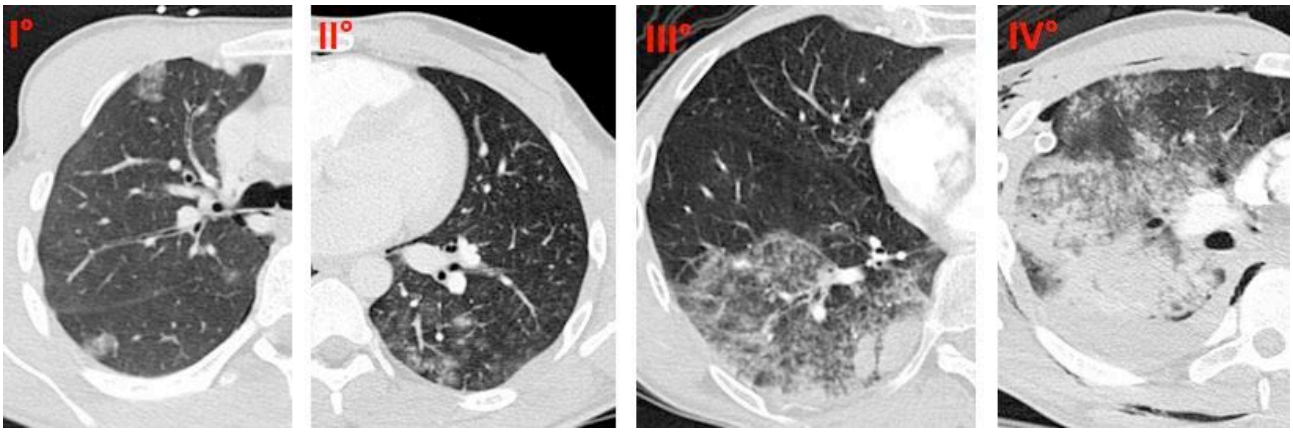

Contusions were evaluated separately for all 5 lung lobes and were graduated into 25 % steps in their extent (grade I-IV)

The sum scores of affected lung damage and the number of affected lobes were evaluated, also the presence of pleural effusion and pneumothorax was registered. For subgroup analysis, trauma mechanism and outcome were evaluated (duration of hospitalization, intubation, necessity of intensive care, death).

Results

In 342/355 patients (96.3 %) IV contrast agent was given. Image quality was perfect in 252/355 cases, good in 55/355 cases and moderate in 48/355 cases. Overall, a pneumothorax was registered in 170/355 (47.8%) patients, a pleural effusion in 150/355 (42.2%) patients.

The mean sum score of lobes with contusions was significantly higher in patients who died as a consequence of their trauma (p= 0.011*), in patients that needed a stay at an intensive care unit (p=0.047*) and in patients who needed intubation (p<0.001*). The mean number of involved lobes in lung contusions was 3.0±1.42, in lacerations 1.0±0.96. The mean number of lobes with contusions was significantly higher in patients who died as a consequence of their trauma (p= 0.037*).

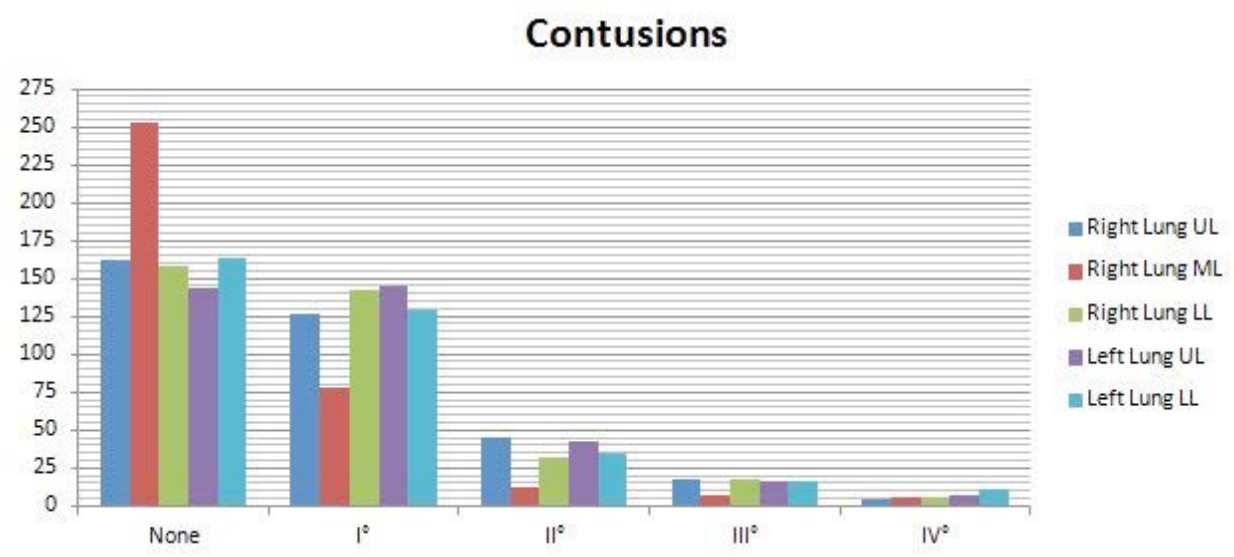

Distribution of contusions

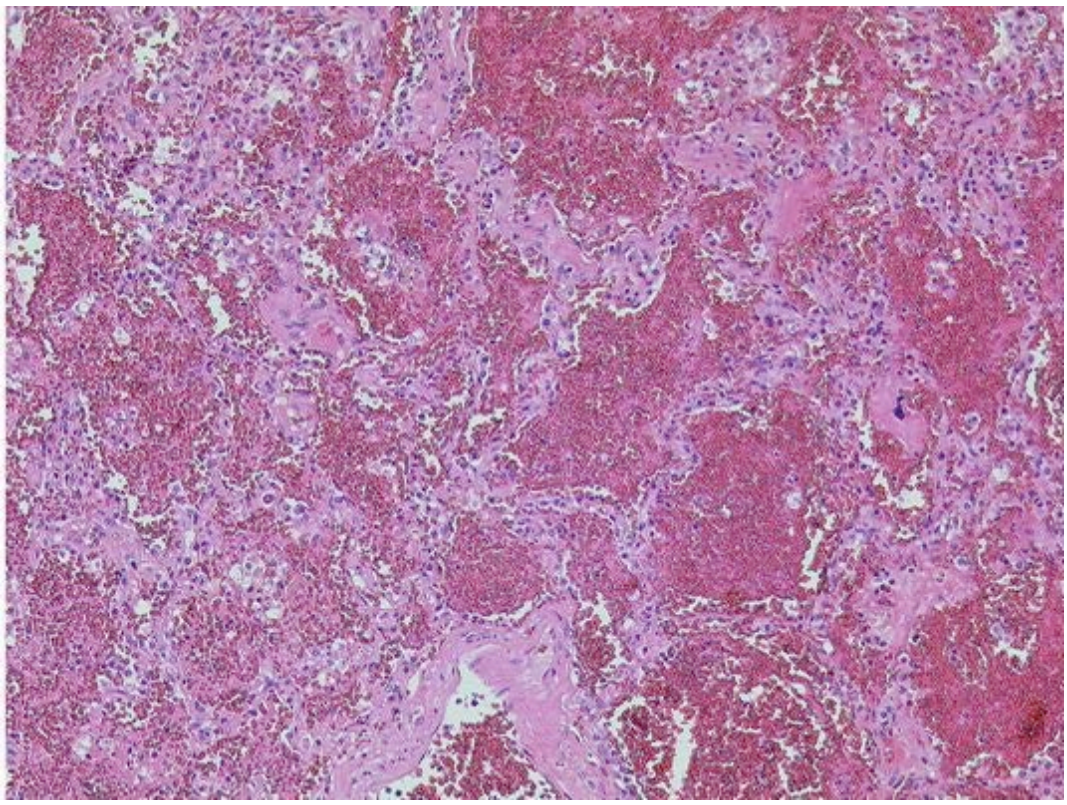

Diffuse contusion/hemarrhage of the lung. HE, original magnification 100:1. The alveolar spaces are filled with blood and fibrin. Changes associated with organization are not seen yet.

A score of 3 and 4 in lobes with contusions was significantly more often registered in patients who died as a consequence of their trauma (n=19 with a score of 3 were registered, expected 10.6, p= 0.01*; n=10 with a score of 4 were registered, expected 4.6, p= 0.01*).
The interobserver agreement was moderate with k = 0.525 (95% CI 0.492-0.558) for the evaluation of contusions ($p < 0.001$*) and also moderate with k = 0.450 (95% CI 0.391-0.509) for evaluation of lacerations ($p < 0.001$*).

Conclusion

Specific structural damages of the lung had a quantitative influence on critical outcome parameters. Scoring of lung contusions correlates more precise with the patient outcome than the number of affected lobes alone. A score of 3 (>50%) and 4 (>75%) in lobes with contusions were significantly more often registered in patients who died as a consequence of their trauma.

A-251

Anatomical CT variations in cystic fibrosis patients under triple therapy: A preliminary report.

J. Collada-Carrasco[1], S. Hernández-Muñiz[1], R. Girón Moreno[2], C. De Benavides Bernaldo de Quirós[1], C. Zorzo Sánchez[3], P. Caballero Sánchez-Robles[1]

[1]Hospital Universitario de la Princesa, Radiology, Madrid, Spain, [2]Hospital Universitario de la Princesa, Pulmonology, Madrid, Spain, [3]Hospital Universitario Sanitas La Moraleja, Radiology, Madrid, Spain

Purpose

Cystic fibrosis transmembrane conductance regulator (CFTR) new triple modulator therapy (elexacaftor-tezacaftor-ivacaftor) has shown benefits since its approval in Spain in late 2021. The aims of our study are:

- To assess anatomical changes on lung CT scans in cystic fibrosis (CF) patients before and after triple therapy.
- To assess the interobserver agreement between two trained radiologists employing Bhalla CT score.
- To compare body mass index (BMI) and lung function parameters in the same group before and after therapy.

Methods & Materials

We conducted an analytical study including CF patients under triple therapy in our tertiary hospital (La Princesa University Hospital, Madrid). Lung CT scans from December 2022 on were reviewed, and patients meeting our inclusion criteria (at least 10 months under therapy) were enrolled by consecutive sampling.

Patients with no previous lung CT in our center were excluded.

Descriptive information was gathered: age, sex, type of CFTR gene mutation.

For every patient, CT images were retrospectively compared by two trained radiologists with the last CT available before treatment. Differences in Bhalla score were analyzed using Wilcoxon signed-rank test.

Agreement between radiologists was assessed using weighted-Kappa index.

BMI and lung function parameters (FVC in mL, FVC%, FEV1 in mL, FEV1%) at the moment of the first and second CT scans were collected retrospectively, and differences were analyzed using paired-sample T-test.

Normality tests were conducted using Shapiro-Wilk test.

For every analysis, a p-value under 0,05 was required for statistical significance.

Results

Twelve patients with median age 23 years old, 50% men. All of them carried *F508del* mutation, 25% in homozygosis. Mean time between CT scans was 31 months, median time under treatment was 12 months.

Median Bhalla score before treatment was 12,5 and 10,5 for radiologists 1 and 2, respectively. After treatment it was 13,5 for both radiologists. Differences were statistically significant ($p<0,05$) (Figures 1 and 2). Agreement between radiologists was moderate (weighted-Kappa 0,6).

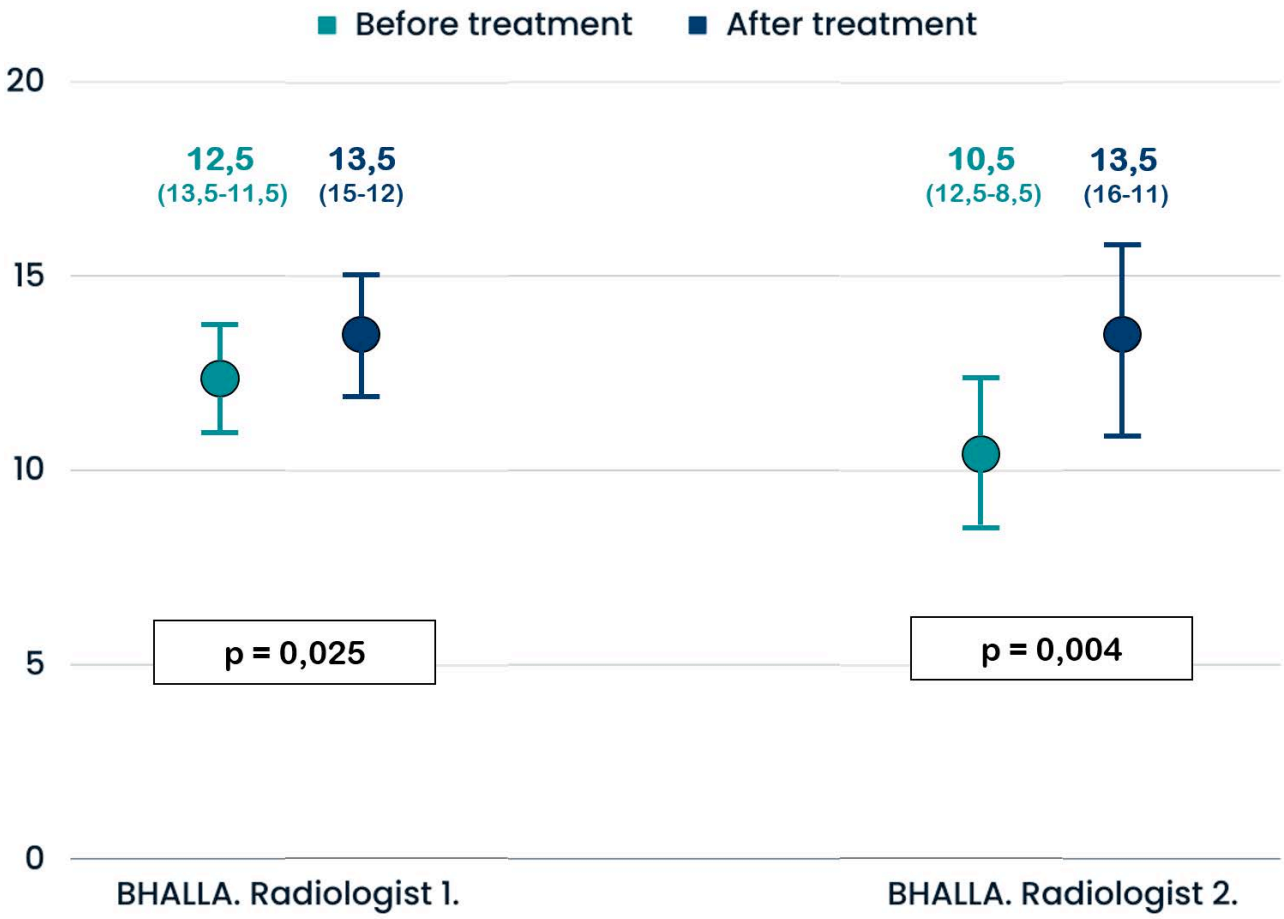

Figure 1. Median (and IQR) Bhalla scores for both radiologists before and after treatment.

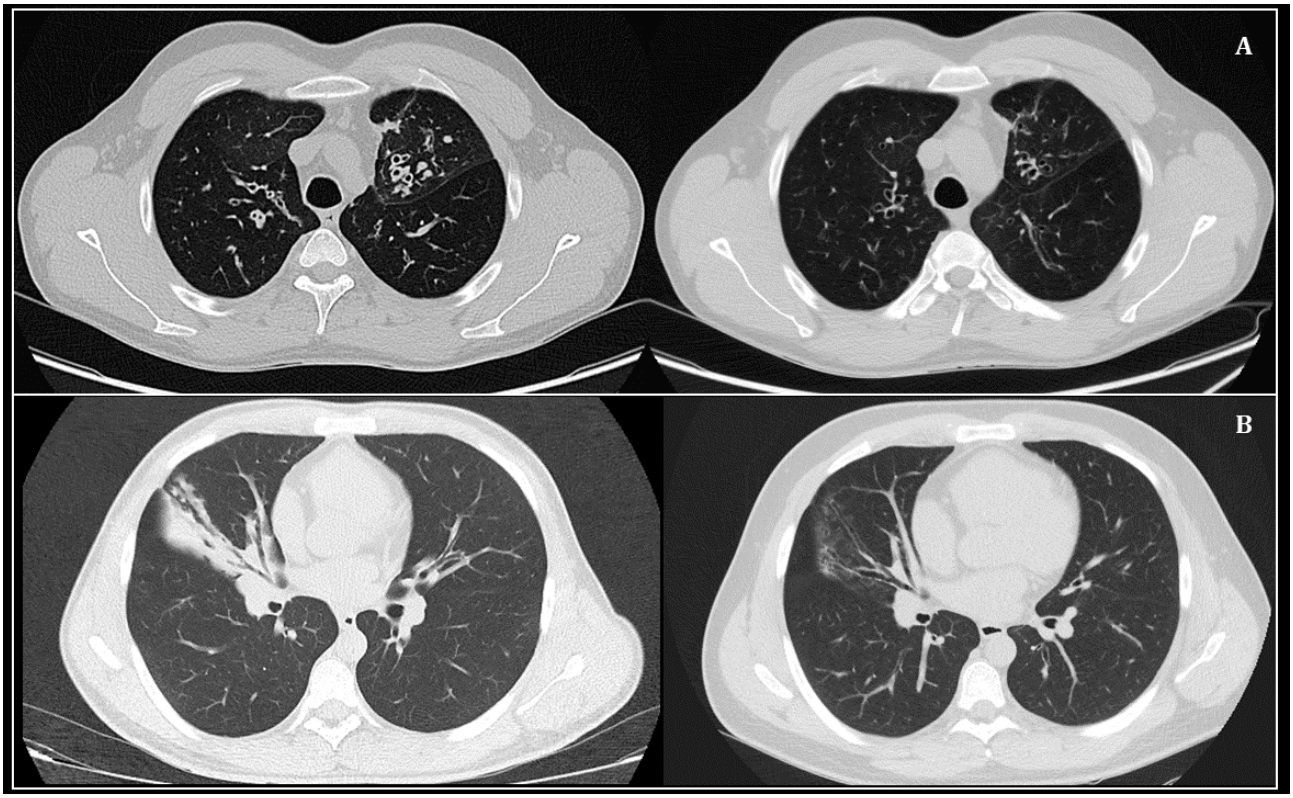

Figure 2. Axial CT lung scans images of two different patients (A and B) from our sample, showing changes in bronchial wall thickening, mucus plugging and atelectasis severity before and after treatment.

A significant improvement in mean FVC (13%, $CI_{95\%}$ 7-19%) and FEV1 (10%, $CI_{95\%}$ 4-16%) was detected ($p<0,01$) (Figure 3). Although a tendency to rise was observed in BMI, differences were not statistically significant in this study.

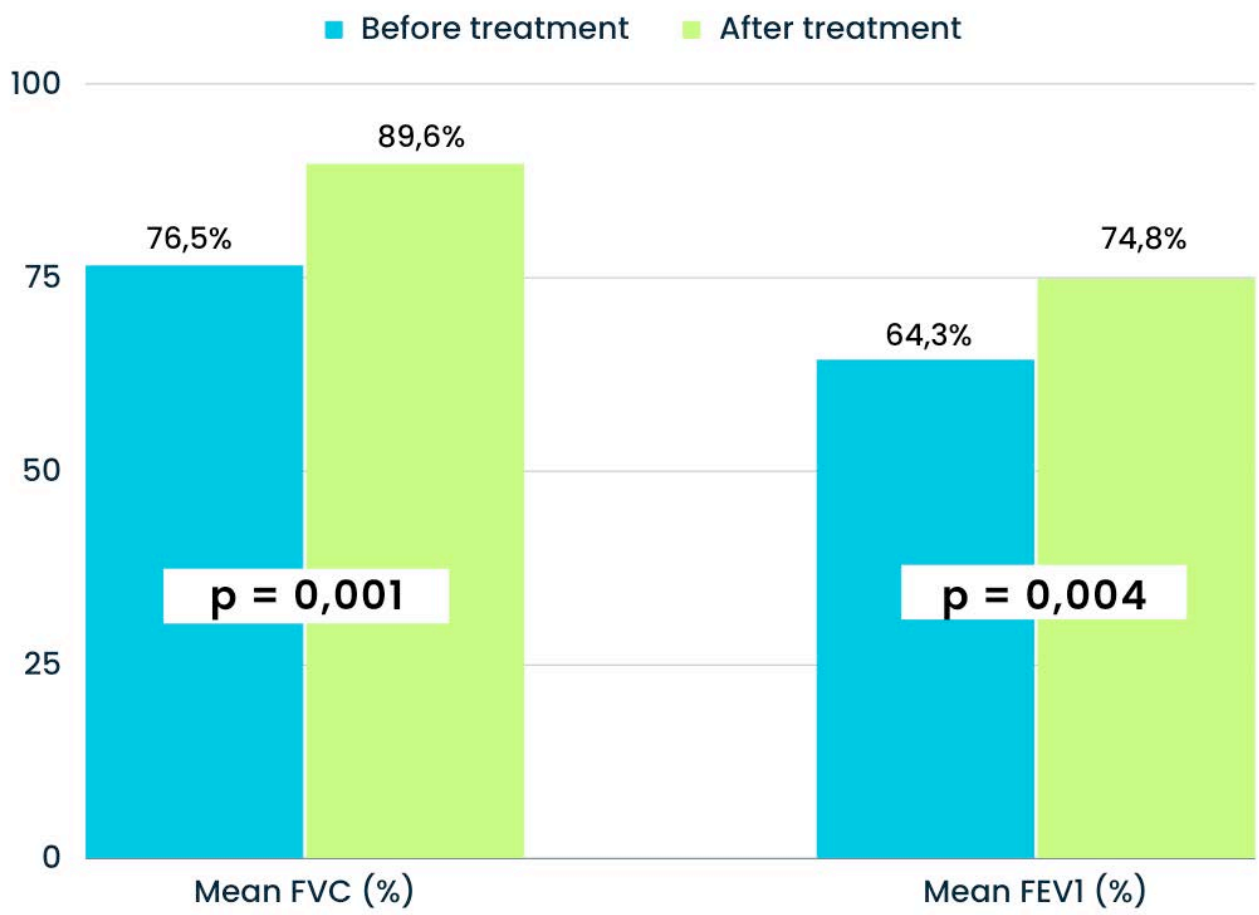

Figure 3. Mean values of lung function parameters before and after treatment.

Conclusion

In our preliminary study in patients under triple therapy for at least 10 months, we detected significant improvements in CT severity assessed through Bhalla score and lung function.

Regarding the results, we aim to continue patient recruiting in order to further and more detailed reports.

References:

[1] Barry P et al, (2021), Triple Therapy for Cystic Fibrosis Phe508del–Gating and–Residual Function Genotypes., N Engl J Med, 385:815-825

[2] Zorzo C, Caballero P, et al, (2020), Predictive value of computed tomography scoring systems evolution in adults with cystic fibrosis, Eur Radiol, 30: 3634-40

[3] Quintana-Gallego E, Delgado-Pecelli´n I, Calero Acuña C., (2014), Tratamientos reparadores de la protei´na CFTR en la fibrosis qui´stica., Arch Bronconeumol, 50:146–50

[4] Bhalla M et al, (1991), Cystic fibrosis: scoring system with thin-section CT. , Radiology, Jun;179(3):783-8.

A-754

Artificial Intelligence (AI) for assessing PVP on radiographic examinations

Y. Liberman, A. Liubauske, R. Liubaskas, D. Litmanovich, R. Eisenberg
Harvard Medical School- Beth Israel Deaconess Medical Center, Radiology, BOSTON, United States of America

Purpose/Objectives
In hospitalized patients, especially in the ICU, the presence or absence of elevated pulmonary venous pressure (PVP) is of clinical significance and is usually based on clinical signs and the chest radiographic appearance. Thus, clinical decisions frequently are made based on the assessment of PVP in radiology reports, but how accurate are they? An additional motivation for this study was recent articles indicating the potential value of Artificial Intelligence (AI) for assessing PVP on radiographic examinations, based on analyzing large numbers of chest images their radiologist reports. Any substantial discrepancy among radiologists in assessing PVP status would raise doubts about the accuracy of AI determinations.
Methods & Materials
150 AP portable chest radiographs were presented to 10 radiologists (5 cardiothoracic; 5 non-cardiothoracic who often interpret chest radiographs). To assess inter-rater variability, each radiologist was asked to place each case in one of four categories: 0 = no elevated PVP; 1 = pulmonary vascular congestion; 2 = interstitial pulmonary edema; or 4 = alveolar pulmonary edema. No instruction was be given regarding the radiographic findings characteristic of these four categories, with readers instead requested to interpret these cases in a manner similar to daily clinical practice.
Results
Both cardiothoracic and non-cardiothoracic radiologists demonstrated wide variability in determining the absence or presence of elevated PVP and, if present, in distinguishing among the three different categories of pulmonary edema. Overall, in the cases in which a majority of
the 10 readers agreed that there was elevated PVP, only in 14% did they agree on a single diagnostic category, while in 32% at least one reader assigned the case to all of the categories of pulmonary edema. For the 5 cardiothoracic radiologists, each of whom twice interpreted the same 150 cases (750 total cases), the intra-observer disagreement rate was 38% (range of 29% to 48.0%). In 151 pairs of readings (42.4%), one of the two was interpreted as the absence of elevated PVP and the other was read as showing some degree of elevated PVP.
Conclusion
Our study demonstrates substantial inter-rater and intra-rater discrepancy among radiologists in determining the absence or presence of elevated PVP, as well as distinguishing among the three categories of elevated PVP. This raises doubts about the accuracy of Artificial Intelligence determinations based on data gleaned from radiologist dictations of PVP

A-535

Artificial intelligence based HRCT-approximated perfusion is comparable to nuclear perfusion imaging

T. D. Koster[1], J.-P. Charbonnier[2], J. Pruim[3], H. A. Gietema[4,5], R. Posthuma[6], L. E. Vanfleteren[7,8], A. van Erp-Zeilstra[3], A. Willems van Beveren[3], M. van Dijk[1], K. Klooster[1], D.-J. Slebos[1]

[1]University Medical Center Groningen, Pulmonary Diseases, Groningen, The Netherlands, [2]Thirona BV, Nijmegen, The Netherlands, [3]University Medical Center Groningen, Nuclear Medicine and Molecular Imaging, Groningen, The Netherlands, [4]Maastricht University Medical Center+, Radiology and Nuclear Medicine, Maastricht, The Netherlands, [5]GROWSchool for Oncology and Reproduction, Maastricht, The Netherlands, [6]Maastricht University Medical Center+, Pulmonology, Maastricht, The Netherlands, [7]COPD Center, Respiratory Medicine and Allergology, Gothenburg, Sweden, [8]Institute of Medicine, Internal Medicine and Clinical Nutrition, Gothenburg, Sweden

Purpose

Artificial intelligence based quantitative analysis of high-resolution computed tomography (HRCT) is an important clinical decision tool in endobronchial valve treatment for COPD patients. Selection of the treatment target lobe is mainly based on emphysema destruction score and fissure completeness. Additionally, total and regional lung perfusion is important in identifying the optimal target lobe for treatment and is commonly assessed using perfusion scintigraphy or single photon-emission computed tomography (SPECT-CT)).
We aimed to investigate whether pulmonary perfusion distribution approximated from a HRCT scan using Thirona's artificial intelligence-based quantitative CT analysis (PXT, Thirona, the Netherlands) provides similar information as the distribution measured by both regular perfusion scintigraphy and SPECT-CT.

Methods & Materials

Patients with severe COPD screened for lung volume reduction who had perfusion scintigraphy or SPECT-CT were included in this analysis. PXT was compared to perfusion distribution for the left and right lung and to SPECT-CT for all individual lobes.

Results

For comparison of PXT to perfusion scintigraphy, we included 207 patients. The Intraclass Correlation Coefficient (ICC) was high (0.96 ($p<0.01$)), the mean difference between the two tests was 0.6% (±3.5). For the comparison of SPECT-CT and PXT on a lobar level we included 85 patients. The ICC range was 0.88 (middle lobe) to 0.97 (left upper lobe). Results are summarized in table 1. The figure shows an individual example of a patient with the results of perfusion on a lobar level measured with both SPECT-CT and PXT. Figure shows the coronal view of matched SPECT and CT (left) and the comparable image of the heatmap acquired with PXT (right).

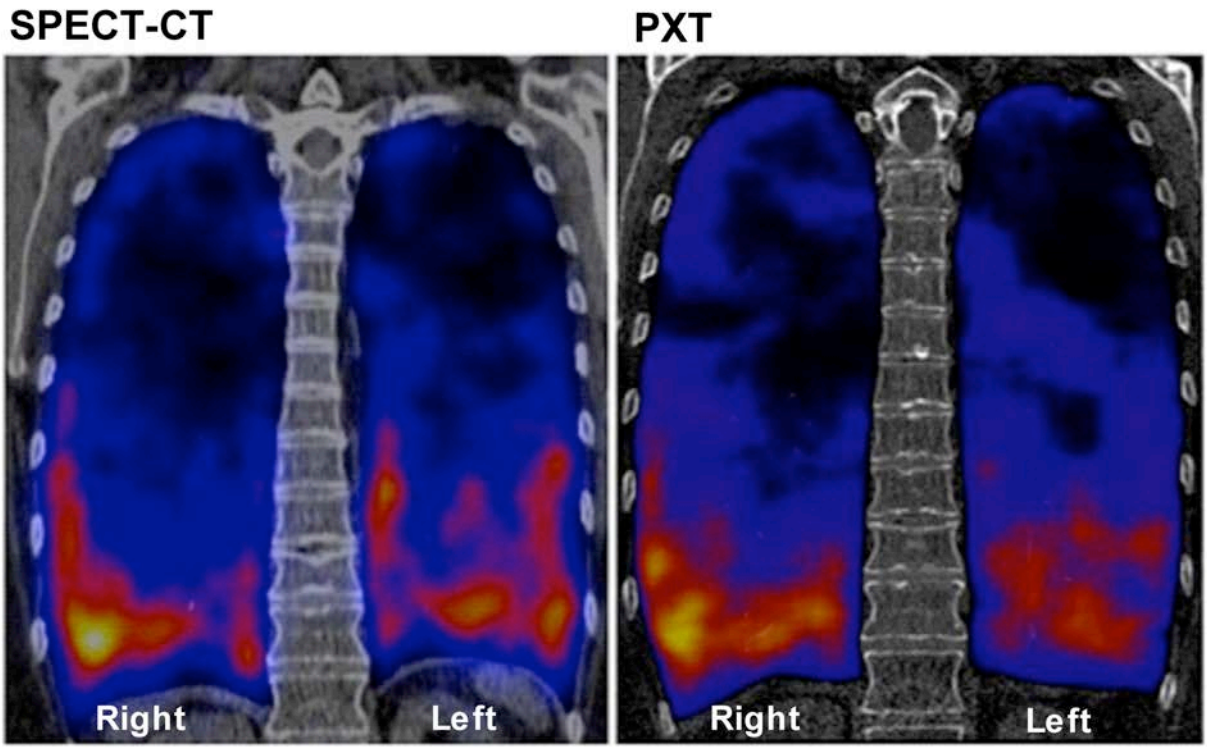

	RUL	RML	RLL	LUL	LLL
SPECT-CT	11	3	37	9	40
PXT	12	6	37	10	35

Example of a patient with the results of perfusion measured with both SPECT-CT and PXT

	Perfusion scintigraphy	PXT			
N=207	**Mean ± SD (%)**	**Mean ± SD (%)**	**Mean difference (%)**	**p-value**	**Intraclass correlation coefficient (95%-CI)***
Left Lung	49 ± 9	48 ± 8	0.6 ± 3.5	**0.02**	0.96 (0.94 – 0.97)
Right Lung	51 ± 9	52 ± 8	-0.6 ± 3.5	**0.02**	0.96 (0.94 – 0.97)
	SPECT-CT	**PXT**			
N=85	**Mean ± SD (%)**	**Mean ± SD (%)**	**Mean difference (%)**	**p-value**	**Intraclass correlation coefficient (95%-CI)***
Left Lung	48 ± 9	46 ± 8	1.5	**<0.01**	0.95 (0.91 – 0.97)
Right Lung	52 ± 9	54 ± 8	-1.5	**<0.01**	0.95 (0.91 – 0.97)
LUL	23 ± 10	22 ± 9	1.6	**<0.01**	0.96 (0.92 – 0.98)
LLL	25 ± 11	25 ± 9	0	0.46	0.97 (0.96 – 0.98)
RUL	22 ± 12	21 ± 10	1.4	**<0.01**	0.96 (0.94 – 0.98)
RML	6 ± 4	6 ± 4	0	0.49	0.88 (0.82 – 0.93)
RUL + RML	28 ± 12	27 ± 10	1.4	**<0.01**	0.97 (0.95 – 0.98)
RLL	24 ± 10	27 ± 9	-2.9	**<0.01**	0.95 (0.70 – 0.98)

Results of comparison between perfusion scintigraphy and PXT, and SPECT-CT and PXT. *: p-value <0.001 for all outcomes.

Conclusion

Pulmonary perfusion can be estimated by HRCT-based artificial intelligence approximation with high accuracy. This can prevent additional examinations beyond CT to quantify pulmonary perfusion.

A-742

Assessment of DE-CTPA derived Virtual Non-Contrast lung images vs low dose unenhanced CT thorax in patients with suspected COVID-19

S. M. Mak, A. Pascoal, D. Hodson, G. Benedetti
Guy's and St Thomas NHS Foundation Trust, London, United Kingdom

Purpose/Objectives

Aim of our study was to compare dual-energy virtual non-contrast CT (VNC) and single-energy low-dose non-contrast CT (LDNC) in terms of image quality in assessing lung parenchyma of patients with suspected COVID-19 pneumonitis.

Methods & Materials

We included inpatients over a 3 month period with suspected COVID-19 pneumonitis, who underwent a LDNC followed by DE-CTPA on a Siemens Somatom Force CT scanner. VNC lung kernel images were post-processed from the DE-CTPA data, which is compared with standard LDNC. Two consultant radiologists evaluated independently the quality of the CT images on a PACS workstation. Severity of pneumonia was assessed and graded from 0 to 3. Then presence of normal lung (NL) parenchyma, ground glass (GG) changes, dense consolidation (DC) and interstitial septal thickening (IST) was assessed on LDNC, and when present, the image quality of each of these changes VNC were compared to LDNC images according to a 4-points Likert scale (1=superior image quality of VNC compared to LDNC, 2 =comparable, 3=poorer but still diagnostic, 4=worse and not diagnostic). Also, overall image noise and diagnostic quality of VNC was compared to LDNC. For quantitative noise comparison, a 1cm2 ROI (average HU ± SD) was drawn by consensus on normal lung parenchyma, on ground glass changes and on dense consolidation. Statistical analyses were performed using SPSS v.20.0. A *p* value of<0.05 was considered statistically significant.

Results

31 patients were enrolled. 7 patients had no pneumonitis, 24 had a certain degree of lung involvement (specifically: 3 pts scored 1, 7 pts scored 2, 14 patients scored 3). 30 patients had at least some extent of normal lung parenchyma, and in all of them VNC were scored as 1 (superior) or 2 (comparable) compared to LDNC according to the Likert scale. 22 patients had a certain degree of GG, all scored 1 or 2 of the Likert scale (20 cases comparable, 2 cases superior). 22 patients had DC and in all those cases DE-VNC was found to be comparable to LDNC. 16 patients had IST, all scored 2 (comparable) according to the Likert scale. When present, IST sharpness was scored as 3 in most cases (poorer, 12 cases), scored 2 in 3 cases and 1 in one case. Lung window overall image noise was scored as 1 (superior) in all cases, while overall diagnostic quality was scored as comparable in 4 cases and superior in 27 cases. Average ROI across both VNC and LDCT lung parenchyma, GG and DC are not statistically significant.

Conclusion

Overall, we found that lung reconstruction on VNC images are non-inferior to LDNC images in assessing lung parenchyma. There was a perception of better SNR, despite sharpness of septal lines was felt to be slightly poorer.

A-456

Benefit of annual screening with chest CT for the early detection of malignancy in patients after lung transplantation

R.-I. Milos[1], E. Alvieva[1], P. Jaksch[2], E. Hielle-Wittmann[2], G. Muraközy[2], L. Beer[1], S. Röhrich[1], M. L. Watzenboeck[1], F. Prayer[1], D. Kifjak[1], B. Heidinger[1], K. Hötzenecker[2], H. Prosch[1]

[1]Medical University of Vienna, Department of Biomedical Imaging and Image-guided Therapy, Vienna, Austria, [2]Medical University of Vienna, Department of Thoracic Surgery, Vienna, Austria

Purpose/Objectives

Lung transplanted patients have an increased risk for developing malignancies due to chronic immunosuppression and underlying diseases leading to transplantation, such as end-stage COPD. Data about effectiveness of cancer screening with chest CT in these patients is currently missing, due to the lack of general guidelines for long-term follow-up [1]. In our institution, lung-transplanted patients undergo annual low-dose non-contrast chest CT for the early detection of subclinical abnormalities. The aim of this study was to assess the utility of this annual screening for the early diagnosis of malignancies in patients after lung transplantation.

Methods & Materials

This retrospective study reviewed the data of all consecutive lung transplants performed at our institution in the last 15-years. Medical records were extracted from the database of the Vienna Lung Transplant Program. Any cancer that was diagnosed during the follow-up period was recorded and the timely performed annual chest CT scans were scrutinized for radiological malignancy-associated manifestations.

Results

A total of 907 Austrian patients were transplanted between January 2006 and December 2021 and 37 patients developed malignancies: posttransplant lymphoproliferative disorder (PTLD) or lymphoma (n=16), lung (n=6), colorectal (n=3), breast (n=2), prostate (n=2), testicular, ovarian, esophageal, liver, laryngeal and bladder cancer (n=1), multiple myeloma (n=1), and sarcoma (n=1). Median time from transplantation to diagnosis was 736 days (range 61 to 3216 days), with 10 cancers diagnosed within one-year posttransplant, most of them being PTLD.

Altogether 696 patients received at least one routine annual chest CT. Six out of the 27 cancers developing at least one year after transplantation presented malignancy-associated lesions on the routine chest CT(see **Figure**).

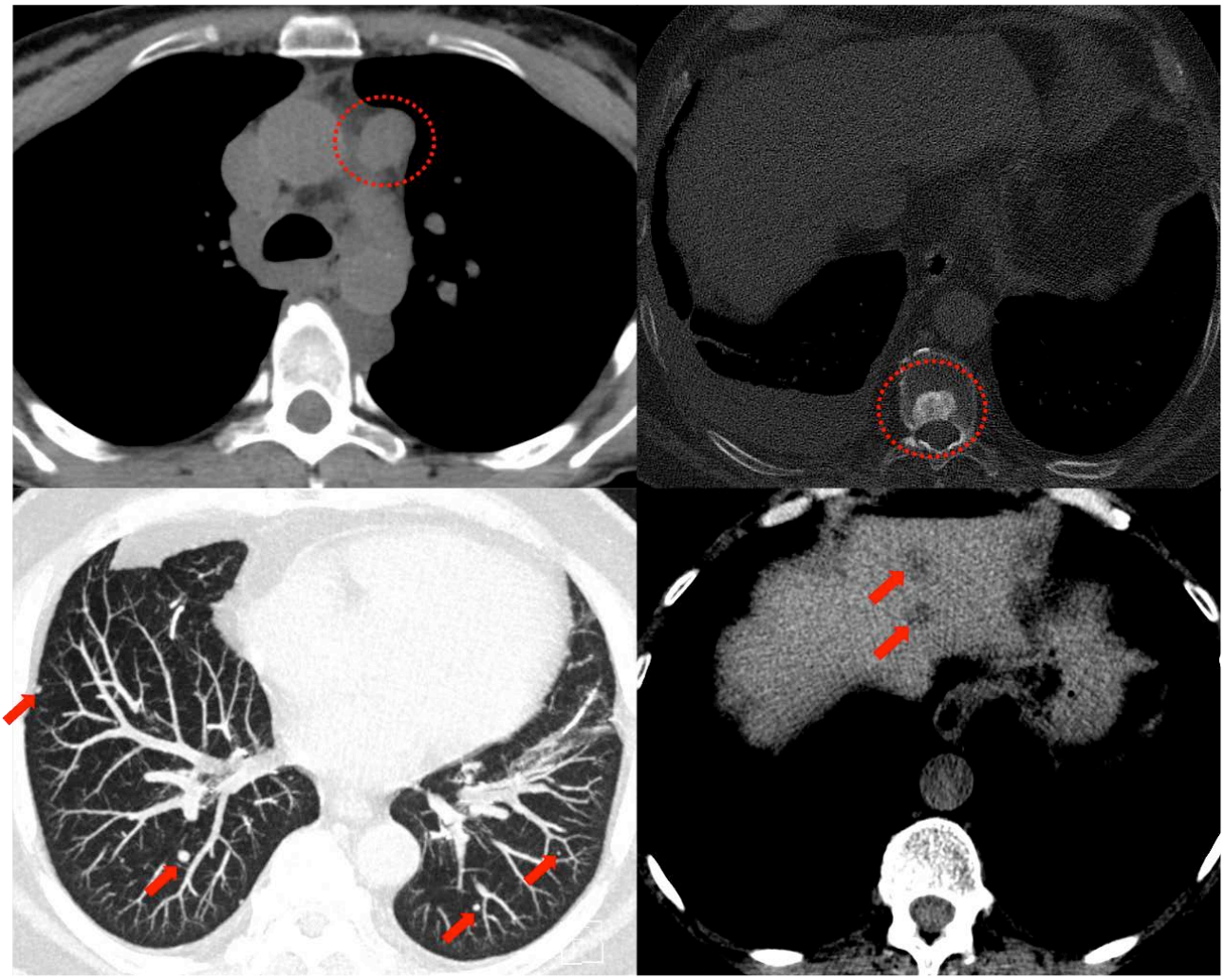

Examples of four different patients with cancer-associated mediastinal, lung, bony or liver lesions detected on the routine annual chest CT

Two further cases were diagnosed with PTLD of the lung only histologically after routine bronchoscopy and did not show any lesions on the timely performed PET-CT (histologically early lesions). In three cases of lung cancers, the last available routine CTs were performed

8, 10 and respectively 22 months before the diagnosis and these did not show any suspicious lesions. One patient diagnosed with lung cancer did not receive routine CT at our institution. The remaining 15 malignancies were not located in the chest.

Conclusion

Annual screening with low-dose chest CT after lung transplantation helps clinicians to identify subclinical malignancy-suspicious chest lesions earlier, thus enabling early diagnosis and multidisciplinary therapeutic actions, involving oncologic and immunosuppression regime.

ESTI Research Support Programme

References:

[1] 1. Delaney FT, Murray JG, Hutchinson BD, et al. , (2022), The role of radiology in addressing the challenge of lung cancer after lung transplantation, Eur Radiol , 8182-8190, Dec;32(12), https://doi.org/10.1007/s00330-022-08942-w

A-523

Changes in radiology staff attitudes after implementation of an AI tool for triaging lung cancer cases

D. Togher[1], J. Moon[1], R. Mayola[1], M. Meheux[1], V. Gnanananthan[1], M. Khalil[1], S. Rickaby[2], G. Dean[1], S. Shelmerdine[3]
[1]Epsom & St Helier NHS Trust, Clinical Radiology, London, United Kingdom, [2]Kingston Hospital NHS Foundation Trust, Clinical Radiology, Kingston, United Kingdom, [3]Great Ormond Street Hospital, Clinical Radiology, London, United Kingdom

Purpose/Objectives
To determine the change in radiology staff opinions and attitudes towards artificial intelligence (AI) after the implementation of an AI tool for triaging lung cancer cases on chest radiographs.
Methods & Materials
An online 19 question survey was distributed to all members of radiology staff across two hospitals within South West London, UK before, and three months after the implementation of an AI tool for chest radiograph triage. Questions specific to the AI tool were included in the second survey from users. Differences in opinions regarding impact and benefits of AI were evaluated.
Results
There were 45/195 (23%) and 26/195 (13%) respondents to the first and second surveys respectively. After AI implementation, staff were less willing for an AI to act autonomously (58% vs 40%) but more likely to believe that AI could improve patient care (50% vs 40% agree) and more willing to allow an AI to triage their own chest radiograph if they were a patient (31% vs 18%). The single most positive factor that staff felt AI would bring to the department was 'time saving for the department and patient' (31%) before the AI implementation, although after AI implementation they were more likely to state 'better patient follow-up care' as the main benefit (31%). After only 3 months of using the AI tool, most users felt they had either no change (37.5%) or a slight improvement in their reporting accuracy (37.5%) but still believed they were confident in knowing when to rely and overrule the tool (50%).
Conclusion
Radiology staff were more likely to agree there was a benefit to patients from an AI tool and more willing to have AI used on their own chest radiograph if in hospital; however early implementation logistical issues meant they no longer felt AI was a time-saving tool. Further surveys will be conducted after another 6 months of using the AI tool.
Early adopters of AI tools for chest radiographs should not overlook staff opinions and crucial feedback when implementing AI,.

A-430

Comparison of Ultra-low and Standard dose computed tomography for Detection and Characterisation of Pulmonary Nodules

A. Harold-Barry[1], M. Waldron[2], M. Maher[2,3]
[1]Cork University Hospital, Cork, Ireland, [2]Cork University Hospital, Dept of Radiology, Cork, Ireland, [3]University College Cork, Cork, Ireland

Purpose/Objectives

Pulmonary nodule size is an important parameter used to estimate the probability of lung cancer. Growth rate and imaging characteristics on computed tomography (CT) are also predictors of benign or malignant aetiology.[Reference1]These imaging features aid management and decision-making. Patients with pulmonary nodules may require multiple follow-up CT's to monitor these nodules; resulting in potentially high cumulative radiation exposure, especially in young patients. It is, therefore, beneficial to aim to reduce the radiation dose, whilst maintaining adequate image quality to detect, characterise and assess for interval growth of these nodules.

Aim

To determine whether ultra-low dose CT with model-based iterative reconstruction (ULDCT-M) allows the follow-up of pulmonary nodules adequately without compromising measurement of nodule size and assessment of imaging characteristics compared to standard dose CT (SDCT).

Methods & Materials

A prospective single-centre study was performed following ethical approval assessing patients with previously detected indeterminate pulmonary nodules on CT thorax imaging. Unenhanced SDCT of the chest followed immediately by an interval ULDCT were acquired with a 64-row multi-detector CT system (Discovery CT750 HD; GE Healthcare). Nodules were identified, characterised and measured on a PACS system. CT dose index volume (CTDIvol) in mGy and dose length product (DLP) in mGy.cm were recorded. SPSS was used to analyse frequencies and means.

Results

Thirty patients with a mean age of 61 years were included. The mean duration between scans was 217 days. One hundred twenty-two nodules were detected on ULDCT (mean 4.1), and 116 were detected on SDCT (mean 3.9). ULDCT failed to identify 1.72% of nodules (n=2).

Eight false positives were identified with ULDCT where areas of vasculature and atelectasis were incorrectly identified as nodules.

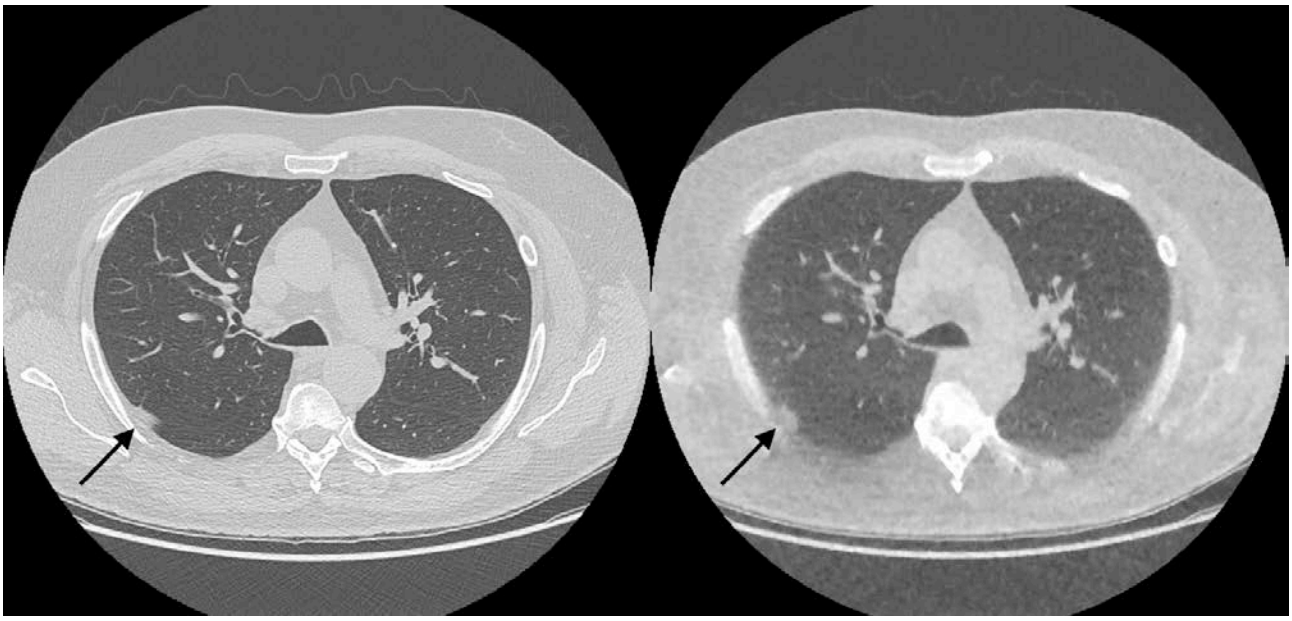

Area of atelectasis on SDCT (left image) was identified as a nodule (false positive) on ULDCT (right image)

Following exclusion, a p-value of 0.09 was obtained, indicating no difference in the characteristics of correctly identified nodules on SDCT compared to ULDCT.

When comparing the two CTs, there was no difference in characterising lesions as cavitating vs spiculated. No significant change in the size of the nodules was detected between ULDCT (mean 4.51mm) and SDCT (mean 4.47mm)($P>0.328$).

Mean DLP for the ULDCT was 5.592 mGy.cm, significantly lower than SDCT mean of 237.095 ($P<0.001$); This represented a dose reduction of 97.6%. Mean CTDI volume for ULDCT was 0.1598 compared with 7.19733 for SDCT ($P<0.001$).

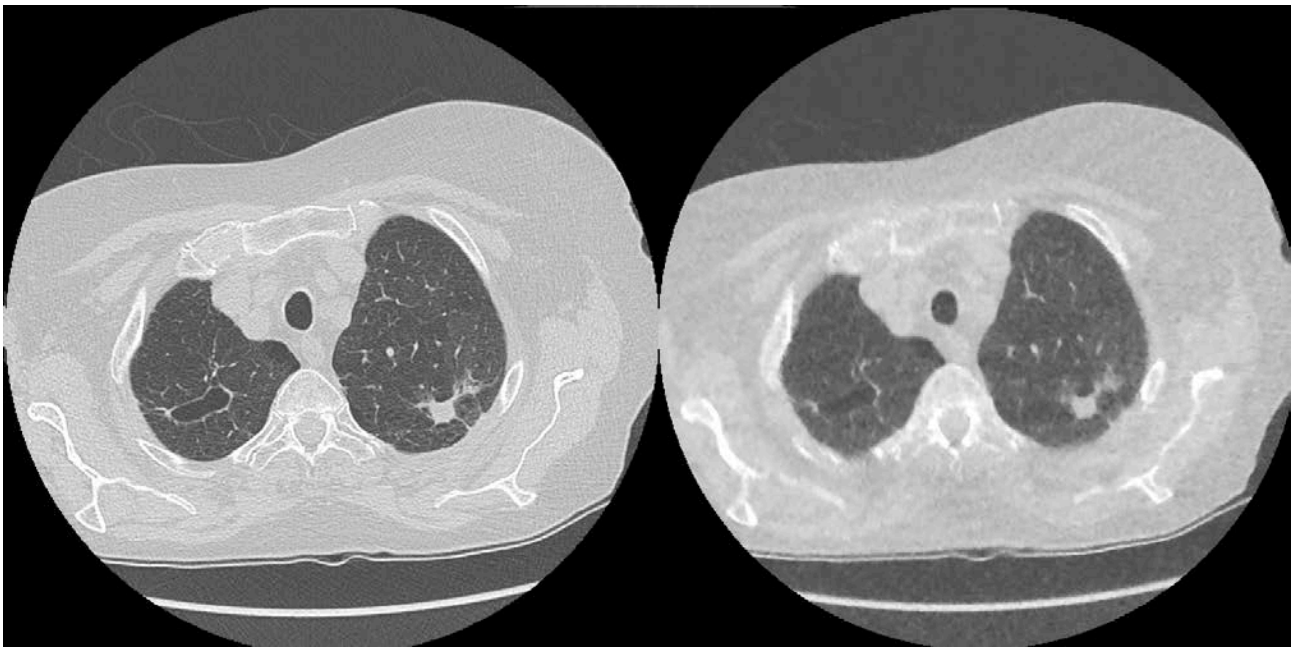

True positive nodule with no difference in size or characteristics identified between SDCT (left image) and ULDCT (right image)

Conclusion

The use of a ULDCT protocol did not significantly influence the number, size or imaging characteristics of nodules detected. Consideration should be given to utilising ULDCT in place of SDCT for follow-up CT, at specific intervals and time-points following initial nodue detection.

References:

[Reference1] Callister ME, Baldwin DR, Akram AR, Barnard S, Cane P, Draffan J, et al., (2015), British Thoracic Society guidelines for the investigation and management of pulmonary nodules. , BMJ, Thorax , 1-54 , 70, 10.1136/thoraxjnl-2015-207168, 2023-03-06, British Thoracic Society

A-139

Computer-Aided Diagnosis of Pulmonary Embolism in Computed Tomography Angiography Imaging

A. Turgut[1], A. Karaman[2], A. Yalcin[2], F. Alper[2]
[1]Erzurum City Hospital, Radiology, Erzurum, Turkey, [2]Ataturk University Faculty of Medicine, Radiology, Erzurum, Turkey

Purpose/Objectives

Pulmonary embolism (PE) is a life-threatening condition in which early and accurate diagnosis is critical for prompt treatment and improved patient outcomes. Computed tomography (CT) is the imaging modality of choice for diagnosing PE. However, the interpretation of CT images can be challenging, and radiologists may miss small or subtle signs of PE. Computer-aided diagnosis (CAD) systems can help overcome these challenges and improve the accuracy and efficiency of PE diagnosis[1]. In this study, we aim to evaluate the performance of a CAD system that assesses the distribution of pulmonary lobar density in PE patients and to compare the histogram-based data with controls.

Methods & Materials

Between August 2016 and December 2018, 93 patients who were diagnosed with PE and 99 individuals who had negative pulmonary CTA for PE were included in this retrospective study. PE patients were classified into three groups namely massive, submassive, and non-massive according to the involvement of pulmonary artery branches in the CTA. All images were analyzed with CAD software integrated into the offline workstation (syngoCTPulmo 3D, Siemens Healthcare, Erlangen, Germany). Lobe-based histogram analyses were conducted automatically using the software and mean lung density (MLD), percentage distribution value (PDV), and kurtosis values were calculated for each patient.

Results

The mean age of the patient population and controls was 61.01 ± 16.9 and 55.3 ± 18.2 respectively. Forty-three percent of the patient population and 34.3% of the controls were male. There was no statistically significant difference by means of age and gender distribution (p=0.678 and 0.205 respectively). Histogram-based analysis showed that kurtosis and PDV calculations showed statistically significant differences between patients and controls whereas no significant differences were observed by means of MLD ($p < 0.01$, < 0.01, and 0.656 respectively)

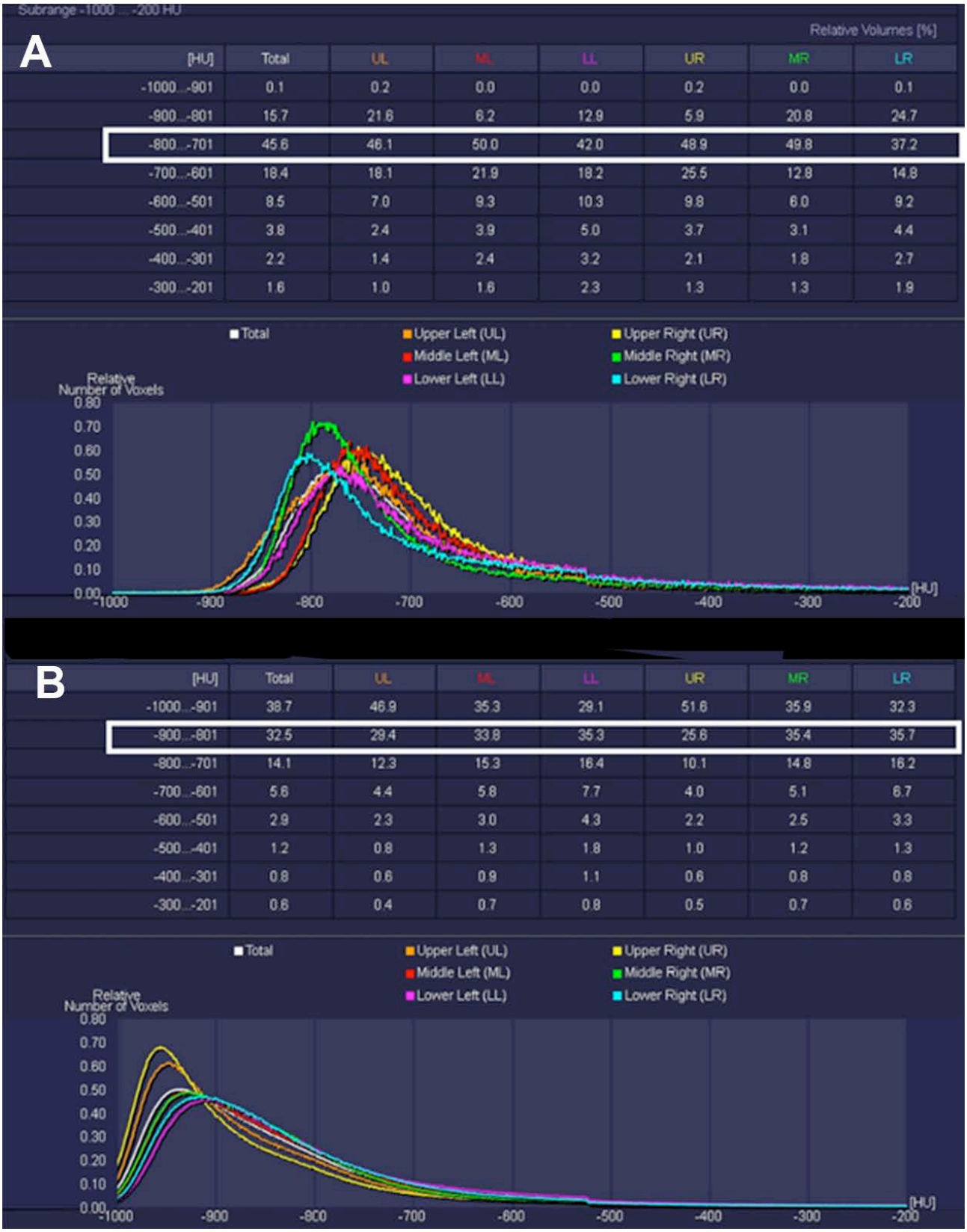

Histogram-based anaylsis of CT image in patients with (A) and without (PE). Density curves belong to different lobes shifted to left and showed negative kurtosin in PE.

.

In subgroup analysis, kurtosis values were significantly different in massive, submissive, and non-massive groups ($p < 0.05$ according to the posthoc test).

Conclusion

In our study, we have found that CAD with histogram-based analysis can help the radiologist to diagnose PE in individuals who presented to the CT unit. Furthermore, the CAD system was also proven to be effective in discriminating massive, submassive and non-massive forms of PE in an acute setting.

References:

[1] Pu, J., Wang, X., Zhang, Y., & Huang, R. , (2019), Computer-aided diagnosis of pulmonary embolism in computed tomography pulmonary angiography based on a deep learning algorithm, European Radiology, 3078-3087, 29(6)

A-667

Correlation of 3D Pulmonary Vessel Morphology with Severity of Chronic Obstructive Pulmonary Disease

T. Fero[1,2], M. Pienn[3], B. Jobst[1,2], J. Biederer[1,2], H.-U. Kauczor[1,2]
[1]Department of Diagnostic and Interventional Radiology, University Hospital Heidelberg, Heidelberg, Germany, [2]Translational Lung Research Center Heidelberg (TLRC), German Lung Research Center (DZL), Heidelberg, Germany, [3]Ludwig Boltzmann Institute for Lung Vascular Research, Graz, Austria

Purpose/Objectives
This study aimed to detect non-invasive markers for diagnosing and characterizing chronic obstructive pulmonary disease (COPD) using non-contrast-enhanced computed tomography (CT) of the chest by evaluating the correlation between structural changes in pulmonary vessels and the severity and time course of the disease.
Methods & Materials
Inspiratory and expiratory low-dose CT of participants in the German COPD cohort study COSYCONET were analyzed using a fully automatic pulmonary vessel analysis software developed at the Ludwig Boltzmann Institute in Graz, Austria. Pulmonary vessel structure changes, including vessel type, tortuosity, and numbers in specific size categories, were evaluated and compared with established clinical and radiological COPD indices. Statistical models were developed to search for effective combinations of parameters to establish a reliable and reproducible concept.
Results
Indices of arterial tortuosity, venous volumes, and vessel numbers demonstrated strong relationships with clinical parameters and quantitative CT outcomes. Expiratory vascular measurements had high predictive value for pulmonary function tests and airway abnormalities, while inspiratory CT scans were more effective in predicting emphysema. Generally, reduced vessel metrics, partly corresponding to decreased %predicted values of forced expiratory volume in 1 second (FEV1), indicated a more severe form of COPD. Combining multiple parameters in models improved the predictive value of vessel metrics, achieving excellent diagnostic accuracy and acceptable severity assessment, with the sum-of-angles metric (SOAM) proving valuable for evaluating tortuosity.

Some diverging findings emerged within this study. Multilevel linear modeling analysis revealed a higher number of distal pulmonary vessels at expiration in patients with severe clinical impairment. Additionally, a relationship was identified between lower tortuosity values, mainly in arteries, and worsening medical conditions alongside progressive pathological changes, contrasting with the limited available literature. Further investigation is required to determine if these conflicting results accurately reflect pathology and if separating emphysema-type and airway-type COPD patients enhances the predictive value of vessel metrics and resolves discrepancies.
Conclusion
CT-based morphometric parameters of the pulmonary vascular tree reflect clinical manifestations in COPD patients. Vessel metrics, notably when combined, have a high predictive value and should be considered promising candidates for image-based disease biomarkers. Further research is warranted to explore the clinical value of this approach.

A-701

Correlation of quantitative analysis of HRCT and pulmonary function tests in interstitial lung diseases

M. Benegas[1], E. Matheus Ramírez[2], M. Noboa-Sevilla[3], A. Frino García[3], F. Hernández-González[3], J. Sellarés[3], M. Sánchez[1]
[1]Hospital Clínic- Barcelona, Radiology, Barcelona, Spain, [2]Hospital General Monte Sinaí, Pulmonology, Guayaquil, Ecuador, [3]Hospital Clínic- Barcelona, Pulmonology, Barcelona, Spain

Purpose
The aim of the study was to analyze the correlation between pulmonary function tests and values obtained using lung texture analysis on quantified HRCT in a group of patients with interstitial lung diseases (ILD) from the ILD unit of our hospital.
Methods & Materials
A total of 121 patients from the ILD Unit of Hospital Clínic from Barcelona were evaluated. Pulmonary function tests (FVC, DL_{co}, and K_{co}) and HRCT were performed. The following parameters of automated quantification of HRCT were obtained by software analysis (Imbio): lung volume (Vol), hyperlucency (HL), ground glass (GG), reticulation (R), honeycombing (HC) and pulmonary vascular volume (PVV).
Results
Of the 121 patients, 67 men (55%) and 54 women (45%) with a mean age of 69±11 years, 20 patients diagnosed with idiopathic pulmonary fibrosis (IPF) (17%), 83 patients with non-IPF ILD (69%)) and 18 patients with sarcoidosis (15%) were included. The correlation analysis was good with an inverse relationship between PVV and DL_{co} (r= -0.60, p= <0.001), FVC (r= -0.46, p= <0.001), and K_{co} (r= - 0.40, p= <0.001). The correlation between FVC and Vol was moderate with a positive linear relationship (r= 0.53, p= <0.001).
Conclusion
Our study shows a correlation between FVC and DL_{co} and quantitative analysis of HRCT (Vol/PVV) in patients with ILD. The use of lung texture analysis with quantitative imaging on HRCT can be an objective assessment tool in the diagnosis and follow-up of patients with ILD.

A-568

Correlations between chest wall muscle atrophy assessed by Computed Tomography and cardiopulmonary function in Systemic Sclerosis

S. Paciulli[1], M. Giannetti[1], A. Gigante[2], G. Cundari[1], C. Pellicano[2], A. Colalillo[2], L. Conia[1], C. Catalano[1], E. Rosato[2], N. Galea[1]
[1]Sapienza University of Rome, Departiment of Radiological, Oncological and Pathological Sciences, Rome, Italy, [2]Sapienza University of Rome, Department of Translational and Precision Medicine, Nephrology Unit,, Rome, Italy

Purpose/Objectives
Systemic sclerosis (SSc) is a multi-organ disease, which can affect the lung parenchyma, resulting in an interstitial lung disease (ILD), and skeletal muscle. Pulmonary function in those patients is influenced by lung disease and chest wall muscles activity. High-resolution CT is a valuable tool to evaluate both ILD progression and chest wall muscle atrophy.
The purpose of our study was to investigate the contribution of chest wall muscle hypotrophy to the impairment of ventilatory efficiency and exercise capacity, in patients with SSc.
Methods & Materials
In this single-center retrospective study, 44 SSc patients (7/37: M/F) underwent cardiopulmonary exercise testing (CPET), high-resolution chest CT (HRCT) and transthoracic echocardiography. The chest wall muscle area was evaluated at the level of the 9th thoracic vertebra on CT images by two independent evaluators blinded to the patient information. We also evaluated BMI, SSc duration and variant, CPET parameters (maximum oxygen uptake [VO2 max], VO2 anaerobic threshold [AT]; arterial oxygen saturation [SpO2]; maximum expired ventilation [VE max]) and transthoracic echocardiography findings.
Results
Median age of our study population was 53 years old [43.5-58] with a BMI of 22.10 kg/m2 [24.25-20.55]. Twenty-two (50%) presented with diffuse cutaneous manifestations (dcSSc variant) and 22 (50%) with localized cutaneous disease (lcSSc variant). Median disease duration was 9.50 years [5.5-15]. Median chest wall area was 617.5 cm^3 [799.5-253.5]. As regards pulmonary functional parameters we found a median %FVC of 100 [107-88]; a %FEV1 of 95 [104.5-86]; a %TLC of 93 [103.5-81,5]; a %DLCO of 77 [86-68.5]; a DLCO/Va of 81.5 % [93.5-69]. Transthoracic echocardiography revealed a median ejection fraction of 60 % [62,5-60]; a right ventricular transverse diameter of 29 mm [31-26]; a left ventricular transverse diameter of 44mm [46-42], a TAPSE of 22 [25-21] and a PAPs of 28 [30-25]. CPET parameters were represented as follows: max_Watts 80% [105,5-62]; VO2max 1211 ml/min [1451.1026.5]; VO2max 20.7 ml/min/Kg [23.82-17.9]; VO2@AT 789.0 ml/min [952-679] ; OUES 1364 ml/min/L/min [1629-1229]; VEmax 49.55 L/min [60.5-44.4]; VTmax 1.51 L [1.88-1.21]; VO2/HRmax 7.95 mL/beat [9.35-6.90] and SpO2max 98% [99-97].
A significant positive bivariate correlation ($P<0.05$) was demonstrated between chest wall volume and BMI and CPET parameters (max_ Watts, VO2max, OUES, VEmax, VTmax, VO2/HRmax, SpO2max).
Conclusion
In SSc-patients chest wall muscle area is associated with ventilatory efficiency and exercise capacity assessed by CPET. Our findings call attention to the role of the hypotrophy of chest wall skeletal muscle in the development of cardiopulmonary complications in SSc patients.

A-154

CT Findings of SMARCA4-deficient Non-Small Cell Lung Cancer in 9 Patients

J. H. Kim[1], Y. K. Cha[1], J. H. Woo[1], J. Han[2], M. J. Chung[1]
[1]Samsung Medical Center, Radiology, Seoul, Republic of Korea (South Korea), [2]Samsung Medical Center, Pathology, Seoul, Republic of Korea (South Korea)

Purpose

Loss of the BAF (SWI/SNF) complex subunit encoded by SMARCA4, also known as BRG1, was reported in 2000 by Wong et al.[1]. SMARCA4 inactivating mutations are described in two thoracic tumors: SMARCA4-deficient undifferentiated tumor (SD-UT, formerly known as SMARCA4-deficient sarcoma) and SMARCA4-deficient non-small cell lung carcinoma (SD-NSCLC)[2].
Currently, only SD-UT is recognized as a separate entity in the 8th edition of the WHO classification that should be differentiated from SD-NSCLC[2]. However, importance of SD-NSCLC, and relationship between these two enitities are emerging as noteworthy subjects. A recent study suggests a biological continuum between these two tumors, that these entities are linked at molecular level, as they share genomic alterations typical of smoking related NSCLC and have a high tumor mutational load[3][4]. Therefore, further investigation is required in order to achieve better understanding of relationship between these two entities.
To the best of our knowledge, there has been no studies regarding imaging features of SD-NSCLC, Aim of our study was to retrospectively assess the clinical, imaging features of SD-NSCLC.

Methods & Materials

We searched medical records between January 2018 to November 2022 at Samsung Medical Center, a tertiary referral hospital located in Seoul, South Korea, by using the term “SMARCA4 deficient Non Small Cell lung cancer”. Retrospectively reviewed for clinical data and histopathologic reports. CT studies were performed using various helical CT scanners (mostly 16- to 64-MDCT scanners) from several vendors.

Results

Demographic features and clinical findings of SD-NSCLC are summarized in Table 1.

Variable	Data
Age (y)	64 (46-74)*
Sex	
Male	9 (100)
Female	0 (0)
Smoking history	
Current smoker	5 (55.6)
Ex smoker	4 (44.4)
Never smoker	0
Average Pack years	51.9
CT Visual classification of Emphysema	
Yes	5 (55.6)
Mild	5
Moderate	0
Confluent	0
Advanced destructive	0
No	4 (44.4)
Symptoms	
Yes	1 (11.1)
No	8 (88.9)
Treatment	
Operation	5 (55.6)
Other	4 (44.4)

Demographic Features and Clinical Findings of Nine Patients with SMARCA4-deficient Non Small Cell Lung Cancer
The primary tumor appeared as a solitary nodule (n = 4) or mass (n = 5), and tumor size ranged from 8 to 62 mm in the greatest dimension (median, 42 mm). All the tumors had well-defined margins with mostly lobulated contour (n=8), and only one tumor showed spiculated contour. The net enhancement value of primary tumor ranged from 8 to 43 HU (median, 24 HU). Most of the tumors (7 cases) were located in the peripheral portion of the lung, and only two cases showed primary tumors located in the central portion. In the aspect of direct invasion from primary tumor to adjacent structures, most of the tumors showed pleural, chest wall invasions (7 out of 9 cases). Even when the tumor was relatively small, the tumor showed direct invasion to the adjacent chest wall (case 3)

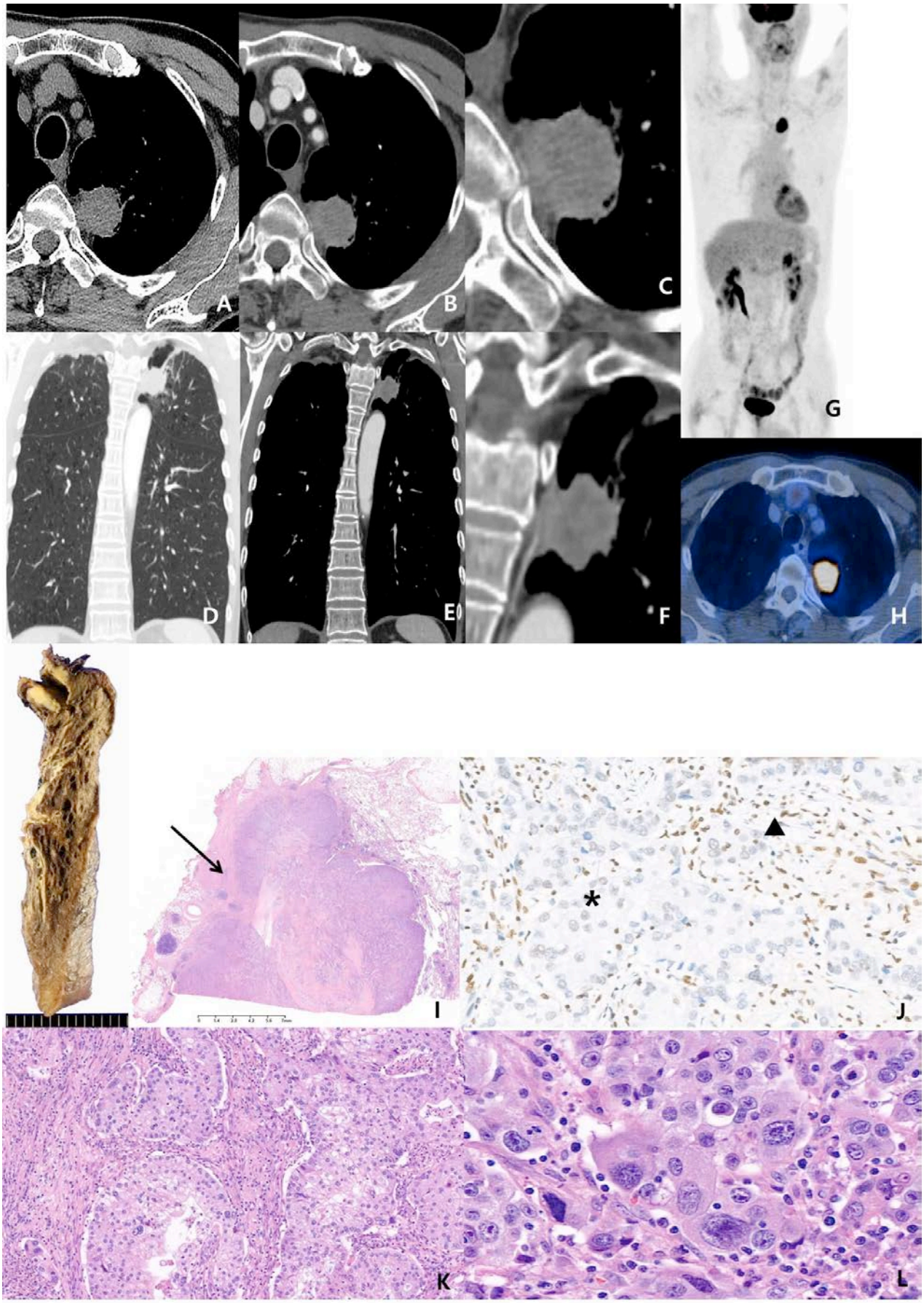

A 26mm enhancing nodule (A,B), shows invasion to adjacent chest wall (C,D,E,F,I). It shows intense FDG uptake(G,H). It consists of poorly differentiated adenocarcinoma(K), large pleomorphic tumor cells(L). BRG1 immunostaining(J), loss of SMARCA4 expression in tumor cells (*) in contrast with normally stained inflammatory cells(Δ).

. Five patient were presumed to have metastastatic lymph nodes on imaging, and two patients showed lymph nodes with necrosis.

CT Imaging Finding	Data
Primary tumor location	
RUL	3
RML	0
RLL	2
LUL	4
LLL	0
Distribution	
Central	2 (22.2)
Peripheral	7 (77.8)
Margin	
Relatively well marginated	9 (100)
Ill defined	0 (0)
Shaped	
Round	0 (0)
Lobulated	8 (88.8)
Spiculated	1 (11.1)
Mean precontrast HU	25.4
Mean postcontrsat HU	52.2
Mean Δ HU	24
Calcification	
Yes	0 (0)
No	9(100)
Necrosis	
Yes	0 (0)
No	9(100)
Pleural tagging	
Yes	1 (11.1)
No	8 (88.8)
Pleural effusion	
Yes	2 (22.2)
No	7 (77.8)
Invasion to adjacent pleura and chest wall	
Yes	7 (77.8)
No	2 (22.2)
Lymph node enlargement	
Yes	5 (55.6)
No	4 (44.4)
Intrathoracic metastasis	
Yes	5 (55.6)
No	4 (44.4)
Extrathoracic metastasis	
Yes	3 (33.3)

Image findings of SMARCA4-deficient Non Small Cell Lung Cancer

			CT Imaging findings							^{18}F FDG PET-CT				
	Age /Sex	Pack years	Lobe (location)	Δ size mm [d](F/U)	Δ HU	shape	pleural involvement on CT	lymph node metastasis on imaging (Necrosis)	Intra-/Extrathoracic metastasis on imaging	SUVmax	FDG uptake pattern	Treatment Modality	pTNM	Clinical outcome
1	67/M	45	RLL (central)	-18 (84)*	18	Lobul-ated	None	Ipsilateral interlobar (Absent)	Mulitple bone metastases	N/A (outside image)	Diffuse	CTx.	N/A	Under treatment
2	59/M	17	LUL (peripheral)	11 (26)	12	Lobul-ated	Pleural tagging	None	None	14.1	Diffuse	Lobectomy+adjuvant CTx.	T4N0	NED
3	67/M	40	LUL (peripheral)	6 (79)	35	Lobul-ated	Pleural thickening	None	None	12.7	Diffuse	Lobectomy+adjuvant CCRTx.	T3N0	NED
4	62/M	40	LUL (peripheral)	37 (111)	40	Lobul-ated	Pleural thickening with effusion	Ipsilateral hilar, paraaortic (Absent)	Mulitple bone metastases	16.5	Diffuse	CTx.	N/A	Death
5	67/M	140	RUL (peripheral)	9 (166)	43	Lobul-ated	None	None	None	12.9	Diffuse	Lobectomy	T1bN0	NED
6	46/M	30	RUL (peripheral)	10 (50)	8	Lobul-ated	Pleural thickening	None	None	N/A (outside image)	Diffuse	Lobectomy+adjuvant CTx.	T3N0	Under treatment
7	74/M	80	LUL (peripheral)	-5 (102)*	40	Spicul-ated	Pleural thickening with effusion	Both supraclavicular, mediastinal, hilar,ipsilateral interlobular (Present)	Multiple bone metastases	9.6	Diffuse	CTx.	N/A	Under treatment
8	63/M	30	RLL (peripheral)	-8 (80)*	21	Lobul-ated	Pleural thickening	Ipsilateral hilar ,interlobar, peribronchial, subcarinal (Present)	Multiple metastatic pulmonary nodules	14.9	Diffuse	CTx.	N/A	Under treatment
9	69/M	45	RUL (central)	4 (22)	24	Lobul-ated	None	None	None	N/A (outside image)	Diffuse	Lobectomy+adjuvant CTx.	T2bN0	Under treatment

Clinical and radiological feature of Thoracic SMARCA4-deficient Non Small Cell Lung Cancer

Conclusion

In conclusion, SD-NSCLC appeared as relatively well-defined mass, with mostly lobulating contour, distributed in the peripheral portion of the lung with frequent pleural, chest wall invasion.

References:

[1] A. K. Wong, F. Shanahan, Y. Chen, L. Lian, P. Ha, K. Hendricks, et al., (2000), BRG1, a component of the SWI-SNF complex, is mutated in multiple human tumor cell lines, CANCER RESEARCH, 6171-7, Issue 21

[2] A. G. Nicholson, M. S. Tsao, M. B. Beasley, A. C. Borczuk, E. Brambilla, W. A. Cooper, et al., (2022), The 2021 WHO Classification of Lung Tumors: Impact of Advances Since 2015, J Thorac Oncol , 362-387, 3

[3] F. Le Loarer, S. Watson, G. Pierron, V. T. de Montpreville, S. Ballet, N. Firmin, et al., (2015), SMARCA4 inactivation defines a group of undifferentiated thoracic malignancies transcriptionally related to BAF-deficient sarcomas, Nat Genet , 1200-5, 47

[4] N. Rekhtman, J. Montecalvo, J. C. Chang, D. Alex, R. N. Ptashkin, N. Ai, et al., (2020), SMARCA4-Deficient Thoracic Sarcomatoid Tumors Represent Primarily Smoking-Related Undifferentiated Carcinomas Rather Than Primary Thoracic Sarcomas, J Thorac Oncol, 231-247, 2

A-209

CT-findings and pattern recognition on ultra-low-dose CT and their relation to the type of pathogen in patients suspected of pneumonia: a multicentre observer study

I. van den Berk[1], M. Kanglie[1], T. van Engelen[2], M. Hovinga de Boer[1], W. de Monye[3], S. Bipat[4], P. Bossuyt[1], J. Stoker[4]
[1]Amsterdam UMC, Department of Epidemiology & Data Science, Amsterdam, The Netherlands, [2]Amsterdam UMC, Internal Medicine, Amsterdam, The Netherlands, [3]Spaarne Hosptial, Radiology, Haarlem, The Netherlands, [4]Amsterdam UMC, Radiology and Nuclear Medicine, Amsterdam, The Netherlands

Purpose/Objectives
In most patients with pneumonia no pathogen is found at microbiology testing. Reliable differentiation between viral and bacterial pneumonia is not possible with chest X-ray (CXR). The objective of this study was to investigate whether CT findings and pneumonia pattern analysis on ultra-low-dose chest CT (ULDCT) can contribute in identifying the likely type of pathogen.
Methods & Materials
In the OPTIMACT trial 1,208 patients with suspected non-traumatic pulmonary disease underwent ULDCT at the emergency department. Of the 281 patients with a final diagnosis of pneumonia, 96/281 (34%) had a positive microbiology result: in 60 patients viral pathogens, in 48 patients bacterial pathogens, in one a fungus, including 13 patients with multiple pathogens. These 96 ULDCT's were blindly and independently evaluated by two chest radiologists, who reported CT findings, pneumonia pattern, and most likely type of pathogen.
Results
For both radiologists, dominant CT findings significantly differed between pathogen groups (p=0.04; p=0.04). Consolidation was the most frequent dominant CT finding in patients with viral and bacterial pathogens, but it was observed significantly more often in those with a bacterial pathogen: 38/48 and 31/48 (79%, 65%) versus 32/60 and 22/60 (53%, 37%) (p=0.005; p=0.004)).
The lobar pneumonia pattern was more frequently observed in patients with a bacterial pathogen by both radiologists: 23/48 and 18/48 (48%, 38%), versus 10/60 and 8/60 (17%, 13%) for viral pathogens (p<0.001; p=0.004). For the bronchopneumonia and interstitial pneumonia patterns the proportions of viral and bacterial pathogens were not significantly different.
Overall, agreement between the radiologists on the dominant CT finding (viral κ 0.45, bacterial 0.41), and the diagnosis pneumonia was moderate (κ 0.47). The lobar pneumonia pattern showed substantial inter-reader agreement (κ 0.61). The bronchopneumonia and interstitial pneumonia patterns had fair (κ 0.27) and slight (κ 0.042) inter-reader agreement.
Both radiologists suggested a viral pathogen correctly (sensitivity) in only 6/60 (10%), and a bacterial pathogen correctly in 34/48 (71%) cases.
Conclusion
At ULDCT a lobar pneumonia pattern had a substantial inter-reader agreement and was significantly more often observed in bacterial infection. However, reliable differentiation between viral and bacterial pneumonia could not be made by pattern recognition on ULDCT.

A-360

Diagnostic performance of synthetic CXR obtained from CT average intensity projection (AIP) reconstruction in the depiction of chest abnormalities

S. Schiro[1], R. E. Ledda[1], G. Milanese[1], L. Leo[1], C. Commisso[1], C. Branchi[2], N. Sverzellati[1]
[1]Università degli Studi di Parma, Parma, Italy, [2]Azienda Ospedaliera Universitaria di Parma, Parma, Italy

Purpose/Objectives

To investigate the diagnostic performance of synthetic chest x-ray (s-CXR) in detecting pleuro-parenchymal abnormalities.

Methods & Materials

A total of 134 subjects (mean age 64 years old ±SD 16; 55% women) who underwent CXR and chest CT within 7 days were enrolled. Average intensity projection (AIP) reconstruction was applied to coronal CT reformatted images to obtain s-CXR. Three radiologists independently reviewed both standard CXR and s-CXR images for the presence of nodule/mass, consolidation, atelectasis, pleural effusion, and soft tissue abnormality.

Sensitivity, specificity, PPV, PPN and accuracy were calculated for standard CXR and s-CXR images. Differences in sensitivity, specificity, PPV, PPN and accuracy were compared with the McNemar test. Inter-observer agreement was tested by Cohen's K test with quadratic weights.

Results

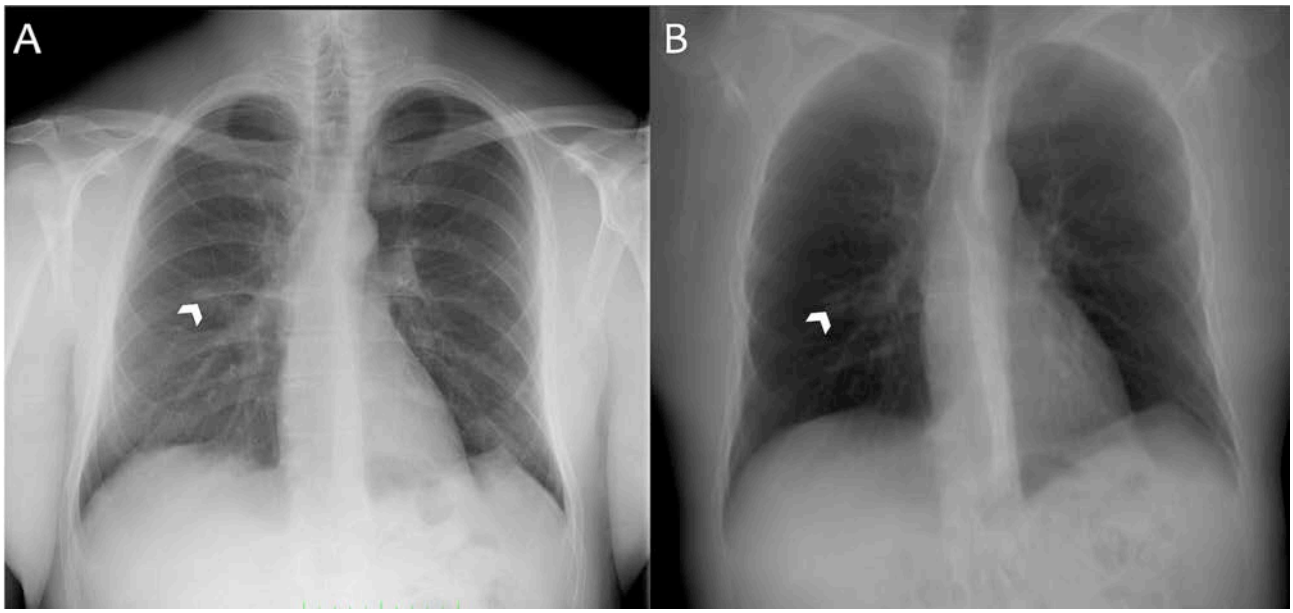

(A) Boa_Image_Frame chest X-ray PA view showing a perihilar nodule on the right lung (chevron), less recognizable on synthetic Chest-Xray obtained by the AIP reconstruction (B).

standard CXR compared to s-CXR showed a higher sensitivity for consolidation (45.2-100%), atelectasis (60-90%) and for soft tissue abnormality (68.4-78.9%) among all readers. s-CXR compared to standard CXR showed a higher specificity for nodule/mass (89.2-96.4%), for pleural effusion (95.7-100%) and soft tissue abnormality (100%), among all readers. Statistically significant differences between standard CXR and s-CXR were found for nodule/mass ($p= 0.019$) and soft tissue abnormality ($p=<0.001$) that were both slightly underestimated by s-CXR. The inter-observer agreement for standard CXR and s-CXR was similar indeed K_w values ranged between 0.30-0.81 and 0.31-0.77, respectively.

Conclusion

We observed a similar diagnostic performance of s-CXR over standard CXR in the depiction of pleuro-parenchymal abnormalities. s-CXR underestimated nodule/mass and soft tissue abnormality depiction compared to standard CXR.

A-500

Difference in the prognostic value of lymphovascular and visceral pleural invasion based on presence of ground-glass opacity in stage I lung adenocarcinoma

H. Park, J. Choe, S. M. Lee, J. B. Seo
Asan Medical Center, Seoul, Republic of Korea (South Korea)

Objectives

Lymphovascular invasion (LVI) and visceral pleural invasion (VPI) have been reported to be risk factors for stage I non-small cell lung cancer. However, only VPI was incorporated into the current 8th Tumor–Node–Metastasis (TNM) classification and there is still a debate regarding the prognostic implication of LVI in stage I lung adenocarcinoma. This study aimed to explore the prognostic effect of LVI and VPI in stage I lung adenocarcinoma based on the presence of ground-glass opacity.

Methods & Materials

We retrospectively evaluated the prognostic value of clinical and radiologic factors regarding the recurrence-free survival (RFS) and overall survival (OS) of patients with clinical stage I lung adenocarcinomas who underwent lobectomy between 2010 and 2019. Patients were categorized based on the presence of GGO (part-solid vs. solid nodule) on chest CT, and multivariable Cox regression analysis for RFS and OS was performed to evaluate the prognostic significance of pathologic LVI and VPI adjusted by other clinical variables.

Results

A total of 924 patients (mean age, 62.5 ± 9.2 years; 505 women) were included with 525 [56.8%] patients having part-solid nodules. LVI was diagnosed in 116 (116/924, 12.6%) and VPI in 139 (139/924, 15.0%) patients, which were both significantly higher in solid nodules compared with part-solid nodules (20.1% vs. 6.9%, $P < .001$ for LVI; 18.5% vs. 12.4%, $P = .012$ for VPI). In multivariable analysis, LVI and VPI was significant prognostic factors (hazard ratio [HR], 1.87, $P = .004$ for LVI; HR, 1.71, $P = .019$ for VPI) for RFS in patients with solid nodules but not in those with part-solid nodules ($P = .78$ for LVI; $P = .98$ for VPI). For OS, LVI and VPI were not a significant prognostic factors in either of patients with solid nodules or part-solid nodules in multivariable analyses (for all, $P > .05$).

Variable (reference)	Model 1, in part-solid nodules - Adjusted HR	Model 1, in part-solid nodules - 95% CI	Model 1, in part-solid nodules - P value	Model 2, in solid nodules - Adjusted HR	Model 2, in solid nodules - 95% CI	Model 2, in solid nodules - P value
Age	1.01	0.98-1.04	.38	1.01	0.99-1.03	.32
Male sex (female)	1.14	0.59-2.23	.69	1.18	0.65-2.16	.59
Ever-smoker (nonsmoker)	0.52	0.63-2.46	.52	0.93	0.51-1.68	.81
Clinical T stage (cT1a)*			.003			.55
cT1b	0.72	0.31-1.67	.80	1.30	0.17-9.68	.80
cT1c	1.92	0.86-4.28	.59	1.73	0.24-12.78	.59
cT2a	2.41	0.96-6.07	.06	1.85	0.25-13.79	.55
Visceral pleural invasion	1.01	0.52-1.98	.98	1.71	1.09-2.68	0.019
Lymphovascular invasion	0.87	0.31-2.44	.78	1.87	1.21-2.88	0.004

Multivariable Cox regression analysis for recurrence-free survival in patients with stage I lung adenocarcinomas–subgroup analysis based on presence of ground-glass opacities.

Conclusion

The presence of LVI and VPI significantly affected RFS in patients with stage I lung adenocarcinoma with solid nodules but not those with in part-solid nodules.

References:

[1] Okubo Y, Kashima J, Teishikata T, et al. , (2022), Prognostic Impact of the Histologic Lepidic Component in Pathologic Stage IA Adenocarcinoma., J Thorac Oncol., 67-75, 17(1), doi: 10.1016/j.jtho.2021.09.006
[2] Higgins KA, Chino JP, Ready N, et al., (2012), Lymphovascular invasion in non-small-cell lung cancer: implications for staging and adjuvant therapy, J Thorac Oncol, 1141-7, 7(7), doi: 10.1097/JTO.0b013e3182519a42
[3] Yun JK, Lee GD, Choi S, et al., (2020), Comparison of prognostic impact of lymphovascular invasion in stage IA non-small cell lung cancer after lobectomy versus sublobar resection: A propensity score-matched analysis., Lung Cancer, 105-111, 146, doi: 10.1016/j.lungcan.2020.04.033
[4] Ruffini E, Asioli S, Filosso PL, et al. , (2011), Significance of the presence of microscopic vascular invasion after complete resection of Stage I-II pT1-T2N0 non-small cell lung cancer and its relation with T-Size categories: did the 2009 7th edition of the TNM staging system miss something?, J Thorac Oncol, 319-26, 6(2), doi: 10.1097/JTO.0b013e3182011f70

A-408

Evaluation of emhysema forms of the chronic obstructive pulmonary disease using 64 slice multidetector computer tomography

U. Batbayar[1], B. Tserendorj[1,2], D. Davaa[3]
[1]Shastin Third State Central hospital, Radiology, Ulaanbaatar, Mongolia, Mongolia, [2]Shastin Third State Central Hospital, Medical Sciences Institute, Ulaanbaatar, Mongolia, [3]Shastin Third State Central Hospital, Radiology, Ulaanbaatar, Mongolia

Purpose/Objectives
To diagnose and characterise emphysema forms of chronic obstructive pulmonary disease using a 64 slice multi detector computer tomography.
Methods & Materials
We evaluated forms of the emphysema (1-centrilobular, 2-paraseptal, 3-panlobular) and a degree of severity (1-mild: few and little sized emphysema, 2-moderate: multiple emphysemas connected with each others, combination with centrilobular and paraseptal, 3-moderate: multiple emphysemas and few bullae connected with each other , 4-extremely severe: multiple bullae with destruction of the lung base structure) for a total of 45 patients who were admitted to the Reference center of Diagnostic Imaging named after R.Purev State Laureate, People's physician and Honorary Professor of the Third State Central Hospital awarded with the Red banner of the Labor with diagnosed chronic obstructive pulmonary disease emphysema by non contrast enhanced, Philips Ingenuity 64 slice lung MDCT between 2020 to 2021. The result of the our study determined by common statistical averages and errors and probabilities of the indicators were determined by Student's criteria.
Results
Of the 45 patients, the youngest age of patients in our study was 45 years and the oldest was 90 years, average age was 69.8±1.4. There were 30 males (66,7%±7.0), 15 females (33,3%±7.0), male:female ratio was 2:1. Among the 45 patients diagnosed with chronic obstructive pulmonary disease emphysema; Centrilobular emphysema was 20(44.4%±7.9), panlobular emphysema was 7(15.6%±5.4), paraseptal emphysema was 18(40.0%±9.2), and by the degree of severity; mild degree of emphysema was 22(48,9%), moderate was 21(46,7%), severe was 2(4,4%). Centrilobular and paraseptal were the predominant emphysema pattern with p value of $P<0.001$.
Conclusion
In our study a patients with COPD emphysema average age was 69.8, male:female ratio was 2:1, centrilobular emhysema incidence was 44.4% and by the severity; 48,9% was mild.

A-358

High-resolution CT in patients after lung transplantation using photon-counting: should we go for higher resolution or lower radiation dose?

A. Dubbeldam[1], V. Van Ballaer[1], E. Muscogiuri[1], L. Cockmartin[1], J. Binst[2], H. Bosmans[2], J. Verschakelen[1]
[1]UZ Leuven, Department of Radiology, Leuven, Belgium, [2]UZ Leuven, Department of Radiology and Medical Physics, Leuven, Belgium

Purpose

As an often young patient population with specific pathology, lung transplant patients could benefit from both high spatial resolution and lower radiation dose [1][2]. We compared image quality on high-resolution photon-counting CT (PCCT) [3] versus conventional high-resolution energy-integrating-detector CT (EIDCT), for both a ultra-high-resolution protocol (Q100) and a radiation-reduced protocol (Q40) [4], in patients after lung transplantation.

Methods & Materials

100 patients post lung transplant, with a PCCT between Dec-2021 and Aug-2022, and with prior EIDCT (<14 months apart), were included. In 49 patients we compared PCCT (0.4mm) at ultra-high-resolution settings (Q100) to previous EIDCT (1.0mm); in 51 patients, we compared PCCT-images (0.4mm) at lower radiation dose settings (Q40) to previous EIDCT (1.0mm). Image quality was scored by 3 thoracic radiologists and one radiologist-in-training, through a 5-point Likert score (-2 to +2) for 7 relevant structures/pathologies (peripheral airways, micronodules, reticulations, pleural thickening, consolidation, GGO and air-trapping) plus an overall quality impression. Statistical analysis used a Mann-Whitney U-test ($p<0.025$ significance level) and a one-sample Wilcoxon signed rank test ($p<0.00625$).

Results

Mean dose length product (DLP) was reduced by 33% in PCCT-Q100 versus EIDCT, by 71% in PCCT-Q40 versus EIDCT, and by 50% in PCCT-Q100 versus Q40 ($p\leq0.001$). For PCCT-Q100, the median visual grading analysis (VGA) score was significantly better (median>0; $p\leq0.003$) for all structures (excluding GGO with N=2), but without a perceived diagnostic impact (median<2; $p\leq0.002$).

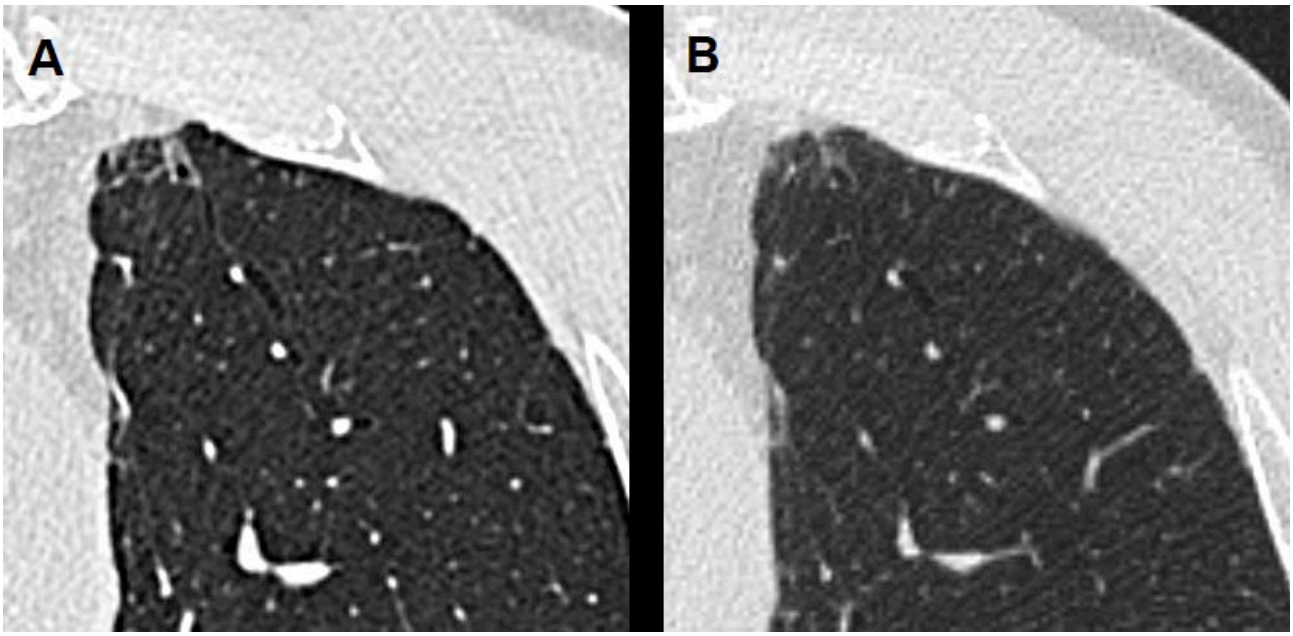

High-resolution CT at PCCT-Q100 dose settings (0.4mm) (A) compared to EIDCT (1.0mm) (B) for peripheral airways. Median VGA-score for readers was 1, suggesting a subjectively better image quality, without impact on diagnosis for this structure. DLP was reduced from 510.10mGy*cm to 93.44mGy*cm (-81,68%).

A score of -1 (worse visibility) was given in 3% of scorings, and +2 (better visibility with diagnostic impact) in 5%. For the PCCT-Q40, the median VGA-score was not significantly better than EIDCT for most structures (median>0; $p\geq0.008$), except peripheral airways, micronodules and overall impression ($p\leq0.002$).

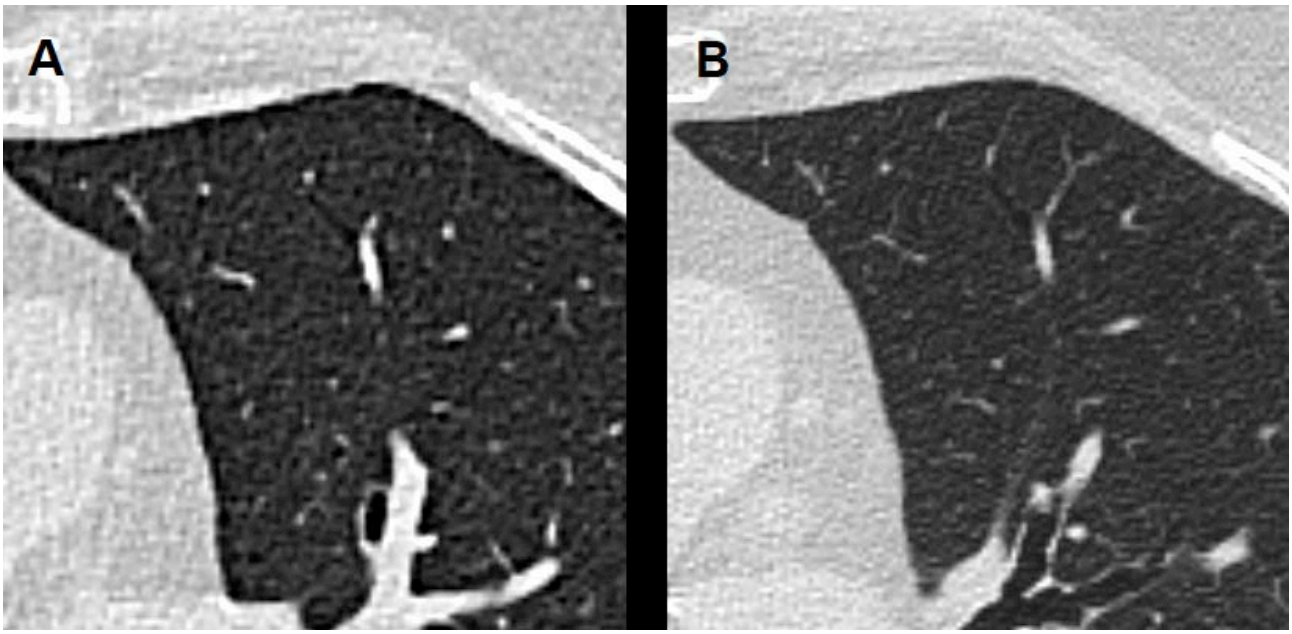

High-resolution CT at PCCT-Q40 dose settings (0.4mm) (A) compared to EIDCT (1.0mm) (B) for peripheral airways. Median VGA-score for readers was 0, suggesting no subjective difference in image quality for this structure. However, DLP was reduced from 550,70mGy*cm to 139,64mGy*cm (-74,64%).
A score of -1 was given in 6% of scorings, and +2 in 1%. Comparing Q100 to Q40, the visual grading characteristics curve for all structures together showed better quality for Q100 (AUC0.67; CI95% 0.62-0.72).

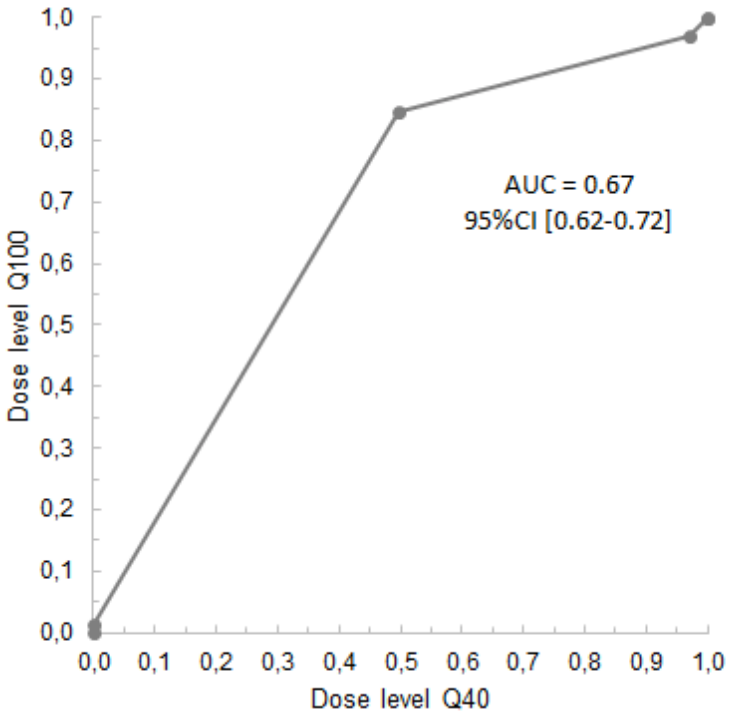

Visual grading characteristic curve, with cumulative relative frequency of each score, for Q100 versus Q40, shows a superior image quality for dose level Q100 compared to Q40 with area under the curve of 0.67.
For individual structures, only peripheral airways, pleural thickening and overall impression were significantly better in Q100 versus Q40. A score of 0 (equal visibility) was given in 26% of scorings in Q100, and 53% in Q40.

Conclusion

A significant dose reduction was achieved switching to the Q40-PCCT protocol. Image quality dropped compared to Q100-PCCT, but was non-inferior to EIDCT. Therefore, a significant radiation dose reduction is feasible, and should be considered for this specific patient population.

References:

[1] Kim SJ, Azour L, Hutchinson BD et al, (2021), Imaging course of lung transplantation: from patient selection to postoperative complications., Radiographics, 1043-1063, 41, 2023-01-01
[2] Fitton I, Revel M-P, Burgel P-R et al, (2019), Cumulative radiation dose after lung transplantation in patients with cystic fibrosis,

Diagnostic and Interventional Imaging, 287-294, 100, 2023-01-01
[3] Si-Mohamed SA, Miailhes J, Rodesch PA et al, (2021), Spectral photon-counting ct technology in chest imaging, J Clin Med , 1-18, 10, 2023-01-01
[4] Graafen D, Tilman E, Halfmann M et al, (2022), Dose reduction and image quality in photon-counting detector high-resolution computed tomography of the chest: routing clinical data, JTI, 315-322, 37, 2023-01-01

A-726

HRCT prevalence of extra-pulmonary findings in patients with idiopathic pulmonary fibrosis

L. Reali[1], C. Scavone[1], S. Galioto[1], E. Sciacca[2], G. Muscato[2], L. A. Mauro[1], C. Vancheri[2], S. Palmucci[1], A. Basile[1]
[1]Policlinico di Catania, Radiology 1, Catania, Italy, [2]Policlinico di Catania, Pneumology, Catania, Italy

Purpose

The aim of this paper is to investigate the prevalence of HRCT extra-pulmonary findings in a population of patients with Idiopathic Pulmonary Fibrosis (IPF).

Methods & Materials

This retrospective study recruited patients exploring – from January 2022 to October 2022 – the radiological archive and the clinical electronic database of interstitial lung diseases of our hospital. We have enrolled patients with a diagnosis of IPF – based on the most recent published guidelines [1] – having a volumetric HRCT scan at the diagnosis; for each clinical case, Pulmonary Function Tests (PFTs) and GAP stage were registered.

HRCT images, were interpreted in consensus by two thoracic radiologists, focusing on the following imaging features: pulmonary artery/ascending aorta diameter (PA:A) ratio, number of enlarged mediastinal lymph nodes (having short axis >1 cm), pericardial effusions, gastro-esophageal junction hernia, dorsal vertebral collapses or/and hyperkyphosis; other extra-pulmonary findings – such as immersed goiter or elastofibroma dorsi – were also listed.

Results

We have found a total of 50 IPF patients in our retrospective analysis, including 18 females and 32 males, with a middle age of 73.3±7.3 years. PA:A ratio>1 was observed in 6 patients (12%); 12 cases (24%) reported a value of ratio ranging from 0,9 up to 1. The remaining patients showed a ratio value<1. Three or more enlarged lymph nodes (having short axis >1 cm) were observed in 6 patients (12%), while 2 enlarged nodes were found in 12 patients (24%). Pericardial effusion was demonstrated in 27 patients (54%). In three patients (6%), dorsal vertebral collapses were detected at HRCT diagnosis.

Conclusion

Extra-pulmonary findings should be highlighted in IPF diseases, since that these comorbidities may influence the prognosis and the management of patients [2]. Namely, enlarged lymph nodes and abnormal PA:A ratio have been associated with intermediate-advanced stage of disease.

References:

[1] Raghu et al., (2022), Idiopathic pulmonary fibrosis (an update) and progressive pulmonary fibrosis in adults: an official ATS/ERS/JRS/ALAT clinical practice guideline, American Journal of Respiratory and Critical Care Medicine 205.9
[2] Raghu et al., (2015), Comorbidities in idiopathic pulmonary fibrosis patients: a systematic literature review, European Respiratory Journal 46.4

A-320

Imaging features and pathology of mediastinal masses of adults and childrenpatients at Sultan Qaboos University Hospital, Oman.

H. Al Dhuhli[1], S. Al Shafaai[2]
[1]Sultan Qaboos University Hospital, Radiolgy, Muscat, Oman, [2]Sultan Qaboos University, College of Medicine, Muscat, Oman

Purpose
The aim of this study is to identify the imaging characteristics of mediastinal masses in adult and children patients at Sultan Qaboos University Hospital with pathology correlation.
Methods & Materials
A retrospective study.The study included adult and pediatric patients diagnosed with mediastinal masses between January 2011 and December 2021. All cases underwent surgery or had biopsy. The location, size, attenuation, presence of fat and/or calcifications vascular encasement, vascular occlusion and signs of invasion were recorded.
Results
A total of 92 cases of mediastinal mass were included in the study. The age range affected by mediastinal tumor was between 6 to 83 years, with the mean age of 44.9 years. Fifty four of the cases were male and 35 cases were female. Most of the mediastinal masses (83%) are malignantfollowed by posterior compartment (15.2%) and middle compartment (4.3%). Lymphoma was the commonest malignant tumor involving the mediastinum (36%) followed by metastasis (27%), thymic masses (17%) and germ cell tumors (7%).

Pathology	Number
Metastasis	25
Hodgkin lymphoma	15
T-cell lymphoblastic lymphoma	11
primary large B cell lymphoma	6
Thymoma	6
Schwannoma	4
invasive thymic ca	4
Mixed grem cell tumor	2
thymic hyperplasia	2
Esophageal cancer	2
Solitary fibrous tumor	1
Langerhans cell histiocytosis	1
Teratoma	1
Cystic Teratoma	1
Malignant epithelioid mesothelioma.	1
NUT carcinoma	1
Invasive thymoma	1
pleomorphic myxoid liposarcoma	1
Mediastinal adenocarcinoma	1
Thymic cyst	1
germ cell tumor	1
Nonseminomatous germ cell tumor	1
burkit lymphoma	1
Thyroid tissue	1

Spectrum of pathology of mediastinal masses
No image found for uniqueTag: IMG:image02#

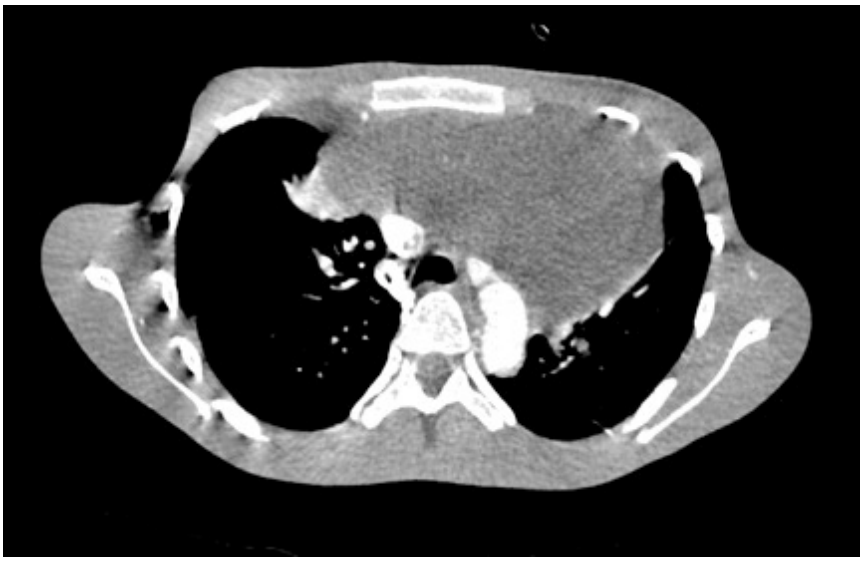

Pleomorphic myxoid liposarcoma. An 18-year-old male with anterior mediastinal of low density mass

Conclusion

CT plays a mojor role in locating medistinal masses and suggests features of certain pathology

A-210

Imaging of Pulmonary Manifestations of Inflammatory Bowel Disease with Clinico-pathologic Correlation.

S. Ghosh
The Cleveland Clinic, Thoracic Imaging, Imaging Institute, Cleveland, United States of America

Purpose/Objectives

The primary objective of our study was to perform a comprehensive review of CT imaging findings of the thoracic manifestations of biopsy-proven inflammatory bowel disease (IBD) in the absence of infection, and characterize different morphologic patterns based on involvement of airways, lung parenchyma including interstitium, and serosal linings with or without involvement of the chest wall, thoracic lymph nodes and/or pulmonary vasculature.

The secondary objective was to ascertain the incidence of infection as a cause for pulmonary manifestations in IBD after correlation with clinical and laboratory data.

Methods & Materials

Ours is a single-center, retrospective review of 32 adult patients with thoracic manifestations of inflammatory bowel disease, performed at a tertiary-care, academic medical center that serves a diverse population.

The study cohort included inpatients and outpatient adults who were diagnosed with thoracic manifestations of inflammatory bowel disease in the last 4 years, consulted the pulmonary medicine service, obtained chest CT scans, and underwent lung biopsy.

Results

32 patients were selected, of whom 15 had infection and 17 patients had thoracic manifestations of IBD which were not accounted by infection. CT imaging of thoracic manifestations was classified into the following compartments: airways (small, intermediate and large), lung parenchyma including interstitium (nodules, consolidations, ground-glass opacities, reticulations), serosal linings (pleural, pericardial), thoracic lymph nodes, pulmonary vasculature and miscellaneous (cardio-mediastinal structures and chest wall). Most of the 17/32 patients showed involvement of more than one compartment. Airway involvement was seen in 8 patients (25%), most commonly bronchiectasis, followed by bronchiolitis and tracheobronchitis. Lung involvement was noted in 15 patients, mostly nospecific nodules of varying sizes (12; 4 = <4 mm, 6 = 4-10 mm, 1 = >10 mm). One had biopsy-proven necrobiotic cavitary nodules. Organizing pneumonia pattern of lung injury was diagnosed in 3 patients (9%), eosinophilic pneumonia in 1 (3%) and nonspecific interstitial pneumonia in 2 patients (6%). Significant small pleural effusions was noted in 1 patient (3%). Thoracic lymphadenopathy (10-15 mm short axis) was noted in 7 patients (22%), and was mostly mild/reactive (10-15 mm in short axis), although one patient had biopsy-proven sarcoidosis. 1 patient developed pulmonary embolism (3%).

Conclusion

Pulmonary manifestations of inflammatory bowel disease present a diagnostic challenge. Our retrospective study highlighted the imaging features with clinico-pathologic correlation in 32 patients with thoracic manifestations of biopsy-proven IBD, and estimated the incidence of infection in this cohort.

A-800

Influence of CT dose reduction on AI-driven malignancy estimation of incidental pulmonary nodules

A. A. Peters
Heidelberg University Hospital, Diagnostic and Interventional Radiology, Heidelberg, Germany

Purpose
The purpose of this study was to determine the influence of dose reduction on a commercially available lung cancer prediction convolutional neuronal network (LCP-CNN) regarding simulated reduced dose scans.
Methods & Materials
CT scans from a cohort provided by the local lung cancer center (n=218) with histologically confirmed malignant pulmonary nodules as well as their corresponding virtual reduced dose simulations (25%- and 5%-dose) were subjected to a commercially available LCP-CNN; 169 patients with 196 malignant nodules were included in the final analysis (mean age±SD, 64.5±9.2y; 49% females). The resulting LCP scores (scale 1-10, increasing malignancy risk) and the proportion of correctly classified nodules were compared. The cohort was subdivided into a low-, medium- and high-risk group based on the respective LCP scores, and group shifts related to virtual dose reduction were studied in order to evaluate the potential clinical impact on lesion management. Two different malignancy risk score thresholds were used; a higher threshold of ≥9 (“rule-in”-approach) and a lower threshold of >4 (“rule-out”-approach).
Results
In total, 169 patients with 196 nodules could be included. Mean LCP scores for original, 25%- and 5%-dose levels were 8.5±1.7, 8.4±1.7 ($p>0.05$ vs. original dose) and 8.2±1.9 ($p=0.003$ vs. original dose), respectively. Using the “rule-in”-approach, the proportion of correctly classified nodules decreased with dose reduction from 58.2% for the original dose to 56.1% for the 25%- ($p=0.337$ vs. original dose) and to 52.0% for the 5%-dose level ($p=0.012$ vs. original dose). For the “rule-out”-approach the respective values were 95.9%, 96.4% and 94.4% ($p=0.115$). When reducing the original dose to 25%/5%, eight/twenty-two nodules shifted to a lower, five/seven nodules to a higher malignancy risk group.
Conclusion
A lower LCP threshold prevents underestimation of the nodule malignancy risk; especially in high-risk cohorts. Significant CT dose reduction may affect the analyzed LCP-CNN regarding the classification of pulmonary malignancies and potentially alter pulmonary nodule management.

A-741

Interstitial lung abnormalities (ILAs) incidentally detected on Coronary CT angiography (CCTA): their prevalence in a cohort of 218 patients

G. La Rosa[1], L. Reali[1], M. T. Cannizzaro[2], L. A. Mauro[1], V. Garretto[2], M. C. Inserra[2], C. Vancheri[3], S. Palmucci[1], A. Basile[1]
[1]University Hospital Policlinico “G. Rodolico-San Marco”, Radiology Unit 1- Department of Medical Surgical Sciences and Advanced Technologies “GF Ingrassia”, Catania, Italy, [2]University Hospital Policlinico “G. Rodolico-San Marco”, Department of Radiology, C.A.S.T., Catania, Italy, [3]University Hospital Policlinico “G. Rodolico-San Marco”, University of Catania, 95123 Catania, Italy, Regional Centre for Interstitial and Rare Lung Disease, Department of Clinical and Molecular Biomedicine, University of Catania, Catania, Italy

Purpose/Objectives

Limited data have been published regarding the association between ILAs and coronary artery disease [1][2][3] – even if same risk factors have been observed in these entities; therefore, our study aims to investigate the prevalence of ILAs in a large cohort of patients scheduled for CCTA. Secondarily, we have evaluated the presence of interstitial lung diseases and other pulmonary disorders, in order to quantify their incidental discovery during CCTA examinations.

Methods & Materials

218 patients – studied by CCTA using a 320-detector row scanner (320s Aquilion Genesis) – were retrospectively evaluated. The study protocol included a basal acquisition – to achieve the Calcium Score – and an enhanced scan obtained by the infusion of a bolus (60-70ml) of iodine contrast (Iomeprol 400, infusion flow rate equal to 5 ml/sec). Parenchymal analysis was retrospectively performed by two senior radiologists (with more than 5 years of experience in thoracic and cardiovascular imaging) and one resident radiologist.
ILAs have been described according to the recent Fleischner Society Statement [4] as non-dependent pulmonary abnormalities affecting more than 5% of any lung zone. Three subcategories were registered: i) ILAs with no predominant subpleural localization; ii) ILAs with predominant subpleural localization and no fibrosis; iii) subpleural fibrotic ILAs. The following categories of abnormalities were registered: ground-glass or reticular abnormalities, diffuse centrilobular nodularity, traction bronchiectasis, honeycombing, and non-emphysematous cysts [5].

Results

ILAs were encountered with a prevalence of 3,2% (7/218 patients); 4 patients with ILAs exhibit significant coronary artery disease on CCTA (a three-vessel involvement in one case and a single vessel in the remaining three cases).
Subpleural localization was the prevalent subtype of ILA encountered, being detected in 6 out of 7 cases (with a prevalence equal to 90%). ILAs with no prevalent peripheral distribution was reported in only one case. Subpleural fibrotic ILAs were observed in 2 out of 7 cases (28,5%).
Concerning the type of interstitial abnormality, reticulations were depicted in all cases, whereas traction bronchiectasis were encountered in 4 out of 7 cases (57%). Ground-glass opacities and honeycombing were respectively depicted in 5 and 1 patients. Non-emphysematous cysts were found in 3 subjects. ILAs were mainly located in the inferior lobes in 3 cases; in one patient, a mixed involvement (inferior and middle lobes) was observed, whereas in only one case ILAs was depicted in the superior lobe.

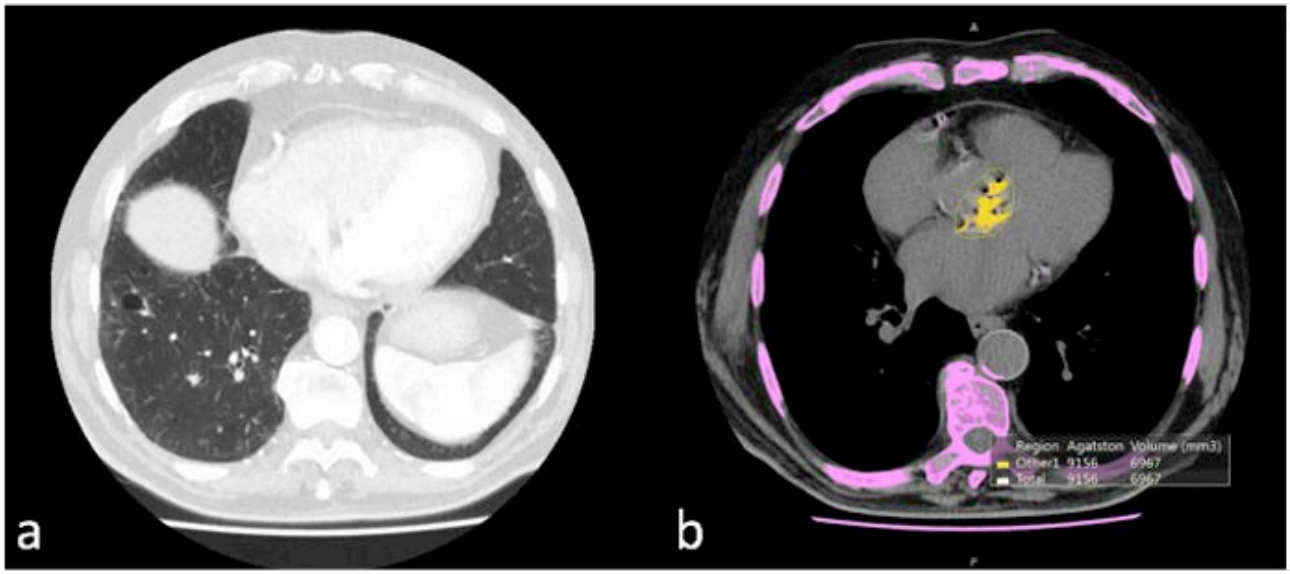

Man patient, basal CT scan (lung window). Interstitial lung alterations (reticulations) spread the lower lobes especially the right one (a); same patient mediatinal sections shows three-vessels coronary artery disease with diffuse calcifications (Totale Agatson score: 9156) (b).

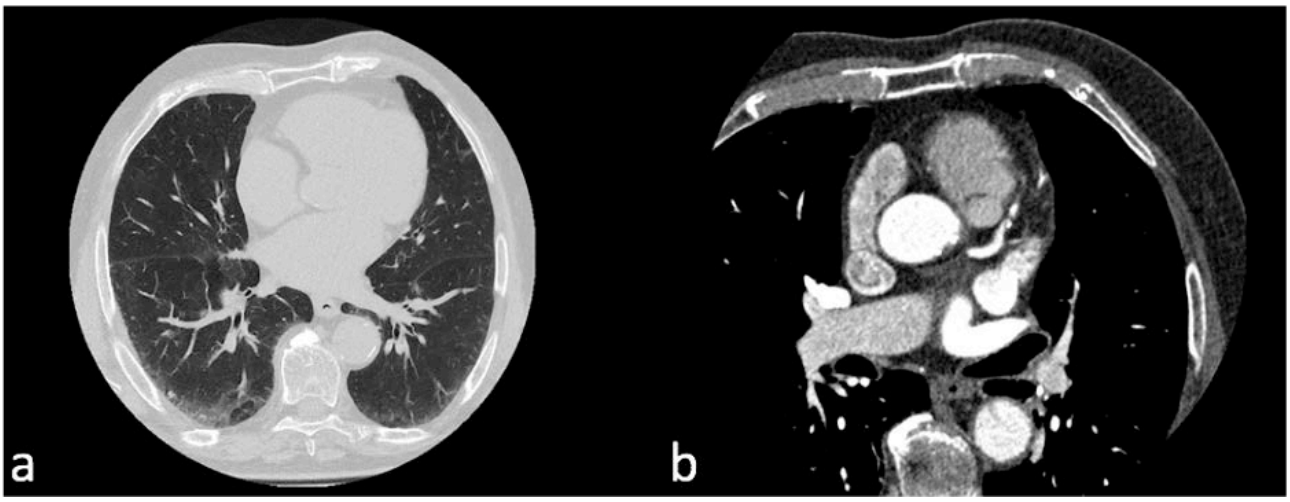

A case of widespread ILA: reticulations >5%; ground glass and also emphysema signs (a). Stenosis of left anterior descending artery (b).

Conclusion

ILAs should be always recognized since they represent a risk factor for ILD development; in addition, they may have influence on patient's prognosis and mortality.

References:

[1] Marchiori E, Taborda-Barata L, Irion K et al , (2022), Incidental chest findings on coronary CT angiography: a pictorial essay and management proposal. , J Bras Pneumol. , 13;48(4):e20220015

[2] Kay FU, Canan A, Abbara S et al , (2019), Incidental Findings on Cardiac CT a Systematic Review, Curr Cardiovasc Imaging Rep. , 12(6):21–21

[3] Macmillan MT, Williams MC. , (2018), Incidental Non-cardiac Findings in Cardiovascular Imaging, Curr Treat Options Cardiovasc Med, Volume 8, Issue 7, 726 – 737

A-447

Long COVID in young patients: impact on lung volume

L. De Pace[1], A. Onori[2], P. Capodiferro[2], D. Bellini[2], M. Rengo[2], S. Vicini[2], I. Carbone[2]
[1]Sapienza Università di Roma, Radiology, Rome, Italy, [2]Sapienza Università di Roma, Rome, Italy

Purpose/Objectives
To evaluate using quantitative analysis on chest CT images a possible lung volume reduction in Long COVID patients who complain mild respiratory symptoms, with chest CT negative for inflammatory findings.
Methods & Materials
CT images of patients from 18 to 40 years old who underwent chest CT scan at our institution were analyzed retrospectively, using AwServer Thoracic VCAR software for a quantitative study. Exclusion criteria were inflammatory findings at CT, previous lung surgery, lung cancer, breath artifacts that invalidate the quality of images. Patients were divided into two groups: in the first one ("post-COVID") patients who had previous SARS-CoV-2 infection, confirmed by an RT-PCR, who underwent chest CT from 3 to 6 months after their negativization for long covid symptoms; in the second one, the control group ("no-COVID"), were enrolled patients who underwent a chest CT scan from January 2018 to December 2019, before the spread of Covid in Italy.
Results
147 TC were evaluated, 77 post-COVID (mean age: 33±6) and 70 no-COVID (mean age: 33±4,9). Non statistical significative differences were obtained between groups in terms of age, sex and other characteristics that affect total lung capacity such as obesity, thoracic malformations and smoking habit. The right-lung volume (RV) in the post-COVID group is 2,76 ±0,14 L vs no-COVID 3 ± 0,14 L (p=0,01); the left-lung volume (LV) in the post-COVID group is 2,48 ± 0,12 L vs no-COVID 2,72±0,12 L (p=0,01); the total lung volume (TV) in the post-COVID group is 5,24 ± 0,25 L vs no-COVID 5,72 ± 0,26 L (p=0,01).
Conclusion
In patients with symptoms suggesting Long COVID, chest CT scans demonstrate a mean value of reduction of lung volume of 10% compared to patients of the same age who never had COVID.

A-162

MDCT analysis of the Arteria Praebronchialis: a rare major branch of the left pulmonary artery

B. M. Gil
Bucheon St. Mary's Hospital, College of Medicine, The Catholic University of Korea, Radiology, Seoul, Republic of Korea (South Korea)

Objectives
To update the incidence and branching patterns of the arteria praebronchialis (AP), a rare variant mediastinal branch of the left pulmonary artery.
Methods & Materials
Since the incidental discovery of the first patient on April 18 2012, contrast-enhanced CT (CECT) was screened by one radiologist for the presence of AP until December 31, 2022. Segmental and lobar branching patterns of the PA were analyzed by three thoracic radiologists.
Results
18 patients with AP were found in CECTs of 26,310 patients (14,553 male) who were screened between April 18, 2022 and December 31, 2022, resulting in an updated incidence of 0.068% from the previously reported 0.03%. Of 18 patients, 16 (88.9%) were male, and the calculated incidence of AP for male and female patients were 0.110%. and 0.017%, respectively. Compared to the normal left descending pulmonary artery (LDPA), the AP was smaller (n = 10), larger (n = 4), or of an equal size (n = 5). AP supplied only the LLL in 10 cases and both the lingular division of LUL and LLL in 9 cases. Dual segmental supply by both the AP and the normal LDPA existed in 16 cases, and exclusive segmental supply by either artery existed in four cases. Contralateral variant, aberrant right A7, was found in three patients.
Conclusion
The AP supplies either the LLL alone or both LLL and the lingular division of LUL, and its incidence (0.110%) is not negligible in the male population, necessitating routine surveillance prior to lobectomy. Radiologists should be aware of this variant and its common branching patterns.

A-542

Migratory ground glass opacities as the radiological manifestation of persistent COVID due to the Omicron variant of SARS-CoV-2 infection in vaccinated immunosuppressed patients.

J. Arenas-Jiménez[1,2,3], M. J. Ballesteros Aparicio[1], A. Ureña Vacas[1,2], E. Merino Lucas[2,4], M. Sirera-Matilla[1,2], E. Feliu Rey[1,2]
[1]Hospital General Universitario Dr. Balmis de Alicante, Radiology, Alicante, Spain, [2]Instituto de Investigación Sanitaria y Biomédica de Alicante (ISABIAL), Alicante, Spain, [3]Universidad Miguel Hernández, Departamento de Patología y Cirugía, Elche, Spain, [4]Hospital General Universitario Dr. Balmis de Alicante, Unidad de Enfermedades Infecciosas, Alicante, Spain

Purpose

Recently, migratory pneumonia has been described as the radiological manifestation of SARS-CoV-2 infection in 7 patients with B-cell lymphoma with B-cell depletion therapies[1] and other similar cases[2][3][4][5][6].

The aim of our study is to review the clinical and CT manifestations of SARS-CoV-2 pulmonary infection in vaccinated immunosuppressed patients who experience prolonged COVID-19 infection.

Methods & Materials

Clinical charts of all patients diagnosed from January to December 2022 of SARS-CoV-2 infection in a tertiary hospital and that fulfilled the criteria to be treated with Remdesivir were reviewed. Of them, those who had undergone more than one chest CT after infection and showed any lung abnormalities attributable to SARS-CoV-2 infection were included in this observational retrospective study. Clinical charts were reviewed for vaccination status, the predisposing condition, duration of SARS-CoV-2 positivity in detection analysis and radiological manifestations across the follow-up studies.

Results

Of 303 patients treated with Remdesevir, 8 had at least 2 chest CT scans during COVID-19 infection. They were 4 males and 4 females, mean age 60.5 years, range 49-75. All of them were fully vaccinated. When an analysis of SARS-CoV-2 variant was avilable, all of them corresponded to Omicron variant, that was the predominant at that time.

The predisposing condition was follicular lymphoma in 4, treated with rituximab in 3 and rituximab and obinutuzumab in 1, mantle cell lymphoma and primary cerebral lymphoma, one patient each, both treated with rituximab, one patient with multiple sclerosis treated with ocrelizumab and one patient with colon cancer under FOLFOX therapy.

Clinical symptoms and signs of SARS-CoV-2 infection or positivity of SARS-CoV-2 in detection analysis were present for 3 weeks to 5 months (median 3 months). CT findings in all patients consisted of patchy ground glass opacites that resolved, and developed new ones in different locations in the follow-up CT examinations that were performed between 2 and 8 weeks (median 3 weeks) after initial scan. There was no case showing progression to consolidation of previous ground glass opacities.

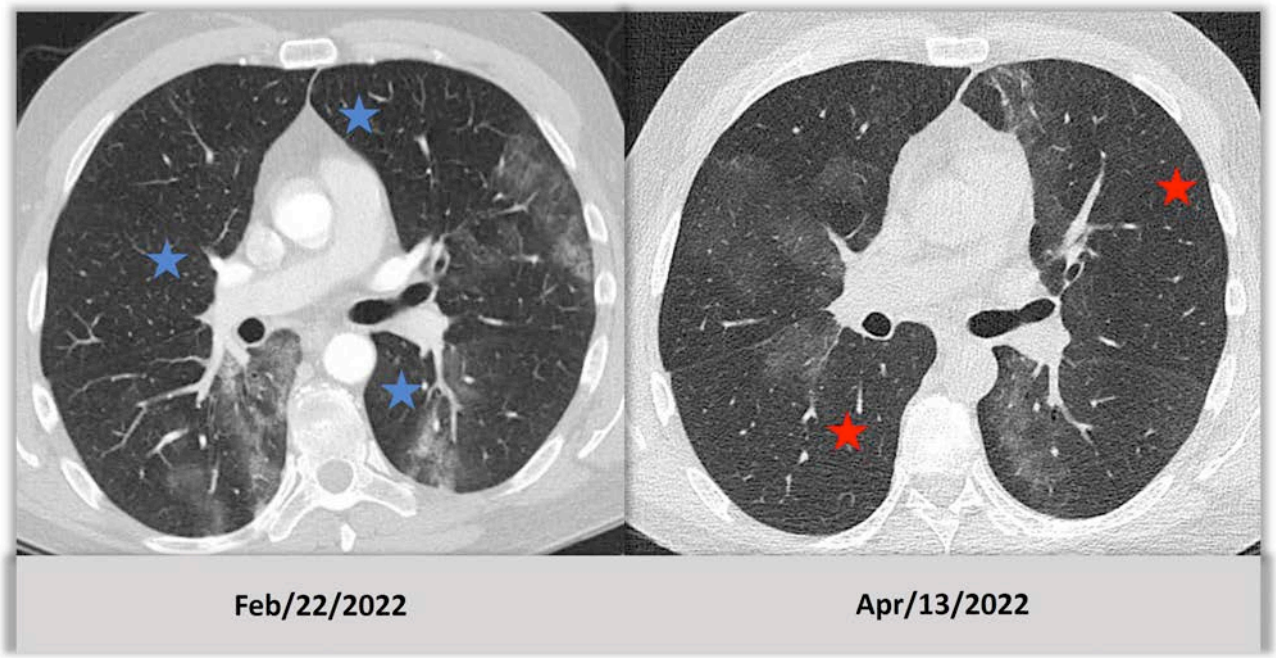

Fifty-four year-old man with multiple sclerosis treated with ocrelizumab with persistent COVID-19 infection. Previous preserved areas in initial scan (blue stars) are affected by new ground glass opacities at follow-up, while previous opacities resolve completely (red stars).

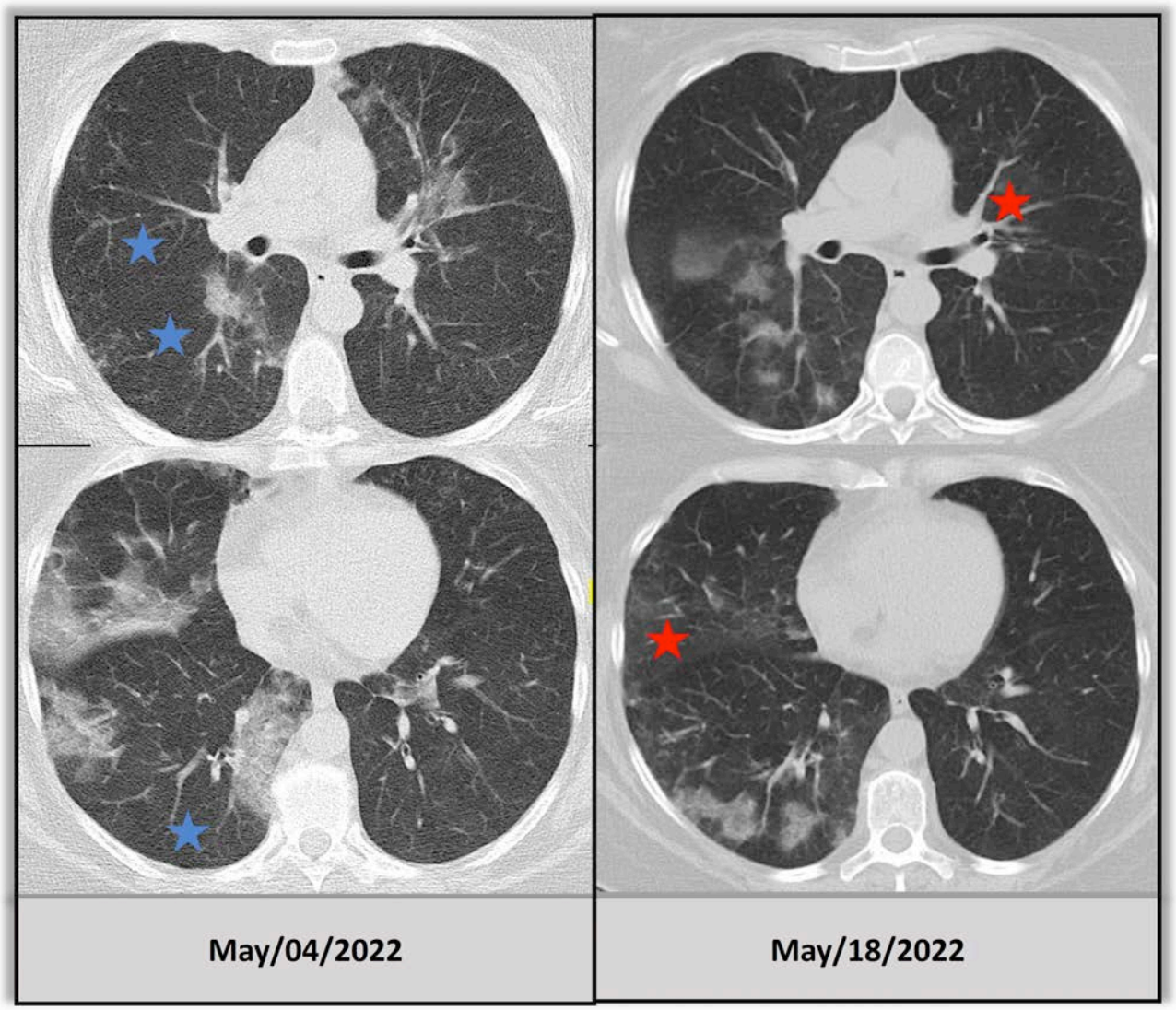

Fifty-six year-old woman with follicular lymphoma treated with rituximab and obinutuzumab with persistent COVID-19 infection. Previous preserved areas in initial scan (blue stars) are affected by new ground glass opacities at follow-up, while previous opacities are improving (red stars).

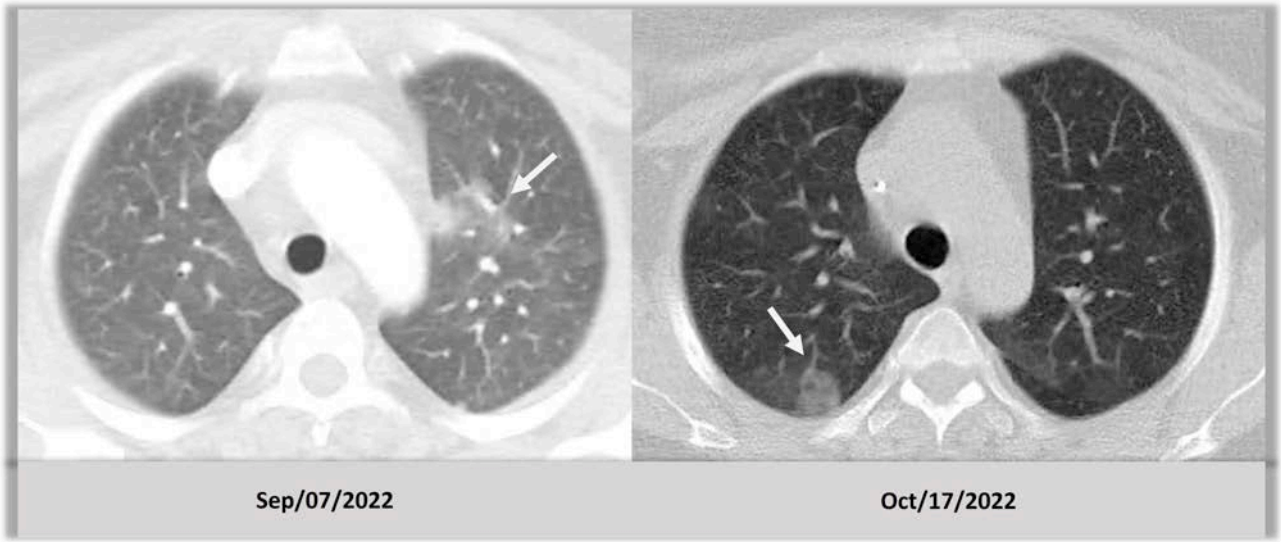

Forty-nine year-old woman with follicular lymphoma treated with rituximab and obinutuzumab with persistent COVID-19 infection. In initial scan a ground glass opacity is seen in left upper lobe (arrow), resolving in CT scan at follow-up, when a new opacity is seen in right upper lobe (arrow).

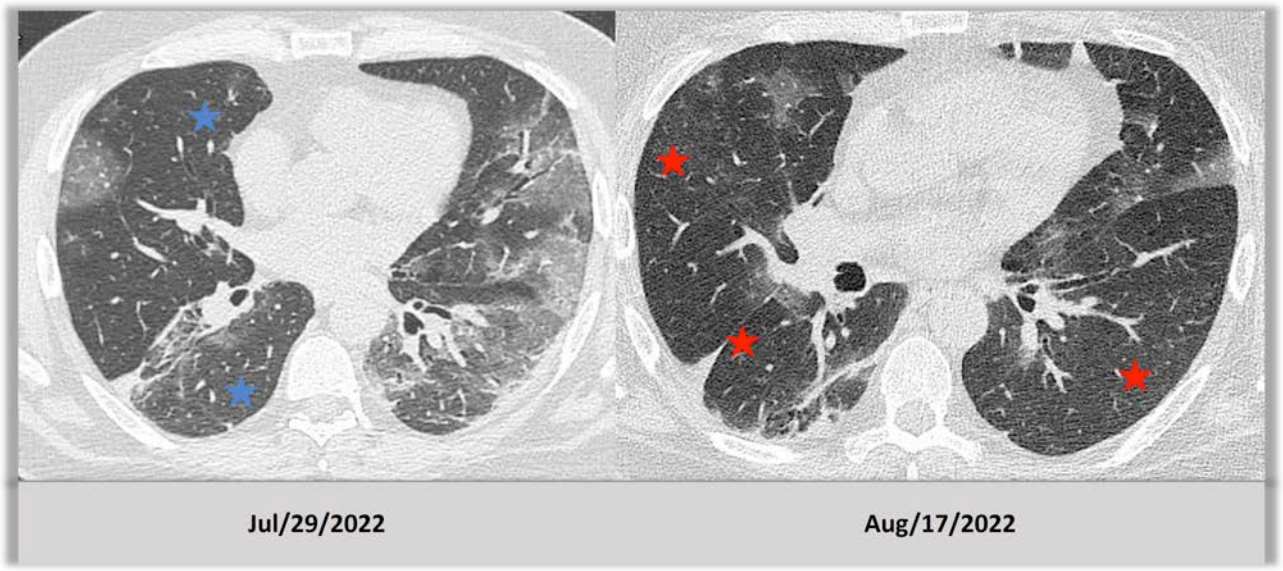

Fifty-eight year-old man with follicular lymphoma treated with rituximab. At diagnosis of COVID-19 infection multiple bilateral ground glass opacities are seen. Three weeks later, most of them have resolved (red stars) and new ones have appeared in previous preserved areas in initial scan (blue stars).

Conclusion

In this series of vaccinated immunosuppressed patients infected by the Omicron variant of SARS-CoV-2, prolonged infection occurs and it manifests as migratory ground glass opacities that wax and wane in a period of weeks. Rituximab and other B-cells-depleting therapies are the cause of this presentation in most of these cases. Radiologists should be aware of this evolution to suggest the diagnosis in the appropriate clinical setting.

References:

[1] Lee J, et al, (2023), Migratory Pneumonia in Prolonged SARS-CoV-2 Infection in Patients Treated With B-cell Depletion Therapies for B-cell Lymphoma. , Korean J Radiol, 362-70, 24, https://doi.org/10.3348/kjr.2022.0844
[2] Kos I, et al., (2020), Prolonged Course of COVID-19-Associated Pneumonia in a B-Cell Depleted Patient After Rituximab., Front Oncol, 1578, 10, https://doi.org/10.3389/fonc.2020.01578
[3] Avouac J, et al., (2021), COVID-19 outcomes in patients with inflammatory rheumatic and musculoskeletal diseases treated with rituximab: a cohort study., Lancet Rheumatol, e419–e426, 3, https://doi.org/10.1016/s2665-9913(21)00059-x
[4] Thornton CS, et al., (2022), Prolonged SARS-CoV-2 infection following rituximab treatment: clinical course and response to therapeutic interventions correlated with quantitative viral cultures and cycle threshold values. , Antimicrob Resist Infect Control, 28, 11, https://doi.org/10.1186/s13756-022-01067-1
[5] Bonuomo V, et al., (2021), COVID-19 (SARS-CoV-2 infection) in lymphoma patients: A review., World J Virol, 312-325, 10, http://dx.doi.org/10.5501/wjv.v10.i6.312
[6] Santana ANC, et al., (2021), Migratory pulmonary infiltrates in a patient with COVID-19 and lymphoma, J Bras Pneumol , e20200528, 47, https://doi.org/10.36416/1806-3756/e20200528

A-709

Miliary pulmonary metastases as presentation of lung cancer: A case-series study

C. F. Munoz-Nunez[1], P. Calvillo-Batlles[1], N. Mancheño-Franch[2], S. Palanca[3], L. Trilles-Olaso[1], E. Ansotegui[4], O. Juan[5]
[1]Hospital Universitario y Politécnico La Fe, Department of Radiology, Valencia, Spain, [2]Hospital Universitario y Politécnico La Fe, Department of Pathology, Valencia, Spain, [3]Hospital Universitario y Politécnico La Fe, Molecular Biology Unit, Service of Clinical Analysis, Valencia, Spain, [4]Hospital Universitario y Politécnico La Fe, Respiratory Department, Valencia, Spain, [5]Hospital Universitario y Politécnico La Fe, Medical Oncology, Valencia, Spain

Purpose
To review imaging and clinical findings of lung cancer cases presenting with a miliary pulmonary pattern due to metastases at our institution.
Methods & Materials
A search of the cases of lung cancer presenting with a miliary pulmonary pattern on imaging at our institution between january 2011 and december 2022 was conducted on our electronic medical records retrieval system. Only the cases with imaging features fulfilling the miliary pattern criteria defined by the Fleischner Society were included (i.e. profuse tiny, discrete, rounded pulmonary opacities (3 mm or less in diameter) generally uniform in size and diffusely distributed throughout the lungs on chest x-ray; widespread, randomly distributed micronodules on CT). In subtle cases MIP reconstructions were also used on the CT studies.
Results
Fourteen patients (57% females) presented with a miliary pulmonary pattern caused by lung cancer metastases. The median age was 58 years [interquartile range (IQR) 47-63 years). The type of lung cancer was in all cases lung adenocarcinoma. Most of the patients complained of cough or chest pain at presentation. Fever or malaise were rare. Most of the patients were no smokers. On imaging all of them had a dominant pulmonary lesion such as a dominant nodule/mass or a consolidation. Most of them presented with hilar and mediastinal nodes metastases, some had malignant pleural effusion or distant metastases in bone, liver or brain. EGFR mutations were present only in 43% of the cases. ALK translocations, ROS1 rearrangements and PD-L1 expressions were usually absent.
Conclusion
A miliary pulmonary pattern on imaging is common in tuberculosis but rare as presentation of lung cancer metastases (usually from lung adenocarcinoma). Radiologist should be aware of this and consider lung cancer in the differential diagnosis of miliary pulmonary nodules, specially if fever and other clinical features of infection are absent.

References:

[1] Chang MH, Chiang KH, Shieh JM, Cheng KC, Ho CH, (2022), Analysis of non-small cell lung cancer with miliary lung metastasis in patients harboring epidermal growth factor receptor mutations, Scientific Reports, 18182, https://www.nature.com/articles/s41598-022-23195-9
[2] Umeki S , (1993), Association of Miliary Lung Metastases and Bone Metastases in Bronchogenic Carcinoma, Chest, 948-50, https://linkinghub.elsevier.com/retrieve/pii/S0012369216389012
[3] Laack E, Simon R, Regier M, Andritzky B, Tennstedt P, Habermann C, et al. , (2011), Miliary Never-Smoking Adenocarcinoma of the Lung: Strong Association with Epidermal Growth Factor Receptor Exon 19 Deletion., Journal of Thoracic Oncology, 199-202, https://www.sciencedirect.com/science/article/pii/S1556086415319171
[4] Kimmig L, Bueno J. , (2017), Miliary Nodules: Not Always Tuberculosis, Annals ATS, 1858-60, https://www.atsjournals.org/doi/full/10.1513/AnnalsATS.201706-436CC
[5] Kim CS, Lee KN, Lee JH. , (2003), Comparison of High-resolution CT Findings between Miliary Metastases and Miliary Tuberculosis, J Korean Radiol Soc , 147-152, https://jksronline.org/DOIx.php?id=10.3348/jkrs.2003.48.2.147
[6] Pillai S, Khan A, Khan S, (2019), Adenocarcinoma of the Lung Presenting with Intrapulmonary Miliary Metastasis, Cureus, e5430, https://www.ncbi.nlm.nih.gov/pmc/articles/PMC6797010/

A-738

Natural hystory of fibrosing interstitial lung diseases: focus on radiological complications

G. La Rosa[1], S. Galioto[2], L. A. Mauro[2], S. Palmucci[2], A. Libra[3], E. Sciacca[3], G. Muscato[3], C. Vancheri[3], A. Basile[2]
[1]University Hospital Policlinico “G. Rodolico-San Marco”, University of Catania, Radiology Unit 1- Department of Medical Surgical Sciences and Advanced Technologies “GF Ingrassia”, Catania, Italy, [2]University Hospital Policlinico “G. Rodolico-San Marco”, University of Catania, 95123 Catania, Italy, Radiology Unit 1- Department of Medical Surgical Sciences and Advanced Technologies “GF Ingrassia”, Catania, Italy, [3]University Hospital Policlinico “G. Rodolico-San Marco” -University of Catania, 95123 Catania, Italy, Regional Centre for Interstitial and Rare Lung Disease, Department of Clinical and Molecular Biomedicine, University of Catania, Catania, Italy

Purpose
This study aims to analyze the complications occurred in patients affected by fibrosing interstitial lung diseases; in addition, it provides a comprehensive and accurate essay for clinicians, radiologists, and surgeons involved in their management.
Methods & Materials
HRTC examinations, performed at our center from June 2018 to December 2019, were considered. We made up a database composed of 499 examinations with a total of 455 patients. Among these patients, we retrospectively identified a total of 207 subjects affected by fibrosing interstitial lung disease; for these cases, one clinician and one radiologist – both having more than 10 years of experience in the field of interstitial lung disease – analysed their clinical and radiological history until 2023. The prevalence of the main complications and their time of onset were examined.
Results
The following fibrosing interstitial lung diseases were included: usual interstitial pneumonia (UIP) (n=132), UIP probable (n=23), non-specific interstitial pneumonia (NSIP) (n=15), combined pulmonary fibrosis and emphysema (CPFE) (n=25), and hypersensivity pneumonitis (HP) (n=4) patterns. Some radiological findings were classified as uncertain between fibrosing NSIP and UIP probable (n=8). The most common complication was the occurrence of nodules (52/207; 25.1%), followed by suspicious consolidations (13/207; 6.3%), acute exacerbations (12/203; 5.9%), cases of pneumothorax (6/207; 2.8%), tumours (8/207; 3.8%) – represented by adenocarcinoma and squamose carcinoma), cases of pneumomediastinum (8/207; 3.8%), infections (7/207; 3.3%), and deaths (49/207; 23.6%). Nodule appearance was the earliest one with an average of 9 months in its appearance. Among UIP patients, complications were observed in 66 cases; a lower number was found in the remaining ILD.

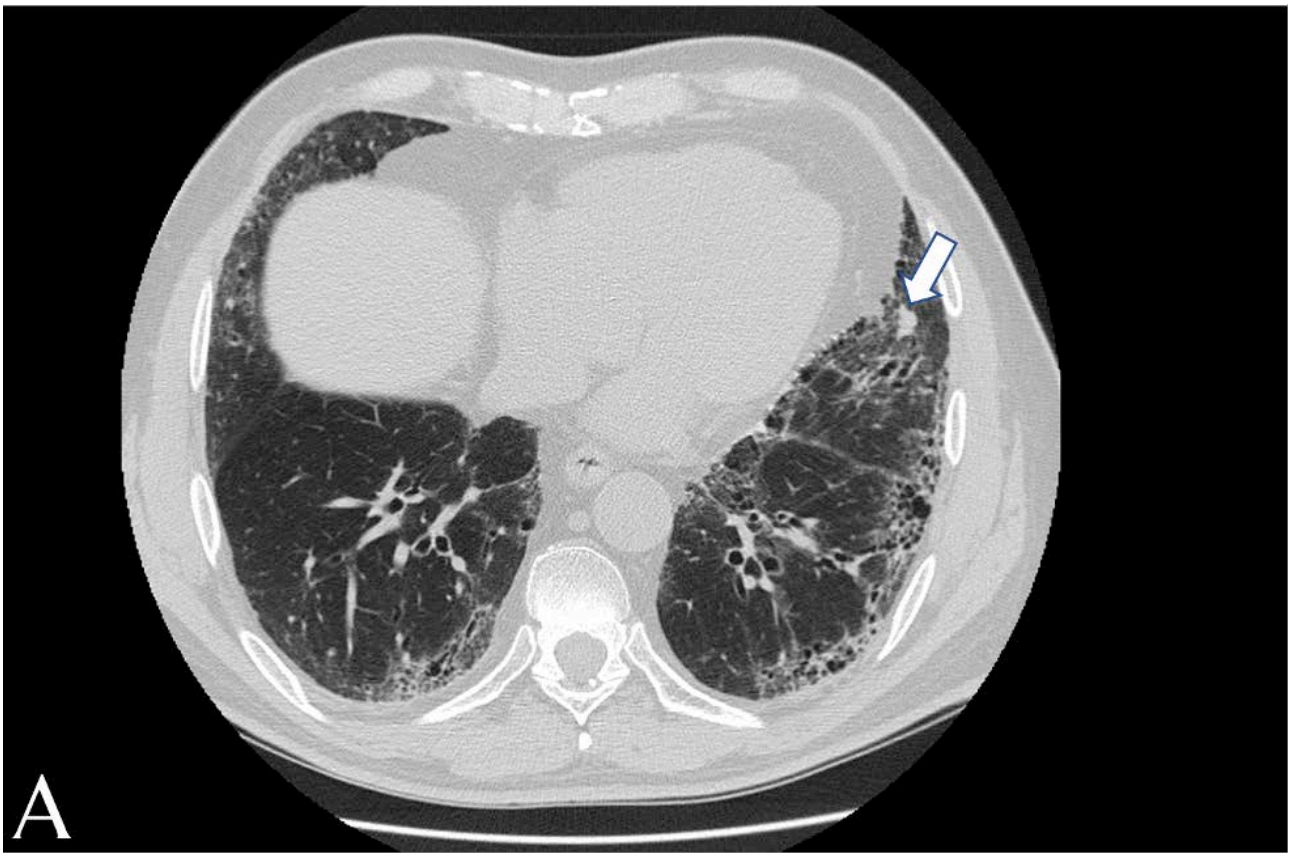

Male patient, 79 years old, UIP pattern, the window for lung parenchyma: in the lower lingular site, pulmonary parenchymal nodule with axial measurements of 10x5 mm is observed.

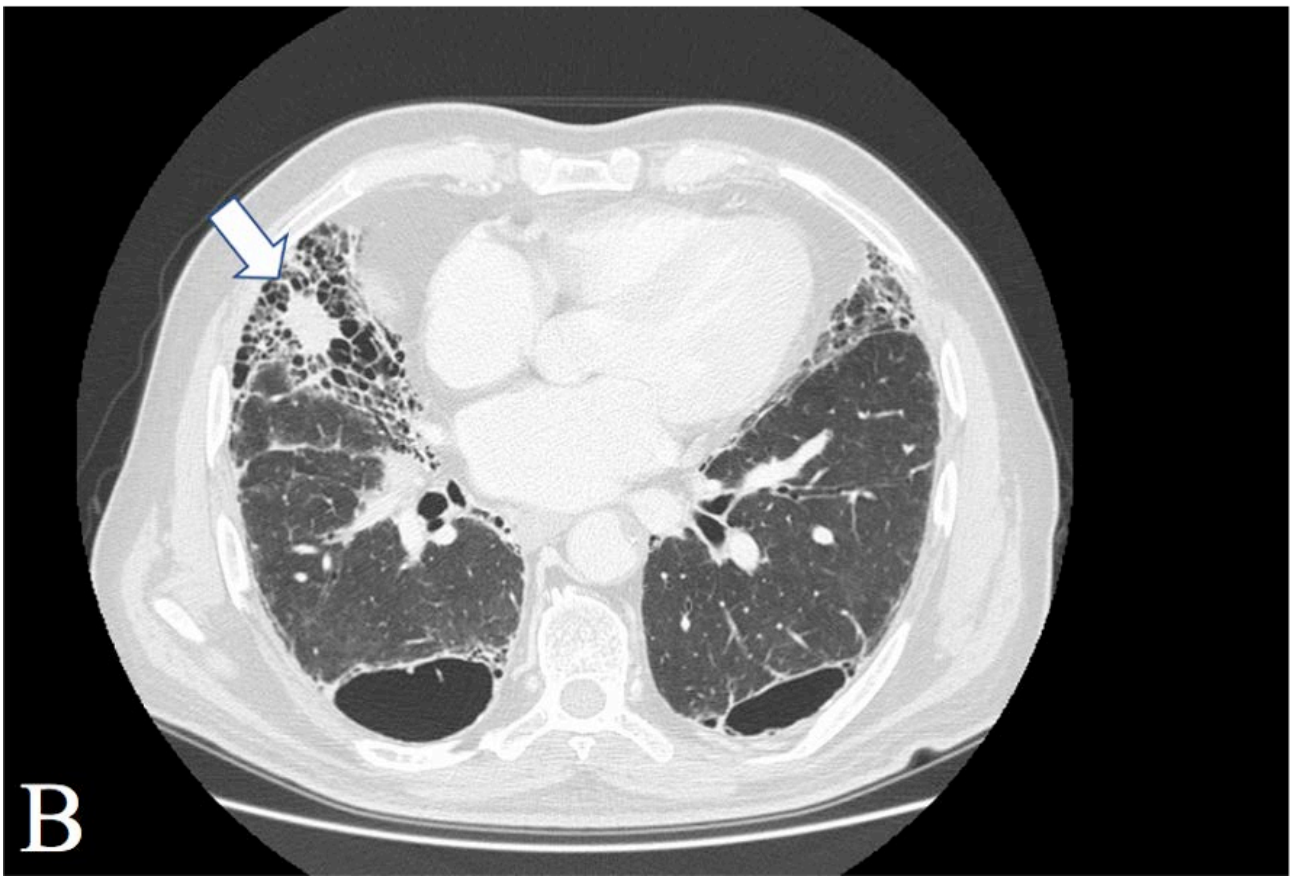

CPFE pattern; man patient 70 years old, diagnosis of squamocellular carcinoma.

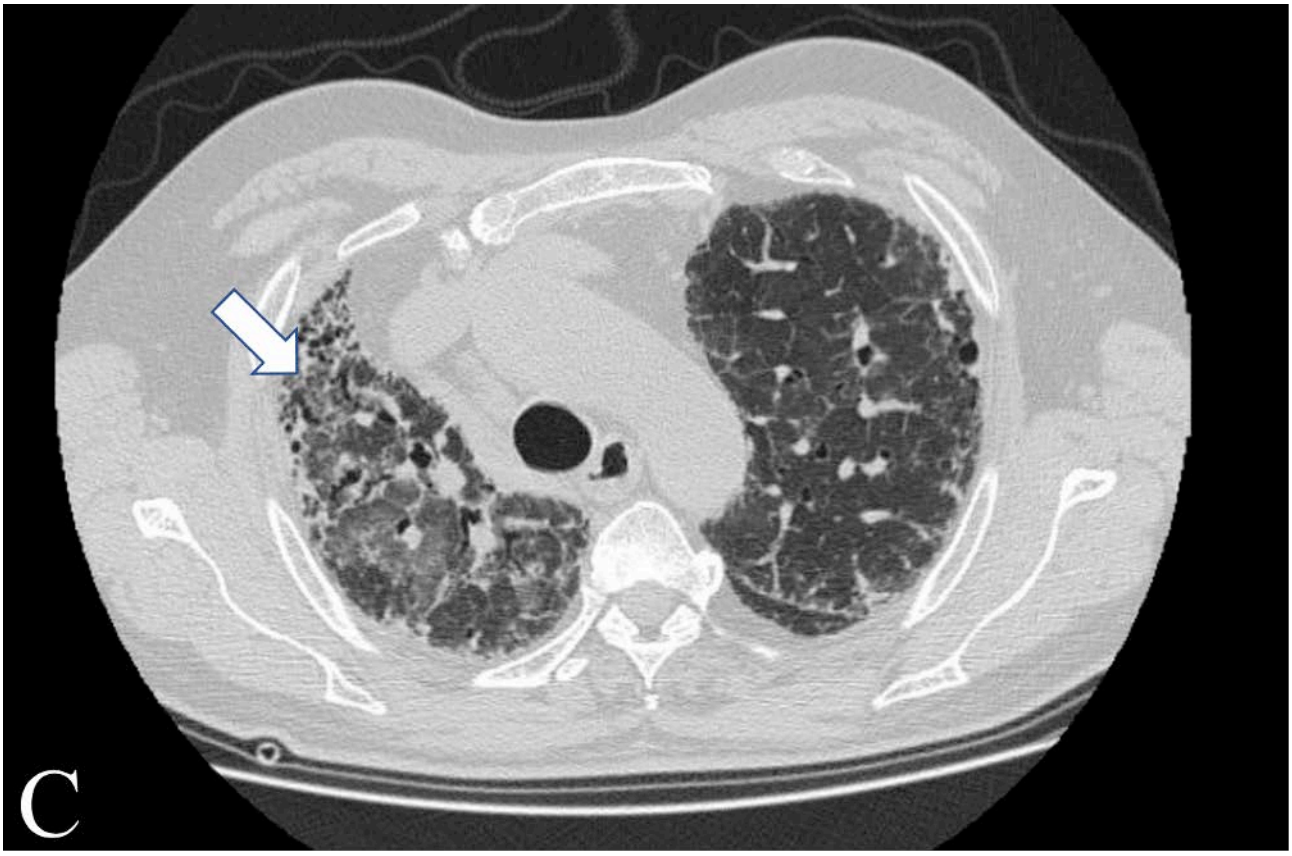

Man patient, 73 years old, UIP pattern, acute respiratory failure, superimposed widespread ground-glass opacity. Acute exacerbation.

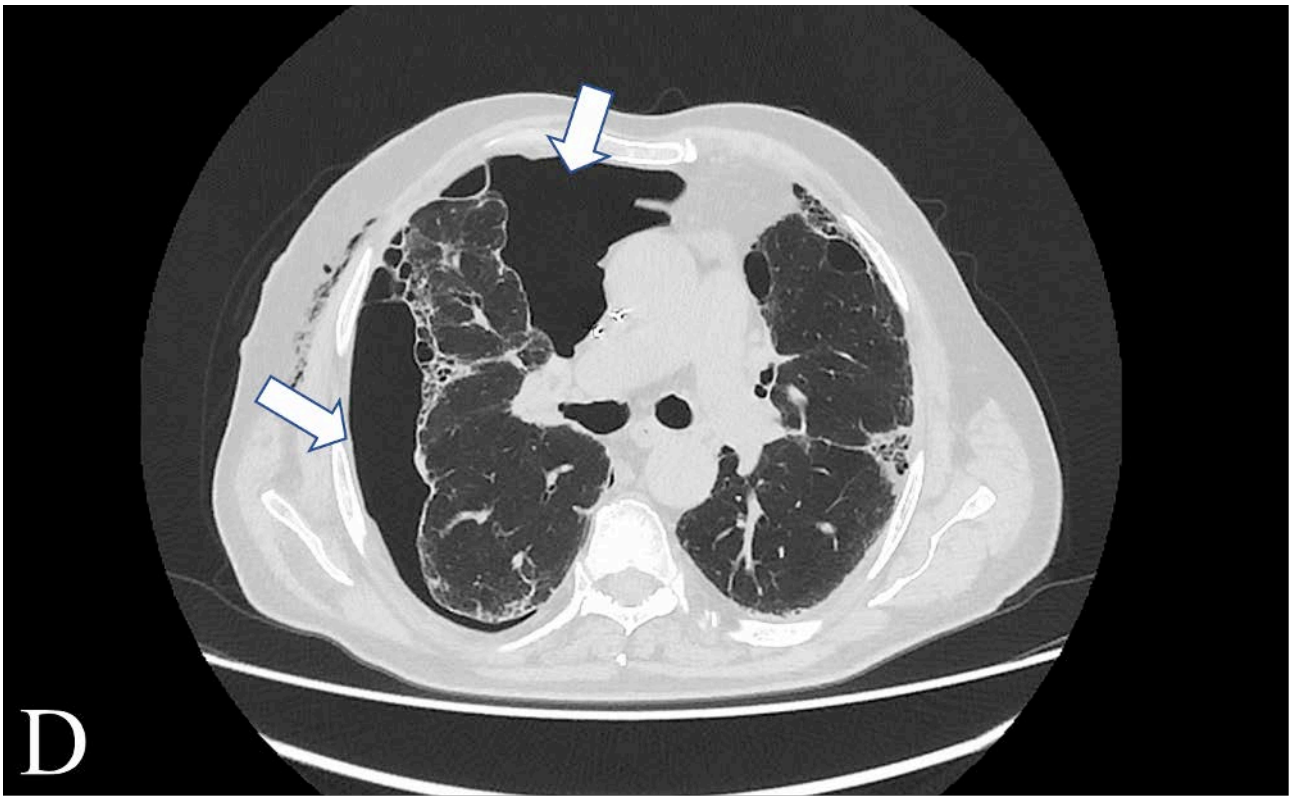

Man patient, 70 years old, CPFE pattern: a large flap of right pneumothorax. There is a minimal amount of subcutaneous emphysema on the right lower thoracic lateral wall. The right lung appears largely collapsed with residual expanded segments.

Conclusion

Pneumologists, radiologists, and pathologists play a key role in the identification of fibrosing ILD disease, and the characterization of its complications. The early identification of complications is crucial and requires an integrated approach among specialists to address the correct treatment.

A-168

Overlooked acute myocardial infarction and intramural hematoma on abdomen CT in patients presented with nonspecific abdominal pain

S. M. Yoo, S. J. Lee, M. J. Son
Bundang CHA medical center, Gyeonggi-do, Republic of Korea (South Korea)

Objectives

Field of view on abdomen CT often includes lower portion of the heart and thoracic aorta. Notably, the authors have encountered multiple occasions in which critical cardiovascular causes overlooked on the previous abdomen CT in patients presented with acute abdominal pain. Critical cardiovascular findings may inadvertently be overlooked on abdomen CT because the protocol is not optimized to identify subtle cardiovascular disease (non-ECG gating), and the primary purpose for the examination is for the identification of abdominal diseases.

The purpose of this paper is to evaluate the incidence of missed triple rule-out abnormalities [acute myocardial infarction (AMI), pulmonary embolism (PE), and acute aortic syndrome (AAS)] on abdomen presented with nonspecific acute abdominal pain.

Methods & Materials

The authors retrospectively identified 913 patients from January 2017 to June 2018 in whom enhanced abdominal CT was performed due to nonspecific acute abdominal pain. Two chest radiologists retrospectively reviewed the abdomen CT by consensus manner, focusing on whether triple rule-out abnormalities (AMI, AAS, and PE) were overlooked or not, and compared with discharge diagnosis.

Results

Mean age of patients was 53.2±17.3 (range=12-93, male/female=404/509). Overall, there were 0.5% missed triple rule-out abnormalities (5/913) [4 cases (2, 1, and 1 cases of left anterior descending, right coronary artery, and left circumflex artery) of AMI, and 1 cases of AAS (intramural hematoma)] on abdomen CT. In contrast, all cases (n=2/2 of PTE were correctly diagnosed. However, majority (71.4%, n=5/7) of the so called triple rule-out abnormalities presented with nonspecific abdominal pain were missed on the initial CT report.

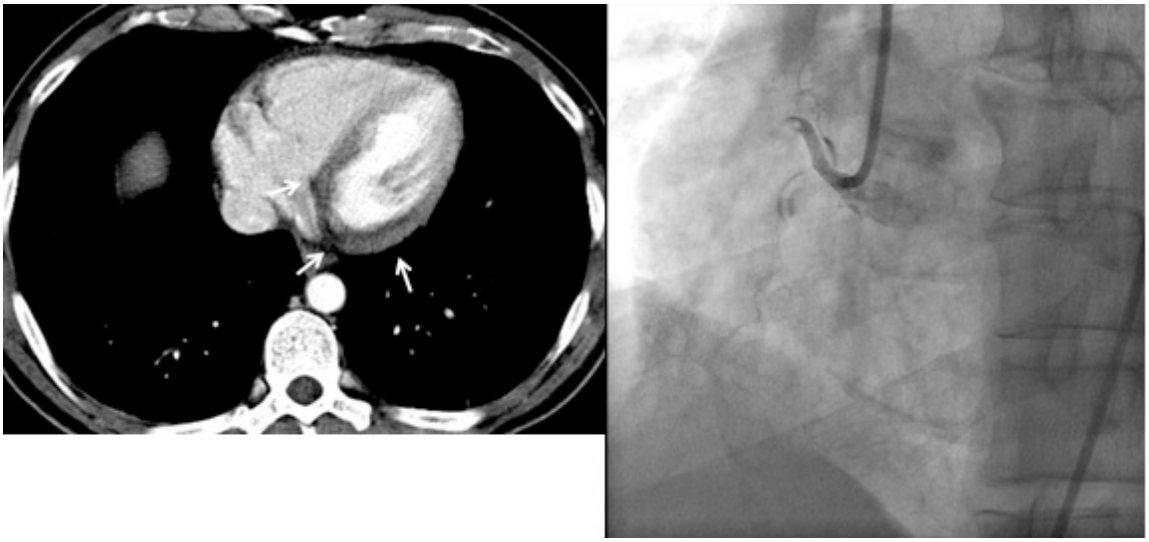

A 51-year-old male presented with nonspecific right upper abdominal pain. There was subendocardial low attenuation in the right coronary artery territory (arrows) on an axial CT image, suggesting AMI. AMI was confirmed on subsequent coronary angiography.

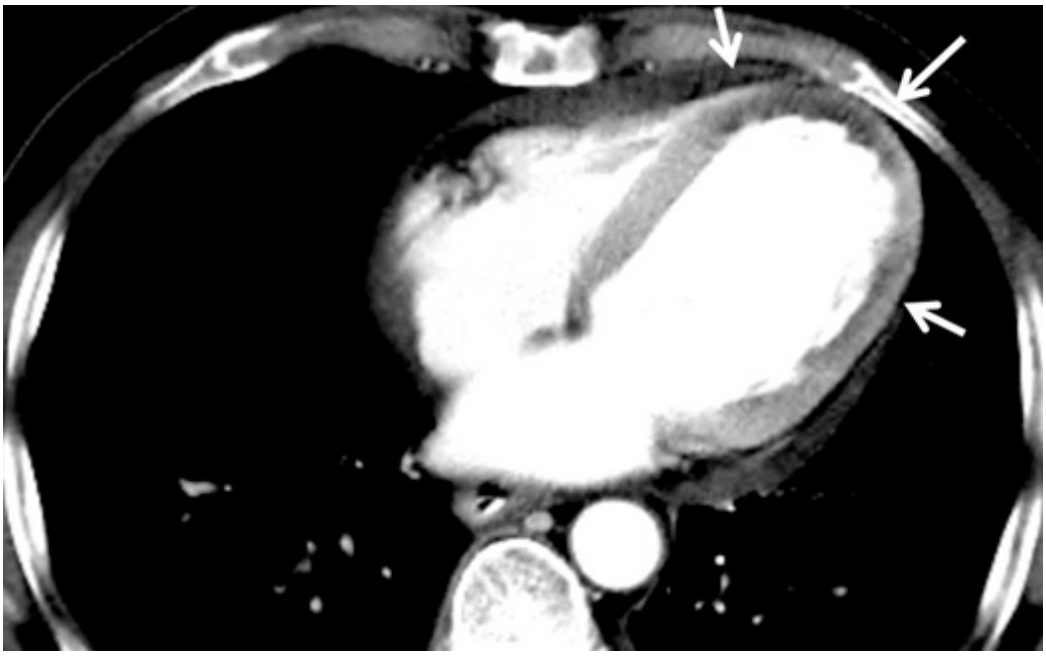

A 73-year-old male presented with nonspecific abdominal pain. There was subendocardial or transmural low attenuation along the left anterior descending coronary artery territory on an axial image CT, suggesting AMI. But the diagnosis of AMI was missed on the initial abdominal CT report.

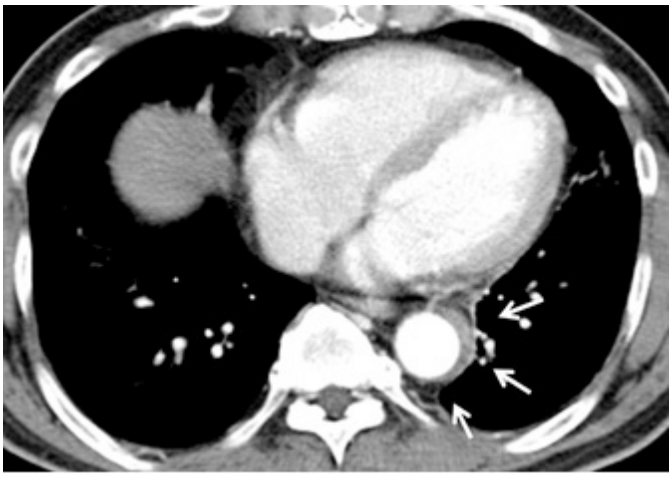

A 73-year-old male presented with nonspecific abdominal pain and nausea. On abdomen CT, there was crescent-shaped wall thickening in descending thoracic aorta, indicating presence of IMH, but the diagnosis was missed on the CT report. Mild aortic wall thickening may be easily missed on enhanced CT alone. It should be compared with non-enhanced CT.

Conclusion

Although rare, AMI or AAS may present with nonspecific abdominal pain. Thus, radiologists should routinely look at cardiovascular system on abdomen CT not to miss critical cardiovascular findings.

References:

[1] Maren Krueger, Paul Cronin, Mohamed Sayyouh, Aine Marie Kelly , (2019), Significant incidental cardiac disease on thoracic CT: what the general radiologist needs to know, Insights into Imaging, 10.1186/s13244-019-0693-y., 2019-02-06, University of Michigan

[2] Kun Young Lim, Seth J Kligerman, Cheng Ting Lin, Charles S White, (2014), Missed pulmonary embolism on abdominal CT, American Journal of Roentgenology., 738-743, 10.2214/AJR.13.11436, 2014-04-01, University of Maryland School of Medicine

A-173

Pilot lung cancer screening program in Serbia after 2-year results and challenges

D. Dragisic[1], G. Vujasinovic[1], J. Djekic Malbasa[2]
[1]Institute for pulmonary diseases of Vojvodina, Center of Radiology, Sremska Kamenica , Novi Sad, Serbia, [2]Institute for pulmonary diseases of Vojvodina, Center of Epidemiology, Sremska Kamenica , Novi Sad, Serbia

Purpose
Lung cancer LC is one of the leading causes of mortality worldwide. Incidence and mortality of LC in Serbia are among the highest in Europe. After smoking cessation, lung cancer screening (LCS) is the best prevention method for reducing LC mortality. Diagnosing the disease in early stages significantly increases survival rate. Therefore, early diagnosis is very important, and it is best achievable by screening. The first pilot LCS program in Serbia started in October 2020. Aims and objectives To present the 2 year results and challenges in implementing LCS.
Methods & Materials
Persons aged 50-74 years, with a smoking history of 30 pack-years or more and/or 20 pack-years with additional risks either active or quit smoking within the previous 10 years undergone low-dose CT evaluation. The screening was performed on a 64 slice CT scanner GE Light speed and Philips Ingenuity using low-dose protocol Eurpean Society of Thoracic Imaging. Total number of nodes and morphology of each node (localization, consistency, diameter, volume, calcifications, margins and other) were analyzed, with the aid of computer aided detection and lung nodule assessment software package. Radiological assessment and further evaluation was done per LUNG RADS version 1.1 American College of Radiology.
Results
During a 2-year period, a total of 3432 LDCT scans were performed on 2138 screen responders. The majority were females (58.1%). Females compared to males were often active smokers (87.1% vs. 78.7%, p<0.001) and frequently reported respiratory symptoms (72.1% vs.65.5%, p=001). Lung RADS score positive screens were found in 9.2% (199/2135). The screening respond rate to control LDCT after 12 months (Lung RADS 1 and 2) was 76.5% (786/1027). The invasive diagnostic was performed in 2.3% of participants, while 0.5% refused invasive procedures. The rate of false positive findings was 1.17 % (25/2138). The LC detection rate was 1.96% (42/2138) and 72.4% of LC were diagnosed on baseline screening. Among LC, 88.1% were NCSLC (adenocarcinoma 54.8%, squamous 21.4% and NOS 9.5%) and 11.9% were SCLC. The stage of disease of 52.4% of participants was I or II. LC was significantly common in males compared to females (1.7% vs. 0.9%, p=0.04). Radiatio dose CTDI vol (mGy) mean±SD)= 0.67 (0.6757±0.301) DLP= 30,501±16,073 mAs=0.427014±0.225 kVp=91.2176±19.142
Conclusion
Decreased irradiation dose, together with higher accuracy (CAD software package) compared to chest X-rays, makes LDCT excellent screening tool, which allows early detection of lung cancer, and therefore improves survival rate.
Innovative approaches, education and a more recognizable campaign are necessary to increase the responds rate among participants with negative baseline LDCT

A-630

Preliminary results analysis demonstrating the prevalence and features of Lung Cancer detected at East Surrey Hospital (ESH) Lung Screening Review Meeting (SRM) as part of the Surrey and Sussex Cancer Alliance (SSCA) Target Lung Health Check (TLHC)

A. Kapoor[1], K. Nimako[2], S. Bax[2], J. Smelt[3], C. O'Driscoll[4], V. Stewart[5], R. Ahmed[6], A. Villanueva[7]
[1]East Surrey Hospital. SASH Trust, ST6. Radiology, Redhill, United Kingdom, [2]East Surrey Hospital. Redhill, SURREY AND SUSSEX HEALTHCARE NHS TRUST, Respiratory Consultant, Redhill, United Kingdom, [3]St Georges University Hospital NHS Foundation Trust. London., Consultant Thoracic Surgeon, London, United Kingdom, [4]East Surrey Hospital. Redhill, SURREY AND SUSSEX HEALTHCARE NHS TRUST, Lead Administrator, Redhill, United Kingdom, [5]Surrey and Sussex Cancer Alliance, Programme Manager, Guildford, United Kingdom, [6]East Surrey Hospital. Redhill, SURREY AND SUSSEX HEALTHCARE NHS TRUST., Consultant Radiologist, Redhill, United Kingdom, [7]East Surrey Hospital. SURREY AND SUSSEX HEALTHCARE NHS TRUST, Consultant Radiologist, Redhill, United Kingdom

Purpose/Objectives

The TLHC lead by SSCA evaluates three locations of Surrey and Sussex (England): Brighton and Hove, Crawley, and Slough. These areas were selected on a basis of population size, smoking prevalence, lung cancer prevalence and mortality. Crawley has the fourth highest lung cancer incidence and smoking prevalence in this region. Each local TLHC may refer patients with some incidental findings or suspicious lung nodules to a local SRM. ESH SRM covers Crawley TLHC

The aim of this work is:

1. To report the prevalence of lung cancer (LC) and to assess the proportion of LC at stage I detected at East Surrey Hospital (ESH) SRM between 1/7/22 and 1/1/23
2. To compare prevalence and proportion of stage I LC detected at ESH SRM with the first round of 8 established lung cancer screening programs (LCS)
3. To define the percentage of LC with or without nodular appearance on CT scans at ESH SRM

Methods & Materials

The SSCA TLHC follows the published standard protocol and quality assurance standards prepared for the Targeted Lung Health Checks Programme by the Lung Clinical Expert Advisory Group (1,2).

Of 1380 invited people living in Crawley, 1148 (83%) were screened between 1/7/22 and 1/1/23. 1061 (92%) of these underwent a low-dose CT scan. Scans with suspicious lung lesions were reviewed at the SRM and were referred and seen in CWT clinics at ESH. Following review appropriate patients underwent lung function, PET CT and biopsy and were discussed in the LC MDM.

Data of histology proven lung cancers were collected via the Somerset Cancer Registry following final MDM review. Comparison with published data from 8 LCS (3).

Results

12 patients out of the 1061 were found to have histologically proven lung cancer (1.1%). 8 out of 12 (66.6%) were stage I, 2 stage II (16.6%), 1 stage III (8.3%) and 1 stage IV (8.3%). Adenocarcinoma was the most frequent histological type (N=8). 7 patients were treated with Surgery. Only two patients required chemotherapy and 4 radiotherapy (Table 1).

Table 1. ESH SRM outcomes for the patient details regarding lung cancers detected at Crawley up to 01.01.2023.

Patient	Cancer diagnosis	Cancer location	Stage	Stage	Treatment
1	Squamous Cell C	LLL	T2aN0M0	IB	Surgery
2	Adenocarcinoma	RLL	T1bN0M0	IA	SABR (patient choice not for surgery)
3	Small cell	LUL	T1aN2M0	IIIA	Chemo/Radiotherapy
4	Adenocarcinoma	LUL	T2aN0M0	IB	Surgery
5	Adenocarcinoma	RUL	T1bN0M0	IA	Radiotherapy
6	Squamous Cell C	RLL	T3N0M0	IIB	Surgery
7	Adenocarcinoma	RUL	T2aN0M0	IB	Surgery
8	Adenocarcinoma	LLL	T2aN2M1a (lung mets)	IVA	Chemotherapy
9	Squamous Cell C	LLL	T1cN0M0	IA	Surgery
10	Adenocarcinoma	LUL	T1cN0M0	IA	Surgery
11	Adenocarcinoma	RLL	T1bN0M0	IA	Radiotherapy
12	Adenocarcinoma	LUL	T3N0M0	IIB	Surgery

LC prevalence and stage found were similar to other LCS such as NELSON or NLST (Table 2).

Table 2. Differences in Lung Cancer Prevalence Rates Between 8 LCS Studies on baseline screening round (*)

Cohort	No.	Participants with lung cancer	Prevalence	Stage I(%)
P-IELCAP a	2989	29	1.0%	89
NLST	26309	270	1.0%	57
DLCST	2052	17	0.8%	59
NELSON a	7557	70	0.9%	64
LUSI	2029	22	1.1%	82
ITALUNG a	1406	20	1.4%	50
DANTE a	1276	28	2.2%	57
DEPISCAN	336	8	2.4%	38
CRAWLEY b	1.061	12	1.1%	66%

Abbreviations: P-IELCAP, Pamplona Early Lung Cancer Detection Program; NLTS, National Lung Screening Trial; DLCST, Danish Lung Cancer Screening Trial; NELSON (Nederlands Leuvens longkanker Screenings Onderzoek; LUSI, German Lung Cancer Screening Intervention trial; DANTE, Detection and Screening of Early Lung Cancer by Novel Imaging Technology and Molecular Essays.

a These studies include individuals with synchronous or metachronous tumors. The prevalence and incidence rates are based on the number of individuals diagnosed with lung cancer rather than the total number of cancers. b Preliminary data of the first 6 months of this study are shown.

(*) Modified from Sanchez-Salcedo P, Berto J, de-Torres JP, Campo A, Alcaide AB, Bastarrika G, et al. Lung Cancer Screening: Fourteen Year Experience of the Pamplona Early Detection Program (P-IELCAP). Arch Bronconeumol. 2015;51:169-176.

11 (91.6%) of the 12 patients with LC showed nodular appearance on CT scans. Examples of some cases will be shown (Figs 1 and 2).

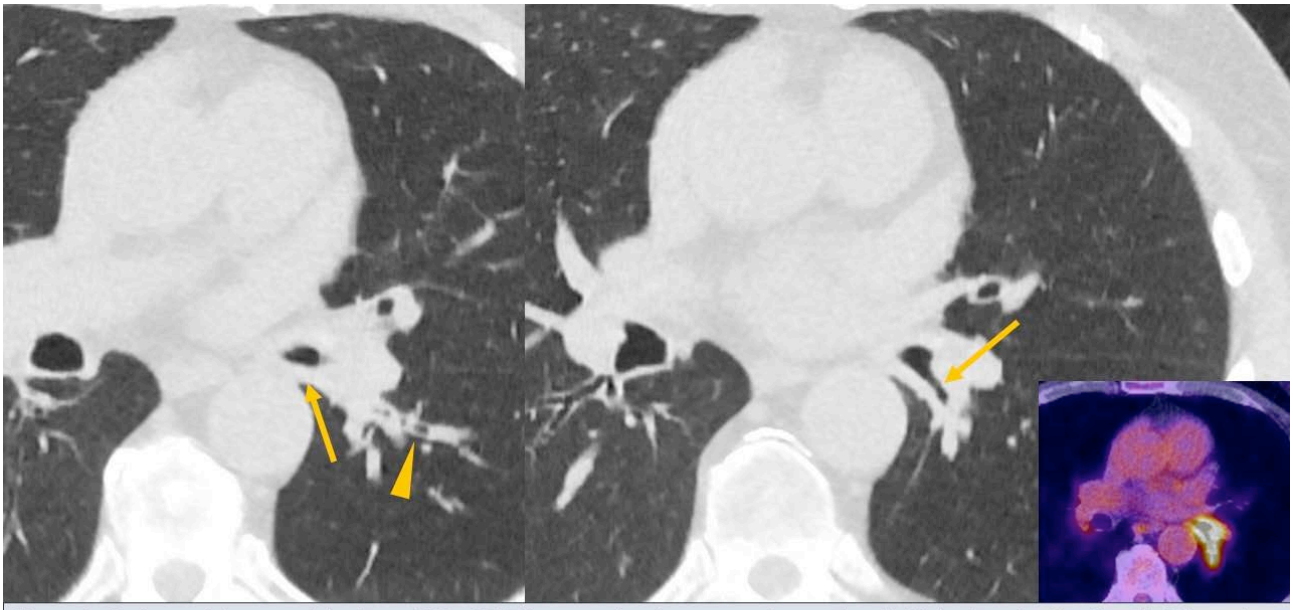

Figure 1. Patient with no nodular Lung SCC: LDCT images showing narrowing and wall thickening in the distal LM bronchus extending into the LLL bronchus and LLL apical bronchus (arrows). Note some focal mucous plug within segmental airway of left segment 6 (arrow head). PET CT detected a bronchial lesion with no lung nodules lymphadenopathy or metastases. Patient underwent left pneumonectomy. Only a patient in this study showed this non nodular pattern on CT scan.

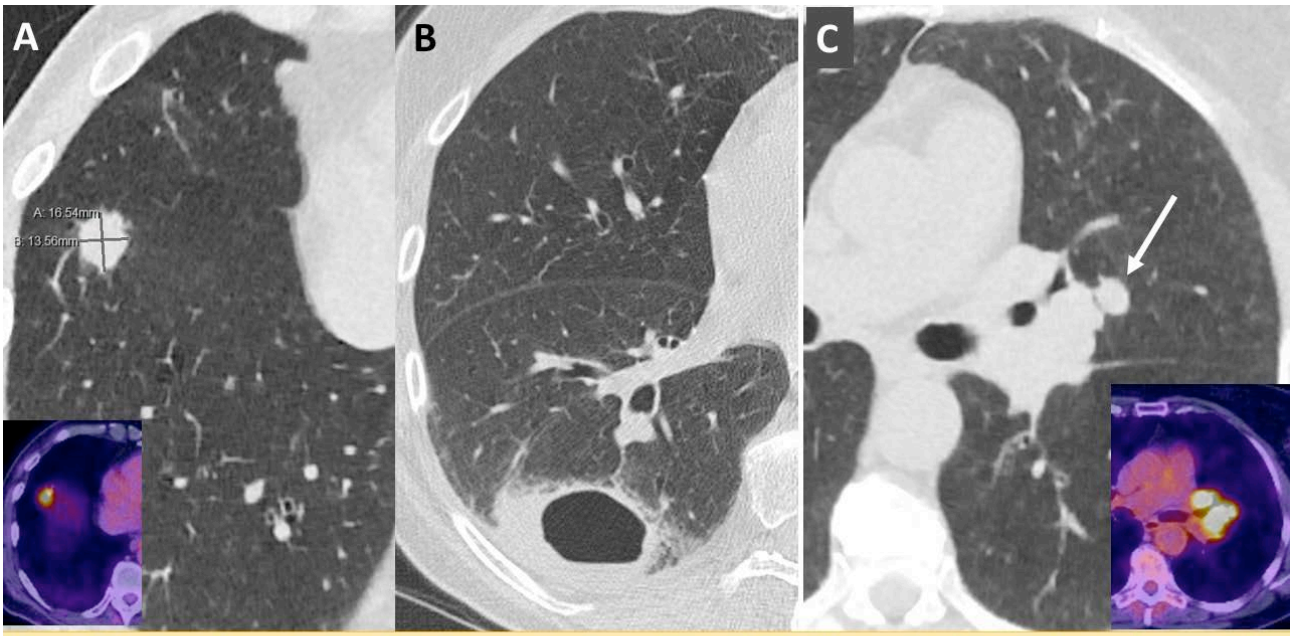

Figure 2. Patients with Lung Cancer with nodular presentation on CT scans**. A)** Solid lung nodule. This was the most frequent CT presentation (N= 9) **B)** Solid lung nodule associated to cyst air space with thickened walls (N=1). **C)** Solid lung nodule (arrow) associated to hilar enlargement (N=1). PET CT did not detect a lung nodule as such in this case.

Conclusion

The prevalence of LC in those screened in Crawley was 1.1% with the majority having early-stage adenocarcinoma and going on to have surgery. The prevalence and proportion of Stage I are similar to the first round of other LCS such as NELSON or NLST. Most of the LC found demonstrated nodular radiographical appearances.

These preliminary results are promising in the aim to find and treat early-stage disease in the population at high risk of LC in England.

References:

[1] NHS England. , (2022), Targeted screening for lung cancer with low radiation dose computed tomography. Standard protocol prepared for the Targeted Lung Health Checks Programme by the Lung Clinical Expert Advisory Group. , NHS England, Publication reference: PR1646.

[2] NHS England. , (2022), Targeted screening for lung cancer with low radiation dose computed tomography. Quality assurance standards prepared for the Targeted Lung Health Checks programme Prepared with guidance from the Lung Clinical Expert Advisory Group. , NHS England

[3] Sanchez-Salcedo P, Berto J, de-Torres JP, Campo A, Alcaide AB, Bastarrika G, et al, (2015), Lung Cancer Screening: Fourteen Year Experience of the Pamplona Early Detection Program (P-IELCAP), Arch Bronconeumol, 169-176, 51

A-230

Pretreatment Interstitial Lung Abnormality Detected on Abdominal Computed Tomography in Prostate Cancer Patients

J. Y. Lee[1], W. G. Jeong[1], Y.-H. Kim[2]
[1]Chonnam National University Hwasun Hospital, Radiology, Hwasun, Republic of Korea (South Korea), [2]Chonnam National University Medical School, Radiology, Gwangju, Republic of Korea (South Korea)

Objectives
Prostate cancer is the most commonly diagnosed cancer in men, particularly in those aged 65 years and above. The purpose of this study was to investigate the prevalence of pretreatment interstitial lung abnormality (ILA) among prostate cancer patients who underwent abdominal computed tomography (CT) within one year at their first visit to the urology department. Additionally, we aimed to assess the association between pretreatment ILA and long-term survival in prostate cancer patients.
Methods & Materials
This study was conducted in patients who had a first visit for prostate cancer at urology department between 2005 and 2016 and underwent an abdominal CT within one year. A thoracic radiologist evaluated the presence of ILA through inspecting the lung base scanned on an abdominal CT. The association between pretreatment ILA and survival was assessed using Kaplan-Meier analysis with log-rank test. Specific survival rates at 12, 36, and 60 months according to the presence of ILA were evaluated using *z*-test. Cox regression analysis was used to assess the risk factors of mortality.
Results
A total of 173 patients were included in this study (mean age: 70.23 ± 7.98). An ILA was observed in 18 patients (10.4%) in abdominal CT scans. Patients with ILA were more likely to be older and current smokers. The survival was significantly poor in patients with ILA compared to those without ILA ($p < 0.001$). Subgroup analysis with localized-stage prostate cancer patients also showed poor survival in patients with ILA ($p < 0.001$). Multivariable Cox regression analysis revealed that age ≥ 70 (hazard ratio (HR), 95% confidence interval (CI); 1.98, 1.24–3.16, $p = 0.004$), metastatic-stage (HR, 95% CI; 2.26, 1.36–3.74, $p = 0.002$), and ILA (HR, 95% CI; 1.96, 1.06–3.60, $p = 0.031$) were independently associated with higher mortality. An ILA (HR, 95% CI; 3.94, 1.78–8.72, $p = 0.001$) was only an independent risk factor of mortality in a subgroup analysis with localized-stage prostate cancer patients.
Conclusion
Approximately 10% of prostate cancer patients showed pretreatment ILA in the lung base scanned on the abdominal CT. Furthermore, the presence of ILA on abdominal CT scans was significantly associated with higher mortality in prostate cancer patients. Therefore, lung bases should be routinely inspected in the abdominal CT scans of prostate cancer patients. In addition, prostate cancer patients who demonstrate a pretreatment ILA on abdominal CT scans should be referred to a pulmonology department for optimal management.

A-334

Prolong intercostal muscle wasting in follow-up of patients with COVID

M. J. Park
Gyeongsang National University School of Medicine, Gyeongsang National University Hospital, Radiology, Jinju, Republic of Korea (South Korea)

Objectives
Sarcopenia is known as the cause of the long-COVID syndrome. We investigated which thoracic muscle was severely affected in follow-up in patients with COVID-19.
Methods & Materials
We retrospectively enrolled 99 patients who were diagnosed with COVID-19. All patients underwent chest CT in the initial and follow-up exams. According to the follow-up period, we separated the patients into groups with less than three month (group 1, n=52) and more than three month (group 2, n=47). The initial and follow-up CT scans were used to examine the intercostal, pectoralis, and T12 smooth muscle masses. A density histogram analysis is used to quantitatively analyze the area of muscle mass. We analyzed the degree of muscle loss by the following formula; (the initial muscle mass-follow-up muscle mass)/initial muscle mass.
Results
In the follow-up CT scan, the loss of intercostal muscle was significantly higher in group 2 than in group 1. (31.6% vs 18.5%). The loss of pectoralis muscle was lower in group 2 than in group 1. (4.8 vs 7.3%). On the other hand, T12 smooth muscle mass in the follow-up was slightly decreased in group 1 (2.3%) but slightly increased in group 2 (-5.3%).
Conclusion
The intercostal muscle wasting was profound compared to the pectoralis and T12 smooth muscle in a follow-up CT scan. The rehabilitation of intercostal muscle should be necessary to reduce the long-COVID syndrome and pulmonary complications.

A-750

Pulmonary Embolism in pregnant patietns- a retrospective study on radiation, doses, and quality

A. Liubauske, D. Litmanovich, Y. Liberman, G. Borisovsky
Harvard Medical School- Beth Israel Deaconess Medical Center, Radiology, BOSTON, United States of America

Purpose/Objectives

Despite 2010 multimodality imaging guidelines suggesting a VQ scan for assessment of pulmonary embolism in pregnancy, CTPA remains the main modality in the majority of clinical centers. Given the wide use of CTPA, constant optimization of its imaging quality and radiation dose is required. This study aims to study the factors influencing image quality, diagnostic accuracy, and radiation dose of CTPA in pregnant patients.

Methods & Materials

All CTPA for suspected PE in pregnant women at BIDMC that were obtained from 01.01. 2006 to 12.31.2022 were retrospectively evaluated. Demographic data (age, weight, height, age of gestation), subjective (visual) and objective (HU and noise index at 3 levels of the pulmonary arteries (PA) image quality (v)), presence of PE, alternative diagnosis, radiation dose (dose-length product – DLP and Volume Computed Tomography Dose Index - CTDI vol) were collected.

Results

451 CTPA were obtained and all were analyzed. The mean age was 31 ± 6 years (range 17–50). PE was diagnosed in 11 patients (2.4%). 49 patients had an alternative diagnosis (10.9%). The median DLP was 119 mGy□cm (IQR 102–155 mGy□cm). The median CTDIvol was 5.2 mGy (IQR 4.8–6.6 mGy). The DLP had a negative correlation with objective evaluation (range 0.07-0.1; p range 0.0028 - 0.045), not correlate with visual assessment of the pulmonary arteries (p = 0.73), 45 cases were non-diagnostical (visual assessment (VA) 1), 102 cases were fair quality (VA 2), 157 cases were good quality (VA 3), and 147 cases were excellent quality (VA 4). The visual evaluation of the pulmonary arteries correlated negatively with the age of gestation in weeks (-0.12; p = 0.0009) and BMI (-0.27; p < 0.0001). . The age of gestations in weeks (but not BMI) correlated with the DLP (0.09; p = 0.01 and p = 0.048).

Conclusion

Decreased radiation dose correlated with an increased objective evaluation of the pulmonary arteries. This can drive the way for modified imaging protocol with even lower radiation doses in this population in subsequent studies. Advanced pregnancy stage increases the risk of suboptimal quality study and increased radiation dose, thus, VQ scan should be encouraged in advanced pregnancy.

A-310

Quantitative computed tomography analysis of pulmonary emphysema in participants in lung cancer screening trials

O. Smorchkova[1], L. Gozzi[1], E. Cavigli[1], D. Cozzi[1], C. Moroni[1], A. Bindi[1], S. Luvarà[1], G. Picozzi[2], K. Ferrari[3], S. Cardellicchio[3], G. Gorini[4], V. Miele[1], M. Mascalchi[2]

[1]Careggi University Hospital, Department of Emergency Radiology, Florence, Italy, [2]Oncologic Network, Prevention and Research Institute (ISPRO), Department of Radiology, Florence, Italy, [3]Careggi University Hospital, Section of Respiratory Medicine, Florence, Italy, [4]Oncologic Network, Prevention and Research Institute (ISPRO), Epidemiology, Florence, Italy

Purpose/Objectives

Some recent studies show that emphysematous changes of lung parenchyma were significantly correlated with the parameters of pulmonary function tests [1]. Further surveys introduced the predictive value of pulmonary emphysematous changes for a definition of the individual risk profile of long-term mortality in smokers and former smokers [2].

The present study aimed to evaluate whether there was a significant correlation between quantitative computed tomography lung analysis of the severity of pulmonary emphysematous changes and gender, age, pack-years, the presence of Coronary Artery Calcifications (CAC), and status of smokers in subjects enrolled in two randomized clinical trials conducted for lung cancer screening in Italy.

Methods & Materials

Two hundred forty-eight smokers and former smokers underwent inspiratory ultra-low-dose chest computed tomography (CT) scans. All CT examinations were performed using the same protocol with standardized scanning parameters on the same CT scanner. The extent of emphysema was visually scored on CT images, in addition quantitative CT analysis was evaluated using the dedicated software tool CT Pulmo 3D (v.B30, Syngo.via, Siemens Healthineers, Germany). The density mask technique was applied by using a threshold cut-off value of – 950 Hounsfield Unit (HU). Parameters measured were lung volume (LV), low attenuation volume (LAV 950), the percentage of low-attenuation areas with density values below 950 HU, mean lung density (MLD), full width at half maximum of lung density histogram, and P15, the CT attenuation value corresponding to the 15th percentile of the histogram.

Results

Pulmonary emphysematous changes were present in 32.2 % of participants.

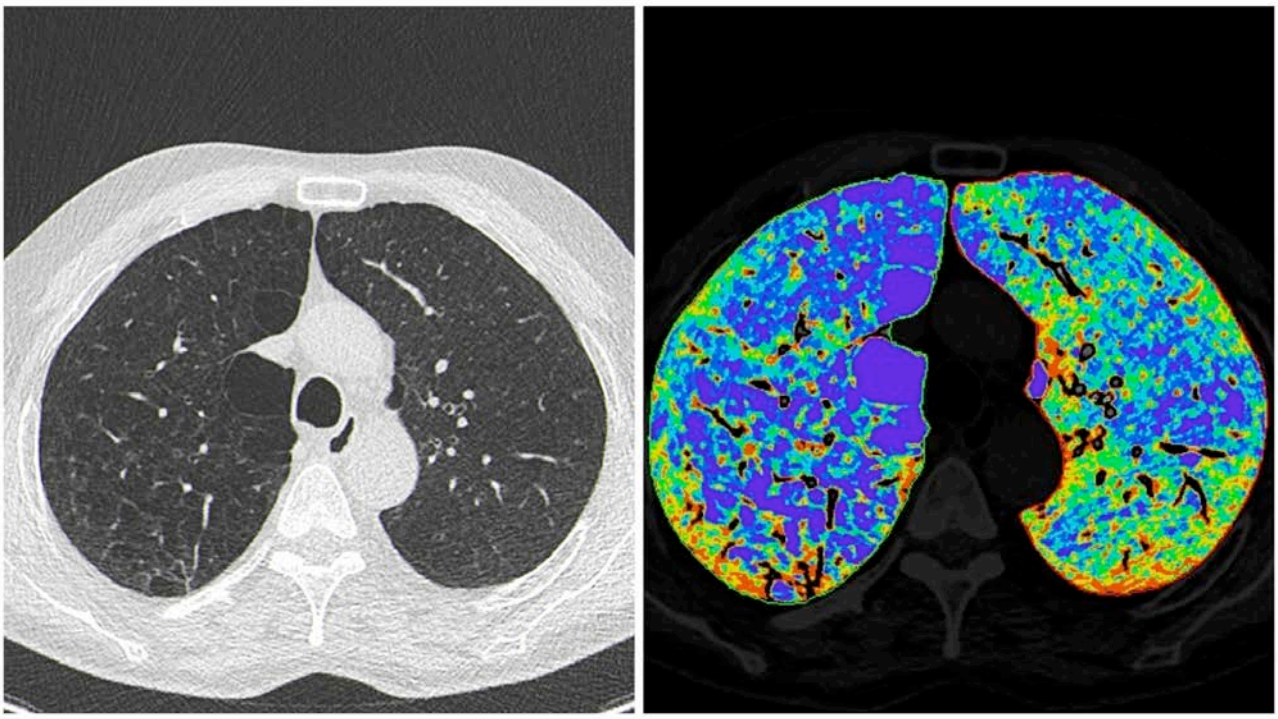

CT scan image in axial section (parenchymal window) shows paraseptal and centrilobular emphysema (left image). The same CT image elaborated with CT Pulmo 3D application(right image).

The mean LAV 950 were 1.6 %, and the mean MLD were –827,8 ± 27.7 HU. The P15 reproducibility coefficient with volume adjustment was -880.2 ± 29.3 HU.

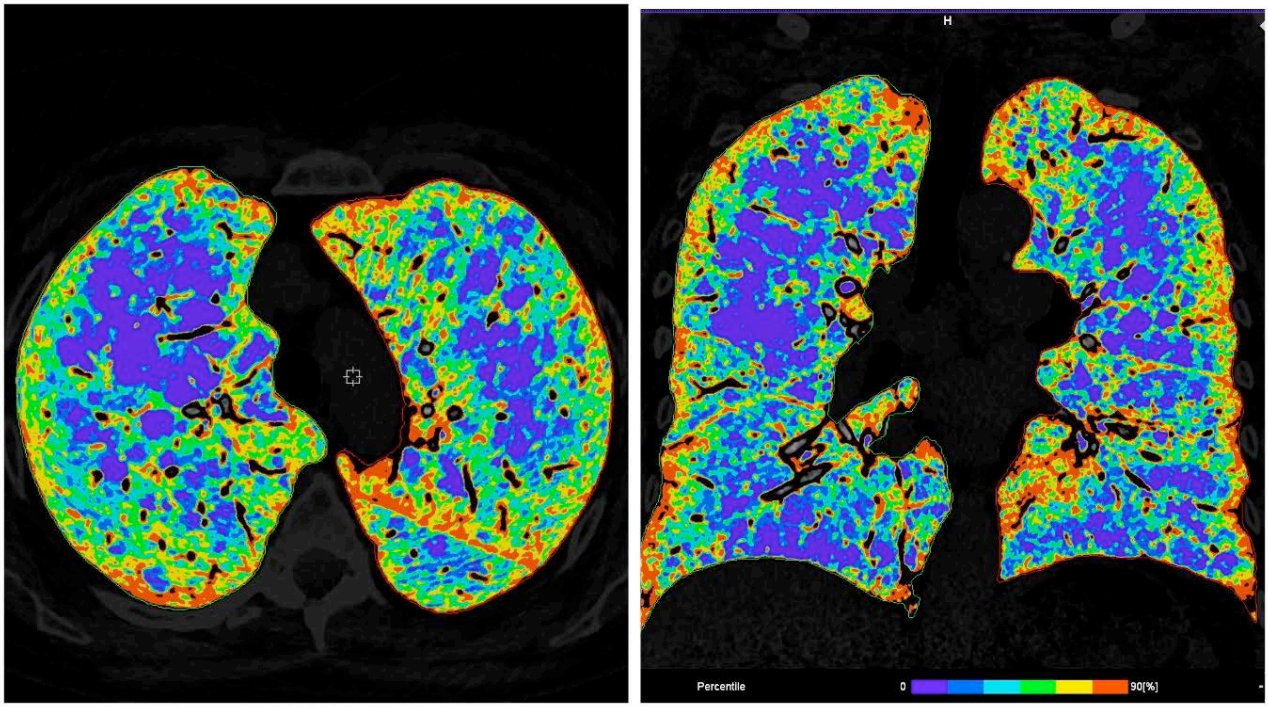

Axial (left) and coronal (right) density mask images of 74 y.o. female smoker show areas of emphysema (blue colour) with a threshold density value of -950 HU (LAV 6.6 %)

The emphysema extent showed a moderate correlation with male sex ($p<0.001$), old age ($p=0.001$), and status of former smoker ($p<0.001$).
Moderate/severe CAC were reported in 30.5% of subjects and it was correlated with male sex ($p=0.001$), old age ($p<0.001$), and > 30 pack-years history of smoking ($p=0.002$).

Conclusion

In this retrospective analysis, nearly one-third of subjects participating in lung cancer screening were affected by emphysematous changes. According to the fact that quantitative CT lung analysis of the severity of pulmonary emphysematous changes seems to predict the severity of lung function decrease [3] and risk of long-term mortality in smokers and former smokers, we suggest considering whether this type of analysis should be performed as a part of routine protocol screening for lung cancer.

References:

[1] Abd Elsalam, S.M., Hafez, M., Mohmed, M.F. et al, (2020), Correlation between quantitative multidetector computed tomography lung analysis and pulmonary function tests in chronic obstructive pulmonary disease patients, Springer, Egyptian Journal of Radiology and Nuclear Medicine, 1-8, 51, https://doi.org/10.1186/s43055-020-00281-4
[2] Pinsky PF, Lynch DA, Gierada DS, (2022), Incidental Findings on Low-Dose CT Scan Lung Cancer Screenings and Deaths From Respiratory Diseases, Chest, 1092-1100, 161(4), DOI: 10.1016/j.chest.2021.11.015
[3] Goldin J G, (2021), The Emerging Role of Quantification of Imaging for Assessing the Severity and Disease Activity of Emphysema, Airway Disease, and Interstitial Lung Disease, Respiration, 277-290, 100, DOI: 10.1159/000513642

A-302

Quantitative CT evaluation and disease progression in patients with asbestosis using CALIPER

L. Colligiani[1], B. Cosci[2], C. Roncella[3], B. J. Bartholmai[4], A. De Liperi[5], G. Guglielmi[6], E. Neri[1], C. Romei[5]
[1]Azienda Ospedaliero Universitaria Pisana, Department of Translational Research, Academic Radiology, Pisa, Italy, [2]Azienda Ospedaliero Universitaria Pisana, Department of Translational Research, Academic Occupational Preventive Medicine, Pisa, Italy, [3]Ospedale Apuane, Department of Radiology, Massa, Italy, [4]Mayo Clinic Rochester, Division of Radiology, Rochester, Minnesota, United States of America, [5]Azienda Ospedaliero Universitaria Pisana, Department of Radiology, 2nd Radiology Unit, Pisa, Italy, [6]Azienda Ospedaliero Universitaria Pisana, Occupational Preventive Medicine Unit, Pisa, Italy

Purpose/Objectives
To evaluate the role of CALIPER, a quantitative texture analysis software, in quantifying and differentiating interstitial lung disease (ILD) patterns such as reticulations (RET), ground glass opacities (GGO), and honeycombing (HC), and their progression over time in high-resolution computed tomography (HRCT) scans of patients with asbestosis compared to patients with IPF.
Methods & Materials
CALIPER was used to evaluate HRCT scans of 22 asbestosis patients and 21 IPF patients at baseline (T0) and after a mean time of 2.9 years (SD=0.65; min=2 years, max=4 years) (T1). The software segments the lung parenchyma and assigns a volume to RET, GGO, and HC in each patient. The volume of each pattern is divided by the total lung volume and summed up to calculate the ILD score, which represents the percentage of lung volume affected by these alterations. To assess disease progression over time, the difference between the ILD score at T1 and T0 was calculated for each patient and divided by the number of months between T0 and T1 (DeltaILD/month).
Differences in HRCT patterns at baseline and progression over time were analyzed between the two groups of patients.
Results
Progression over time (DeltaILD/month) was significantly slower in patients with asbestosis (median=0.40%/month; IQR=1.23) compared to patients with IPF (median=1.35%/month; IQR=4.38) (p=0.039).
Patients with asbestosis showed a significantly lower ILD score at T0 (median=3.42%; IQR=11.74) than patients with IPF (median=11.48%; IQR=9.52) (p=0.035).
Total lung volume was significantly higher at T0 in patients with asbestosis (median=4459.66 cc; IQR=866.33) compared to IPF patients (median=5482.29 cc; IQR=1784.33) (p=0.018).
Conclusion
CALIPER was capable of quantifying a slower progression over time in patients with asbestosis compared to patients with IPF, a finding which is in accord with clinical experience.

A-373

Quantitative evaluation of COVID-19 CT examinations using an AI-based CT Pneumonia Analysis prototype and correlation with outcome and clinical parameters

N. Trif[1], S. A. Schmidt[1], B. Grüner[2], S. Stenger[3], T. Stamminger[4], C. Kloth[1], M. Beer[1]
[1]University Hospital Ulm, Department for Diagnostic and Interventional Radiology, Ulm, Germany, [2]Ulm University Medical Center, Division of Infectious Diseases, Ulm, Germany, [3]Ulm University Medical Center, Institute of Medical Microbiology and Hygiene, Ulm, Germany, [4]Ulm University Medical Center, Institute of Virology, Ulm, Germany

Purpose

The study aimed to use an AI-based software prototype for the quantitative analysis of COVID-19 pneumonia in CT datasets of the lung, correlate it with clinical and laboratory parameters, and determine their impact on patient outcomes and intensive care medicine.

Methods & Materials

This single-center retrospective analysis consecutively included 66 patients (31 female, mean age 64.66 ± 16.28 years) with CT datasets of the lung from 12/2020 to 05/2021, all with confirmed COVID-19 pneumonia by PCR as gold-standard. The CT datasets were evaluated using the AI-based *Pneumonia Analysis Prototype* (Siemens Healthineers, Germany), an example is given in figure 1.

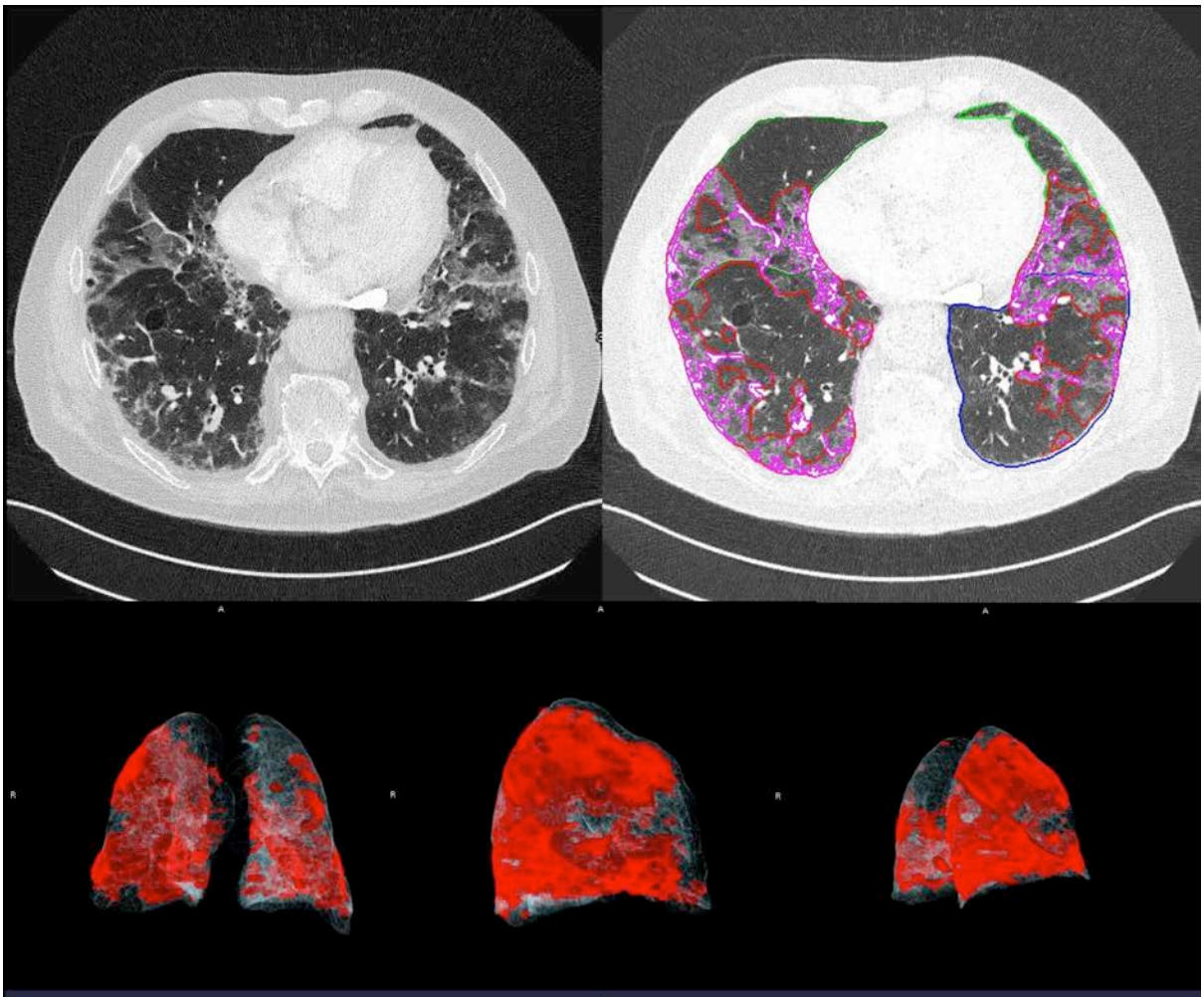

COVID-19 Probability: 1.00
Total Opacity Score: 9
Percentage of opacity: 24.20

L/R Lobes

	Both lungs	Left upper lobe	[illegible]	Right upper lobe	Right middle lobe	Right lower lobe
Affected	Yes	Yes	Yes	Yes	Yes	Yes
Opacity Score	9	1	2	2	2	2
Lung volume (ml)	6462.58	1738.45	1349.25	1588.87	652.53	1133.47
Volume of opacity (ml)	1563.78	146.29	340.42	438.33	210.65	428.08
Percentage of opacity	24.20	8.42	25.23	27.59	32.28	37.77
Volume of high opacity (ml)	143.31	14.04	35.09	21.94	23.69	48.55
Percentage of high opacity	2.22	0.81	2.60	1.38	3.63	4.28
Mean HU total	-752.59	-811.16	-703.62	-782.80	-763.52	-672.39
Mean HU of opacity	-613.16	-611.86	-581.27	-678.26	-603.91	-576.87
Standard deviation total	251.15	217.36	265.80	225.51	245.51	284.94
Standard deviation of opacity	268.93	275.60	270.66	232.55	286.37	278.83

Mean ct-value was 26.14±5.81 and the mean time between CT examination and microbiological proof was 0.33±0.67 days. All CT datasets were evaluated according to their quality (perfect-good-moderate-inadequate). Underlying diseases, patient outcomes including intubation and necessity of intensive care unit, and laboratory parameters were also evaluated.

Results

Overall, 26/66 (39.3%) CT examinations had perfect quality, 33/66 (50.0%) had good quality and 7/66 (10.7%) had moderate quality. Inadequate examinations were excluded. A distribution into minor and major corrections was performed: in 26/66 (39.3%) cases, major corrections and in 40/66 patients (60.7%), minor corrections were necessary. The mean post-processing time to complete the full analysis was 27.31±18.02 minutes.

The mean evaluated COVID-19 probability in the complete cohort was 0.81±0.36. Lung Severity Score (LSS), reflecting the severity of all lung lobes was 7 ± 4.7, overall lung volume was 3903.65 ±1185.67 ml and the mean volume of opacities was 866.52 ± 8219.29 ml. Overall, 12/66 patients died (18.2%), 10/66 patients (15.2%) required intubation, and in 27/66 (40.9%) cases, a stay at the intensive care unit was necessary, with a mean time of 5.72 ± 10.87 days. The mean time of intubation was 3.05 ± 8.42 days and the mean time at hospital was 16.12 ±13.73 days.

The mean CT value was significantly lower (p=0.045*, figure 2) and the mean age was with 74.54 years significantly older (p= 0.001*, figure 3) in patients who died.

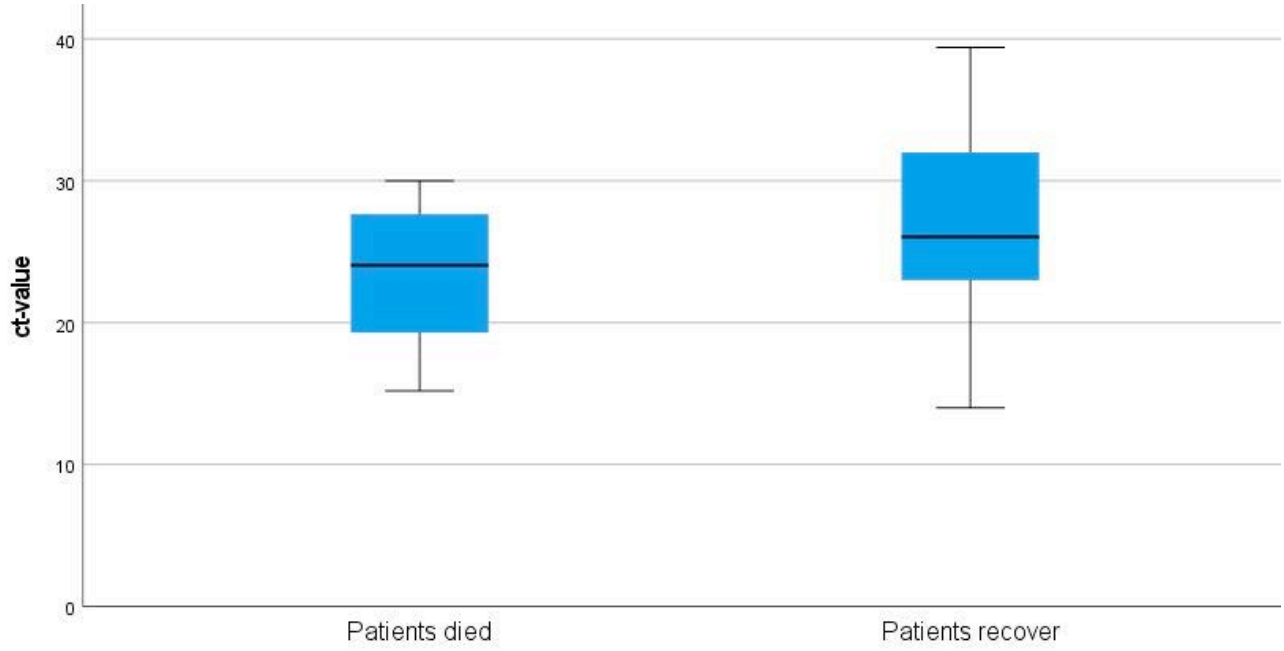

CT values in pateints that died and patients that recover

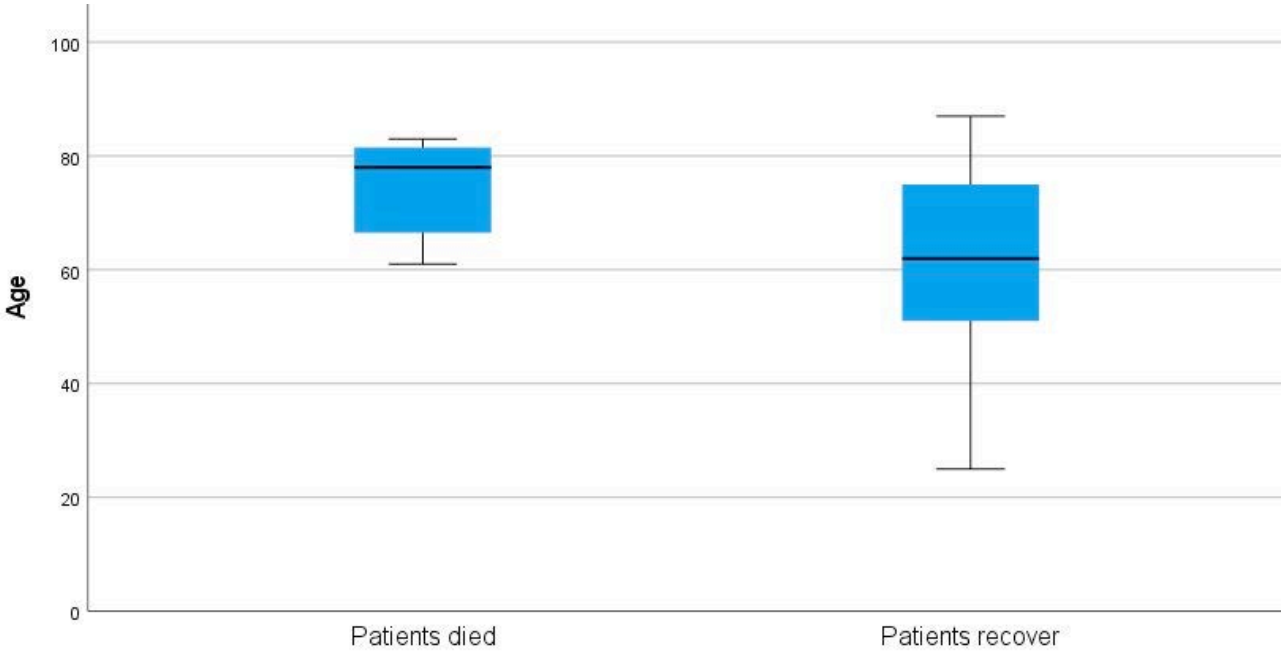

Comparison of mean age

The time spent in the intensive care unit was significantly longer (p=0.005*). There was no significant difference in the mean COVID-19 probability in patients who died (p=0.184). However, the volume of opacities (figure 4) and high opacities was significantly higher (p= 0.006* and 0.029*, respectively).

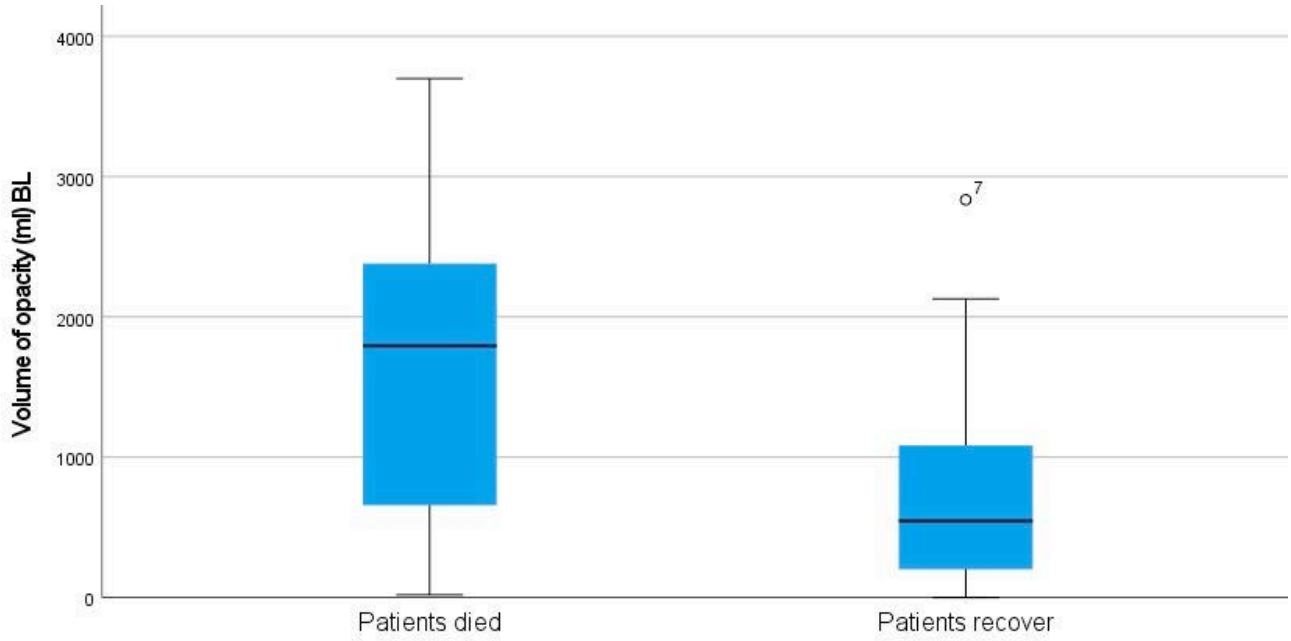

Comparison of volume of opacities

Conclusion

The *Pneumonia Analysis Prototype* is a precise tool for the detection and quantification of COVID-19 pneumonia. Quantifications allow for precise information about the volume of opacities, patient outcomes, and the necessity of intensive care medicine.

A-198

Radiomics-based Differentiation of Lung Adenocarcinoma and Squamous Cell Carcinoma in Contrast-Enhanced Computer Tomography

F. Palmeri, D. Caruso, D. De Santis, M. Zerunian, M. Polici, B. Masci, I. Nacci, S. Nardacci, F. Pucciarelli, A. Laghi
Sapienza - University of Rome, Department of Medical Surgical Sciences and Translational Medicine - Radiology Unit - Sant'Andrea University Hospital, Rome, Italy

Purpose/Objectives

To assess radiomics performances in differentiating lung adenocarcinoma from squamous cell carcinoma, aiming at avoiding lung biopsy.

Methods & Materials

A total of twenty patients (10 with lung adenocarcinoma and 10 with lung squamous cell carcinoma) with availability of baseline contrast-enhanced CT scans were retrospectively enrolled between August 2017 and January 2022. Pathological diagnosis was collected for each patient. Patients were divided into two groups: adenocarcinoma and squamous cell carcinoma. An expert radiologist manually segmented lung cancers on baseline CT scan at portal venous phase, by using a dedicated software (3DSlicer v5.2.2). 107 radiomics features were extracted and compared between two groups (T-test or Mann-Withney-U). Radiomics performance was assessed by receiver operating characteristic curves; univariate logistic regression was performed to investigate the correlation with pathology. P < .05 was considered significant.

Results

Each group consisted of 10 patients. Nine radiomics features showed significant differences between two groups: 1) Contrast, 2) DifferenceAverage, 3) DifferenceEntropy, 4) DifferenceVariance, 5) GrayLevelVariance, 6) ID, 7) RunLengthNonUniformityNormalized, 8) ShortRunEmphasis and 9) SumSquares. Among these, DifferenceEntropy

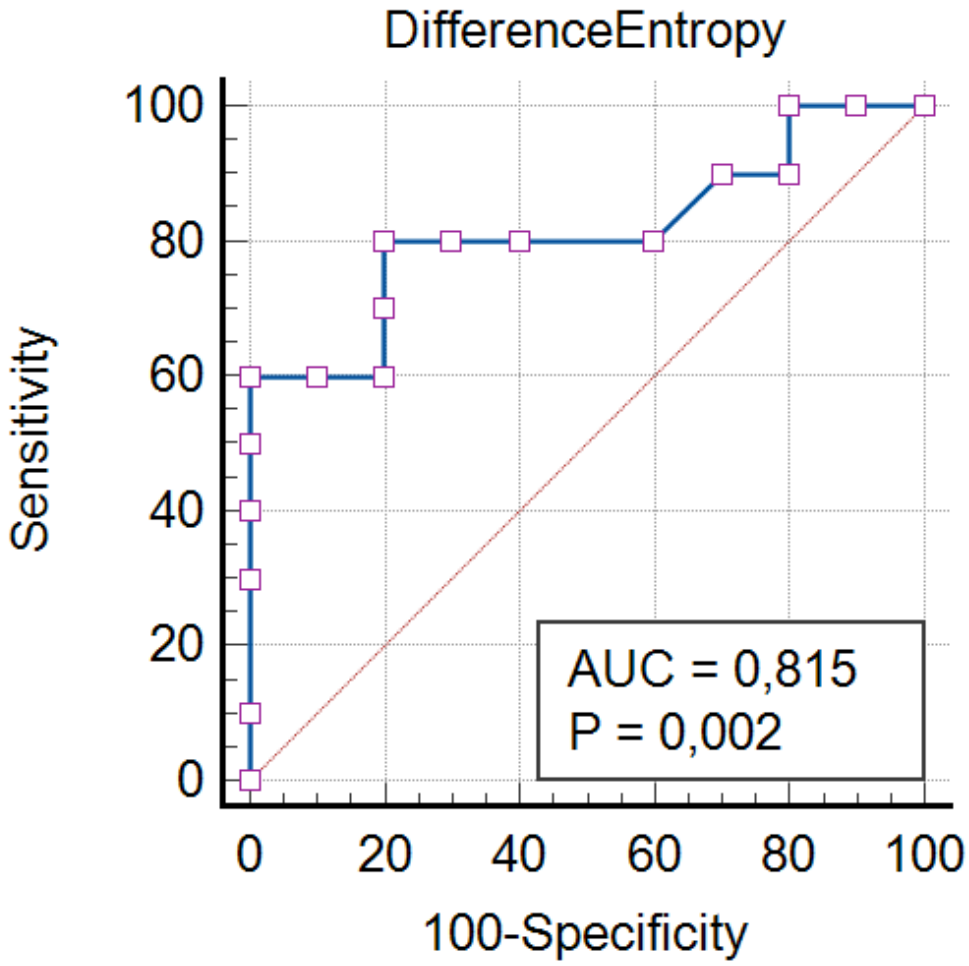

Performance of DifferenceEntropy to differentiate Lung Adenocarcinoma from Squamous Cell Carcinoma reaching AUC of 0.815 and DifferenceVariance

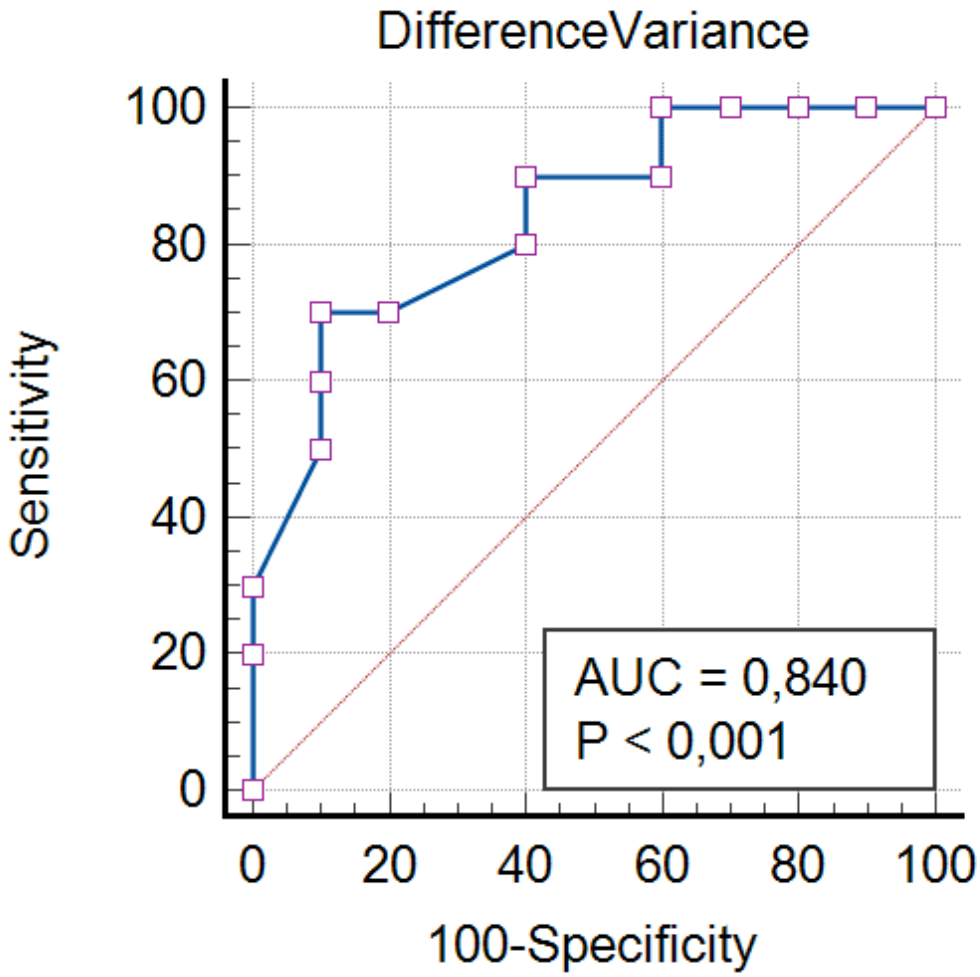

Performance of DifferenceVariance to differentiate Lung Adenocarcinoma from Squamous Cell Carcinoma reaching AUC of 0.815 had the best performance (AUC: 0.81 and 0.84, respectively P < .003). Univariate analysis showed five radiomic features independently correlated with histology: 1) SurfaceVolumeRatio, 2) DependenceNonUniformity, 3) LongRunEmphasis, 4) SizeZoneNonUniformity, and 5) SmallAreaLowGrayLevelEmphasis. Among these LongRunEmphasis had the highest AUC (0.73, P= .04).

Conclusion

Radiomics can be used as a non-invasive imaging biomarker to differentiate lung adenocarcinoma from squamous cell carcinomas, potentially overcoming biopsy tissue undersampling. Further studies are needed to standardize and strengthen our results.

A-352

SARS-CoV-2 Omicron variant infection in immunocompromised patients: clinical and imaging characteristics

K.-I. Kim[1], J. W. Kim[1], Y. J. Jeong[1], J. E. Lee[2]
[1]Pusan National University Yangsan Hospital, Radiology, Yangsan, Republic of Korea (South Korea), [2]Chonnam National University Hospital, Radiology, Gwangju, Republic of Korea (South Korea)

Objectives
To evaluate clinical and imaging features of SARS-CoV2 Omicron variant infection in immunocompromised patients.

Methods & Materials
Consecutive adults hospitalized for confirmed COVID-19 between January 2022 and December 2022 at a single center were retrospectively included. Chest radiographs or CT were available in all patient. Patients were divided into two groups according to the immune status; immunocompetent vs immunocompromised. Immunocompromised status was defined as having an active solid organ or hematological cancer, solid organ transplantation, active immune mediated inflammatory disorders, and HIV/AIDS. Pearson $\chi 2$ test, Fisher exact test, or the independent t-test were used to analyze the differences of clinical and imaging features between two groups. Multivariable logistic regression analyses were used to evaluate the effect of immune status on imaging features of pneumonia and clinical severity.

Results
Of the 340 patients (mean age, 68years ± 14, 117 women), 93 patients (27%) were classified as immunocompromised status. The proportions with severe pneumonia were 53% of immunocompromised patients (49 of 93) and 53% of immunocompetent patients (131 of 247) on chest radiographs. The immune status was not significantly associated with clinical severity, but the patients with solid organ transplantation were associated with higher odds of severe pneumonia based on chest radiograph (OR, 2.08 [95% CI: 1.11, 3.91; P = .02]). The proportions with typical pattern pneumonia were 41% of immunocompromised patients (30 of 74) and 24% of immunocompetent patients (36 of 150) ($p<0.001$).

Conclusion
The clinical severity of patients with SARS-CoV-2 Omicron variant infection was not significantly different depending on the immune status of patients. However, patients with solid organ transplantation had a higher risk of severe pneumonia based on chest radiograph. Immune-compromised patients with SARS-CoV2 Omicron variant infections had significantly higher proportions of typical pattern pneumonia compared with immunocompetent patients.

A-427

Semi-automated segmentation and ventilated lung quantification on chest CT in SARS-Cov-2 hospitalized patients: can Artificial Intelligence improve diagnostic accuracy and enhance clinical management?

D. Gandola, M. Ragusi, T. P. Giandola, C. Maino, C. Talei Franzesi, R. Corso, D. Ippolito
IRCCS San Gerardo, Monza, Italy

Purpose/Objectives
To use an artificial intelligence (AI)-based prototype algorithm to perform a fully automated segmentation and ventilated lung quantification on chest computed tomography (CT) to assess lung involvement in patients affected from COVID19.
Methods & Materials
A total of 68 patients with confirmed SARS-CoV-2 infection was enrolled between March 1st, 2020, and April 5th, 2020. All patients undergoing chest CT in three hospitals in Northern Italy. All images underwent quantitative analyses with a dedicated workstation using the COPD software (IntelliSpace Portal, Philips Healthcare, Eindhoven, the Netherlands) for automatic lung segmentation and ventilated lungs volume calculation, ground glass opacities volume and consolidation volume. A qualitative evaluation, including the presence, distribution and number of pure ground glass opacity, focal alveolar consolidation and mixed lesion for each lobe was also performed.
Results
Thirty-two percent of patients required mechanical ventilation (22/68), while all other patients were managed with non-invasive techniques. Ground glass opacities were present in 90% (61/68) of patients, mostly with a bilateral and subpleural distribution. More than half of patients (38/68, 56%) revealed the presence of consolidation. A total of 21/68 patients (30.8%) presented fibrotic bands. The mean of total lung volume was 2848±1310 ml, the mean of ventilated lung volume was 3894±1157 ml. A significative correlation was found between ground glass opacities volume and white blood cells count ($p<0.05$), neutrophils ($p<0.0001$), C-reactive protein ($p<0.05$), peripheral oxygen saturation ($r= -0.356$, $p<0.05$). No significant differences were found with hard clinical outcomes, including need for mechanical ventilation, non-invasive ventilation or mortality.
Conclusion
The use of an artificial intelligence (AI)-based prototype algorithm for.CT elaboration effectively correlates with laboratory and clinical parameters. Further studies are needed to assess its impact on clinically relevant outcomes, including need for intensive care and mortality.
An artificial intelligence-enhanced algorithm for CT elaboration may help clinicians to forecast severity and need for intensive care in COVID19 patients.

A-366

Subsolid pulmonary nodules: the role of quantitative CT features to predict malignancy

N. Antunes[1], C. Romei[2]
[1]Hospital de Cascais, Radiology, Lisbon, Portugal, [2]Azienda Ospedaliero-Universitaria Pisana, Pisa, Radiology, Pisa, Italy

Purpose
To study the relationship between quantitative CT features of subsolid pulmonary nodules in CT imaging and the severity of the corresponding histopathological diagnosis.
Background
Persistent subsolid pulmonary nodules (SSNs), which comprise pure ground glass and part-solid nodules, can be identified incidentally or as part of lung cancer screening in chest CT and represent a spectrum of neoplastic growth ranging from atypical adenomatous hyperplasia (AAH) to adenocarcinoma in situ (AIS), minimally invasive adenocarcinoma (MIA) and invasive adenocarcinoma (IAC). However, follow-up guidelines are variable and SSNs management remains a clinical challenge.
Methods & Materials
We retrospectively reviewed the clinical, histopathological and CT characteristics of 73 SSNs detected incidentally in chest CT which underwent surgical resection between January 2012 and September 2021 at our institution. Quantitative CT features (maximal orthogonal diameter, volume, mean CT attenuation and its standard deviation and WHO area) were assessed for each lesion using a semi-automated volumetry algorithm (Syngo VIA, version VB30).

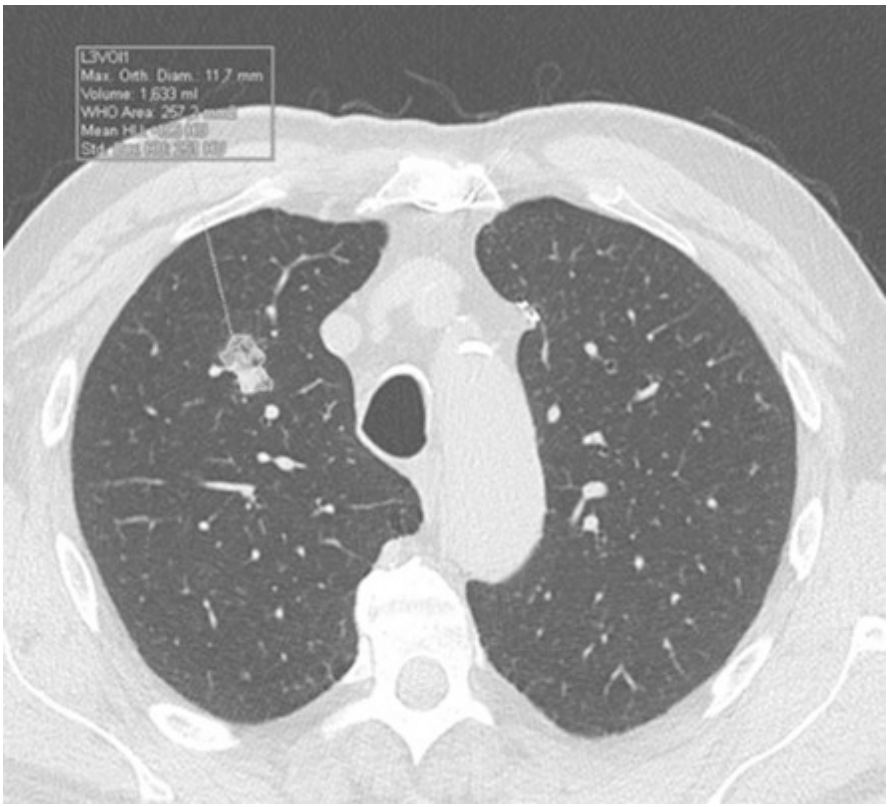

Unenhanced chest CT (lung window) shows measurements obtained of a part-solid nodule using semi-automated volumetry algorithm (Syngo VIA, version VB30; Siemens Healthcare). The reader draws a linear stroke across each lesion in the axial plane, after which the program automatically generated 3D masks.

Results
Most of the lesions were part-solid nodules (48; 65,8%) while the remainder were pure GGOs (25; 34,2%). 6,8% of cases were categorized as non-malignant, 2,7% as AAH, 2,7% as AIS, 19,2% as MIA and 68,5% were diagnosed as IAC. The maximal orthogonal diameter, the volume and the WHO area tend to increase with increasing histological result severity, from non-malignant to AAH to AIS to MIA and especially to IAC; and the differences are statistically significant. The mean CT attenuation tends to increase with increasing histological result severity; but the differences are not statistically significant, although very close to being significant. No statistically significant difference was found between the standard deviation of HU and histological result severity.
Conclusion
CT quantitative features may be used to guide follow-up and management in patients with incidentally detected SSNs. A risk calculator for SSNs could include patient characteristics, nodule growth and CT quantitative features.

A-252

Synchronous primary lung tumors awareness: chest CT review as primer clue

J. Ip[1], A. Gaivao[1], C. Carvalheiro[2], S. Granadeiro[3], I. Rolim[4], N. Gil[5]
[1]Champalimaud Foundation, Radiology, Lisbon, Portugal, [2]Champalimaud Foundation, Thoracic Surgery, Lisbon, Portugal, [3]Champalimaud Foundation, Interventional Pulmonogy, Lisbon, Portugal, [4]Champalimaud Foundation, Pathology, Lisbon, Portugal, [5]Champalimaud Foundation, Oncology, Lisbon, Portugal

Purpose

This study aimed to investigate the radiological features of synchronous primary lung tumors (SPLT) and to determine the frequency of different histological types and their pairings in patients with SPLT[1][5].

Methods & Materials

A retrospective analysis was performed of the chest-CT (CT) images of 18 patients (11M:7F, mean age 66.6 ± 5.7 years) diagnosed with SPLT between May 2015 and December 2022. Each subject was characterized in terms of i) smoking, both history (yes/no) and packs per year; ii) both nodal (N) and metastases (M) staging; and iii) respiratory comorbidities (yes/no). Each tumor (2x18) was then characterized in terms of type (adenocarcinoma - ADC, squamous cell carcinoma - SCC, small cell lung carcinoma - SCLC, or neuroendocrine - NE), size (largest axial axis), location, density, and contours.

Relative frequencies were obtained for each tumor characteristic, as well as for pairs of tumor types. A oneway ANOVA was then performed to assess if there was a difference between such pairs and number of packs per year. The Fisher Exact Test was then applied in order to ascertain if there was an association between both smoking history and histological pairs versus N staging, M staging, and respiratory comorbidities. All statistical analyses were performed in IBM SPSS Statistics for Windows, v28.0. Significance was set at 0.05.

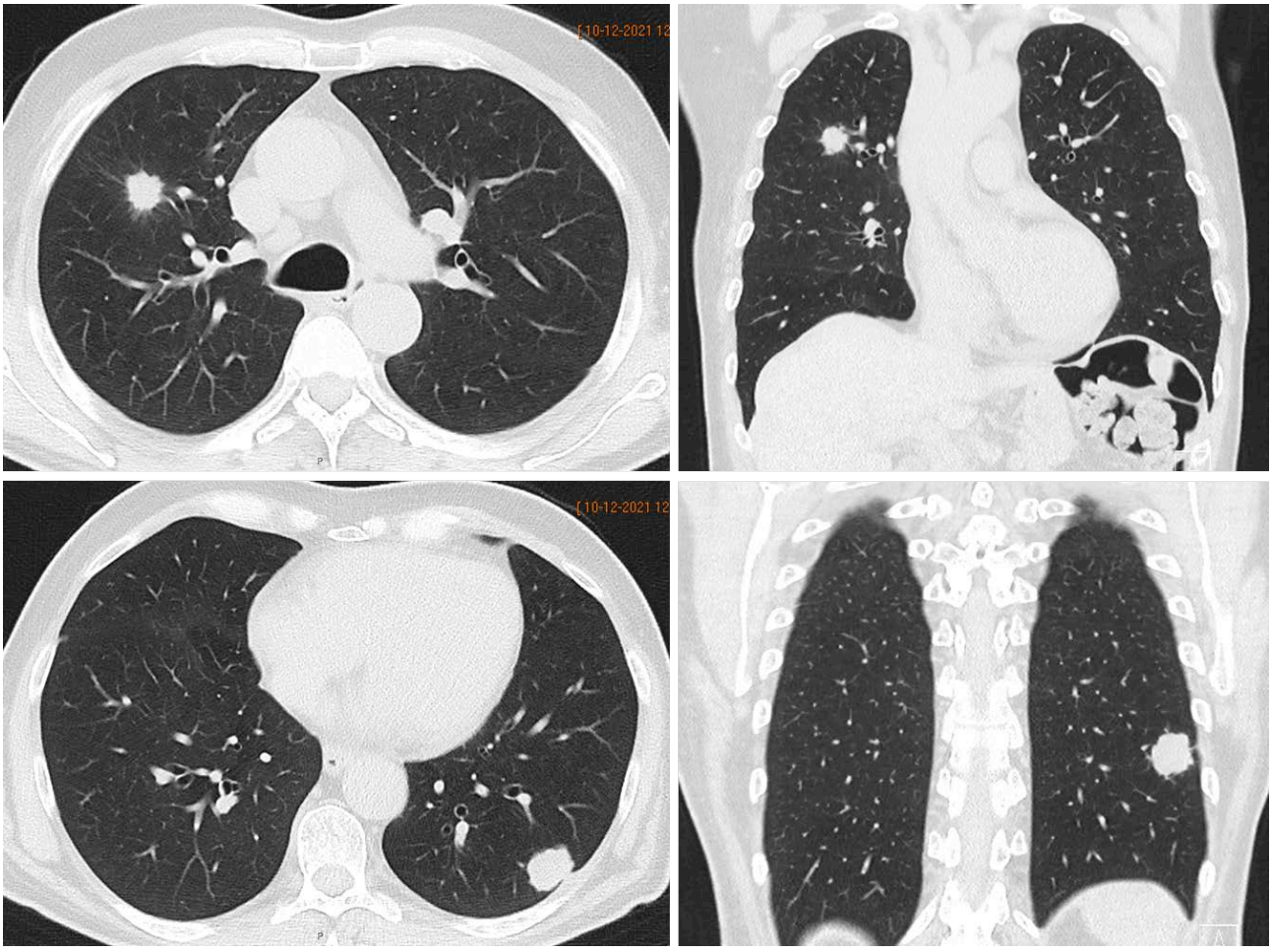

71-year-old patient, previous smoker (50-pack-year). Chest CT showed two pulmonary lesions: 1. a 27 mm spiculated-dense-nodule in the right upper lobe (RUL) and 2. 20 mm smooth-dense-nodule in the left lower lobe (LLL), ADC and SCC respectively

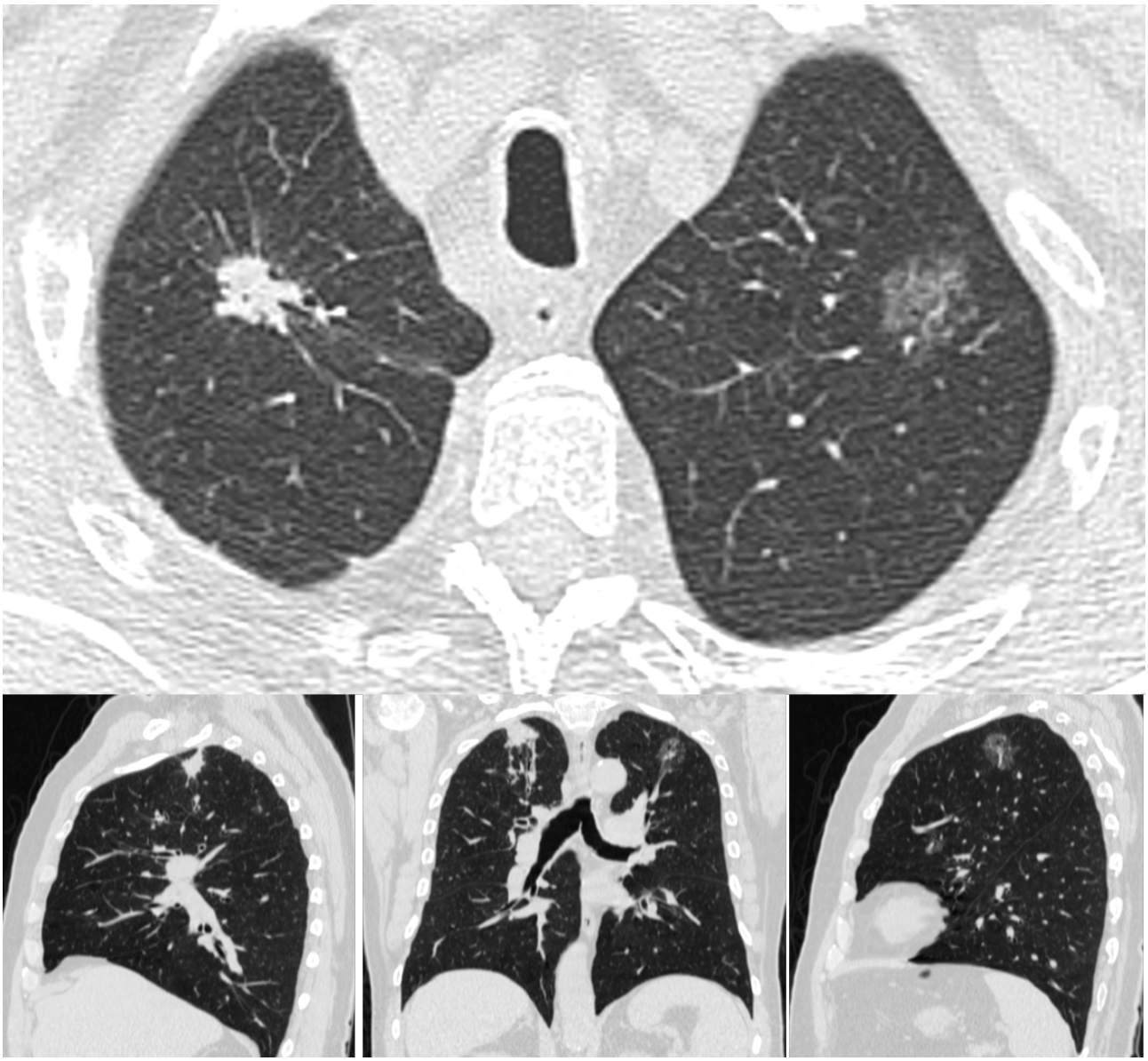

71-year-old patient, previous smoker (50-pack-year). Chest CT showed two pulmonary lesions: 1. a 35 mm spiculated-dense-nodule in the right upper lobe (RUL) and 2. 32 mm smooth-ground glass-nodule in the left upper lobe (LUL), both ADC

Results

Of the 36 tumors analyzed individually, the most common histological type was ADC (61.1%), followed by SCC (16.7%), NE (13.9%), and SCLC (8.3%).The majority of the tumors were located in the right upper lobes (33.3%) had a solid density (72.2%) and the majority had a spiculated contour (52.8%). The mean size of the tumors was 2.9 cm (range 0.2-8.7 cm).

The most frequent pairing was ADC+ADC (50%), followed by SCC+ADC (16.7%), SCLC+SCC (16.7%), NE+NE (11.1%) and ADC+NE (5.6%). There was a significant difference between pairs in terms of packs per year ($F = 3.923$, $p = 0.027$), with the highest consumption seen for ADC+SCC. Smoking history only presents an association trend ($p = 0.082$) with the presence of respiratory comorbidities. The type of histological pairs were significantly associated with the N staging ($p < 0.001$), suggesting lower stages for ADC+ADC[2][3][4].

Gender		
	M	11
	F	7
	Mean age	66.6 ± 5.7
Smoking		
	Current	8
	Former	6
	Non smoker	4
Pulmonary comorbidities		
	Yes	50%
	No	50%
Pairs		
	ADC+ADC	50%
	ADC+SCC	16,7%
	SCLC+SCC	16,7%
	NE+NE	11,1%
	ADC+NE	5,6%

Histological Type		
	ADC	22
	SCC	6
	SCLC	3
	NE	5
Location		
	RUL	12
	RML	2
	RLL	6
	LUL	9
	LLL	7
Density		
	Ground glass	6
	Subsolid	4
	Solid	26
Contours		
	Smooth	15
	Lobulated	2
	Spiculated	19

Demographics and radiological individual features of synchronous primary lung tumors (SPLT)

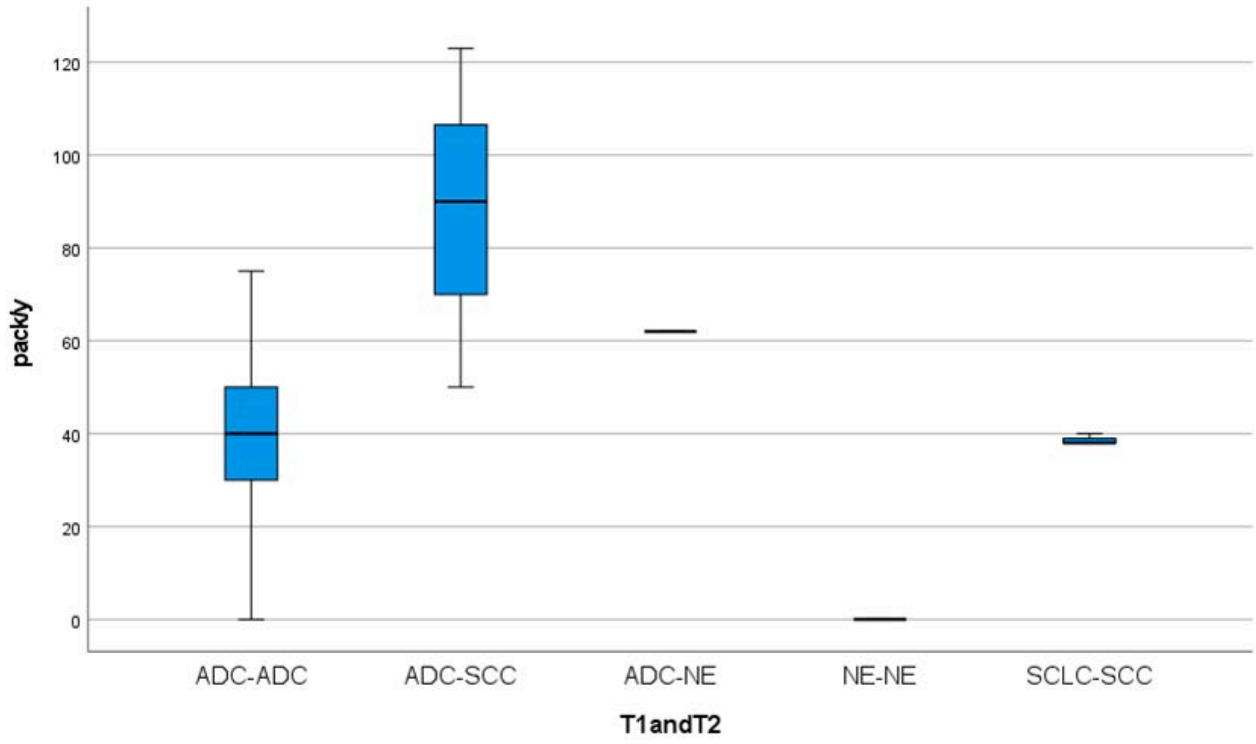

Pairs and smoking distribution

Conclusion

SPLT have better prognosis that lung cancer with intrapulmonary metastases. In this sample, SPLT are most commonly ADC+ADC, which also presents an association with lower N staging. A heavier smoking history was seen for all ADC pairs, notably ADC+SCC. Further studies are needed to confirm these findings for the broader population.

References:

[1] Georgia Hardavella , Ioannis Karampinis , Aggeliki Mpairaktari , Gerasimos Aravantinos , Nikolaos Anastasiou, (2018), Synchronous primary lung cancers;a clinical challenge inmodern thoracic oncology, European Respiratory Journal, 10.1183/13993003.congress-2018.PA1743

[2] Long Jiang, Jiaxi He, Xiaoshun Shi, Jianfei Shen, Wenhua Liang, Chenglin Yang, Jianxing He, (2022), Prognosis of synchronous and metachronous multiple primary lung cancers: Systematic review and meta-analysis, Elsevier, Lung Cancer, 303-310, 87, 10.1016/j.lungcan.2014.12.013
[3] Yangki Seok, (2015), Prognosis of Synchronous Double Primary Lung Cancer Based on Immunohistochemical Staining, Soonchunhyang Medical Science, 1-6, 28, https://doi.org/10.15746/sms.22.001
[4] Thomas E Stinchcombe, Shamus R Carr, (2022), Multiple primary lung cancers, Wolters Kluwer, UpToDate, https://www.uptodate.com/contents/multiple-primary-lung-cancers/
[5] Jingxu Li, Xinguan Yang, Tingting Xia, Yubao Guan, Nanshan Zhong, (2017), Stage I synchronous multiple primary non-small cell lung cancer: CT findings and the effect of TNM staging with the 7th and 8th editions on prognosis, Jounal of Thoracic Disease, 5335-5344, vol 9, n12, 10.21037/jtd.2017.12.101

A-699

The added value of the structured report in fibrosing lung pathologies: a model to follow even when not embedded in the RIS.

E. Tona[1], C. Timpanaro[1], G. La Rosa[1], S. Galioto[1], L. Reali[1], L. A. Mauro[1], C. Vancheri[2], S. Palmucci[1], A. Basile[1]
[1]University Hospital Policlinico "G.Rodolico - San Marco", Radiology I, Catania, Italy, [2]University Hospital Policlinico "G.Rodolico - San Marco", Pneumology, Catania, Italy

Purpose

Aim of this poster is to evaluate – in patients having fibrosing interstitial lung disease (fILD) – the concordance of radiological features described in the free text report – with those reported in the structured model.

Methods & Materials

60 HRCT studies – extracted from our RIS-PACS archive and performed in the period between January 2019 and November 2022 – were retrospectively analysed; HRCT examinations were reported by two radiologists with different level of expertise: i) in 40 cases, they were compilated by a radiologist with more than ten years of experience in the thoracic field; ii) in 20 cases, reports were redacted by a radiologist with no specific expertise.

All cases were redacted again according to the structured template: in this way, for each study, we examined the radiological findings described in free text report – assessing the degree of concordance with the items listed in the structured report template (not embedded in our RIS-PACS system).

Results

The items of the structured report template were satisfied in a percentage equal to 75.86 – in the group of HRCT examinations redacted by expert radiologists; in a quarter of cases, the free text report did not fill the specificities of the template, especially for disease quantification and fILD pattern. Another misalignment was observed in 16 patients (26.6%) – due to the fact that the "unclassifiable disease" item was not included among the "pattern items" yet.

The cases reported by inexperienced radiologist, on the other hand, showed a percentage of 64.9 in mentioning structured report template objects. In 2 cases, the presence of two main radiological features of fibrosing diseases – honeycombing and traction bronchiectasis – were not mentioned by the general radiologist. Pathology indicators such as cranio-caudal and axial distribution of fibrotic lesions and enlargement of mediastinal lymph nodes were described by the general radiologist in 66% of cases.

An element neglected by expert and general radiologists was the lack of quantification of the extension of fibrosis, rarely described in our sample, as well as any signs of loss of parenchymal volume, which represent new important imaging features that need to be addressed – considering the possibility of progressive fibrosing pathology.

Conclusion

The structured report represents a guide for radiologists without thoracic expertise; it constitutes an important weapon to reduce the risk of omitting essential elements. Based on our analysis, it should be followed during the redaction of thoracic reports – even if its template is not included in the RIS. Some needs emerge, including a standardized system for fibrosis quantification and an update of the classification items and radiological patterns.

A-319

The Benefits of Chest CT Imaging after Breast Cancer Treatment

J. H. Kim, S. H. Lim, H. Kwon, S. S. Kim
Chungnam National University Hospital, Radiology, Daejeon, Republic of Korea (South Korea)

Objectives
This study aims to present diverse chest CT findings in patients with breast cancer during or following therapy, which could be a valuable clinical practice reference, not only for radiologists but also surgeons and oncologists responsible for treating breast cancer patients
Methods & Materials
Chest computed tomography (CT) scans performed in patients with breast cancer between January 2018 and February 2023 were included. The study focused on image analysis of lesions in the chest, scanned upper abdomen, breast implants, and treatment-related complications, but excluded metastatic cancer.
Results
These lesions are grouped into several categories: 1. new lumps or growths that appear in either the breast that was previously treated for cancer or the opposite breast or chest wall. 2. changes or abnormalities seen on chest CT after breast reconstruction surgery. 3. changes or abnormalities following chemotherapy or radiation therapy. 4.incidentally discovered lung cancer.
Conclusion
Computed tomography (CT) is commonly performed in breast cancer patients for staging and monitoring as chest CT imaging, during or after treatment, can provide important information regarding metastasis, local recurrence, treatment-related changes, and possible complications in the thorax. Furthermore, local and regional tumor recurrence can be diagnosed earlier using CT than through physical examination. However, in some cases, treatment-related changes and complications concerning the recurrence of tumors and metastasis can be confusing for radiologists. Thus, radiologists must understand the various spectrum of findings when assessing treatment outcomes and care planning.

A-622

The impact of mediastinal nodes in progressive and non-progressive ILDs patients: a preliminary report

L. Reali[1], S. Galioto[1], C. Scavone[1], G. La Rosa[1], C. Timpanaro[1], E. Tona[1], C. Vancheri[2], L. A. Mauro[1], S. Palmucci[1], A. Basile[1]
[1]Policlinico di Catania, Radiology 1, Catania, Italy, [2]Policlinico di Catania, Pneumology, Catania, Italy

Purpose/Objectives

To investigate the impact of mediastinal lymph nodes in patients with Interstitial Lung Disease (ILDs) – focusing on their correlation with disease progression.

Methods & Materials

This retrospective study recruited 48 patients from our radiological RIS-PACS system and electronic database of "Regional Referral Center for Rare Lung Diseases". We have selected 17 females and 31 males (middle age 65.7 years) with ILD diagnosis obtained after multidisciplinary evaluation, having at least two volumetric HRCT scans (baseline and 1-year); for each clinical case, Pulmonary Function Tests (PFTs) – acquired nearest to the CT scan – were collected.

HRCT images, were interpreted in consensus by two thoracic radiologists: for each patient, the 2 larger mediastinal lymph nodes (exceeding 1 cm in short axis) – were registered. Semiautomatic volume segmentation of lymphatic nodes was achieved using Radiomic extension of 3D Slicer © (SlicerCIP4-8-1).

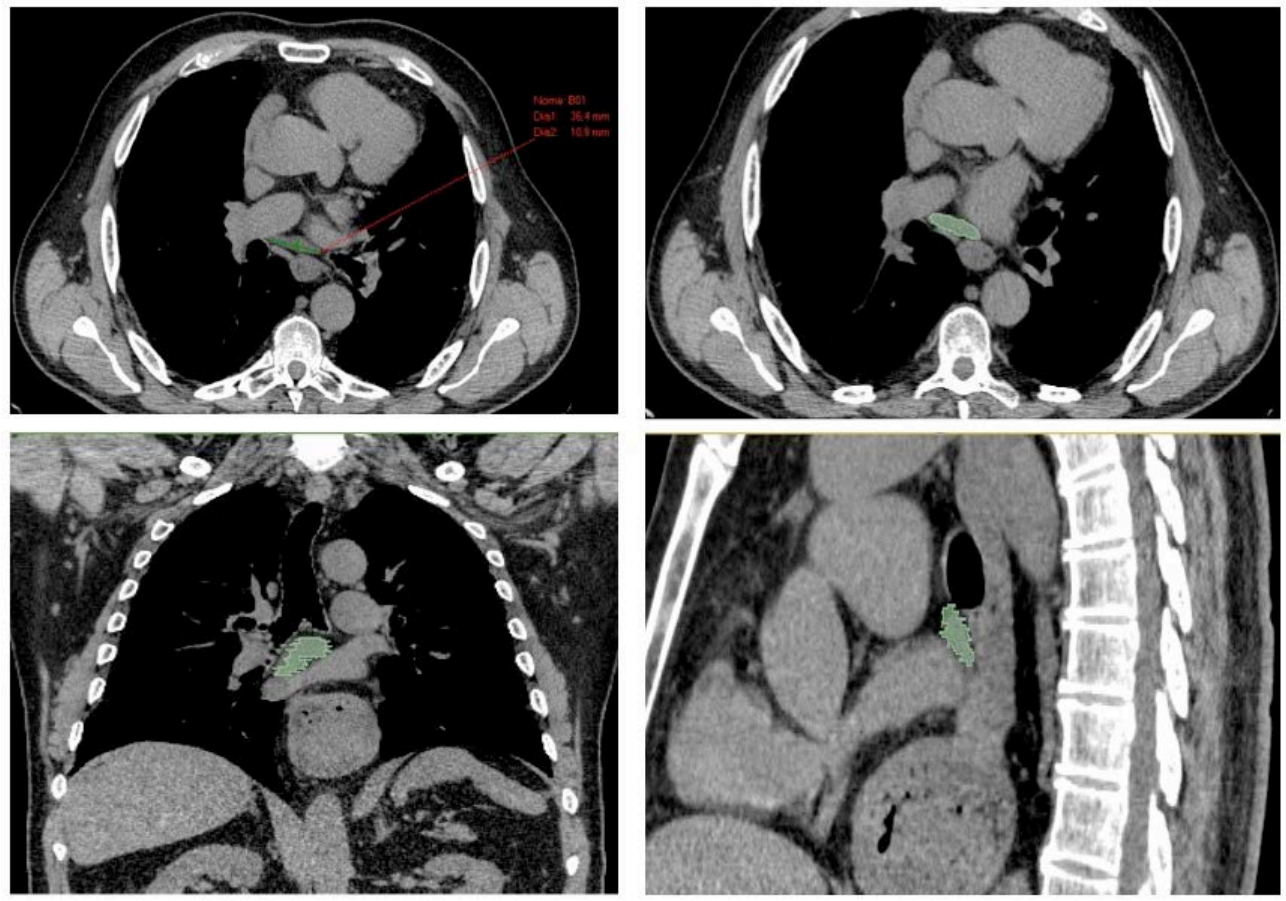

Subcarinal lymph node (7-IASLC), with axial diameters 36x11mm, analyzed through Radiomic extension of 3D Slicer © (SlicerCIP4-8-1).

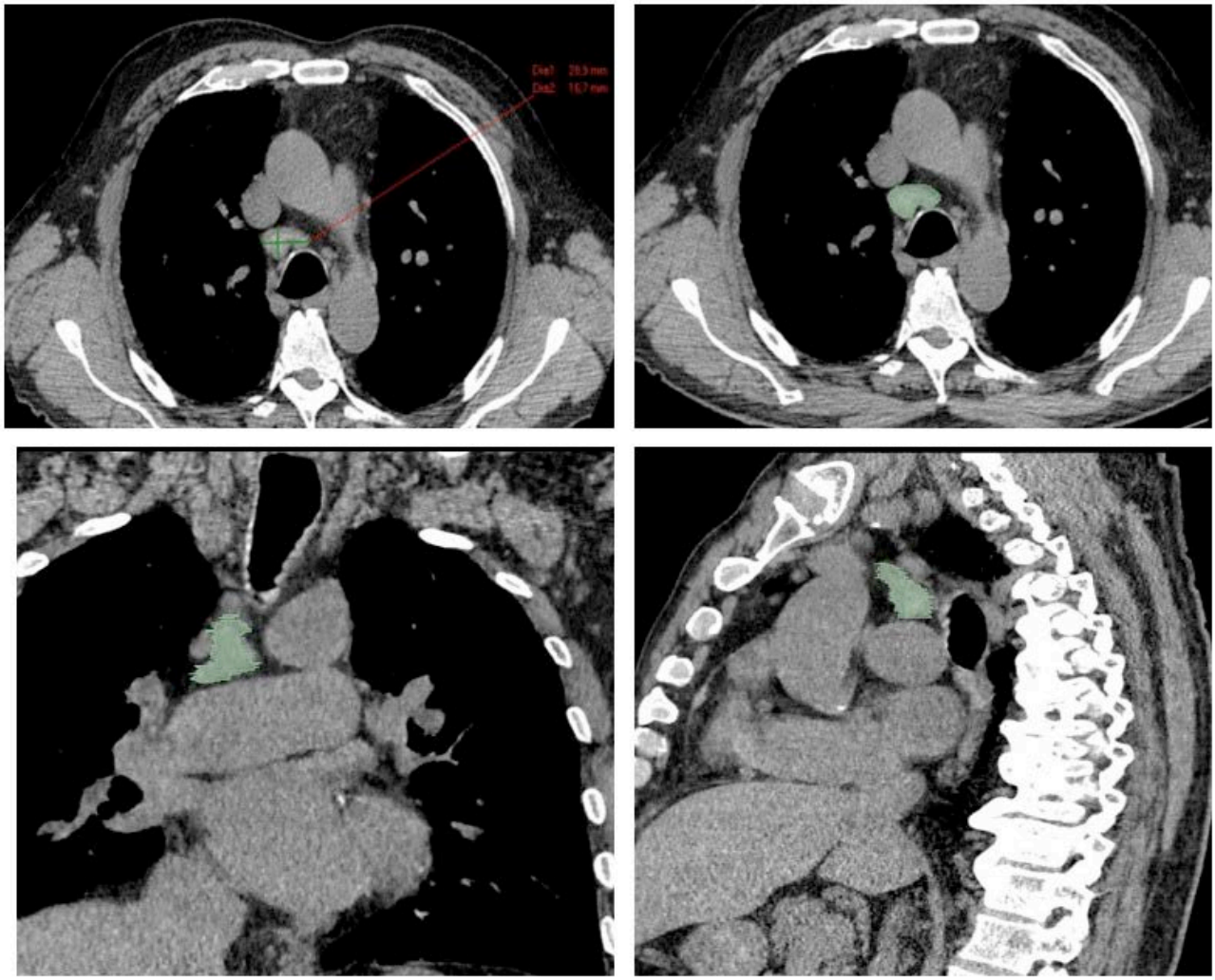

Paratracheal lymph node (4R-IASLC), with axial diameters 29x17mm, analyzed through Radiomic extension of 3D Slicer © (SlicerCIP4-8-1).

Baseline volumes of most enlarged nodes (at least 2 for each patient) were compared using the Mann-Whitney U-test. ROC analysis was performed to assess quantitative disease progression – based on the presence of enlarged mediastinal nodes.

Results

Disease progression was depicted in 16 cases (progressive group), whereas the remaining 32 cases were classified as stable disease. In non-progressive group, at baseline the mean volume of most enlarged nodes was equal to 1698 mmc (±1.103), whereas in the progressive group we reported a value of 2085 mmc (±682). At baseline, no statistical difference was reported between the 2 groups (p=0.08).

Receiver Operating Characteristic (ROC) curve reported an Area Under the Curve equal to 0.619, with sensitivity and specificity respectively of 90% and 46.2% - using a threshold value of volume >1394.9.

Conclusion

Extra-pulmonary findings should be highlighted in ILDs. Enlarged lymph nodes can be associated with a progression of the disease.

A-331

The unilateral pleural effusion: when is it malignant, when benign. A smalls study

T. Lou[1], C. Sai[2]
[1]QE gateshead, radiology, Gateshead, United Kingdom, [2]UHND, durham, United Kingdom

Purpose

To investigate probability of unilateral pleural effusion being malignant, for those who do not have well documented CT malignant features, but may have non specific CT features.

Methods & Materials

We reviewed CT findings of 30 patients; 13 malignant, and 17 benign. These patient all had pleural VAT procedure. Patient who showed clear signs of malignant CT features were excluded. Non specific features smooth mediastinal and peripheral pleural thickening of less than 5mm, and loculated appearing pleural effusion were included and these features evaluated.

Results

1) All large volume pleural effusions (6 in total) were malignant, regardless the pattern of non specific pleural changes were malignant.
2) All small volume pleural effusion (9 in total) were benign. The CT features here varied from none to quite prominent non specific changes.
3) There were equal malignant and benign diagnoses in the moderate pleural effusion group (15 in total). Pleural thickening of more than max of 2mm, and average of 1mm, tended to be malignant. Otherwise, there was no differences between the two groups .

Conclusion

This is a small study. However, allowing for this limitation:
1) Pleural effusion volume is a predictor for malignancy.
2) Non specific pleural changes, in particular mild mediastinal pleural thickening can be seen in small volume benign effusion. However, on the other spectrum, there may be no CT pleural features in a large volume malignant pleural effusion.
3) Moderate pleural effusion is still an unknown with no feature, apart from wall thickness differentiating the malignant and benign diagnosis.
4) These findings will be important for clinicians in deciding whether patients will need a further invasive biopsy procedure.

A-195

Aspergillus within the lung: a guide for the radiologist.

J. Collada-Carrasco[1], S. Hernández-Muñiz[1], P. Olmedilla-Arregui[2], C. De Benavides Bernaldo de Quirós[1], R. Gutiérrez-Rodríguez[1], P. Caballero Sánchez-Robles[1]
[1]Hospital Universitario de la Princesa, Radiology, Madrid, Spain, [2]Hospital Universitario Fundación Alcorcón, Radiology, Alcorcón, Spain

Learning Objectives
To review the spectrum of lung *Aspergillus*-related diseases and describe their main features for the radiologist to report.
Background
Aspergillus spp. are mold species ubiquitous on dust and soil, some of which (*A. fumigatus, A. flavus*) may affect human lungs through inhalatory pathway. The consequences will depend on host's immunity and previous lung pathology, defining a spectrum of diseases whose classification is still a pain in the neck for radiologists.
Acute angioinvasive aspergillosis (AAIA) is the most feared form; however, chronic variants (chronic cavitary pulmonary aspergillosis – CCPA- the most frequent) affect up to 250000 people around Europe and associate morbidity.
Imaging findings OR Procedure details

Immune status	Lung	Diseases
Hyperimmune	Normal // Asthma or Cystic fibrosis	Hypersensitivity pneumonitis (HP) // Allergic bronchopulmonary aspergillosis (ABPA)
Normal	Previous pathology	Aspergilloma // Aspergillus nodules // Chronic cavitary pulmonary aspergillosis (CCPA) // Chronic fibrosing pulmonary aspergillosis (CFPA)
Immunosupressed	Usually normal	Chronic necrotizing, Subacute invasive or semi-invasive pulmonary aspergillosis (SAIA) // Acute airway-invasive pulmonary aspergillosis // Acute angioinvasive pulmonary aspergillosis (AAIA)

Aspergillosis spectrum based on host's immunity and lung previous pathology.

HP: it does not differ from other acute or chronic HP. Historical farmer's lung or stipatosis were due to *Aspergillus.*
ABPA: suspected in asthma / cystic fibrosis patients with increasing symptoms or treatment needs, diagnosis is lab-based (eosinophils, IgG, IgE) and treatment involves steroids and/or targeted antibodies. Radiological features include "finger-in-glove" bronchiectasis with mucus "A or V shape" plugging (Figure 1). High-attenuation mucus is nearly pathognomonic.

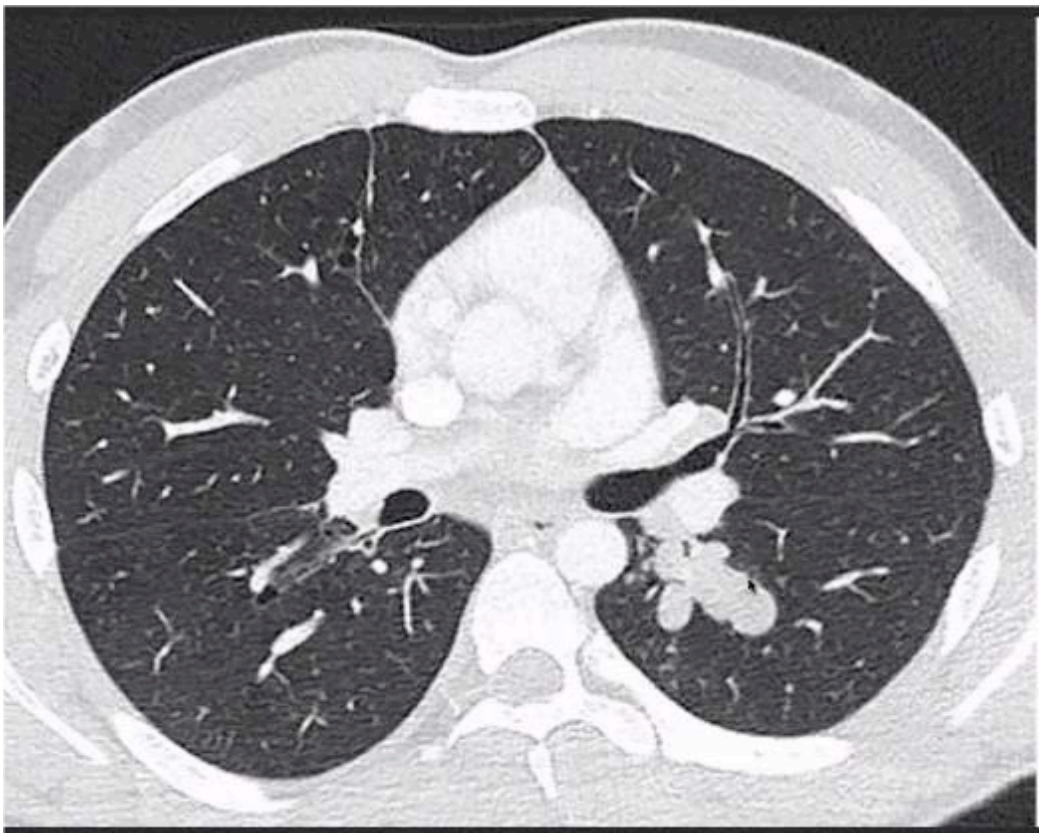

Central bronchiectasis with "A-shape" mucus plugging in a cystic fibrosis patient with ABPA

Aspergilloma: found alone or with other chronic forms, arises on a previous cavity and stays invariable, requiring embolization or surgical treatment only if symptomatic (hemoptysis). On CT it is a rounded non-enhancing mass that grows defining the Monod sign (Figure 2).

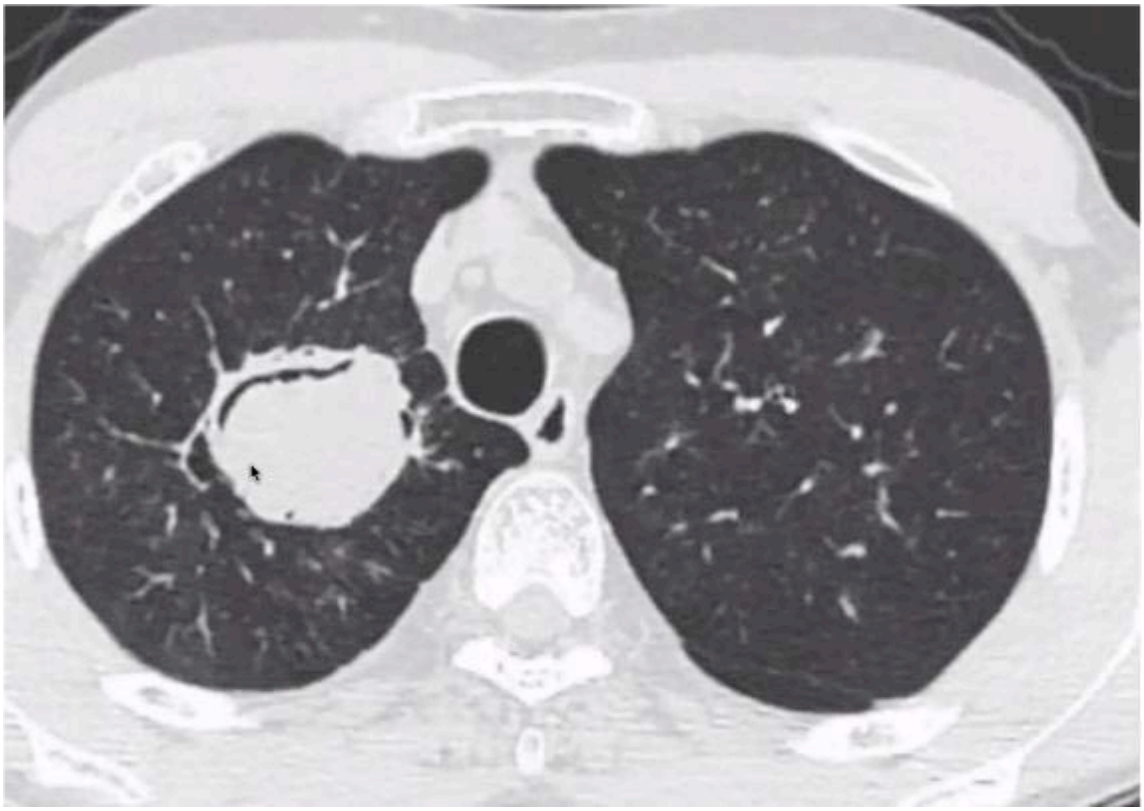

Aspergilloma within a lung cavity. Crescent-shaped gas around the micetoma is referred to as Monod sign.

CCPA: previous or new lung cavities (w/wo aspergillomas) slowly evolving with wall thickening and lung-pleural distortion (Figure 3). It

requires microbiology confirmation and is treated with antifungals to prevent **CFPA**, the end-stage form affecting at least two lobes and leading to pulmonary function loss.

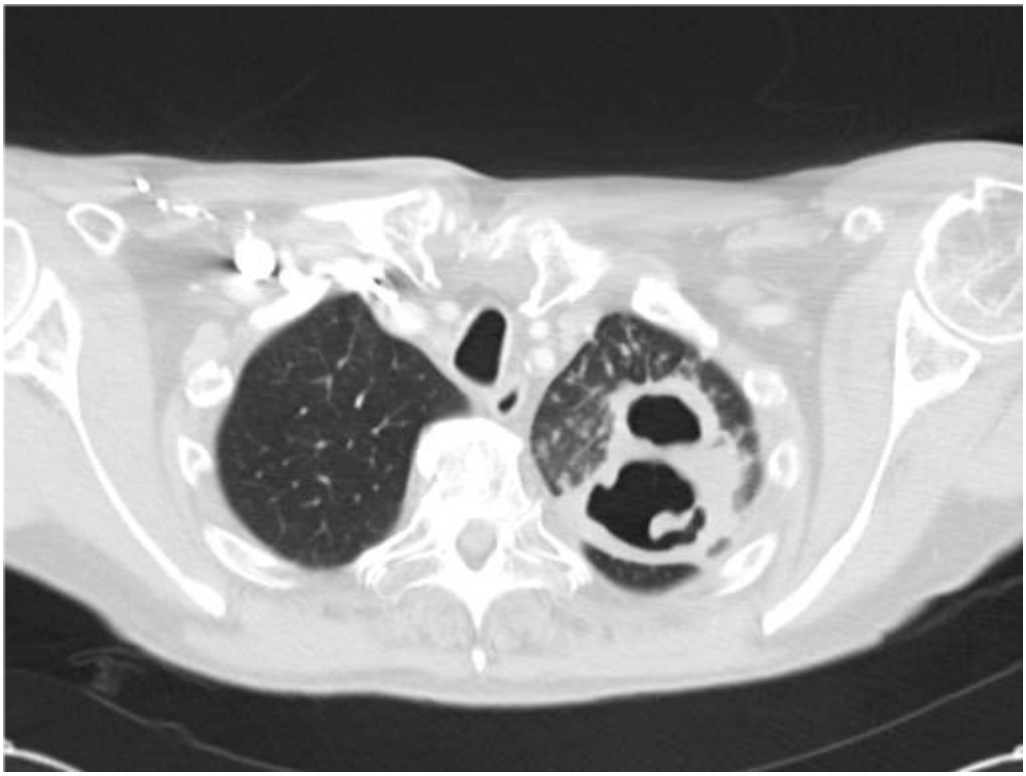

Chronic cavitary pulmonary aspergillosis (CCPA)

SAIA: mimics CCPA but evolves faster (weeks), takes place in the mildly immunosuppressed and markers (galactomannan on BAL and serum) and tissue samples show invasion, so it requires aggressive treatment.
AAIA: a cause of febrile neutropenia in the immunosuppressed, it results of small vessels invasion and associates great mortality. “Halo sign” (lung infarction and bleeding) and “air-crescent sign” (lung healing) should be reported. Invasion taking place in small airways is called **acute airway-invasive aspergillosis**. Both must be treated intravenously.

Conclusion

Aspergillosis are a wide spectrum of diseases depending on host and lung status, some of them morbidity-associated, other potentially fatal. As clinical and microbiological features can be non-specific, and in some cases histological sampling is not viable, the radiologist remains cornerstone in their diagnosis.

References:

[1] David W Denning et al., (2016), ESCMID/ERS GUIDELINES. Chronic pulmonary aspergillosis: rationale and clinical guidelines for diagnosis and management. , Eur Respir J, 45-68, 47(1), https://erj.ersjournals.com/content/47/1/45.long
[2] Prasad Panse et al, (2016), The many faces of pulmonary aspergillosis: Imaging findings with pathologic correlation., Radiology of Infectious Diseases, 192-200, 3 (4), https://www.sciencedirect.com/science/article/pii/S2352621116300821

A-260

Chest manifestations in chronic liver disease: a topic to keep in mind

P. Olmedilla[1], S. Hernández-Muñiz[2], P. Caballero[2], V. Quintana[1], F. Fernández-Alarza[1], I. Salmerón[2]
[1]Hospital Universitario Fundación Alcorcón, Radiology, Alcorcón, Spain, [2]Hospital Universitario de La Princesa, Radiology, Madrid, Spain

Learning Objectives
- To review clinical presentation, pathogenesis and treatment of the complications that occur in patients with cirrhosis
- To describe imaging findings in these entities

Background
Patients with chronic liver disease are at risk of extra-hepatic complications that compromise their quality of life, increasing their morbidity and mortality. Advanced liver disease is associated with the development of potentially severe pulmonary complications, such as hepatopulmonary syndrome, portopulmonary hypertension and acute respiratory distress syndrome (ARDS). Other chest manifestations include hepatic hydrothorax, infections and drug toxicity.

Imaging findings OR Procedure details
Hepatopulmonary syndrome is an indication for liver transplantation. Triad of liver disease, arterial hypoxemia and intrapulmonary vascular dilatation is the hallmark of the disease. On CT dilated pulmonary vessels are seen in subpleural location. This syndrome is due to the excessive production of vasodilators, particularly nitric oxide.

Portopulmonary hypertension is defined as pulmonary artery hypertension in a situation of portal hypertension. Its etiopathogenesis is multifactorial and vasoconstriction related to vasoactive substances is one of the underlying mechanisms. Imaging techniques show the classical features of pulmonary arterial hypertension.

The incidence of ARDS is increased in chronic liver diseases. CT shows dependent consolidations and diffuse ground glass opacities. It is difficult to distinguish from pulmonary edema and alveolar hemorrhage.

Hepatic hydrothorax consists of significant pleural effusion in the absence of cardiopulmonary cause in a cirrhotic patient with portal hypertension. The effusion is a trasudate usually on the right side. The infection of this fluid can develop an spontaneous bacterial empyema.

The immune status of cirrhotic patients is the predisposing factor for the development of infections, being pneumonia the third more common type after bacterial peritonitis and urinary tract infections. Radiological presentation depends on the responsible microorganism.

Sarcoidosis associated with interferon therapy and interstitial pneumonitis related to methotrexate therapy have been reported.

Conclusion
Radiologist should be aware of the thoracic manifestations related to chronic liver diseases.
An accurate diagnosis requires a close correlation between the clinical scenario and imaging findings and it is crucial to plan a proper management.

A-266

A case of Hermansky-Pudlak syndrome presenting lung fibrosis and intraparenchymal hemorrhage

L. Gozzi[1], D. Cozzi[2], E. Cavigli[2], C. Moroni[2], A. Bindi[2], B. Lugli[1], E. Rosi[3], V. Miele[2]
[1]University of Florence, Florence, Italy, [2]Careggi University Hospital, Emergency Radiology, Florence, Italy, [3]Careggi University Hospital, Respiratory Diseases, Florence, Italy

Learning Objectives
Hermansky-Pudlak syndrome (HPS) is a rare multisystem disease. Patients affected by HPS are generally young and suffer from oculocutaneous albinism, bleeding secondary to platlet disfunction, cardiac disfunction and early progressive pulmonary fibrosis. Death usually occurs between 30-50 years from restrictive lung disease or hemorrhage. [1] Therefore, high resolution chest computed tomography (HRCT) plays a key role in the diagnosis of lung fibrosis and in assessing the progression of the disease.
Background
HPS is transmitted in an autosomal recessive manner and up to now ten subtypes are described in literature. Lung fibrosis is the most concerning complication since is the primary cause of death in young age. Most frequently lung fibrosis occurs in HPS-1, HPS-2 and HPS-4 subtypes, being diagnosed since young age by onset of symptoms as dyspnea and progressive hypoxemia, leading to death usually within 10-15 years. [2]
Imaging findings OR Procedure details
We describe a case of a 31-year-old male patient who was admitted at our Emergency Department with hemoptysis and dyspnea. A lung HRCT was performed which revealed intralobular and interlobular interstitial thickening with confluent bronchiectasis/bronchiolectasis and honeycombing in the anterior subpleural region of both superior lung lobes, medium lobe, lingula with a lesser involvement of both lower lobes (UIP pattern). Adjacent to left lung fissure, a hazy consolidation surrounded by centrilobular ground-glass halo was descripted, in agreement with clinical symptoms, as a focal hemorrhage.

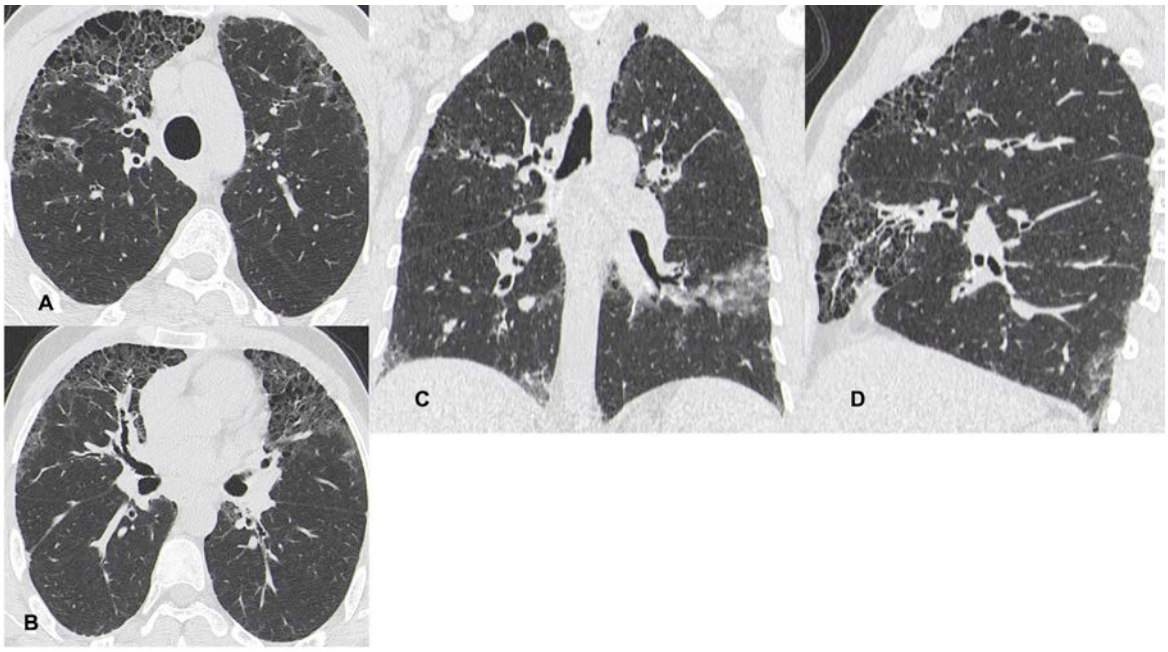

Figure 1. High resolution CT scan showing interstitial lung involvement (A, B axial; D sagittal) with predominant anterior involvement and areas of honeycombing. Figure in C shows focal alveolar hemorrhage in left lower lobe.
In addition, multiple hyperdense cysts were found in the left kidney, possible expression of proteinaceous/hemorrhagic cysts.
This lung presentation, along with oculocutaneous albinism and genetic examination, led to diagnosis of HPS-2.
Conclusion
Since lung fibrosis is the major negative prognostic factor, a correct diagnosis with HRCT is mandatory in order to describe the pattern, quantify the extension of the disease and set a correct follow-up. No treatment is available for this disease. Pirfenidone could be useful in slowing the progression of fibrosis, but the only possible effective treatment is lung transplantation. [3]

References:

[1] Hengst M, Naehrlich L, Mahavadi P, Grosse-Onnebrink J et al., (2018), Hermansky-Pudlak syndrome type 2 manifests with fibrosing lung disease early in childhood, Orphanet J Rare Dis.
[2] Matsuyuki K, Ide M, Houjou K et al., (2022), Novel AP3B1 mutations in a Hermansky-Pudlak syndrome type2 with neonatal interstitial lung disease, Pediatr Allergy Immunol.
[3] Bin Saeedan M, Faheem Mohammed S, Mohammed TL, (2015), Hermansky-Pudlak syndrome: high-resolution computed tomography findings and literature review, Curr Probl Diagn Radiol.

A Pictorial Review of Cystic Lung Disease

B. Vekaria, N. Sivarasan
Guys and St. Thomas' Hospital Trust, Medical Imaging, LONDON, United Kingdom

Learning Objectives
See and identify some of the characteristic findings of several of the commonest cystic lung diseases.
Background
Cystic lung disease continues to be a fascinating and varied finding on computerised tomography (CT) imaging. With CT becoming a commonly used tool in daily practice, diagnosis of cystic lung changes are becoming more frequent and it is useful to become familiar with the characteristic findings.
There is a wide spectrum of appearances with some overlap which can make specific diagnosis challenging. Although a multidisciplinary discussion including imaging is generally used to reach the final diagnosis, there are several aspects of each of the most common cystic lung diseases that can reduce ambiguity and help to establish the most likely diagnoses. In particular, the location of cysts, the appearances of their walls, size, other parenchymal and extra thoracic findings within the field of view.
We present imaging examples of Birt Hogg Dube, Lymphangioleiomyomatosis, Langerhans Cell Histiocytosis and Neurofibromatosis related cystic lung disease.
Imaging findings OR Procedure details
Birt Hogg Dube – bilateral cysts varying in size, lower lobe predominant. Tip - review any available imaging of the kidneys for chromophobe oncocytomas, these patients care at increased risk of pneumothoraces.
Lymphangioleiomyomatosis – uniform, thin walled cysts, small to medium in size. Tip - these patients can have chylous effusions, if renal angiolipomas are present, think tuberous sclerosis complex.
Langerhans Cell Histiocytosis – centrilobular nodules, confluence of cysts have resulted in irregular or "bizarre" shaped cysts.
Neurofibromatosis related cystic lung disease – thin walled cysts, lower zone interstitial fibrosis. Tip - look for extra thoracic findings within the field of view e.g. plexiform and soft tissue neurofibromas.
Conclusion
Although there is a wide spectrum of cystic lung disease, this pictorial review shows the classical imaging features of these commoner varieties. CT imaging findings in conjunction with clinical history and MDT discussion is a useful approach to identifying the underlying cause.

A-336

All asthmatic patients need a chest CT? The evolving role of imaging in Asthma

M. L. Urbano[1,2], M. Cunha[3], C. Lopes[4], J. R. Inácio[5]
[1]Centro Hospitalar Lisboa Norte, Lisboa, Portugal, [2]Centro Hospitalar Lisboa Norte, Serviço de Imagiologia Geral, Lisboa, Portugal, [3]Hospital de Vila Franca de Xira, Pneumologia, Vila Franca de Xira, Portugal, [4]Centro Hospitalar Lisboa Norte, Pneumologia, Lisboa, Portugal, [5]Centro Hospitalar Lisboa Norte, Serviço de Imagiologia Geral, Lisbon, Portugal

Learning Objectives

Asthma is defined by variable airflow obstruction and chronic inflammation leading to airway thickening. Recent literature shows that airflow limitation correlates with chest Computed Tomography (CT) measures of airway diameter and wall thickness.

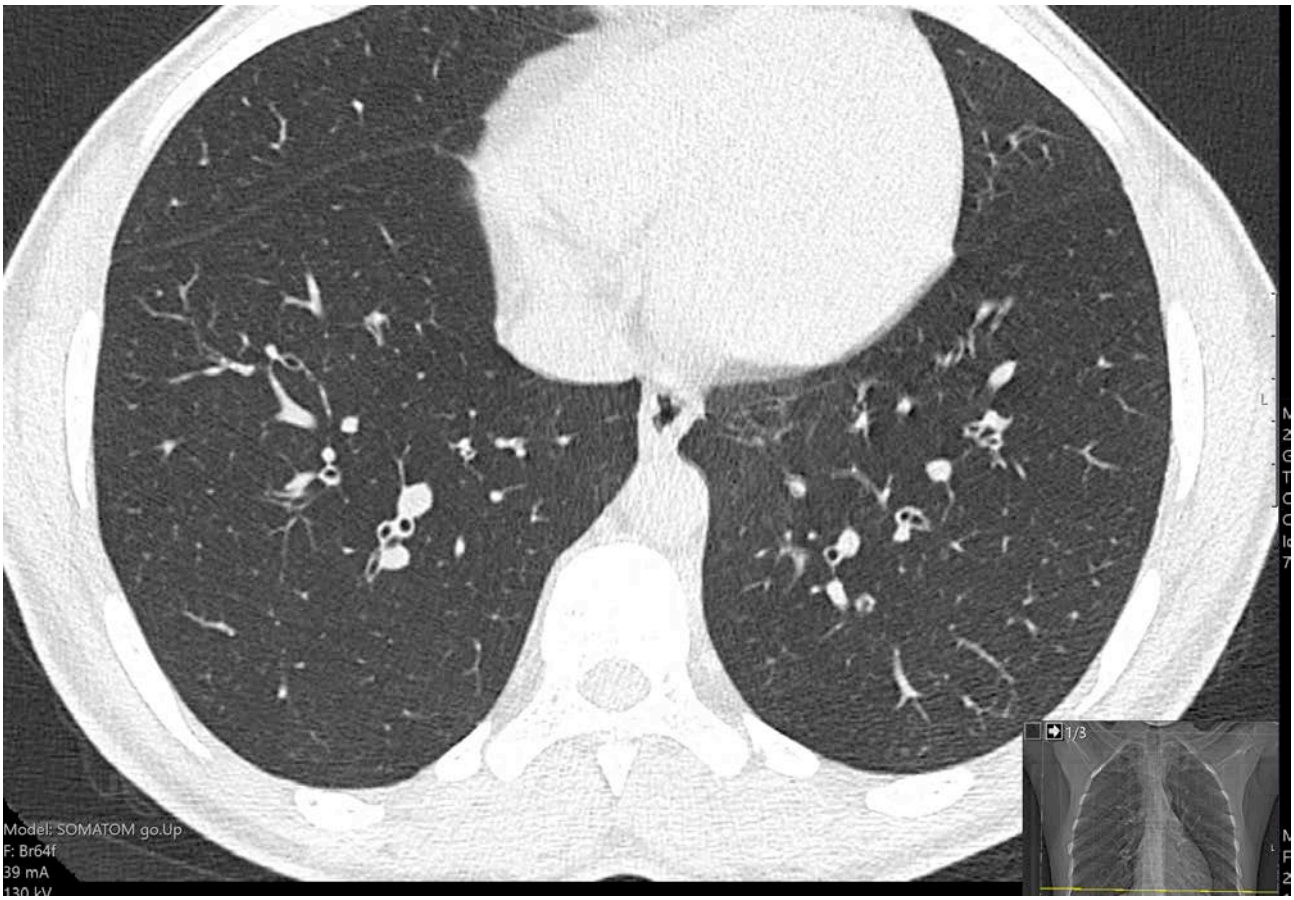

Axial CT (lung window) showing diffuse bronchial wall thickening and mucoid impactation

In this poster we aim to review the latest indications and perspectives of CT in the evaluation of asthma.

Background

Asthma is a common and heterogenous disease characterized by chronic airway inflammation comprising various etiologies and manifestations, therefore classified in different phenotypes with potential to adjust and individualize therapy.

Imaging is an essential tool for the correct clinical management of the asthmatic patient, allowing exclusion of other diseases with similar clinical presentation, particularly in the setting of treatment failure, assessment of complications, classification of disease severity and phenotype description.

Imaging findings OR Procedure details

Chest CT is useful in the diagnosis of acute complications of severe asthma including pneumonia, atelectasia, pneumothorax and pneumomediastinum. Imaging also plays an important role in the evaluation of subacute and chronic complications of asthma, such as bronchiectasis, lung destruction, allergic bonchopulmonary aspergillosis (ABPA) and eosinophilic granulomatosis with polyangiitis (Churg-Strauss Disease).

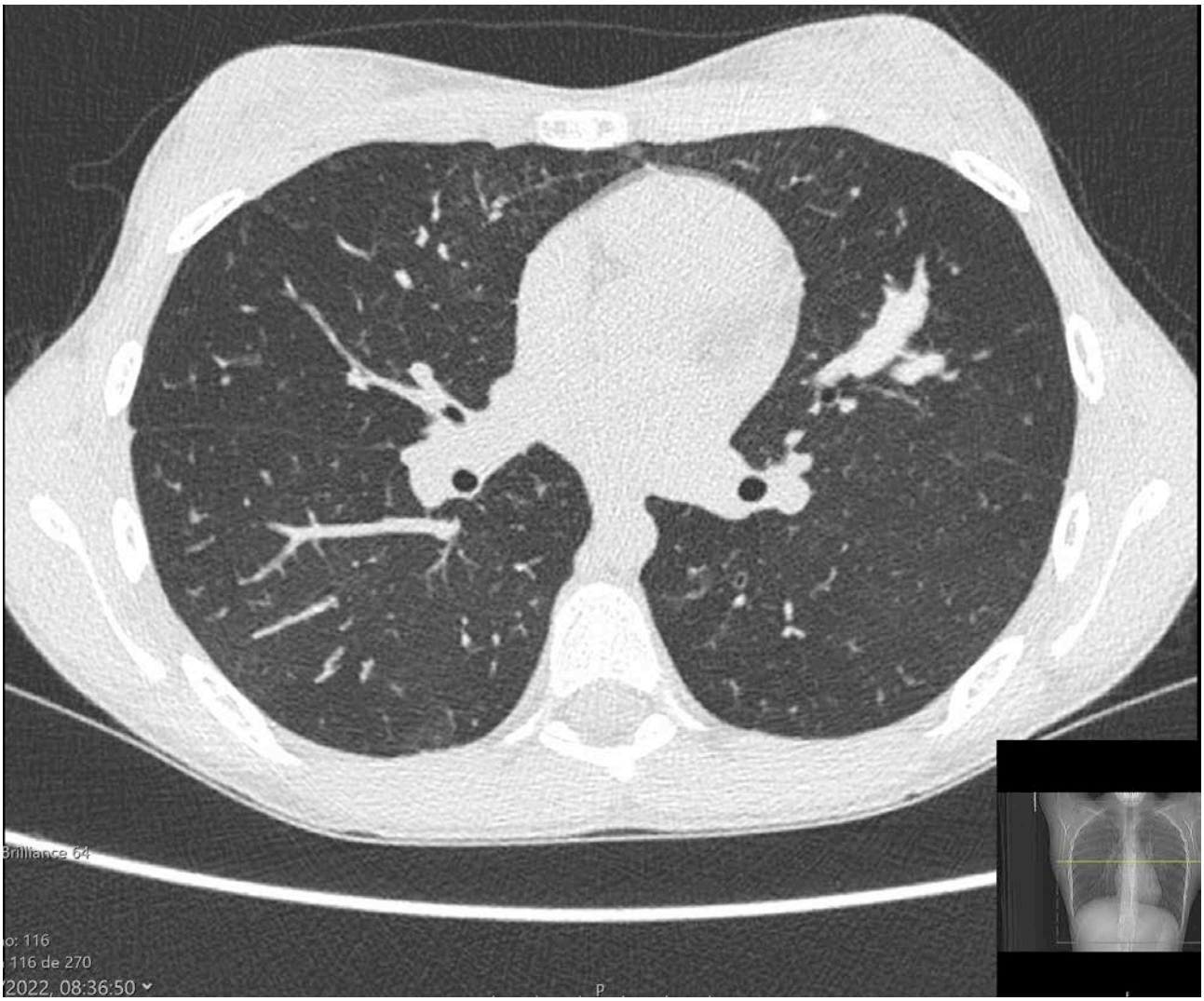

Axial CT (lung window) showing bronchial mucocele

However, novel applications of CT have been recently described for the initial stages of diagnosis of asthma, such as cluster phenotyping, functional respiratory imaging with spirometry-controlled CT, measurement of lung densities in inspiration/expiration to evaluate and quantify air trapping or CT pre and post bronchodilator therapy in cases of severe asthma.
Additionally, quantitative CT can be used in the evaluation of proximal airways assessing bronchial luminal diameter and wall thickening that correlate with functional parameters of asthma severity; assessment of various degrees of airway remodeling can identify different clusters that correlate to the heterogeneous clinical manifestations.

Conclusion

The role of CT in asthma was previously restricted to severe cases and assessment of complications. Recent evidence suggests that CT might be an important tool in advanced stages of disease as well as at time of diagnosis, including evaluation of lung function, response to treatment and a better understanding of its different phenotypes.

A-499

An illustrative guide to coronary artery anomalies.

S. Billingsley[1], D. Oswal[2], C. Ramakumaran[2]
[1]Leeds teaching hospitals nhs trust, Radiology, Leeds, United Kingdom, [2]Mid Yorkshire NHS Trust, Wakefield, United Kingdom

Learning Objectives

Aims to demonstrate in a clear and concise format the important and commonly encountered coronary artery anomalies.
Discuss clinical and radiological significance of varied anatomical abnormalities.
Demonstrate coronary artery abnormalities in a clear, pictorial manner to aid learning.

Background

Coronary artery anomalies (CAAs) are a group of conditions characterised by abnormal origins or course of the three major coronary vessels. There is a spectrum of clinical relevance regarding CAAs, with outcomes varying from sudden cardiac death to incidental findings (1). Clinical difficulties regarding CAAs are multifaceted, including difficulty diagnosing and identifying abnormalities on non-dedicated cardiac imaging as well as organising correct management. The latter in particular can be challenging given the lack of evidence regarding prognostication of individual CAAs, in spite of approximately 7% of the population demonstrating identifiable anomalies (2).

One step in improving the care of CAAs is improved awareness and subsequent diagnosis within a radiology setting. After identification comes classification, in turn improving prognostication based on imaging findings (3) with subsequent improvement in therapeutic management and correct follow up.

Imaging findings OR Procedure details

Imaging with descriptions of multiple CAAs are exhibited, including but not limited to those listed below.

Anomalies of origin

Anomalous left coronary artery from the pulmonary artery (ALCAPA)
Left circumflex origin from the right coronary artery (RCA)
Double left anterior descending artery (LAD)
Left main coronary artery from RCS with a double LAD

Anomalies of course

Crossing of the LAD and ramus intermedius
Anomalous RCA with a malignant course
Hyper dominant LAD

Conclusion

This poster illustrates the type of cases encountered in a busy district general hosptial in the UK. Radiology has a key role in identifying, highlighting and following up patients with CAAs. The hope is that improved awareness and identification will enhance the understanding and management of these varied anomalies.

References:

[1] Gentile F, (2021), Coronary Artery Anomalies, Circulation, 144, 12
[2] Namgung et al, (2014), The prevalence of coronary anomalies in a single center of Korea: origination, course, and termination anomalies of aberrant coronary arteries detected by ECG-gated cardiac MDCT, BMC Cardiovasc Disord, 48, 14
[3] Baumgertner et al, (2021), ESC Scientific Document Group. 2020 ESC guidelines for the management of adult congenital heart disease, Eur Heart J, 563 , 42

A-694

Application of Artificial Intelligence (AI) in lung cancer screening with low-dose CT: beyond lung nodules

F. Scrocca[1], G. Cicchetti[2], A. del Ciello[2], L. Calandriello[2], A. Farchione[2], A. G. Castelli[1], A. Ceccherini[1], G. Chiffi[1], E. Moliterno[1], R. Marano[1,2], L. Natale[1,2], A. R. Larici[1,2]
[1]Università Cattolica del Sacro Cuore, Section of Radiology, Department of Radiological and Hematological Sciences, Rome, Italy, [2]Fondazione Policlinico Universitario "A. Gemelli" IRCCS, Advanced Radiodiagnostic Center, Department of Diagnostic Imaging, Oncological Radiotherapy and Hematology, Rome, Italy

Learning Objectives
-To learn about artificial intelligence (AI) tools application in lung cancer screening (LCS) with low-dose Computed Tomography (LDCT)
-To provide insights into the potential role of AI-based algorithms in lung nodules detection and characterization and in identification and quantification of other smoking-related diseases
Background
LCS based on LDCT has been shown to significantly reduce lung cancer mortality in high-risk populations according to randomised controlled trials performed both in the United States and in Europe, and various countries are currently considering the implementation of LCS programs.
Together with lung cancer detection, LDCT allows the assessment of other smoking-related pulmonary and cardio-vascular diseases, mainly chronic obstructive pulmonary disease (COPD), interstitial lung disease (ILD) and coronary artery calcifications (CAC).
In the last decades AI tools have been developed and applied in thoracic imaging; particularly, deep-learning algorithms have shown great potential application in LCS.
Imaging findings OR Procedure details
AI has been widely applied in the detection and classification of pulmonary nodules, especially as a second reader alongside experienced thoracic radiologists; indeed, algorithms have been trained to efficiently classify lesions according their malignancy risks (for example applying the Lung-RADS).
Apart from nodule evaluation, AI analysis is useful in the identification and grading of COPD, with high accuracy in pulmonary emphysema quantification and in detection of airway abnormalities (i.e. bronchial wall thickness measurement). Furthermore, AI may be used for detection, quantification and characterization of lung fibrotic changes, configuring the so-called interstitial lung abnormalities (ILA) or an ILD, which more frequently affecting heavy smokers. AI can also provide rapid and reproducible measure of CAC, widely proved to be a strong predictor of cardiovascular events.
In this educational exhibit we will present an overview of the potential applications of AI tools to LDCT in the setting LCS screening, focusing not only on lung nodule detection and characterization (which is the primary purpose of LCS), but also in the identification and quantification of smoking-related pulmonary and cardio-vascular diseases.
Conclusion
Despite potential limitations to the lack of standardization, AI demonstrates a wide potential application in LCS settings with LDCT, providing useful tools for lung cancer detection and for the identification and quantification of coexisting lung and cardio-vascular abnormalities due to the smoking habit. Thus, AI may allow a more comprehensive assessment of subjects and enhancing the global scope of LCS.

References:

[1] Adams SJ, Stone E, Baldwin DR, Vliegenthart R, Lee P, Fintelmann FJ, (2023), Lung cancer screening, Lancet, 401(10374):390-408
[2] Regan EA, Lowe KE, Make BJ, et al., (2019), Identifying Smoking-Related Disease on Lung Cancer Screening CT Scans: Increasing the Value, Chronic Obstr Pulm Dis, 6(3):233-245
[3] Grenier PA, Brun AL, Mellot F., (2022), The Potential Role of Artificial Intelligence in Lung Cancer Screening Using Low-Dose Computed Tomography, Diagnostics, Basel, 12(10):2435
[4] Labaki WW, Xia M, Murray S, et al., (2021), Quantitative Emphysema on Low-Dose CT Imaging of the Chest and Risk of Lung Cancer and Airflow Obstruction: An Analysis of the National Lung Screening Trial, Chest, 159(5):1812-1820

A-731

Applications of pulmonary MRI: the future is now?

G. La Rosa, M. Contino, S. Barbarino, L. Reali, S. Galioto, E. Tona, C. Timpanaro, S. Palmucci, A. Basile
University Hospital Policlinico “G. Rodolico-San Marco”, University of Catania, 95123 Catania, Italy, Radiology Unit 1- Department of Medical Surgical Sciences and Advanced Technologies “GF Ingrassia”, Catania, Italy

Learning Objectives

The purpose of this educational exhibit is: i) to provide a pictorial review of most pathological conditions which may be evaluted by MRI; ii) to show which protocols and sequences should be used in the evaluation of lung parenchyma and pulmonary vascular diseases.

Background

MRI provides a structural and quantitative functional image of the lungs – without ionizing radiation exposure: this makes it an ideal modality for pediatric examinations, pregnant women, and patients requiring a serial and longitudinal follow-up. Recently – thanks to ultrashort echo time and zero echo time techniques, multi-coil parallel acquisitions, and acceleration methods – apnea troubles were solved. T1 and T2 weighted, diffusion, and perfusion sequences play a crucial role to approach a lot of benign and malignant formations.

Imaging findings OR Procedure details

Clinical pulmonary MRI indications range from oncological diseases to inflammatory and vascular pathological conditions.
Numerous MRI sequences have been evaluated for pulmonary nodule characterization [1]. Currently, diffusion-weighted imaging (DWI) is considered the most useful sequence to achieve the differentiation between malignant and benign lesions [1]. In this setting, the breath-hold T2-weighted fast spin-echo sequence can show the presence of mucin in lung adenocarcinoma – especially in the previuos histological type labeled as bronchioloalveolar carcinoma [2]. Three-dimensional GRE with ultra-short echo time, when compared with CT, showed almost perfect agreement for imaging lung nodules or masses, interstitial lung abnormalities, emphysema, and bullae [1]. GRE-MRI can be used to reveal air trapping [1] and steady-state free precession methods to distinguish mucus from airway wall thickening in cystic fibrosis [3].
In pulmonary embolism MRI, perfusion defects can reveal even a small airway obstruction, which is difficult if not impossible to detect using CT. In addition to quantitative contrast-enhanced MR angiography, triggered true FISP MRI imaging and re-circulation 3D GRE MRI imaging are innovative tools for the assessment of the severity of pulmonary hypertension and the longitudinal assessment of therapy effect [4]. Magnetic resonance is a promising imaging modality in pericardial cysts - the fluid produces a hyperintense signal on T2-weighted MRI images- [5].
Finally, exogenous lipoid pneumonia appears like an abnormal area of consolidation with irregular margins, with a fairly high signal intensity on T1- weighted images; in tuberculosis MRI is an accurate predictor of node and pleural involvement [6].

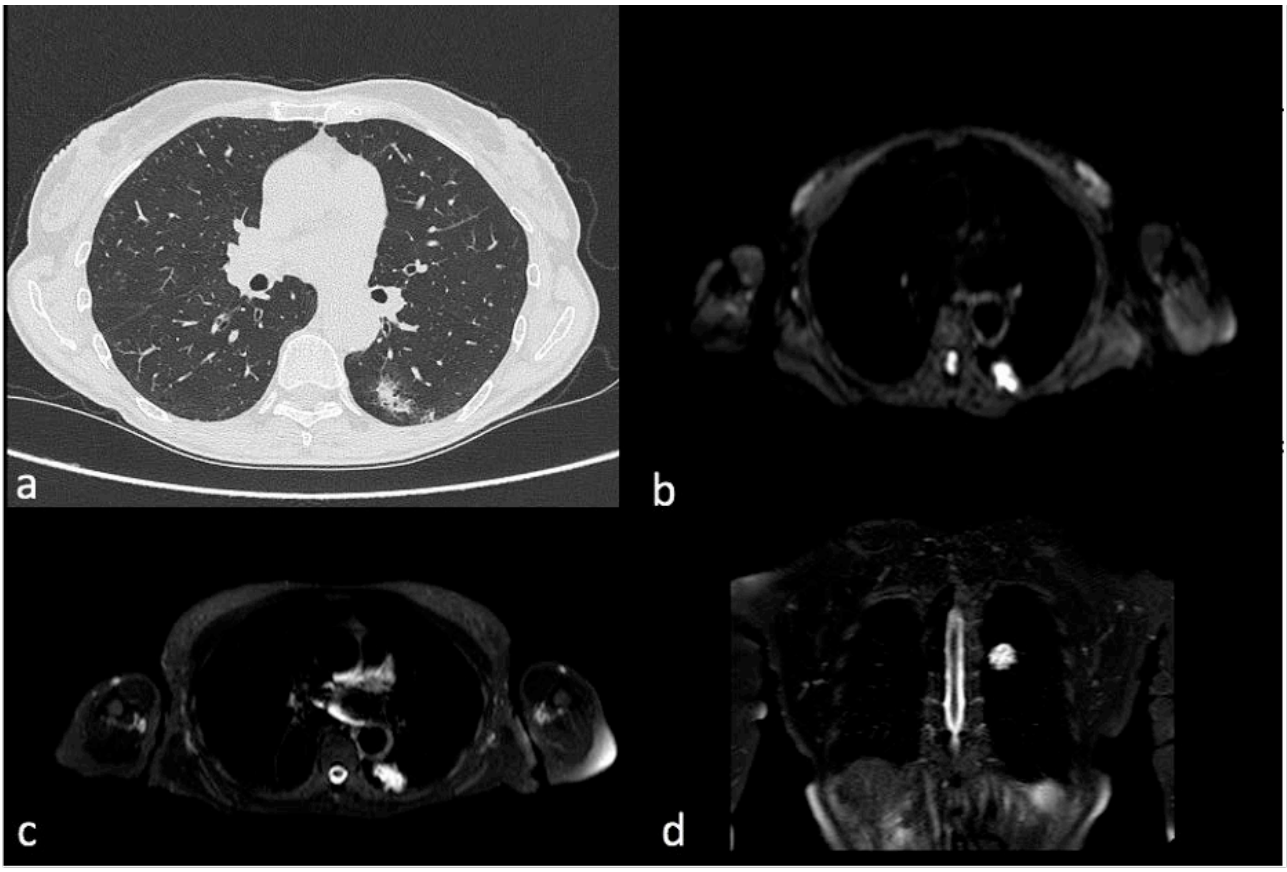

Woman patient 68 years old, CT image shows adenocarcinoma located on left lower lobe (a) ; MRI images show restriction of diffusion on DWI sequence (b), T2 weighted images with fat suppression show fairly hyperintense aspect of the lesion (c-d)

Conclusion

Although CT will remain the principal imaging tool for routine pulmonary imaging examinations, MRI is going to increase its diagnostic capability in the diagnosis of some pulmonary disorders.

References:

[1] Hatabu H, Ohno Y, Gefter WB, Parraga G, Madore B, Lee KS, Altes TA, Lynch DA, Mayo JR, Seo JB, Wild JM, van Beek EJR, Schiebler ML, Kauczor HU; Fleischner Society. , (2020), Expanding Applications of Pulmonary MRI in the Clinical Evaluation of Lung Disorders: Fleischner Society Position Paper, Radiology, 297(2):286-301
[2] Gaeta, Michele M.D.; Blandino, Alfredo M.D.; Scribano, Emanuele M.D.; Vinci, Sergio M.D.; Minutoli, Fabio M.D.; Pergolizzi, Stefano M.D.; Pandolfo, Ignazio M.D., (2000), Magnetic Resonance Imaging of Bronchioloalveolar Carcinoma, Journal of Thoracic Imaging , 15(1):p 41-47
[3] Failo R, Wielopolski PA, Tiddens HA, Hop WC, Mucelli RP, Lequin MH. , (2009), Lung morphology assessment using MRI: a robust ultra-short TR/TE 2D steady-state free precession sequence used in cystic fibrosis patients, Magn Reson Med , 61(2):299–306
[4] Bobby Kalb, Puneet Sharma, Stefan Tigges, Gaye L. Ray, Hiroumi D. Kitajima, James R. Costello, Zhengjia Chen, and Diego R, (2012), 8. MR Imaging of Pulmonary Embolism: Diagnostic Accuracy of Contrast-enhanced 3D MR Pulmonary Angiography, Contrast-enhanced Low–Flip Angle 3D GRE, and Nonenhanced Free-Induction FISP Sequences, Martin,Radiology , 263:1, 271-278
[5] Kar SK, Ganguly T et al , (2017), Current concepts of diagnosis and management of pericardial cysts, Indian Heart J, 69(3):364-370
[6] Edson Marchiori, Gláucia Zanetti, Claudia Mauro Mano, Bruno Hochhegger, (2011), Exogenous lipoid pneumonia. Clinical and radiological manifestations, Respiratory Medicine, Volume 105, Issue 5,2011, Pages 659-666, ISSN 0954-6111

A-732

Bronchial artery-pulmonary artery malformations: an imaging review.

S. Pamparino[1], A. Amlani[2], M. Narbone[2], R. Preston[2]
[1]Ospedale Policlinico San Martino, Oncology and Interventional Radiology Department, Genova, Italy, [2]Guy's & St Thomas' NHS Foundation Trust, Department of Radiology, London, United Kingdom

Learning Objectives
To review the imaging appearances of pulmonary artery to bronchial artery malformations.
Background
Systemic artery to pulmonary artery malformations are rare entities with only sporadic case reports documented [1]. They can be both congenital and non-congenital; potentially developing from any inflammatory, infective, neoplastic, or traumatic process. They are a distinct entity from major aortopulmonary collateral arteries (MAPCAs), as these usually occur in the setting of congenital cardiac disease and have peripheral fistulae. These malformations are often incidentally diagnosed during adulthood because their symptoms are absent or manifest late [2].
Imaging findings OR Procedure details
We report two cases of pulmonary artery to bronchial artery fistulae. Case 1, a 51-year-old male, was an outpatient who underwent a CT coronary angiogram for stable angina. Case 2, a 39-year-old male, attended our emergency department with haemoptysis and pleuritic chest pain and underwent CT thoracic angiography. Both had no significant prior medical history. In both cases, the CT findings demonstrated a network of tortuous bronchial arteries, at least one of which was enlarged, with a connection to a proximal segmental pulmonary artery.
In both cases the malformation was seen within the right lower lobe. In case 1, there was also evidence of pulmonary arterial hypertension with a dilated pulmonary trunk (32 mm) and evidence of right ventricular hypertrophy. This suggests the presence of a significant left-to-right shunt.

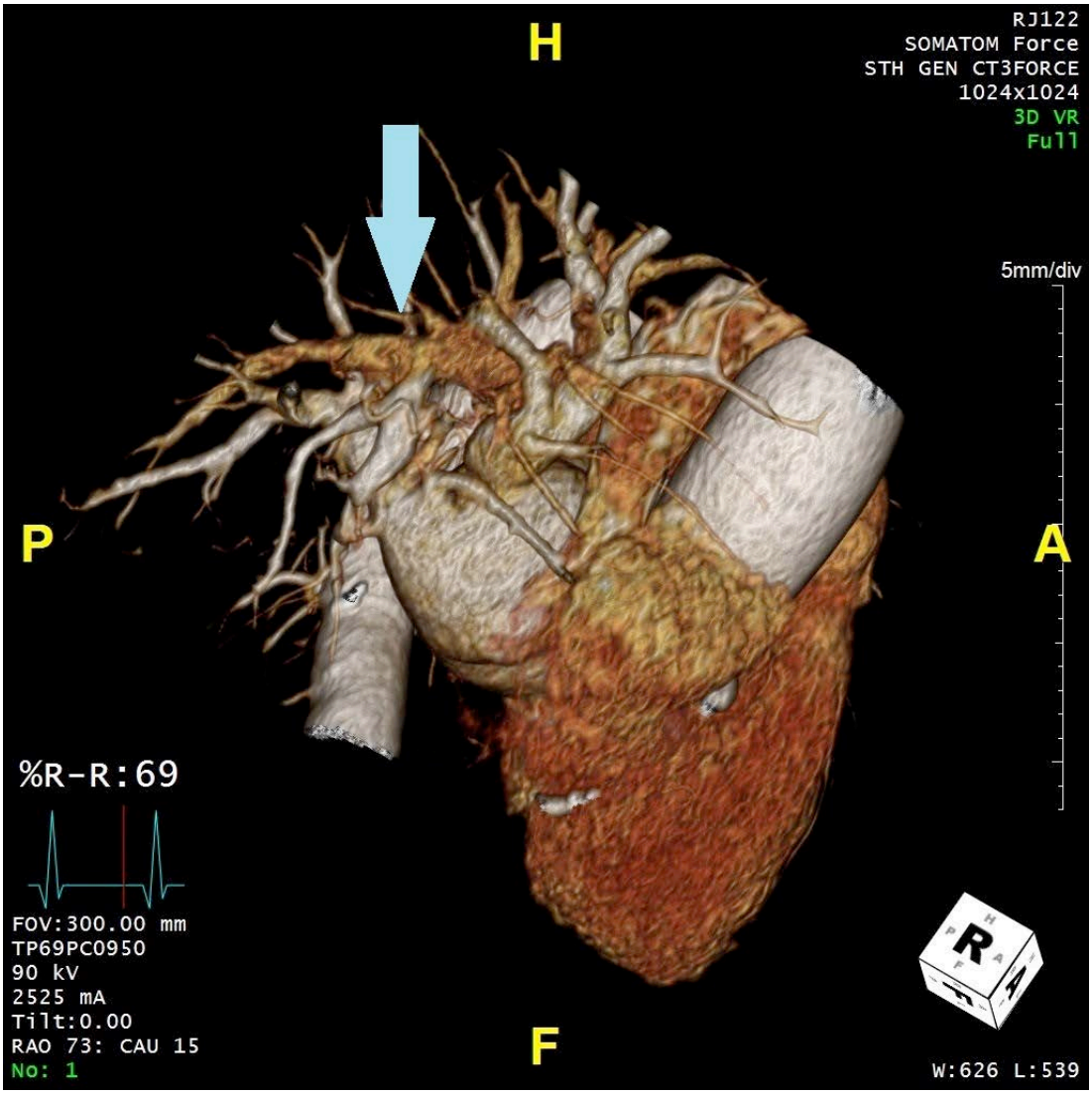

CASE 1: CT Coronary Angiogram – 3D volume rendered image demonstrating the pulmonary artery – bronchial artery fistula (blue arrow)

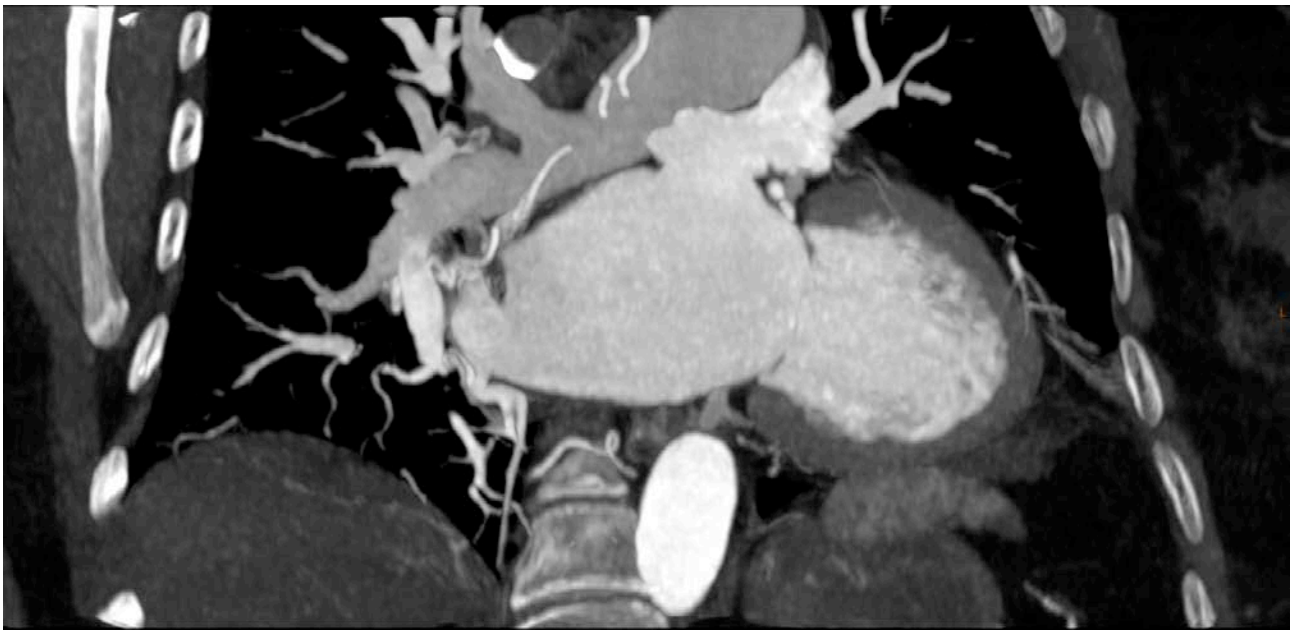

CASE 1: CT Coronary Angiogram – Coronal maximum intensity projection image again demonstrating the pulmonary artery – bronchial artery fistula within the right lower lobe. There was no associated pulmonary haemorrhage in this case.

In case 2, there was patchy centrilobular ground glass opacification and consolidation within the right lung, suggestive of pulmonary haemorrhage. This is a recognised, albeit extremely rare, complication.

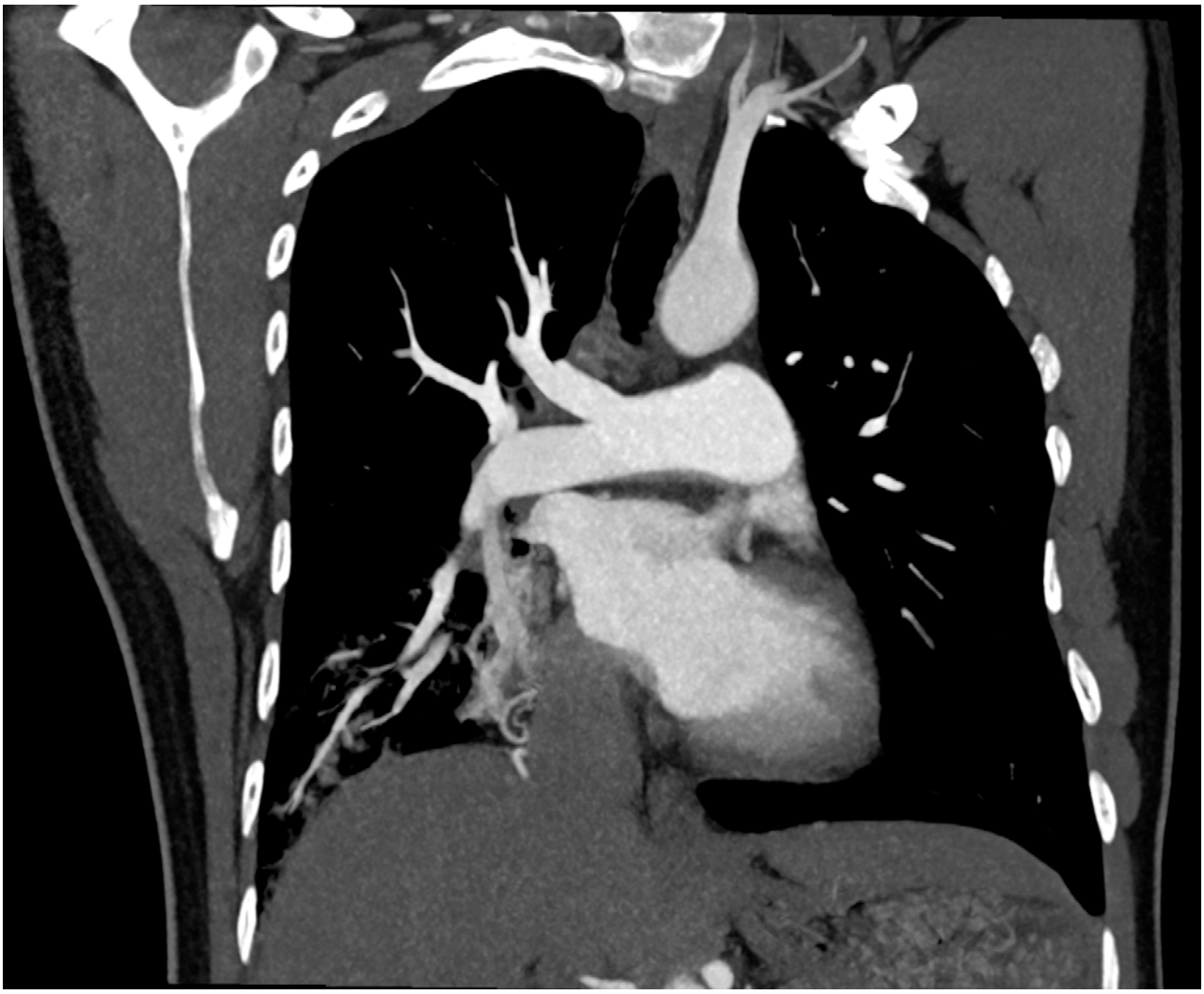

CASE 2: CT Coronary Angiogram – Coronal maximum intensity projection image again demonstrating the pulmonary artery – bronchial artery fistula within the right lower lobe. There was no associated pulmonary haemorrhage in this case.

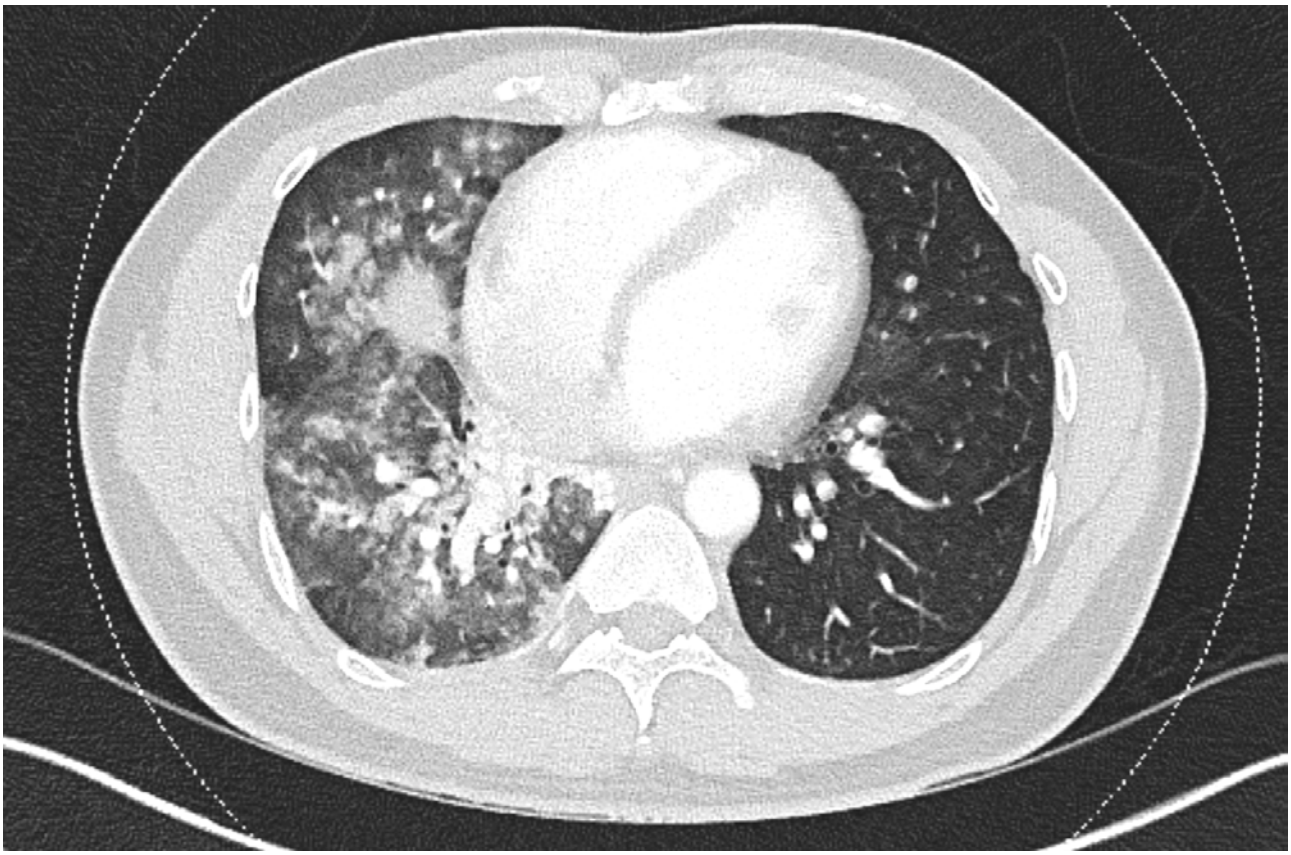

CASE 2: CT Pulmonary Angiogram – Axial image (lung window) demonstrating patchy ground glass opacification and consolidation within the right lung, in keeping with pulmonary haemorrhage.

The first patient was asymptomatic and is currently undergoing further outpatient investigation to quantify the shunt and extent of pulmonary arterial hypertension.
The second patient required inpatient admission due to the haemoptysis and subsequently underwent IR guided embolization of this malformation.

Conclusion

Systemic artery to pulmonary artery malformations are exceedingly rare entities however prompt recognition of the CT imaging features is essential due to the potential complications.

References:

[1] Kyung-Hyun Do, Jin Mo Goo, Jung-Gi Im, Kyoung Won Kim, Jin Wook Chung, Jae Hyung Park , (2001), Systemic Arterial Supply to the Lungs in Adults: Spiral CT Findings , RadioGraphics
[2] Wojciech Jacheć, Andrzej Tomasik, Marcin Kurzyna, Radosław Pietura, Adam Torbicki, Jan Głowacki, Ewa Nowalany-Kozielska & Celina Wojciechowska , (2019), The multiple systemic artery to pulmonary artery fistulas resulting in severe irreversible pulmonary arterial hypertension in patient with previous history of pneumothorax, BMC Pulmonary Medicine

A-400

Bronchiectasis: the role of imaging in the etiologic assessment

A. L. Amado Costa, D. Antunes, M. L. Lobo, J. Leitão
Centro Hospitalar Universitário Lisboa Norte/ Hospital de Santa Maria, Serviço de Imagiologia Geral, Lisboa, Portugal

Learning Objectives

1. To describe the different types of bronchiectasis and to illustrate their imaging findings.
2. To review the role of imaging in the differential diagnosis of the etiologies of bronchiectasis based on anatomic location, distribution pattern, and associated findings.

Background

Bronchiectasis is defined as irreversible dilatation of diseased bronchi. It is often a complication of repeated cycles of airway infection and inflammation. It can be caused by a wide variety of pathologic entities, including inflammatory and infectious diseases, obstructive processes, systemic and congenital diseases. Many of these conditions require a specific therapy and thus, a systematic etiologic assessment should be performed for each patient. High-resolution computed tomography (HRCT) is the best imaging method currently available for the detection and characterization of bronchiectasis, playing an important role in the study of patients with this condition.

Imaging findings OR Procedure details

Based on our department database, we will present and illustrate the imaging characteristics of bronchiectasis and we will review a wide range of potential etiologies. Three types of bronchiectasis have been described, based on their morphology: cylindrical, varicose and cystic. Bronchiectasis may be focal or diffuse. Causes of focal bronchiectasis include bronchial obstruction by an endobronchial lesion, extrinsic compression and previous infection. Etiologies of diffuse bronchiectasis include systemic and congenital conditions such as cystic fibrosis, congenital tracheobronchomegaly (Mounier-Kuhn syndrome) and multifocal infections. Central-predominant bronchiectasis are typically seen in allergic bronchopulmonary aspergillosis, cystic fibrosis, congenital tracheobronchomegaly and Williams Campbell syndrome. Upper lobe bronchiectasis is characteristic of tuberculosis and cystic fibrosis, but it may also occur in other conditions. Middle lobe bronchiectasis may occur in some conditions such as non-tuberculous mycobacterial infections and middle lobe syndrome. Lower lobe bronchiectasis can be seen in aspiration, immunodeficiency disorders such as hypogammaglobulinemia, and after recurrent infections, among other conditions.

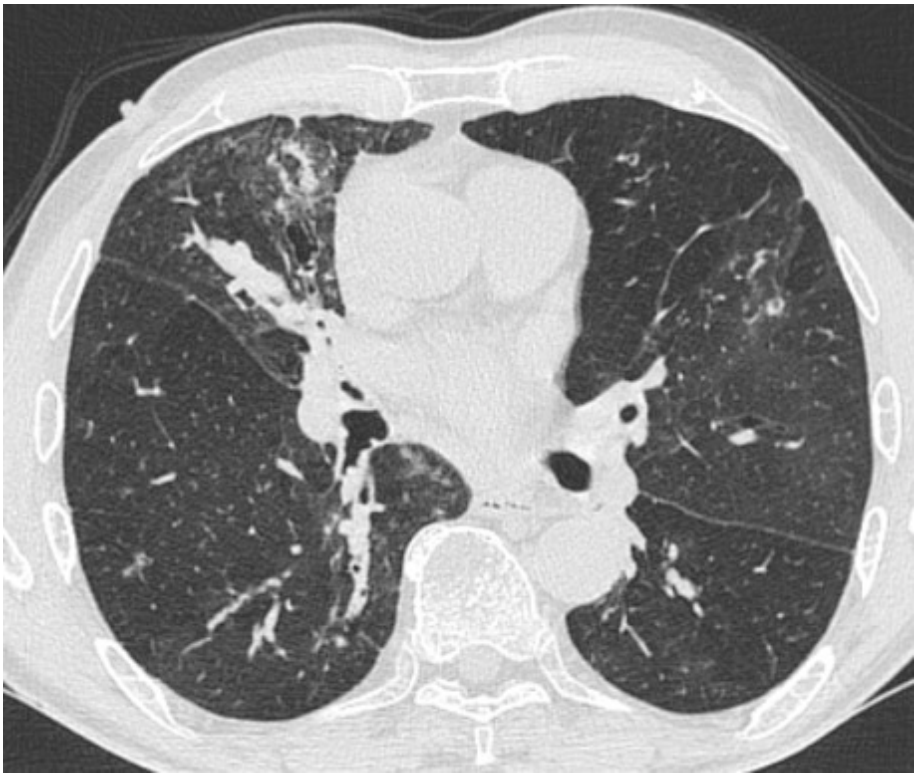

Axial CT image (lung window) of a patient with allergic bronchopulmonary aspergillosis, presenting central-predominant bronchiectasis in the middle lobe and in the right lower lobe, some with mucoid impaction.

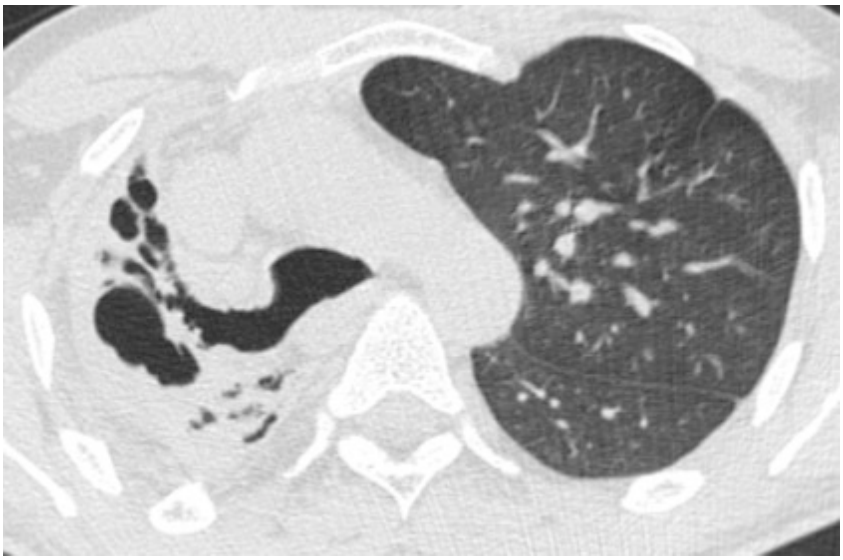

Axial CT image (lung window) of a patient with right upper lobe colapse, with post-tuberculosis bronchiectasis. Tracheal deviation is also noted.

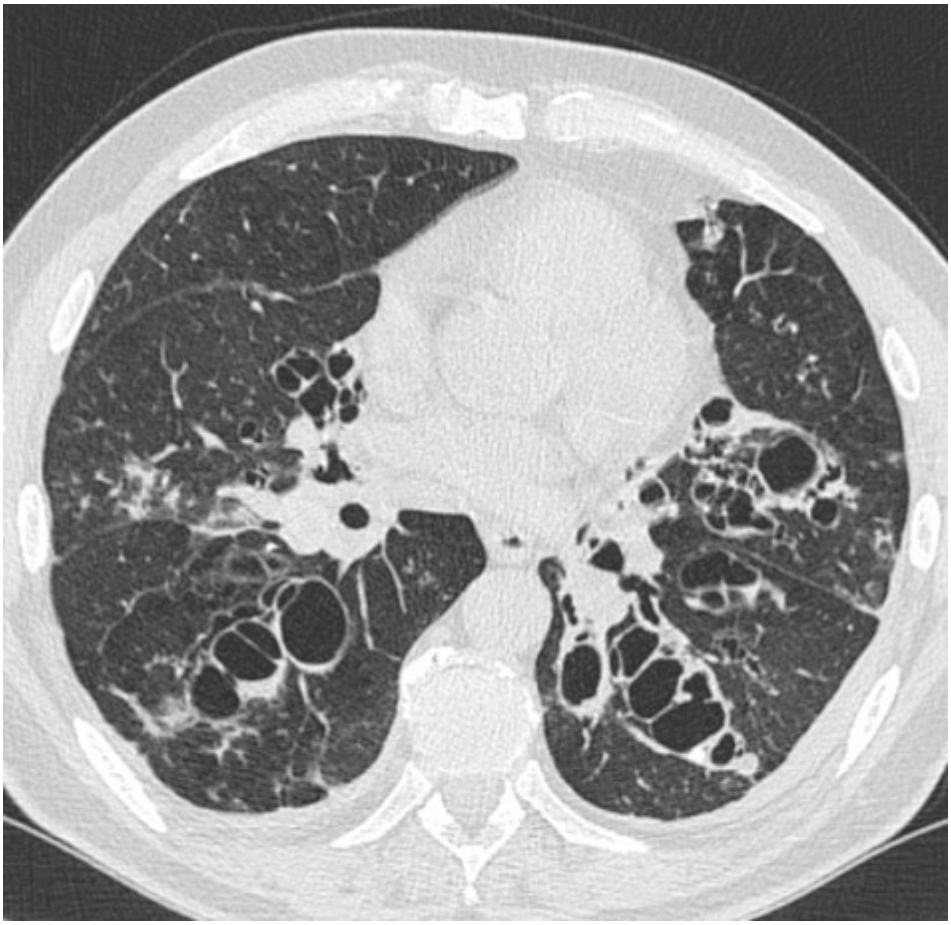

Axial CT image (lung window) of a patient with Mounier-Kuhn syndrome, presenting multiple central-predominant cystic and varicose bronchiectasis in several pulmonary lobes. Centrilobular nodules in a tree-in-bud pattern and multifocal lung consolidations are also noted.

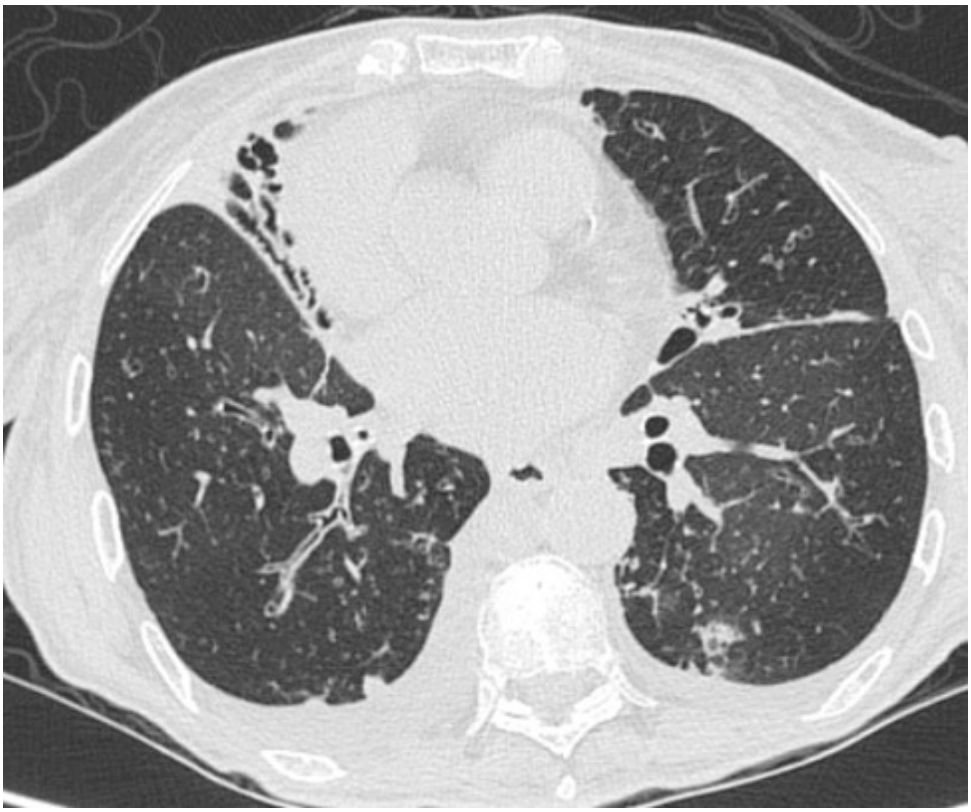

Axial CT image (lung window) of a patient with pulmonary Mycobacterium avium complex infection, presenting bronchial wall thickening and varicose bronchiectasis in the right middle lobe, which is collapsed. Centrilobular nodules and some small consolidations are also noted in the lower pulmonary lobes. Bilateral pleural effusion is also present.

Conclusion

Bronchiectasis can result from a wide variety of pathologic entities. The assessment of the location, distribution, and associated findings on imaging can narrow down the differential diagnosis.

A-191

Cases from daily clinical practices : use of AI-CAD in screening chest radiographs

H. Song
Seongnam Citizens Medical Center, Radiology, Seongnam, Republic of Korea (South Korea)

Learning Objectives

The objective of this educational poster is to present cases from daily clinical practices on screening chest radiographs using the AI-CAD system.

Background

The chest radiograph is important and commonly used as the initial imaging modality for diagnosing thoracic diseases in health screening centers. However, radiologists and physicians tend to overlook subtle abnormalities while interpreting chest radiographs. Nowadays, artificial intelligence-computer-aided detection (AI-CAD) has demonstrated the excellent diagnostic performance in detecting abnormalities on chest radiographs.

The AI-CAD improves accuracy and sensitivity, but there is a possibility of increased false positives. The AI-CAD system can be utilized in various clinical settings.

Imaging findings OR Procedure details

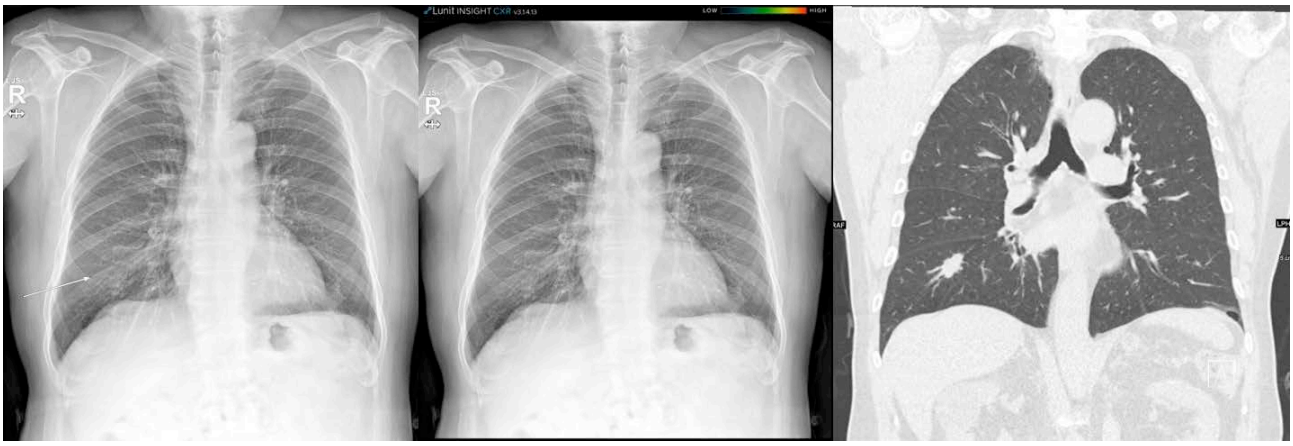

1. CXRs of a man with 69 years old,

1) Radiologist detected lung abnormalities in right lower lung field, without AI.
2) AI-CAD did not display any abnormalities.
3) Coronal CT scan demonstrates a spiculated mass in right lower lobe, suggesting lung cancer.

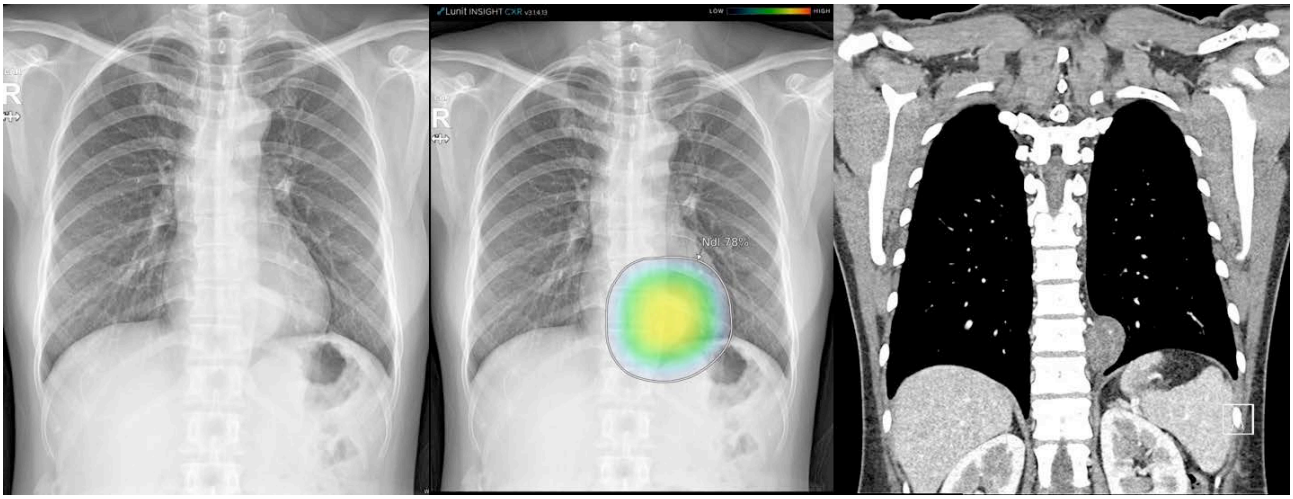

2. CXRs of a woman with 51 years old,

1) Radiologist detected posterior mediastinal mass in retrocardiac area, without AI.
2) AI-CAD also showed nodule.
3) Coronal CT scan demonstrates a posterior mediastinal mass, suggesting neurogenic tumor.

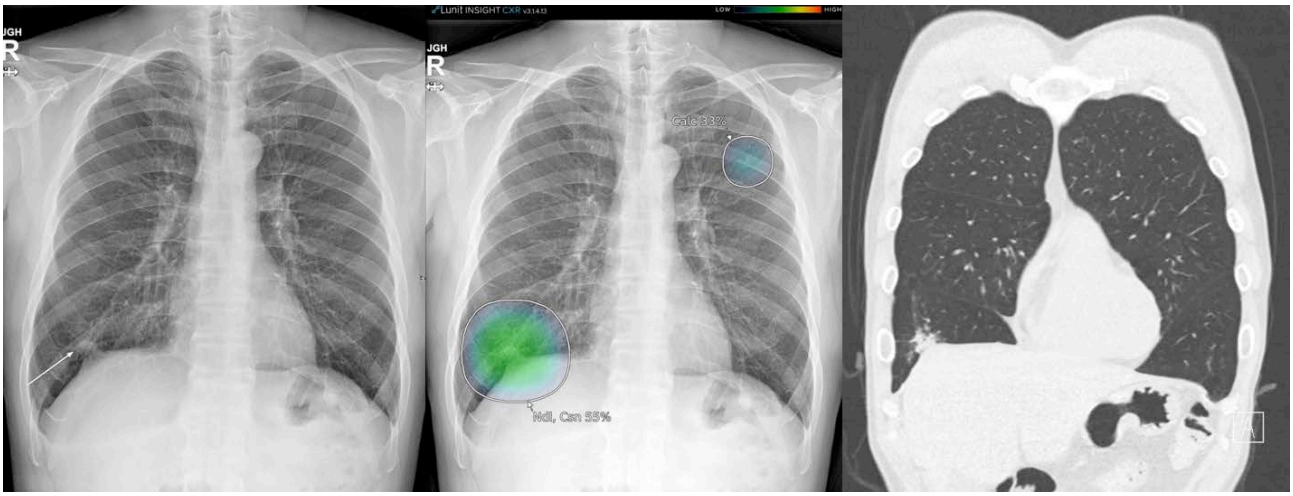

3. CXRs of a man with 65 years old,

1) Radiologist detected lung abnormalities in right lower lung field, without AI.
2) AI-CAD detected right lower lobe abnormalities.
3) Coronal CT scan demonstrates focal consolidation in right lower lobe, suggesting focal pneumonia.

Conclusion

In our institution, AI-CAD system was implemented on chest radiographs for routine health screening exams.
This educational exhibit illustrates cases of abnormalities discovered on chest radiograph using the AI-CAD settings for screening.

A-280

Chest airway devices: an overview for radiologists

A. Ceccherini[1], A. Farchione[2], D. Magnigi[3], L. Calandriello[2], G. Cicchetti[2], A. Del Ciello[2], F. Castaldo[1], F. Scrocca[1], C. Strappa[1], L. Natale[1,2], A. R. Larici[1,2]

[1]Università Cattolica del Sacro Cuore, UCSC, Section of Radiology, Department of Radiological and Hematological Sciences, Università Cattolica del Sacro Cuore, Italy, Roma, Italy, [2]Fondazione Policlinico Universitario "A. Gemelli" IRCCS, Advanced Radiodiagnostic Center, Department of Diagnostic Imaging, Oncological Radiotherapy, Roma, Italy, [3]Fondazione Policlinico Universitario "A. Gemelli" IRCCS, Interventional Pneumology Division, Roma, Italy

Learning Objectives

Provide an overview of chest airway devices, in terms of types/indications, appearance/positioning and complications that can be observed at imaging.

Background

Airway devices belong to a heterogeneous group ranging from endotracheal tubes to endobronchial valves, whose function differs from ventilation support, to airflow maintenance or lung volume reduction. They are used in critically illpatients, especially in intensive care, as well as in elective settings. Chest X-ray (CXR) remains the first-line exam to evaluate the correct appearance/positioning and complications; Computed Tomography (CT) is useful to overcome CXR technical limits and to better define complications.

Imaging findings OR Procedure details

Endotracheal/tracheostomy tubes support patient ventilation or maintain airway patency. The tip of endotracheal tube should be positioned in the mid trachea (5 cm above the carina with 2 cm excursion) and the balloon shouldn't be inflated more than 1.5 times the tracheal diameter. Correct site of the tip of tracheostomy tube is at one-half to two-thirds of the distance from the stoma to the carina. Main complications are malposition, acute/chronic tracheal injury, barotrauma, aspiration pneumonitis and occlusion. Endobronchial stents are placed to maintain or restore airway patency in benignant or malignant diseases.They are silicon or metallic endoluminal prostheses, visible on CXR if metallic with a lattice-like structure, while on CT with uniform uninterrupted structure and different degree of density. Principal complications are malposition,migration (especially for silicone ones) and obstruction. Endobronchial valves and coils are used in patients affected by severe emphysema to reduce lung hyperinflation. Valves are positioned in the bronchi from the lobar level that supply a single lobe, allowing expiration but preventing re-inflation; they appear as umbrella-like structures with radiopaque struts located centrally in a lobe, associated to progressive lobar collapse. Coils are positioned into sub-segmental bronchi usually belonging to two different contralateral lobes treated sequentially, determining airways distortion/re-tension and lung tissue compression/shrinking;the correct position is in the mid-third of the lung and atelectasis is rare. Complications are pneumothorax, post-obstructive pneumonia, valve migration, haemorrhage, COPD exacerbation and respiratory failure.

Conclusion

A variety of airway devices are currently used in the clinical setting thanks to continuous innovations in interventional pneumology. Post-procedure imaging assessment is essential to define procedure effectiveness or possible complications, even when not clinically apparent, therefore radiologists should be familiar whit normal and abnormal thoracic imaging findings.

References:

[1] Green DB, Groner LK, Lee JJ, Shin J, Broncano J, Vargas D, Castro M, Shostak E., (2021), Overview of Interventional Pulmonology for Radiologists. , Radiographics

[2] Milanese G, Silva M, Sverzellati N. , (2016), Lung volume reduction of pulmonary emphysema: the radiologist task., Curr Opin Pulm Med

[3] Godoy MC, Leitman BS, de Groot PM, Vlahos I, Naidich DP. , (2012), Chest Radiography in the ICU: Part I, Evaluation of Airway, Enteric, and Pleural Tubes., AJR

[4] Slebos DJ, Ten Hacken NH, Hetzel M, Herth FJF, Shah PL. , (2018), Endobronchial Coils for Endoscopic Lung Volume Reduction: Best Practice Recommendations from an Expert Panel., Respiration

A-710

Chest diffusion-weighted MRI in lung cancer imaging

A. Sudarkina, A. Dergilev
Novosibirsk State Medical University, Novosibirsk, Russian Federation

Learning Objectives

1. To describe the basics of diffusion-weighted MRI enabling tissues/fluids characterization.
2. To highlight the main directions of application of DWI in lung cancer imaging.
3. To discuss the obstacles and pitfalls in chest DWI data acquisition and interpretation.

Background

Lung cancer remains the most commonly diagnosed cancer and the leading cause of oncologic-related death worldwide over the last few decades.

Among all modalities in chest imaging MRI is the least used although the latest advances of hardware and software have made it possible to obtain a high-quality MR images of the chest providing beneficial morphologic and functional information.

Nowadays diffusion-weighted MRI is a widely used technique for cancer detection, staging and treatment follow-up in body imaging however its application in the workup of patients with lung cancer still remains limited.

We aimed to discuss the diagnostic scope of chest diffusion-weighted MRI which could provide a valuable information in lung cancer detection and radiological follow-up.

Imaging findings OR Procedure details

1. Diagnostic performance of DWI in lung nodules/lesions detection and characterization, malignant from benign lesions differentiation[1][3].
2. Using of DWI in lung cancer staging including tumor from atelectasis/peritumoral inflammation delineation[5], nodal status assessment[4], contribution of chest DWI to M-staging[2].
3. Potential of DWI in lung cancer radiological follow-up including tumor response to chemotherapy and/or radiation evaluation and recurrence diagnosis[6].

Conclusion

DWI is a useful complementary tool in lung cancer imaging providing valuable information for tumor detection and characterization, staging and treatment follow-up.

References:

[1] Basso Dias A, Zanon M, Altmayer S, et al, (2019), Fluorine 18-FDG PET/CT and Diffusion-weighted MRI for Malignant versus Benign Pulmonary Lesions: A Meta-Analysis, Radiology, 290(2): 525-34

[2] Luna A, Sánchez-Gonzalez J, Caro P, (2011), Diffusion-weighted imaging of the chest, Magn Reson Imaging Clin N Am, 19(1): 69-94

[3] Shen G, Jia Z, Deng H, (2016), Apparent diffusion coefficient values of diffusion-weighted imaging for distinguishing focal pulmonary lesions and characterizing the subtype of lung cancer: a meta-analysis, Eur Radiol, 26(2): 556-66

[4] Shen G, Lan Y, Zhang K, et al, (2017), Comparison of 18F-FDG PET/CT and DWI for detection of mediastinal nodal metastasis in non-small cell lung cancer: A meta-analysis, PLoS ONE, 12(3): e0173104

[5] Qi L, Zhang X, Tang L, et al, (2009), Using diffusion-weighted MR imaging for tumor detection in the collapsed lung: a preliminary study, Eur Radiol, 19: 333–341

[6] Usuda K, Iwai S, Funasaki A et al, (2019), Diffusion-weighted magnetic resonance imaging is useful for the response evaluation of chemotherapy and/or radiotherapy to recurrent lesions of lung cancer, Transl Oncol, 12(5): 699-704

A-621

Chest radiograph beyond lungs and heart

A. Sabu, R. k. Ramachandran, Z. Pkm
Kimshealth hospital trivandrum, Radiology, Trivandrum, India

Learning Objectives

To promt radiologiat to look to for subtle findings in chest radiograph which may be usually missed during routine evaluation

Background

Usually chest radiographs are taken for diseases of the lungs and heart. But involvement of other structures can also be made out. There are some hidden areas which can be easily missed in our routine evaluation. A variety of pathology is found in those areas.

Imaging findings OR Procedure details

Hidden areas in chest radiograph include apices, mediastinum,hila, diaphragm, soft tissue and bone. While looking for lung or heart pathologies a radiologist may miss some subtle finding in these areas. This poster showcases various findings that was incidentally detected in chest radiograph which was usually taken for other purposes

Methods

Chest radiograph of patients admitted to our hospital was evaluated and the findings obtained was correlated with further investigations and various pathologies were identified

Results

8 cases are demonstrated in this poster

Case 1: Chest Radiograph showing calcification in splenic area which was due to portal hypertension

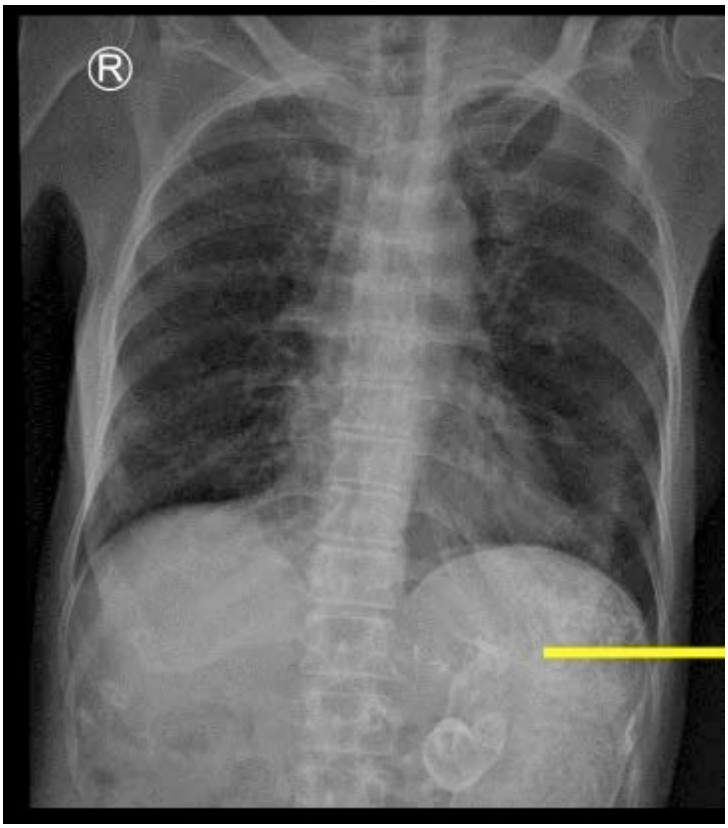

Calcified spleen

Case2: Calcification in liver area which was identified to be due to polycystic liver disease

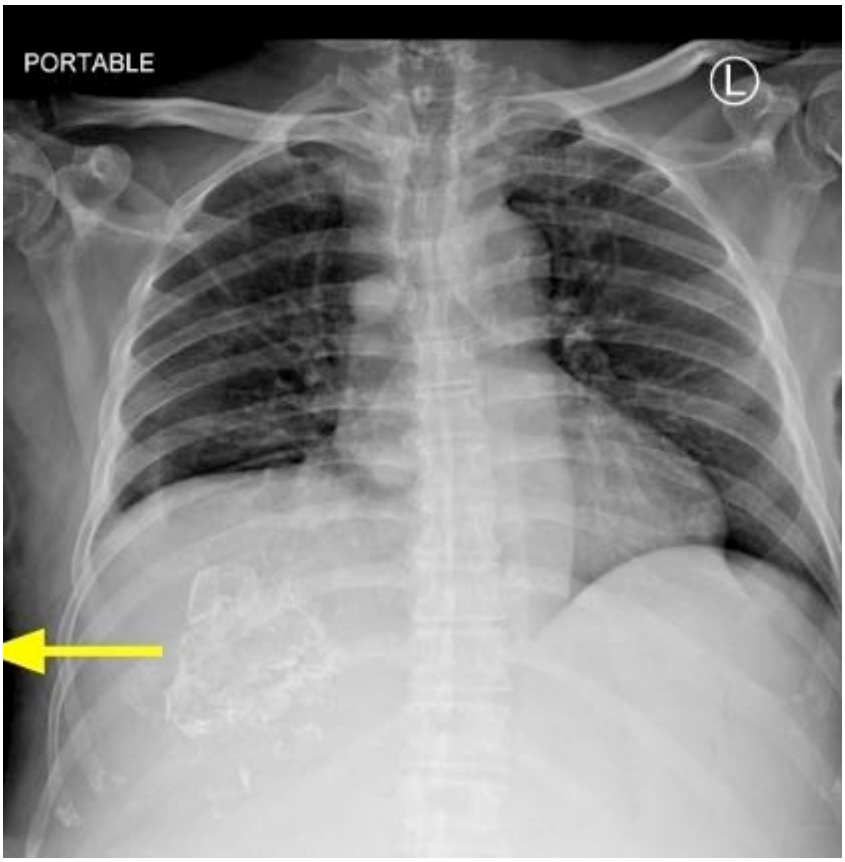

Calcified liver

Case 3:soft tissue calcification in the area of chest due to dermatomyositis

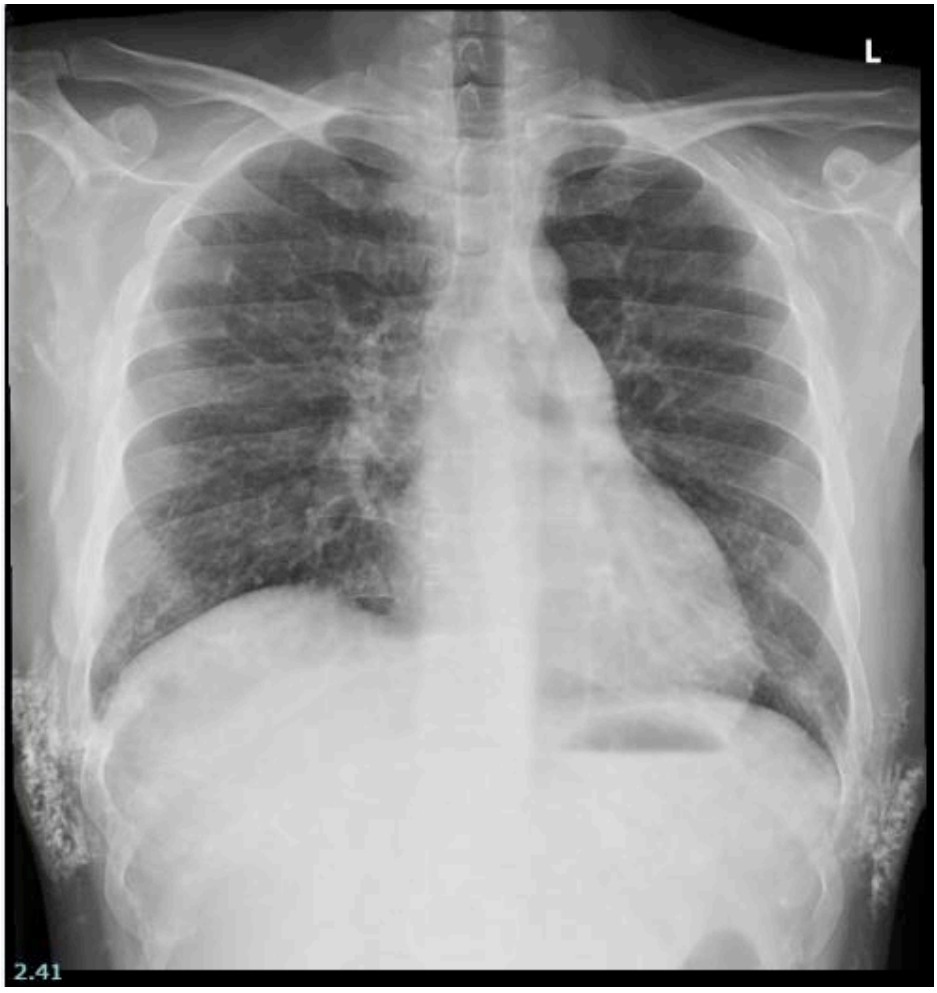

Dermatomyositis

Case 4:Costal osteomas renal osteodystrophy
Case 5:Ginko leaf sign in surgical emphysema
Case 6:Opacity noted in right humerus suggestive of bone infarct.
Case 7: widening of shoulder joint space due to Pigmented villonodular synovitis

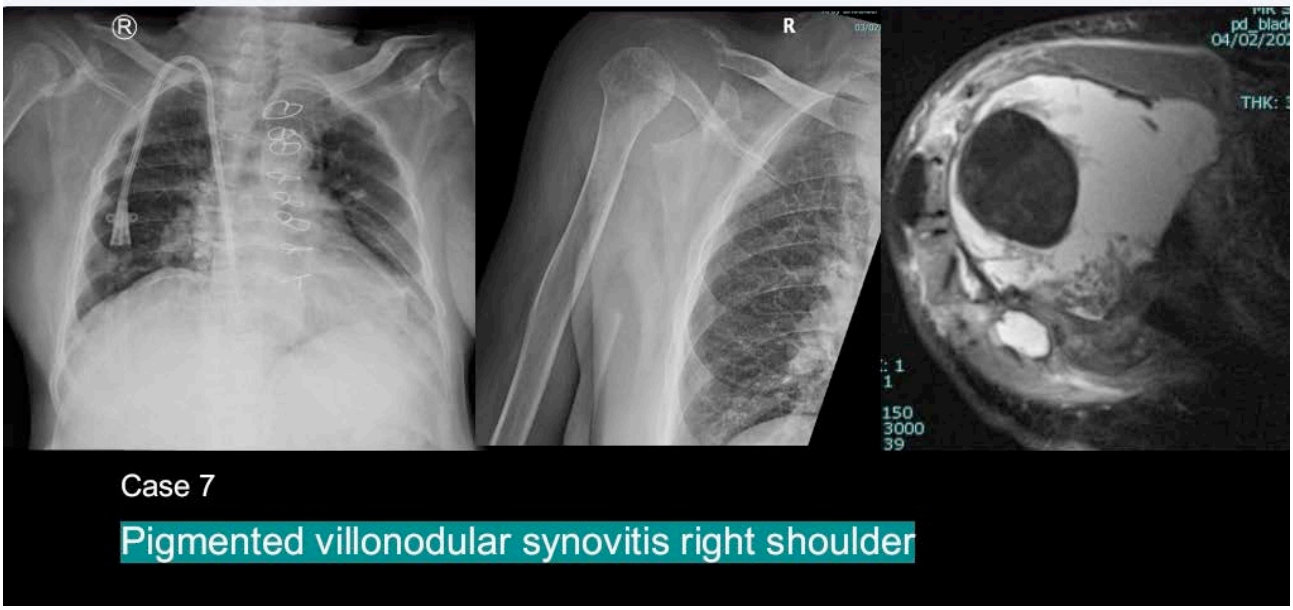

Pigmented villonodular synovitis

Case 8: Calcification in splenic area due to embolic material in angiomyolipoma

Conclusion

Chest radiograph should be evaluated systematically so that these subtle findings wont be missed. Early detected of these clues can help in early management and better outcome for the patient.

A-690

Chest Trauma: what Radiologists need to know

L. Reali[1], S. Galioto[1], C. Scavone[1], E. Tona[1], C. Timpanaro[1], G. La Rosa[1], L. A. Mauro[1], C. Vancheri[2], S. Palmucci[1], A. Basile[1]
[1]Policlinico di Catania, Radiology 1, Catania, Italy, [2]Policlinico di Catania, Pneumology, Catania, Italy

Learning Objectives
Chest trauma, is a leading cause of mortality and morbidity, either for causes directly related to thoracic injuries or for indirectly related ones. The aim of this study is to analyze the role and technique of the CT; in addition, this pictorial essay focuses on possible injuries and radiological findings detectable in these patients.

Background
Chest injuries usually occur above all in motor vehicle crashes, falls from heights, sports injuries and violent acts and according to the underlying cause, the injuries are classified as blunt and penetrating injuries [1]; the latter, for the high probability of vascular involvement, have higher mortality.
Although chest radiography and ultrasound are the fastest feasible methods for triage, especially in unstable patients, MDCT plays a key role not only in diagnosis. In fact, thanks to its multiplanar reconstructions and 3D reformations it allows excellent spatial and temporal resolution and provides useful information to the surgical treatment. CT technique is summarized in the table.

DETECTORS (layers)	> 16
COLLIMATION (mm)	0.6-1.2
ROTATION TIME (s)	0.3 - 0.5
PITCH	1-1.5
KILOVOLT PEAK (KVp)	120
MILLIAMPERE SECOND (mAs)	80-120
PATIENT'S POSITION	SUPINE
SCAN DIRECTION	CRANIO-CAUDAL
RECONSTRUCTION ALGORITHMS	SMOOTH AND SHARP
RECONSTRUCTION SECTION THICKNESS (mm)	0.625 - 1

Chest trauma MDCT protocol for adults.

Imaging findings OR Procedure details
Pleural space: A) pneumothorax: through MDCT is possible to have a qualitative and quantitative evaluation of the amount of intrapleural air and to detect the typical sign of tension pneumothorax (which requires immediate drainage); B) hemothorax: MDCT is important to differentiate simple fluid effusion from hemothorax and to detect active bleeding. **Lungs***:* A) pulmonary contusion, which may be assessed as ground-glass areas or ill-defined consolidations; chest CT scan help to predict the need for mechanical ventilation [2][3]. B) pulmonary laceration; C) traumatic lung herniation. **Airways***:* A) bronchial and tracheal lacerations; B) Macklin effect. **Esophagus**: the segment that is generally more involved is the cervical one. **Heart**, **aorta and great vessels:** A) thoracic aortic injury; B) injury to the internal mammary artery and injuries to the aortic arch branches. **Diaphragm***:* MDCT with reformation can show even a small diaphragmatic discontinuity. **Chest wall**: A) rib fracture; B) flail chest, it is a marker for significant intrathoracic associated injuries requiring surgical treatment [4]; C) fractures of the scapula; D) sternal fractures; E) sternoclavicular dislocations, can be associated with mediastinal blood vessels so that they could require contrast-enhanced CT to avoid vascular injuries; F)Thoracic spine fractures: MDCT aids in fracture characterization and stability [5].

Conclusion
MDCT and multiplanar and volumetric reformation is considered the primary imaging method in patients with high-energy trauma and is fundamental for a quick and accurate diagnosis and injuries classification that are important for the management of the patients.

References:

[1] Mirka et al., (2012), Multidetector computed tomography of chest trauma: indications, technique and interpretation, Insights into imaging 3.5
[2] Guerrero-Lopez F. et al., (2000), Evaluation of the utility of computed tomog- raphy in the initial assessment of the critical care patient with chest trauma, Crit Care Med
[3] Trupka A. et al., (1997), Value of thoracic computed tomography in the first assessment of severely injured patients with blunt chest trauma: results of a prospective study, J Trauma
[4] Athanassiadi K. et al., (2004), Management of 150 flail chest injuries: analysis of risk factors affecting outcome, Eur J Cardiothorac Surg
[5] Rivas et al., (2003), Multislice CT in thoracic trauma, Radiologic Clinics 41.3

A-399

Chest wall disorders: a pictorial review

A. L. Amado Costa, D. Antunes, J. Leitão
Centro Hospitalar Universitário Lisboa Norte/ Hospital de Santa Maria, Serviço de Imagiologia Geral, Lisboa, Portugal

Learning Objectives
1. To review various chest wall disorders and to illustrate their imaging findings

2. To review the imaging features that help narrow down the differential diagnosis of chest wall lesions

Background

Chest wall disorders include congenital anomalies and deformities, anatomical variants, inflammatory and infectious diseases, as well as soft-tissue and bone benign and malignant lesions. Radiography may be useful for the diagnosis of some chest wall deformities and variants; it is rarely useful for the diagnosis of most chest wall lesions, but it may help in the study of bone lesions and in the identification of calcifications in calcified chest wall lesions. Ultrasound is useful for detecting superficial lesions and to help guide biopsy. Computed tomography (CT) and Magnetic Resonance Imaging (MRI) enable accurate localization and characterization of chest wall lesions, as well as assessment of surrounding structures. CT is superior to MRI in depicting calcifications in calcified lesions and it can be useful in showing the anatomy of severe chest wall deformities, particularly in patients who are being considered for surgery. MRI provides superior contrast resolution of soft-tissue lesions, allowing better tissue characterization.

Imaging findings OR Procedure details

Based on our department database, we will present and illustrate the imaging characteristics of several chest wall disorders, including chest wall deformities and anomalies (namely pectus excavatum, pectus carinatum, Poland's syndrome, cervical ribs, and bifid ribs), chest wall variants (such as sternalis muscle, sternal foramen, and manubriosternal joint fusion), intercostal hernias (including intercostal lung hernia and inverted intercostal hernia), inflammatory and infectious diseases (such as arthritis and osteomyelitis), chest wall benign lesions (e.g.: lipomas, hematomas, *elastofibroma dorsi,* and neurogenic tumors), and malignant lesions (including sarcomas, metastasis, and plasmacytomas).

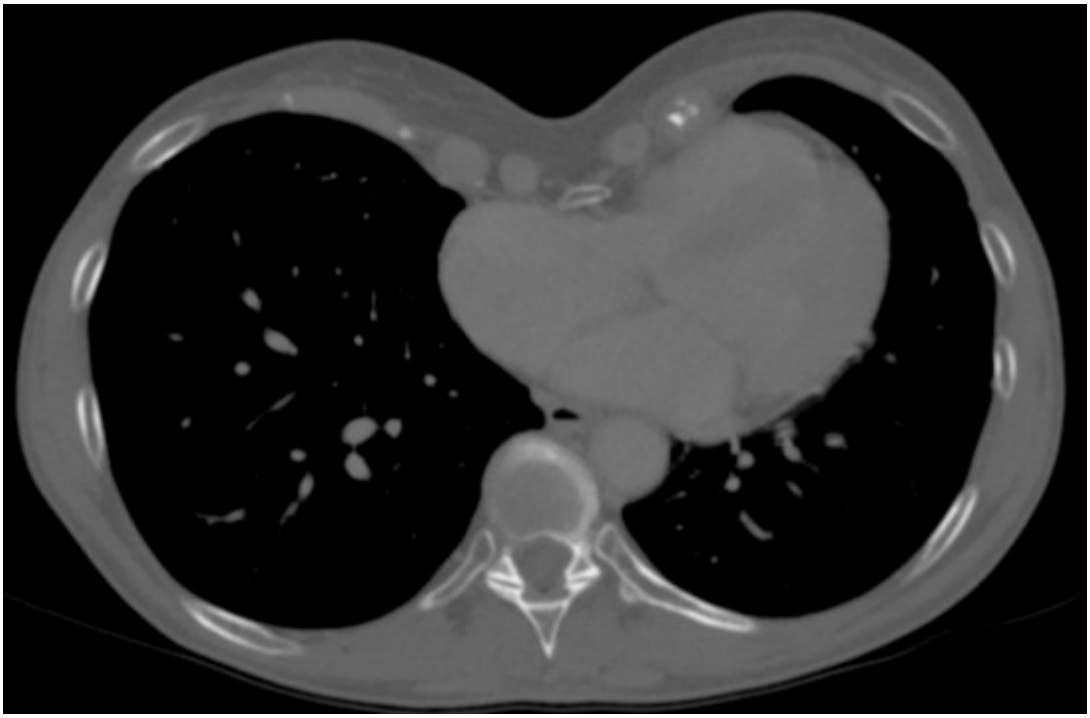

Axial contrast-enhanced CT image (bone window) of a patient with pectus excavatum.

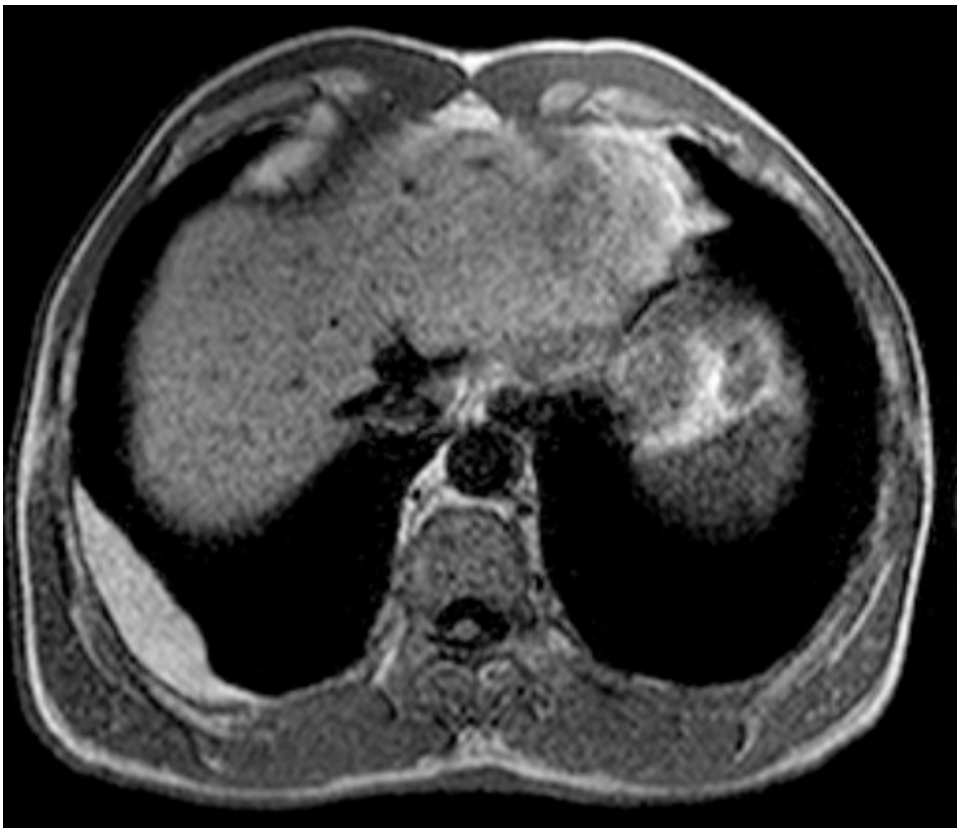

Axial T1-weighted MRI image of a patient with a right-sided chest wall lipoma.

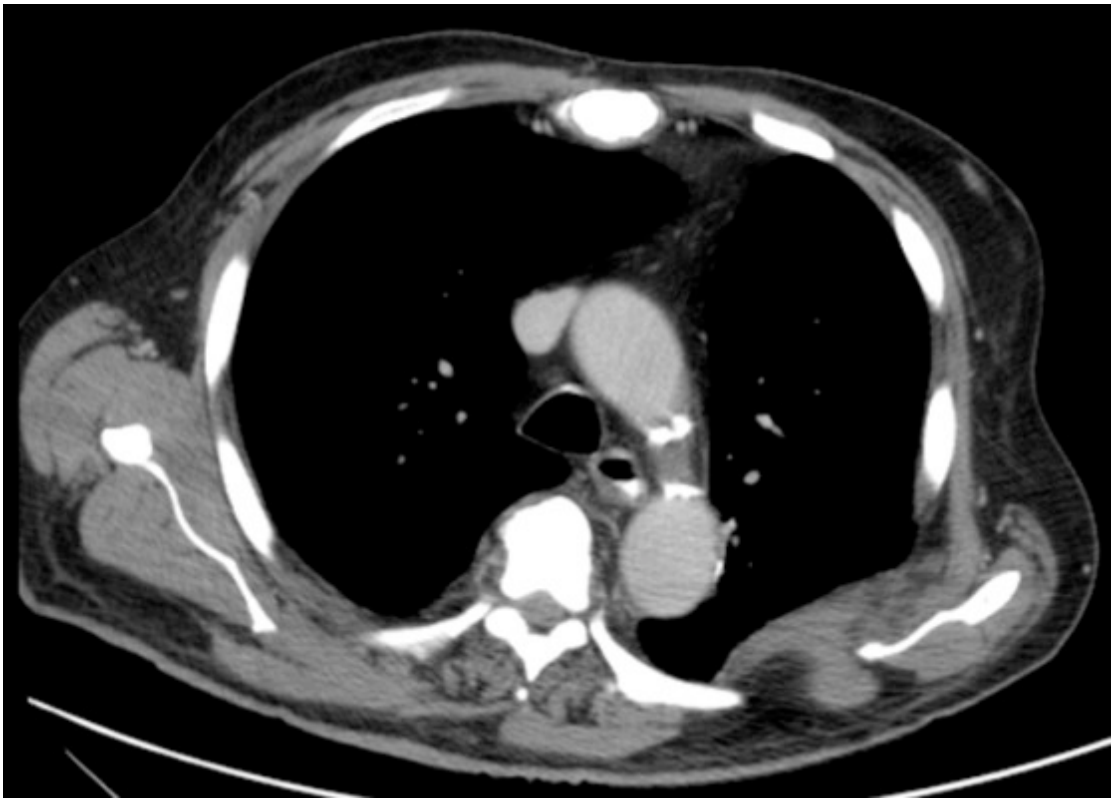

Axial contrast-enhanced CT image of a patient with a left-sided inverted intercostal hernia of soft tissue of the chest wall

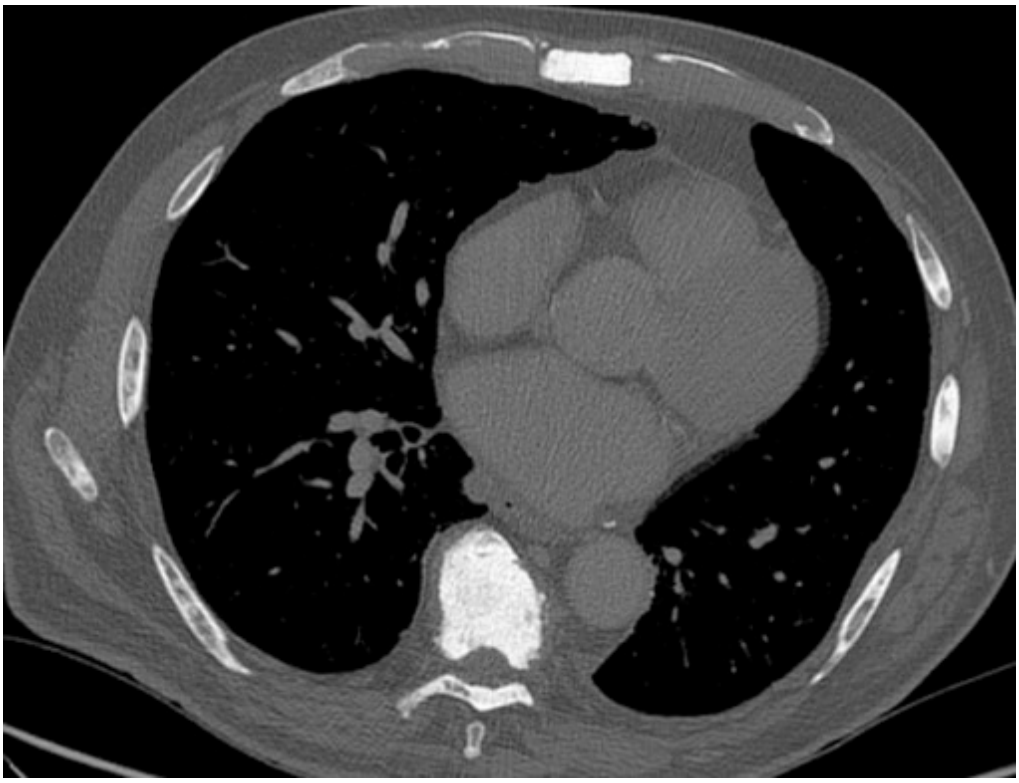

Axial contrast-enhanced CT image (bone window) of a patient with multiple osteoblastic metastasis in several ribs, the sternum, the right scapula and dorsal vertebra.

Conclusion

Many chest wall disorders have characteristic imaging features that allow a confident diagnosis. However, some chest wall lesions can be challenging to diagnose. The radiologist plays a crucial role in diagnosing and advising further workup and management of these conditions.

A-590

Chronic Graft versus Host disease involving the lung: CT scan features

R. Barbante[1], C. Ravaglia[2], A. Vizzuso[3], R. Galeotti[4], E. Giampalma[3], V. Poletti[2], S. Piciucchi[5]
[1]Ospedale Morgagni Pierantoni di Forlì, Radiology, Forlì, Italy, [2]Department of Diseases of Thorax; GB Morgagni Hospital/University of Bologna, Forli, Italy, [3]Department of Radiology; GB Morgagni Hospital/University of Bologna, Forli, Italy, [4]Interventional Radiology Unit, Ferrara University Hospital, Radiology, Ferrara, Italy, [5]Department of Radiology; GB Morgagni Hospital/University of Bologna, FORLI', Italy

Purpose/Objectives
To describe computed tomography findings in patients suffering for chronic Graft Versus Host Disease (GVHD) after allogeneic hematopoietic stem cell transplantation (HSCT) involving also the lungs
Methods & Materials
Patients with diagnosis of pulmonary graft versus host disease were retrieved from the database of our hospital in the period between 2010 to 2023 and enrolled in this observational retrospective study. The ethical Committee approved this study (CEROM approval n° 30/2020 I.5/284)). The inclusion criteria were: criteria for chronic GVHD, age above 18 year-old, availability of CT scan at the moment of the diagnosis.
Clinical data collected included: pulmonary function tests, time lapse between transplant and symptoms, donors sources and farmacological treatment.
CT findings were analyzed in consensus by two radiologists with respectively 2 and 17 years of experience and categorized according the Fleischner glossary terms. A final radiological and clinical correlation of data was achieved.
Results
The group consisted of fourty-three patients (22 males; mean age range 20- 72 years old). Haematological history included: acute lymphocytic leukemia (n= 16); chronic myeloid leukaemia (n= 9), acute myeloid leukaemia (n=9); plasmacytoid leukaemia (n=1); non-lymphoid acute leukaemia (n=2); multiple myeloma (n= 2); non-Hodgkin lymphoma (n= 3); Hodgkin lymphoma (n= 1), myelofibrosis (n= 1).
Nine patients showed bronchiectasis and tree-in-bud pattern (two of them with air trapping in expiratory scan); fifteen mosaic attenuation with air trapping in the expiratory scan; five patients centrilobular ground glass nodules; two patients organizing pneumonia pattern (reverse halo and nodules); thirteen cases showed a prevalent fibrotic pattern with PPFE. PPFE showed three main phenotypes: PPFE-ILD (n=2) in which the ILD was represented by UIP pattern; PPFE-airways disease (n=5) in which PPFE was associated with signs of bronchiolitis as tree-in-bud, centrilobular nodules and/or bronchiectasis with mucus plugging, and standalone PPFE (n=4). In six patients of our cohort GVHD appeared with a rapidly progressive form. In these six patients CT findings were patchy ground glass (n=4), crazy paving (n=1), centrilobular nodules (n=1).
Conclusion
CT scan features confirm that chronic GVHD involving the lungs may manifest with two main patterns: the bronchiolocentric one with mosaic oligoemia, expiratory air trapping but also inflammatory bronchiolitis (tree in bud pattern) and bronchiectasis ; the restrictive pattern being PPFE the main feature.Other interstitial aspects were also documented (UIP, organizing pneumonia).

A-219

Chronic Thromboembolic Pulmonary Hypertension (CTEPH): A Review of Imaging Features on radiograph and CT

V. S. Ponnalagu[1], T. Hui[2]
[1]WOODLANDS HEALTH, Diagnostic Radiology, SINGAPORE, Singapore, [2]TAN TOCK SENG HOSPITAL, Diagnostic Radiology, SINGAPORE, Singapore

Learning Objectives

-Understand the imaging features of pulmonary hypertension
-Understand the imaging features of chronic thromboembolic pulmonary hypertension (CTEPH)
-Appreciate the treatment options for CTEPH

Background

Pulmonary hypertension due to chronic thromboembolism is recognised as the only type of pulmonary hypertension (PH) that is potentially curable. The clinical symptoms and signs could be non-specific leading to under-diagnosis and eventual increased mortality rate. By developing an understanding of the features of pulmonary hypertension on chest radiographs and CT scans, the radiologist could raise the diagnosis and facilitate early treatment and improved outcomes.

Imaging findings OR Procedure details

Chest radiograph imaging features of pulmonary hypertension include the following:
-Elevated cardiac apex due to right ventricular hypertrophy (RVH)
-Enlarged right atrium (RA)
-Enlarged pulmonary arteries (PA)
-Hilar enlargement (bilateral)
-'Pruning' of the peripheral pulmonary vessels
CT features of pulmonary hypertension include:
-Enlarged main pulmonary trunk and/or PA
-Mural calcification in the central PA
-RVH (wall thickness > 4mm), straightening or bowing towards left ventricle (LV)
-Right ventricular dilatation
-IVC and hepatic vein dilatation
-Pericardial effusion
-Carina crossover sign
In addition to these features, in chronic thromboembolic pulmonary hypertension (CTEPH), CT imaging may demonstrate:
-Chronic or acute central and/or peripheral pulmonary emboli (PE)

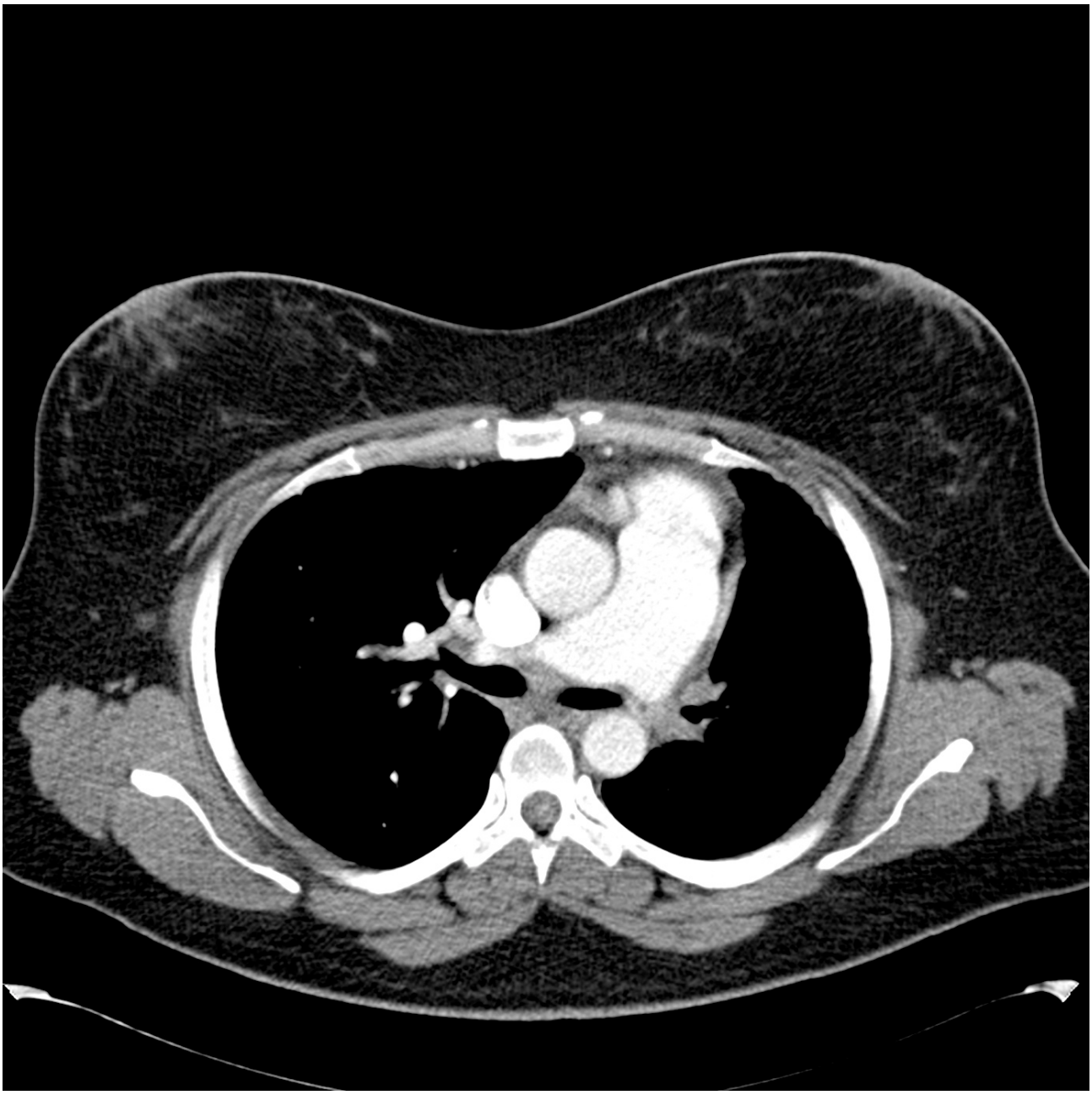

Chronic pulmonary embolism causing complete obliteration of the left pulmonary artery as well as dilatation of the pulmonary trunk

-Right atrial thombus
-Mosaic attenuation
-Parenchymal changes: bands, wedge consolidation, cavitation
-Bronchial/non-bronchial collaterals
-Bronchial dilatation or wall thickening
-Pleural or pericardial effusion[CTEPHFeatures]

Treatment options for CTEPH include surgical and non-surgical modalities, in addition to lifelong anticoagulation.
Pulmonary endarterectomy is the modality of choice in most cases. However, in patients who may not be surgical candidates, targeted medical therapy with or without balloon pulmonary angioplasty (BPA) could be viable. The procedure is performed under general anaesthesia, with targeting of webs in segmental and subsegmental vessels using hydrophilic guidewires. The aim is to restore normal flow with rapid filling of draining pulmonary veins. The lower lobe vessels are prioritised and right lung over left lung, due to the greater physiological impact. Although complications could occur peri- and post-procedure, BPA has shown durable results and improvment in mortality, with pulmonary artery pressure (PAP) and pulmonary vascular resistance (PVR) remaining >50% lower than baseline values[5].

Conclusion

CTEPH is a potentially curable cause of pulmonary hypertension. Yet it is under-diagnosed.
By looking out for imaging features, we can recommend referral to appropriate specialists for early treatment.
References:

[5] Takumi Inami, Masaharu Kataoka, Ryoji Yanagisawa, Haruhisa Ishiguro, Nobuhiko Shimura, Keiichi Fukuda, Hideaki Yoshino and Toru Satoh, (2016), Long-Term Outcomes After Percutaneous Transluminal Pulmonary Angioplasty for Chronic Thromboembolic

Pulmonary Hypertension, Circulation, 2030–2032, 134, https://doi.org/10.1161/CIRCULATIONAHA.116.024201, 2023-03-02
[CTEPHFeatures] Alexandra Grosse, Claudia Grosse, Irene Lang, (2018), Evaluation of the CT imaging findings in patients newly diagnosed with chronic thromboembolic pulmonary hypertension, PLoS One, e0201468, 13(7), https://doi.org/10.1371%2Fjournal.pone.0201468, 2023-03-02

A-501

Combined pulmonary fibrosis and emphysema (CPFE): a threatening distinct entity?

S. Giedrys, E. Baltakytė, J. Zaveckienė
Lithuanian University Of Health And Sciences, Radiology, Kaunas, Lithuania

Learning Objectives

To overview the current state of recognition of CPFE as a standalone disease with unique clinical, radiologic, and pathologic characteristics.
To present imaging features of CPFE as variety of patterns that include fibrosis and emphysema.
To improve awareness of CPFE by presenting case examples with complications increasingly linked to CPFE.

Background

Combined pulmonary fibrosis and emphysema (CPFE) was not recognized as a distinct disease until 2005, when Cottin et al. described CPFE as coexistence of emphysematous and fibrotic changes of the lungs[1]. The syndrome generally occurs in male smokers and presents with a various degree of dyspnoea, emphysema, fibrosis and reduced capacity of gas exchange. In a combination of symptoms and pulmonary function tests, high-resolution computed tomography (HRCT) is the essential imaging technique used in making the diagnosis[2]. However, to this day a consensus definition of CPFE syndrome, classification and quantitative grading does not exist.

Imaging findings OR Procedure details

The degree of each finding in making the diagnosis is yet to be established, however practical points in evaluation can be divided into four categories.

Emphysema.

The emphysematous part of lung damage may include centrilobular, paraseptal emphysema and bullae formation, while centrilobular distribution is considered more common in smokers, CPFE frequently presents with dominant paraseptal subtype which may be considered distinctive of this syndrome[5]. Another unique radiological and pathological sign of CPFE are thick-walled cystic lesions (TWCLs), which are found more frequently than in emphysema or fibrosis alone (Fig. 1)[3].

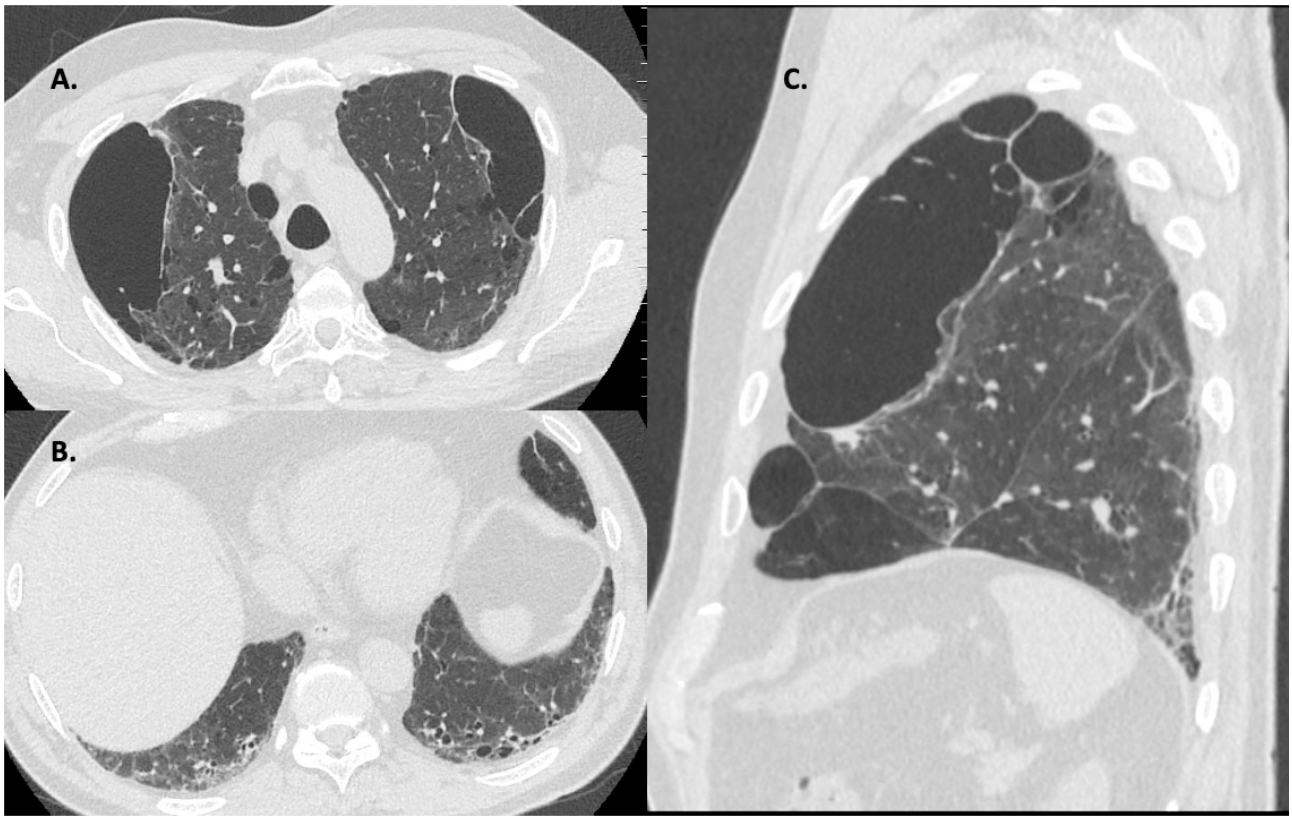

Fig. 1. HRCT appearance of CPFE with thick-walled cystic airspaces, found more frequently than in in emphysema or fibrosis alone. A, B, C) Patient with a smoking history of 25 years and restrictive pattern on pulmonary function test.

Fibrosis.

The fibrotic part of lung damage show various patterns of honeycombing, reticulations and traction bronchiectasis, while addition of ground glass opacities are also common in CPFE suggesting potential smoking related ILD (Fig. 2)[4].

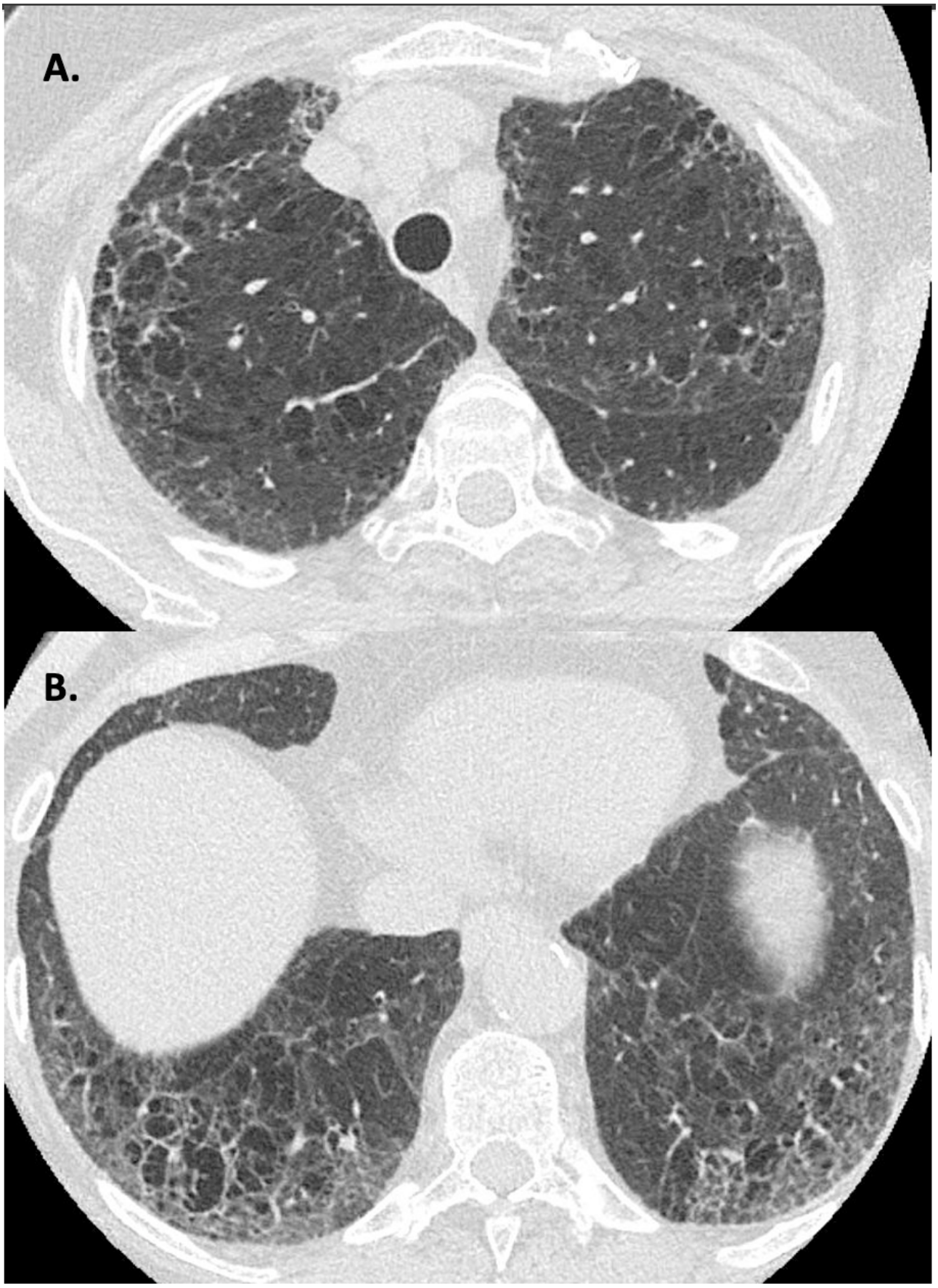

Fig. 2. A, B) HRCT appearance of CPFE: dominant upper lobe paraseptal and centrilobular emphysema and lower lobe fibrosis, characterised by thickening of interlobular septa, honeycombing and traction bronchiectasis.

Combination and mixed patterns.
Different distribution patterns in CPFE have been described as upper lobe emphysema with fibrotic interstitial disease predominantly in the lower lobes (Fig. 3)[5].

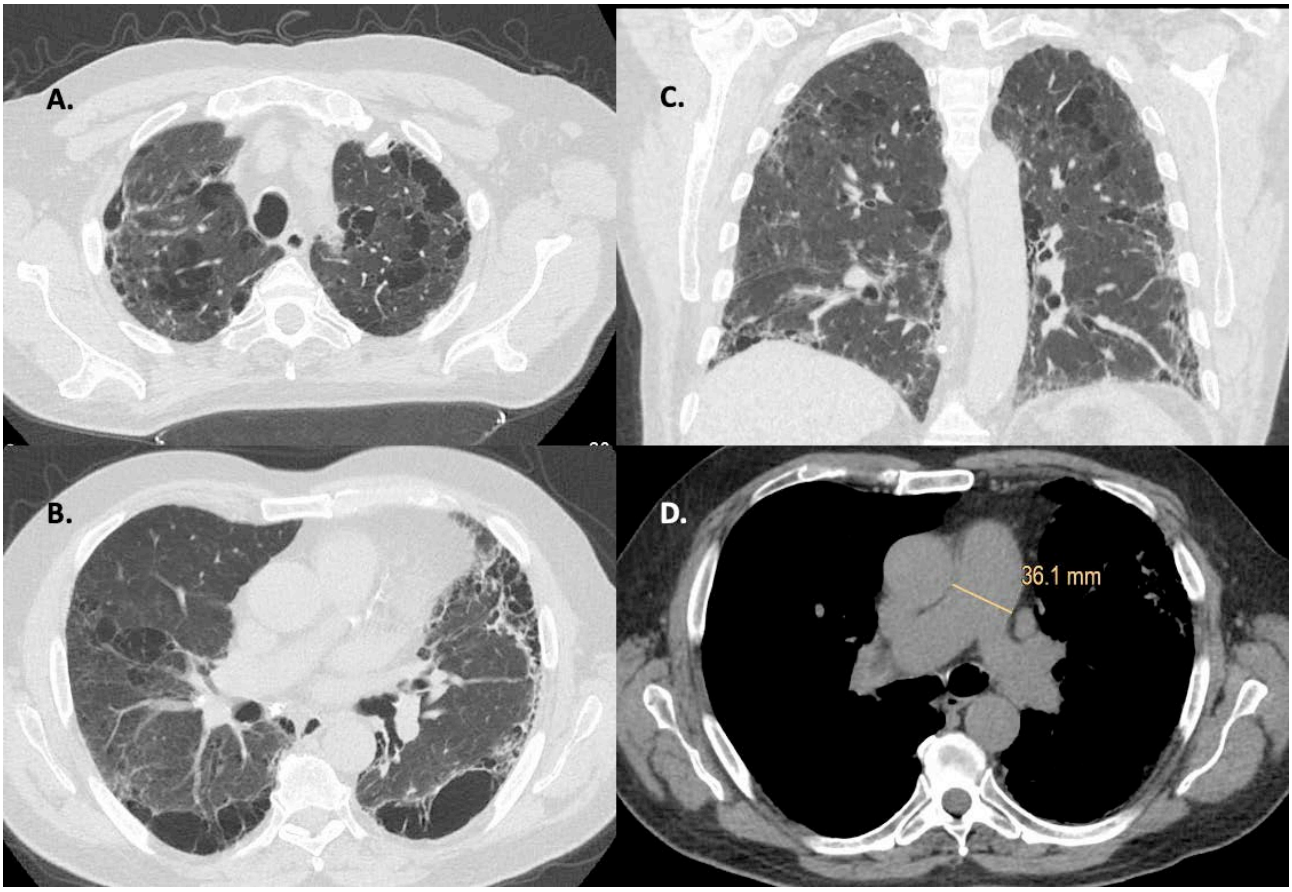

Fig. 3. A, B, C) HRCT appearance of common subtype described as diffuse emphysema with zone of transition with honeycombing. D) Patients with CPFE are at higher risk of developing pulmonary hypertension, which can be suspected even on non-contrast enchanced CT by enlargment of pulmonary arteries and right heart chambers (not shown).

Complications.
Furthermore, an increased risk of lung cancer, pulmonary hypertensions and acute lung injury is established (Fig. 4.)[5].

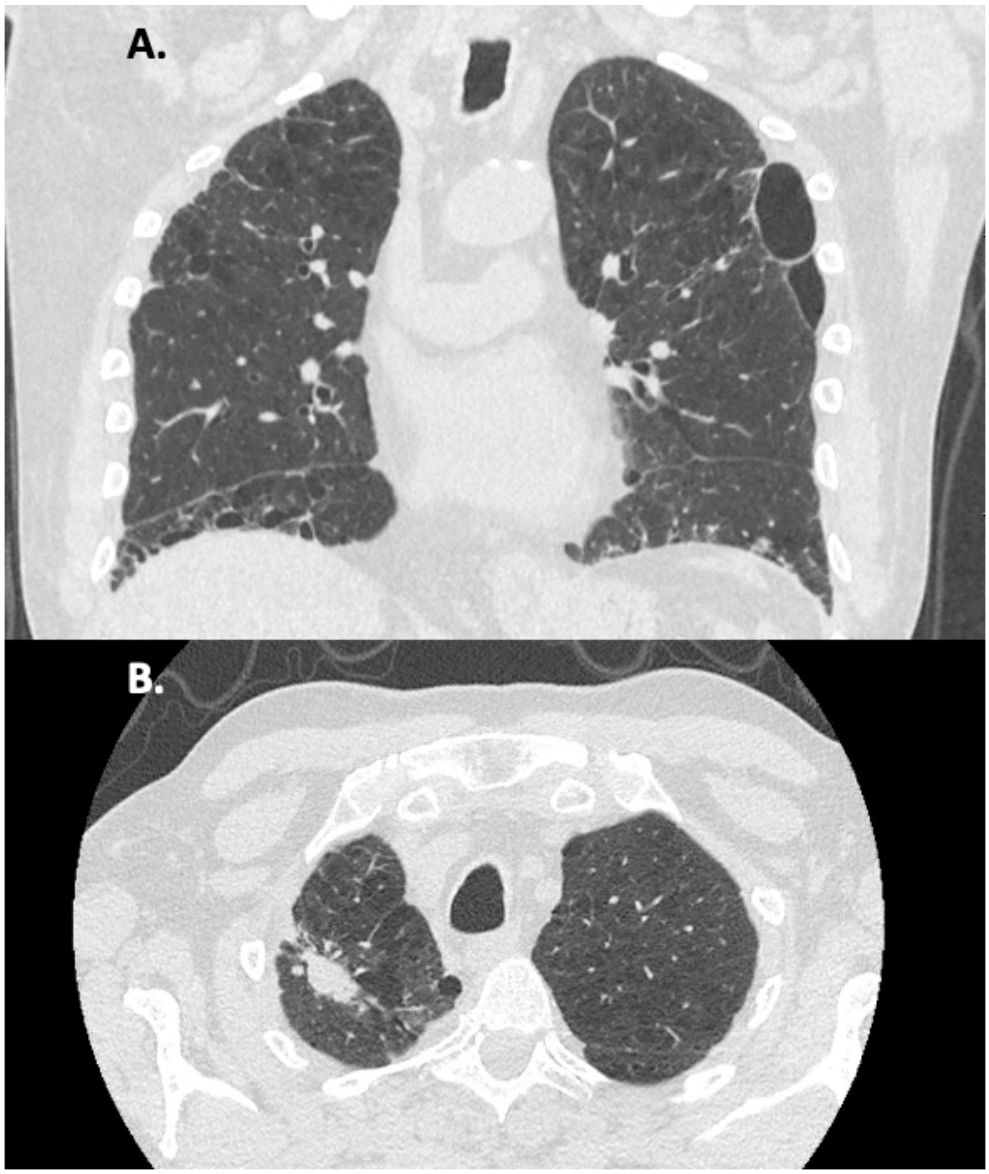

Fig. 4. Patients with CPFE are at higher risk of developing lung cancer. A, B) Patient with a smoking history of 30 years showing signs of CPFE, right upper lobe mass verified as infiltrative squamos cell carcinoma.

Conclusion

Over the last two decades there is an increase in radiological and clinical understanding of CPFE. HRCT remaining the diagnostic standard, radiologists should be able to identify coexisting patterns of lung emphysema and fibrosis and their subsequent complications. Further studies are needed in possible diagnostic criteria and differences of CPFE with its standalone parts, other smoking related lung diseases, COPD, independent ILD with the aim of improved patient management.

References:

[1] Ciccarese, F., Attinà, D. & Zompatori, M. , Combined pulmonary fibrosis and emphysema (CPFE): what radiologist should know, Radiol med 121, 564–572 (2016). https://doi.org/10.1007/s11547-016-0627-4.
[2] Lin H, Jiang S. , Combined pulmonary fibrosis and emphysema (CPFE): an entity different from emphysema or pulmonary fibrosis alone., J Thorac Dis. 2015 Apr;7(4):767-79. doi: 10.3978/j.issn.2072-1439.2015.04.17. PMID: 25973246; PMCID.
[3] V. Cottin, H. Nunes, P-Y. Brillet, P. Delaval, G. Devouassoux, I. Tillie-Leblond, D. Israel-Biet, I. Court-Fortune, D. Valeyre, J-F. Cordier, Combined pulmonary fibrosis and emphysema: a distinct underrecognised entity., European Respiratory Journal Oct 2005, 26 (4) 586-593; DOI: 10.1183/09031936.05.00021005.
[4] Andriana I. Papaioannou, Konstantinos Kostikas, Effrosyni D. Manali, Georgia Papadaki, Aneza Roussou et. al., Combined pulmonary fibrosis and emphysema: The many aspects of a cohabitation contract., Respiratory Medicine, Volume 117, 2016, Pages 14-26, ISSN 0954-6111, https://doi.org/10.1016/j.rmed.
[5] V. Cottin, M. Selman, Y. Inoue, A. W. Wong, T. J. Corte et. al. , Syndrome of Combined Pulmonary Fibrosis and Emphysema: An Official ATS/ERS/JRS/ALAT Research Statement., American Journal of Respiratory and Critical Care Medicine., e7-e41, 206-4, 10.1164/rccm.202206-1041ST.

Common and uncommon tracheal disorders – a pictorial review

R. Rodrigues Bexiga, C. Mendonça, A. L. Amado da Costa, J. Leitão
Centro Hospitalar Universitário Lisboa Norte, Serviço de Radiologia Geral, Lisboa, Portugal

Learning Objectives

To review the imaging features of neoplastic and nonneoplastic disorders of the trachea to help narrow down the differential diagnosis.

Background

An extensive range of disorders can affect the trachea. These conditions can be categorized in different groups, namely congenital or acquired, benign or malignant, focal or diffuse, and narrowing or widening of the trachea. Chest radiography is usually the first step in the evaluation of suspected central airway disease. However, computed tomography (CT) improves both the detection and characterization of central airway disease; meanwhile, it enables the assessment of the surrounding structures. Consequently, the recognition of the imaging characteristics of tracheal disorders is essential to generate a differential diagnosis and then aid in the planning of bronchoscopy or therapeutic interventions.

Imaging findings OR Procedure details

Based on our department database, we will present and illustrate the imaging characteristics of diverse tracheal disorders, mainly on radiography and CT, emphasizing their imaging features. Tracheal disorders include nonneoplastic conditions, as well as benign and malignant neoplasms. We will review and illustrate the main radiological characteristics of several non-neoplastic conditions, including: congenital anomalies, such as tracheal bronchus; Mounier-Kuhn syndrome; innominate artery compression syndrome; tracheal diverticulum; tracheomalacia; tracheal calcification; saber-sheath trachea; some etiologies of tracheal stenosis, such as post-tracheostomy and post-intubation tracheal stenosis, tracheobronchopathia osteochondroplastica, among others. We will also review and illustrate some benign tracheal tumors and some malignant tracheal tumors, including primary and secondary tracheal tumors. Tracheal tumors are uncommon, and the vast majority are malignant [1]; they often cause tracheal stenosis. The most common primary malignant tumors are squamous cell carcinoma and adenoid cystic carcinoma [1]. Secondary malignancies most frequently occur as a result of direct invasion by a malignancy or, less commonly, by hematogenous spread [2]. Benign tumors of the tracheobronchial tree are extremely rare; hamartoma and squamous cell papilloma account for most of the benign tumors arising in the tracheobronchial tree [2].

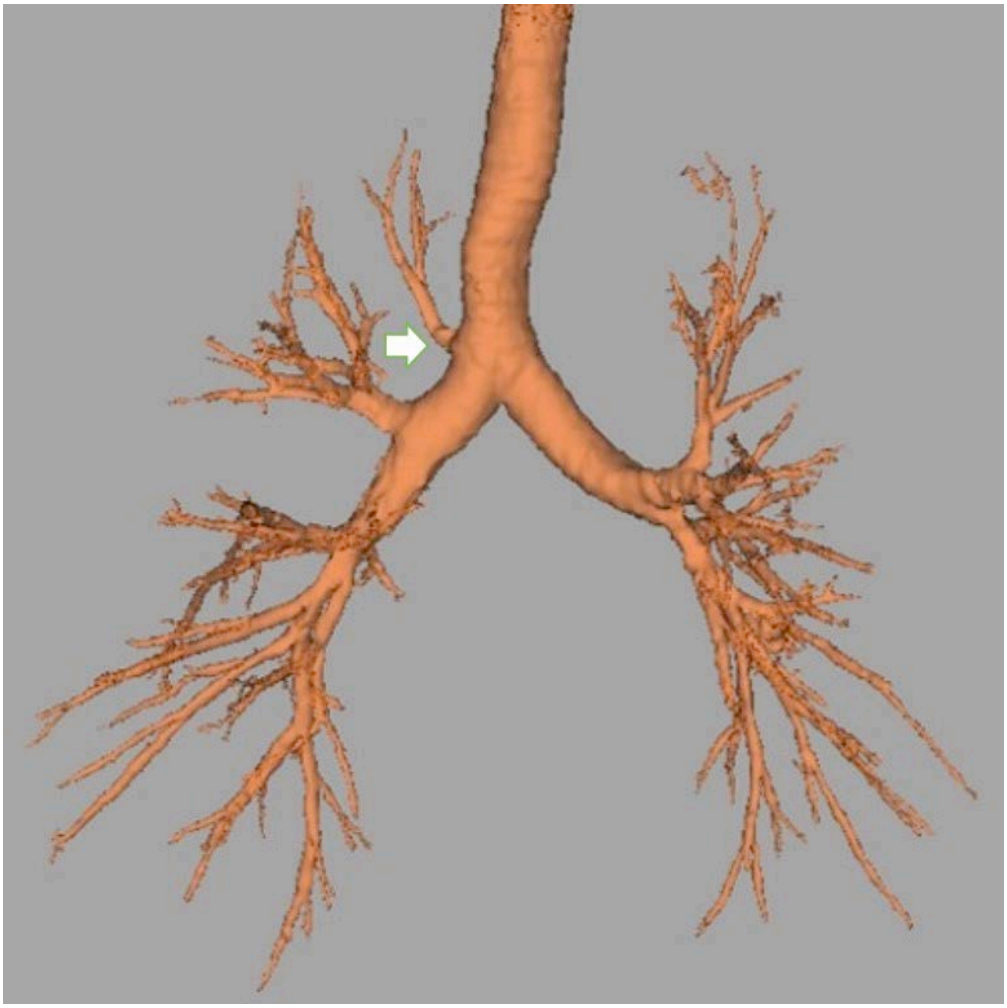

Anteroposterior view of a 3D reconstruction of the CT of a patient with a tracheal bronchus (arrow).

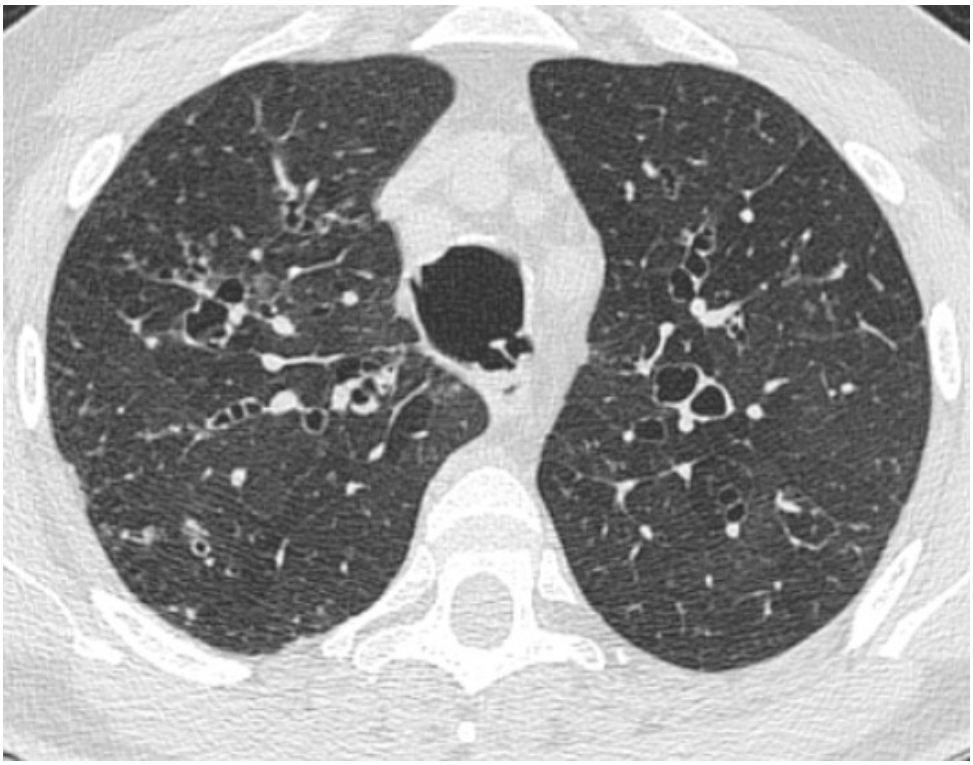

Axial CT image (lung window) of a patient with Mounier-Kuhn syndrome, presenting tracheomegaly, tracheal diverticula and bronchiectasis.

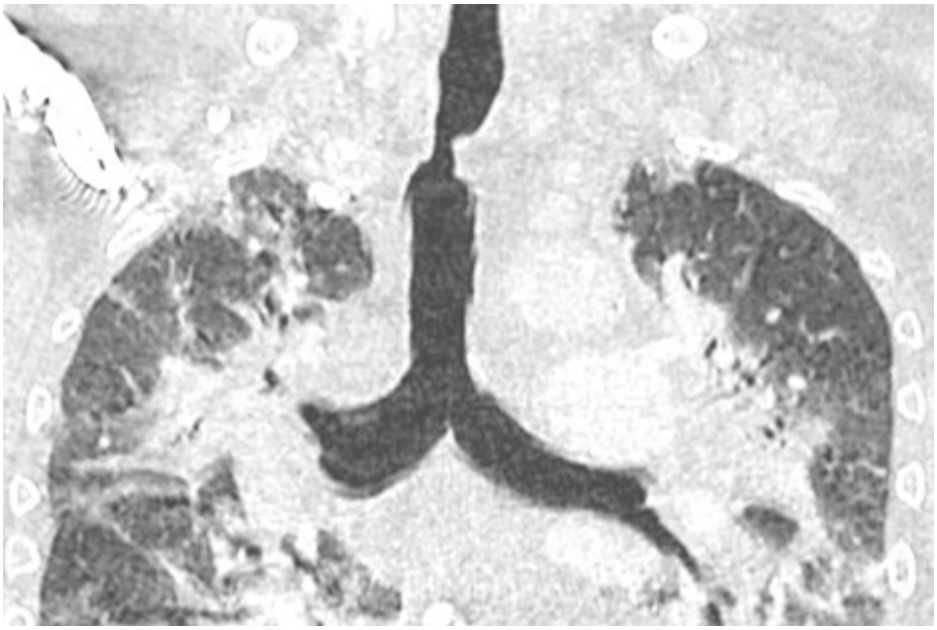

Coronal oblique CT image (lung window) of a patient with post-intubation tracheal stenosis.

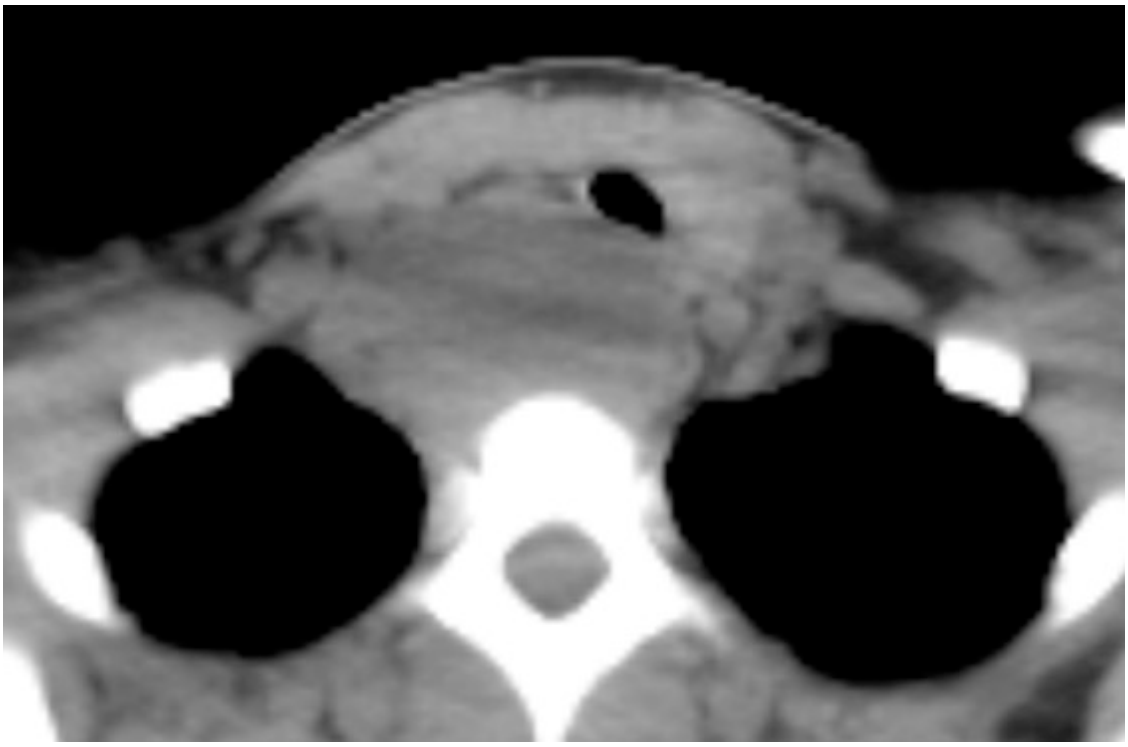

Axial CT image (mediastinal window) of a patient with tracheal stenosis due to adenoid cystic carcinoma.

Conclusion

A wide range of tracheal disorders can be found on imaging. Knowledge of the radiologic appearance of these conditions is crucial in generating a differential diagnosis and determining the next step in management.

References:

[1] Macchiarini P., (2006), Primary tracheal tumours, Lancet Oncol , 83-91, 7
[2] Park CM, Goo JM, Lee HJ, Kim MA, Lee CH, Kang MJ, (2009), Radiographics, 29, 55–71

A-660

Congenital Malformations of the Pulmonary Airways: What the Radiologists Need to Know

P. P. Saturnino[1], F. Dell'Aversana[2], A. Fabozzi[2], E. Basco[1], N. Rosano[1], D. Pourmolkara[3], L. Cagini[4], A. D'Antonio[5], F. Tamburro[1]
[1]Ospedale del Mare-ASL NA1 Centro, Department of Radiology, Naples, Italy, [2]Università degli studi della Campania "Luigi Vanvitelli", Department of Radiology, Naples, Italy, [3]Università degli studi di Perugia, Thoracic Surgery Unit, Perugia, Italy, [4]Ospedale del Mare-ASL NA1 Centro, Thoracic Surgery Unit, Naples, Italy, [5]Ospedale del Mare-ASL NA1 Centro, Department of Pathologic Anatomy, Naples, Italy

Learning Objectives

Although most congenital pulmonary airway malformations (CPAM) are diagnosed before birth, it's not uncommon for them to remain asymptomatic or minimally symptomatic into adulthood, where they may be found incidentally. Since CPAM can present a malignant evolution, especially type 1, it's essential to diagnose this rare pathological entity.

Background

CPAM is a rare non-hereditary abnormality of lung parenchymal development with an estimated incidence of 1 in 25,000–35,000 newborns[1]. The imbalance between cell proliferation and apoptosis is believed to be the main mechanism behind CPAM development. CPAMs are characterized by the presence of multiple cysts or air-filled spaces of varying sizes within lung. Cysts are typically distributed throughout the lung and can result in compression of adjacent lung tissue, leading to symptoms such as cough, shortness of breath and recurrent pulmonary infections. It's typically recognized in early childhood, with symptoms appearing at the age 2 or 3[2]. However, it can also occur in children and young adults usually presenting as an incidental finding on imaging studies such as chest X-ray and CT scan or during evaluation for unrelated respiratory symptoms. Adult onset of CPAM is uncommon, occurring in only about 15-20% of cases. [2]Treatment typically involves surgical removal of the affected lung tissue to prevent complications and improve symptoms. In some cases, CPAM may be asymptomatic and require no treatment[3].

Imaging findings OR Procedure details

33-year-old patient with no history of recurrent lung disease underwent post-covid chest-X-ray. The radiograph demonstrates a large retrocardiac pseudonodular hypodiaphanous area in the lower zones.

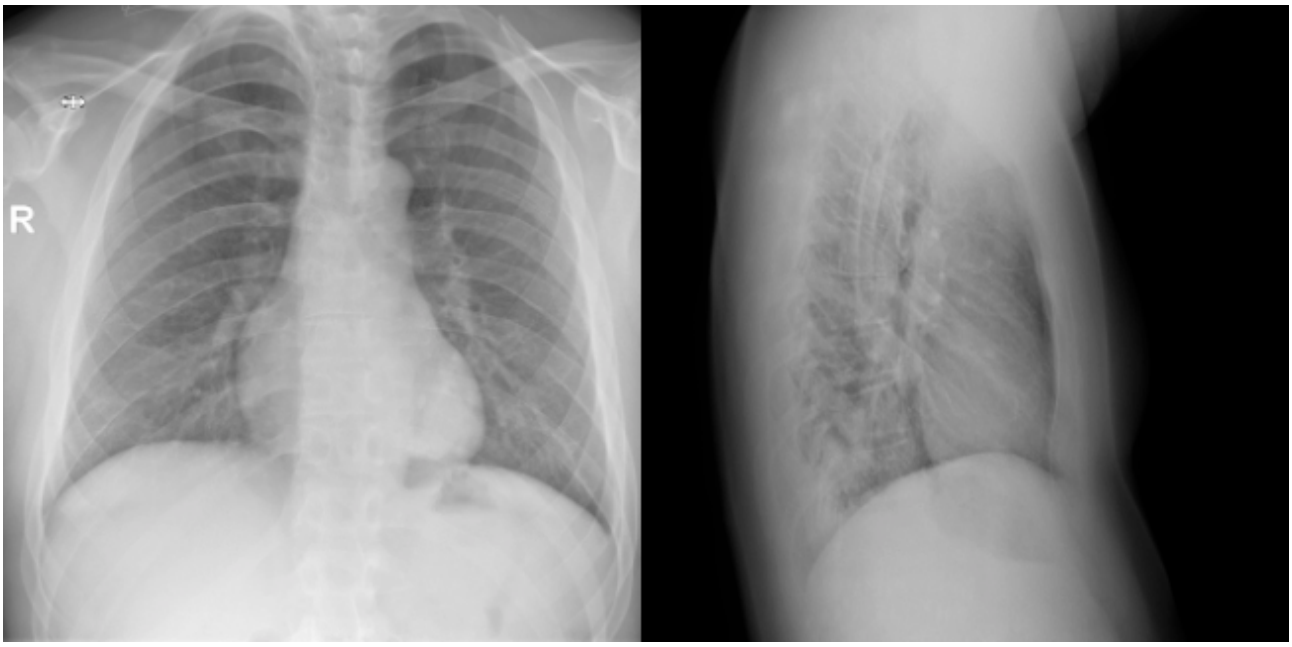

The radiograph demonstrated a large retrocardiac pseudonodular hypodiaphanous area in the lower zones.
Chest-CT confirmed the presence of a non-enhancing irregularly oval consolidation of lung parenchyma measuring about 3cm located at the postero-basal segment of the left lower lobe.

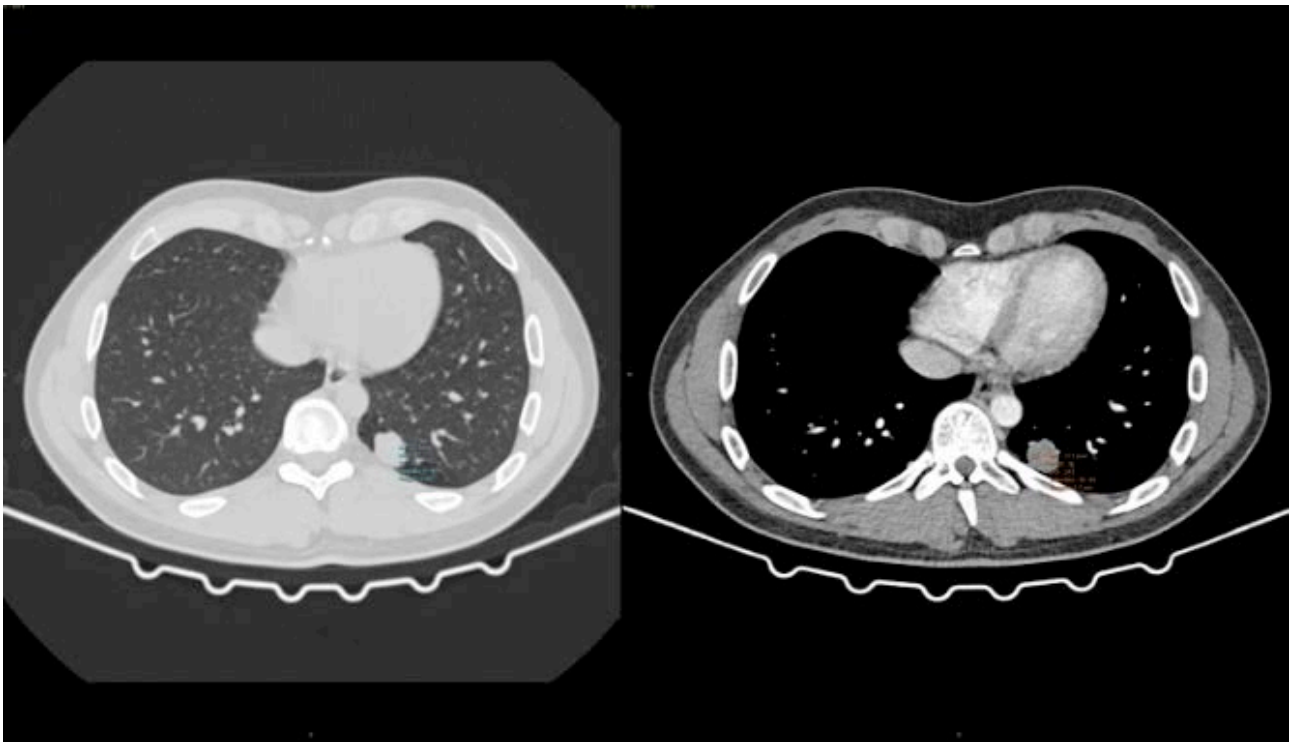

Chest CT performed before and after the administration of non-ionic iodinated contrast medium confirmed the presence of an irregularly oval consolidation of the lung parenchyma of approximately 28x26x35 mm located in the postero-basal segment of the left lower lobe. Emphysematous rarefaction of the surrounding parenchyma was also demonstrated.

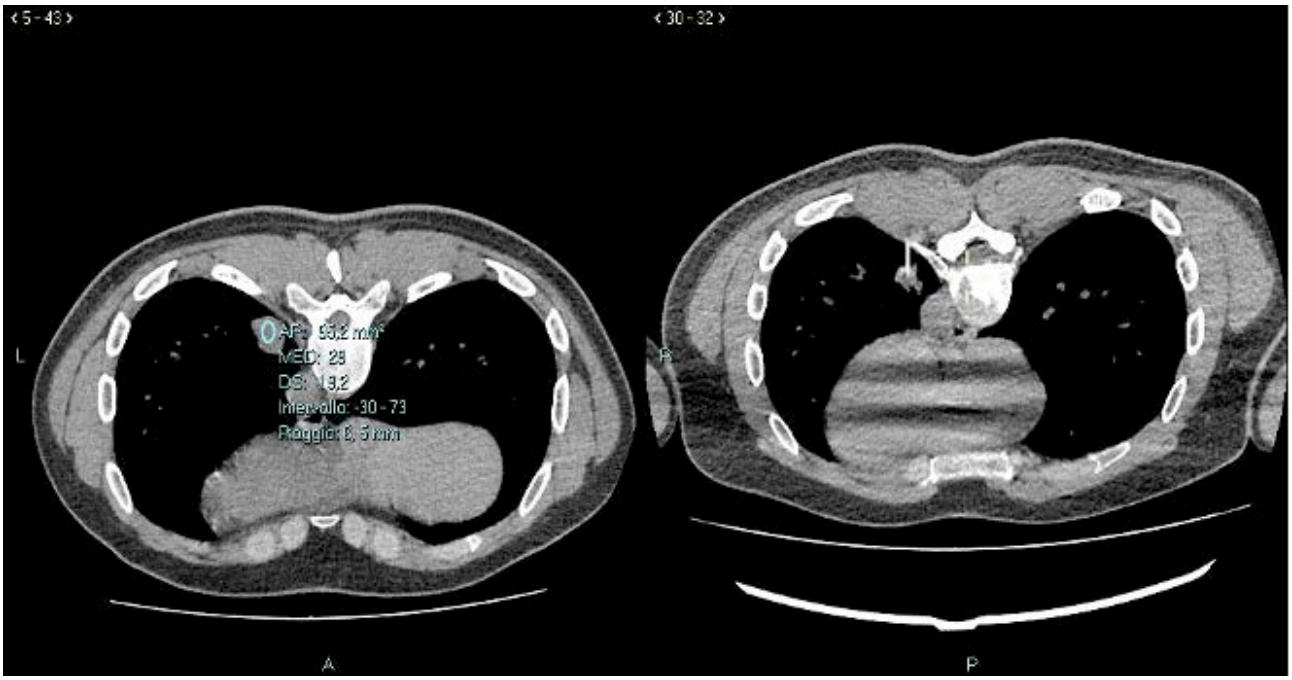

The mass does not show significant post-contrast enhancement. Measurement of the density of a small region of interest in the lesion showed an average density of approximately 29 HU before administration of the iodinated non-ionic contrast medium, which increased to approximately 36 HU in post-contrast acquisitions.
Mass showed a 1.3 SUV at PET scan. Biopsy was performed on the lesion and the histological evaluation showed a very small fragment of superficial of squamous carcinoma within cancer-free lung tissue. Patient underwent inferior left lobectomy and histologic examination revealed the CPAM diagnosis.

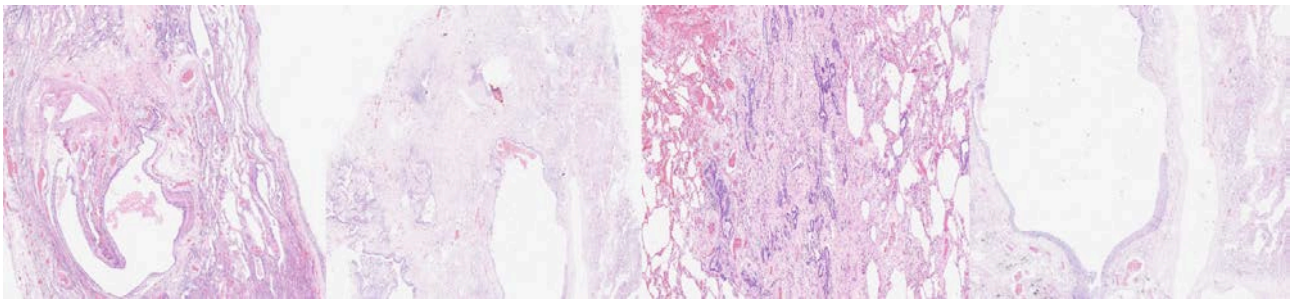

Macroscopically, the lower lobe of the lung showed a 4.2 cm subpleural mass surrounded by sub centimeter cysts. The major mass was cystic with thickened walls and contained necrotic-like material and blood. Most of the cysts were lined by respiratory epithelium with focal atypical squamous metaplasia and an adenomatoid glandular proliferation.

Conclusion

The diagnosis of CPAM can be challenging, and other etiologies such as bronchogenic cysts or pulmonary sequestration should be ruled out before making a definitive diagnosis. The imaging finding of an intraparenchymal lesion with micro or macrocystic component in a young adult especially if associated with history of PNX, recurrent infections and chest pain should lead to suspect a congenital adenomatoid misdiagnosed pathology[4]. The most correct therapeutic option seems to be surgical resection because neoplastic evolution can occur in 1% of cases[5].

References:

[1] Bolde S, Pudale S, Pandit G, Ruikar K, Ingle SB. , (2015), Congenital pulmonary airway malformation: A report of two cases. , World J Clin Cases

[2] Frick AE, Decaluwé H, Weynand B, Proesmans M, Van Raemdonck D., (2021), Invasive mucinous adenocarcinoma of the lung arising in a type 1 congenital pulmonary airway malformation in a 68-year-old patient: a case report., Acta Chir Belg.

[3] Garg S, Singh RS, Singh H, (2018), . Congenital cystic adenomatoid malformation of the lung in adults: report of two cases and review of the literature. , Indian J Thorac Cardiovasc Surg

[4] Leblanc C, Baron M, Desselas E, Phan MH, Rybak A, Thouvenin G, Lauby C, Irtan S. , (2017), Congenital pulmonary airway malformations: state-of-the-art review for pediatrician's use., Eur J Pediatr.

[5] Kantor N, Wayne C, Nasr A. , (2018), Symptom development in originally asymptomatic CPAM diagnosed prenatally: a systematic review, Pediatr Surg Int.

A-496

Congenital Pulmonary Malformations: pictorial review

R. Rodrigues Bexiga, A. Viegas, C. Sousa, J. Leitão
Centro Hospitalar Universitário Lisboa Norte, Serviço de Radiologia Geral, Lisboa, Portugal

Learning Objectives

1. To describe the normal embryologic development of the respiratory system.
2. To discuss postnatal imaging features and pathologic basis of various congenital lung abnormalities.

Background

Congenital pulmonary malformations are a group of rare lung abnormalities affecting the airways, parenchyma, and vasculature. They result from aberrant embryological lung development that occurs at different stages of intrauterine life. Congenital pulmonary malformations are usually diagnosed in the prenatal and neonatal periods, and childhood. However, some remain asymptomatic and may be encountered incidentally in adulthood. Anomalies can be confused with other lung pathologies, even though they may have distinctive radiological findings. Consequently, recognition of the imaging features of these anomalies is essential to generate a differential diagnosis from other pulmonary diseases and management of these diseases. We will briefly discuss the embryologic development of the lungs, review and illustrate imaging findings of various congenital lung abnormalities.

Imaging findings OR Procedure details

Congenital pulmonary malformations in adults can be classified into three broad categories: bronchopulmonary anomalies, vascular anomalies, and combined lung and vascular anomalies. Bronchopulmonary anomalies include lung agenesis/hypoplasia complex, congenital pulmonary airway malformations (CPAMs), bronchial atresia, bronchogenic cysts, and congenital lobar emphysema. Vascular anomalies include absence of the main pulmonary artery, anomalous origin of the left pulmonary artery or pulmonary sling, anomalous pulmonary venous drainage, and pulmonary arteriovenous malformations. Combined lung and vascular anomalies encompass scimitar syndrome and bronchopulmonary sequestration. This pictorial review aims to comprehensively define the radiological characteristics of each congenital lung disease.

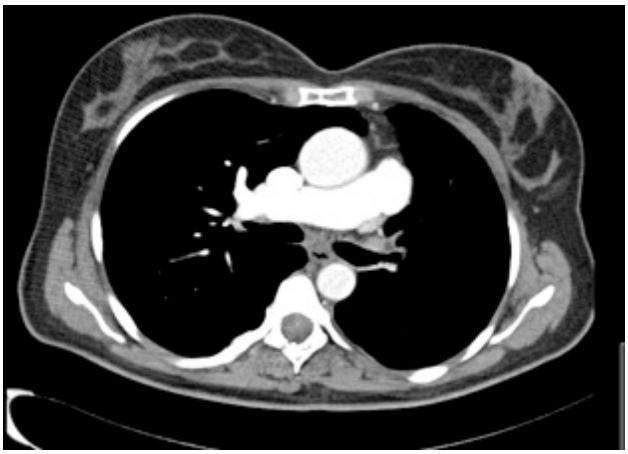

Axial contrast-enhanced CT image of a patient with agenesis of left pulmonary artery

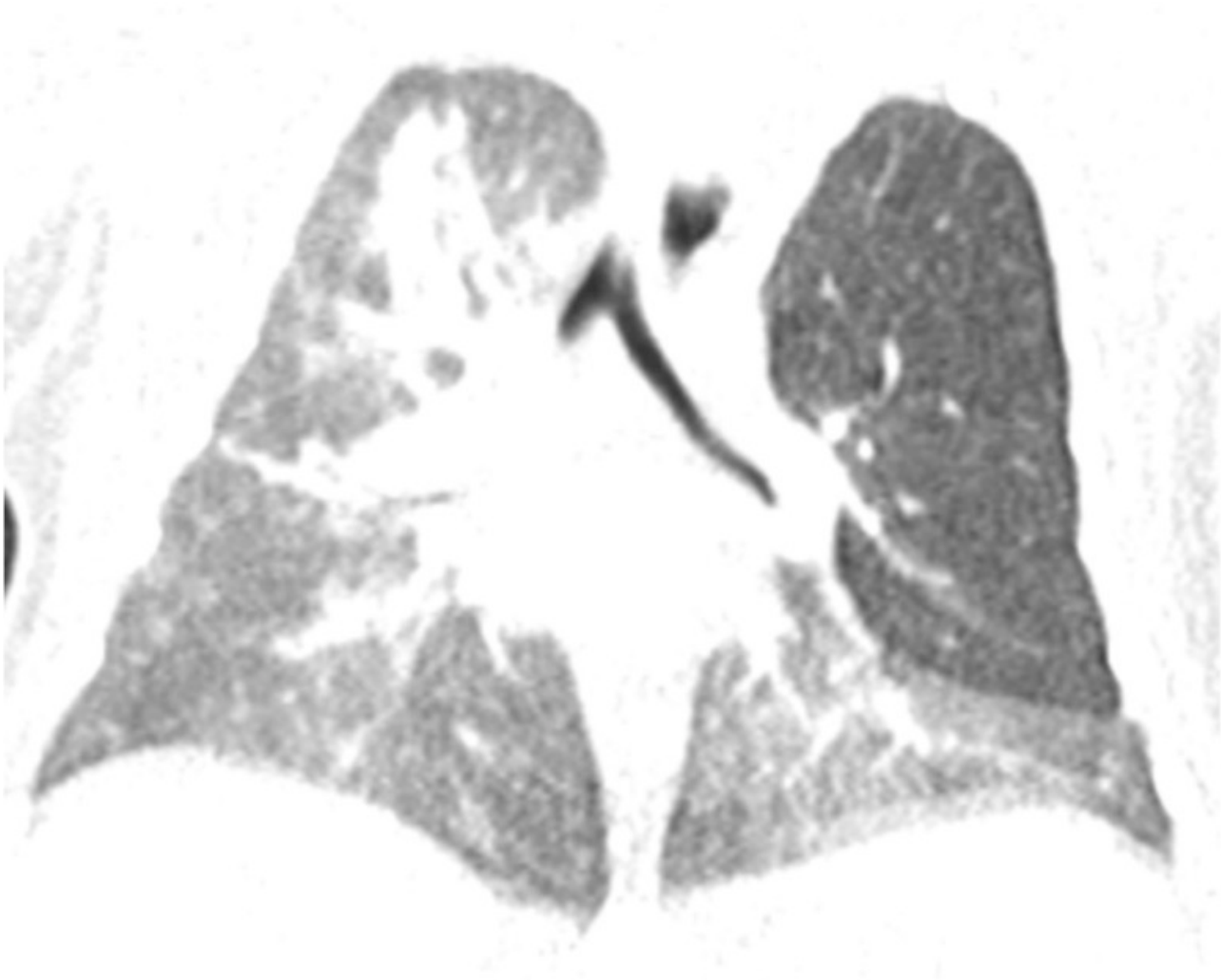

Coronal CT image (lung window) shows of a patient with congenital lobar emphysema.

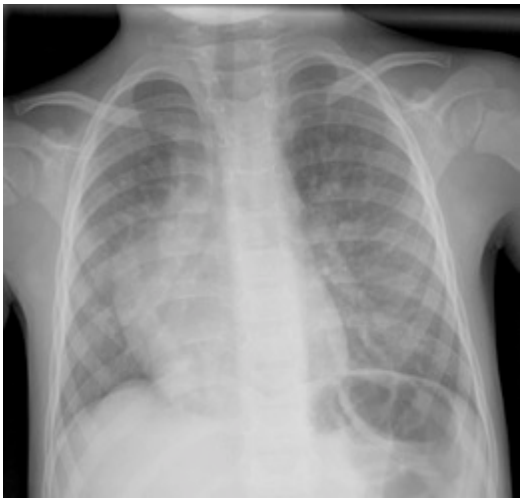

Chest radiograph of an asymptomatic 7 year old boy with Scimitar syndrome shows an hypoplastic right lung with a longitudinal dense shadow in right pulmonary base.

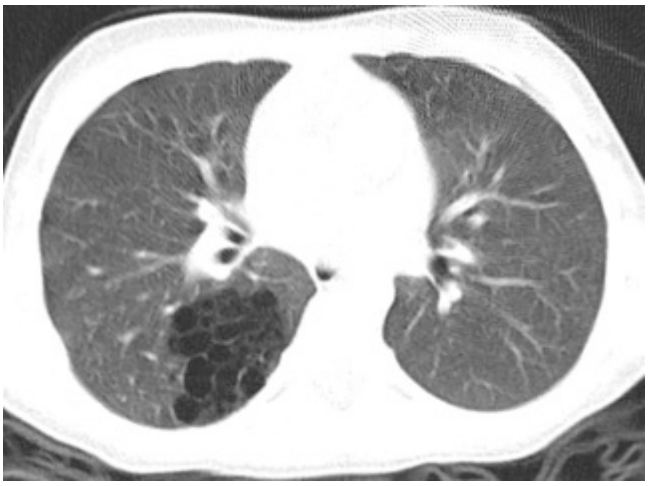

Axial CT image (lung window) of a patient with CPAM type 2, with multiple small cysts

Conclusion

Congenital lung malformations include a heterogeneous group of anomalies involving the lungs. They can be categorized in different groups, namely bronchopulmonary anomalies, vascular anomalies, or combined lung and vascular abnormalities. Even though many of these anomalies are detected at routine prenatal ultrasound, some remain asymptomatic until childhood or later life. Familiarity with imaging findings of different types of congenital lung diseases enables prompt diagnosis, determines management and therapeutic approach.

A-556

CT findings in asthma: what the radiologist should know

A.-L. Brun, R. Quint
Hôpital Foch, Imaging, Suresnes, France

Learning Objectives

- Knowing the radiological features associated with uncomplicated asthma
- Knowing the main complications and differential diagnosis of asthma
- Recognizing the findings that should prompt an associated or alternative diagnosis

Background

Asthma is one of the most common diseases of the lung and is still associated with high morbi-mortality.
High-resolution computed tomography (HRCT) is not recommended in the routine evaluation of patients with a typical history and / or controlled asthma. When referring an asthmatic patient for a CT scan, clinicians are usually concerned about uncontrolled or atypical disease, and radiologists reviewing the imaging of these patients are challenged to search for potential complications and alternative diagnosis.

Imaging findings OR Procedure details

1- CT findings related to asthma:

- Expected findings

HRCT findings of asthma include bronchial wall thickening and air trapping, which are both subjective and nonspecific

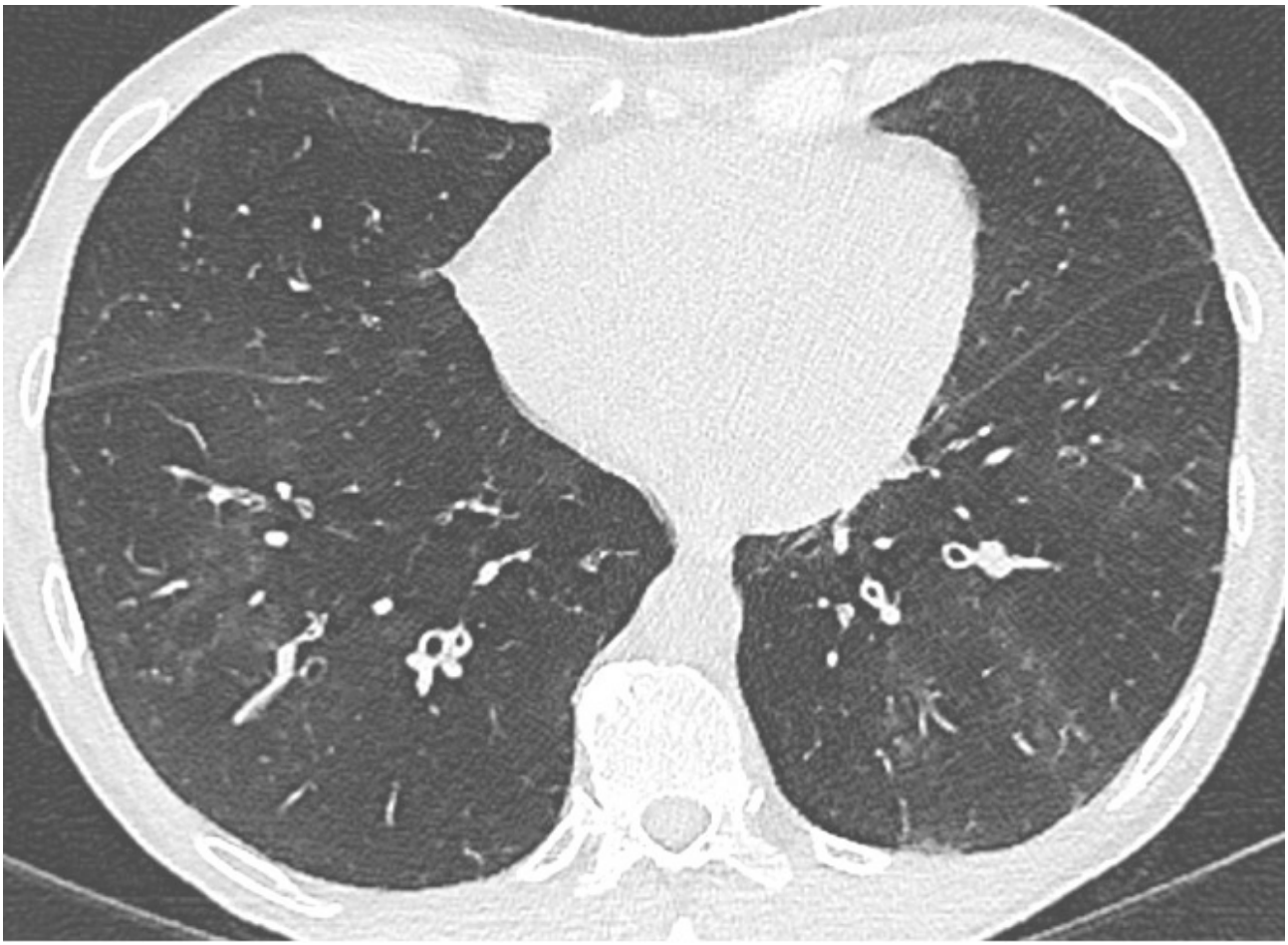

Bronchial wall thickening and mosaicism in patient with sever asthma

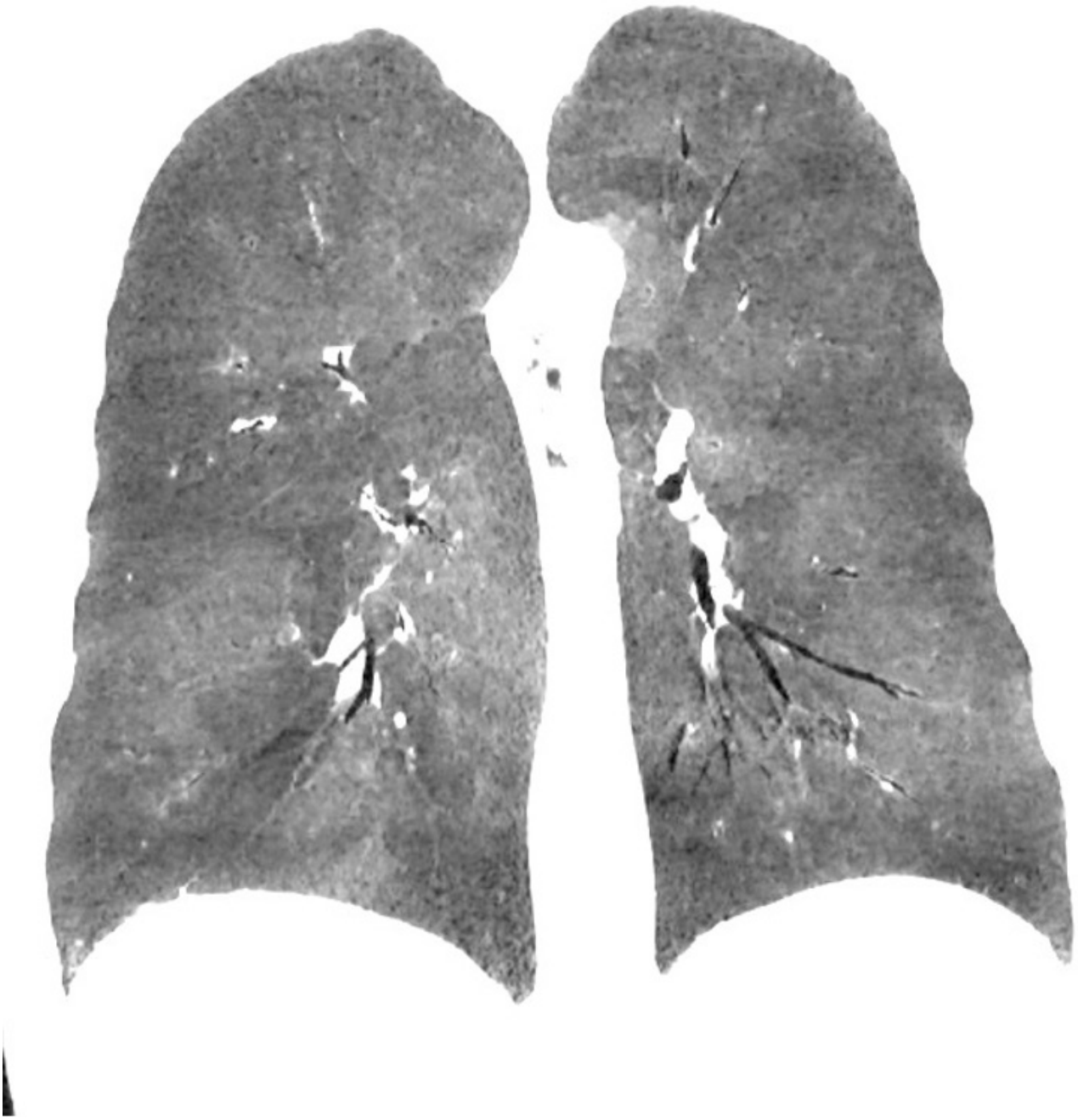

Mosaicim mIP

. Quantitative techniques have been developed to improve objectivity, reproducibility, and efficiency in the evaluation of these abnormalities. Bronchiectasis, if present, should be limited and cylindrical.

- Associated conditions

Features worth mentioning as potential worsening factors include hiatus hernia or findings suggestive of esophagitis, rhinosinusitis, evidence of tobacco exposure (extensive emphysema, saber-sheath trachea…).

- Acute complications: pneumonia, atelectasis, pneumothorax, ...

2- Associated diseases

Conditions frequently developing on an asthmatic background include allergic bronchopulmonary aspergillosis

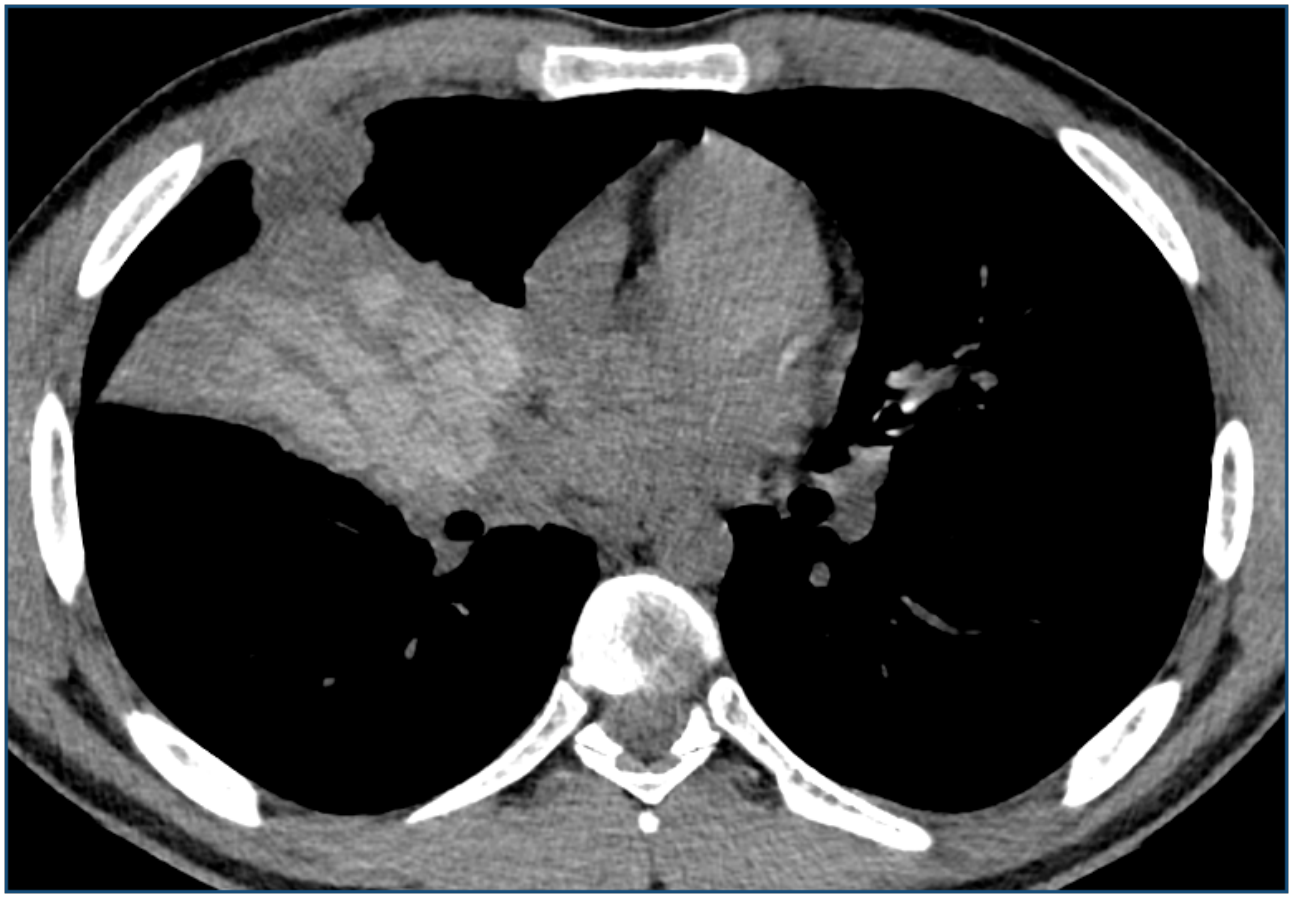

Allergic bronchopulmonary aspergillosis
, eosinophilic pneumonia, and eosinophilic granulomatosis with polyangiitis

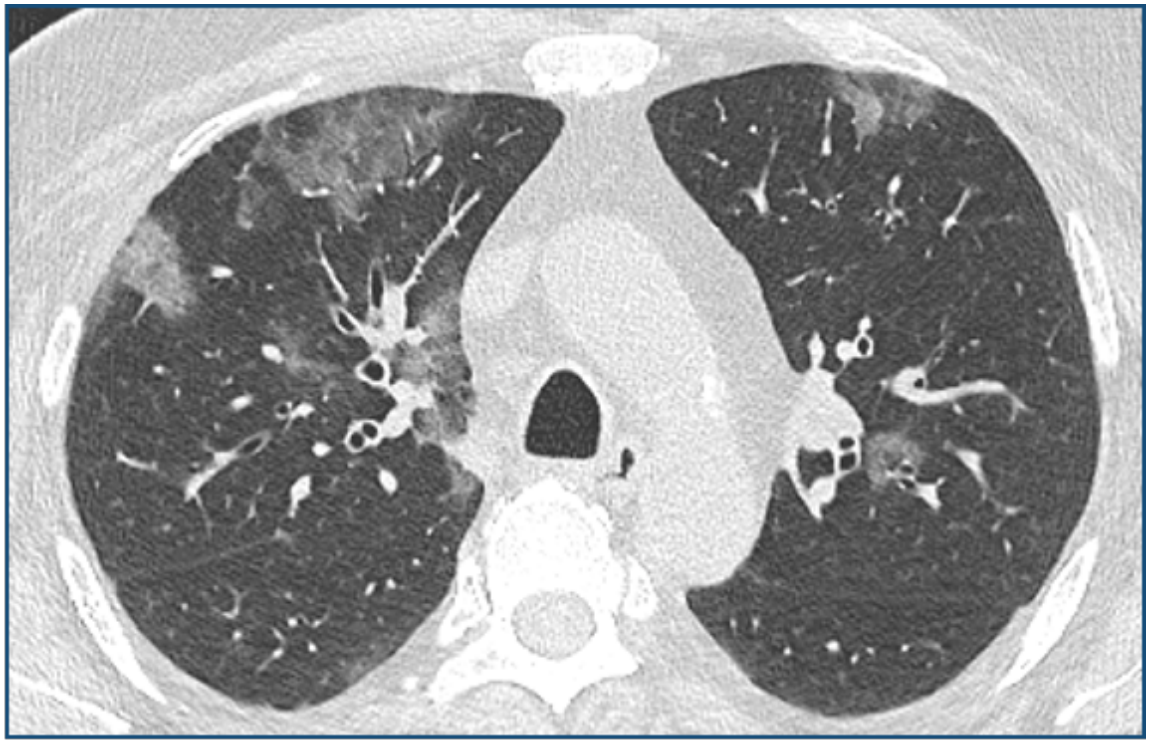

Eosinophilic granulomatosis with polyangiitis
. The presence of severe and extensive bronchiectasis, mucus plugging especially with high attenuation, ground glass opacities and consolidation should alert the radiologist.

3- Differential diagnosis

Misdiagnosis of nonasthmatic conditions as uncontrolled asthma is common. Patients presenting with wheezing and dyspnea can suffer tracheal obstruction, infiltrative diseases involving the proximal airways such as amyloidosis or relapsing polychondritis. The main differential diagnosis of asthma-related air trapping is irreversible obliterative bronchiolitis. Diffuse idiopathic neuroendocrine cell hyperplasia is a rare disease mimicking asthma in middle aged women.

Conclusion

Asthma is a frequent and potentially life-threatening disorder with suggestive but nonspecific imaging features. HRCT is of high value in patients presenting with severe and / or atypical disease, as it may identify complications or suggest an alternative diagnosis. Quantitative CT is a promising tool to monitor patients under treatment and help identify different asthma phenotypes.

A-734

CT patterns in sarcoidosis and their possible implications for biopsy yield

P. Agarwal[1], L. Jouanjan[2], C. Terschluse[2], J. Nattenmüller[1], F. Bamberg[1], C. L. Schlett[1], M. Feineis[2], D. Stolz[2], B. C. Frye[2]
[1]University of Freiburg, Department of Diagnostic and Interventional Radiology, Freiburg im Breisgau, Germany, [2]University of Freiburg, Department of Pneumology, Medical Center-University of Freiburg, Faculty of Medicine, Freiburg im Breisgau, Germany

Purpose/Objectives
Sarcoidosis is a heterogeneous disease, in clinical as in radiological presentation. We aim to give an overview of common and uncommon CT patterns found in sarcoidosis and their possible implications for biopsy yield.
Methods & Materials
We retrospectively analysed patients followed at our institution for sarcoidosis between 2010 and 2022. CT-scans were reviewed and patterns scored by a thoracic radiologist using semi-quantitative scoring system.
Results
324 patients with sarcoidosis were screened, of whom 282 had available CT-scans. Of them 269 of which were of sufficient quality to be further analysed. Scadding stages as per CT were distributed as follows: 8.6% stage 0, 24.2% stage I, 59.7% stage II, 4.8% stage III and, 3.7% stage IV. Lymphadenopathy was found in 85,5%, most frequently in both hilar and mediastinal stations. Lymph node size with short-axis more than 1 cm was associated with endobronchial ultrasound guided transbronchial needle aspiration positivity ($p<0.01$, OR=3.52 (1.31-9.61)). Parenchymal involvement was frequent, the most common finding being nodules (61.0%), mostly in perilymphatic distribution, followed by reticulations (32.4%). A galaxy sign was present in 17.4%, ground-glass opacities in 16.6%, consolidations in 13.3%, fibrosis in 10.4%, mass-like lesions in 7.9%. Emphysema was found in 8.3% and was the sole feature significantly associated with current/ex-smoker vs. never smoker status ($p<0.01$, OR=5.44 (1.65-17.89)). Airway involvement was less common, with wall thickening in 20.3%, external compression in 17.0%, distortion in 12.4% and hyperinflation in 12.9%. The presence of nodules was associated with transbronchial forceps biopsy positivity ($p=0.04$, OR=2.91 (1.00-7.49)). A high nodule profusion (>15 nodules) was associated with cryobiopsy positivity ($p=0.01$, OR=5.33 (1.33-19.0)). Airway wall thickening was associated with endobronchial biopsy positivity ($p=0.01$, OR=10.5 (1.37-119.3)).
Conclusion
Our cohort reflects the vast array of imaging features found in sarcoidosis. The CT morphology can help to guide the selection of ideal biopsy approach. We plan to evaluate a diagnostic algorithm based on these findings.

A-325

Current advances in Imaging of pneumoconiosis

J. S. Park
Soonchunhyang University Hospital, Bucheon, Radiology, Bucheon, Republic of Korea (South Korea)

Learning Objectives

1. Recognize the imaging manifestations of pneumoconiosis, including pathophysiology and CT-pathologic correlation
2. Describe the CT features of early (p-type) pneumoconiosis
3. Discuss the imaging features of progressive massive fibrosis (PMF) and the differential diagnosis from lung cancer

Background

The opacities caused by dust inhalation are divided according to their shape (round or irregular). According to size, the round opacities are classified as p, q, or r, and the irregular opacities as s, t or u (p and s, up to 1.5 mm in diameter; q and t, 1.5 ~ 3 mm; r and u, 3 ~ 10 mm).

On the basis of CT-pathologic correlation, these centrilobular opacities or small branching structures correspond to irregular fibrosis around and along the respiratory bronchiole.

The large opacity of PMF is defined as an opacity having the longest dimension exceeding 10 mm.

MR is potentially a useful tool in distinguishing lung cancer from PMFs in patients with coal worker's pneumoconiosis.

Imaging findings OR Procedure details

1. The common CT findings of p-type pneumoconiotic nodules were ill-defined micronodules and bi-branching structures. And other frequent finding were bronchiectasis and well-defined micronodules. However, centrilobular emphysema, tree-in-bud appearance, and GGA were uncommon.
2. On T1WI of MR, there was no significant signal intensity difference between lung cancer and PMF. On T2WI, all lung cancer showed high signal intensity, as opposed to all PMFs which showed low signal intensity except for one PMF. For the dynamic contrast study, lung cancer showed faster and slightly stronger enhancement than PMFs. For a delayed image, most of the lung cancers showed washout, as opposed to a plateau in most of PMF.

Conclusion

1. The most common CT findings of pneumoconiosis with p-type pneumoconiotic nodules were diffusely distributed, ill-defined and well-defined micronodules, bi-branching structures and bronchiectasis.
2. MR is potentially a useful tool in distinguishing lung cancer from PMFs in patients with silicosis and coal worker's pneumoconiosis.

A-231

Diagnosing processes involving the extrapleural space: usefulness of the extrapleural fat sign

M. Andreu Magarolas, C. Lozano Roca, M. Cufí Quintana, X. Gallardo Cistaré, T. Movsisyan, E. Castañer González
Hospital Universitari Parc Taulí, Thoracic Radiology, Sabadell. Barcelona, Spain

Learning Objectives

To identify the normal anatomy of the extrapleural space (EPS).

To describe the extrapleural fat sign (internal displacement of the adipose tissue layer), a key finding for locating different conditions in the EPS.[1]

To recognize the various conditions that may affect the EPS, emphasizing the role of CT.[2]

Background

The EPS lies between the parietal pleura and the chest wall and diaphragm. It is a poorly understood anatomical compartment which can lead to diagnostic errors.

Imaging findings OR Procedure details

A. Anatomic review

The EPS is located in the chest wall periphery (between parietal pleura, diaphragm and inner surface of the ribs). It is composed of three layers: extrapleural fat, endothoracic fascia, and the innermost intercostal muscle. However, these layers are not distinguishable in CT.

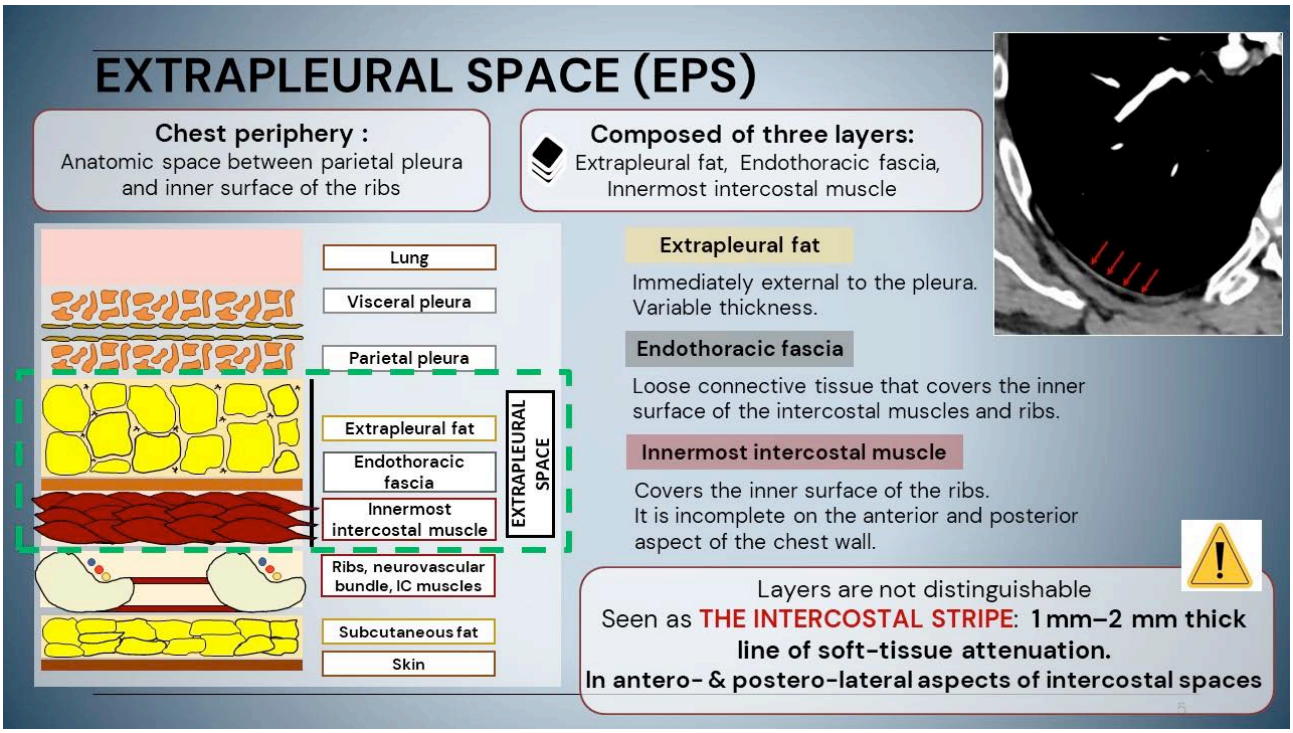

B. Extrapleural fat can be displaced, enlarged, or affected by [3]:

Blood (extrapleural hematoma): from trauma, iatrogenic lesion of a thoracic vessel, aortic dissection or aneurysm rupture, spontaneous bleeding.

Extrapleural hematoma. Blunt trauma

Frequently misdiagnosed as hemothorax, it is an accumulation of blood between the parietal pleura and the endothoracic fascia. It can occur as a result of chest trauma, aortic rupture, or placement of medical devices.
Clues to locating the lesion are convex morphology of the blood collection and fat stripe displacement.

Fig. 1. A 75-year-old man with chest pain, dyspnea, and a recent history of chest trauma

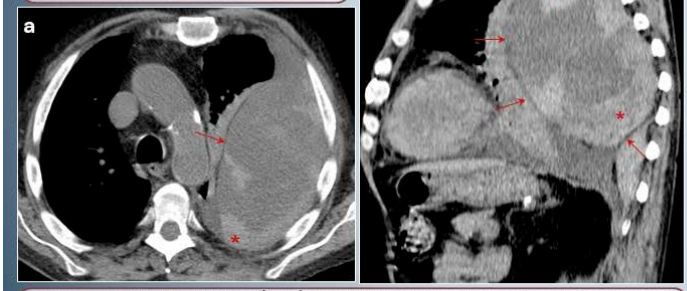

Non-contrast CT images (a, b) show a voluminous and heterogeneous collection in the left hemithorax, with areas of greater density inside (recent bleeding *). Note the displaced extrapleural fat stripe (→).

Management of EH depends on it size and cause.
Thoracotomy should be performed for large collections.
Placement of a drainage tube is not indicated.

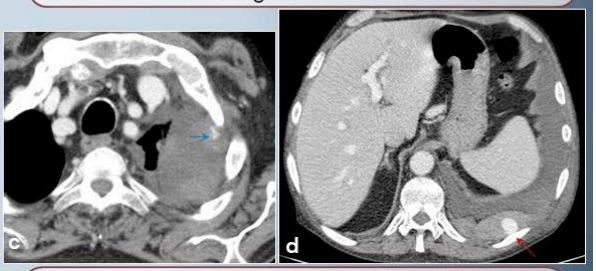

Arterial-phase contrast CT images show focal extravasation of contrast (→) in the upper part of the collection (c). A highly enhanced nodular image (→) is also seen anterior to the posterior arch of the 10th rib, due to an intercostal artery pseudoaneurysm (d).

Air (extrapleural emphysema): barotrauma.

Extrapleural emphysema. Barotrauma

Air within the EPS caused by the extrapleural extension of pneumomediastinum is mainly associated with barotrauma.
An increase in intraalveolar pressure may lead to alveolar rupture, resulting in air escaping along the peribronchovascular sheaths toward the lung hilum and mediastinum (Macklin effect). This sign is known as pulmonary interstitial emphysema (PIE).
Air collections in the EPS can mimic pneumothorax.
Looking for web-like linear opacities within the air collection is the key to the diagnosis.

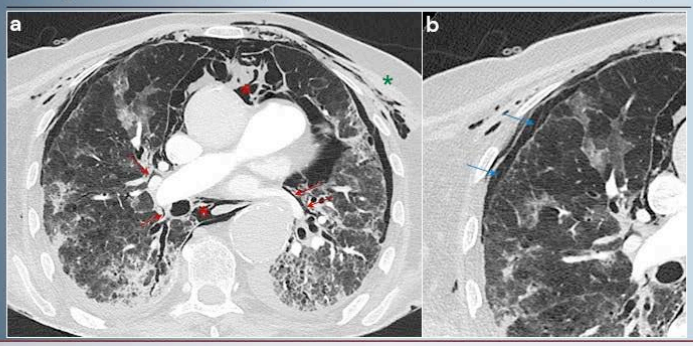

Fig. 3. Pulmonary barotrauma in an 83-year-old man with underlying interstitial disease and acute respiratory distress syndrome associated with COVID-19. a) Axial CT images show air (→) surrounding the lung interstitium, corresponding to PIE, and pneumomediastinum (*). b) Web-like linear septa are present in the extrapleural air collection (→). Subcutaneous emphysema is also present (*).

Differential diagnosis: Pneumothorax

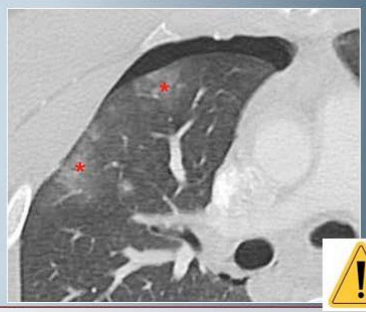

Fig.4. Pulmonary pneumothorax (*note the lack of linear opacities inside the air collection*) in a young patient with blunt chest trauma and lung contusions (*).

Fat: non-pathologic (obesity or estrogens), lipoma, chronic pleural conditions.
Edema/infection: acute pleural exudates, empyema necessitatis.

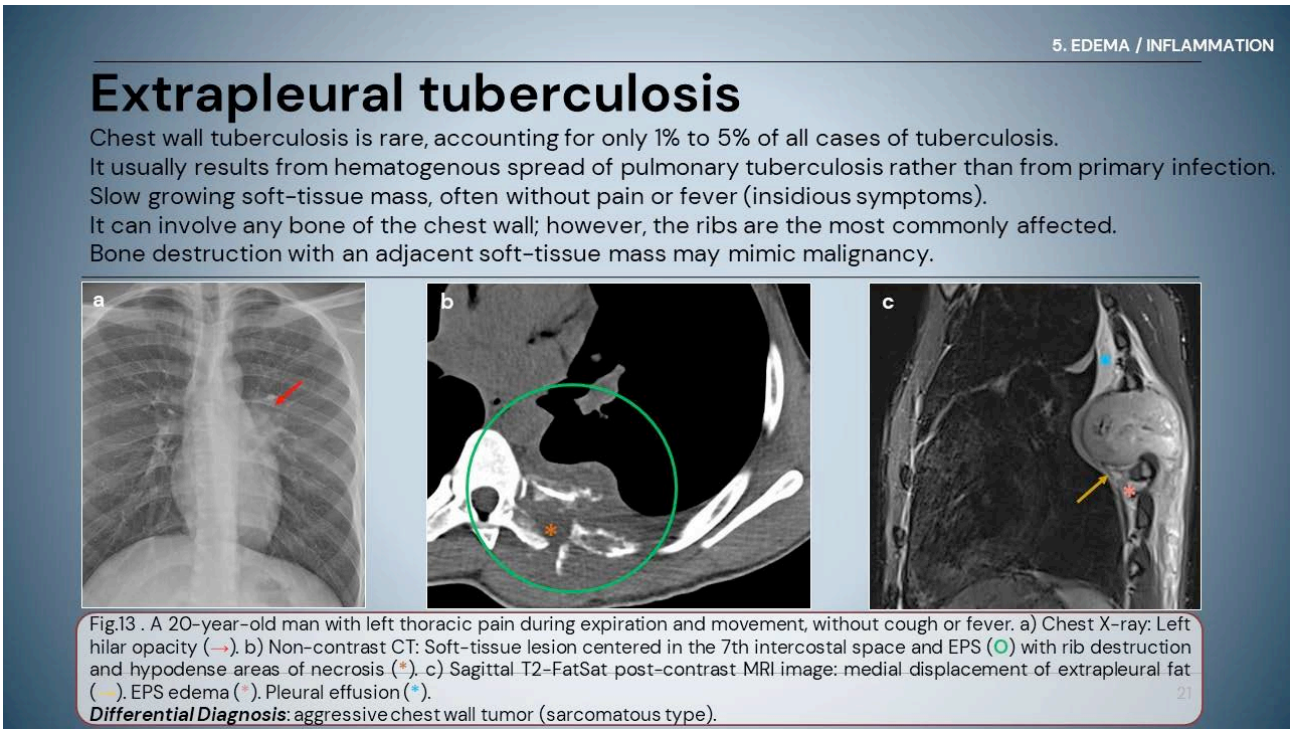

Soft tissue: extramedullary hematopoiesis, neurogenic lesions, primary or metastatic pleural tumors, infiltration of lung tumor, chest-wall malignancies.

Calcium: chronic hematoma/empyema, asbestos-related pleural disease.

Conclusion

The extrapleural fat sign is useful in distinguishing between pleural and extrapleural lesions.

Conditions involving the EPS may require different treatment approaches than pleural or lung diseases.

References:

[1] Dharshan R. Vummidi, Jonathan H. Chung, Eric Stern., (2012), Extrapleural Fat Sign, J Thorac Imaging. , 5

[2] Ravishankar Pillenahalli Maheshwarappa , Maharshi Rajdev , Prashant Nagpal , Ali Gholamrezanezhad , Neetu Soni , Amit Gupta, (2021), Multimodality imaging of the extrapleural space lesions., Clinical imaging, 64-68, 79

[3] Mario G Santamarina, Ignacio Beddings, Guillermo V. Lermanda Holmgren, Hector Opazo Sanchez, (2017), Multidetector CT for Evaluation of the Extrapleural Space., Radiographics, 1352-1370, 37

A-462

Diagnosis in the making: Excessive dynamic airway collapse

G. Jurkeviciute Kucinskiene, S. Giedrys
Lithuanian University of Health Sciences, Radiology Department, Kaunas, Lithuania

Learning Objectives

To review the clinical manifestations of EDAC.
To review the appearances of EDAC on radiological exams.

Background

Excessive dynamic airway collapse (EDAC) is a respiratory disorder that is characterized by recurrent collapse of the airway during inspiration, resulting in breathing difficulty and wheezing. EDAC and tracheobronchomalacia (TBM) are underdiagnosed distinct clinical entities that require more attention to enable prompt diagnosis and guide proper management

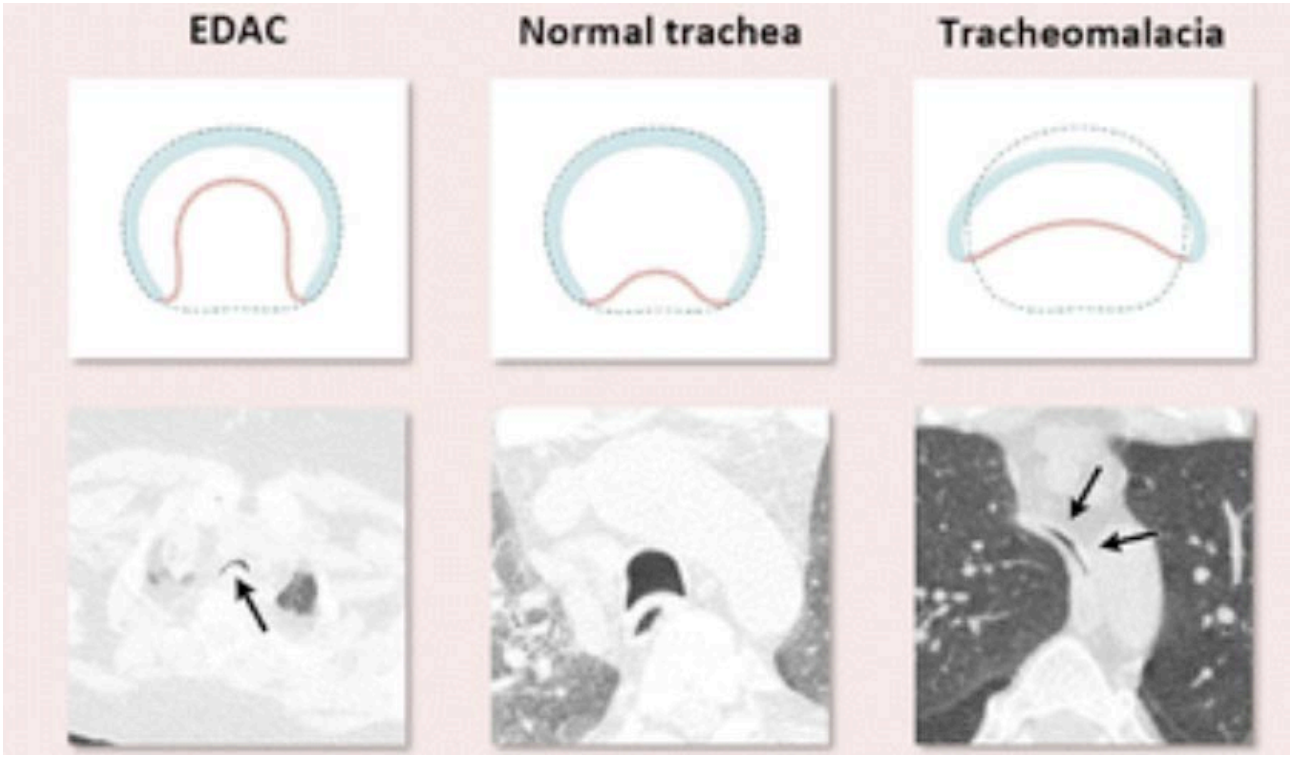

Visual comparison of tracheobronchomalacia, EDAC and normal trachea appearances on CT.
. TBM and EDAC are airway abnormalities that share a common feature of expiratory narrowing but are distinct

Imaging findings OR Procedure details

Diagnosis of EDAC begins with a detailed history and physical examination. Symptoms, such as wheezing, shortness of breath, cough, are important in determining the presence of airway collapse. Physical examination may reveal signs of airflow obstruction, such as hyperinflation and decreased breath sounds. Furthermore, spirometry can reveal decreased lung function and airflow obstruction. Bronchoscopy can aid in diagnosing airway changes. One of the key diagnostic tools for EDAC is computed tomography CT of the chest. EDAC is typically characterized by exaggerated bulging of the posterior wall within the airway lumen during exhalation with an excessive flattening in AP diameter

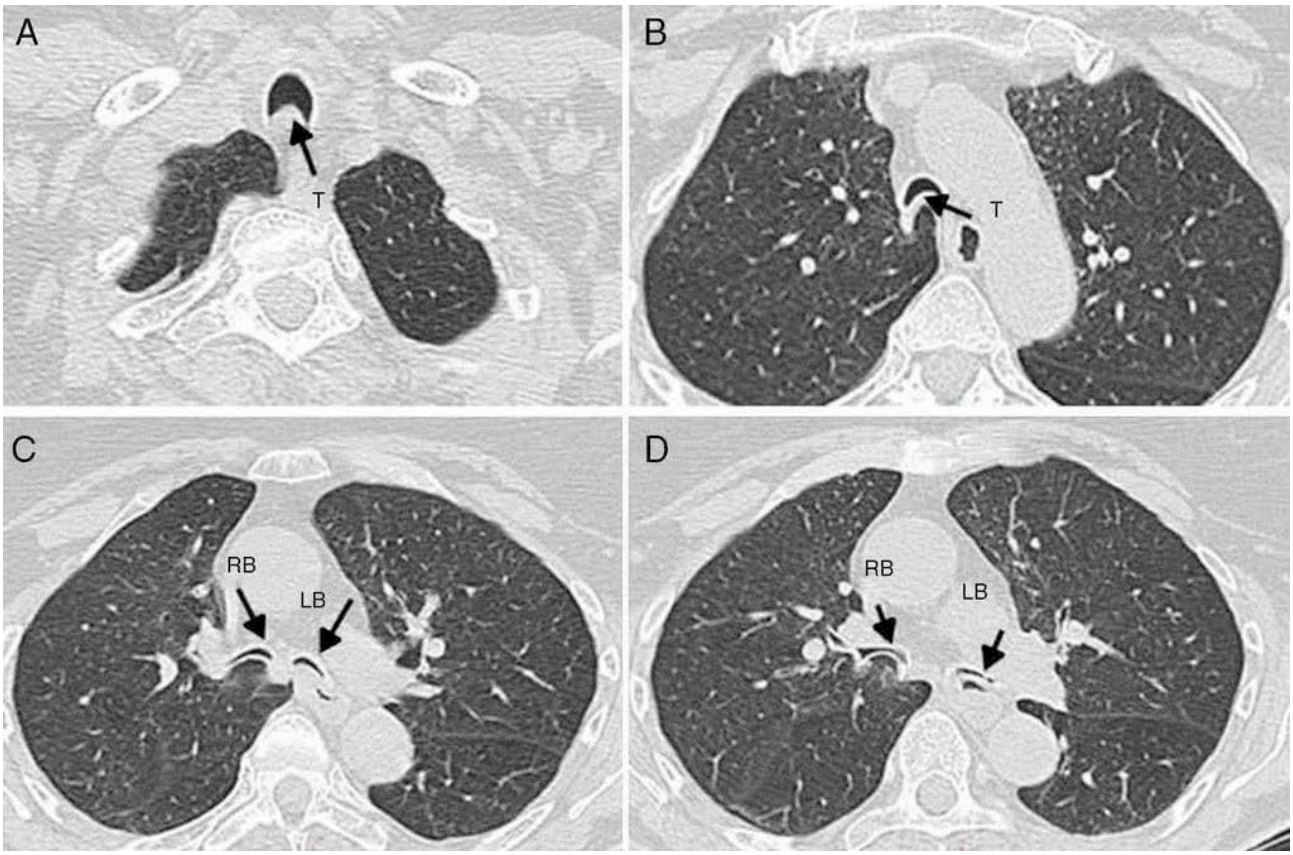

Chest CT scans of the studied patient show invagination of the posterior wall membrane of trachea (T) (A, B) and of the main bronchi (Panels C, D) with narrowing of airways lumen.

. The tracheobronchial lumen should decrease in size more than 50% (recent publications suggest >70%). MRI is an alternative tool, although it is not as widely available and is not currently used as frequently for this indication. Advanced techniques can be implemented in diagnosis and treatment, e.g. trachea volumetric rendering and personalized 3D printed stents. These tools can provide a roadmap to clinicians and surgeons for planning treatment.

Conclusion

EDAC is an underdiagnosed clinical entity that requires more attention. Chest CT is an excellent tool for the diagnosis of EDAC and has distinct radiological signs.

A-351

Diagnosis of Hypersensitivity Pneumonitis in Adults: a Case-based Approach to the 2020 ATS/JRS/ALAT Guidelines.

I. Pulzato, M. Gutierrez, M. Radike
Liverpool Heart and Chest Hospital, Radiology, Liverpool, United Kingdom

Learning Objectives
To define the principal imaging features of hypersensitivity pneumonitis (HP) by computerized tomography.
To present a case-based, illustrative approach to establish a diagnosis on high-resolution CT (HRCT) according to the current guidelines.
Background
HP is typically an immune-mediated disease that manifests as ILD in susceptible individuals after environmrntal exposure.
In 2020 the ATS/JRS/ALAT guidelines classified the disease as fibrotic hypersensitivity pneumonitis (FHP) and non-fibrotic hypersensitivity pneumonitis (NFHP) by the predominant presence or absence of radiological and/or histopathological fibrosis.
In daily practice, HP represents a challenging diagnosis because the clinical manifestations are broad and the radiologic and histologic patterns can mimic those of other diseases. Therfore, HRCT may have a key role in the diagnosis and classification of the diseased.
Imaging findings OR Procedure details
HRCT detects and evaluates lung abnormalities through suggesting patterns and distinguishing fibrosis.
Typical HP, Compatible with HP, and Indeterminate for HP are the classification schemes provided by the ATS/JRS/ALAT guidelines for HRCT patterns related with NFHP and FHP.

The usual HRCT presentations of non-fibrotic HP are *ill-defined ground-glass nodules* that are distributed throughout all lung zones in keeping with bronchiolocentric inflammation. This may cause airway constriction, resulting in lobular *air-trapping.*
Ground-glass opacities (GGO) and increased lung density are due to extensive interstitial inflammation with a patchy distribution which is referred to as mosaic attenuation.
The presence of patchy GGO and/or increase lung density areas, air trapping and normal lung was referred as “headcheese sign” renamed by the ATS/JRS/ALAT guidelines *“three-density pattern”.*

The current guidelines classify the disease as:
- *Typical NFHP pr*esents with infiltrative parenchymal abnormalities with GGO or mosaic attenuation and at least one abnormality suggesting small airway disease.
- *Compatible with NFHP* is reserved for uniform or subtle GGO, airspace consolidation or cysts
- *Typical FHP* presents with bronchiolar obstruction with lung fibrosis in the mid/lower lung zone or it is evenly distributed with basilar sparing and no central or peripheral predominance.
- *Compatible with FHP* shows fibrosis with UIP pattern or extensive GGO with superimposed fibrosis (on axial peri-broncho-vascula, or subpleural) and upper lobe predominance. Small airway disease may also be present.
- *Indeterminate for FHP* when non of the FHP categories is compatible.
Conclusion
According to the new ATS/JRS/ALAT guidelines confident diagnosis of FHP or NFHP on high-resolution CT is based on the presence of small airways disease and interstitial inflammation in the appropriate contest.
References:

[01] Ganesh Raghu, Martine Remy-Jardin, Christopher J. Ryerson, Jeffrey L. Myers, Michael Kreuter, Martina Vasakova, Elena Bargagli, Jonathan H. Chung, Bridget F. Collins, Elisabeth Bendstrup, Hassan A. Chami, Abigail T. Chua, Tamera J. Corte, Jean-Charles Dalphin†, Sonye K. Danoff, Javier Diaz-Mendoza, Abhijit Duggal, Ryoko Egashira, Thomas Ewing, Mridu Gulati, Yoshikazu Inoue, Alex R. Jenkins, Kerri A. Johannson, Takeshi Johkoh, Maximiliano Tamae-Kakazu, Masanori Kitaichi, Shandra L. Knight, Dirk , (2020), Diagnosis of Hypersensitivity Pneumonitis in Adults An Official ATS/JRS/ALAT Clinical Practice Guideline, Am J Respir Crit Care Med, 36 - 69, Volume 202 Issue 3, DOI: 10.1164/rccm.202005-2032ST
[02] Irich Costabel, Yasunari Miyazaki, Annie Pardo, Dirk Koschel, Francesco Bonella, Paolo Spagnolo, Josune Guzman, Christopher J. Ryerson, and Moises Selman, (2020), Hypersensitivity pneumonitis, Springer Nature Limited 2020, NATURE REVIEWS DISEASE PRIMERS , 6:65, https://doi.org/10.1038/ s41572-020-0191- z
[03] C. Isabela S. Silva, Andrew Churg, Nestor L. Müller, Silva CIS, Churg A, Müller NL, (2005), Hypersensitivity Pneumonitis: Spectrum of High-Resolution CTand Pathologic Findings, AJR 2007; 188:334–344, DOI:10.2214/AJR.05.1826
[04] Dabiri M, Jehangir, M, Khoshpouri P, Chalian H., (2022), Hypersensitivity Pneumonitis: A Pictorial Review Based on the New ATS/JRS/ALAT Clinical Practice Guideline for Radiologists and Pulmonologists, Diagnostics MDPI , 12, 2874, https://doi.org/10.3390/ diagnostics12112874
[05] Andrew Churg, (2022), Hypersensitivity pneumonitis: new concepts and classifications, Springer Nature, Modern Pathology , 15–27, 35, https://doi.org/10.1038/s41379-021-00866-y

A-672

Differential diagnosis in cystic lung lesions on HRCT

M. Mastandrea, G. Mancò, M. Servietti, M. Scutti, M. Mereu, R. L. Patea, M. Caulo
Santissima Annunziata Hospital, Chieti, Italy

Learning Objectives
To recognize the main HRCT findings of cystic lung disease (CLD) and cystic lung cancer.
Background

CLD is a group of lung disorders characterized by multiple cysts, defined as air-filled lucencies or low-attenuating areas, bordered by a thin wall (usually < 2 mm). Among these we have to take in consideration cystic lung cancer, defined as a single or multiple “cyst-like” lesions, with areas of ground glass or consolidation abutting the wall of the cystic lesion or spreading between the cystic components. The purpose of this paper is to underline HRCT findings of CLD and cystic lung cancer.

Imaging findings OR Procedure details

We described the most common HRCT findings in cystic lung disease, such as lymphangioleiomyomatosis (LAM), pulmonary Langerhans cell histiocytosis (PLCH), lymphocytic interstitial pneumonia (LIP) and the most common appearance of cystic lung cancer . HRCT findings in LAM area characterized by round and small thin-walled cysts (typically more than 10), usually 2 to 5 mm in diameter but as large as 30 mm, without zonal predominance. Small centrilobular nodules in the upper lobe are seen in patients with tuberous sclerosis complex.

The most common HRCT findings in PLCH are bizarre cysts and nodules, predominantly in the upper and middle lobes, with almost complete sparing of the costophrenic angles. As the disease progresses, nodules gradually lead to cavitation and then become thick/thin-walled cysts.

The main HRCT findings in LIP are randomly distributed cysts, which measure < 30 mm in diameter, and are typically fewer than in LAM. They frequently coexist with GGOs, centrilobular nodules, or septal thickening.

In cystic lung cancer the main HRCT findings are non-uniform cyst walls, septation(s) within the cyst, wall nodule(s), GGO around the cyst, irregular margins, gradual expansion of the cystic airspaces. This appearance is distinct from that of benign cystic disease, which typically have thin symmetrical walls without nodularity.

While the cysts in LAM and LIP show a diffuse or random distribution, those in PLCH typically have an upper/middle zone predominance. The thickness of the cyst wall is another diagnostically useful feature. Furthermore, protruding or solid internal structures in the pulmonary cyst are suggestive of LIP or cystic lung cancer.

Conclusion

This new type of neoplastic lesion is often missed or misinterpreted because of its imaging appearance overlapping with benign entities especially at initial stage. Radiologists should recognize the main CT features of cystic lung disease to avoid a late diagnosis. The right clinical scenario, as well as biopsy, can help to diagnose it correctly.

References:

[1] Sheard S, Moser J, Sayer C, Stefanidis K, Devaraj A, Vlahos I, (2018), Lung Cancers Associated with Cystic Airspaces: Underrecognized Features of Early Disease

[2] Park S, Lee EJ. , (2017), Diagnosis and treatment of cystic lung disease

[3] Y. Tan et al., (2019), CT Characteristics and Pathologic Basis of Solitary Cystic Lung Cancer

A-704

Diffuse pulmonary meningotheliomatosis: a case report and a literature review

C. F. Munoz-Nunez[1], N. Mancheño-Franch[2], E. Baettig-Arriagada[1], P. Calvillo-Batlles[1], C. Fonfría-Esparcia[1]
[1]Hospital Universitario y Politécnico La Fe, Department of Radiology, Valencia, Spain, [2]Hospital Universitario y Politécnico La Fe, Department of Pathology, Valencia, Spain

Learning Objectives

1. To present a case of Diffuse Pulmonary Meningotheliomatosis (DPM) detected by CT.
2. To review clinical, radiological and pathological findings of DPM.

Background

DPM is a diffuse lung disease characterized by multiple bilateral disseminated minute pulmonary meningothelial-like nodules. First described by Korn et al (1960) as “pulmonary nodules resembling chemodectomas” their meningothelial origin was discovered by Gaffey et al (1988) who coined the term "minute pulmonary meningothelial nodules". The exact etiology of DPM remains elusive today and why some individuals present the disease is unknown. DPM is usually asymptomatic (72%) and an incidental finding on CT done for a different purpose, probably representing a reactive process. DPM has predilection for females (92%) in their 50-60s. DPM is a not uncommon coincidental finding on surgical biopsies and are seldom reported in the radiological literature.

Imaging findings OR Procedure details

On CT DPM appears as ground-glass small nodules or micronodules. The ground-glass nodules may show central lucency representing alveolar spaces enlargement. CT findings are nonspecific and differential diagnoses include metastasis, miliary tuberculosis and atypical adenomatous hyperplasia.

We present a 57-years-old female patient complaining of recurrent respiratory infections, chronic productive cough and a previous history of fibrolamellar hepatocarcinoma resected several years ago. Her chest CT showed multiple minute ground-glass nodules with basal predominance. A final pathological diagnosis of DPM was reached after transbronchial-pulmonary-cryobiopsy.

Conclusion

- DPM is a rare disease seldom reported in the radiological literature.
- Radiologist should know this entity and consider the diagnosis in case of typical CT features in proper clinical scenario in females in their 50-60s.

References:

[1] Asakawa A, Horio H, Hishima T, Yamamichi T, Okui M, Harada M. , (2017), Clinicopathologic features of minute pulmonary meningothelial-like nodules, Asian Cardiovascular & Thoracic Annals, 509-12, 7-8, https://doi.org/10.1177/0218492317731390
[2] Gleason J, Valentin R, Almeida P, Martinez N, Bejarano P, (2017), Diffuse pulmonary meningotheliomatosis: A literature review of a rare diffuse parenchymal lung disease with unclear clinical significance, The Journal of Association of Chest Physicians, 18-25, https://www.jacpjournal.org/text.asp?2017/5/1/18/196647
[3] Harada M, Aono Y, Yasui H, Uto T, Sato J, Imokawa S, et al., (2019), 1. Harada M, Aono Y, Yasui H, Uto T, Sato J, Imokawa S, et al. Minute Pulmonary Meningothelial-like Nodules Showing Multiple Ring-shaped Opacities, Internal Medicine , Tokyo, 3149-3152, https://www.jstage.jst.go.jp/article/internalmedicine/58/21/58_2108-18/_article
[4] Mizutani E, Tsuta K, Maeshima AM, Asamura H, Matsuno Y, (2009), Minute pulmonary meningothelial-like nodules: clinicopathologic analysis of 121 patients, Human Pathology, 678-682, https://doi.org/10.1016/j.humpath.2008.08.018
[5] Suster S, Moran CA, (2007), Diffuse pulmonary meningotheliomatosis, The American Journal of Surgical Pathology, 624-631, https://doi.org/10.1097/01.pas.0000213385.25042.cf
[6] Wang Y xia, Lei Z, Yang M, Wang Z yuan, Zhang X, Pan G qing. Case Report: Clinicopathological Analysis of Minute Pulmonary Meningothelial-Like Nodules: Report of 7 Cases. Front Oncol [Internet]. 19 de julio de 2022 [citado 15 de abril de 2023];12:942517. , (2022), Case Report: Clinicopathological Analysis of Minute Pulmonary Meningothelial-Like Nodules: Report of 7 Cases, Frontiers in Oncology, 942517, https://www.ncbi.nlm.nih.gov/pmc/articles/PMC9345627/

A-643

Dual energy CT Pulmonary angiography; Principles, indications and applications in our practice.

L. Cosbey, K. S. Babar, S. Raza
Royal Stoke University Hospital NHS Trust, Radiology Department, Stoke-on-Trent, United Kingdom

Learning Objectives

To explain the physics of Dual Energy Computed Tomography (DECT).
To discuss the clinical applications of Dual Energy Computed Tomography Pulmonary Angiography (DE-CTPA), including its role in the investigation of persistent symptoms following COVID-19.

Background

DECT is based on simultaneous acquisition at low and high kVp allowing detection of differences in X-ray attenuation at different photon energies, thereby enabling characterisation of the constituents of each voxel [1]. In the case of dual energy CT pulmonary angiography, pulmonary blood volume images representing iodine concentration allow for visualisation of perfusion defects. The morphology of these perfusion defects differ from case to case and can be categorised as wedge-shaped (as seen in patients with acute pulmonary embolism), mottled (typical of chronic thromboembolic pulmonary hypertension) or amorphous [2].

Imaging findings OR Procedure details

In this educational poster, we review cases where DE-CTPA has been of clinical value, including in the diagnosis and quantification of microembolic disease, more than what would have been obtained through conventional CTPA imaging. Most topically, DE-CTPA plays an integral role in the investigation of patients with persistent symptoms following COVID who are observed to have normal lung parenchyma without macroscopic pulmonary embolism on conventional imaging. Included in our case review is a case of a 37 year-old male who continued to complain of shortness of breath at his 3 month post COVID follow up. His initial DE-CTPA during COVID infection showed patchy consolidation, bilateral subsegmental PE and corresponding iodine map perfusion defects

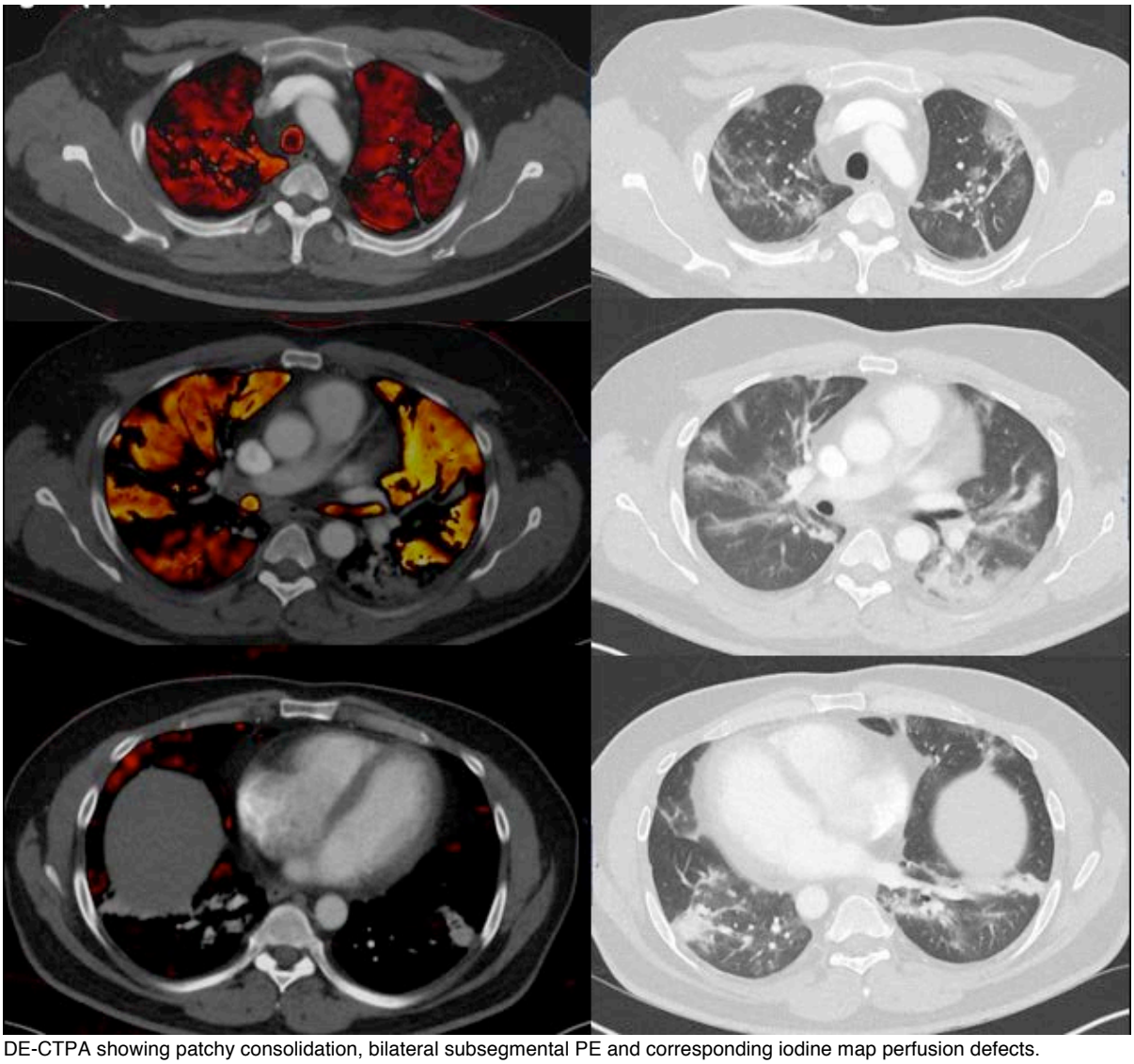

DE-CTPA showing patchy consolidation, bilateral subsegmental PE and corresponding iodine map perfusion defects.
. He was managed for COVID pneumonia requiring non-invasive ventilation and eventually discharged to complete 6 months of anticoagulation. Repeat DE-CTPA 3 months following COVID showed normal lungs with no pulmonary embolism or post-COVID fibrosis although confirmed multiple subpleural defects on perfusion imaging compatible with post-COVID microangiopathy

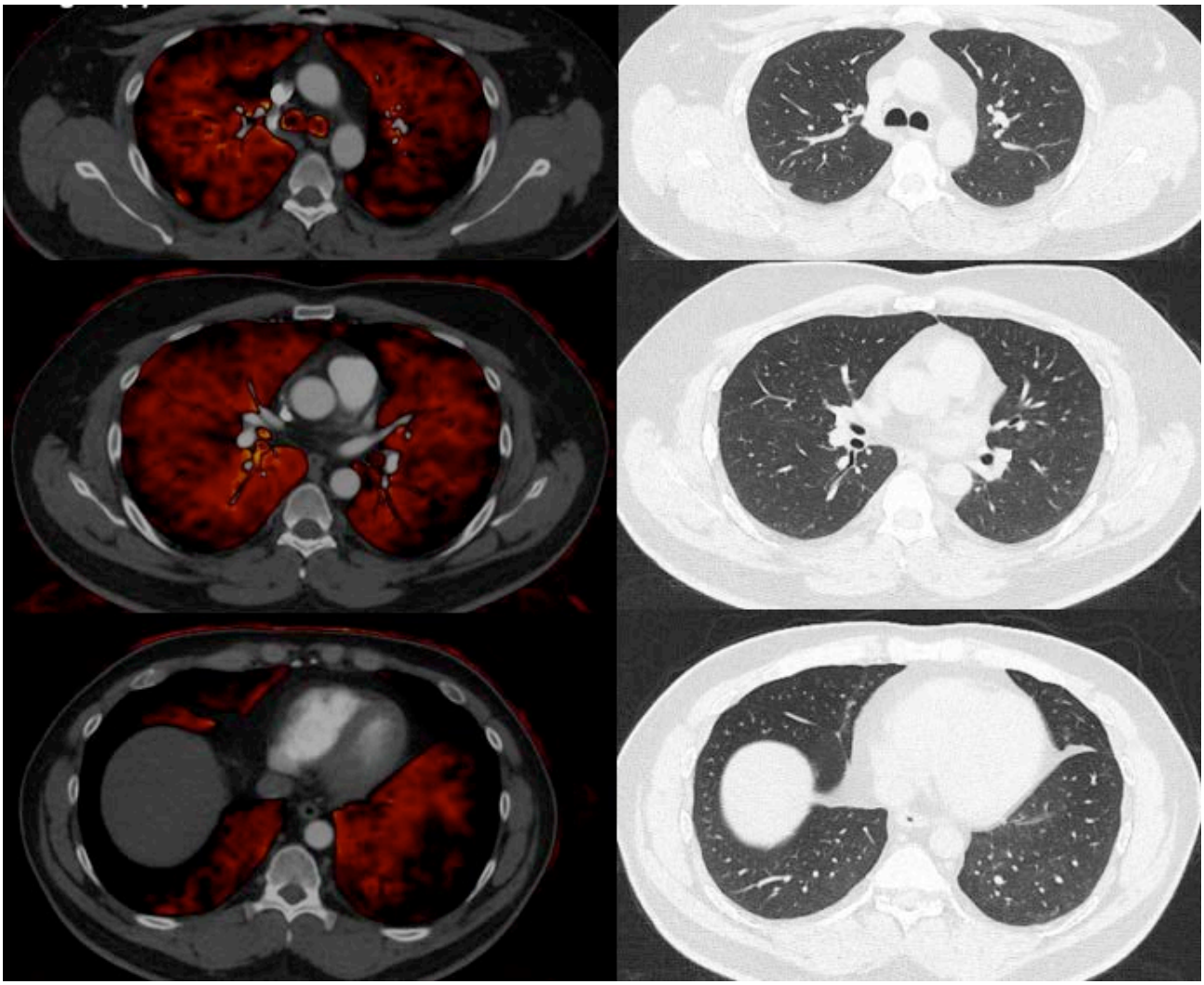

Repeat DE-CTPA showing normal lungs with no pulmonary embolism or post-COVID fibrosis although confirmed multiple subpleural defects on perfusion imaging compatible with post-COVID microangiopathy

.

Conclusion

The clinical applications of DE- CTPA continue to increase. Most topically, the utilisation of DE-CTPA in the detection and quantification of pulmonary microembolic disease is of clinical significance, increasingly so in the post COVID-19 era.

References:

[1] Seyed Ameli-Renani, MBBS, FRCR Farzana Rahman, MBBS, FRCR Arjun Nair, MD, MRCP, FRCR Laurie Ramsay, BMBCh Jenny Louise Bacon, BM, MRCP Alex Weller, MBBS, FRCR Heminder K. Sokhi, MBBCh, FRCR Anand Devaraj, MD, MRCP, FRCR Brendan Madden, MBBS, FRCP, FRCPI Ioannis Vlahos, MRCP, FRCR, (2014), Dual-Energy CT for Imaging of Pulmonary Hypertension: Challenges and Opportunities, Radiographics, Radiographics, 34:1769–1790, Published online 10.1148/rg.347130085

[2] Ridge CA, Desai SR, Jeyin N, Mahon C, Lother DL, Mirsadraee S, Semple T, Price S, Bleakley C, Arachchillage DJ, Shaw E, Patel BV, Padley SP, Devaraj A., (2020), Dual-Energy CT Pulmonary Angiography (DECTPA) Quantifies Vasculopathy in Severe COVID-19 Pneumonia., PMID: 36980509; PMCID: PMC10047841., Radiology. Cardiothoracic imaging, vol. 2,5, https://doi.org/10.1148/ryct.2020200428

A-505

Era of Rib Fracture Using Artificial Intelligence in Chest CT in Trauma Patients: Can we solve it?

G. Y. Jin
Jeonbuk National University Medical School and Hospital, Radiology, Jeon Ju, Republic of Korea (South Korea)

Objectives
To evaluate diagnostic accuracy of rib fracture using artificial intelligence (AI) in chest CT in trauma patient in emergency
Methods & Materials
1,209 patients' chest CT (rib fracture chest CT, n=1,159, normal chest CT, n=50) were enrolled in this study. Nine rib fractures were randomly selected as a training set from 1,159 rib fracture on chest CTs, and tests were performed with 150 rib fracture on chest CTs and 50 normal CTs. The finally developed model was internally verified with chest CT of the remaining 1000 ribs fracture. Through testing, sensitivity, specificity, positive predictive value, negative predictive value, F1-score for detection of rib fracture of AI were investigated, and the diagnostic accuracy of acute rib fracture with rib fracture location diagnosis of AI were investigated through internal verification.
Results
In the developed AI model, the diagnostic accuracy of detection of rib fractures was 93% and 96% in testing and internal verification, respectively. In the tests, sensitivity (93.3%), specificity (94%), positive predictive value (97.9%), negative predictive value (82.5%), and F1-score (95.6%) for detection of rib fracture. However, in internal validation for acute rib fracture with rib fracture location diagnosis of AI, diagnostic accuracy of rib fracture was 77.7% (777/1000).
Conclusion
The developed AI model diagnoses the presence or absence of acute rib fracture very well, but there are limitations in accurately reporting the location of rib fractures.

A-518

Extra Skeletal Ewing's Sarcoma of the chest wall: a Case Report and literature review.

E. Kadakovska[1], A. Meijere - Cirsa[1], I. Rasa[2], A. Karklins[1]
[1]North Kurzeme state hospital, Diagnostic, Ventspils, Latvia, [2]Riga East Clinical University Hospital, Clinic of Internal diseases, Riga, Latvia

Learning Objectives
Extraosseous Ewing sarcomas (EESs) are rare tumours originating from soft tissues. Their clinical picture depends mainly on the primary site of the sarcoma.

Background
Ewing sarcoma (ES) is a poorly differentiated, highly malignant, round cell tumour without cellular or structural differentiation. It shows an aggressive clinical behaviour with high rate of local recurrence and distant metastasis. ES is the second most common malignant bone tumour in children and young adults, although, rarely, it may be of extraskeletal origin. Commonly affected extraskeletal sites include the paravertebral spaces, lower extremities, head and neck and pelvis. Other rare locations of EES include the retroperitoneum, omentum, orbit, skin and chest wall.

Imaging findings OR Procedure details
A 25-year-old male annual chest radiograph was done under the the procedure provided for in the legislation. Partial opacification of the right hemithorax was noticed. Six days later a noncontrast CT scan was subsequently performed. A relatively small soft-tissue mass was noticed clos to the apical part of the right lung, but localised mostly in the chest wall (close to the aperthura thoracica superior), without internal calcifications, without costal destructions, without evidence for invasion in the surrounding soft tissues, without mass, without extension to the pleural surface.
Since there were no signs of malignancy, but a formation was detected - surgical intervention was performed.
Upon receiving the results of histological examination (pT1 Extra Skeletal Ewing's Sarcoma, Grade 3 (Ewing)), a PET-CT examination was performed, no metastatic disemination were found.

Conclusion
1. As for the differential diagnosis of solitary lung lesions, primary lung neoplasms are rare in young people.
2. Primary neoplasms in young patients are more frequently malignant than benign.
3. Although a regular chest examination required by law is a rare phenomenon (which in our case allowed early detection of the mass), the possibility of neoplasms in the chest should always be kept in mind even in young patients.

A-213

Fibrotic Lung Diseases – A Comprehensive Guide

I. Mata, C. Leal, O. Fernandes
Centro Hospitalar Universitário Lisboa Central, Radiology, Lisboa, Portugal

Learning Objectives

Discuss in detail radiological manifestations of fibrotic lung diseases (FLDs) with a focus on the characteristic patterns of lung fibrosis seen on HRCT.

Background

Fibrosing lung diseases are a group of chronic lung conditions characterized by thickening and scarring of lung tissue, resulting in respiratory dysfunction. The pathogenesis of these conditions is not fully understood and involves various factors, such as genetic predisposition, environmental exposures, and immune dysregulation. The diagnosis of fibrosing lung diseases involves a combination of clinical, radiological, and histopathological evaluations. High-resolution computed tomography (HRCT) is the most sensitive and specific imaging modality for the detection and assessment of lung fibrosis. Radiologists play a crucial role in identifying a typical usual interstitial pneumonia (UIP) pattern that is typically related to idiopathic pulmonary fibrosis (IPF), which has the worst prognosis among fibrosing lung diseases.

Imaging findings OR Procedure details

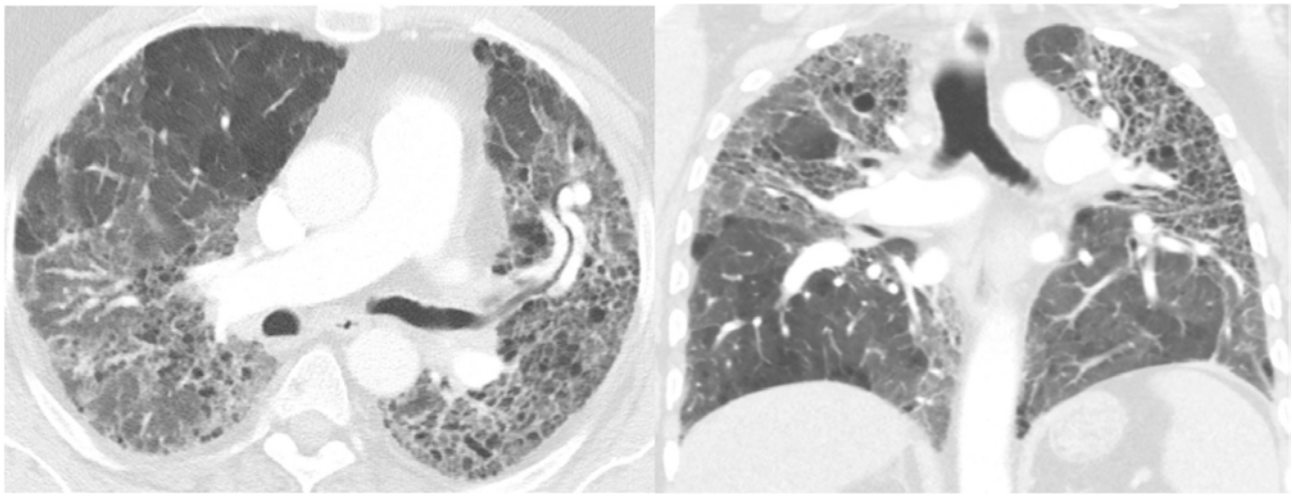

Chronic HP as manifestation of suberosis. Upper-lung zone predominance of reticulation, bronchiectasis and honeycoombing (no sub-pleural or peri-bronchovascular predominance). The presence of ground-glass opacities, mosaic pattern attenuation and lobular air-trapping suggest small airways disease.

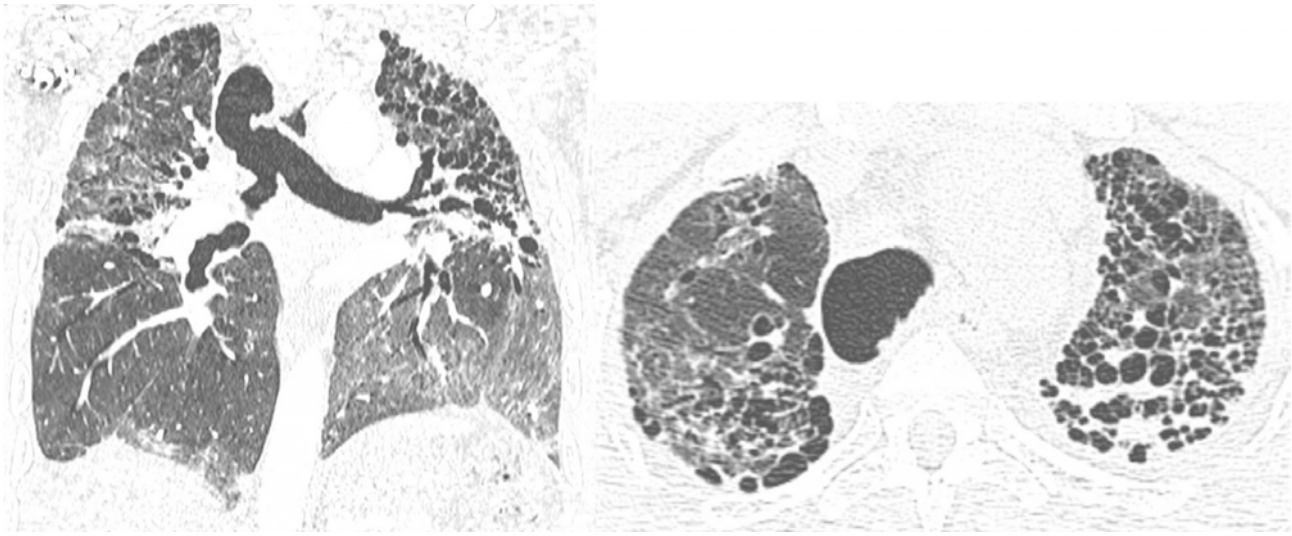

Fibrotic Sarcoidosis. Typical upper lobe perihilar distribution of traction bronchiectasis and fibrocystic areas with volume loss and architectural distortion.

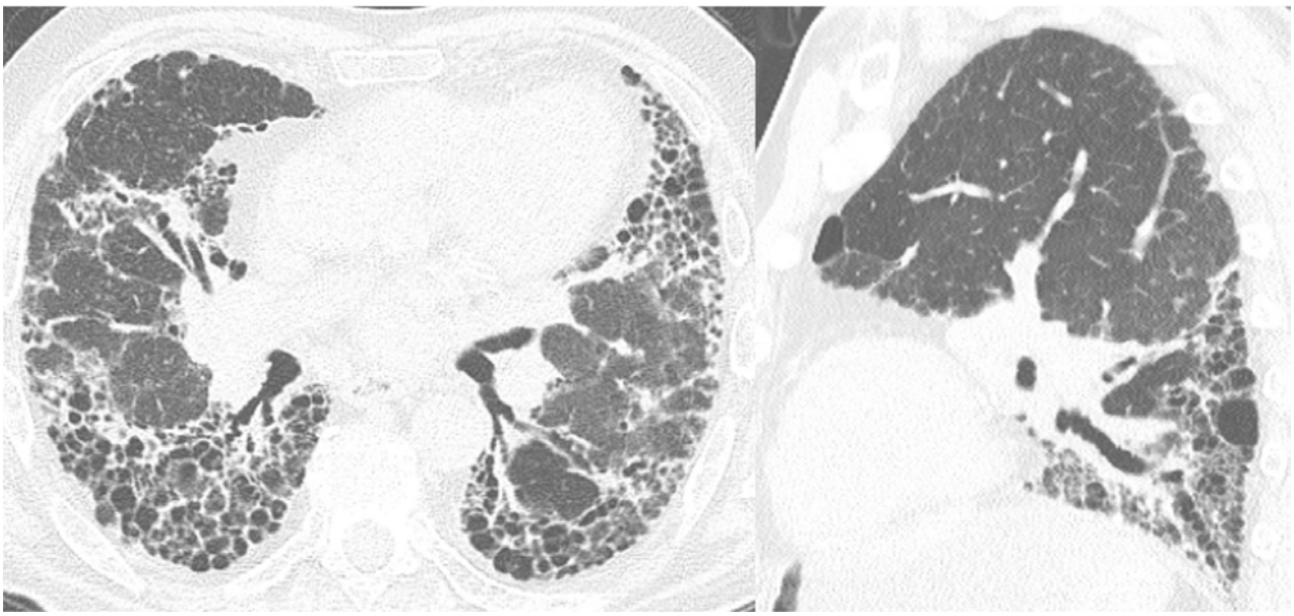

Classical UIP pattern characterized by clustered sub-pleural cystic spaces (honeycoombing), coarse reticulation and bronchiectasis with a predominant basal distribution.

The three primary features that suggest the existence of pulmonary fibrosis are the presence of honeycombing, traction bronchiectasis, and volume loss, which has a predominant basal and subpleural distribution in the case of the typical UIP/IPF pattern. Additional features include reticulations and ground-glass opacities, which are less prominent in UIP. UIP pattern is not exclusive to IPF and can be seen in other interstitial lung diseases, including connective tissue disease-associated interstitial lung disease (CTD-ILD), chronic hypersensitivity pneumonitis (CHP), asbestosis, or in combination with emphysema as combined fibrosis and emphysema (CPFE).

The predominance of other lung changes such as ground-glass opacities, mosaic attenuation pattern, consolidations, micronodules, and cysts, along with the absence of a apicobasal gradient and predominant subpleural distribution, indicates an interstitial fibrosing pattern inconsistent with UIP. According to the 2013 ATS/ERS guidelines, other "non-UIP" fibrotic interstitial idiopathic pneumonias include non-specific interstitial pneumonia (NSIP) and the fibrosing variant of organizing pneumonia (fOP), which may be associated with connective tissue diseases or drug-induced interstitial lung diseases.

CHP and fibrotic sarcoidosis are other diagnoses to consider on evaluation of pulmonary fibrosis.

Conclusion

Familiarity with the radiological patterns of these diseases improves accurate diagnosis and guide treatment decisions. Nevertheless different fibrosing lung diseases may have overlapping CT patterns. An multidisciplinary team approach to combine imaging and clinical data has proven to be the new diagnostic gold-standard.

References:

[1] William D. Travis, Ulrich Costabel, David M. Hansell, Talmadge E. King, Jr.,, (2013), An Official American Thoracic Society/European Respiratory Society Statement: Update of the International Multidisciplinary Classification of the Idiopathic Interstitial Pneumonias, Am J Respir Crit Care Med , 733–748, 188/6

[2] David A Lynch, Nicola Sverzellati, William D Travis, Kevin K Brown, (2018), Diagnostic criteria for idiopathic pulmonary fibrosis: a Fleischner Society White Paper, Lancet Respiratory Medicine, 138–53, 6

[3] Horst C, Gholipour B, Nair A, Jacob J., (2019), Differential diagnoses of fibrosing lung diseases, BJR Open, https:// doi. org/ 10. 1259/ bjro. 20190009

[4] Ganesh Raghu, Martine Remy-Jardin, Jeffrey L. Myers, Luca Richeldi, et al., (2018), Diagnosis of Idiopathic Pulmonary Fibrosis An Official ATS/ERS/JRS/ALAT Clinical Practice Guideline, Am J Respir Crit Care Med, e44-e68, 198

[5] Joseph Jacob, David M. Hansell, (2015), HRCT of fibrosing lung disease, Respirology, 859–872, 20

A-632

From lungs to beyond: the radiological odyssey of aspergillosis

C. Sousa
Centro Hospitalar Lisboa Norte, Radiology, Lisbon, Portugal

Learning Objectives

Describe the radiological features of chronic and invasive pulmonary aspergillosis and some of the usually unexpected extrapulmonary findings of disseminated disease.

Background

Aspergillosis is a mycotic infection caused by a ubiquitous soil fungus. The transmission is through the respiratory tract by inhalation of the *Aspergillus* conidia. The clinical presentation depends on organism and host particularities, with immune deficiency and pre-existing lung disease as two of the most critical risk factors. The incidence of fungal infection has increased significantly over the last few decades, partly because of the increased number of transplants and the widespread use of chemotherapy and immune-suppressive drugs. The spectrum of clinical presentation can range from an asymptomatic or indolent infection to a rapidly progressive and life-treating disease. Invasive infection may also spread to extrapulmonary sites, causing infections at distant organs.

Imaging findings OR Procedure details

At computed tomography, chronic pulmonary aspergillosis (CPA) has many appearances, namely aspergilloma, aspergillus nodule, allergic bronchopulmonary aspergillosis (ABPA), chronic cavitary or fibrosing pulmonary aspergillosis (CCPA and CFPA, respectively), and subacute invasive aspergillosis (SAIA). Aspergilloma is characterized by a mass within a lung cavity separated from the wall by an air crescent; ABPA consists primarily of mucoid impaction and bronchiectasis predominantly involving the segmental and subsegmental bronchi of the upper lobes; CPA appears as lung cavities with thin or thick walls, which may progress if untreated to CFPA, i.e. severe fibrotic destruction of at least two lobes with significant loss of lung function. The findings of SAIA are similar to CPA, however, with a subacute clinical presentation. Invasive pulmonary aspergillosis has an angio-invasive and airway-invasive form. The classic finding of angio-invasive aspergillosis is the halo sign, characterized by a ground-glass opacity surrounding a solid pulmonary nodule, mass or consolidation. Usually, the nodular and mass-like infiltrates subsequently progress to cavitation and air crescent formation. The findings of airway-invasive aspergillosis indistinguishable from bronchopneumonia caused by other common microorganisms, including tracheal and bronchial wall thickening, luminal secretions, peribronchial areas of consolidation and ground-glass, and patchy centrilobular nodules.

Conclusion

Recognition and familiarity with the different radiological findings in the appropriate clinical setting are crucial for patient management and starting prompt life-saving therapy.

A-371

From qualitative to quantitative chest CT analysis: four strategies to assess COVID-19 pneumonia outcome

L. Colligiani[1], S. C. Fanni[1], F. Volpi[1], C. A. D'Amore[1], A. Milazzo[1], C. Airoldi[2], M. Tonerini[3], L. Novaria[4], B. J. Bartholmai[5], A. De Liperi[4], E. Neri[1], C. Romei[4]

[1]University of Pisa, Department of Translational Research, Pisa, Italy, [2]University of Eastern Piemonte, Department of Translational Medicine, Novara, Italy, [3]University of Pisa, Department of Surgical, Medical, Molecular and Critical Area Pathology, Pisa, Italy, [4]Pisa University-Hospital, Department of Diagnostic Imaging, 2nd Radiology Unit, Pisa, Italy, [5]Mayo Clinic, Division of Radiology, Rochester, United States of America

Purpose/Objectives

This study aims at investigating the relationship between COVID-19 pneumonia outcomes and the outputs of four different analysis approaches of chest CT scans

Methods & Materials

A cohort of 192 patients who performed a real-time PCR test positive for SARS-COV2 and non-contrast chest CT was retrospectively enrolled between March and April 2020. All chest CTs were assessed with 4 approaches.

A radiologist performed a qualitative evaluation using a structured report with 18 radiological items (yes/no)

A quantitative analysis was performed using the Total Severity Score (TSS) by an emergency (TSS1) and a thoracic radiologist (TSS2). A score (range 0-4) representing the percentage of affected parenchyma was assigned to each lobe: none (0%), minimal (1-25%), mild (26-50%), moderate (51-75%), or severe (76-100%). The final TSS was calculated by summing up the scores (range 0-20).

A quantitative analysis was carried out using a density mask technique (DMT) to compute the percentage of normal and more dense parenchyma. The defined thresholds were: -949 -750 for normal parenchyma (DM_Norm), -749 -300 for ground glass opacities (DM_GG), and -299 +40 for consolidations (DM_Cons).

A texture analysis (TA) was performed through CALIPER software to quantify the percentage of normal parenchyma (TA_Norm) and interstitial lung disease (TA_ILD).

Inter-reader variability between TSS1 and TSS2 was assessed through the intraclass correlation coefficient (ICC), and Bland-Altman analysis was performed to calculate bias and limits of agreement (LOA).

Patients were divided into survivors and non-survivors, and ventilated and not-ventilated. The association between the outcomes and analysis outputs was assessed using the Chi-square and the Mann-Whitney test for categorical and quantitative variables, and for the latter also with a logistic regression analysis.

Results

At qualitative analysis, only left hilar lymph nodes and emphysema were found significantly prevalent among non-survivors, while GGO among ventilated ($p<0.05$).

The median TSS were 9 [IQR 6;13] for TSS1 and 7 [5;10] for TSS2. The ICC value was 0.83 (95% CI 0.76;0.88] and the Bland-Altman plot showed a bias (LOA) of 1.55 (-4.69,7.78). A significant difference for both TSS was found between ventilated and not ($p < 0.001$), but only for TSS1 between survivors and not ($p=0.017$). The strongest differences between survivors and not were demonstrated at quantitative analysis for DM_Cons ($p=0.002$) and TA_Norm ($p=0.003$). At multivariate analysis, the same features showed the higher AUC (0.70) with OR of 1.07 and 0.97, respectively.

Conclusion

Quantitative methods as TA and DMT provide an objective and reliable severity assessment in COVID-19 patients, outperforming qualitative evaluation and TSS.

A-176

Hilar abnormalities on chest radiograph

E. S. Lee
Hangang Sacred Heart Hosp., Medical college, Hallym Univ, Diagnostic Radiology, Seoul, Republic of Korea (South Korea)

Objectives

Hilar abnormalities are very hard part in chest radiograph for understanding. The principal opacities of the normal hilum, as seen on both the frontal and lateral plain chest images, are the two main pulmonary arteries as they enter the lungs.

Methods & Materials

Though both hila should be indistinguishable in size and density, we do not get equal hila in majority of CXRs.

Results

There are numerous causes of hilar abnormalities.

Conclusion

I will show interpreting hilum by three factors shape, radiopacity, position.

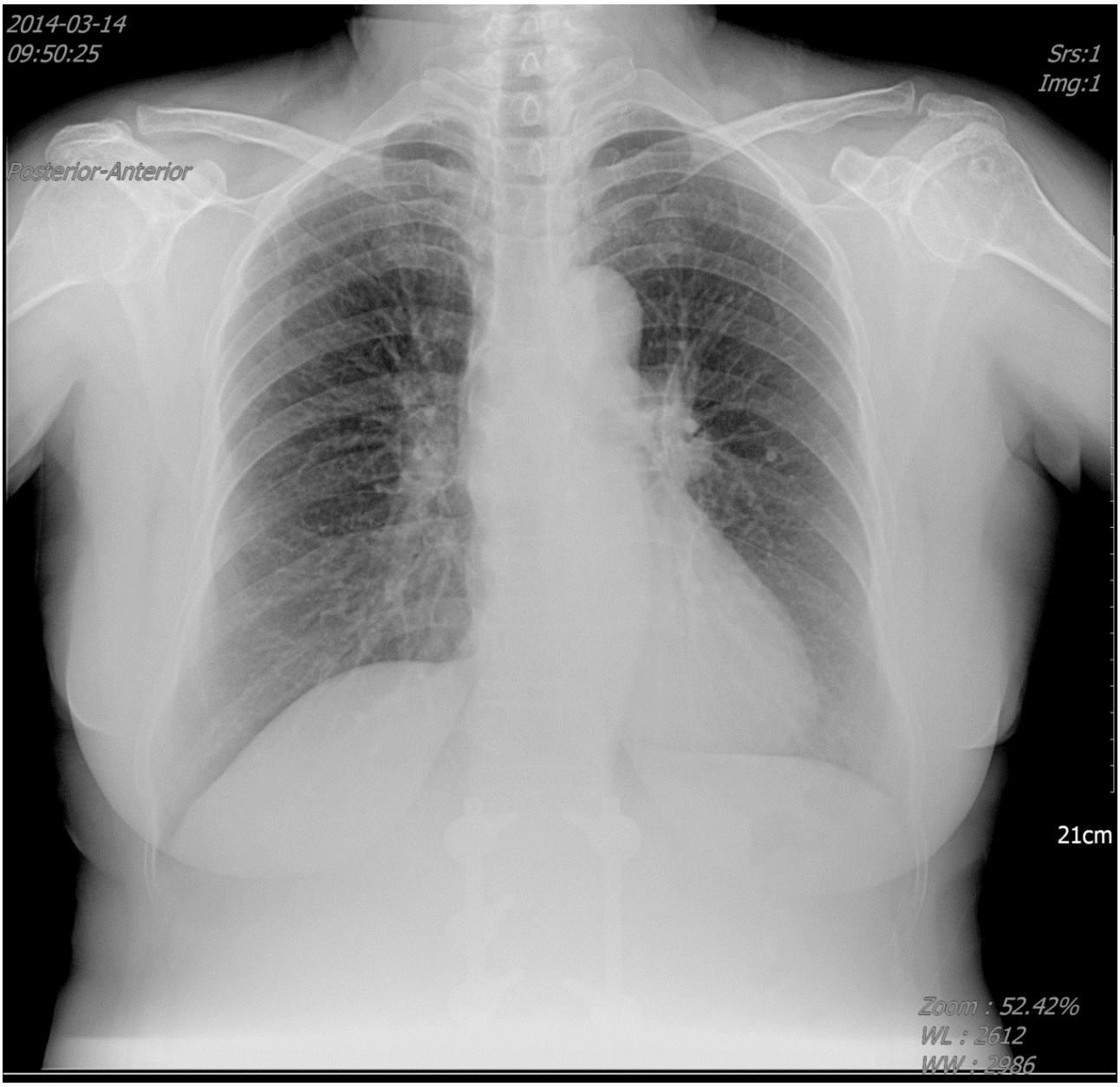

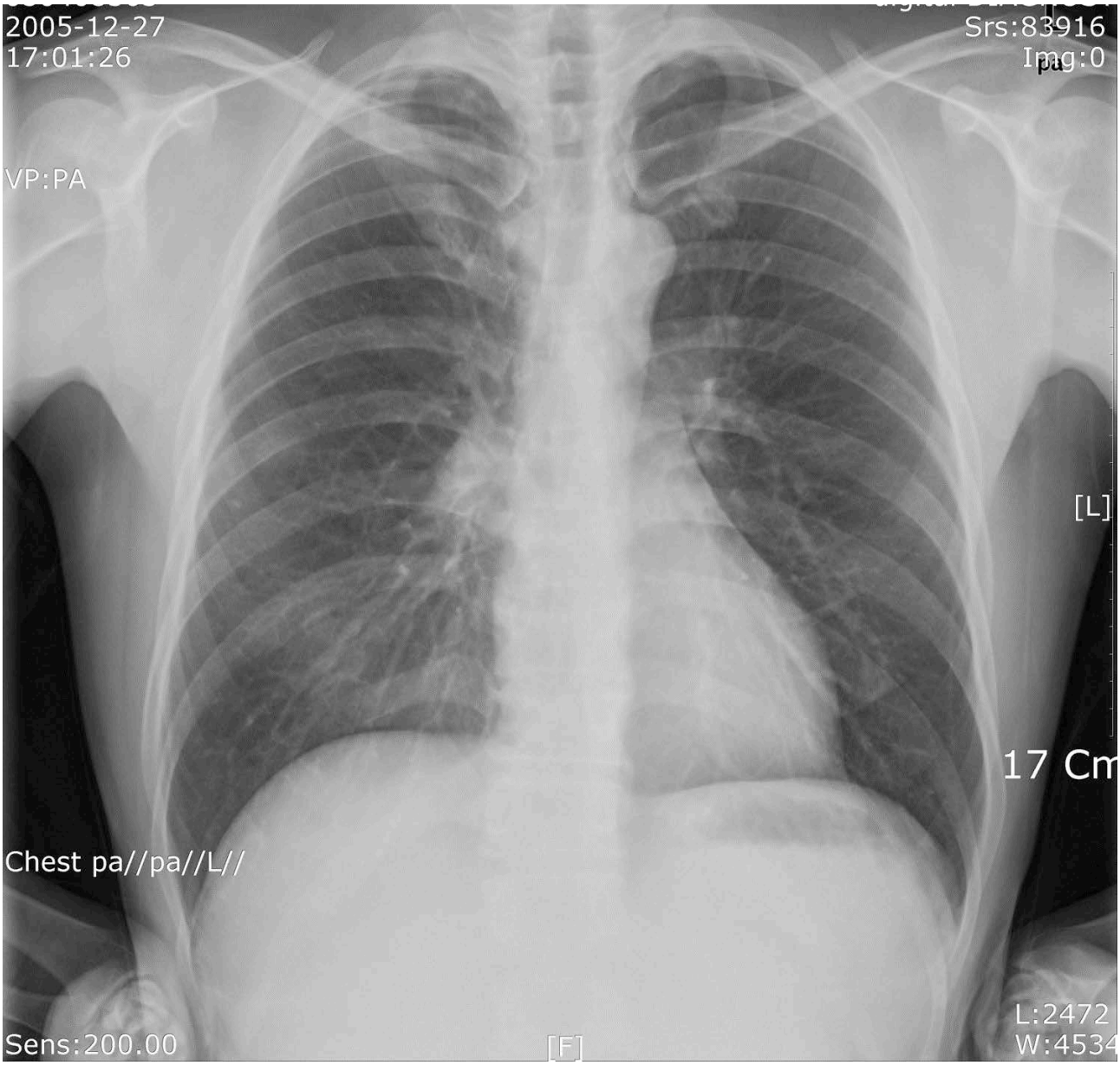
2005-12-27
17:01:26
Srs:83916
Img:0
VP:PA
[L]
17 Cm
Chest pa//pa//L//
L:2472
Sens:200.00
[F]

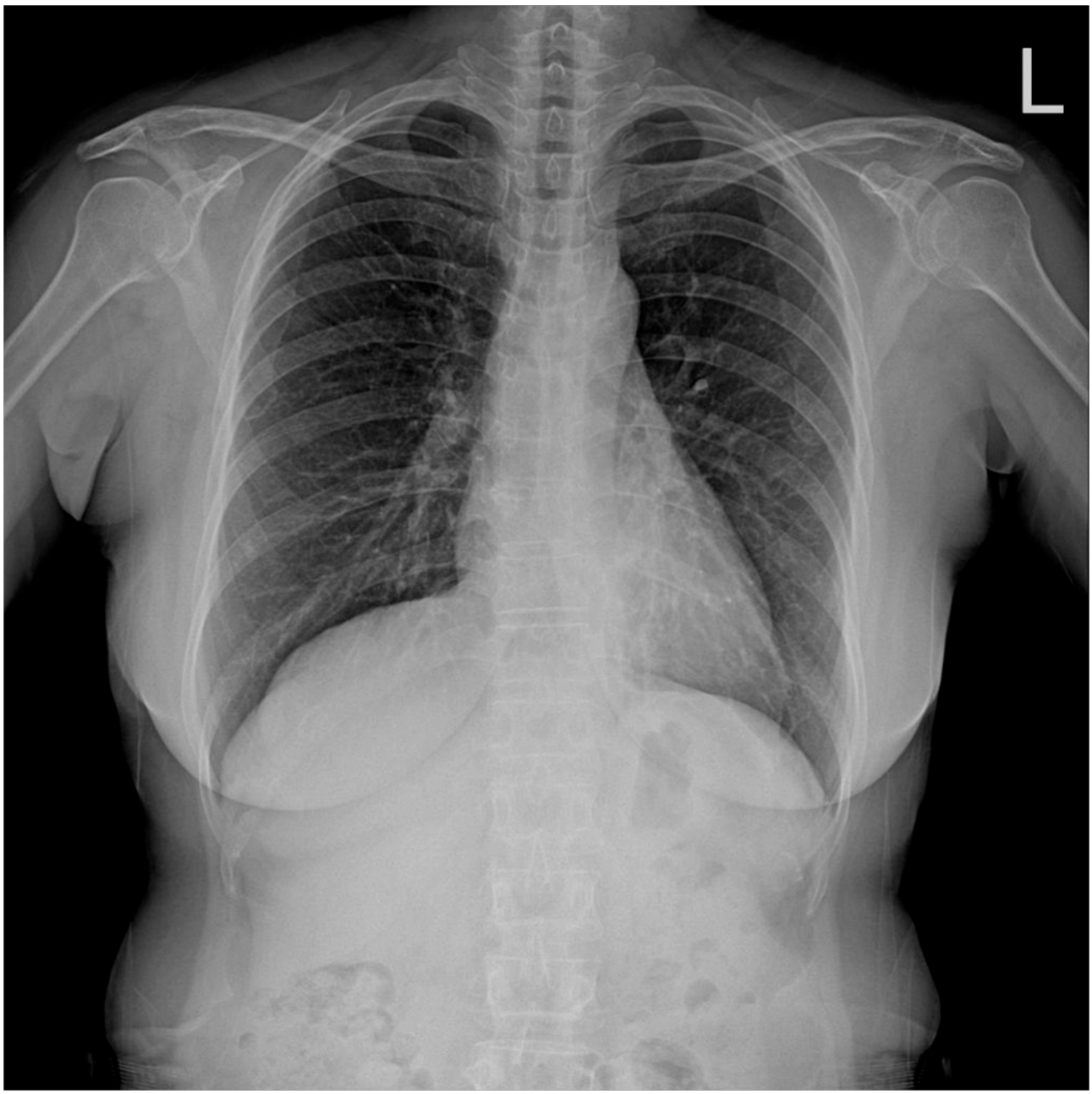
L

A-633

Imaging Findings In Hypersensitivity Pneumonitis: A Pictorial Essay

Z. N. Tekin[1], H. Prosch[2]
[1]Istanbul Medeniyet University Goztepe Prof Dr Suleyman Yalcin City Hospital, Radiology, Istanbul, Turkey, [2]Medical University of Vienna, Department of Biomedical Imaging and Image-guided Therapy, Vienna, Austria

Learning Objectives

To appreciate the HRCT findings in inflammatory and chronic hypersensitivity pneumonitis (HP) and to know the most important differential diagnoses.

Background

HP, also called extrinsic allergic alveolitis, is allergic reaction of the lung parenchyma in response to inhaled antigens in genetically susceptible individuals. HP shares clinical and radiological features with other acute and chronic interstitial lung diseases.
Two distinct phenotypes of HP have been recognized: inflammatory (acute/subacute) HP, which lasts a few weeks, is mostly reversible, and has a good prognosis; and chronic HP, which develops over several months and is associated with worse survival.

Imaging findings OR Procedure details

Non-fibrotic (inflammatory) HP is characterized by inflammation in the small airways and the pulmonary interstitium[Ref1]. Consequently, HRCT frequently shows bilateral and symmetric, patchy, ground-glass opacities. The distribution usually shows a predominance for the mid- or lower lung field. In some patients, numerous centrilobular ground glass nodules are seen.

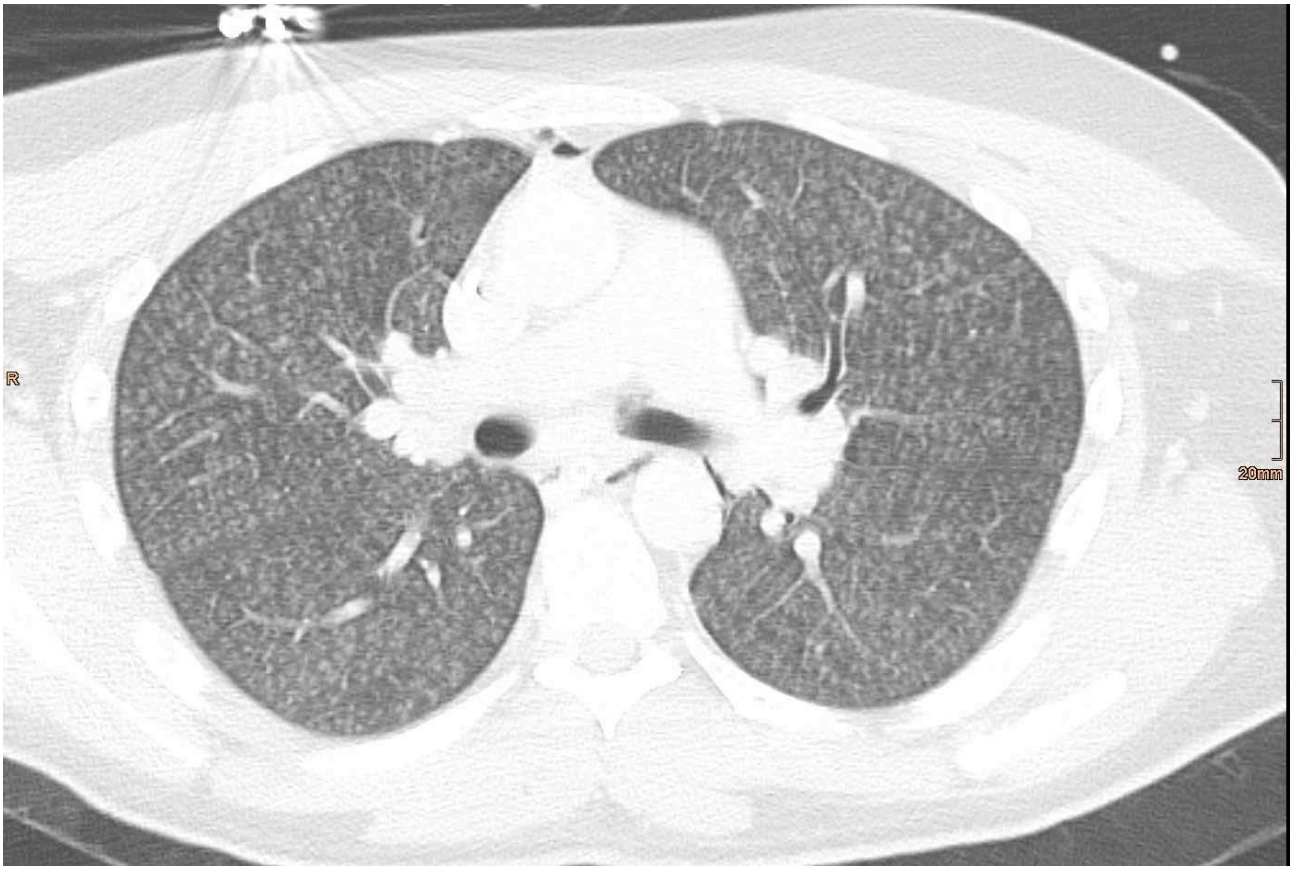

Non-fibrotic HP defined as bilateral and symmetric numerous centrilobular ground glass nodules on HRCT

Inflammation of the small airways may lead to air-trapping, which is one of the hallmarks of hypersensitivity, particularly if seen in the context of the so-called the three-density pattern (formerly the head-cheese sign), which is defined as a combination of lobules with normal density, lobules with an increase in density, and lobules with a decrease in density

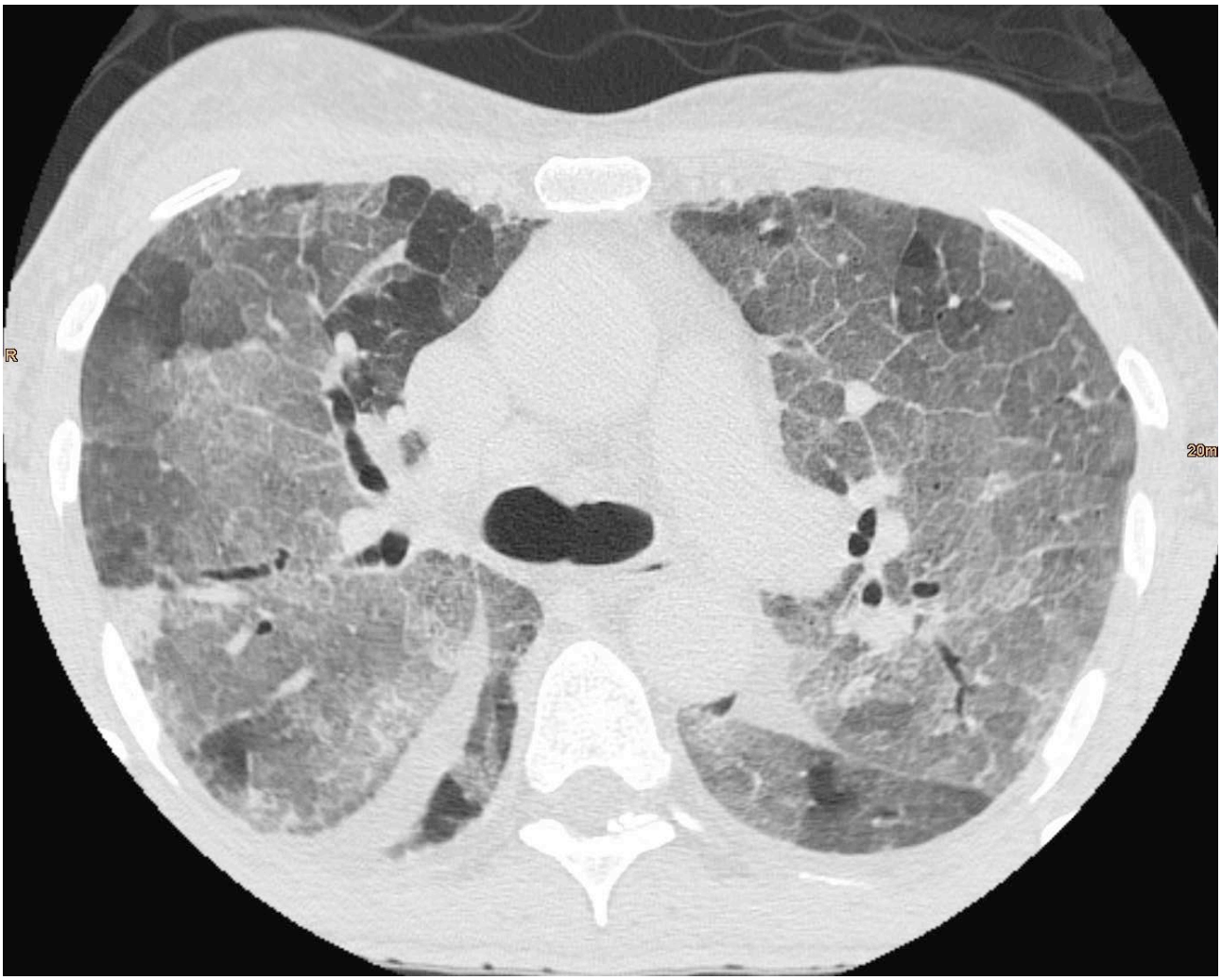

Three-density pattern characterized by the combination of lobules with normal density, lobules with an increase in density, and lobules with a decrease in density

.

Fibrotic HP (mixed inflammatory and fibrotic or purely fibrotic) is characterized by signs of fibrosis (reticular abnormalities, traction bronchiectasis with or without honeycombing) with or without signs of inflammatory HP [Ref2].

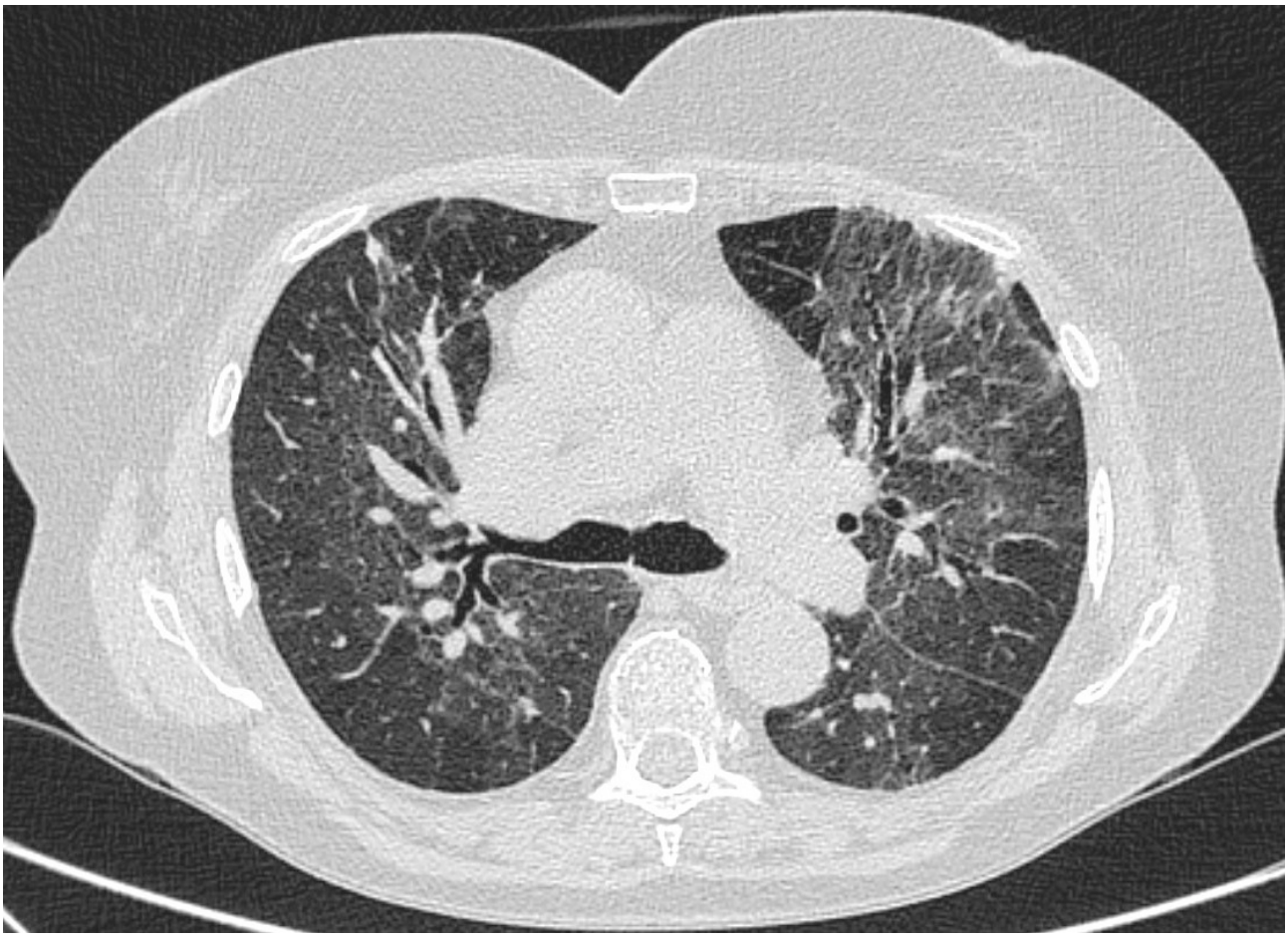

Typical fibrotic hypersensitivity pneumonitis on axial HRCT. Mosaic attenuation with signs of fibrosis (reticular abnormalities and traction bronchiectasis)

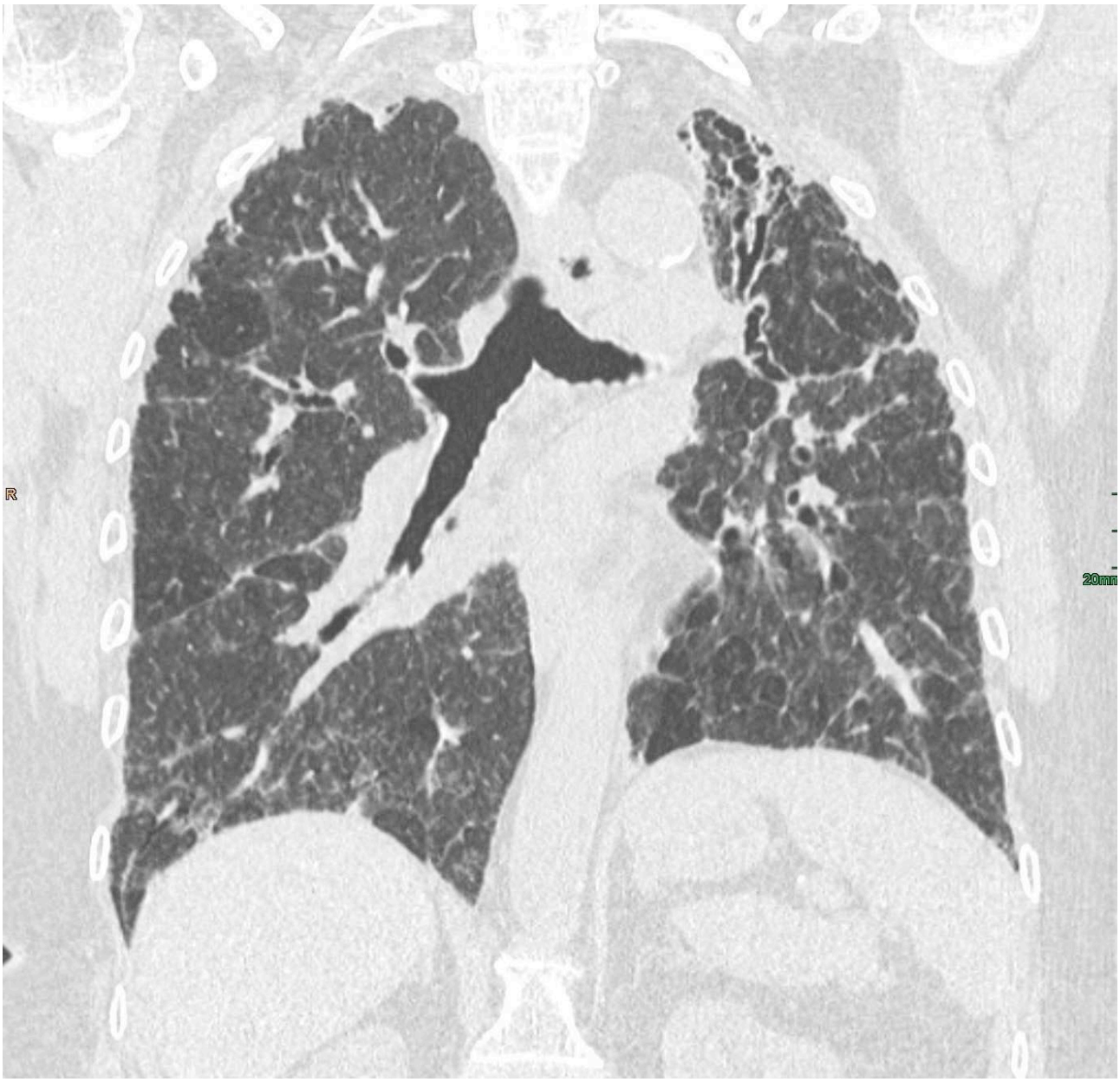

Typical fibrotic hypersensitivity pneumonitis on coronal HRCT. Mosaic attenuation at inspiration affecting all lung zones with signs of fibrosis (reticular abnormalities and traction bronchiectasis)

The differential diagnosis of fibrotic HP is challenging at times and includes the usual interstitial pneumonia and non-specific pneumonia. The best discriminating finding has been reported to be the three-density pattern[Ref3].

Thin-walled lung cysts are also found in around 15% of patients with HP and may resemble those seen in lymphoid interstitial pneumonia.

Conclusion

HRCT is an important tool for the diagnosis of HP. The diagnosis of HP, however, requires additional diagnostic tests, such as a bronchioloalveolar lavage, the history of antigen exposure, and, at times, a biopsy.

References:

[Ref1] Raghu G, Remy -Jardin M, Ryerson CJ, et al, Diagnosis of hypersensitivity pneumonitis in adults. An official ATS/JRS/ALAT clinical practice guideline, Am J Respir Crit Care Med, https://pubmed.ncbi.nlm.nih.gov/32706311/

[Ref2] Fernández Pérez ER, Travis WD, Lynch DA, et al. , Executive summary diagnosis and evaluation of hypersensitivity pneumonitis: CHEST guideline and expert panel report., Chest , https://pubmed.ncbi.nlm.nih.gov/33865835/

[Ref3] Takei R, Yamano Y, Kataoka K, et al. , Usefulness of new diagnostic criteria for chronic hypersensitivity pneumonitis established on the basis of a Delphi survey: A Japanese cohort study, Respir Investig. , https://pubmed.ncbi.nlm.nih.gov/31718936/

A-323

Imaging of the diaphragm: anatomy and disorders

M. Cufí Quintana[1], M. Gallego Casals[2], M. Andreu Magarolas[1], C. Lozano Roca[1], X. Gallardo[1], E. Castañer González[1]
[1]Hospital Parc Taulí, Thoracic Radiology, Sabadell, Spain, [2]Hospital Parc Taulí, Radiology, Sabadell, Spain

Learning Objectives

- To describe the anatomy and physiology of the diaphragm.
- To review the primary diaphragm disorders.
- Learn the image techniques available for its study.

Background

The diaphragm is the physical barrier that separates the thorax from the abdomen and is the main muscle involved in ventilation. Its dysfunction can be a cause of dyspnea, and despite its importance, it is often underrated and incompletely evaluated by clinicians as well as by radiologists.

Imaging findings OR Procedure details

1. Brief description of embryology and anatomy of the diaphragm.
2. Abnormalities cases, classified as:

- Dysfunction: paralysis, weakness or eventration and consequences of diaphragmatic inversion.
- Hernias: congenital (Morgagni, Bochdalek) and acquired.

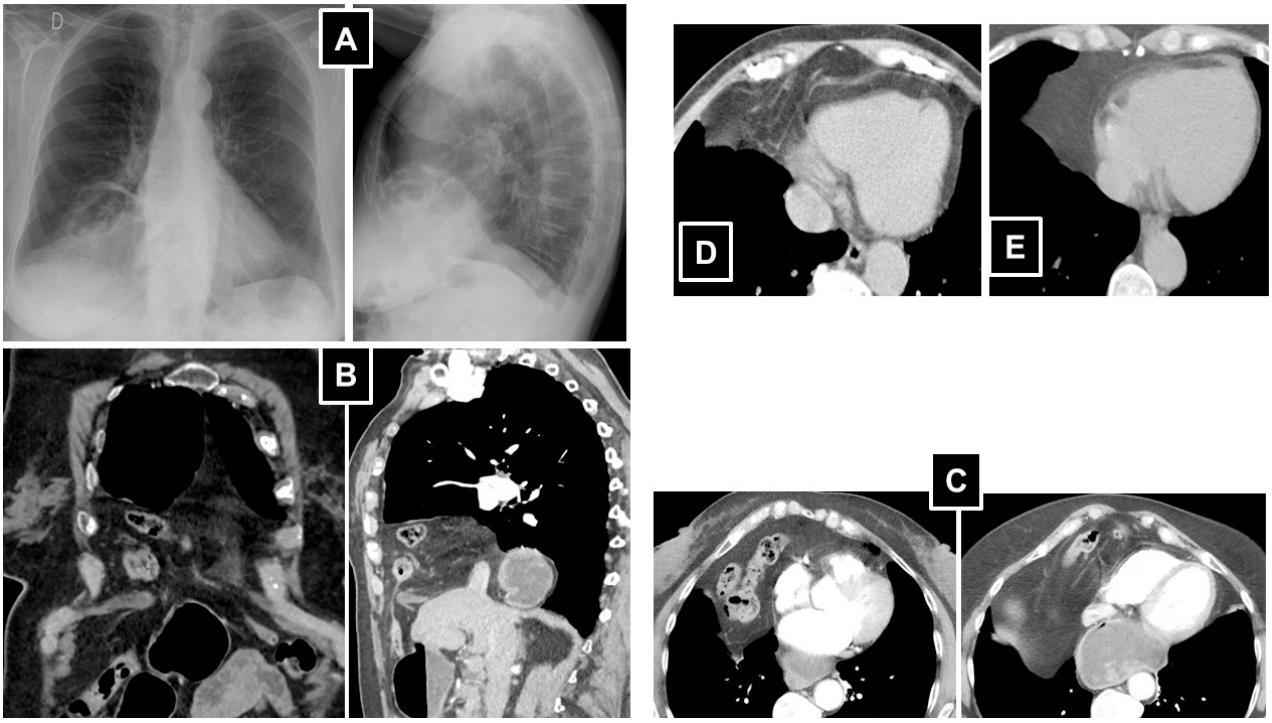

Morgagni and hiatal hernias.

- Rupture: traumatic and post-surgery.
- Secondary: neoplastic and infectious involvement by contiguity from the abdominal cavity.

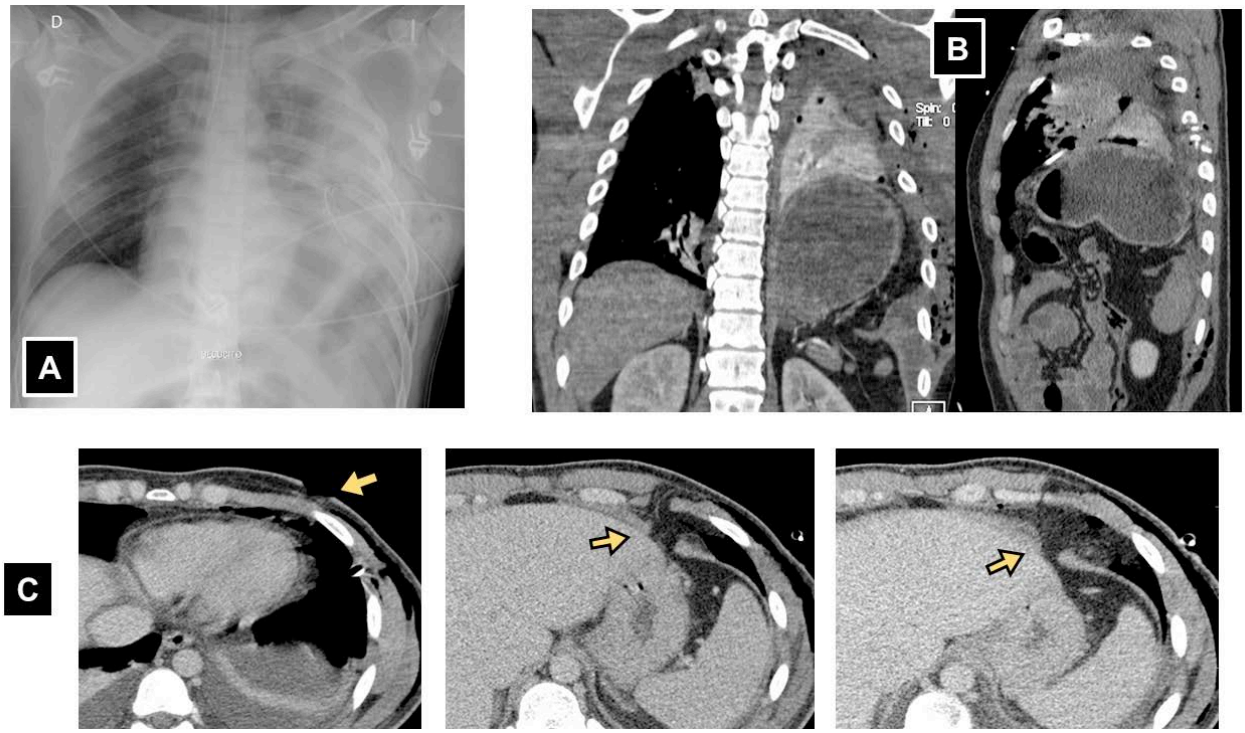

Diaphragmatic rupture with herniation of several abdominal viscera to the thoracic cage and a disruption of the left anterior diaphragm by a knife.

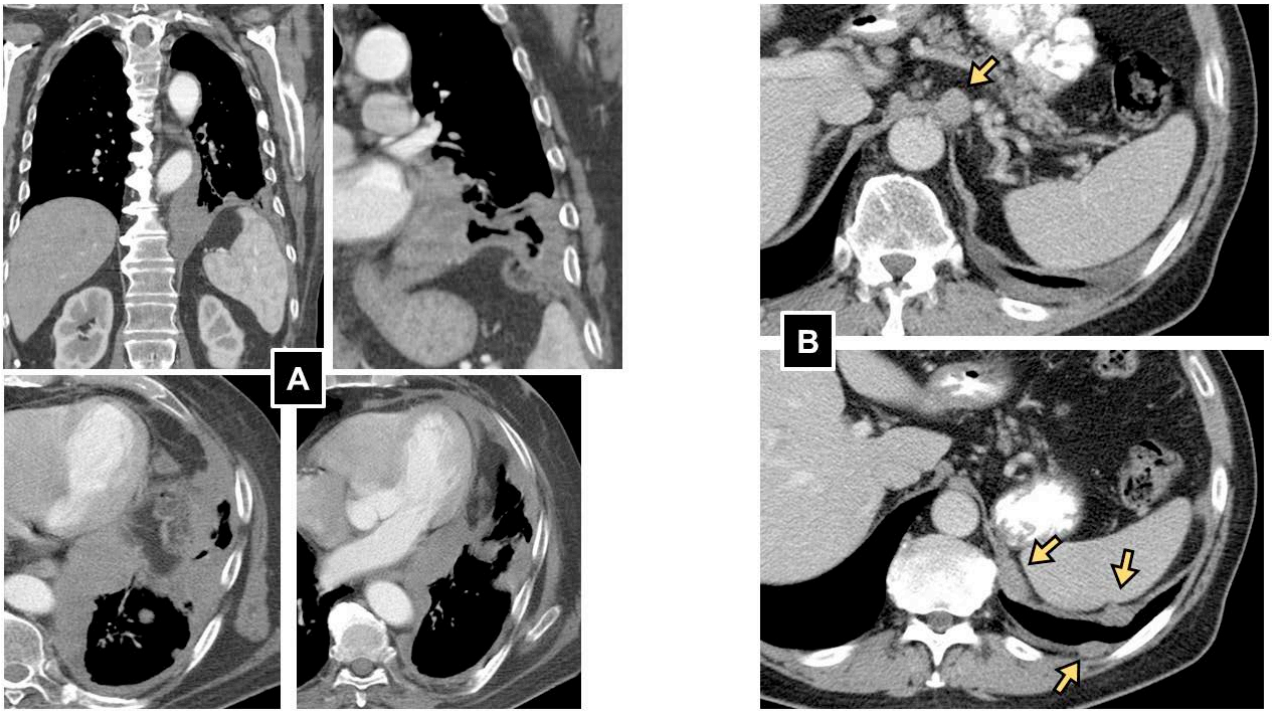

Neoplastic involvement of the diaphragm.

- Miscellanea: Median arcuate ligament syndrome and increased uptake on PET/CT (respiratory effort, hipo).

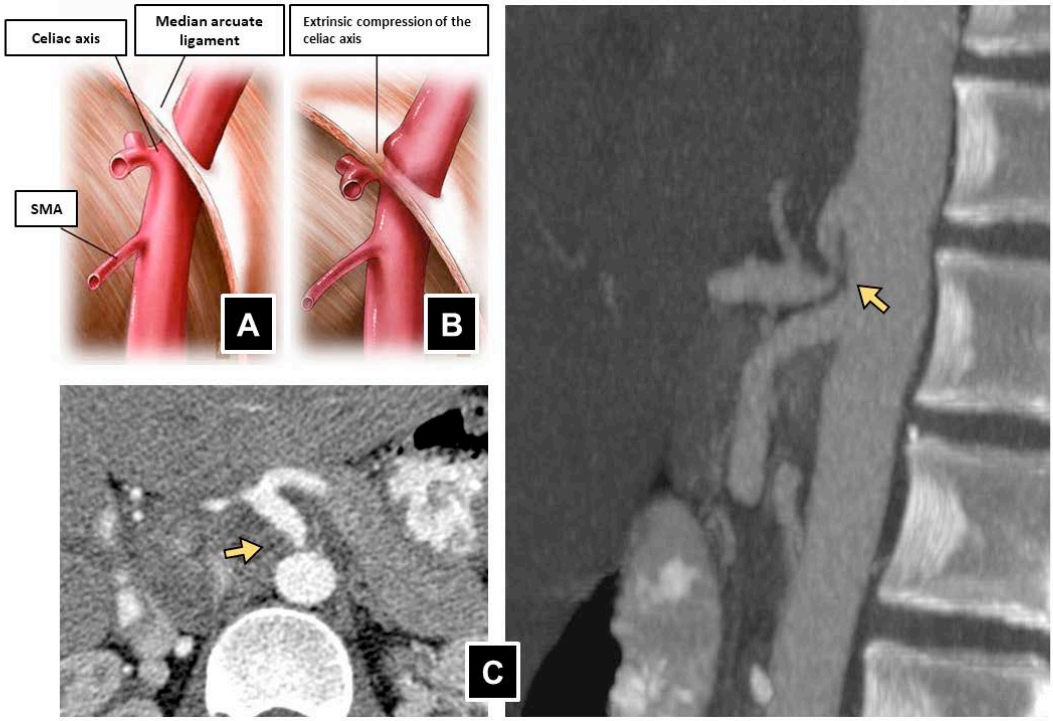

A low insertion of the medial arcuate ligament which leads to a stenosis of the ostium of the celiac axis.

3. Finally, we explain the main imaging techniques we have for both the functional and morphological study of the diaphragm, including chest radiographs, fluoroscopic tests, ultrasounds, CT, and MRI.

Conclusion

The diaphragm is ventilation's primary muscle, and its dysfunction is an underrated cause of respiratory difficulties. The radiologist must know its different pathology and also the indications of the most appropriate imaging techniques for each case.

A-686

Incidental breast findings on chest CT – what to do?

A. Azeiteiro, L. Urbano, C. Mendonça, A. L. Amado Costa
Centro Hospitalar Lisboa Norte, EPE, Serviço de Imagiologia Geral, Lisbon, Portugal

Learning Objectives

- To review and illustrate breast incidentalomas on CT.
- To present the CT characteristics of breast lesions requiring referral.
- To emphasize imaging features suggestive of malignancy on CT, indicating a need for urgent referral.

Background

Even though chest computed tomography (CT) is not the first-line imaging method for breast assessment, the whole breast tissue is usually scanned in the exam, enabling the detection of breast incidentalomas, even when the exam is performed for other indications. Breast abnormalities are frequently overlooked or inaccurately assessed on CT. However, some Studies have reported the importance of chest CT for the identification of unexpected breast lesions, which may include primary and secondary malignancies, as well as benign lesions.

Radiologists should be able to identify and characterize breast lesions incidentally detected on chest CT as benign, indeterminate, or sufficiently suspicious to require further work-up. They should also be aware of the normal and abnormal imaging findings after breast surgery, in order to recognize signs of breast cancer recurrence and potential complications, such as seromas.

Imaging findings OR Procedure details

Based on our department database, we will present and illustrate the imaging characteristics of several breast incidentalomas on CT, including malignant breast lesions and breast cancer recurrence, benign lesions (such as lipomas, gynecomastia, fat necrosis, seromas, abscesses, and fibroadenomas), as well as imaging findings after mastectomy and breast reconstruction surgery (including breast prosthesis and flap reconstruction).

Some breast incidentalomas have characteristic imaging findings on CT that allow a confident diagnosis. However, often CT cannot provide sufficient information for a definitive diagnosis, and further workup is necessary.

Some breast lesion characteristics such as spiculated and irregular margins, irregular shape, and rim enhancement suggest malignancy. However, Studies have not been able to accurately define benign features or those that can exclude malignancy, therefore all breast lesions identified on CT should still be further evaluated.

Some breast postoperative changes are easily recognized. However, others may mimic a malignancy and require further assessment.

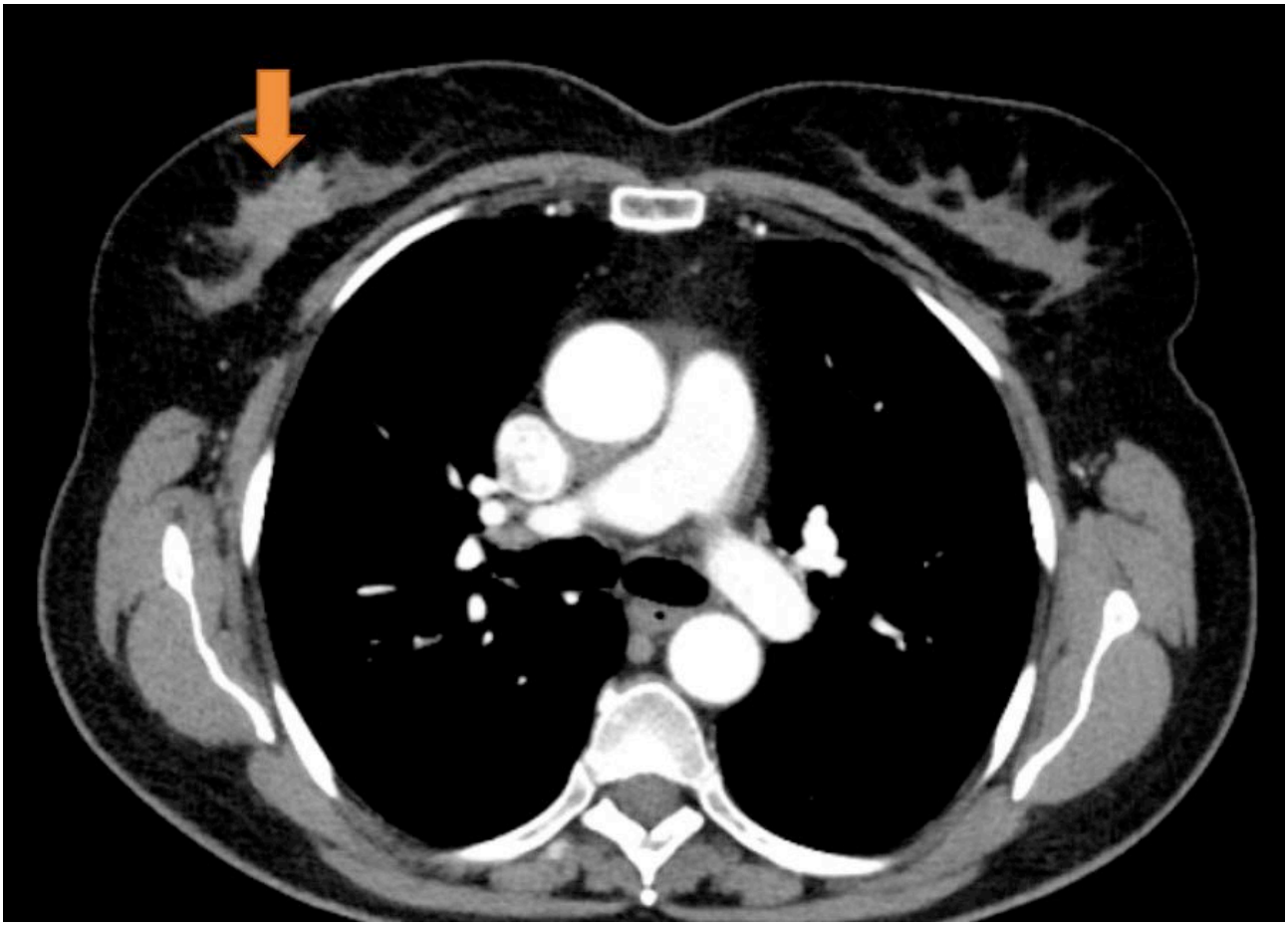

Axial contrast-enhanced chest CT image reveals an enhancing lesion with irregular margins in the right breast (arrow), which corresponded to a breast cancer.

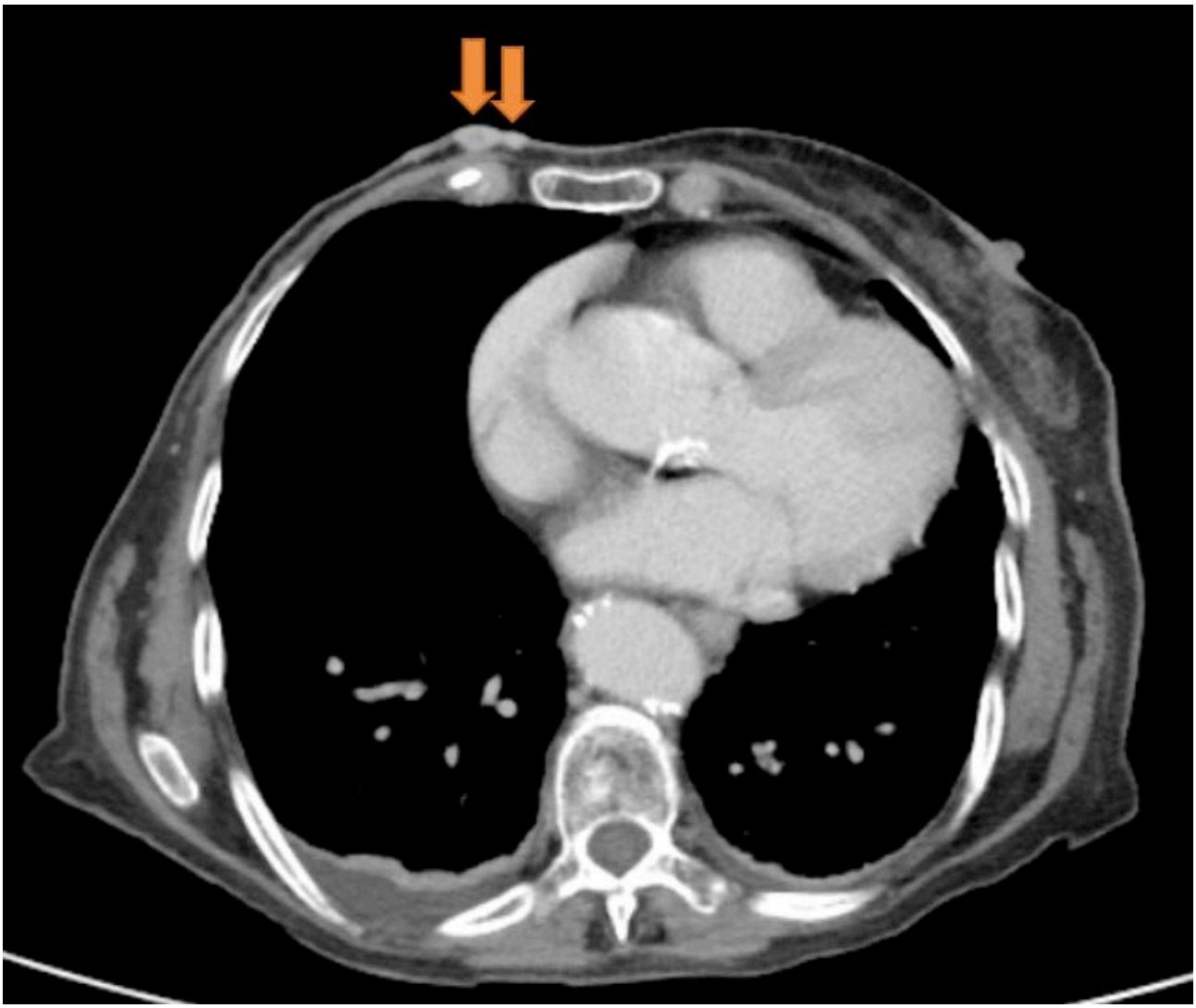

Axial contrast-enhanced chest CT image of a patient who had underwent previous right breast mastectomy due to breast cancer. Small enhancing nodules are seen on the chest wall (arrows), in keeping with recurrent breast cancer. Bilateral pleural effusion is also present.

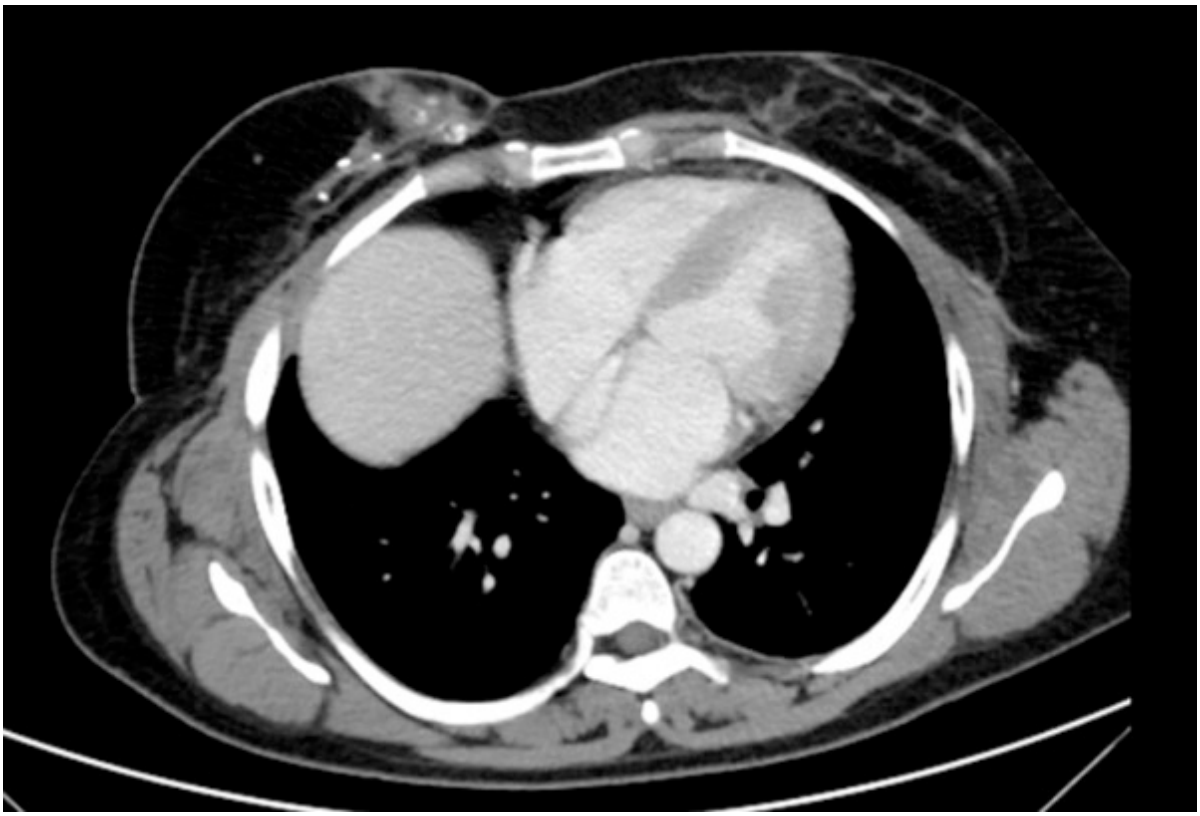

Axial contrast-enhanced chest CT image of a patient who had underwent right breast mastectomy with TRAM flap reconstruction reveals partially calcified lesions in the reconstructed breast, due to fat necrosis.

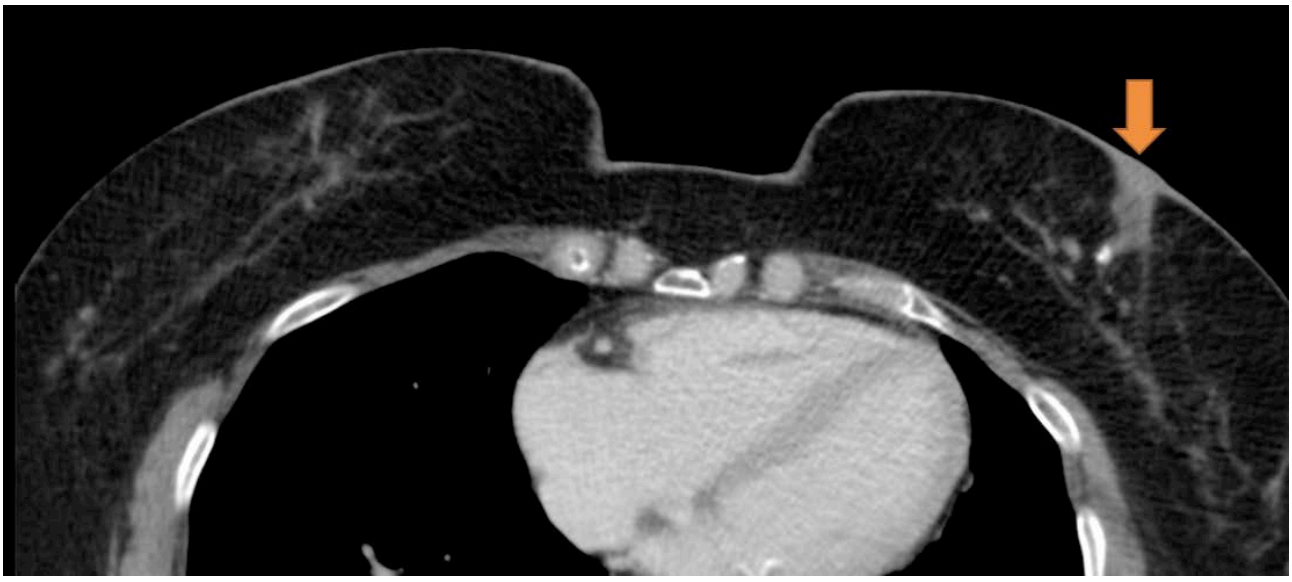

Axial contrast-enhanced chest CT image reveals a retroareolar non-enhancing and elongated image with a small calcification (arrow), which corresponded to a ductal ectasia caused by an intraductal papilloma.

Conclusion

A dramatic rise in the use of CT imaging has led to the increased detection of breast incidentalomas, some of which may be clinically significant.

It is important for the radiologists, particularly for those who perform chest and cardiac CT, to carefully assess the breasts on CT scans. Radiologists should be able to recognize and report abnormal breast findings, as well as to advise further workup when needed.

A-673

Is it a Pulmonary Embolism or is actually a Pulmonary Artery Sarcoma?

B. Vekaria, N. Sivarasan
Guys and St. Thomas' Hospital Trust, Medical Imaging, LONDON, United Kingdom

Purpose/Objectives

Imaging examples of Pulmonary Artery Sarcoma (PAS)
Potential ways to distinguish between PAS and Pulmonary emoblism (PE) with the use of imaging

Methods & Materials

PAS is a rare tumour of the intimal layer of the pulmonary arteries, on computerised tomography (CT) imaging alone it can be difficult to distinguish from PE.
We present the case of a patient who presented with PAS in our tertiary hospital, their journey through radiology and the pertinent imaging findings. An additional companion case is also presented to illustrate the variety of imaging appearances of PAS.

Results

Case 1. Patient was found to have a large filling defect in the main pulmonary artery extending into bilateral main pulmonary arteries. This was initially thought to be a large saddle embolus and patient was commenced on medical treatment, after a period there was little to no change in the appearances and the patient was transferred to our centre. The patient underwent angiographic thrombectomy, at the time of procedure it was noted that the filling defect remained and a tissue sample was taken and was found to be pulmonary artery sarcoma on pathology. Post procedure, the patient was clinically well and saturating normally on room air.

Case 2. Patient presented locally with chest pain, a CT suggested irregular thickening of the main and bilateral proximal pulmonary arteries walls. A PET CT was performed which showed marked uptake in the areas of CT thickening and the patient was treated with steroids for a presumed vasculitis. They were later found to have pulmonary hypertension and a pulmonary thromboendarterectomy was performed, tissue sample revealed PAS.

Conclusion

Some case reports have suggested PAS can show heterogeneous enhancement on contrast CT which would not be the case with clot. Others have shown MRI to be a useful discriminator. Ultimately, persistent filling defects on CT that are unresponsive to medical treatment should trigger further investigation, this may be in the form of further imaging or interventional tissue sample and can prove to be key to diagnosis.

References:

[1] Alan M. Ropp , Allen P. Burke, Seth J. Kligerman, Jay S. Leb, Aletta A. Frazier, (2021), Intimal Sarcoma of the Great Vessels, Radiographics, Vol. 41, No. 2
[2] Shanda H. Blackmon, David C. Rice, Arlene M. Correa, Harsh Singh, Ara A. Vaporciyan, Michael Reardon, (2008), Management of Primary Pulmonary Artery Sarcomas, The Annals of Thoracic Surgery, vol 87, issue 3, https://www.annalsthoracicsurgery.org/article/S0003-4975(08)01671-8/fulltext
[3] Eva Cervilla-Muñoz, Francisco Galeano-Valle, Jorge Del-Toro-Cervera, Enrique Calleja-Cartón, Pablo Demelo-Rodríguez, (2020), Differential diagnosis and treatment approach to pulmonary artery sarcoma: a case report and literature review, ERJ open research, 6, https://openres.ersjournals.com/content/6/3/00124-2020

A-684

Lung cancer screening made simple: a roadmap for implementation

N. Antunes[1], C. A. Ruano[1,2], F. Reis[1]
[1]Hospital de Cascais, Radiology, Lisbon, Portugal, [2]Hospital da Luz, Radiology, Lisbon, Portugal

Purpose/Objectives

- To explain the importance of a standardized lung cancer screening (LCS) program.
- To propose a unified model for LCS, with a detailed “step-by-step” plan that can be applied in every country setting, enabling simple implementation.

Methods & Materials

Lung cancer is the most frequent cause of death due to cancer worldwide. In the year 2020, it represented 18% of mortality attributable to cancer, a higher percentage than the combined mortality of breast and prostate cancer.

Low-dose chest CT screening has proven to detect lung cancer at an earlier stage and to reduce lung cancer-specific mortality by 20-25% in a high-risk population. However, the implementation of lung cancer screening in Europe has been variable and heterogeneous. A proposed “step-by-step” program could facilitate its implementation while yielding uniform results.

Results

The initial phase, or *eligibility for screening*, is performed by family/primary care physicians, who apply the designated inclusion criteria to asymptomatic patients in their consultation. The next phase involves carrying out the screening method (low-dose chest CT, LDCT) in specialized centers, strictly following the guidelines issued by the European Society of Thoracic Radiology (ESTI). The result of the LDCT returns to the requesting physician, who is in charge of the next phase, or *follow-up*. If there is no suspicion of lung cancer, the patient returns to the annual screening, scheduled by the primary care physician. If there are suspicious alterations or a shorter follow-up is required, the patient is referred to a *Pulmonology consultation* designated for this purpose, also in a specialized center. All patients included in the screening and who maintain active smoking habits are referred to the *Smoking Cessation Consultation*.

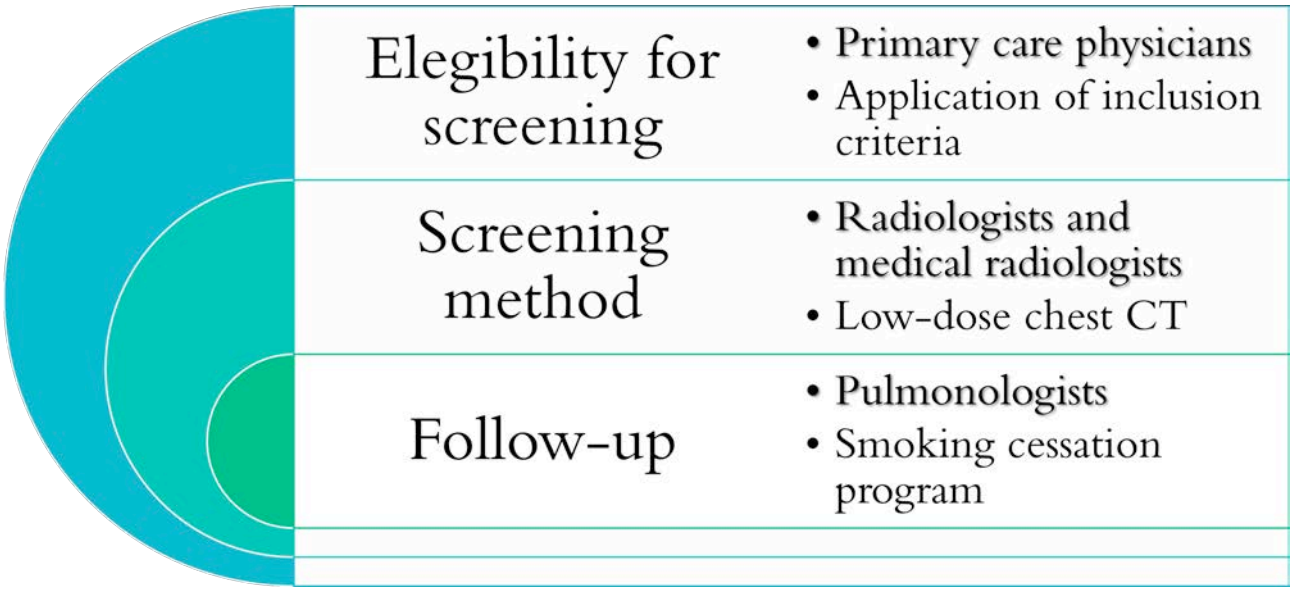

Explanatory diagram of the sequential steps that the lung cancer screening program must follow.

All the referral phases are carried out by health professionals through a **digital application** (resident in Cloud services) that they can access on their computer and/or mobile phone. In addition to recording the patient's data, the application allows access to a **scheduling module**, both for screening availabilities and for the Pulmonology consultation (if the follow-up so requires). The requesting physician is also notified of the **result of the CT report** through the application and is reminded to schedule the patient’s new annual screening (one month in advance). This significantly reduces the waiting time for diagnosis and, potentially, for treatment. Finally, the use of the application reduces dependence on health infrastructures, by streamlining the entire screening process.

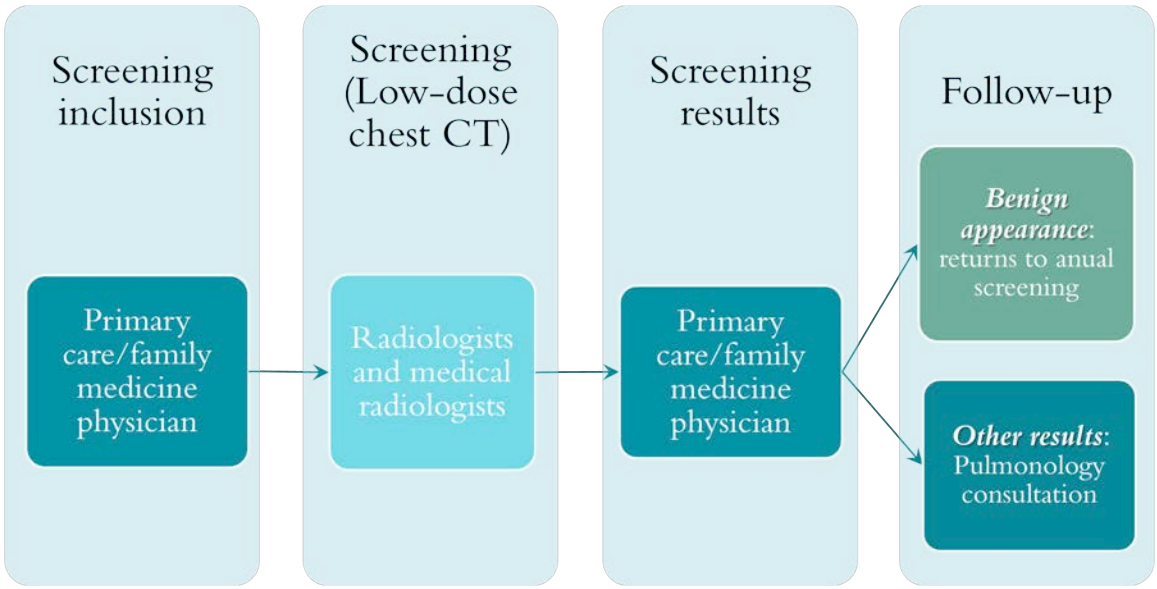

Diagram of the sequential steps and follow-up options after the screening result.

Conclusion

The application of a LCS program should follow a set of sequential steps and requires a multidisciplinary team. The use of a digital application further expedites and uniforms the process.

A-706

Magnetic Resonance Imaging guided Stereotactic Body Radiation Therapy (MRIgSBRT) for lung malignancies: lung toxicity patterns at Computed Tomography (CT).

G. Chiffi[1], C. Strappa[1], A. Del Ciello[2], L. Calandriello[2], G. Cicchetti[2], A. Farchione[2], A. G. Castelli[1], L. Nardini[1], L. Boldrini[3], A. Martino[3], L. Natale[4], A. R. Larici[4]
[1]Università Cattolica del Sacro Cuore, Section of Radiology, Department of Radiological and Hematological Sciences, Rome, Italy, [2]Fondazione Policlinico Universitario "A. Gemelli" IRCCS, Advanced Radiodiagnostic Center, Department of Diagnostic Imaging, Oncological Radiotherapy and Hematology, Rome, Italy, [3]Fondazione Policlinico Universitario "A. Gemelli" IRCCS, Radiation Oncology Unit, Department of Diagnostic Imaging, Oncological Radiotherapy and Hematology, Rome, Italy, [4]Università Cattolica del Sacro Cuore, Fondazione Policlinico Universitario "A. Gemelli" IRCCS, Section of Radiology, Department of Radiological and Hematological Sciences, Rome, Italy

Learning Objectives
- To learn about radiation-induced lung injury (RILI) occurring during the first 12 months after Stereotactic Body Radiation Therapy (SBRT) in patients treated for primary and secondary lung cancers with a 0.35T MR-linear accelerator system (MRIdian, ViewRay Inc, USA).
- To highlight the appearance of MRIgSBRT-induced RILI observed at CT in the early and late phases and their relative frequency in our population.
- To propose a grading system for MRIgSBRT-induced RILI based on their CT extent.

Background
SBRT is currently the treatment of choice in patients with early-stage non-small cell lung cancer (NSCLC) not suitable for surgery. Also, a growing approach to treating oligometastatic lung disease with SBRT is employed.
Despite the widespread use of standard CT based imaging-guided radiotherapy, delivering ablative doses while efficaciously sparing organs at risk (OAR) still represents a challenge.
The recent integration of on board MRI into conventional linear accelerators not only allows for reduced radiation exposure but also enables daily online adaptation of the single treatment fraction. Furthermore, currently the MRIdian system is the only machine that allows a real time direct gating up to 8 frames per second of the therapy volumes.
These unprecedented technological solutions permit significant clinical target volume (CTV) to planning target volume (PTV) margins reduction, thus minimizing OAR dose and potentially toxicity.

Imaging findings OR Procedure details
RILI is a common finding at CT following lung SBRT. Lung abnormalities are conventionally distinguished into *early* and *late*, based on their occurrence after treatment completion, respectively within or after 6 months.
Early lung abnormalities may include areas of ground-glass and consolidation with variable combination and extent, while the late ones consist of fibrotic changes. According to the CT pattern definition already described in the literature in this educational exhibit we will provide a pictorial review of RILI induced by MRIgSBRT in patients treated for early-stage primary lung cancer and pulmonary metastases. We will present the lung abnormalities identified in both early and late phases, describing their CT features in terms of morphology, extent and prevalence, proposing a grading system of RILI based on their CT appearance.

Conclusion
Radiologist should become familiar with innovative RT techniques, as MRIgSBRT, and their potential induced lung abnormalities, in order to allow for correct recognition of expected CT findings, thus contributing to a proper patient management in a multidisciplinary context, while avoiding unnecessary further workup.

References:

[1] Febbo JA, Gaddikeri RS, Shah PN, (2018), Stereotactic Body Radiation Therapy for Early-Stage Non-Small Cell Lung Cancer: A Primer for Radiologists, Radiographics, 1312-1336, 38(5)
[2] Chassagnon G, Martini K, Giraud P, Revel MP, (2020), Radiological assessment after stereotactic body radiation of lung tumours, Cancer Radiotherapy, 379-387, 24(5)
[3] Rammohan N, Randall JW, Yadav P, (2022), History of Technological Advancements towards MR-Linac: The Future of Image-Guided Radiotherapy, Journal of Clinical Medicine, 4730, 11(16)
[4] Corradini S, Alongi F, Andratschke N, Belka C, Boldrini L, Cellini F, Debus J, Guckenberger M, Hörner-Rieber J, Lagerwaard FJ, Mazzola R, Palacios MA, Philippens MEP, Raaijmakers CPJ, Terhaard CHJ, Valentini V, Niyazi M. , (2019), MR-guidance in clinical reality: current treatment challenges and future perspectives, Radiation Oncology , 92, 14(1)
[5] Finazzi T, Haasbeek CJA, Spoelstra FOB, Palacios MA, Admiraal MA, Bruynzeel AME, Slotman BJ, Lagerwaard FJ, Senan S, (2020), Clinical Outcomes of Stereotactic MR-Guided Adaptive Radiation Therapy for High-Risk Lung Tumors, International Journal of Radiation Oncology, Biology, Physics, 270-278, 107(2)
[6] Al-Umairi R, Tarique U, Moineddin R, Jimenez-Juan L, Kha LC, Cheung P, Oikonomou A, (2022), CT patterns and serial CT Changes in lung Cancer patients post stereotactic body radiotherapy (SBRT), Cancer Imaging, 51, 22(1)

A-494

Mediastinal lesions on CT and MRI: a pictorial review

R. Rodrigues Bexiga, C. Mendonça, A. L. Amado da Costa, J. Leitão
Centro Hospitalar Universitário Lisboa Norte, Serviço de Radiologia Geral, Lisboa, Portugal

Learning Objectives
1. To review the International Thymic Malignancy Interest Group (ITMIG) classification of mediastinal compartments.

2. To Describe and illustrate the imaging characteristics of common and uncommon mediastinal lesions on computed tomography (CT) and magnetic resonance imaging (MRI).

Background

The mediastinum contains vascular and nonvascular structures and organs. Division of the mediastinum into compartments is important for the identification and characterization of numerous mediastinal abnormalities. An anatomic scheme based on cross-sectional imaging findings was developed by the ITMIG that can be exploited to localize and characterize mediastinal lesions. The ITMIG classification system divides the mediastinum into prevascular, visceral and paravertebral compartments [1]. Some mediastinal lesions present specific characteristics on CT that allow radiologists to reach a diagnosis, while others may present suggestive but inconclusive imaging findings [1]. MRI provides a more thorough assessment of mediastinal masses due to its superior tissue characterization and excellent contrast resolution, presenting an important role in surgical and treatment planning.

Imaging findings OR Procedure details

Based on our department database, we will present and illustrate the CT and MRI characteristics of common and uncommon mediastinal lesions, emphasizing their imaging features to guide the imager in diagnosing these diverse lesions. Prevascular lesions include thymic lesions (such as thymic hyperplasia, thymic cysts, thymoma, and thymic carcinoma), germ cell neoplasms, metastatic lymphadenopathy, lymphoma, pericardial cysts and intrathoracic goiter. Mediastinal lesions in the visceral compartment include metastatic lymphadenopathy, lymphadenopathy due to granulomatous diseases, cystic lesions such as bronchogenic cysts and esophageal cysts, and vascular lesions arising from the heart or great vessels. Paravertebral compartment lesions include neurogenic tumors, primary osseous tumors and metastases, thoracic spinal infections due to bacterial and mycobacterial agents, thoracic meningocele and neurenteric cyst, and extramedullary hematopoiesis.

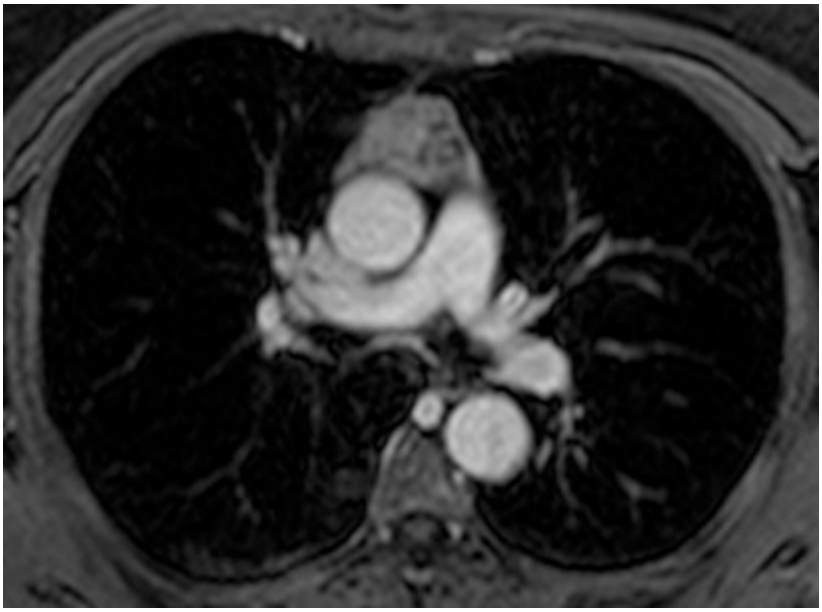

Axial T1-weighted fat-suppressed contrast-enhanced MRI image of a patient with thymoma, presenting as a heterogeneous prevascular mediastinal mass.

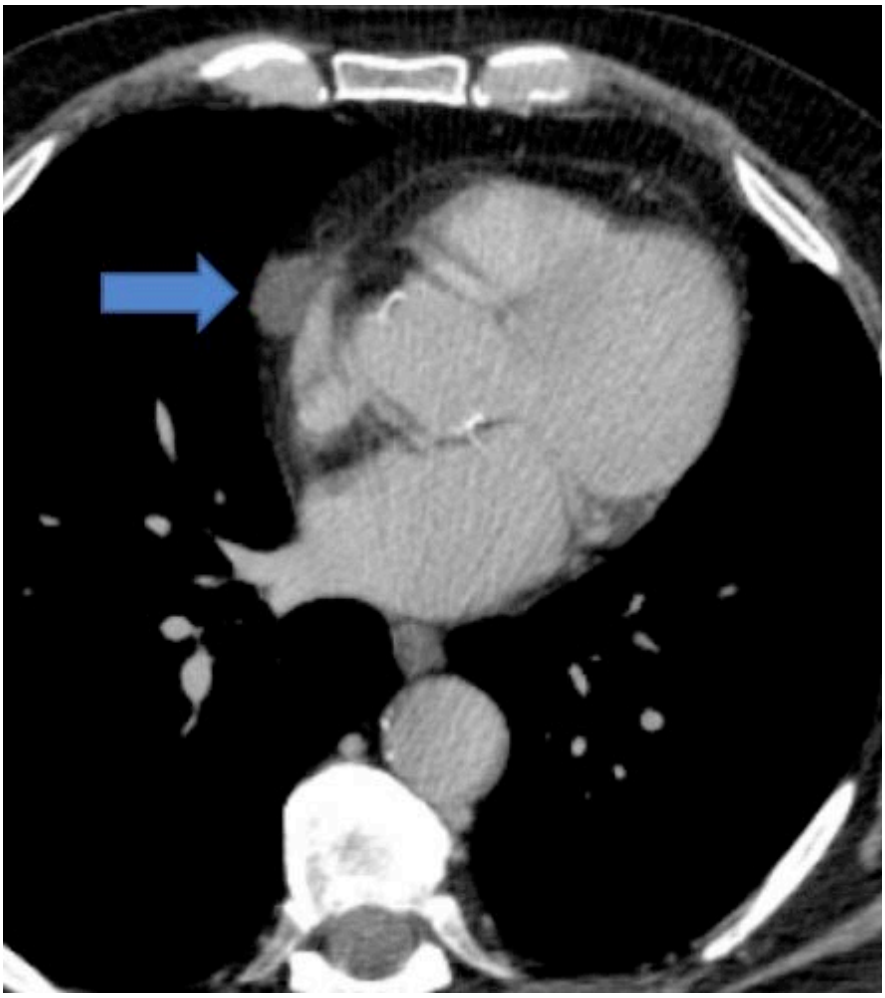

Axial contrast-enhanced CT image of a patient with a pericardial cyst (arrow).

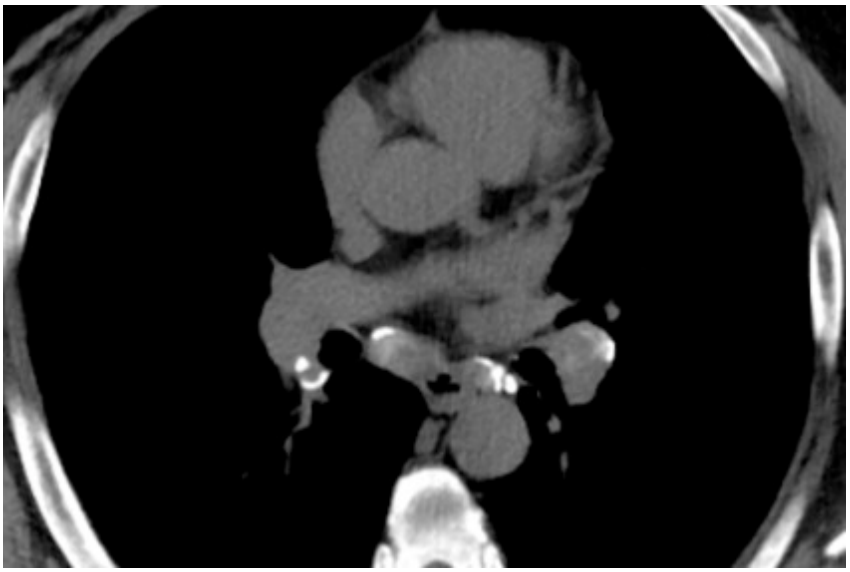

Axial CT image of a patient with sarcoidosis, with calcified mediastinal lymph nodes in the visceral compartment.

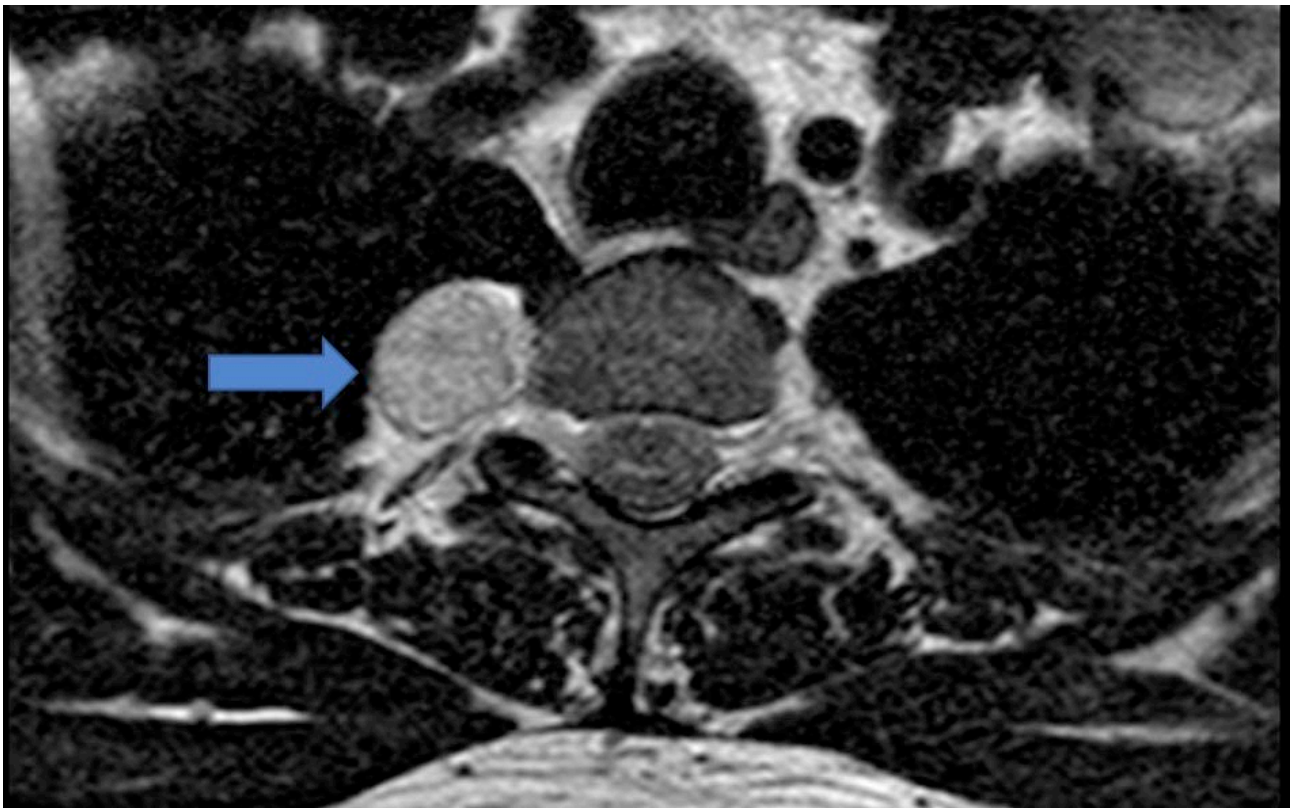

Axial T2-weighted MRI image of a patient with a neurogenic tumor, presenting as a heterogeneously hyperintense lesion in the paravertebral compartment (arrow).

Conclusion

Mediastinal lesions comprise a variety of solid and cystic lesions. Recognition of the mediastinal anatomy and accurate localization and assessment of the imaging characteristics of mediastinal masses is essential in determining the appropriate differential diagnosis.

References:

[1] Carter BW, Benveniste MF, Madan R, Godoy MC, de Groot PM, Truong MT, Rosado-de-Christenson ML, Marom EM., (2017), ITMIG Classification of Mediastinal Compartments and Multidisciplinary Approach to Mediastinal Masses. , RadioGraphics, 413-436, 37

A-544

Metastatic pulmonary calcifications

K. Maurer, O. W. Hamer
University Medical Center Regensburg, Radiology, Regensburg, Germany

Learning Objectives

- Etiology of and patients at risk for metastatic pulmonary calcifications
- Radiographic and CT morphology of metastatic pulmonary calcifications
- Differential diagnoses of metastatic pulmonary calcifications
- Clinical significance of metastatic pulmonary calcifications

Background

Metastatic pulmonary calcifications (MPC) are the morphological correlate of a metabolic disease. They occur most often in association with conditions that cause hypercalcemia and/or hyperphosphatemia. The typical patient at risk suffers from chronic renal failure and consecutive hyperparathyroidism. However, many more conditions, both benign and malignant, can cause MPC. Most patients are asymptomatic but some develop dyspnea and chronic dry cough.

Imaging findings OR Procedure details

Chest radiographs can be normal or demonstrate patchy to confluent airspace opacities. High resolution CT most often shows characteristic “fluffy” centrilobular ground glass opacities sized 3-10 mm. At the beginning calcific nature is not obvious but becomes visible with ongoing disease. In severe cases consolidation occurs. The upper lobes are predominantly involved because the alcalic milieu in the apices facilitates the deposition of calcium salts. An associated finding frequently observed is wall calcification of vessels in the chest wall.

Differential diagnoses

Although in the correct clinical setting the CT morphology is virtual pathognomonic the ground glass appearance can be misleading and trigger the diagnosis of an airspace disease like pneumonia or
alveolar hemorrhage. Also edema, hemosiderosis, metastases and alveolar microlithiasis might be mistakenly suspected.

Conclusion

The educational poster will review the etiology, physiology and clinical setting of MPC. Morphology of MPC on chest radiograph and CT will be demonstrated in detail. Differential diagnoses will be discussed.

A-711

Minute pulmonary meningothelial-like nodules – role of radiology in MPMNs.

W. Bernard, M. Jelitto, E. Szurowska
University Clinical Centre of Gdańsk, Department of Radiology, Gdansk, Poland

Learning Objectives

 To list radiological features of minute pulmonary meningothelial-like nodules (MPMNs) and to increase awareness of the disease.
 To summarise up-to-date knowledge concerning clinical considerations and management.
 We enclose a case of diffuse pulmonary meningotheliomatosis diagnosed in our clinical centre, as an example of an uncommon MPMNs manifestation.

Background

Lung cancer screening programmes implemented worldwide have popularised the concept of performing low-dose computed tomography (CT) of the chest. Obtaining such immense amount of data has led to revealing multiple accessory findings in lung parenchyma, such as minute pulmonary meningothelial-like nodules (MPMNs).
MPMNs are sporadic lesions of benign nature, though a common incidental finding in surgical specimens and autopsy examinations. MPMNs are reported to coexist with malignant pulmonary tumours and can mimic neoplastic lesions. Radiologically, it is difficult to distinguish MPMNs from early-stage lung cancer, therefore active surveillance should be considered.
Particular types of immunohistochemical staining can reveal features consistent with MPMN diagnosis.

Imaging findings OR Procedure details

MPMNs typically manifest on CT imaging as tiny (or: minute) round centrilobular nodules with smooth margins, mostly of ground-glass density. Usually the lesions measure up to 5 mm in diameter and exhibit a tendency to be located in subpleural lung zones.
When nodules are diffusely distributed in the lungs they are termed diffuse pulmonary meningotheliomatosis.
Due to lack of specific CT features of MPMNs, they should be considered in differential diagnosis with other entities of similar pattern, such as non-fibrotic hypersensitivity pneumonitis, vasculitis or adenocarcinoma in situ.

We report a case of a 75-year old man, asymptomatic former smoker who presented with innumerable diffuse centrilobular ground-glass nodules located mostly in the lung periphery. Due to suspicion of malignancy, lung cryobiopsy was performed. Histopathological examination of obtained tissue samples was indicative for MPMN. Pulmonary lesions remained stable on CT imaging within 2-year follow-up period.

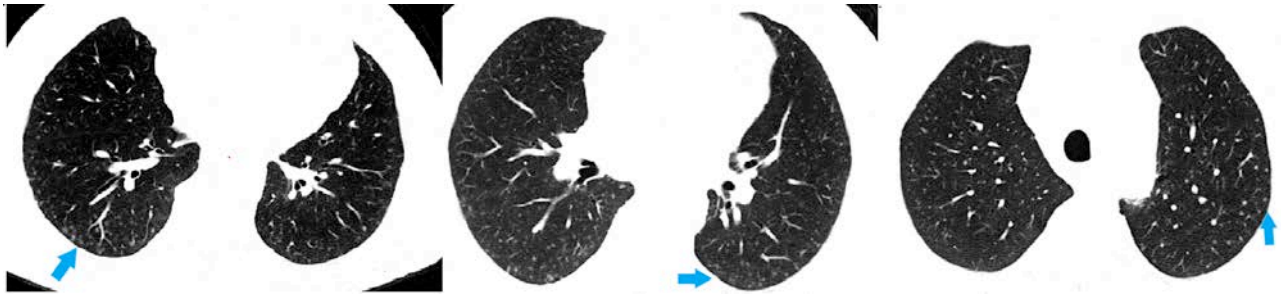

CT images of our patient show multiple subcentimeter ground-glass nodules, visible in both lungs..

Conclusion

Minute pulmonary meningothelial-like nodules are considered infrequent entities, however should be considered in differential diagnosis of diffuse micronodular pattern.
Histopathological examination is required to confirm the diagnosis.
Active CT surveillance may be essential for avoiding misdiagnosis, especially in cases of clinical suspicion of lung malignancy.

A-528

MRI: the key to understanding thymus

G. Mancò, M. Scutti, V. Caruso, A. Travaglini, M. Mereu, R. L. Patea, M. Caulo
Università degli studi, Chieti, Italy

Learning Objectives

Try to be more confident with MRI mediastinal and thymic lesions.

Background

Mediastinal masses and in particular thymic lesions are often difficult to characterize with computerized tomography (CT) and CT images are frequently indeterminate, instead Magnetic Risonance Imaging (MRI) in many cases is decisive. MRI provides excellent soft tissue contrast and so represent a noninvasive way to further characterize mediastinal lesions, their site of origin and their involvement of adjacent structures.

The most commonly used MRI sequences for thymus evaluation include[1]: T1-weighted (T1WI; in- and out of phase, useful for individuate the presence of fat within a lesion); T2-weighted (T2WI-useful for evaluating the tissue characteristics of the thymus); Gradient-echo imaging (used to evaluate the presence of hemorrhage or calcification); Contrast-enhanced imaging (tumor vascularity and can aid in the diagnosis of thymic malignancies); Diffusion-weighted imaging (DWI-useful for evaluating the cellular density of thymic tumors and for differentiating benign from malignant thymic lesions).

Imaging findings OR Procedure details

Among benign lesion, there is thymic hyperplasia that typically appears as a well-defined, homogeneous mass that is isointense to muscle and on in-phase and opposed-phase demonstrate an apparent decrease in signal intensity[2].

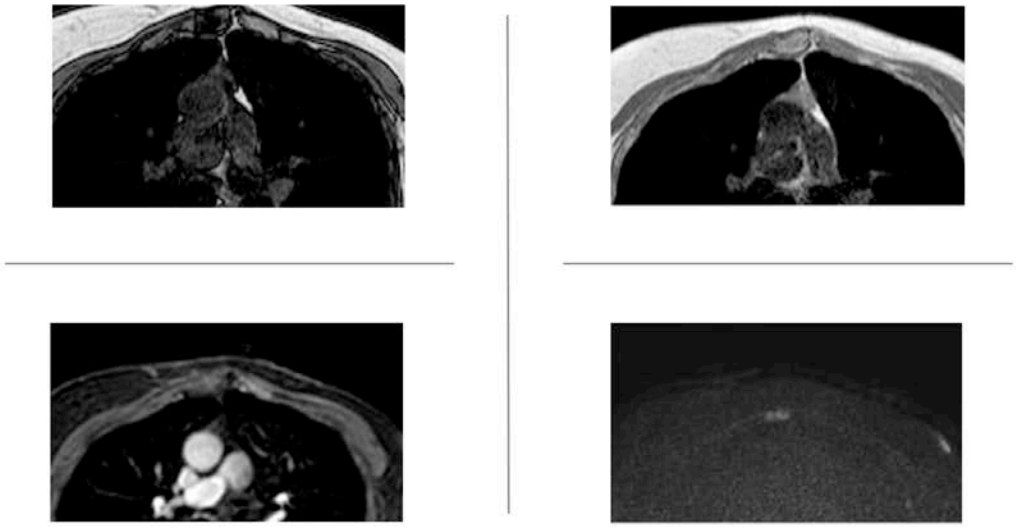

THYMIC HYPERPLASIA

In-phase and opposed-phase are also essential for thymolipoma; indeed, in these sequences there is a decrease in signal intensity because of the fat component, while the soft tissue component may have variable signal intensity on both T1 and T2-WI.

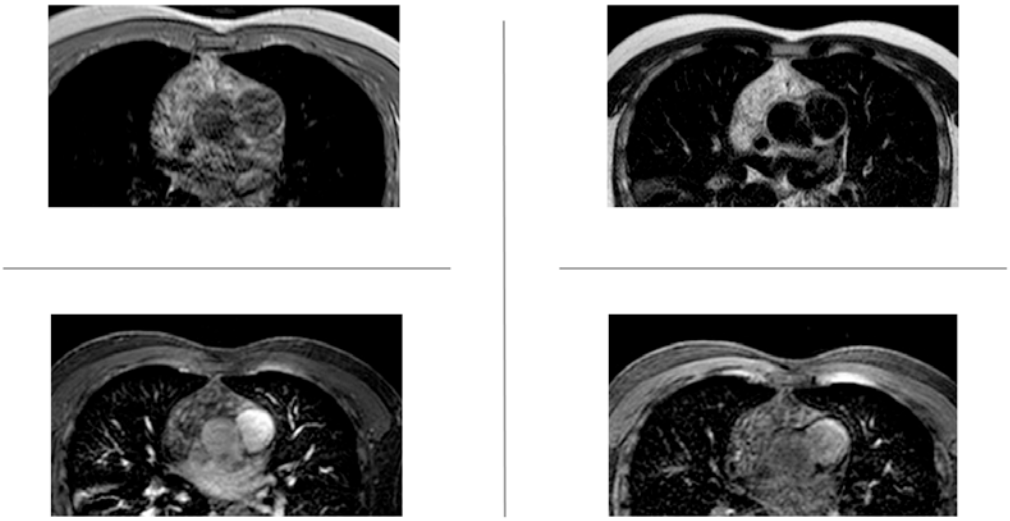

THYMOLIPOMA

Thymic cyst typically appears as well-circumscribed, T1-hypointense and T2-hyperintense lesions. The signal intensity of the cyst contents may vary depending on the fluid content and protein concentration.

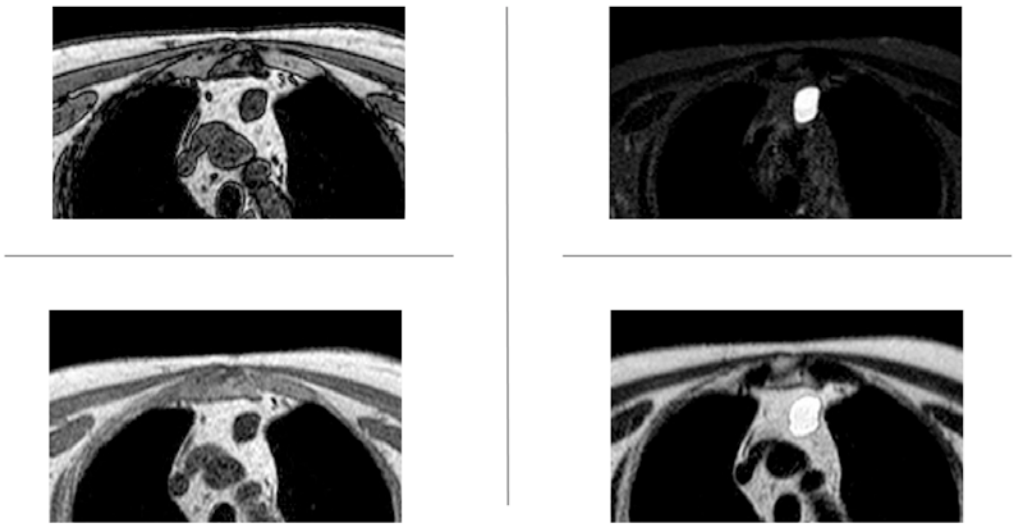

THYMIC CYST

Contrast-enhanced MRI and DWI can also be useful in the evaluation of benign lesion, as it can help differentiate hyperplasia from other thymic pathologies, such as thymomas or lymphomas, which typically show heterogeneous enhancement and high signal intensity due to increased cellular density. Thymic tumors have different signal abnormalities; in particular, in- and out of phase T1WI demonstrate no change in signal intensity in thymic epithelial tumors. T2-WI could also show a lobulated border, fibrous septa, and lobulated internal architecture, characteristic mostly of invasive tumor. It may also demonstrate areas of necrosis of hemorrhage, which can be seen as area of T1 hyperintensity or T2 ge hypointensity, respectively.[3]

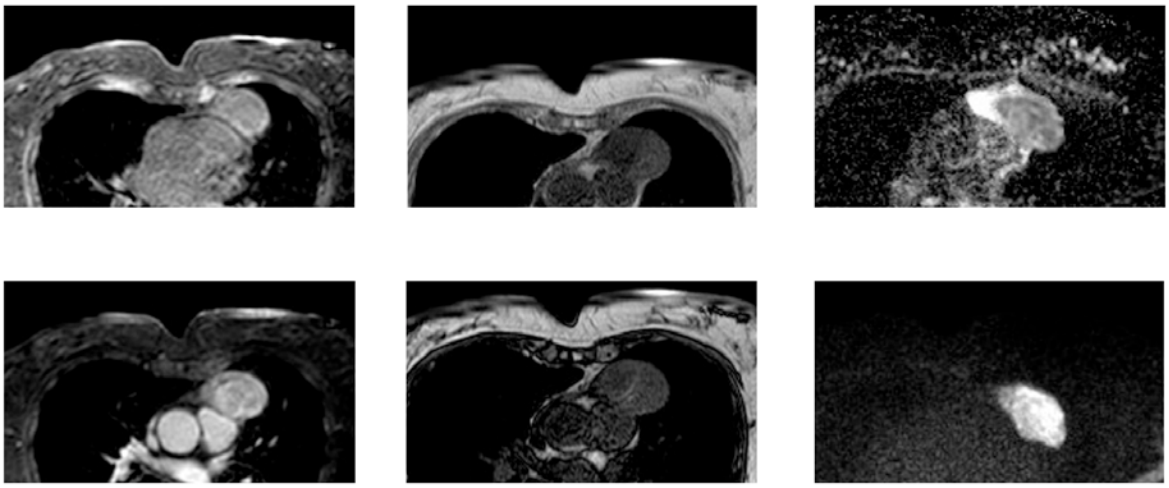

THYMOMA

Conclusion

Even if is underutilized, MRI is not only a winning weapon for the characterization of the thymic lesions, but it is also fundamental for correct patient management and for choosing the most suitable diagnostic and therapeutical iter.

References:

[1] Jeanne B.Ackmann and Carol C.Wu, (2011), MRI of the thymus, AJR online

[2] Dania Daye and Jeanne B. Ackman , (2017), Characterization of mediastinal masses by MRI: techinques and application – , Applied Radiology

[3] Tsutomu Inaoka, Koji Takashi, Masayuki Mineta, Tomonori Yamada, Noriyuki Shuke, Atsutaka Okizaki, Kenichi Nagasawa, Hiroyuki Sugimori, Tamio Aburano , (2007), Thymic Hyperplasia and Thymus Gland Tumors: differentiation with chemical shift MR imaging , Radiology

A-484

Multimodal Imaging Findings of Axillary Lymphadenopathy Associated with COVID-19 Vaccination

J. Y. Rho, S. R. Kang
Wonkwang University Hospital, Wonkwang University College of Medicine, Diagnostic radiology, IKsan, Republic of Korea (South Korea)

Learning Objectives
The purpose of this study was to review the multimodal imaging findings for axillary LAP associated with COVID-19 vaccination and investigate how they changed on follow-up imaging.

Background
The incidence of axillary lymphadenopathy (LAP) associated with COVID-19 vaccination is increasing, and it is being observed on breast, chest, and PET/CT imaging in patients with cancer, especially those who have received treatment involving the axillary lymph nodes (e.g., breast cancer). Axillary LAP may persist for several weeks after vaccination in these patients and can be misdiagnosed as metastatic LAP.

Imaging findings OR Procedure details
Axillary lymphadenopathy (LAP) associated with COVID-19 vaccination has been reported in up to 16% of cases to date. It is more likely to occur within two weeks after vaccination and is frequently noted within four weeks, indicating that immediate LAP after vaccination is more likely to be caused by the vaccine. Most abnormal lymph nodes showed local or diffuse cortical thickening >3mm on axillary ultrasound, and hypoechoic lymph nodes were more commonly involved. There is an overlap in the imaging findings between reactive and malignant LAP, which makes it challenging to differentiate from metastatic disease based on morphology or location. Axillary LAPs were identified in chest CT as an incidental finding or during a targeted screening or diagnostic procedure. PET/CT images revealed FDG-avid lymph nodes ipsilateral to the vaccine injection in 54% of cases, with a mean SUVmax of 5.1 ± 2.1 (range 2.0 – 17.3). Additionally, axillary lymphadenopathy with FDG uptake appeared most often one to seven days after vaccination and exhibited a negative correlation with time after vaccination.

Conclusion
By showing multimodal imaging results for axillary LAPs associated with COVID-19 vaccination for patients with cancer, particularly breast cancer, it can help radiologists avoid useless diagnostic imaging and invasive procedures. Additionally, the importance of providing accurate vaccination histories to radiologists is even more evident.

A-752

Multimodality Imaging Strategies for Safe and Effective Diagnosis in Pregnancy

Y. Liberman, G. Gittens, A. Liubauske, G. Borisovsky, R. Liubaskas, D. Litmanovich
Harvard Medical School- Beth Israel Deaconess Medical Center, Radiology, BOSTON, United States of America

Learning Objectives

Maternal mortality in the US is on the rise, with cardiopulmonary diseases as the leading cause at ~15.5% of all pregnancy-related deaths. Cardiovascular imaging modalities may be needed because of a variety of reasons, such as a previous known cardiovascular disease, hemodynamic changes during pregnancy, trauma and more.

Certain modalities used for cardiac imaging may present a risk to either or both mother and fetus. At the same time, certain emergency situations may require cardiovascular screening in which the risk of the exam is outweighed by the risk of cardiovascular damage on the fetus and/or mother.

It is important for every clinician to know which imaging methods are available to them when dealing with a pregnant patient to offer the best and safest care, and how to modify tests as needed depending on the needs and wants of the patient.

Background

In this educational exhibit we aim to review the different imaging tools that can be used for cardiovascular imaging in pregnancy, and identify which medical conditions they can be used to diagnose. We will cover different scenarios in which we can adjust the screening process to meet the needs of the patient while inflicting minimal risk to the mother and fetus. We will provide a suggested algorithm for appropriate use of various imaging modalities based on clinical condition, patient pregnancy age and local existing expertise.

Imaging findings OR Procedure details

We will address both radiation dose related risks and contrast material pertinent pregnancy related issues and potential strategies to overcome those challenges.

Conclusion

Cardiovascular imaging during pregnancy is usually done in life-threatening conditions. It is necessary to be cautious about possible risk and side effects. Imaging modality should be selected from the least risky for both mother and fetus and benefits have to justify the potential risk.

A-204

Non-tuberculous mycobacterial pulmonary disease (NTM-PD): imaging findings of a diagnostic and therapeutic challenge

L. Nardini[1], G. Cicchetti[2], L. Iaccarino[1], L. Calandriello[2], A. del Ciello[2], A. Farchione[2], F. Castaldo[1], F. Taccari[3], G. Montemurro[4], L. Natale[1,2], A. R. Larici[1,2]

[1]Università Cattolica del Sacro Cuore, Section of Radiology, Department of Radiological and Hematological Sciences, Rome, Italy, [2]Fondazione Policlinico Universitario "A. Gemelli" IRCCS, Advanced Radiodiagnostic Center, Department of Diagnostic Imaging, Oncological Radiotherapy and Hematology, Rome, Italy, [3]Fondazione Policlinico Universitario A. Gemelli IRCCS, Department of Laboratory and Infectious Diseases Sciences, Rome, Italy, [4]Fondazione Policlinico Universitario "A. Gemelli" IRCCS, Department of neuroScience, Sensory Organs and Chest, Rome, Italy

Learning Objectives

- To review the most common radiological findings of non-tuberculous mycobacterial pulmonary disease (NTM-PD).
- To learn about the role of radiologists in diagnosis and follow-up of NTM-PD.

Background

NTM-PD represents a chronic pulmonary infection caused by a wide range of mycobacteria species, characterized by both airways and parenchymal involvement. The incidence and prevalence of NTM-PD has recently increased worldwide. Nonetheless, its diagnosis is still challenging due to its non-specific clinical features, poor knowledge of the disease and wide range of radiological findings. Moreover, NTM-PD therapy requires long antibiotic regimens, which may last till 24 months, burdened by the risk of developing treatment intolerance or failure.

Thoracic imaging plays a key role in both diagnosis and follow up of NTM-PD. Indeed, chest X-ray is a low-dose, low-cost and widely available technique, thus representing the initial investigation, although it may often underestimate the disease burden or show non-diagnostic features. On the other hand, high- resolution computed tomography (HRCT), due to its major sensitivity, represents the main diagnostic examination for NTM-PD evaluation, despite the higher costs, and radiation exposure.

Imaging findings OR Procedure details

NTM-PD demonstrates two main radiological presentations. Fibrocavitary NTM- PD is commonly seen in elderly males, with smoking history and pre-existing lung disease and it is characterized by consolidations/opacities and cavities, with an upper lobe predominance, therefore mimicking pulmonary tuberculosis.

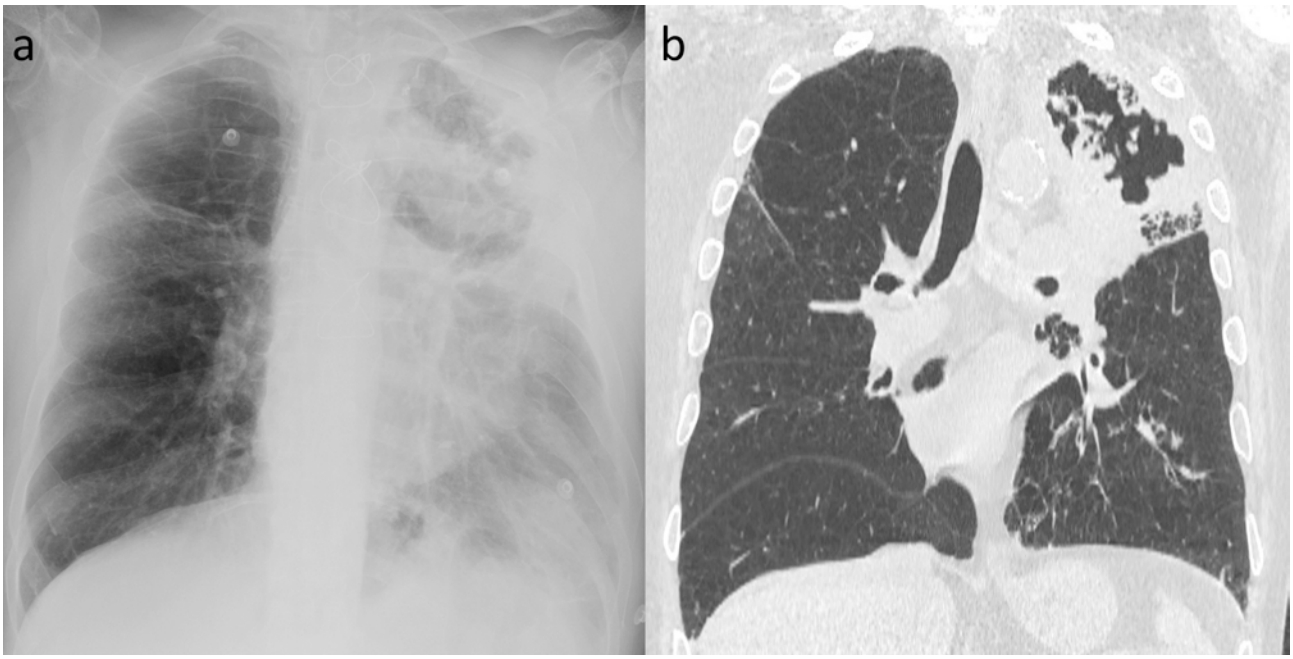

Fig1. Fibrocavitary form of NTM-PD. Chest X-ray (a) and coronal multiplanar CT scan reconstruction (b) showing a large, thick-walled cavitation with irregular margins in the left upper lobe, in a 82-year-old man with a lifetime smoking history of 50 pack-yrs; note CT signs of confluent emphysema and diffuse bronchial wall thickness.

On the contrary, nodular-bronchiectatic NTM-PD shows bronchiectasis, bronchial wall thickening with mucoid impaction, multiple centrilobular nodules and "tree-in-bud" pattern, more frequently in the right middle lobe and in the lingula, and it often affects women during post- menopause or patients without previous smoking history. This form requires differential diagnosis with other causes of bronchiolitis, such as atypical infections and cystic fibrosis among the others.

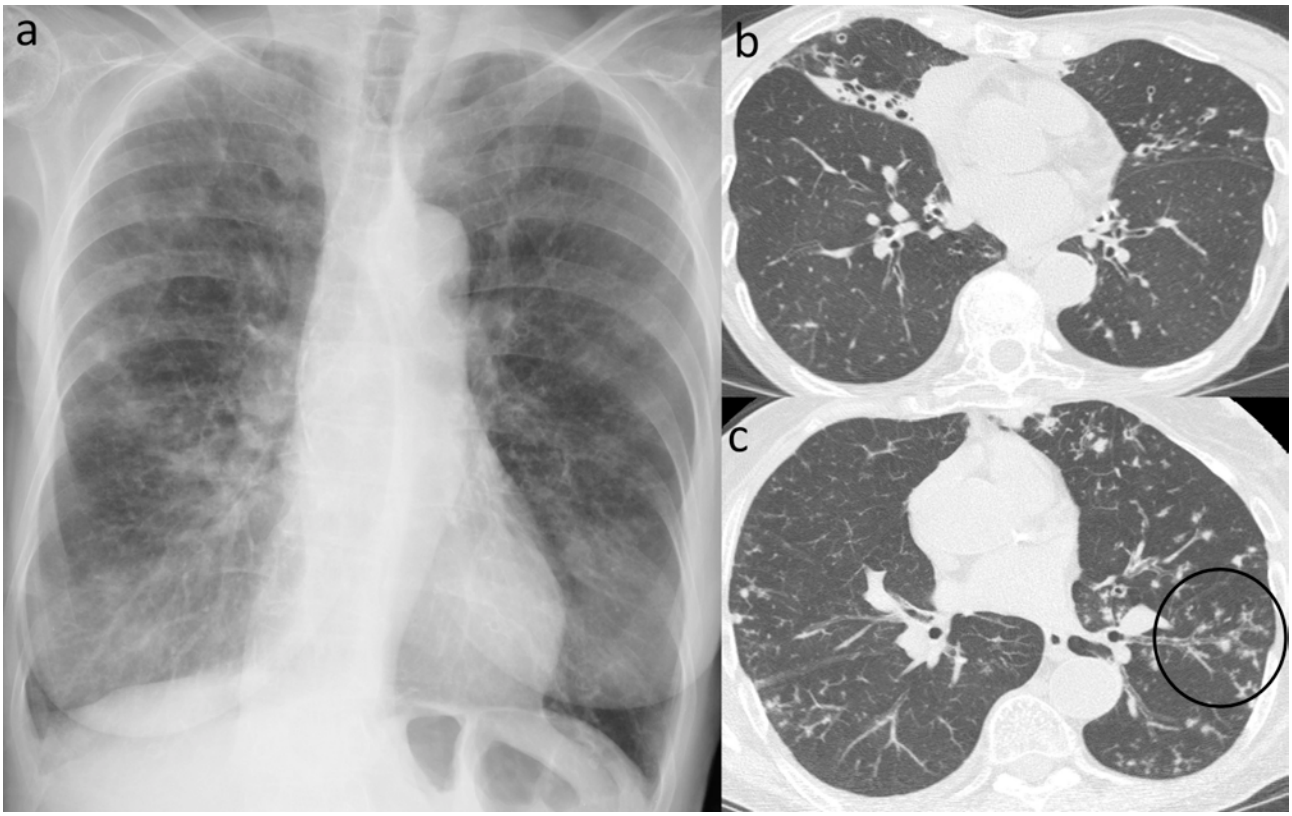

Fig2. Nodular-bronchiectatic form of NTM-PD. Chest X-ray (a) and axial CT scans (b, c), depicting multifocal bronchiectasis, partial atelectasis of the right middle lobe and extensive signs of bronchiolitis, with diffuse bronchial wall thickening, mucoid impaction and multiple centrilobular nodules with 'tree in bud' pattern (black circle).

In this educational exhibit we will focus on the imaging spectrum of NTM-PD, taking into consideration possible differential diagnosis, prognostic factors and response to treatment.

Conclusion

Radiologists should be aware of the wide range of CT appearance of NTM-PD, in order to postulate the diagnosis (which requires microbiological confirmation), to categorize the different forms of disease and to define radiological prognostic factors. Furthermore, in a multidisciplinary setting, they play a central role in the evaluation of treatment response at follow-up, favoring a proper management of NTM-PD patients.

References:

[1] Haworth CS, Banks J, Capstick T, Fisher AJ, Gorsuch T, Laurenson IF, Leitch A, Loebinger MR, Milburn HJ, Nightingale M, Ormerod P, Shingadia D, Smith D, Whitehead N, Wilson R, Floto RA, (2017), British Thoracic Society guidelines for the management of non-tuberculous mycobacterial pulmonary disease (NTM-PD), Thorax, 72(Suppl 2):ii1-ii64

[2] Griffith DE, Aksamit T, Brown-Elliott BA, Catanzaro A, Daley C, Gordin F, Holland SM, Horsburgh R, Huitt G, Iademarco MF, Iseman M, Olivier K, Ruoss S, von Reyn CF, Wallace RJ Jr, Winthrop K; ATS Mycobacterial Diseases Subcommittee; American Thoracic Society; Infectious Disease Society of America, (2007), An official ATS/IDSA statement: diagnosis, treatment, and prevention of nontuberculous mycobacterial diseases, Am J Respir Crit Care Med, 175(4):367-416

[3] Musaddaq B and Cleverley JR, (2020), Diagnosis of non-tuberculous mycobacterial pulmonary disease (NTM-PD): modern challenges, Br J Radiol , 93: 20190768

[4] Anjos LRBD, Parreira PL, Torres PPTS, Kipnis A, Junqueira-Kipnis AP, Rabahi MF, (2020), Non-tuberculous mycobacterial lung disease: a brief review focusing on radiological findings, Rev Soc Bras Med Trop, 53:e20200241

[5] Lee G, Lee KS, Moon JW, Koh WJ, Jeong BH, Jeong YJ, Kim HJ, Woo S, (2013), Nodular bronchiectatic Mycobacterium avium complex pulmonary disease. Natural course on serial computed tomographic scans., Ann Am Thorac Soc, 10(4):299-306

[6] Cowman SA, Jacob J, Obaidee S, Andres Floto R, Wilson R, Haworth CS, Loebinger MR, (2018), Latent class analysis to define radiological subgroups in pulmonary nontuberculous mycobacterial disease, BMC Pulm Med, 18(1):145

A-175

Organizing Pneumonia - A pictorial essay of HRCT manifestations

I. Mata, C. Leal, O. Fernandes
Centro Hospitalar Universitário Lisboa Central, Radiology, Lisboa, Portugal

Learning Objectives

To review and illustrate the imaging findings spectrum of organizing pneumonia (OP) on high-resolution CT (HRCT).
To emphasize the importance of recognizing the classical and atypical patterns of OP for diagnosis and treatment management.

Background

OP is a non-specific tissue repair reaction to multiple types of acute lung injuries (namely, infections, drug toxicity, connective tissue diseases, organ transplant or radiotherapy) or another lung patology (such as vasculitis, neoplasms or interstitial lung diseases). On the other hand, cryptogenic organizing pneumonia (COP) is a rare idiopathic form of OP.
Clinical and radiological features are similar in secondary organizing pneumonia (SOP) and COP. Classical symptons include mild dyspnea, cough and malaise that can became severe and usualy have a subacute course. Differentiating between secondary organizing pneumonia and cryptogenic organizing pneumonia is crucial, as treatment strategies vary according to the underlying cause.
The definitive diagnosis of OP is histologically established, even though a multidisciplinary approach with radiological and clinical expertise could support the diagnosis and eliminate unnecessary lung biopsies.

Imaging findings OR Procedure details

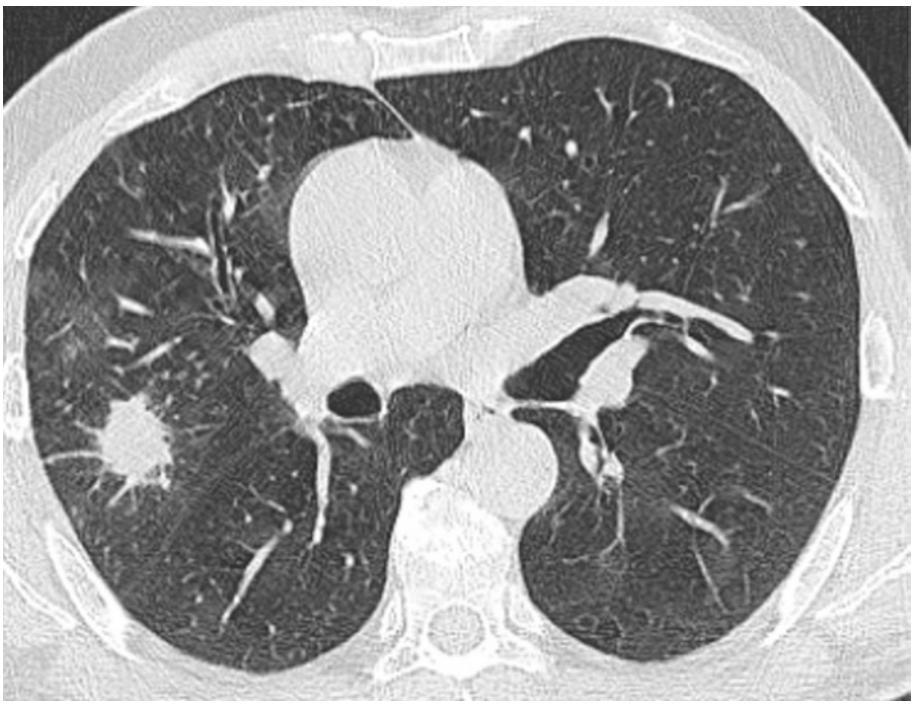

Nodular form of OP. OP diagnose was establish on lung biopsy.

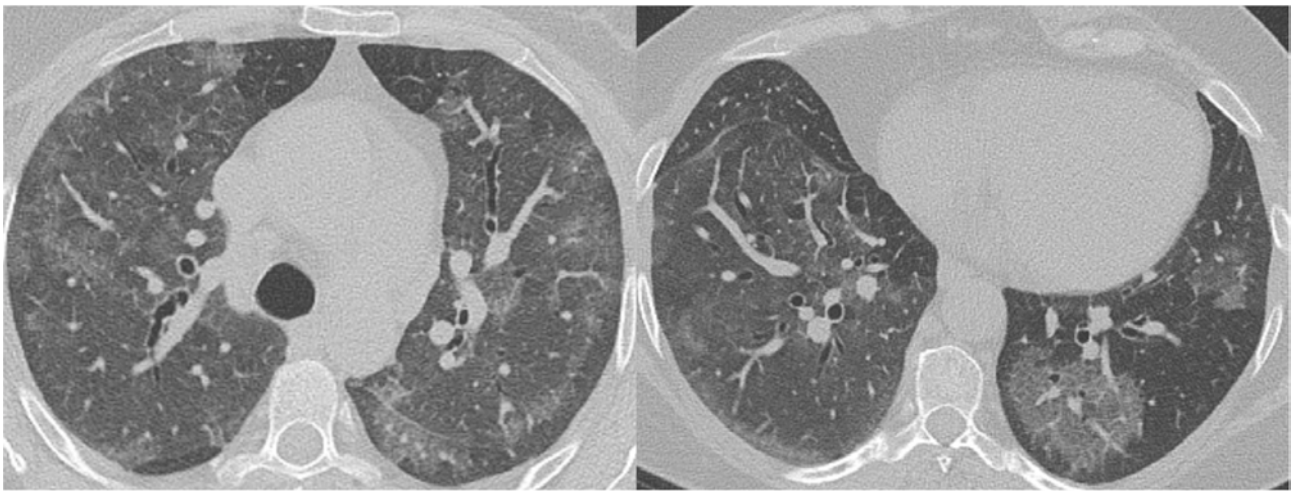

Female patient with history of undifferentiated connective tissue disease and secondary OP presenting on HRCT as bilateral sub-pleural and peri-bronchovascular areas of ground gland opacities.

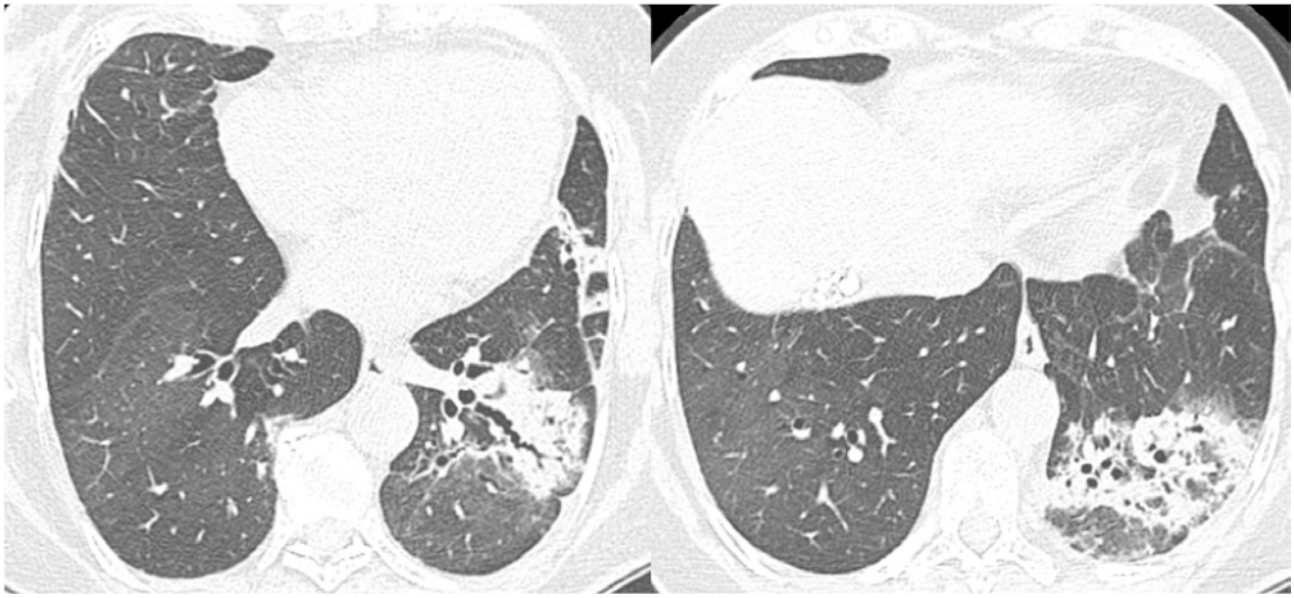

Sub-pleural and peri-broncovascular consolidations in left lower lobe secondary to OP in a female patient with history of breast cancer who underwent lumpectomy and radiotherapy.Complete regression of parenchymal lung changes was observed after initiation of corticosteroid therapy.

We retrospectively have reviewed some of the HRCT lung studies of our hospital to illustrate the different patterns of organizing pneumonia (OP).

Classic manifestations include: migratory areas of consolidation that may be associated with traction bronchiectasis and ground-glass opacities (GGO). Focal consolidation, nodular forms, linear/band-like, perilobular opacities, reversed halo opacity are another variants patterns of OP described in literature.

Conclusion

The HRCT patterns of OP are heterogeneous, given that, there are a multiple differential diagnoses to consider. Radiologists must be familiarized with spectrum manifestations of OP to successfully establish diagnosis since untreated cases can progress into a chronic fibrosing form of OP which negatively affect patient's prognosis. A multidisciplinary approach that combines patient history and clinical findings could suggest a diagnosis.

References:

[1] R. Polverosi, M. Maffessanti, G. Dalpiaz, (2006), Organizing pneumonia: typical and atypical HRCT patterns, La radiologia medica, 111, 202–212

[2] Talmadge E. King, Jr., M.D., Joyce S. Lee, M.D., (2022), Cryptogenic Organizing Pneumonia, The New England Journal of Medicine, 1058-69, 386

[3] Anastasia Oikonomou David M Hansell, (2002), Organizing pneumonia: the many morphological faces, European Radiology, 1486–1496, 12

[4] M. Baque-Justona, A. Pellegrin, S. Leroyb, C.H. Marquetteb, B. Padovania, (2014), Organizing pneumonia: What is it? A conceptual approach and pictorial review, Diagnostic and Interventional Imaging , 771—777, 95

[5] Sujith V. Cherian, Dhara Patel, Stephen Machnicki, David Naidich, Diane Stover, et al., (2022), Algorithmic Approach to the Diagnosis of Organizing Pneumonia: A Correlation of Clinical, Radiologic, and Pathologic Features, Chest, 156-178, 162

A-442

Osteoporosis in smokers

I. Willekens
UZ Brussel, Brussels, Belgium

Learning Objectives
Screening for osteoporosis is necessary in cigarette smoking people.
Background
Osteoporosis is a common disease that is characterized by deterioration in bone strength. Cigarette smoking is associated with reduced bone mineral density (BMD) and increased fracture risk.
Imaging findings OR Procedure details
Dual-energy x-ray absorptiometry (DXA) is the most widely used method for measuring BMD.
Quantitative computed tomography (QCT) measures volumetric bone density of the spine and can analyze cortical and trabeculair bone separately.
Conclusion
Cigarette smoking is a reversible risk factor for osteoporosis and osteoporotic fractures.Screening for osteoporosis is necessary in smokers.

A-353

Pericardial diverticulum arising from the right lateral superior aortic recess of the pericardium: demonstration of representative cases

S.-J. Yoo, M. S. Kim, Y. W. Choi
Hanyang University Hospital, Seoul, Republic of Korea (South Korea)

Objectives

Pericardial diverticula may appear as a mediastinal cystic mass and may be distinguished from pericardial cysts because the former retain communication with the pericardial space and change in size with changes in body position or breathing as opposed to pericardial cysts which have a constant size. We recently reported that a pericardial diverticulum may arise from the right lateral portion of the superior aortic recess (SAR) which is the most superior division of the transverse sinus. We'll demonstrate representative cases of the pericardial diverticulum arising from the right lateral superior aortic recess (RSAR).

Methods & Materials

We defined a pericardial diverticulum of the RSAR as a well-circumscribed, fluid-attenuation lesion in the anterior mediastinum with communication with the RSAR, no enhancing wall, molding by adjacent structures, and an acute angle with the cardiac border or an imaginary line connecting the anterior margins of the ascending aorta and superior vena cava on CT. We'll demonstrate serial CT features of the diverticulum.

Results

The pericardial diverticulum present as a cystic anterior mediastinal mass communicating with the RSAR. Although the largest diverticular part is usually on the same axial image with the RSAR, it is sometimes above or below the RSAR. On follow-up CT studies, the diverticulum shows size fluctuations, which sometimes disappears or decreases in size with loss of a connection with the RSAR.

Conclusion

If there is an anterior mediastinal cystic mass, a careful search for its connection to the RSAR on all available CT images, including past studies, is required for the diagnosis of pericardial diverticulum of the RSAR.

A-387

Pericardial mesothelioma: a case report.

B. Hervás-Sanz[1], P. C. Notta[1], L. M. Gràcia-Sánchez[1], L. Rodríguez-Bel[1], S. A. Bolívar-Cuevas[2], D. Castellón-Plaza[2], I. E. Sánchez-Rodríguez[1], D. Plaza-González[3], M. Cortés-Romera[1]
[1]Bellvitge Universitary Hospital-IDIBELL, Nuclear Medicine-PET (IDI) Department, L'Hospitalet de Llobregat, Spain, [2]Bellvitge Universitary Hospital-IDIBELL, Radiology Department, L'Hospitalet de Llobregat, Spain, [3]Bellvitge Universitary Hospital-IDIBELL, Administrative Department, L'Hospitalet de Llobregat, Spain

Learning Objectives

The aim of this poster is to perform a correct differential diagnosis (DD) and to recognize the characteristic features visualized on [18F]FDG-PET/CT, of an uncommon neoformative process, such as pericardial mesothelioma (PM).

Background

Primary PM is an extremely rare neoplasm, more frequent in males with a mean age of 46 years.
Clinically it is manifested by dyspnea and pericardial effusion.
Its final diagnosis is obtained by biopsy, although frequently, it is obtained directly in post-mortem analysis.
Our case is a 48-year-old man who came to the emergency department with chest tightness and dry cough of one month's evolution, for which a chest X-ray was performed, showing cardiomegaly with suspected pericardial effusion, hence he was admitted for study.
Several imaging tests were performed, including [18F]FDG-PET/CT, biopsies and anatomopathological analysis in which mesenchymal cells were visualized, making the final diagnosis of metastatic MP.

Imaging findings OR Procedure details

On MIP we observed a large uptake in mediastinum as well as small thoracic deposits and visualization of bone marrow that would show underlying infiltration.
In the axial fusion images we located the extensive heterogeneous mediastinal uptake, with cardiac extension, corresponding to primary tumorization, as well as severe pericardial effusion.
Multiple metastatic pulmonary nodules and small deposits corresponding to suspicious adenopathies.
Such findings raise the DD between lymphoproliferative process and pericardial tumorization.

Conclusion

MP is a very infrequent process, with unfavorable prognosis. The [18F]FDG-PET/CT allows to study its metabolism, extension, as well as to make a DD between the different possibilities.

A-283

Pleuroparenchyal Fibroelastosis

M. Pringle, P. Garmany
NHS Greater Glasgow and Clyde, Radiology, Queen Elizabeth University Hospital, Glasgow, United Kingdom

Learning Objectives
Discuss pathophysiology and characteristic imaging findings of pleuoroparenchymal fibroelastosis (PPFE).
Background
PPFE is a rare but increasingly recognised interstitial lung disease (ILD), which predominantly involves the upper lobes. Onset is typically between 40-70 years and no gender predilicition [1]. It may be idiopathic, or occur in association with connective tissue diseases or previous insults such as chemotherapy. The disease can co-exist with other forms of ILD or can occur in isolation [2].

Symptoms of PPFE include non-productive cough, dyspnoea and weight loss[1]. Diagnosis is made by a combination of imaging and histology, however wedge resection is rarely possible in patients with advanced disease. Therefore, the role of imaging is particularly important. Histological features include a subpleural distribution of elastofibrosis: dense accumulation of elastic fibres with collapsed alveoli, intra-alveolar collagenous fibrosis with septial fibrosis and collagenous thickening of the visceral pleura[3].

PPFE has a progressive clinical course, and there is no disease-specific management.

Imaging findings OR Procedure details
PPFE is characterised by upper lobe predominate pleural thickening and course subpleural reticulation, associated with traction bronchiectasis and volume loss. Findings are progressive over several years, typically with increased volume of pleuroparenchymal thickening [1]. Pneumothoraces are a recognised complication.

Platythorax, antero-posterior narrowing of the thorax, can be identified on imaging by posterior indrawing of the trachea and deepening of the sternal notch [1] and progressive platythorax is associated with worsening fibrosis [4].

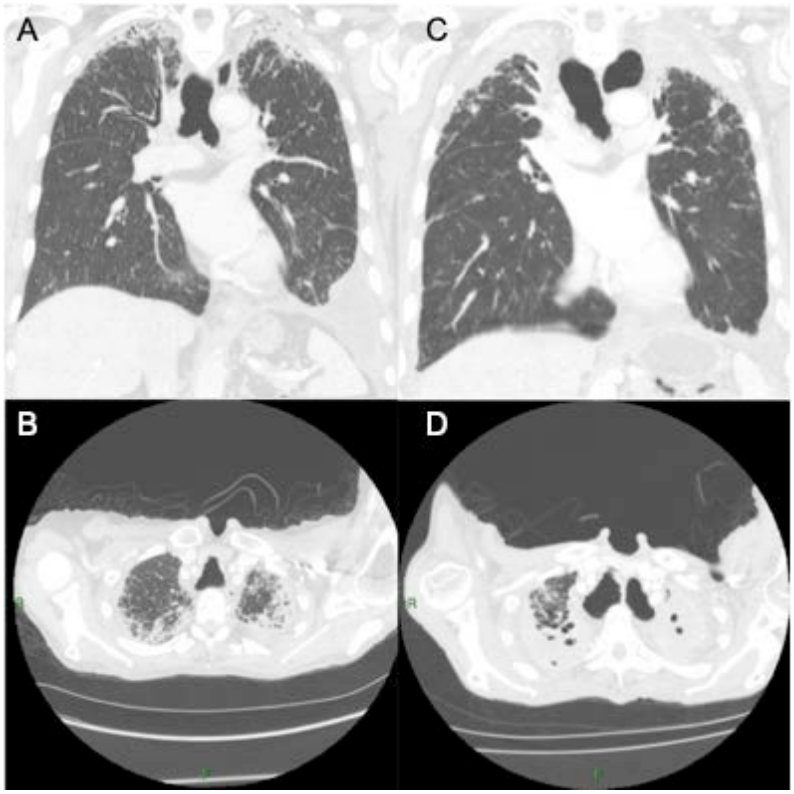

Case 1

Case 1 - 81 year old male: Coronal and axial CT index (A; B) demonstrating upper lobe pleuroparenchymal thickening, architectural distortion, volume loss and hilar retraction. On the axial images, there is deepening of the suprasternal notch with retraction of the trachea and overlap of posterior border of trachea with vertebral body. On the follow up images at 3 years (C;D), these findings are all progressive in severity with new dilatation of the oesophagus.

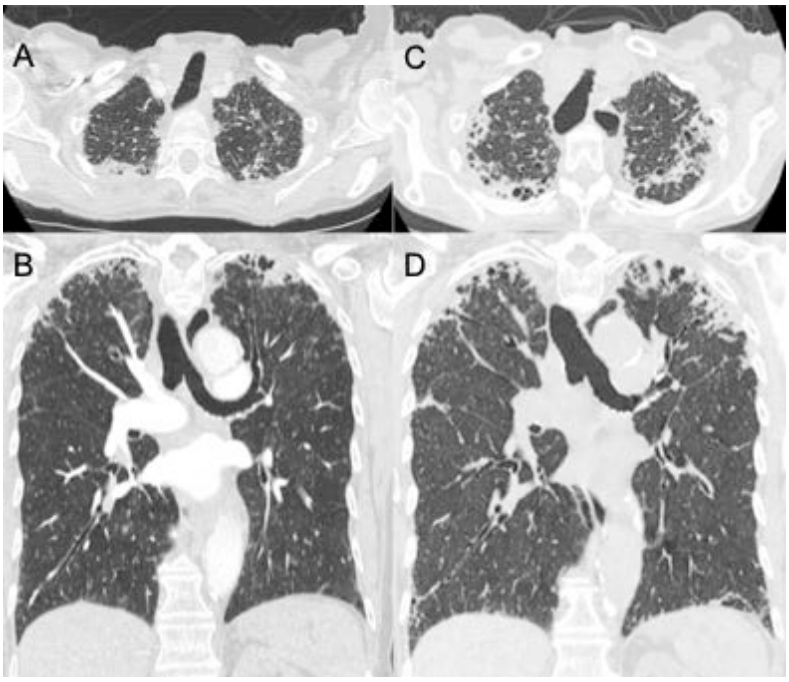

Case 2

Case 2 - 88 year old male: Axial and coronal CT index (A;B) shows marked tracheal retraction with associated subpleural coarse reticulation and superior hilar retraction. On subsequent CT 5 years later (C;D), there is progressive tracheal retraction and deepening of the suprasternal notch with increasing volume of subpleural tissue and progressive volume loss. Reticular changes extend to involve the lower lobes and there is new dilatation of the oesophagus.

Conclusion

PPFE is an increasingly recognised form of ILD and radiologists should be aware of the characteristic imaging findings including features of platythorax to consider the diagnosis.

References:

[1] Chua F, Desai SR, Nicholson AG, Devaraj A, Renzoni E, Rice A, Wells AU, (2019), Pleuroparenchymal Fibroelastosis. A Review of Clinical, Radiological, and Pathological Characteristics, Ann Am Thorac Soc, 1351-1359, 16(11), 2023-03-27

[2] Kato M, Sasaki S, Kurokawa K, Nakamura T, Yamada T, Sasano H, Arano N, Komura M, Ihara H, Nagashima O, Shiota S, Takahashi F, Takahashi K., (2019), Usual Interstitial Pneumonia Pattern in the Lower Lung Lobes as a Prognostic Factor in Idiopathic Pleuroparenchymal Fibroelastosis, Respiration, 319-328, 97(4), 2023-03-27

[3] Kinoshita Y, Ishii H, Nabeshima K, Watanabe K, (2021), The pathogenesis and pathology of idiopathic pleuroparenchymal fibroelastosis, Histol Histopathol, 291-303, 36(3), 2023-03-27

[4] Ikeda T, Kinoshita Y, Miyamura T, Ueda Y, Yoshida Y, Kushima H, Ishii H, (2022), Platythorax progresses with lung involvement in pleuroparenchymal fibroelastosis, Respir Investig, 293-299, 60(2), 2023-03-27

A-572

Pneumocystis jirovecii pneumonia in lung cancer patients

A. Jöbstl[1], F. Kocher[2], J. Rudzki[2], A. Pircher[2], G. Widmann[3]
[1]Department of Radiology, Tirol Kliniken, Innsbruck, Austria, [2]Department of Hematology and Oncology, Internal Medicine V, Medical University of Innsbruck, Innsbruck, Austria, [3]Department of Radiology, Medical University of Innsbruck, Innsbruck, Austria

Learning Objectives

To be aware of pneumonitis in lung-cancer-patients under radiochemotherapy and/or ICI.
To consider PjP in patients treated for pneumonitits without improvement of chest-CT-findings.
To ask clinicians about status of PjP-prophylaxis in immunocompromised patients.

Background

Pneumocystis jirovecii can affect immunocompetent as well as immunocompromised subjects, but remains asymptomatic in immunocompetency. [1]
Although PjP is best known in HIV-patients with low CD4+ cell count, it is more severe and more often lethal in non-HIV-patients with some other kind of immunodeficiency. [1]
The most important risk factor in non-HIV-patients is a high-dose- or long-standing steroid treatment [1], as for example during treatment of pneumonitis.
In lung cancer patients, pneumonitis can be a consequence from treatment with immune checkpoint inhibitors (ICI). The incidence is about 5% and most cases respond well to steroids. [2] Furthermore, pneumonitis can be caused by radiotherapy of lung cancer with an incidence of 0-40% depending on radiation dose and irradiated lung volume. [3]

Imaging findings OR Procedure details

There is a variety of CT-patterns in pneumonitis, but the most common is the OP-like pattern consisting of bilateral ground-glass and/or consolidations with peribronchovascular distribution and predominance of the middle and lower lungs. [4]
The classic appearance of PjP is particularly central ground-glass with predominance of the upper lungs. In advanced disease crazy paving and consolidations can be seen, and multiple pulmonary cysts are rare in non-HIV-patients compared to HIV-patients. [5]
A critical finding that has to make us think of PjP is lack of improvement or even deterioration of the chest-CT-findings of pneumonitis during steroid-therapy.

Conclusion

Radiotherapy as well as ICI therapy can induce pneumonitis in lung-cancer-patients. Treatment with high-dose and long-standing steroids poses a high risk for developing PjP, a frequently lethal complication for which PjP-prophylaxis is strongly recommended [6].
Radiologists should be very cautious and consider PjP if CT findings in steroid-treated pneumonitis do not improve or even deterioriate

References:

[1] Apostolopoulou A, Fishman J A, (2022), The Pathogenesis and Diagnosis of Pneumocystis jiroveci Pneumonia, Journal of Fungi , 1167, 8(11)
[2] Naidoo J, Wang X, Woo K M, Iyriboz T, Halpenny D et al, Pneumonitis in Patients Treated With Anti-Programmed Death-1/Programmed Death Ligand 1 Therapy, J Clin Oncol , 709-717, 35
[3] Schoenfeld J D, Nishino M, Severgnini M, Manos M, Mak R H, Hodi F St, (2019), Pneumonitis resulting from radiation and immune checkpoint blockade illustrates characteristic clinical, radiological and circulating biomarker features, J Immunother Cancer, 112, 7
[4] Kalisz K R, Ramaiya N H, Laukamp K R, Gupta A, (2019), Immune Checkpoint Inhibitor Therapy-related Pneumonitis: Patterns and Management, RadioGraphics, 1923-1937, 39
[5] Kanne J P, Yandow D R, Meyer C A, (2012), Pneumocystis jiroveci Pneumonia: High-Resolution CT Findings in Patients With and Without HIV Infection, AJR, 555-561, 198
[6] Fragoulis G E, Nikiphorou E, Dey M, Zhao S S, Courvoisier D S et al, (2022), 2022 EULAR recommendations for screening and prophylaxis of chronic and opportunistic infections in adults with autoimmune inflammatory rheumatic diseases, Ann Rheum Dis , 1-12

A-156

Present and Future of GL-ILD as Distinct Entity Among the Interstitial Lung Diseases

G. Jurkeviciute Kucinskiene, S. Giedrys
Lithuanian University of Health Sciences, Radiology Department, Kaunas, Lithuania

Learning Objectives

To review the radiological exams for GL-ILD
To learn the imaging signs of GL-ILD
To discuss the future possibilities of using hybrid imaging in the GL-ILD management

Background

Granulomatous Lymphocytic Interstitial Lung Disease (GL-ILD) is a rare complex non-infectious lung disorder that presents in about one-fifth of patients with common variable immunodeficiency disorders (CVID). Due to a poorly understood pathogenesis, GL-ILD diagnosis and management criteria still lack consensus. GL-ILD patients may show signs of lymphoproliferative pulmonary disease, including lymphocytic interstitial pneumonia, follicular bronchiolitis or lymphoid hyperplasia in combination with granulomas. Diagnosis is made by performing both radiological and histopathological examinations of the lungs.

Imaging findings OR Procedure details

Currently a non-invasive gold standard to assess GL-ILD-related structural lung changes is chest computed tomography (CT). Radiologically, GL-ILD has been characterized by CT findings including reticulation, bronchial wall thickening, pulmonary nodules, patchy consolidation, ground glass opacities and traction bronchiectasis

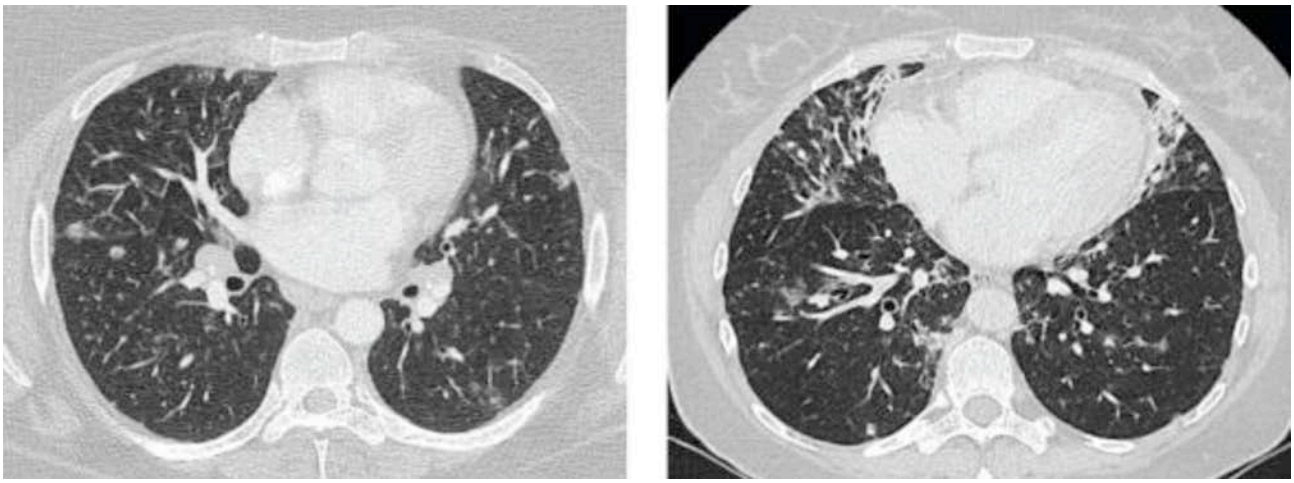

Features of granulomatous lymphocytic interstitial lung disease (GLILD). Different appearance of GLILD in two different patients. Left: diffuse nodules and lymphadenopathy. Right: combination of diffuse nodules, reticulation and ground-glass opacities.

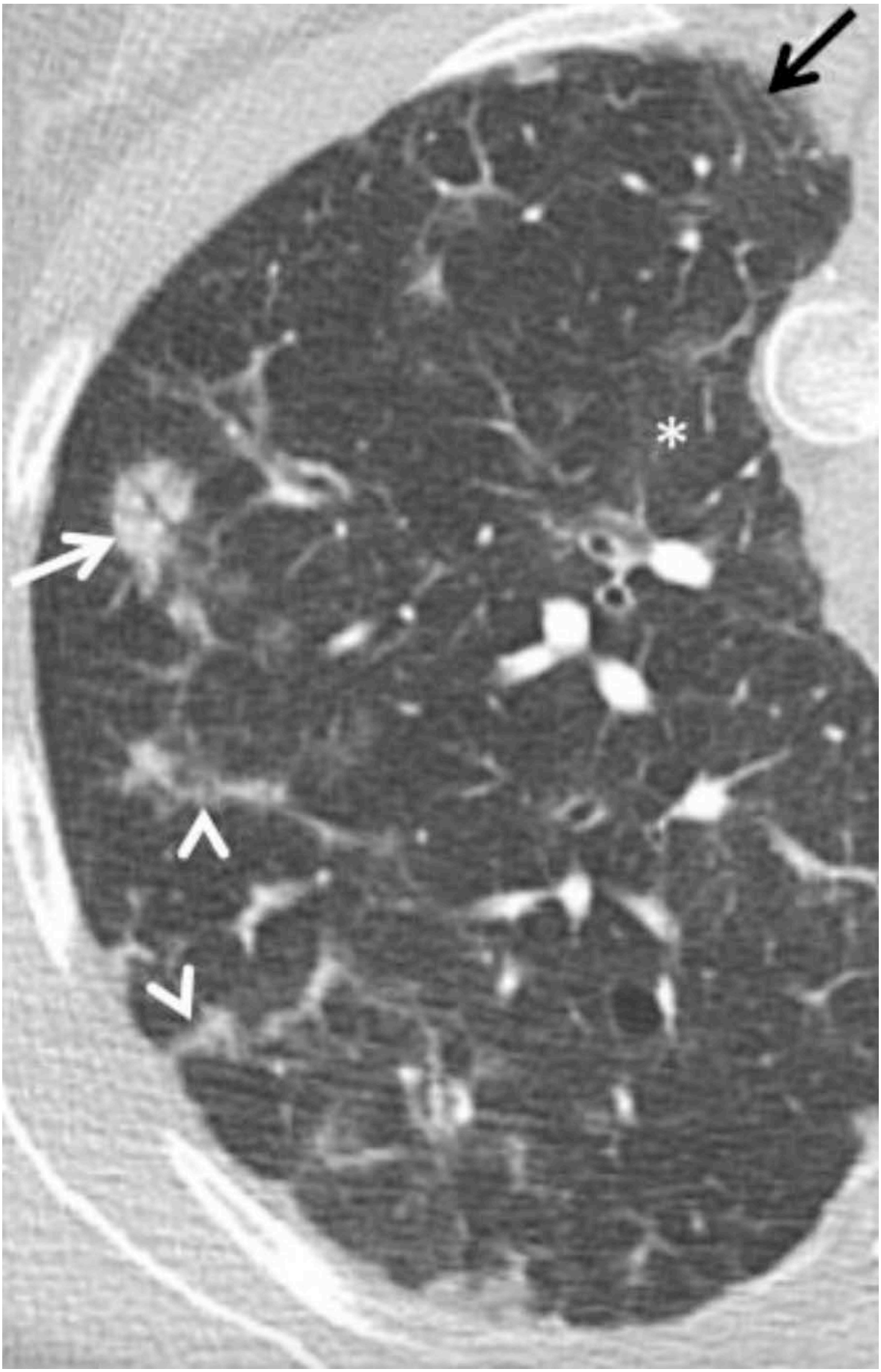

HRCT image of the right upper lobe of a 40-year-old woman with characteristic findings of GLILD with irregular peribronchovascular interstitial thickening (white arrow), interlobular septal thickening (arrowheads), subtle ground glass opacities (asterix), and traction bronchiectasis (black arrow

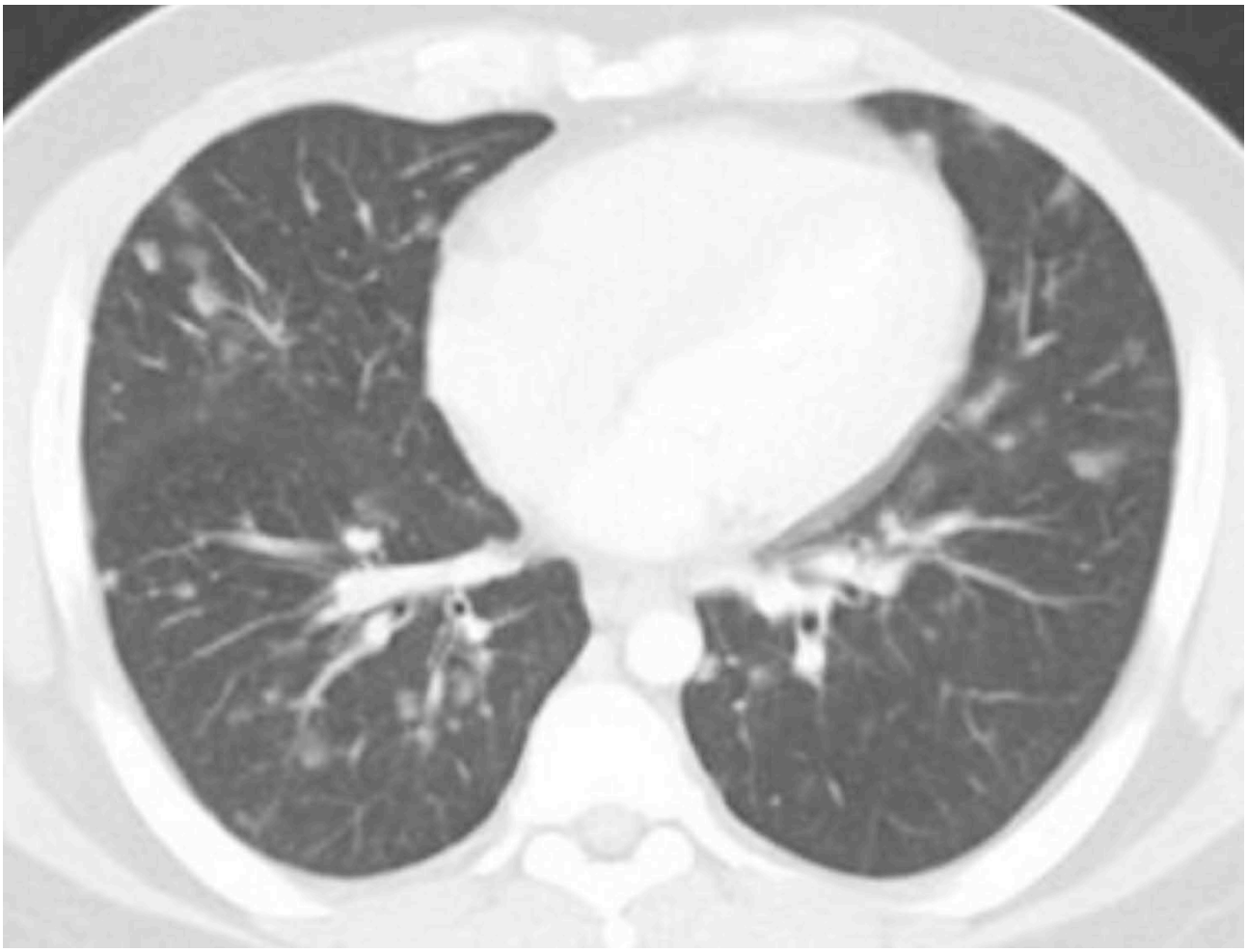

CT chest at lower level shows multiple bilateral solid as well as ground glass nodules in CVID patient.

. GL-ILD is often associated with extrapulmonary involvement that may be diagnosed with CT. Recently two methods were developed for scoring CVID CT scans: the Baumann method and the Hartmann method. Both methods may come into use in clinical practice in the future. FDG-PET/CT imaging has been reported in case studies of GLILD and is a promising possibility in the evaluation of inflammatory disease.

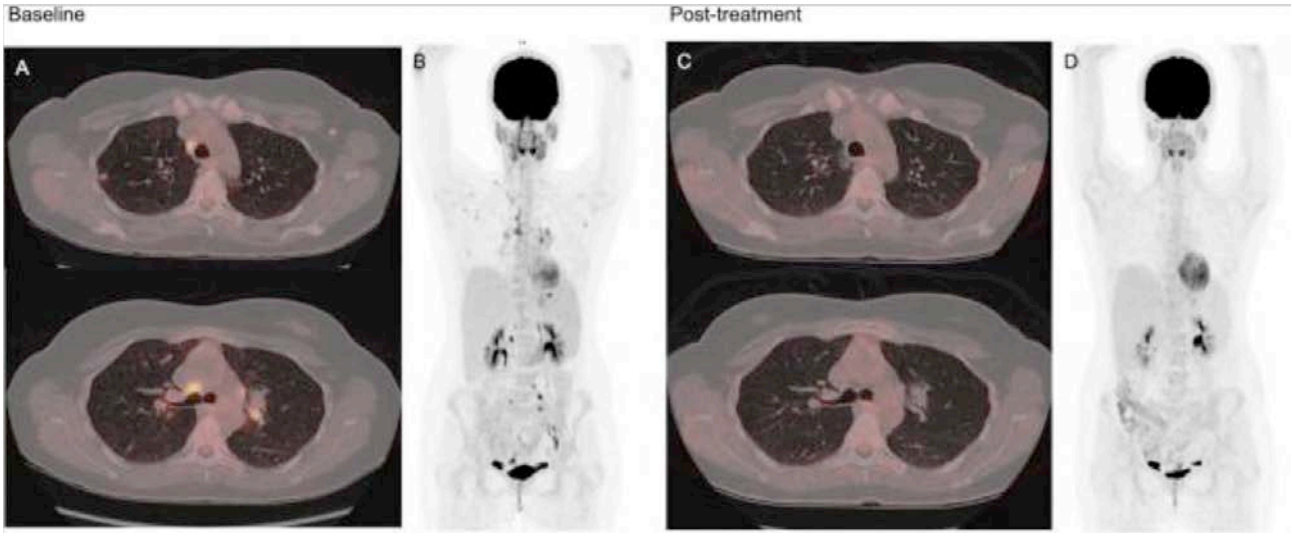

Image A baseline PET/CT images with scattered nodular and confluent consolidation in the lungs and mediastinal lymphnodes with moderate to high FDG uptake.Image B baseline MIP showing FDG uptake in the lungs lymph nodes. Images C, D show post-treatment FDG PET/CT and MIP with complete resolution of previous findings.

FDG-PET/CT may show metabolic activity in consolidated parts of the lungs and recent studies show that patients with progressive disease may have significantly higher SUVmean in the lungs compared to patients with stable disease.

Conclusion

GL-ILD diagnosis and management still lack consensus. CT is the gold standard non-invasive imaging modality that can reveal

characteristic findings such as diffuse and bilateral bronchial wall thickening and nodular or reticular opacities. PET/CT may be used in management of GL-ILD in the future.

References:

[1] Fraz MSA, Moe N, Revheim ME, et al., (2021), Granulomatous-Lymphocytic Interstitial Lung Disease in Common Variable Immunodeficiency-Features of CT and 18F-FDG Positron Emission Tomography/CT in Clinically Progressive Disease., Front Immunol., https://www.ncbi.nlm.nih.gov/pmc/articles/PMC7874137/
[2] Meerburg JJ, Hartmann IJC, Goldacker S, et al., (2020), Analysis of Granulomatous Lymphocytic Interstitial Lung Disease Using Two Scoring Systems for Computed Tomography Scans-A Retrospective Cohort Study. , Front Immunol., https://www.ncbi.nlm.nih.gov/pmc/articles/PMC7662109/
[3] Cinetto F, Scarpa R, Carrabba M, et al., (2021), Granulomatous Lymphocytic Interstitial Lung Disease (GLILD) in Common Variable Immunodeficiency (CVID): A Multicenter Retrospective Study of Patients From Italian PID Referral Centers., https://pubmed.ncbi.nlm.nih.gov/33777011/
[4] Park JH, Levinson AI. , (2010), Granulomatous-lymphocytic interstitial lung disease (GLILD) in common variable immunodeficiency (CVID)., https://pubmed.ncbi.nlm.nih.gov/19900842/

A-669

Principle HRCT findings in pulmonary fungal disease: what radiologist should know

M. Mastandrea[1], G. Lezzi[1], M. Servietti[1], S. Conte[1], L. Migliorato[2], M. Mereu[1], R. L. Patea[1], M. Caulo[1]
[1]Santissima Annunziata Hospital, Chieti, Italy, [2]Presidio Ospedaliero, Pescara, Italy

Learning Objectives
To describe the principal HRCT patterns of pulmonary fungal disease; to help physicians to reach the proper diagnosis.
Background
Fungal diseases kill more than 1.5 million and affect over a billion people worldwide. Pulmonary fungal diseases include several ranges of infections related to fungal sources. They can particularly affect immunocompromised patient, due to AIDS, cancer, organ transplantation and corticosteroid therapies. The most common pulmonary fungal diseases are chronic pulmonary aspergillosis, invasive candidiasis, Pneumocystis jirovecii pneumonia (PJP), invasive aspergillosis, cryptococcosis and mucormycosis. Symptoms are aspecific, similar to other lung infections, and can include dyspnea, cough, fever and weight loss.
Imaging findings OR Procedure details
We describe the most common HRCT findings in pulmonary fungal diseases, such as *consolidation, nodules, halo sign, reverse halo sign, hypodense sign, air crescent sign, feeding vessel sign.* The presence of nodules, with halo or reverse halo sign, could be an indicator of fungal infection. Aspergillomas are mass-like lesions (fungus ball) typically composed of Aspergillus fumigatus and are a non-invasive form of pulmonary aspergillosis. Fungus ball can occur in patients with structurally abnormal lungs, with pre-existing cavities such as bullae, pneumatocoeles, bronchiectasis and cavitated lesions due to tuberculosis. Invasive aspergillosis can appear on HRCT as nodules with halo sign in the early phase, and cavitary lesions with air crescent sign in the late phase. Hypodense sign (central hypodensity in a consolidation due to central area of necrosis) and feeding vessel sign (a vessel directed into the center of a nodule) can occur in some cases of angioinvasive pulmonary aspergillosis. Nodules and cavitation are common findings in cryptococcosis, and nodules with centrilobular or random distribution are common in candidiasis. Reverse halo sign and nodules may be encountered in mucormycosis. Diffuse ground glass opacities and cystic lesions are frequently encountered in PJP. HRCT findings mentioned above are nonspecific and can mimic other pulmonary infection. So, it is mandatory to associate these findings with other ancillary CT findings (pleural effusion, bronchial wall thickening, lymphadenopathies), clinical history and laboratory data in order to narrow the differential diagnosis.
Conclusion
The HRCT findings in pulmonary fungal diseases are nonspecific and they can mimic other pulmonary infection. Radiologists, in the appropriate clinical setting, can help physicians to diagnose them in time and allow a prompt antifungal therapy.

References:

[1] Bongomin F, Gago S, Oladele RO, Denning DW, (2017), Global and Multi-National Prevalence of Fungal Diseases-Estimate Precision. J Fungi (Basel)
[2] - Kunihiro, Y., Tanaka, N., Kawano, R. et al. , (2019), Differential diagnosis of pulmonary infections in immunocompromised patients using high-resolution computed tomography
[3] Sousa C, Marchiori E, Youssef A, Mohammed TL, Patel P, Irion K, Pasini R, Mançano A, Souza A, Pasqualotto AC, Hochhegger B, (2022), Chest Imaging in Systemic Endemic Mycoses

A-554

Pulmonary alveolar hemorrhage - useful radiological and clinical features

E. Baltakytė, S. Giedrys, J. Zaveckienė
Lithuanian University of Health Sciences Hospital Kaunas Clinics, Lithuania, Radiology, Kaunas, Lithuania

Learning Objectives

1.To describe possible causes and clinical features of a pulmonary hemorrhage in different clinical scenarios
2.To discuss computed tomography (CT) features of intraparenchymal pulmonary hemorrhage
3.To illustrate distinguishing features and possible combinations of CT signs in different clinical context

Background

Pulmonary hemorrhage is a potentially lethal condition, mostly accompanied with clinical symptoms such as dyspnoe, hemoptysis, anemia, fatigue. In about 1/3 cases it can appear rather “silent” clinically and therefore one should always keep in mind that absence of a hemoptysis does not exclude diffuse alveolar hemorrhage (DAH). Moreover, in these asymptomatic cases, changes in the chest CT may be the first clue to differential, helping narrow down and specify a possible cause. Correct identification of the etiology for DAH is important as the treatment varies based on the cause.

Imaging findings OR Procedure details

Pulmonary hemorrhage is a condition characterized by a disruption of the alveolar – capillary membrane basement that results in an intraalveolar hemorrhage. On a radiological imaging it can manifest as a focal or more likely diffuse alveolar opacities. There are many possible etiologies which differ drastically in their pathophysiological origin, clinical impact, burden and treatment too. Both clinical and radiological features are non-specific, however particular combinations of CT signs can help to separate possible etiological groups (for example connective tissue diseases, vasculitides, drug effect, marrow transplant, cardiac disease..). In some cases, especially in asymptomatic patients, chest CT are the first step in the diagnosis, making a radiologist role a crucial factor as a delay in correct diagnosis leads to delayed initiation or suboptimal treatment and may attribute to a higher morbidity and mortality

Conclusion

Absence of hemoptysis does not exclude pulmonary hemorrhage. Knowing CT features and accompanying symptom helps to achieve right diagnosis.

A-638

Pulmonary Arterial Interventions: A Pictorial Review

V. S. Ponnalagu[1], K. Chokkappan[2], S. Srinivasan[2], R. Chung[2], S. B. Balasubramanian[2]
[1]WOODLANDS HEALTH, Diagnostic Radiology, SINGAPORE, Singapore, [2]KHOO TECK PUAT HOSPITAL, Diagnostic Radiology, SINGAPORE, Singapore

Learning Objectives

To review the percutaneous catheter based interventions of pulmonary arteries in various clinical conditions.
To describe the imaging findings wherever required.
The technique of pulmonary arterial catheterisation is also reviewed.

Background

Percutaneous pulmonary arterial intervention was first reported in the 1970s. With advent of sophisticated hardware and imaging techniques, minimally invasive interventions of pulmonary arteries are possible obviating the need to invasive surgeries. Pulmonary arterial interventions are safe. However, understanding the physiology and pathophysiology of various clinical conditions is necessary and requires experience. This pictorial review provides an overview of imaging findings and percutaneous endovascular management in various pulmonary arterial conditions.

Imaging findings OR Procedure details

Percutaneous catheter guided pulmonary interventions include thrombectomy and thrombolysis, embolisation in patients with hemoptysis[1], embolisation of pulmonary AVMs

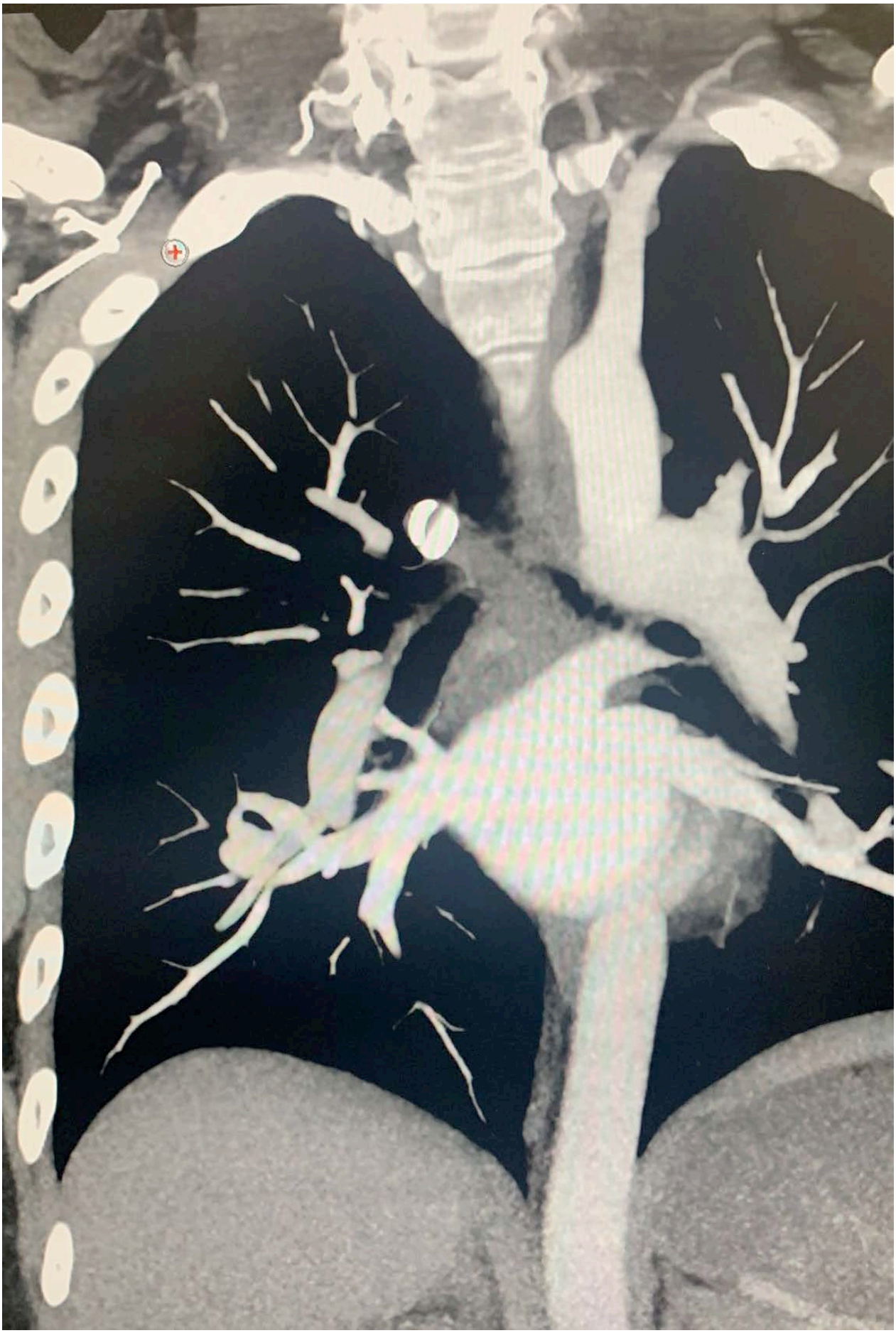

CT pulmonary angiogram MIP reconstruction showing a right lower lobe pulmonary arteriovenous malformation (AVM).

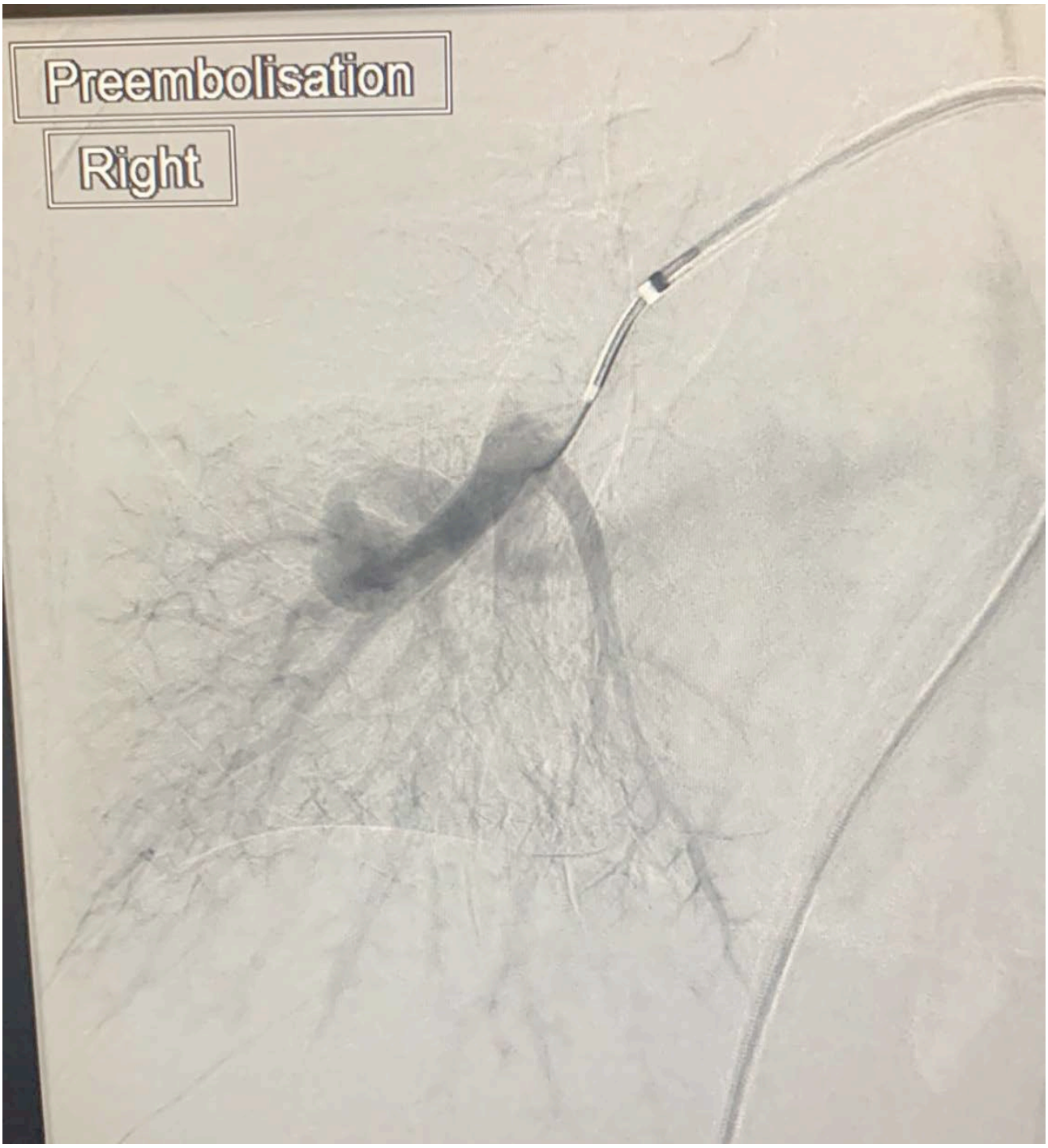

Right pulmonary angiogram demonstrating a right lung arterivenous malformation pre-embolisation

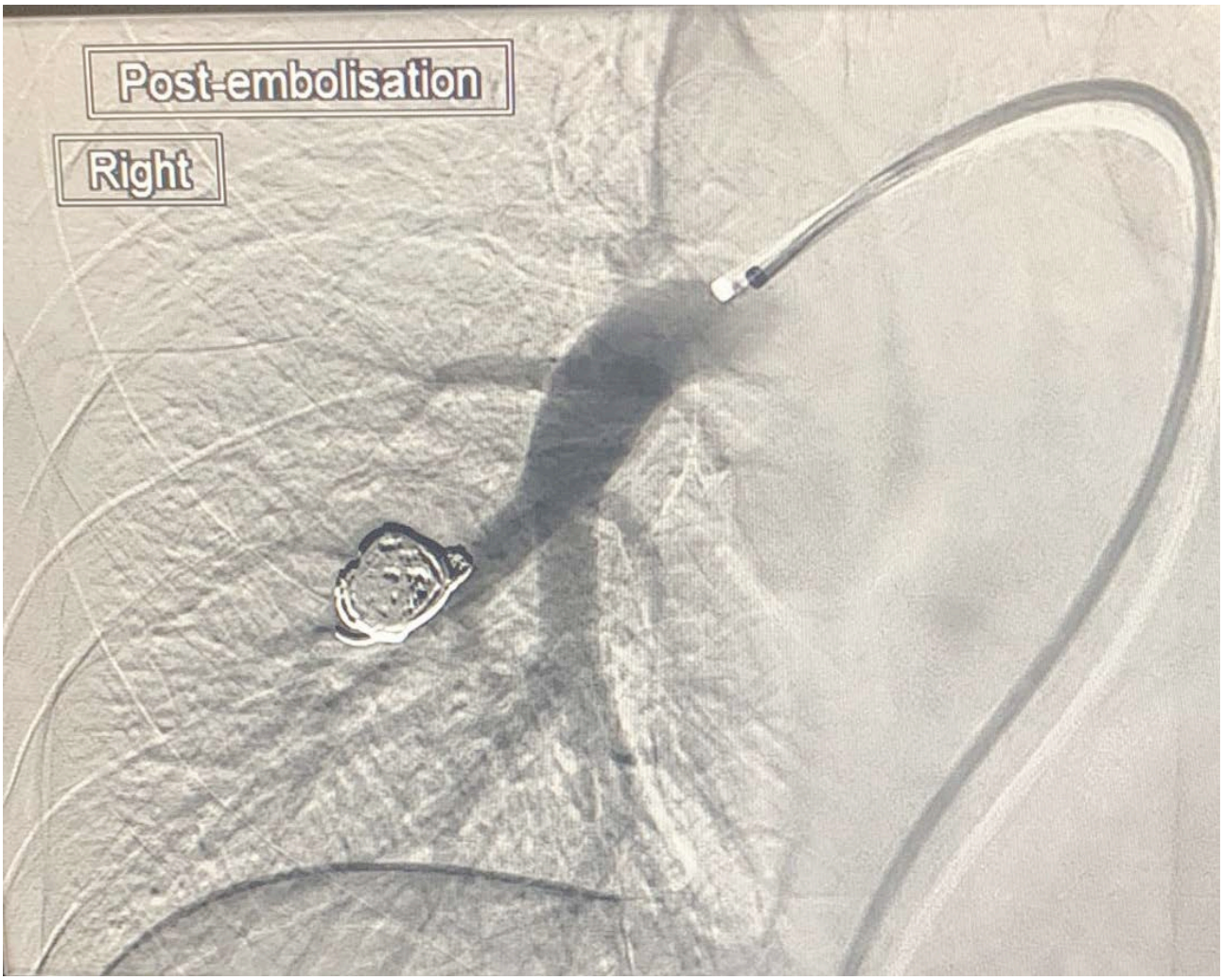

Right pulmonary angiogram post-embolisation showing occlusion of the lesion.
, retrieval of foreign bodies and balloon dilatation. Other rarely described interventions include endovascular biopsy, temporary occlusion before pulmonary resection and endovascular ultrasound.

Conclusion

Multiple percutaneous catheter directed pulmonary interventions are possible and it is important for radiologists to be aware of these procedures[2]. Interventional Radiologists should not only be trained in these procedures, but also understand the disease process and pathophysiology. Collaboration between the chest, emergency and referring physicians and the interventional radiologists is very important for better patient outcomes.

References:

[1] Kaitlin M. Marquis, Constantine A. Raptis, M. Zak Rajput, Kacie L. Steinbrecher, Travis S. Henry, Santiago E. Rossi, Daniel D. Picus, and Sanjeev Bhalla, (2021), CT for Evaluation of Hemoptysis, Radiological Society of North America, RadioGraphics, 742 - 761, https://doi.org/10.1148/rg.2021200150, 2023-04-05

[2] Jean-Pierre Pelage, Mostafa El Hajjam, Christine Lagrange, Thierry Chinet, Antoine Vieillard-Baron, Sophie Chagnon, Pascal Lacombe, (2005), Pulmonary Artery Interventions: An Overview, Radiological Society of North America, RadioGraphics, 1653–1667, 25/6, https://doi.org/10.1148/rg.256055516., 2023-04-15

A-390

Pulmonary Artery Angiosarcoma: case based review

M. Sbaraini, A. P. Sartori, T. Krieger Bento da Silva, C. Simoes dos Santos, S. Marcantonio Camargo, M. Bellon dos Santos, B. Canela Furian, S. Adamour Soder
Pavilhão pereira filho, Radiology, Porto Alegre, Brazil

Learning Objectives
To review the clinical and imaging findings of pulmonary artery sarcomas, more specifically those differentiated in angiosarcomas, using four cases from our institution.

Background
Sarcomas are rare malignant tumors of mesenchymal origin. They can originate in bones or in soft tissues such as fat, cartilage, muscle and endothelial cells. Primary sarcomas of the major blood vessels are most commonly found in the pulmonary arteries and the aorta, and can be divided in two types - mural (involving the wall) and intraluminal or intimal (growing inside the vessel). Primary sarcomas of the pulmonary artery can be histologically undifferentiated (most common) or differentiated in angiosarcomas and liposarcomas, among others. Angiosarcoma is one of the rarest subtypes of sarcomas, comprising up to 3.6% of pulmonary artery sarcomas. Few cases have been reported in the literature - a review from 2019 found 21 cases of pulmonary artery angiosarcomas published. Angiosarcomas are usually aggressive and treatment has a poor prognosis.
PA intimal sarcomas (PAIS), including angiosarcomas, are often misinterpreted at presentation as acute or chronic pulmonary thromboembolism (PT), as the clinical findings are similar and they can coexist. Some studies show that more than half of all patients with PAIS have an initial diagnosis of PT. Most patients present with dyspnea, cough, chest pain, hemoptysis and syncope, although some can be asymptomatic. Many patients can have locally advanced or metastatic disease at the time of initial diagnosis.

Imaging findings OR Procedure details
Computed Tomography shows intraluminal filling defects at the main pulmonary artery, which can extend into other branches, or at the right and/or left pulmonary arteries. Findings of pulmonary hypertension and right heart strain can be found, as the tumor gradually grows over weeks to months. Magnetic Resonance Imaging can improve differentiation between angiosarcomas and PT, although findings can vary, ranging from isointense to mildly hyper-intense at T1-weighted imaging and isointense to highly intense at T2-weighted imaging. Angiosarcomas usually exhibit a heterogeneous enhancement of the gadolinium contrast, unlike a thrombus, that will not show any enhancement. Positron-emission tomography CT with 18F-fluorodeoxyglucose (FDG) can further increase the diagnostic sensitivity, demonstrating metabolic activity, characterized by an uptake of FDG in the lesion. In immunohistochemical analysis, angiosarcomas express typical vascular and endothelial markers, such as CD31, CD34, ERG and FVIII.

Conclusion
Although pulmonary artery angiosarcomas are rare, they are an important differential diagnosis of PT that must be considered, especially in patients who don't respond to antithrombotic therapy.

A-604

Pulmonary Manifestations in Patients with HIV/AIDS: A Pictorial Review

A. Fevereiro[1], C. Silva[2], F. Gomes[1]
[1]Pedro Hispano Hospital, Radiology, Matosinhos, Portugal, [2]Nossa Senhora da Oliveira Hospital, Radiology, Guimarães, Portugal

Learning Objectives

- Review and illustrate the most common pulmonary manifestations in patients with HIV/AIDS, including infectious and non-infectious complications;
- Provide a pattern based approach in high-resolution computed tomography (*HRCT*) imaging, according to CD4+ cell count.

Background

Since the first descriptions of HIV/AIDS, the lung has been the most frequently affected site. The introduction of antiretroviral therapy (ART) has significantly reduced morbidity and mortality; however, respiratory conditions remain the leading cause of complications in AIDS, mainly of infectious etiology[1].

The lung mucosa seems to be an important HIV reservoir site. Since ART does not eliminate the virus, residual levels of HIV remain in the mucosa, leading to chronic immune activation and pulmonary inflammation, which in turn cause immune cell exhaustion and progressive depletion of T-cell immunity, displayed by a decrease in CD4+ cell count [2].

The degree of immunosuppression influences the risk of developing specific pulmonary diseases based on CD4+ cell count: when below 500 CD4+ cells, there is an increased risk for developing bacterial pneumonia, pulmonary tuberculosis, and lymphoproliferative disorders; if CD4+ cell count is less than 200 cells there is also an increased risk for *Pneumocystis* jirovecii pneumonia and disseminated tuberculosis; Fungal infections, Cytomegalovirus pneumonia, AIDS-related lymphoma, and Kaposi's sarcoma should be considered when < 100 CD4 cells [3]

Achieving an etiological diagnosis of pulmonary infection in these patients is vital in terms of prognostic.

Imaging findings OR Procedure details

We overview the most common pulmonary complications in patients with HIV/AIDS by providing a systematic pattern-based approach in high-resolution computed tomography (*HRCT*) and conventional chest radiography, according to the degree of immunosuppression / stage of infection.

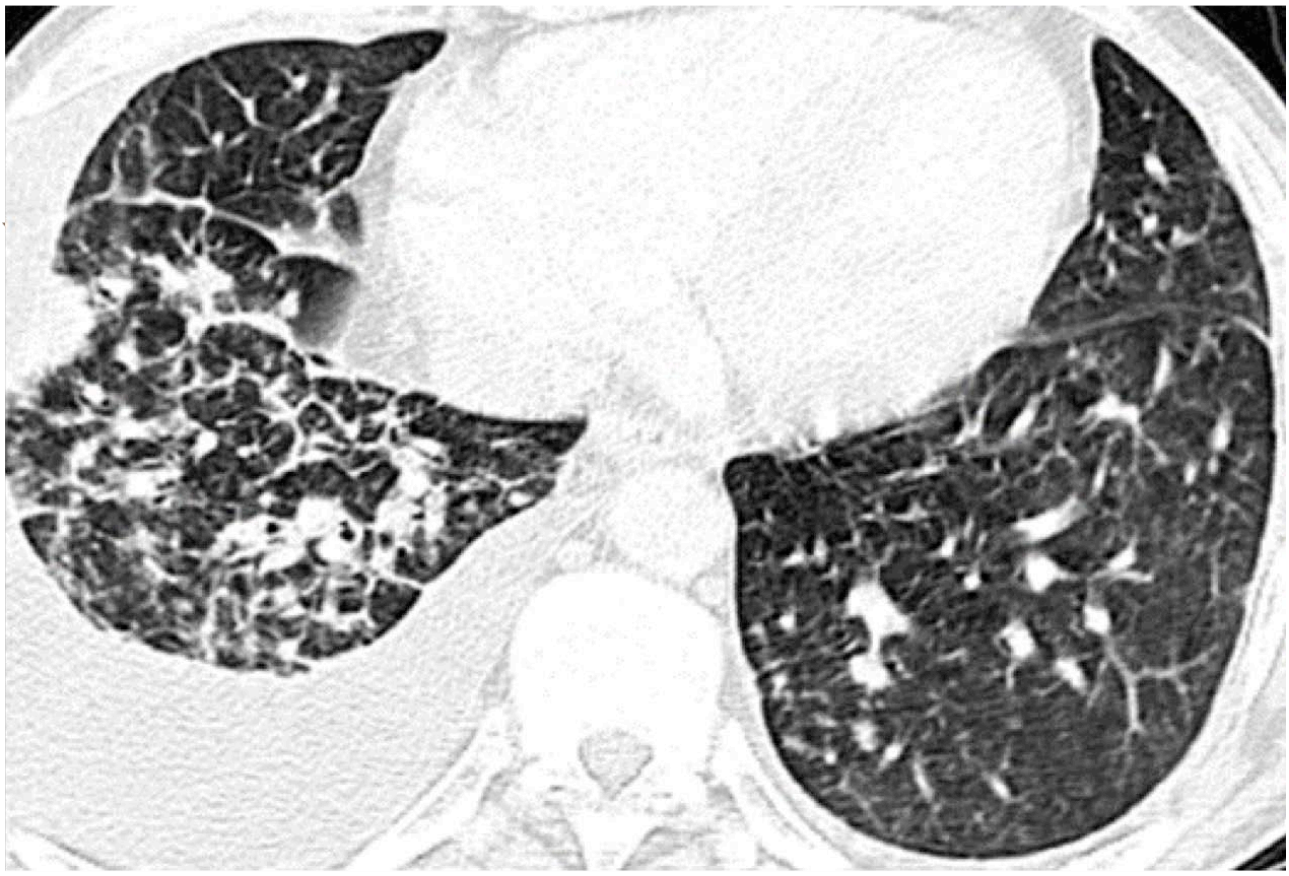

Kaposi Sarcoma. Peribronchovascular consolidation extending from the hilum to the periphery as the disease progresses; Ill-defined irregular nodules with peribronchovascular distribution, which may coalesce and form consolidations. Lower/medium lobes more affected; May be associated with pleural effusion and adenomegaly.

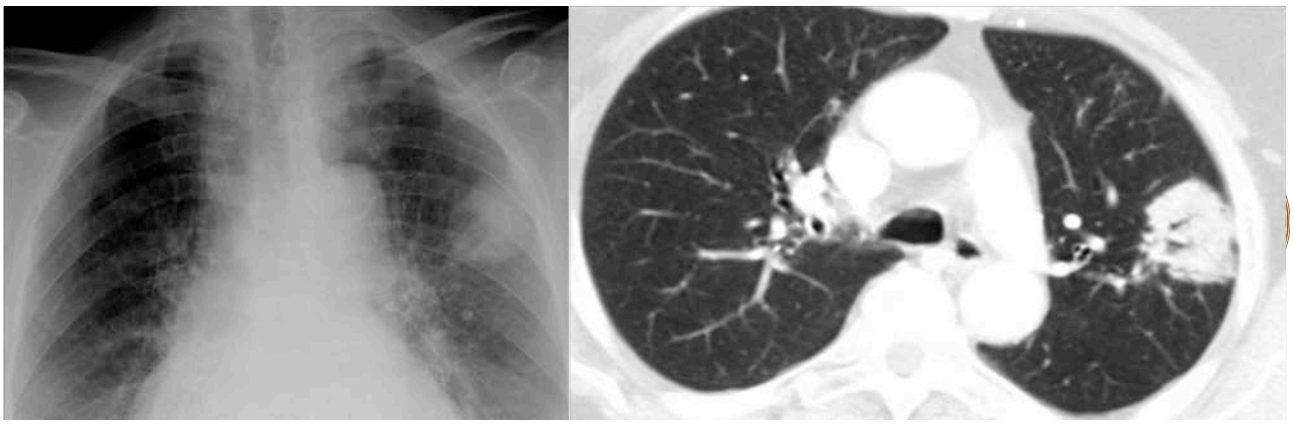

Non-Hodgkin Lymphoma. Solitary/multiple nodules >1cm, predominantly peripheral and at the bases. Pleural effusion is common.

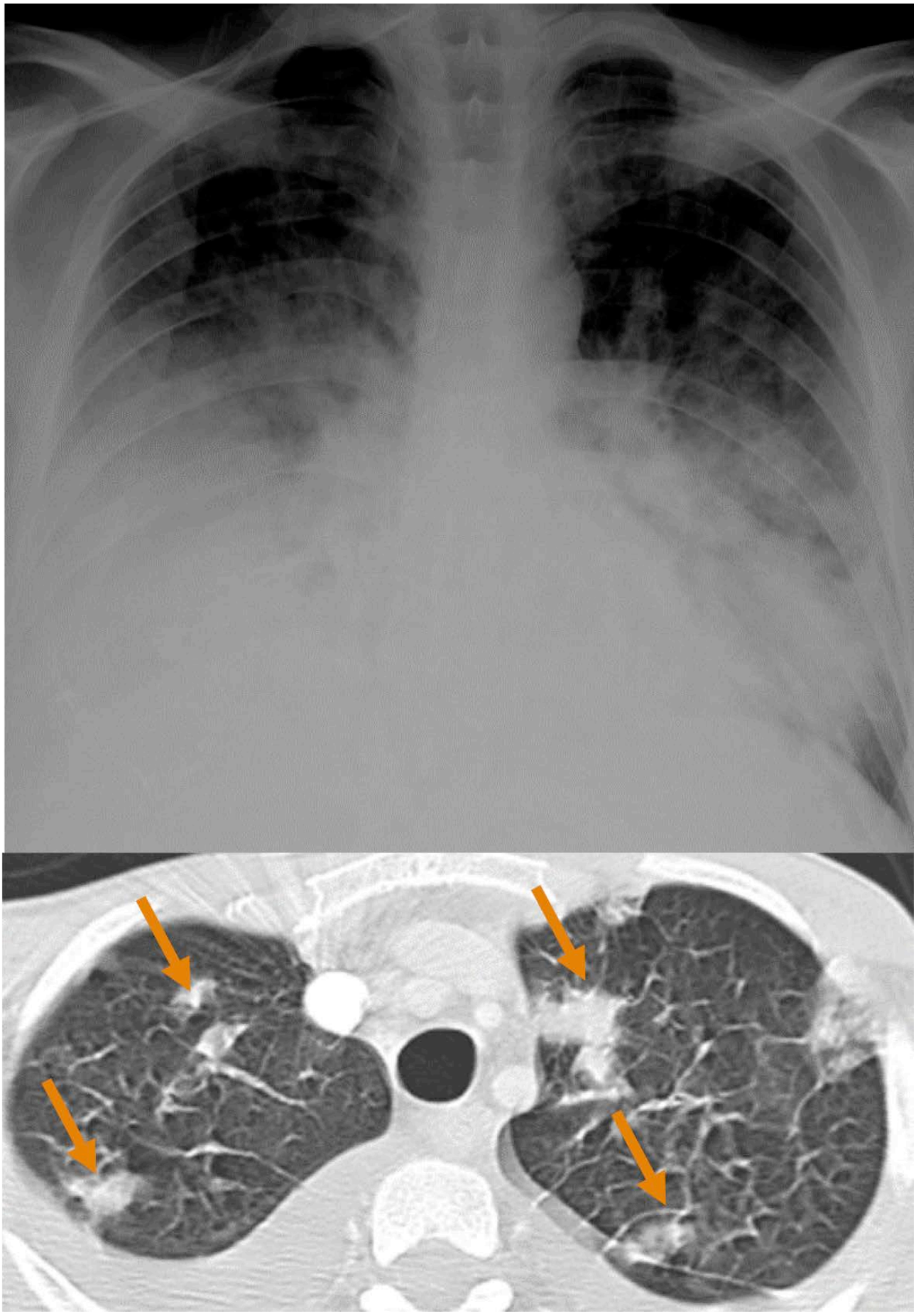

Mycobacterium Avium Complex (MAC) Pulmonary Infection: Diffuse interstitial and/or alveolar opacities / consolidations (arrows). Cavitations are a less common finding, but may be present.

Conclusion

Pulmonary complications in HIV/AIDS patients display a wide variety of imaging findings. While there is considerable overlap between the radiographic findings of different pulmonary complications, a particular condition may manifest in various radiological appearances. Computed tomography plays a preponderant role in the management of these patients, as it narrows the differential diagnosis and allows treatment optimization.

References:

[1] N. Benito, A. Moreno, J.M. Miro , (2012), Pulmonary infections in HIV-infected patients: an update in the 21st century, European Respiratory Journal, 730-745

[2] Yulia Alexandrova, Cecilia T. Costiniuk, Mohammad-Ali Jenabian, (2022), Pulmonary Immune Dysregulation and Viral Persistence During HIV Infection, Immunol.

[3] Marchiori. E. et. al., (2005), Pulmonary Disease in Patients with AIDS: High-Resolution CT and Pathologic Findings, American Journal of Roentgenology., 757-764, 184

A-393

Pulmonary manifestations of common variable immunodeficiency

A. Azeiteiro, A. Viegas, L. Urbano, D. Antunes
Centro Hospitalar Lisboa Norte, EPE, Serviço de Imagiologia Geral, Lisbon, Portugal

Learning Objectives

- To review the pulmonary findings and complications in common variable immunodeficiency
- To characterize and review the imagological characteristics of granulomatous lymphocytic interstitial lung disease

Background

Common variable immunodeficiency disorder (CVID) is an heterogeneous disorder characterized by B-lymphocyte dysfunction and decreased serum immunoglobulin levels (low immunoglobulin G, low immunoglobulin A and/or immunoglobulin M).
Patients with CVID present with recurrent upper and/or lower respiratory tract infections. Recurrent upper respiratory tract infections can lead to chronic sinusitis and hearing loss and recurrent lower respiratory tract infections can result in the development of bronchiectasis. Parenchymal and interstitial changes of the lung lead to both obstructive and restrictive abnormalities. In restrictive lung disease both granulomatous and lymphoproliferative histopathological patterns are demonstrated. Malignancy is also described in CVID and occurs in up to 15% of patients. The prevalence of non-Hodgkin lymphoma and gastric carcinoma are particularly increased in CVID.

Imaging findings OR Procedure details

Pulmonary involvement occurs due to recurrent infections, airways, granulomatose and lymphoproliferative diseases. There is considerable overlap in imaging findings between acute and chronic, infectious and non-infections complications in patients with CVID.

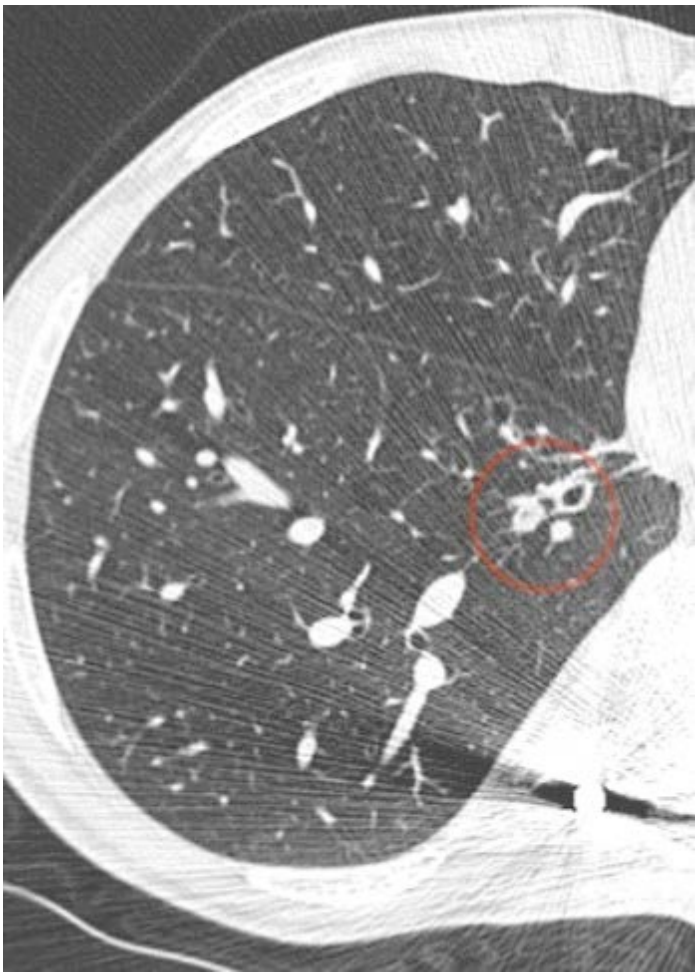

Bronchiectasis with thickening of bronchial walls and mucoid impactation

Up to 20% of patients with CVID experience a systemic inflammatory/granulomatous form of the condition, characterised by lymphocytic and/or granulomatous infiltration of several organs, most commonly the lungs. Granulomatous-lymphocytic interstitial lung disease (GLILD) is a distinct form of interstitial lung disease in patients with CVID.
GLILD may correspond to granulomas, lymphocytic interstitial pneumonia (LIP), lymphoid hyperplasia or follicular bronchiolitis, which are histological patterns that usually coexist and may be different expressions of the same phenomenon.
On CT imaging, GLILD is characterized by lower lung–predominant nodularity, consolidation, and interlobular septal thickening, with perilymphatic distribution. Nodules may be solid or groundglass in attenuation and although bronchiectasis is not a dominant finding in GLILD, it may be present and associated with air trapping. These findings may vary over time.

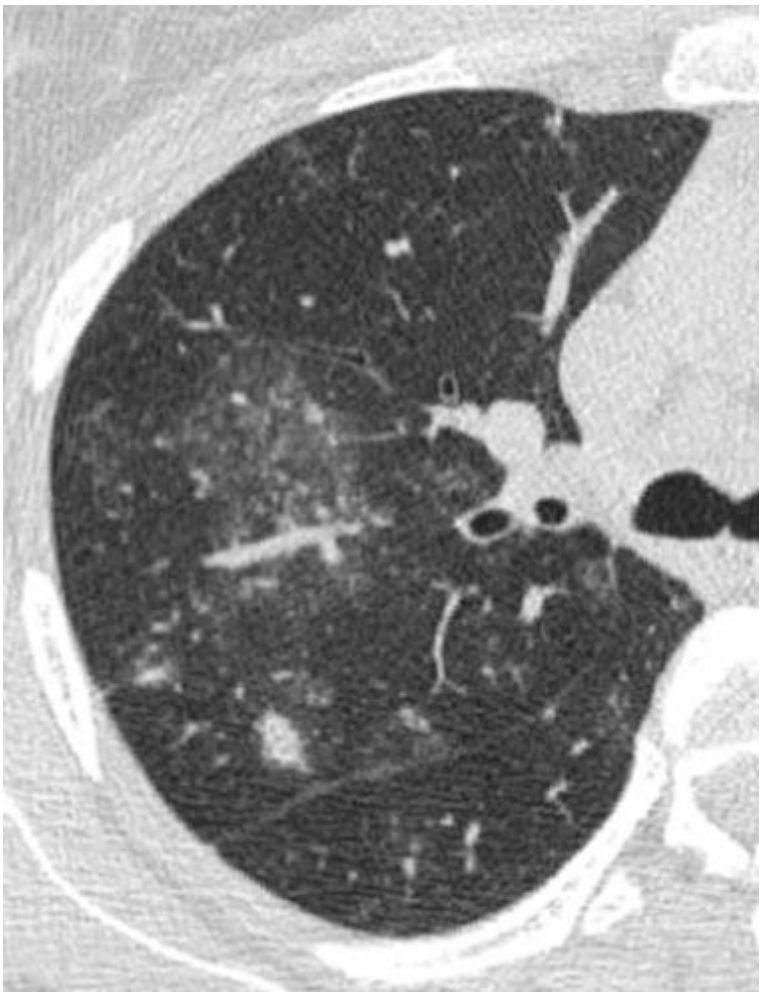

GLILD - diffuse micronodules, small consolidation focci and ground glass areas

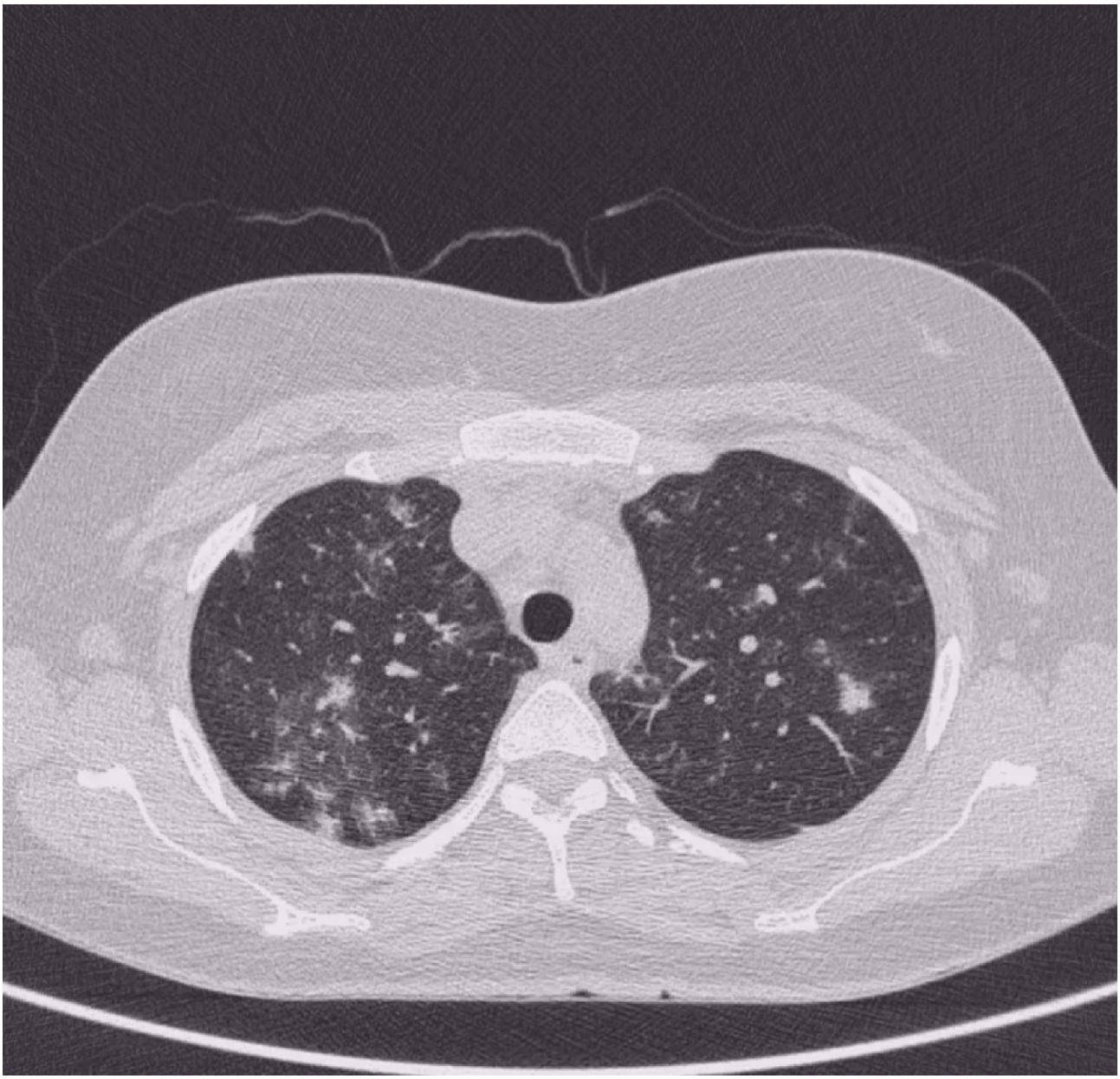

GLILD - diffuse micronodules, small consolidation focci and ground glass areas

Conclusion

CVID is a complex mix of immunologic disorders, associated with recurrent infections, autoimmunity, and chronic lung disease. The radiologist can add value to the diagnosis by understanding the spectrum of abnormalities that may be found, and by early identification of complications, which may result in better outcomes.

A-611

Pulmonary metastasis from spinal meningioma.

D. Orlovs[1,2], D. S. Putriņš[1], I. Priedīte[1], E. Kreitāle[1], R. Mikijanskis[3]
[1]Pauls Stradiņš University Hospital, Institute of Diagnostic Radiology, Riga, Latvia, [2]Rīga Stradiņš University, Faculty of Residency, Rīga, Latvia, [3]Pauls Stradiņš University Hospital, Department of Neurosurgery, Rīga, Latvia

Learning Objectives

Although extremely rare, pulmonary metastasis from a meningioma can prove to be a diagnostic challenge and might delay or otherwise negatively influence treatment strategies. Therefore, if a radiologist should find themselves dealing with unexpected pulmonary findings in a patient with a primary meningioma, it merits further examination.

Background

Meningiomas are common tumours of the meninges, mostly found intracranially, with a much smaller proportion being spinal.[1] Although mainly considered benign and indolent, in rare cases they can exhibit malignant behaviour.[2] Distal metastases of meningiomas are very uncommon and mostly occur in high grade tumours;[3],[4] however, relevant current literature is scarce,[5] with reports of imaging findings being even rarer.

Imaging findings OR Procedure details

A 58-year-old female was referred to a university hospital due to complaints of progressing lower back pain and inconclusive findings on lumbar spine CT. At the time, no respiratory symptoms or signs were observed. Thoracic and lumbar spine contrast-enhanced MRI revealed a pathologic intradural extramedullary mass spanning the thoracolumbar junction with extensive contrast accumulation.

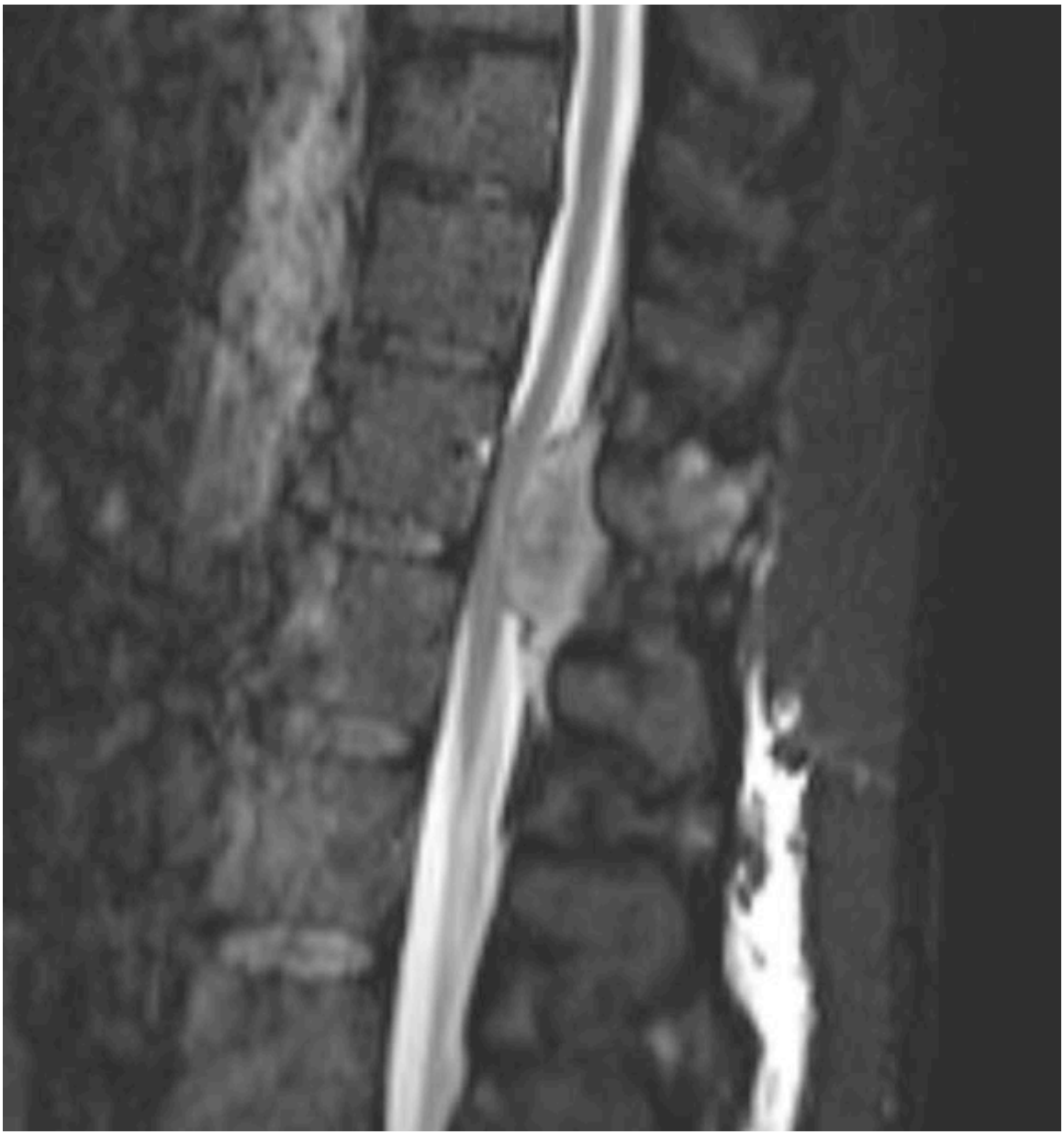

Sagittal fat suppressed T2 scan of the primary spinal lesion on 3T MRI showing an intradural extramedullary thoracic-lumbar spine lesion with spinal cord compression.

A preoperative thoracic contrast enhanced CT examination showed an incidental second lesion within the left lung. The pulmonary lesion abutting the left heart border was ovoid, well circumscribed, approximately 3.5 cm in average size, consisting of parts of vividly enhancing solid tissue density intertwining with areas of necrotic degeneration, with some pleural retraction.

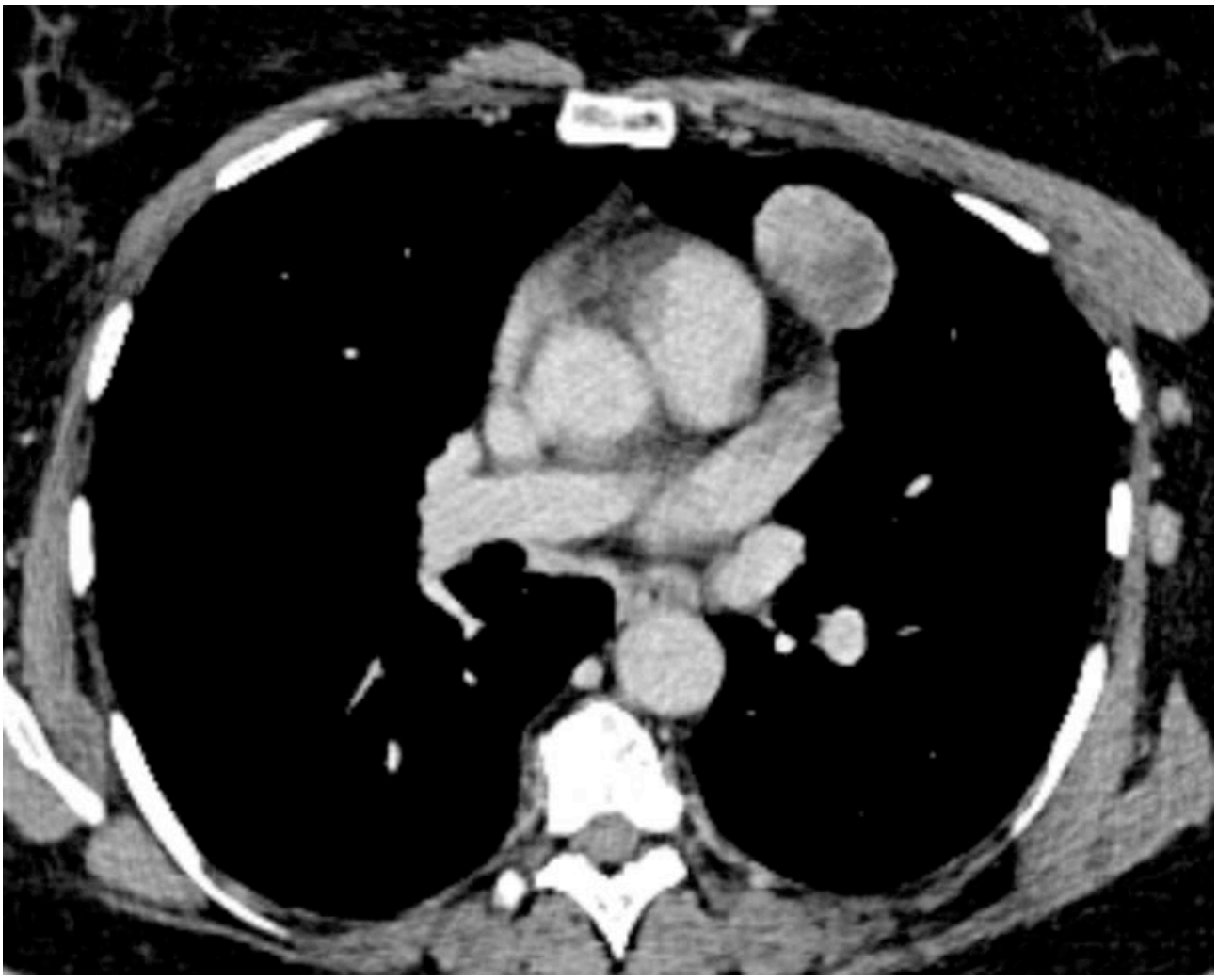

Axial venous phase thoracic CT scan showing a rounded vividly enhancing intrapulmonary mass in the same patient.

It was at first assumed to be associated with the spinal lesion, although the precise relationship was unclear. After tumour board review, a decision to remove the spinal cord compressing mass was made, followed by a successful operation. Based on the pathological diagnosis of meningioma, the masses were treated as separate entities for a short while thereafter. The patient underwent subsequent adjuvant radiotherapy and was scheduled for radical left upper lobe resection and lymphadenectomy a few months later. A final interdisciplinary meeting, after thorough review of tumour histology, concluded that the pulmonary lesion was indeed most likely a metastasis of an atypical Grade 2 (WHO) spinal meningioma.

Conclusion

This clinical case demonstrated a very rare finding of an atypical spinal meningioma metastasizing to the lung. Few similar cases have been documented containing thorough imaging review of pulmonary findings, with the presented lesion resembling most previous reports. Further patient management remains unclear due to a lack of standardised treatment protocols, and multimodal imaging findings such as MRI and PET-CT are as of yet undescribed, potentially warranting further inquiries.

References:

[1] Kobayashi K, Ando K, Matsumoto T, et al., (2021), Clinical features and prognostic factors in spinal meningioma surgery from a multicenter study., Sci Rep, doi:10.1038/s41598-021-91225-z

[2] Utsumi, T., Saito, T., Ishida, M. et al., (2022), Solitary pulmonary metastasis after meningioma surgery of the head: a case report, Surg case rep, https://doi.org/10.1186/s40792-022-01379-9

[3] Kessler RA, Garzon-Muvdi T, Yang W, et al. , (2017), Metastatic Atypical and Anaplastic Meningioma: A Case Series and Review of the Literature, World Neurosurgery.

[4] Louis, DN, Ohgaki, H, Wiestier, OD, et al., (2016), WHO Classification of Tumours of the Central Nervous System. 4th ed.

[5] Montgomery EY et al., (2023), Metastatic Meningioma: A systematic review of incidence and risk factors, Interdisciplinary, Neurosurgery, https://doi.org/10.1016/j.inat.2023.101720

A-315

Pulmonary sarcoidosis and tracheal amyloidosis: an unusual association in a young woman.

B. Lugli[1], D. Cozzi[2], E. Cavigli[2], C. Moroni[2], S. Luvarà[2], L. Gozzi[1], V. Pasini[3], R. Piperio[4], G. Camiciottoli[5], S. Tomassetti[6], V. Miele[2]

[1]Univerisity of Florence, Florence, Italy, [2]Careggi University Hospital, Radiology Emergency Department, Florence, Italy, [3]Careggi University Hospital, Department of Experimental and Clinical Medicine, Florence, Italy, [4]Careggi University Hospital, Department of

Interventional Pneumology, Florence, Italy, [5]Univerisity of Florence, Department of Biomedical, Experimental and Clinical Sciences, Florence, Italy, [6]Univerisity of Florence, Department of Experimental and Clinical Medicine, Florence, Italy

Learning Objectives

1. To describe thoracic imaging findings in a patient with pulmonary sarcoidosis and tracheal amyloidosis.
2. To describe the patient's diagnostic work-up.

Background

Sarcoidosis is a disease that typically manifests with bilateral hilar adenopathy and pulmonary reticular opacities. A multi-organ assessment is necessary for suspected cases to obtain additional diagnostic data, confirm the diagnosis, and identify extrapulmonary organ involvement [1][2].

Amyloidosis encompasses various diseases characterized by the extracellular deposition of amyloid fibrils [3]. The clinical manifestations of amyloidosis are dependent upon the site of the amyloid deposits [4][5].

In this report, we present the case of a 42-year-old woman who presented with a persistent cough without fever. The patient's medical history did not reveal any prior pulmonary conditions, except for a smoking habit ten years earlier. A chest radiograph revealed mild pulmonary interstitial thickening in the mid-upper lung fields bilaterally, and further diagnostic tests were subsequently conducted.

Imaging findings OR Procedure details

The HRCT exam showed perilymphatic nodules between 2 and 8 mm in size with a predominantly broncho-vascular and fissural distribution in the upper-to-mid regions in both lungs in the absence of mediastinal lymphadenopathy. With regard to the trachea some focal and partly calcified thickenings of the maximum dimension of 4mm, affecting the right anterior and lateral wall of the trachea in the thoracic tract were noticed.

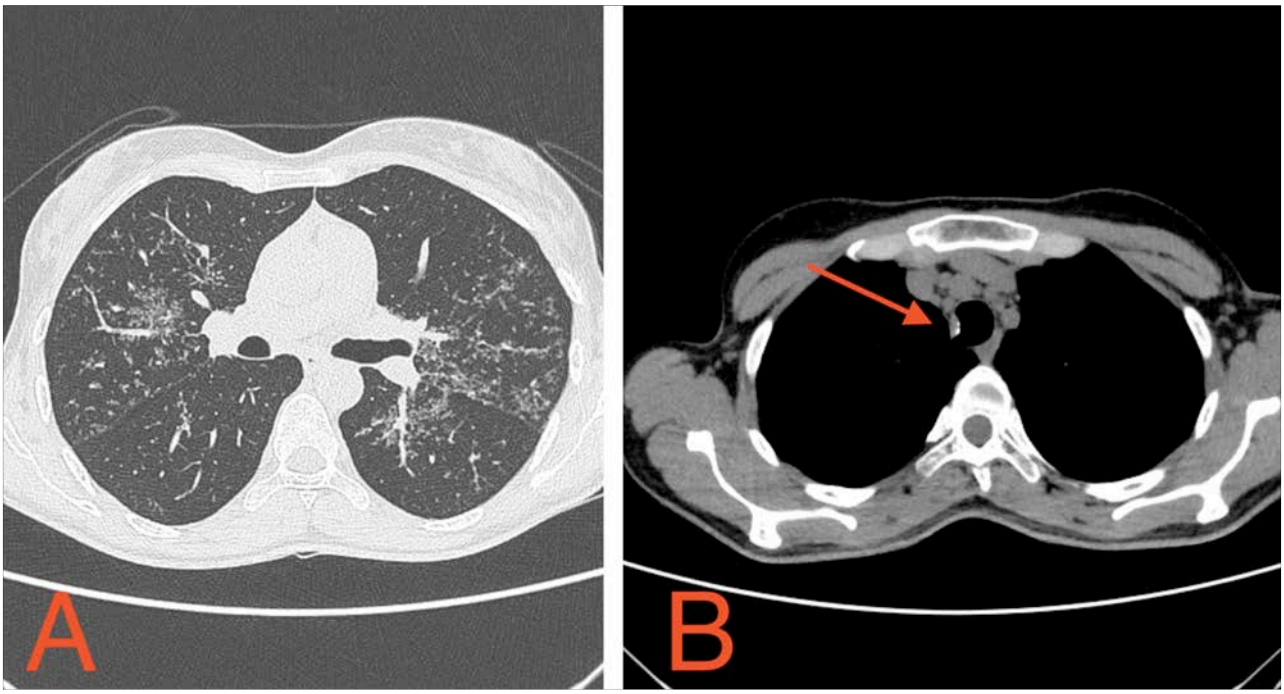

Figure 1- A) CT axial image of the patient showing perilymphatic nodules with predominantly broncho-vascular and fissural distribution in the upper-to-mid regions in both lungs and B) CT axial image showing one of the partly calcific thickenings of the lateral wall of the trachea (red a

These findings appeared suspicious for pulmonary sarcoidosis with tracheal involvement. A PET/CT examination showed hypermetabolism in the regions of the lungs corresponding to the nodules described on the CT scan, and multiple mediastinal lymphadenopathies, compatible with an active granulomatous inflammatory process. The patient received a bronchoalveolar lavage examination, consistent with lymphocytosis without infection, and tracheal biopsies, which stained positive for immunoglobulin light chain amyloid fibrils (AL).

To evaluate the extent of the amyloidosis, the patient received several diagnostic tests, which resulted negative for systemic amyloidosis or monoclonal components.

Because of new-onset dyspnea a new HRCT examination was performed, showing an increase in size of the nodules. These new findings prompted a new bronchoscopy with transbronchial and tracheal biopsies. The lung biopsies were consistent with a sarcoidosis diagnosis, while the tracheal ones confirmed the tracheal AL amyloidosis.

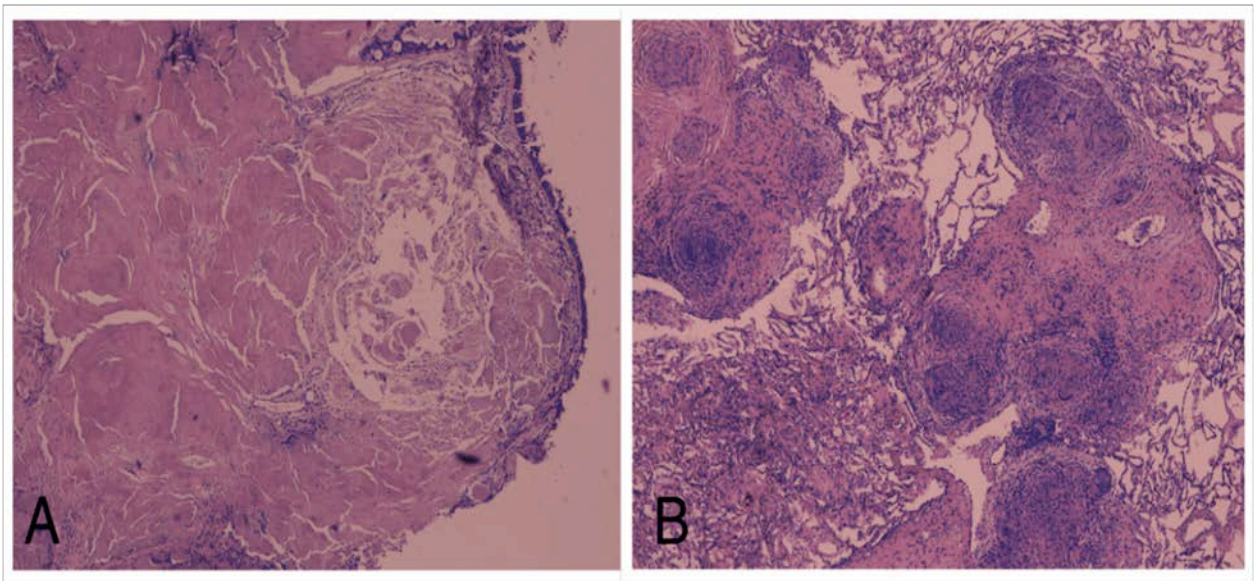

Figure 2 - Histological findings of: A) deposits of amyloid fibrils in the trachea and B) non-caseous granulomatous infiltrates in the lung indicative of Sarcoidosis.

Conclusion

Radiologists should be familiar with the potential connections between sarcoidosis and AL amylodiosis and know the plausible imaging characteristics.

References:

[1] Judson, M. A. , (2008), The diagnosis of sarcoidosis. , Clinics in chest medicine, 29, 415-427, 3
[2] Judson, M. A. , (2007), Extrapulmonary sarcoidosis. In seminars in respiratory and critical care medicine , Thieme Medical Publishers, Inc., 28, 333 Seventh Avenue, New York, NY 10001, USA, 083-101, 01
[3] Wechalekar, A. D., Gillmore, J. D., & Hawkins, P. N. , (2016), Systemic amyloidosis. , The Lancet, 387, 2641-2654, 10038
[4] Pitz, M. W., Gibson, I. W., & Johnston, J. B. , (2006), Isolated pulmonary amyloidosis: case report and review of the literature. , American journal of hematology, 81, 212-213, 3
[5] Oka, H., Ishii, H., Iwasaki, T., Amemiya, Y., Otani, S., Yoshioka, D.,….& Kadota, J. I. , (2009), Tracheobronchial amyloidosis in a patient with sarcoidosis. , Internal Medicine, 48, 1715-1716, 18

A-712

Radiology as a key point in the evaluation of post-surgery thoracic imaging

C. Timpanaro[1], E. Tona[1], S. Galioto[1], L. Reali[1], G. La Rosa[1], L. A. Mauro[1], G. Cusumano[2], S. Palmucci[1], A. Basile[1]
[1]University of Catania, Policlinico "G.Rodolico-San Marco", Radiology 1, Catania, Italy, [2]University of Catania, Policlinico "G.Rodolico-San Marco", Thoracic Surgery, Catania, Italy

Learning Objectives

To show the most common thoracic anatomic variations after surgical intervention for treatment of pulmonary neoplasia; to describe main expected post-surgical alterations and potential complications after intervention.

Background

Thoracic radiographs and/or CT are essential in the post-operative evaluation of patients surgically treated for lung cancer; radiologists should be able to distinguish normal post-surgical alterations from any complications, in order to avoid misinterpretations or diagnostic mistakes. From our RIS-PACS archive, we have revised chest X-rays and thoracic CT examinations of 100 patients surgically treated for lung cancer.

Imaging findings OR Procedure details

The treatment of patients with lung cancer is decided on the extension of the tumor and on disease stage. Sub-lobar resection (wedge and segmentectomy), lobectomy and pneumonectomy are the most common surgical techniques. In the early post-operative period patients undergo daily bedside chest radiographs, since that they can easily detect the correct position of thoracic devices and possible complications. Sub-lobar resection could be identified as a parenchymal linear opacity in the peripheral region – with high-attenuating stripes due to the presence of suture materials. Lobectomy consists of the resection of an entire anatomical lobe of the lung. It causes a significant reduction in the parenchymal volume, and the remaining lobes develop a compensatory mechanism. Pneumonectomy is the surgical resection of an entire lung, which is associated with hilar dissection, ligation of the ipsilateral bronchus and hilar vessels. Chest radiograms will show a progressive filling by fluid of the residual cavity, which will appear full of air on the first day, and full of liquid, up to complete opacification, in the following weeks. The presence of a new air-fluid interface always indicates complications, including anastomotic leak or bronchopleural fistula. Other complications could be represented by hemothorax and thrombosis of the main or lobar pulmonary artery stump.

Conclusion

The radiologist plays an essential role in the follow-up of pulmonary resection because the early identification of any complications in these patients, often critical, allows timely and appropriate treatment, improving the outcome. Radiology, once again, proves to be a key point in the post-operative multidisciplinary management for the correct identification and interpretation of the expected versus unforeseen complications.

A-676

Rasmussen's aneurysm: a lesser-known, but serious complication of pulmonary tuberculosis

D. Musetescu[1], C. Caraenache[2], A. Eddan[1]
[1]Marius Nasta Institute of Pneumology, Bucharest, Romania, [2]Craiova Clinical Emergency Hospital, Craiova, Romania

Learning Objectives
To acknowledge the importance of Rasmussen's aneurysm diagnosis. To present the radiological appearance of this entity, reviewing a case of a patient with previous pulmonary tuberculosis who presented with hemoptysis. To discuss the possible outcomes of Rasmussen's aneurysm and treatment options.

Background
Pulmonary tuberculosis (TB) remains a common disease in many parts of the world, especially in developing countries. Many patients pose an important risk of developing complications, mostly because of the destructive potential of Mycobacterium tuberculosis. Hemoptysis can be encountered in the active stage of tuberculosis, but also following completion of treatment. Usually, this is caused either by reactivation, bronchiectasis or another infectious process developed in a residual cavitary lesion. Sometimes, a vascular abnormality can be the source of a significant bleeding that may require embolization or surgical treatment.

Imaging findings OR Procedure details
Rasmussen's aneurysm, first described in 1968, represents an aneurysmal dilatation of a pulmonary artery branch inside or in the proximity of a tuberculous cavity. In clinical practice, it is a very rare complication, found in less than 1% of TB cases. Therefore, it might be also little known among physicians. However, it has a considerable risk of rupture with major hemorrhage. CT pulmonary angiography has a key role in detecting this abnormality in order to take adequate measures and prevent fatal outcomes.

Conclusion
Although Rasmussen's aneurysm is an uncommon cause of hemoptysis in complicated TB, it is crucial to recognize its appearance as the implications can be life-threatening.

A-182

Rising to the challenge of the multidisciplinary discussion; regarding interstitial lung disease: tips for the radiologist.

D. García Casado[1], F. León Román[2], I. Álvarez Silva[3], M. Yasuda[4], G. Fernández Pérez[5]
[1]Hospital Recoletas, Radiology, Segovia, Spain, [2]Hospital de Recoletas, Neumología, Valladolid, Spain, [3]Complejo Asistencial de Segovia, Radiología, Segovia, Spain, [4]Hospital de Recoletas, Radiología, Valladolid, Spain, [5]Grupo Recoletas, Radiología, Valladolid, Spain

Learning Objectives
Our objectives are to establish our role in the MDT, to provide a simplified but effective reading structure of the HRCT images, to describe the main radiological patterns and questions asked in the MDD, and to summarize some basic, yet useful and updated tools which include some of the latest guidelines and consensus papers.

Background
The primary goals for any MDT are the etiological assesment, and the diagnosis and management of the diseases. There should be present at least one clinician, one pathologist and a radiologist for this purpose, and when it comes to the diagnosis of the interstitial lung disease (ILD), rheumatologists are also required to be part of the team, due to the high prevalence of lung involvement in connective tissue diseases (CTDs). Participation might extend in some institutions to thoracic surgeons, nurses or other professionals who are engaged in the ILD management.

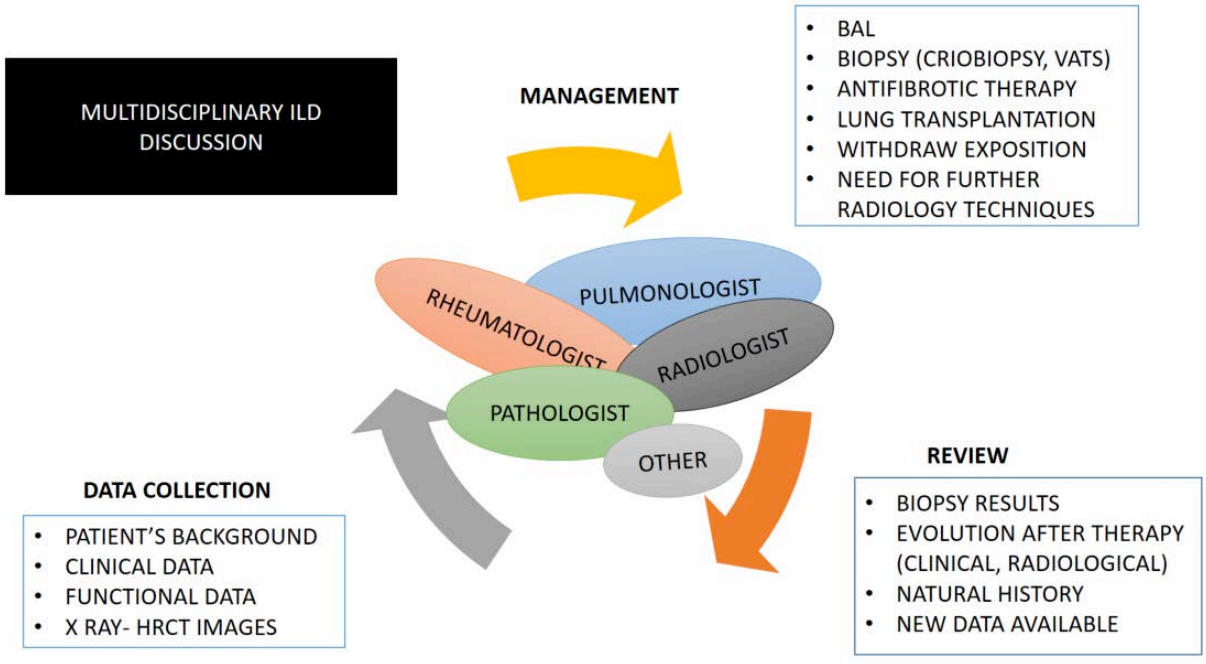

The role of the radiologist in the multidisciplinary discussion (MDD) as regards the ILD diagnosis is both essential and challenging; many unspecific radiological findings or the coexistence of patterns on HRCT are to be found on a daily basis, and so radiological expertise in this field is usually required in order to take part in the team. However, every beginning is difficult and every institution is different.[1]

Imaging findings OR Procedure details
The diagnosis in the MDT is a dynamic process; the more we understand it, the better we will be able to succesfully ask the right questions and provide the correct answers.
A simplified reading structure of the HRCT is a quick tool to unconsciously start narrowing the differential diagnosis of ILD. At least coronal images should be available to rapidly assess lung volume and distribution of the findings.
The guidelines are there to help us speak a common language. Deciding when to apply them and when not to is part of the individualized patient care and one of the main reasons why there is the need of an ILD-MDD. We put the emphasis on the diagnosis of UIP and CTD-related ILDs, but also other frequently seen entities (such as hypersensitivity pneumonitis, smoking related lung disease) [2][4][5].We also give some quick tools to understand their clinical management, so that we can give the clinicians the information they need [3].

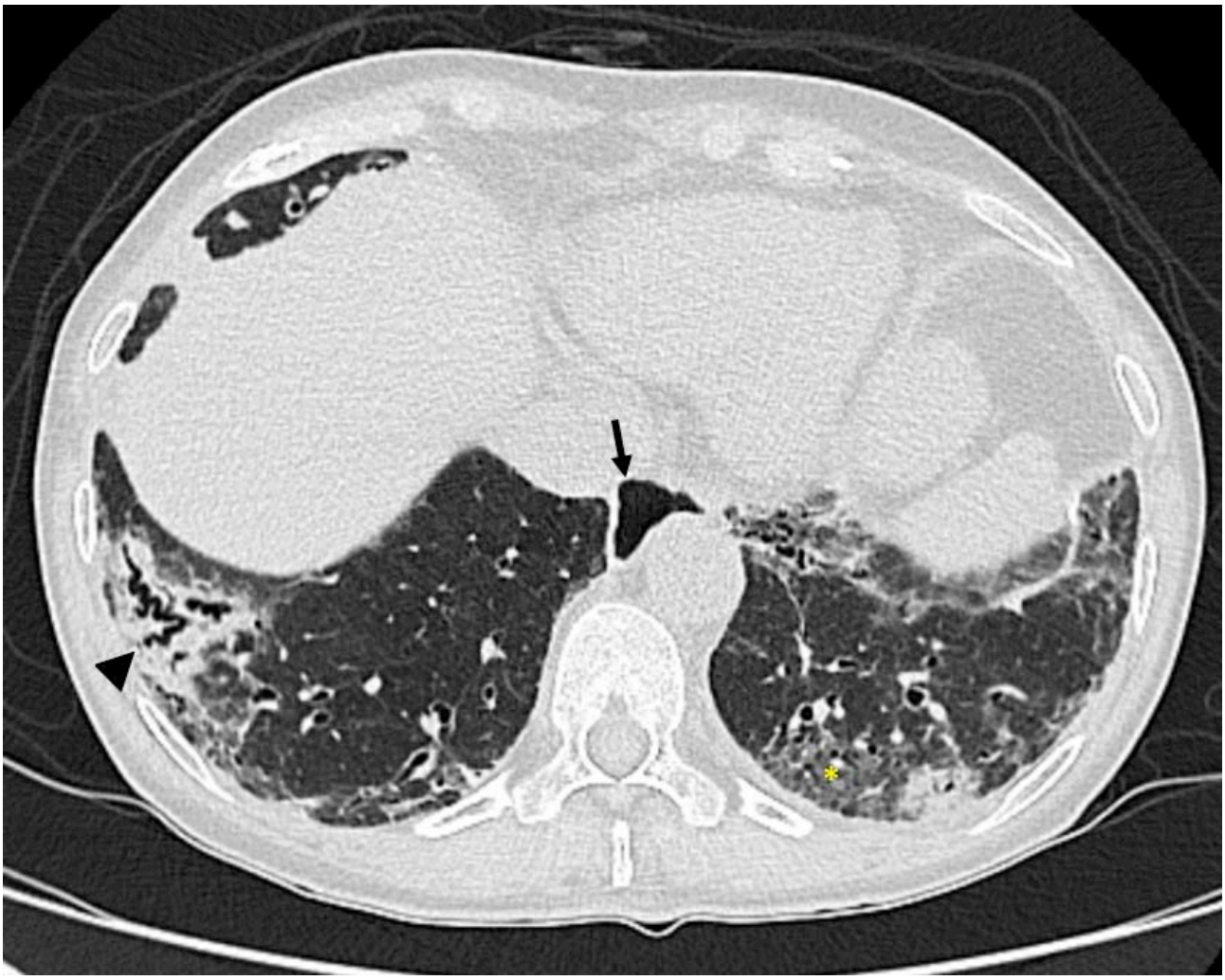

NSIP in a patient with systemic sclerosis. Note the sinusoidal bronchiectasis (arrowhead), the groundglass opacities with subjacent reticulation (yellow star) and the esophageal dilatation (arrow)

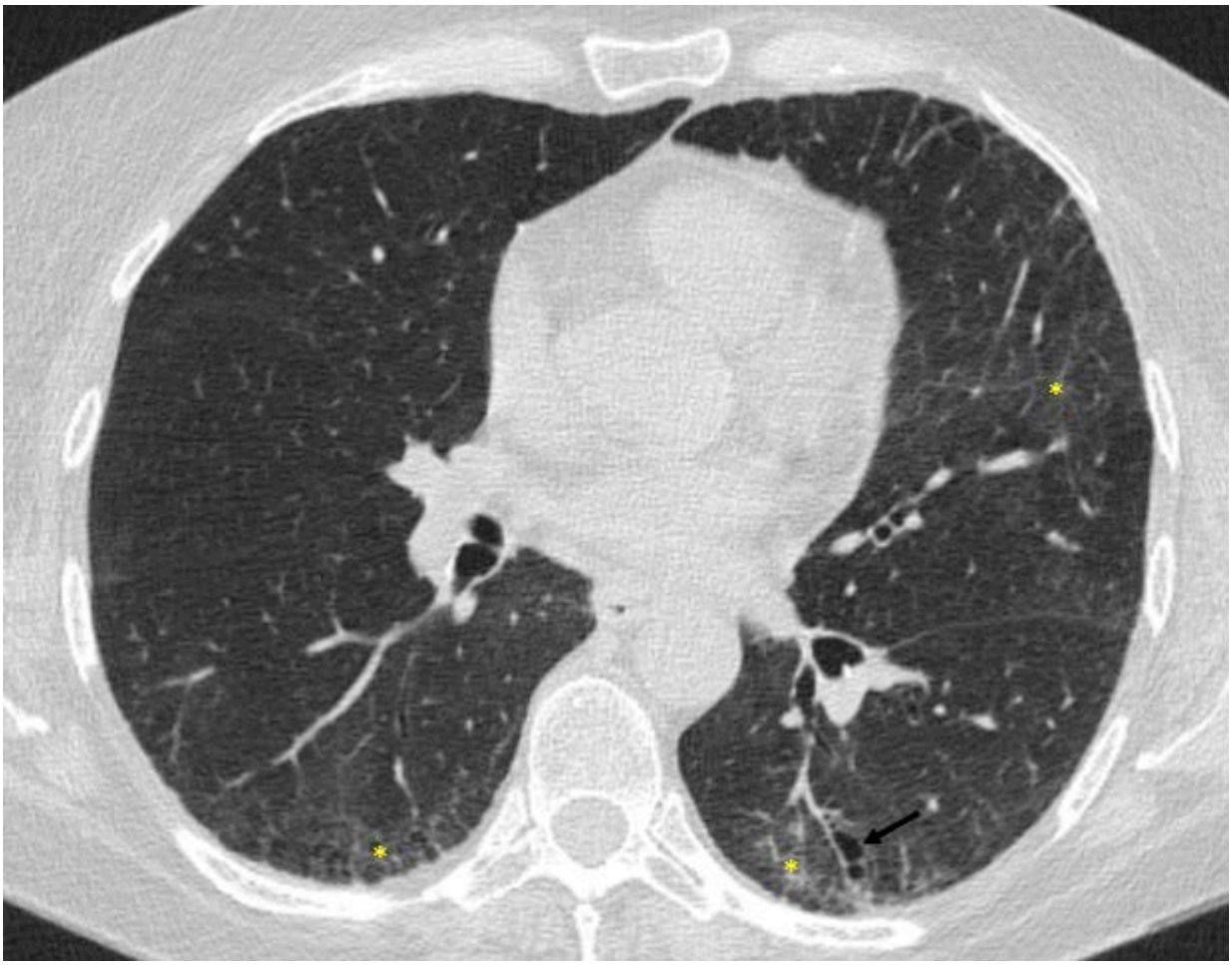

Patient with lymphoplasmacytic lymphoma with no current treatment and without known autoimmune disorder presents with respiratory symptoms. HRCT image shows reticulation within ground glass opacities (yellow stars) and bronchiectasis (arrow) with no subpleural sparing. Criobiopsy was performed with the diagnosis of unspecific interstitial fibrosis

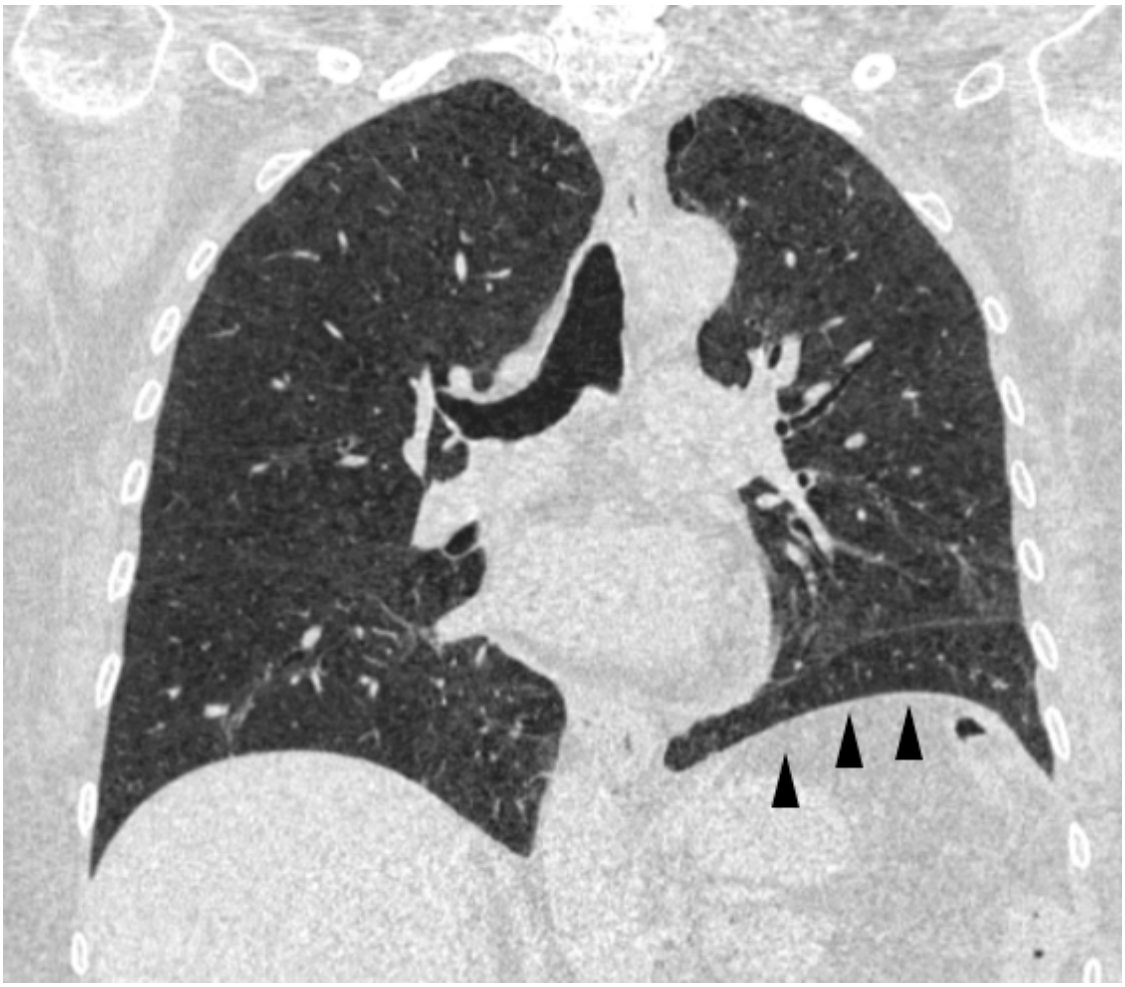

Coronal HRCT image shows elevation of the left hemidiaphragm due to volume loss of the lower left lobe.

Conclusion

We hope that with these tools we can help the less experienced radiologists to succesfully rise to the challenge of ILD-patient care in the MDT environment, by providing a starting point to minimize the fears and doubts that might discourage their participation.
Our role as radiologists in the ILD-MDT is essential, but it is just one piece of the puzzle. Fluid, constructive, dialogue between the participants and the creation of a good learning environment is the way forward towards excellence.

References:

[1] Walsh SLF, Multidisciplinary evaluation of interstitial lung diseases: current insights
[2] Raghu G, (2020), Diagnosis of Hypersensitivity Pneumonitis in Adults. An Official ATS/JRS/ALAT Clinical Practice Guideline.
[3] Maldonado F, (2020), Transbronchial Cryobiopsy for the Diagnosis of Interstitial Lung Diseases: CHEST Guideline and Expert Panel Report. Chest.
[4] Travis WD, An official American Thoracic Society/European Respiratory Society statement: Update of the international multidisciplinary classification of the idiopathic interstitial pneumonias.
[5] Raghu G, (2022), Idiopathic Pulmonary Fibrosis (an Update) and Progressive Pulmonary Fibrosis in Adults: An Official ATS/ERS/JRS/ALAT Clinical Practice Guideline.

A-700

Signs to suspect congenital chest malformations in the plain radiograph

C. Vila[1], R. Vidal[2], A. Narbona[3], M. Huguet[3], J. Caceres[3]
[1]Centro Medico Teknom, Radiology, Barcelona, Spain, [2]Centro Medico Teknon, Radiology, Barcelona, Spain, [3]Teknon Medical Center, Radiology, Barcelona, Spain

Learning Objectives

To identify levocardia with abdominal inversion in the plain film
To detect signs of pulmonary artery agenesis
To show signs of bronchial atresia and scimitar sindrome

Background

Many congenital chest malformations (CCM) are asymptomatic and not discovered until adulthood. They may show bizarre images that may be confused with other processes. Their features in the chest film are easily recognizable if one knows their imaging manifestations. The suspected diagnosis is easily confirmed with cross-sectional techniques

Imaging findings OR Procedure details

We plan to present our experience in four selected CCMs, which in our opinion have specific signs in the chest radiograph that allow to suspect them

1. LEVOCARDIA AND ABDOMINAL INVERSION

In this malformation the thoracic structures are in normal position, whereas the abdominal viscera are inverted. This anomaly is accompanied by polysplenia and proximal interruption of IVC with azygos continuation
Typical signs in the chest film are a large azygos arch and gastric bubble under the right hemidiaphragm
CT findings: inversion of abdominal viscera as well as polysplenia in the abdominal RUQ Interruption of IVC with azygos continuation is also visible.

2. CONGENITAL INTERRUPTION OF PULMONARY ARTERY

In this malformation the main right/left pulmonary artery is absent. It occurs with the same frequency in both sides. Right aortic arch occurs in half of cases
Signs in the chest film: small lung with small hilum and decreased vascularity. Right aortic arch supports the diagnosis of this anomaly. Expiratory films do not show air-trapping, excluding McLeod syndrome
Findings in CT are pathognomonic, demonstrating an absent main pulmonary artery

3. CONGENITAL BRONCHIAL ATRESIA

Due to focal interruption of a segmental bronchus, which results in associated mucous impaction and hyperinflation of the obstructed lung segment.
Findings in the chest radiographs: focal area of hyperlucent lung parenchyma with tubular shadows that represent mucous plugs. Expiration films confirms air-trapping
Enhanced CT is diagnostic showing the mucous plugs better and excluding organic causes of bronchial obstruction (endobronchial tumors or inflammatory stenosis)

HYPOGENETIC RIGHT LUNG (SCIMITAR SYNDROME)

Due to agenesis of one/two lobes of right lung. Usually accompanied by anomalous vein (scimitar vein) which drains the right lower lobe into to the IVC
Chest findings: small right lung with small hilum and mediastinal displacement. When present, scimitar vein is visible in 50% of cases
CT findings: Absent lobe(s), anomalous bronchial branching. Scimitar vein. Accompanying malformations such as duplicated diaphragm or horseshoe lung can be seen

Conclusion

Some congenital chest malformations can be suspected in the plain film if we know their main manifestations

A-433

Spectrum of diseases associated with diffuse pulmonary haemorrhage: a diagnostic challenge

C. Lozano, X. Gallardo, M. Cufí, M. Andreu, E. Castañer
Hospital Parc Tauli, Thoracic radiology, Sabadell, Spain

Learning Objectives

-To Learn the different causes of diffuse pulmonary haemorrhage, its pathophysiology and radiological signs.
-To know that the correlation with the clinical history and laboratory data will be the key for the diagnosis.

Background

Diffuse pulmonary haemorrhage (DPH) is an uncommon entity resulting in intra-alveolar haemorrhage. The histopathologic diagnosis includes diseases associated with pulmonary capillarity and those associated with normal vessels (bland haemorrhage).
Clinical and radiological imaging are non-specific, so diagnosis can be a major challenge.

Imaging findings OR Procedure details

A wide group of diseases are associated with DPH. We propose a review of the aetiologies through a series of clinical-radiological cases.
To simplify we will approach the causes of DPH from the histopathological pattern.

-Pulmonary capillaritis: neutrophilic infiltration of the alveolar septa leading to necrosis of the lung interstitium.
 -Small vessel vasculitis / Anti-GBM (GoodPasture) (all pulmonary-renal syndromes).
 -Rheumatic diseases (Lupus).
 -Drugs.
-Bland pulmonary haemorrhage: alveolar haemorrhage without destruction or inflammation of the alveolar spaces.
 -Anticoagulant, bleeding disorders.
 -Heart failure, mitral stenosis.
 -Idiopathic pulmonary hemosiderosis.

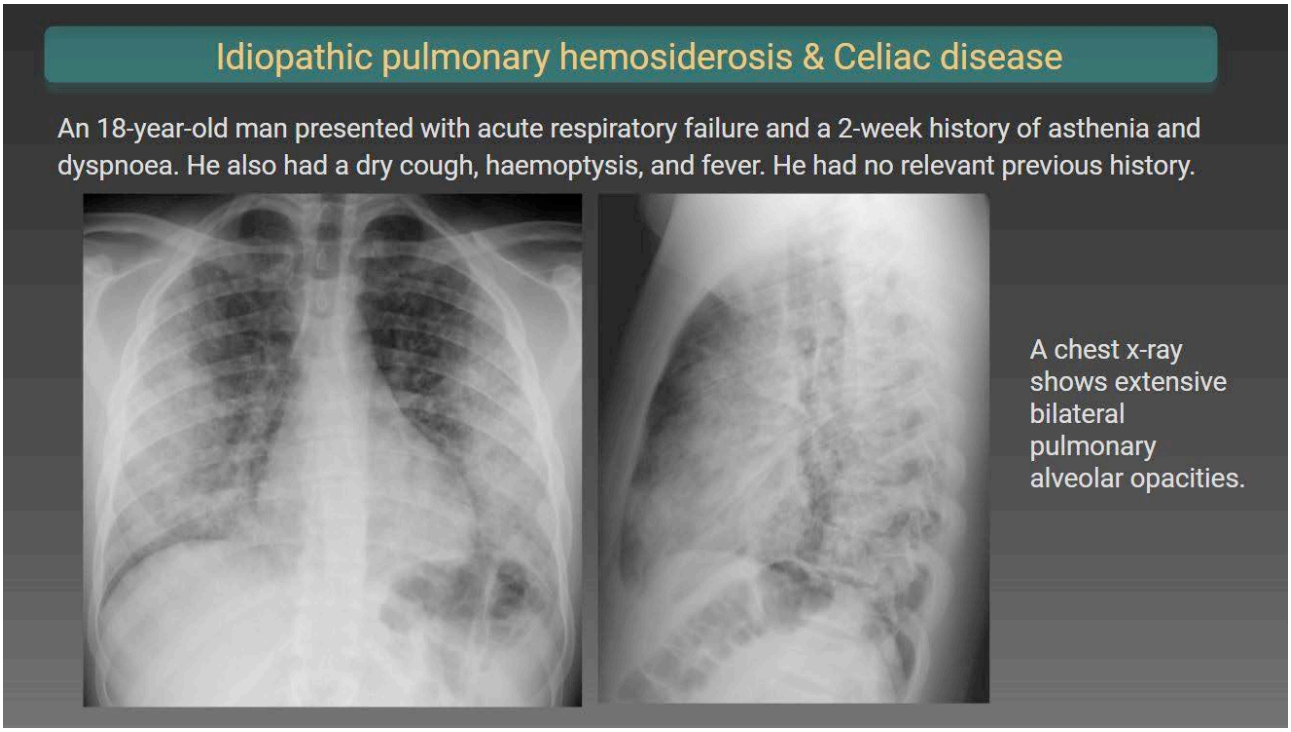

Idiopathic pulmonary hemosiderosis & Celiac disease

An 18-year-old man presented with acute respiratory failure and a 2-week history of asthenia and dyspnoea. He also had a dry cough, haemoptysis, and fever. He had no relevant previous history.

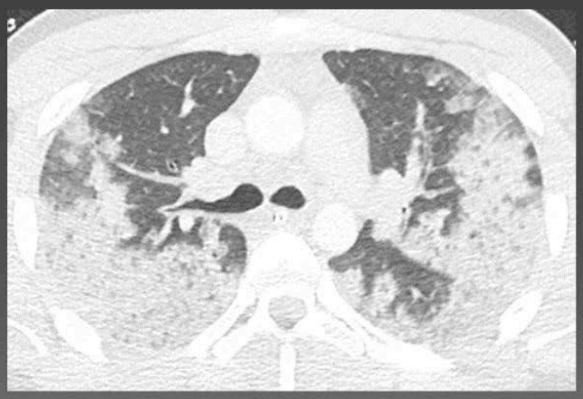

➔ A CT scan was performed which confirmed the extensive alveolar lung involvement.

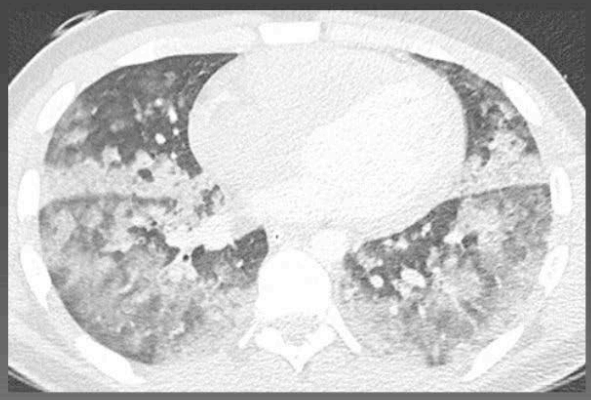

Idiopathic pulmonary hemosiderosis & Celiac disease

An 18-year-old man presented with acute respiratory failure and a 2-week history of asthenia and dyspnoea. He also had a dry cough, haemoptysis, and fever. He had no relevant previous history.

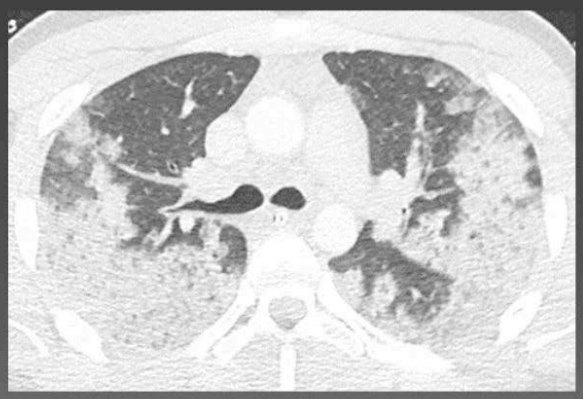

Laboratory study:

- *Hb 7 g/dL*
- *+ Transglutaminase IgA and Endomysial IgA antibodies*
- ***BAL:** Haemorrhage and 27% hemosiderophages*

Idiopathic pulmonary haemosiderosis

Bland pulmonary haemorrhage.
Recurrent PH with no aetiology.
Can occur at any age but typically affects children and young adults.
Iron-deficiency anaemia.
30% present coeliac disease: **Lane-Hamilton syndrome.**

-Diffuse alveolar damage: alveolar edema and hyaline membranes covering alveolar spaces.
-Infection.
-Drugs.
-Rheumatic diseases (Lupus).

Conclusion

The radiological findings of DPH are nonspecific and we need to incorporate other information (clinical, laboratory, exposure to drugs) to reach the diagnosis.

Small-vessel vasculitis is the most frequent aetiology of DPH. Heart failure (HF) is probably an underrecognized cause of DPH; in the context of HF, think about this possibility if the patient has lung opacities that do not resolve.

A-376

The many faces of mosaic attenuation pattern

B. Freixo, R. Martins, S. Lopes Rodrigues
Instituto Português de Oncologia do Porto Francisco Gentil, Radiology, Porto, Portugal

Learning Objectives

Discuss the various causes of mosaic attenuation pattern on computed tomography (CT).
Explore an approach to narrow the differential diagnosis.
Explore the role of the radiologist in the detection of the underlying disease.

Background

Mosaic attenuation pattern is a nonspecific term used to describe a patchwork of regions of differing pulmonary attenuation on CT imaging. It refers to a pattern that occurs in a variety of lung diseases that can involve the airways, pulmonary vasculature, alveoli, and interstitium[1].

There are three main categories of disease causing a mosaic pattern attenuation that include: 1) small airways disease; 2) pulmonary vascular disease; 3) parenchymal disease[2].

Causes of small airways inflammation include cellular bronchiolitis, respiratory bronchiolitis, hypersensitivity pneumonitis, and follicular bronchiolitis.

The most common vascular causes resulting in mosaic attenuation are chronic thromboembolic pulmonary hypertension and primary pulmonary arterial hypertension.

Parenchymal diseases include acute processes (infection, pulmonary edema and hemorrhage), and subacute and chronic processes (such as organizing pneumonia and fibrotic diseases).

There are strategies to help narrow the differential diagnosis, specifically: -analysis of vascularity in low attenuation area; -using paired inspiratory and expiratory CT scans; -analysis of pulmonary artery, airways and of the heart;-find additional clues [3].

Imaging findings OR Procedure details

Analysis of the size of the pulmonary vessels should be an early step in distinguishing among the causes of a CT mosaic pattern of lung attenuation. In small-airway disease and pulmonary vascular disease, the pulmonary vessels within the lucent regions of the lung are narrowed or occluded compared to the vessels in the attenuated regions of the lung. This difference in vessel caliber is caused by local hypoxic reflex vasoconstriction in small-airway disease, whereas the difference in vessel size in primary vascular lung disease is due to the underlying hypoperfusion.

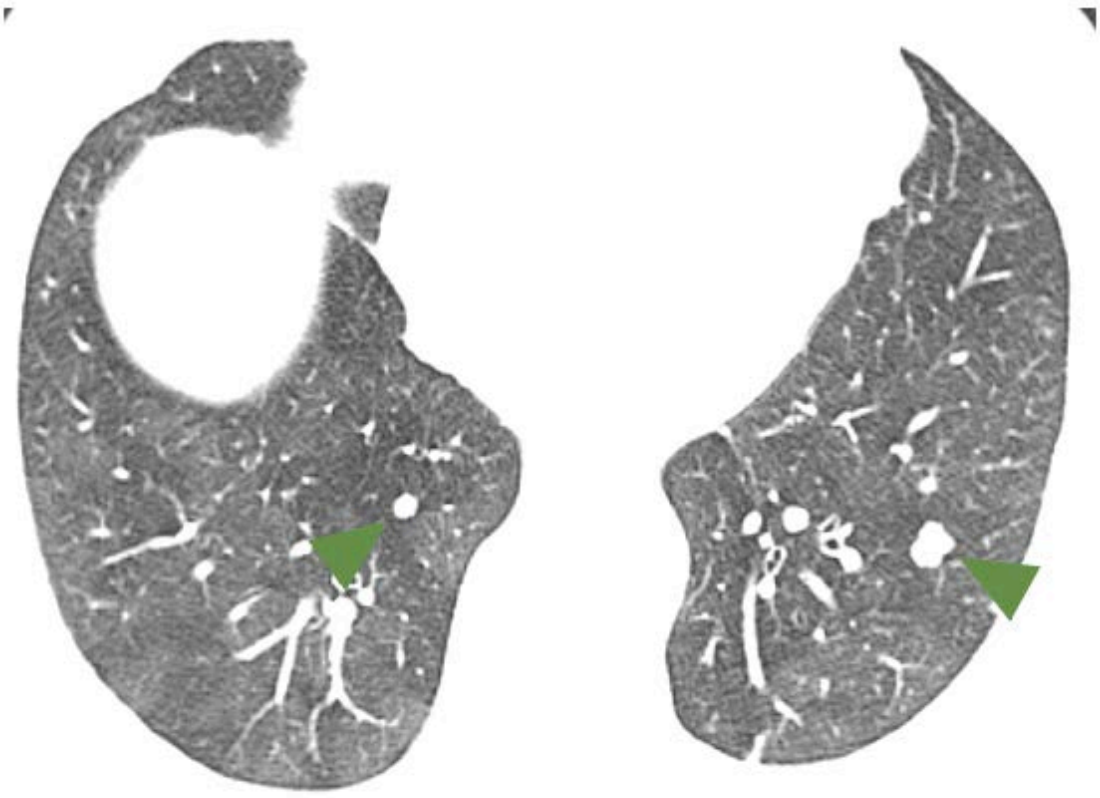

Diffuse idiopathic neuroendocrine cell hyperplasia in a 72-year-old female patient with chronic cough. CT imaging shows bilateral, small, nodules (arrowheads) and mosaic perfusion pattern with relative paucity and reduced size of the subsegmental pulmonary arteries in the areas of reduced attenuation.

On the other hand, in parenchymal diseases, the vessels are uniform in size throughout the different regions of lung.

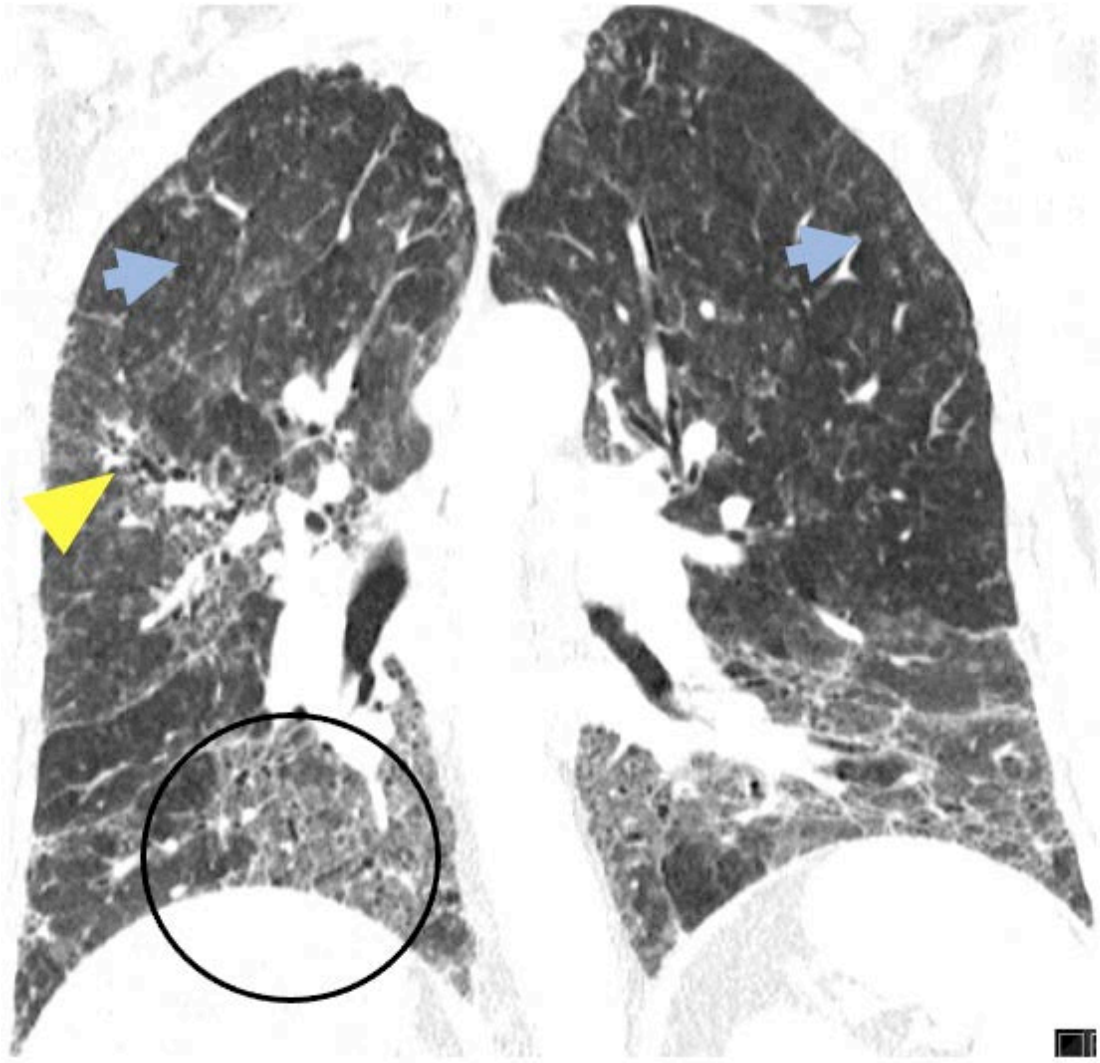

Hypersensitivity pneumonitis. CT scan shows diffuse small centrilobular opacities (arrows), and mosaic attenuation with multiple varying areas of lung attenuation (circle). The presence of mid and upper lung fibrosis with reticulation and bronchiectasis (arrowhead), and areas of airtrapping suggest fibrotic hypersensitivity pneumonitis.

Other imaging clues that can assist the radiologist in pinpointing a diagnosis are air trapping in expiratory CT, large airway dilatation of wall thickening in the low attenuation area, and small centrilobular nodules which suggest small airway disease. Dilated pulmonary artery, dilated right heart or thromboembolic filling defects are other clues that should prompt evaluation for pulmonary vascular disease.

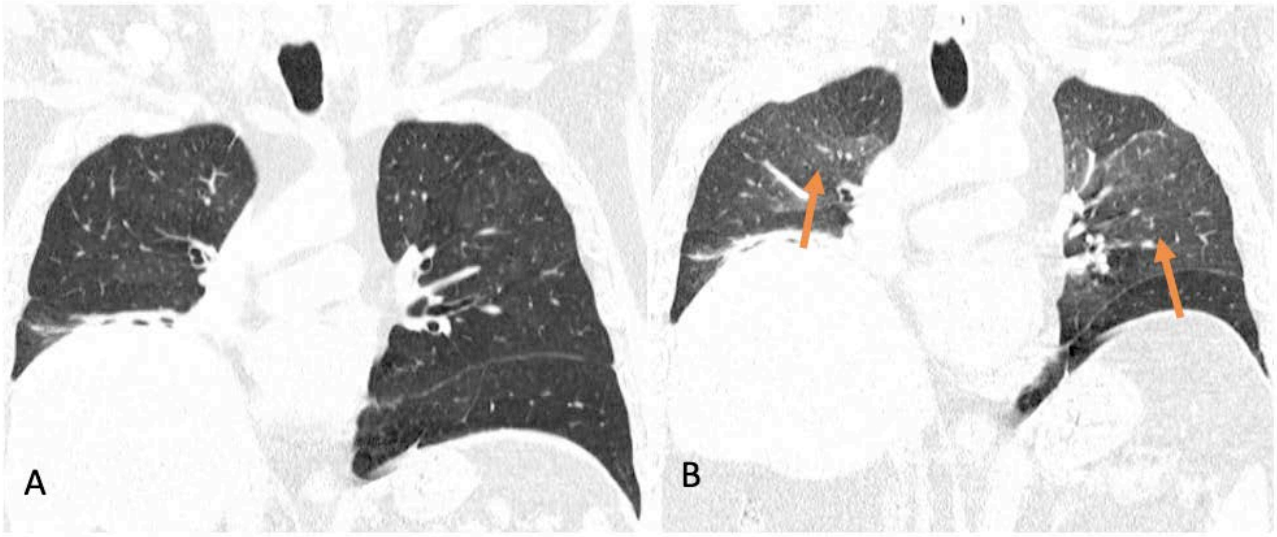

Constrictive bronchiolitis obliterans following allogeneic hematopoietic stem cell transplantation in a 42-year-old patient. Comparison between inspiratory (A) and expiratory (B) axial CT shows much more pronounced multifocal hypoattenuated areas (arrows) at the

same level.

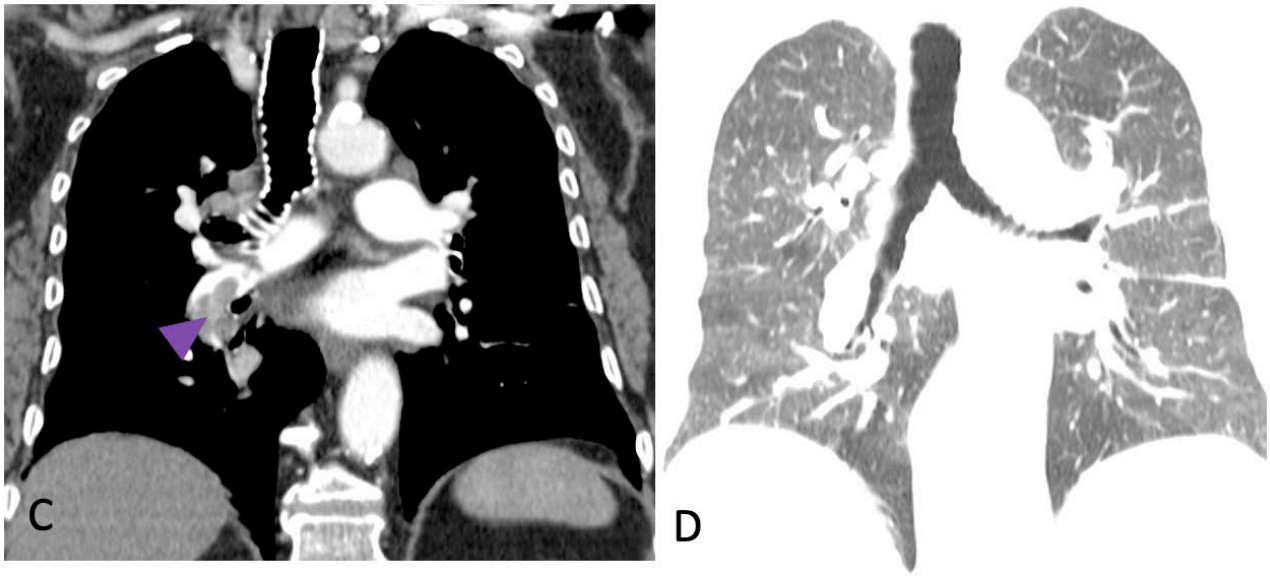

Chronic thromboembolic pulmonary hypertension in a 84-year-old female with breast cancer. Thromboembolic filling defects in proximal right lower lobar artery are seen (arrowhead). Hypoattenuated areas of both lungs (E) imply mosaic attenuation caused by vascular origin.

Conclusion

The mosaic attenuation pattern is a common radiographic finding that can provide valuable diagnostic information for clinicians and help guide the management of patients with various lung diseases.

References:

[1] David M. Hansell, Alexander A. Bankier, Heber MacMahon, Theresa C. McLoud, Nestor L. Müller, and Jacques Remy Radiology 2008 246:3, 697-722, (2008), Fleischner Society: Glossary of Terms for Thoracic Imaging , Radiology, 697-722, 3, https://pubs.rsna.org/doi/abs/10.1148/radiol.2462070712?journalCode=radiology

[2] Seth J. Kligerman, Travis Henry, Cheng T. Lin, Teri J. Franks, and Jeffrey R. Galvin, (2015), Mosaic Attenuation: Etiology, Methods of Differentiation, and Pitfalls, RadioGraphics, 1360-1380, https://pubs.rsna.org/doi/abs/10.1148/rg.2015140308?journalCode=radiographics

[3] Stern EJ, Müller NL, Swensen SJ, Hartman TE, (1995), CT mosaic pattern of lung attenuation: etiologies and terminology, J Thorac Imaging, 294-7, https://pubmed.ncbi.nlm.nih.gov/8523510/

A-736

The many faces of pulmonary edema on CT imaging

S. Pochepnia, R. Milos, S. Röhrich, H. Prosch
Medical University of Vienna, Dept. of Biomedical Imaging and Image-guided Therapy, Vienna, Austria

Learning Objectives

To recognize common and uncommon radiologic appearance of pulmonary edema
To understand different variants of pulmonary edema in various etiology

Background

Pulmonary edema is one of the most common disorders diagnosed during chest examinations in both inpatient and outpatient settings. The pathophysiological mechanism of this disorder is the movement of extracellular fluid from vessels into the pulmonary interstitium and alveoli and can be caused by a variety of etiological factors. Based on the physiological determination of the edema, pulmonary edema can be divided into four main categories: hydrostatic edema (cardiac edema), permeability edema with and without diffuse alveolar damage (non-cardiac edema), and mixed edema, in which both have an increase in hydrostatic pressure and membrane permeability. While the usual imaging manifestations of cardiogenic edema are very familiar to radiologists, atypical manifestations of cardiogenic edema as well as noncardiogenic edema can present a diagnostic challenge to radiologists.

Imaging findings OR Procedure details

Both hydrostatic and permeability edema can be characterized by typical CT manifestations that depend on disease severity and underlying parenchymal disorders: pulmonary vein dilatation, thickening of the interlobular septa, thickening of the bronchovascular bundles, ground glass opacity, pleural and pericardial effusions. However, pulmonary edema may also present with unusual appearance on CT and can be mistaken for other diseases. The role of CT in routine practice is invaluable as it provides the opportunity to detect or rule out pulmonary edema and to assess the possible causes contributing to the manifestation of this disease.

Conclusion

The role of CT in routine practice is invaluable as it offers the opportunity to detect or rule out pulmonary edema, also to evaluate the possible causes contributing to the manifestation of this disease.

A-685

The many faces of pulmonary sarcoidosis

F. Carvalho, C. Mota, L. Resende, L. Ferreira, L. Batista
Centro Hospitalar de Vila Nova de Gaia/Espinho, Radiology, Vila Nova de Gaia, Portugal

Learning Objectives

This poster aims to review the role of radiology in the diagnosis, differential diagnosis and monitoring of pulmonary sarcoidosis, as well as to share images from both usual and unusual cases of this pathology.

Background

Sarcoidosis is a multisystemic granulomatous disease that most commonly affects the lung and the lymphatic system. Radiographic and high-resolution CT (HRCT) imaging plays a critical role in the diagnosis and management of this disease, as the clinical presentation is often nonspecific. Nonetheless, sarcoidosis is known as the “the great mimicker” and may have a wide variety of imaging findings (some of them also seen in other diseases, such as tuberculosis and lymphoma), making its diagnosis particularly challenging.

Imaging findings OR Procedure details

Chest X-ray is the initial imaging modality of choice for pulmonary sarcoidosis and helps stage the disease. Its characteristic findings are bilateral hilar lymphadenopathy and/or diffuse interstitial lung disease. HRCT provides more detailed information and can reveal additional findings, including the typical multiple micronodules with perilymphatic distribution (ie. peribronchovascular, subpleural and interlobular septal distribution), mainly in the upper and middle lung zones. Sarcoidosis can also present with several atypical findings such as ground-glass opacities, consolidation (alveolar sarcoid pattern), cystic disease, airway disease and pleural involvement. Its progression can lead to parenchymal fibrotic changes, presenting with linear/reticular opacities, architectural distortion, traction bronchiectasis and volume loss. HRCT plays an important role in differentiating active inflammation from fibrosis, subsequentially aiding therapeutic decisions.

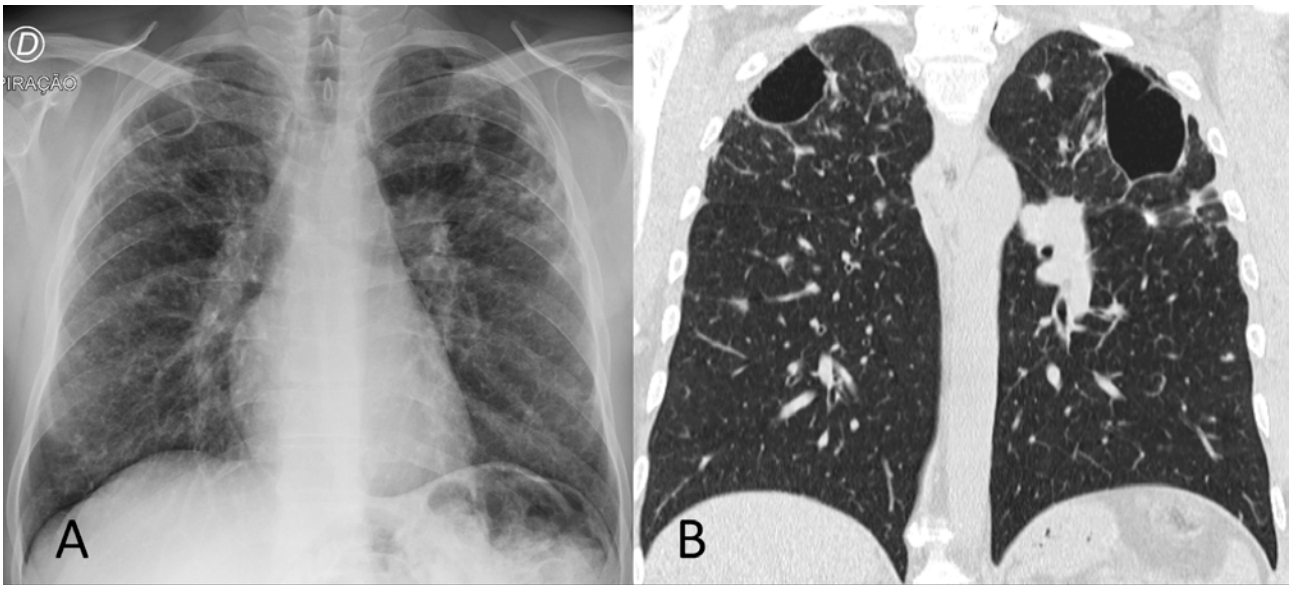

Lung sarcoidosis presenting with cystic pattern and micronodules. (A) Chest-ray demonstrates hilar lymph nodes, diffuse reticular pattern and round hyperlucent areas in pulmonary apices. (B) Coronal high-resolution CT scan shows bilateral apical cysts and micronodules. Bacilar infection was excluded and biopsy confirmed sarcoidosis related cysts.

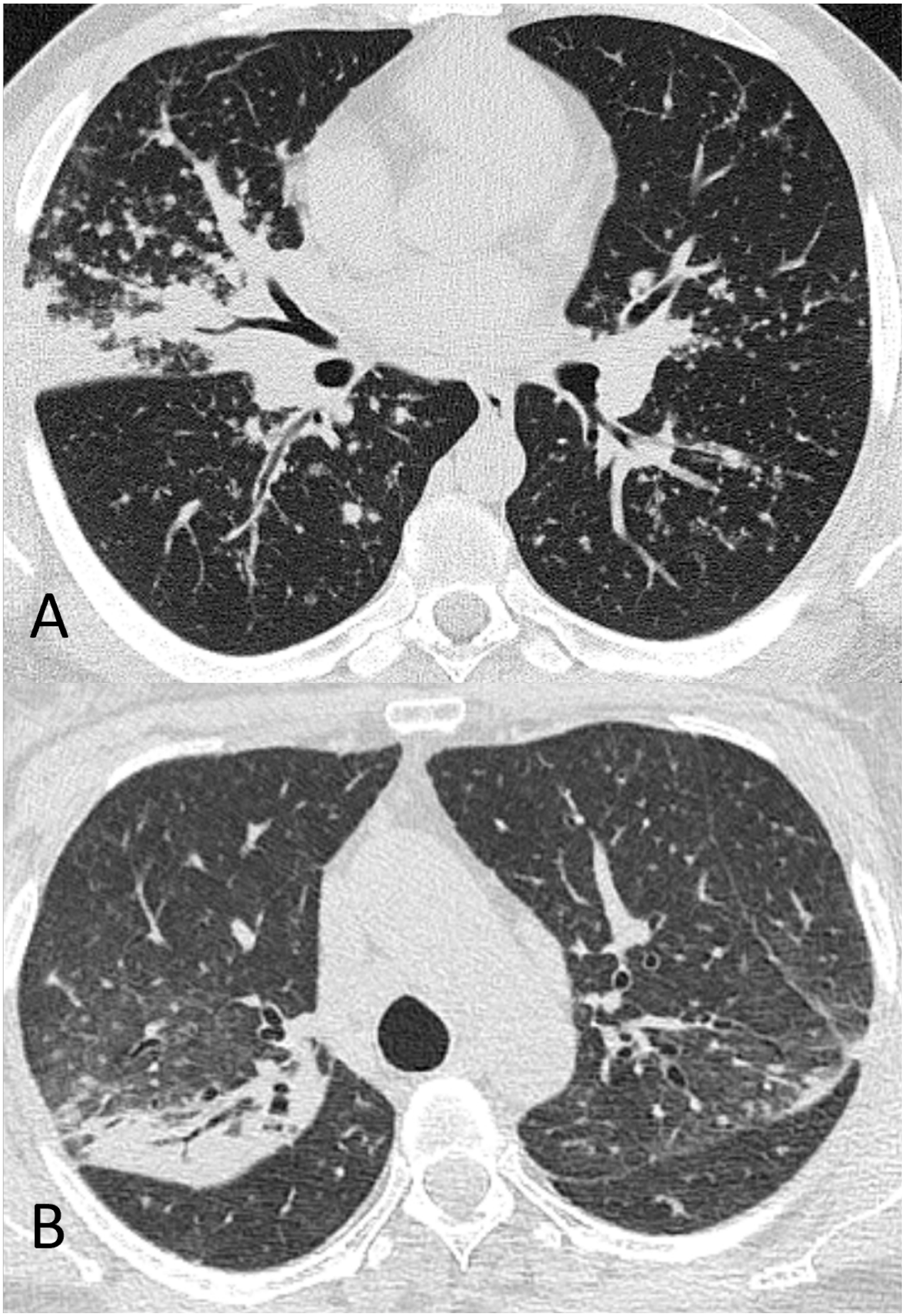

Patterns of lung sarcoidosis. Axial high-resolution CT scan images of (A) typical bilateral perilymphatic distribution of micronodules and (B) alveolar sarcoid pattern with a consolidation in the right upper lobe.

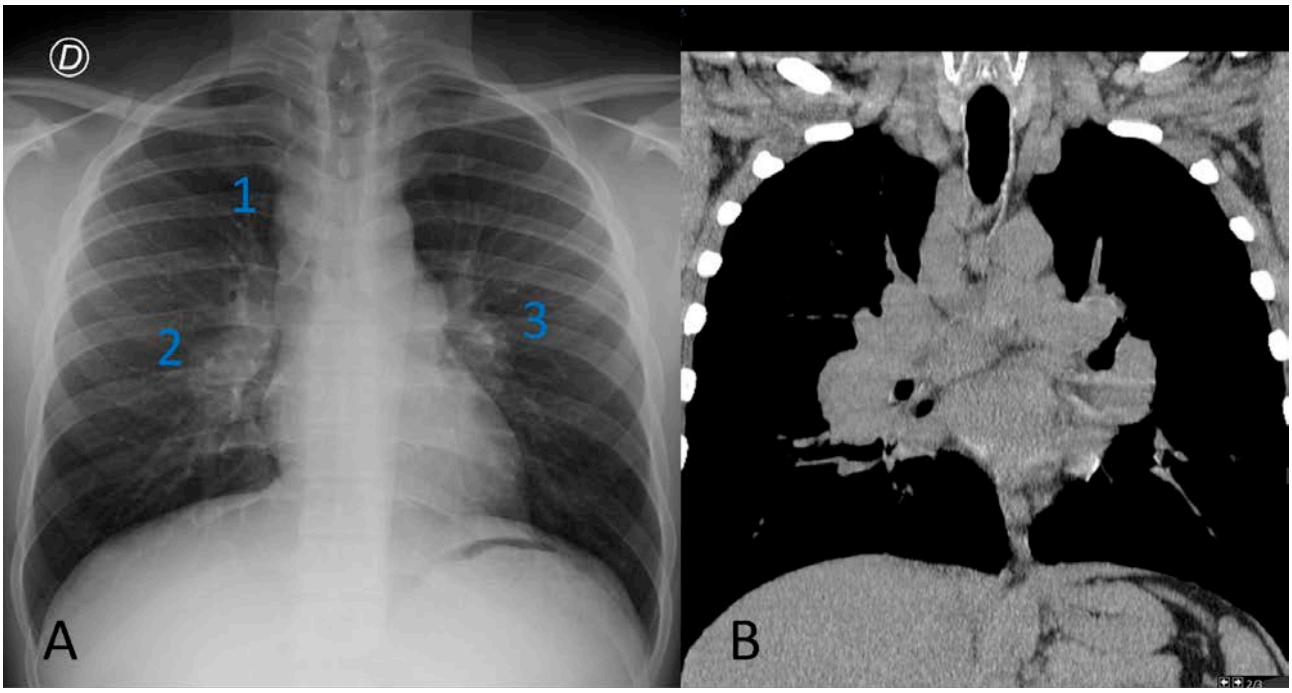

Bilateral enlargement of mediastinal and hilar lymph nodes. (A) 1-2-3 sign on chest radiographs and (B) coronal CT images of the same patient.

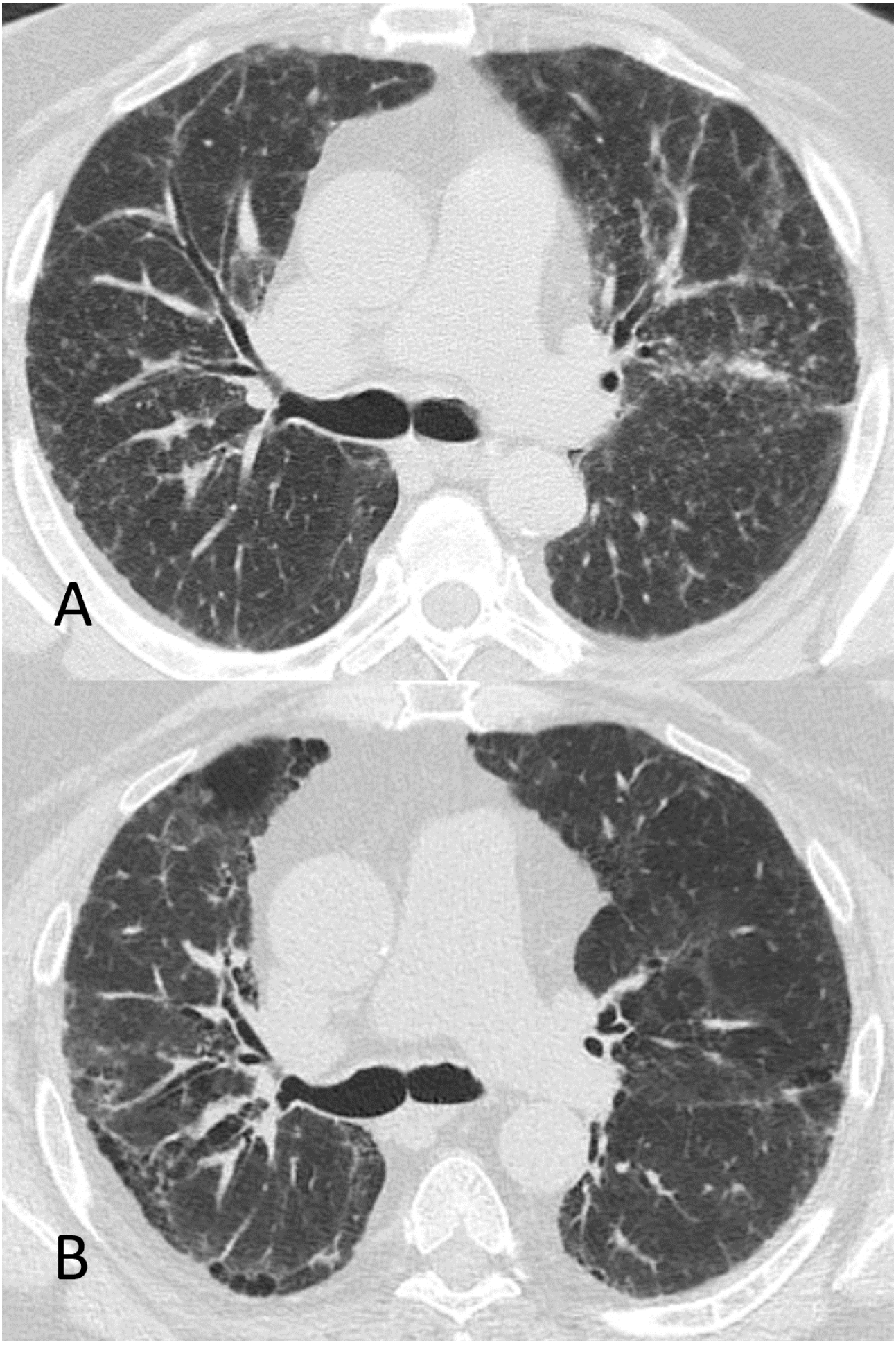
A
B

Progression of fibrosis in the same patient with sarcoidosis. Axial high-resolution CT scans show (A) perilymphatic micronodules associated with incipient fibrosis. (B) Ten years later it is evident the progression of fibrosis with characteristic features including traction bronchiectasis, architectural distortion, volume loss, and honeycomb cysts.

Conclusion

Understanding the characteristic imaging features of this disease is crucial. Nonetheless, sarcoidosis can have a variety of radiological manifestations, some of them overlapping with other diseases. Thus, these must be correlated with clinical, laboratory and histopathologic findings for accurate diagnosis and proper patient management.

A-634

The Role of Interventional Radiology in the Diagnosis and Treatment of Lung Malignancies

E. Arik[1], O. Taydas[2], O. F. Ates[2], G. Danisan[2], M. Ozdemir[2], M. H. Ozturk[2]
[1]İgdir State Hospital, Radiology, İgdir, Turkey, [2]Sakarya University, Radiology, Sakarya, Turkey

Learning Objectives

To evaluate the interventional radiological methods used for the diagnosis and treatment of lung cancer.

Background

Lung cancer is an important health problem with increasing frequency worldwide. There is a wide range of interventional radiological methods ranging from diagnosis to treatment and palliation of the disease. Of these, percutaneous transthoracic needle biopsy (PTTNB) is used for diagnosis, imaging-guided percutaneous ablation (PA) for treatment, and bronchial artery embolization (BAE) for the treatment of hemoptysis, which is an important cause of morbidity and mortality. Our aim in this study is to examine the interventional radiological methods used in the diagnosis and treatment of lung cancer with examples.

Imaging findings OR Procedure details

Percutaneous transthoracic needle biopsy (PTTNB) is a frequently used method for pathological diagnosis. It is often applied to peripheral lesions or central lesions with negative bronchoscopy. PTTNB procedure is often performed under local anesthesia with CT guidance. In addition, ultrasound can be used in pleural-based lesions [1]. The coaxial technique is used in the procedure so that multiple biopsies can be taken [2].

Imaging-guided percutaneous ablation (PA) is a proven treatment modality for early-stage non-small cell lung cancer and oligometastatic lung disease. It is based on killing tumor cells by applying extreme temperatures to the tumor and safety margin. The modalities used for PA are radiofrequency ablation, microwave ablation, and cryoablation. Appropriate PA modality should be selected considering the characteristics of the lesion and the patient [3].

Bronchial artery embolization (BAE) is applied to treat massive or recurrent hemoptysis originating from a lung tumor [4]. The cause of hemoptysis in lung tumors is abnormal angiogenesis in the vessels feeding the tumor. Various agents (Gelfoam, PVA particles, etc.) and coils can be used for UAE [5]. Reflux of embolizing agents to the branches feeding the aorta and spinal cord must be prevented during the procedure [6].

Conclusion

Interventional radiological methods are safe and effective methods that can be used in the diagnosis and treatment of lung cancer.

References:

[1] Priola AM, Priola SM, Cataldi A, Errico L, Di Franco M, Campisi P, et al., (2007), Accuracy of CT-guided transthoracic needle biopsy of lung lesions: factors affecting diagnostic yield , Radiol Med, 1142-1159, 112(8)
[2] 2. Kaufman JA, Lee MJ, (2014), Vascular and Interventional Radiology: The Requisites, Elsevier, 395-399
[3] Páez-Carpio A, Gómez FM, Isus Olivé G, Paredes P, Baetens T, Carrero E, et al., (2021), Image-guided percutaneous ablation for the treatment of lung malignancies: current state of the art, Insights Imaging, 57, 12(1)
[4] Ferris EJ, (1981), Pulmonary hemorrhage. Vascular evaluation and interventional therapy, Chest, 710-714, 80(6)
[5] Duka E, Ierardi AM, Floridi C, Terrana A, Fontana F, Carrafiello G., (2017), The Role of Interventional Oncology in the Management of Lung Cancer, Cardiovasc Intervent Radiol, 153-165, 40(2)
[6] Andersen PE, (2006), Imaging and interventional radiological treatment of hemoptysis, Acta Radiol, 780-792, 47(8)

A-137

The use of lung ultrasound in COVID-19

I. Blazic[1], C. Cogliati[2], N. Flor[3], G. Frija[4], M. Kawooya[5], M. Umbrello[6], S. Ali[5], M.-L. Baranne[7], Y.-J. Cho[8], R. Pitcher[9], I. Vollmer[10], E. van Deventer[11], M. del Rosario Perez[11]

[1]CHC Zemun, Radiology, Belgrade, Serbia, [2]Internal Medicine, L.Sacco Hospital, ASST Fatebenefratelli-Sacco; University of Milan, Department of Biomedical and Clinical Sciences, Milan, Italy, [3]Unità Operativa di Radiologia Luigi Sacco University Hospital Milan, Milan, Italy, [4]Université de Paris; International Society of Radiology Paris, Paris, France, [5]Ernest Cook Ultrasound Research and Education Institute (ECUREI), Kampala, Uganda, [6]SC Anestesia e Rianimazione II; Ospedale San Carlo Borromeo, ASST Santi Paolo e Carlo – Polo Universitario, Milan, Italy, [7]APHP (Assistance Publique –Hôpitaux de Paris); PICUS (Paris Institute for Clinical Ultrasound), Paris, France, [8]Division of Pulmonary and Critical Care Medicine, Seoul National University College of Medicine, Seoul National University Bundang Hospital, Department of Internal Medicine, Seoul, Republic of Korea (South Korea), [9]Division of Radiodiagnosis, Faculty of Medicine and Health Sciences, Stellenbosch University, Department of Medical Imaging and Clinical Oncology, Cape Town, South Africa, [10]Hospital Clínic de Barcelona, Barcelona, Spain, [11]World Health Organization, Geneva, Switzerland

Learning Objectives

Lung ultrasound (LUS), a simple imaging procedure, can contribute to the early identification of patients with clinical conditions suggestive of COVID-19 allowing early management and isolation measures and can support decisions about home discharge versus hospital admission, including the decisions about admission to a regular ward versus an intensive care unit. It can also be used to monitor progression of COVID-19 pneumonia and development of thoracic complications (e.g. heart failure, pleural effusion and pneumothorax), and inform therapeutic strategy.

Background

Advanced applications, such as contrast-enhanced ultrasonography and elastography, can provide information regarding lung peripheral perfusion, areas of infarction and degree of interstitial lung edema. LUS can support a rapid, point-of-care diagnosis in various clinical settings (primary care facilities, emergency departments, hospital wards, intensive care units) and can also be performed in outpatient settings (assisted living facilities, retirement residences, home care) using portable devices, which is relevant for appropriate resource allocation.

Imaging findings OR Procedure details

Typical LUS findings for COVID-19 pneumonia (interstitial pattern, pleural abnormalities and consolidations) are described, as one component of COVID-19 diagnostic workup that otherwise includes other imaging modalities, clinical and laboratory evaluation, taking into account patient's medical history (e.g. comorbidities such as cardiovascular disease, lung interstitial disease or fibrosis). Advantages and limitations of LUS use in COVID-19 are presented, along with equipment requirements and training needs. The use of LUS in the management of COVID-19 in different regions and countries is inferred from a literature search of related published papers.

Conclusion

LUS is a noninvasive, rapid and reproducible procedure that can be performed at the point of care, usually by a physician who clinically monitors the patient, allowing interpretation of LUS imaging features along with other significant clinical and laboratory findings. It requires simple sterilization and involves non-ionizing radiation allowing repeated exams on the same patient, with special benefit in children and pregnant women. However, physical proximity between the patient and the ultrasound operator is a limitation in a pandemic context, emphasizing the need to implement specific infection prevention and control measures. Availability of qualified staff adequately trained to perform LUS remains a major barrier to lung ultrasound utilization. Training, advocacy and awareness raising can help build up capacities of local providers to facilitate LUS use for COVID-19 management, with particular focus on low- and middle-income countries.

References:

[1] Akl EA, Blažić I, Yaacoub S, et al., (2021), Use of chest imaging in the diagnosis and management of COVID-19: a WHO rapid advice guide, Radiology, E63–E69, 298

[2] World Health Organization, (2022), WHO guidelines on the use of chest imaging in COVID-19

[3] Blazic I, Cogliati C, Flor N, Frija G, Kawooya M, Umbrello M, Ali S, Baranne ML, Cho YJ, Pitcher R, Vollmer I, van Deventer E, Del Rosario Perez M., (2022), The use of lung ultrasound in COVID-19, ERJ, 00196-2022, 9(1)

A-698

Thoracic calcifications: a practical guide to discern their significance on chest X-rays

E. Tona[1], C. Timpanaro[2], L. Reali[2], L. A. Mauro[2], S. Palmucci[2], A. Basile[2]
[1]University Hospital Policlinico "G.Rodolico - San Marco", Radiology I, Catania, Italy, [2]University Hospital Policlinico, Radiology I, Catania, Italy

Learning Objectives
The purpose of this study is to describe thoracic calcifications depicted on chest x-ray examination, outlining their location and main features – in order to achieve a correct identification and to provide a differential diagnosis. Although calcifications could be less relevant in the evaluation of several acute pathologies, in some circumstances they may provide useful information on the patient's clinical condition – and they could be representative of some specific diseases.
Background
We have revised thoracic radiographs extracted from our RIS-PACS archive – in the period between January 2022 and February 2023; from a total of 1500 radiological reports, we have retrospectively selected those containing “calcifications” as keyword through the text. A practical guide – based on their different radiological features – has been summarized.
Imaging findings OR Procedure details
The calcifications can be distinguished on the basis of their localization: lung parenchyma, pleura, lymph nodes, skeleton bone and cartilaginous, soft tissue and vascular structures. Moreover, they can be classified on an etiological basis: long-lasting inflammatory process, such as in cases of tuberculosis and histoplasmosis, benign primitive neoplasms (hamartoma), malignant (exposure to asbestos), secondary diseases (metastasis from mucinous colorectal adenocarcinoma) and metabolic disorders. A diffuse distribution could be observed in pulmonary ossification, amyloidosis and alveolar microlithiasis. The shape is another discriminating factor, and sometimes pathognomonic for the diagnosis: the popcorn-like appearance is typical of hamartoma, whereas a central nidus could be representative of a granulomatous lesion (sarcoidosis). Various cardiac and pericardial calcifications could be considered a marker for atherosclerosis and may be identified on chest radiographs. Vascular calcifications are common and they may involve the coronary arteries, aorta, cardiac valves, annuli, myocardium, pericardium. Coronary calcifications, for example, are the result of calcium deposited along the course of the vessel, assuming a tubular image; calcifications of the mitral annulus have an irregular appearance such as a “C” in the early stages, when they are localized only in the posterior leaflet, and an “O” when also the anterior leaflet is involved.
Conclusion
Chest radiography is often the first diagnostic technique to evaluate the lung parenchyma, cardiovascular and mediastinal structures, soft tissues and supporting structures. Calcifications cannot have clinical relevance, or they can suggest critical pathologies for the patient: knowing their significance and disease association is necessary to obtain an appropriate diagnosis.

A-606

Thoracic endemic fungi: Review of common imaging findings

M. L. Urbano[1,2], A. Viegas[3], C. Sousa[3], J. Leitão[3]
[1]Centro Hospitalar Lisboa Norte, Lisboa, Portugal, [2]Centro Hospitalar Lisboa Norte, Serviço de Imagiologia Geral, Lisboa, Portugal, [3]Centro Hospitalar Lisboa Norte, Serviço de Imagiologia Geral, Lisbon, Portugal

Learning Objectives

Endemic mycoses can cause various clinical manifestations including respiratory infections with high rates of morbidity and mortality. We aim to review the presentation and differential diagnosis of endemic fungal infections based on most common chest imaging findings.

Background

Fungi may have a ubiquitous or endemic geographic distribution, therefore a correct anamnesis regarding clinical status, demographics and travel history are crucial to help the correct diagnosis.

Clinical presentation is often insidious, moreover both symptoms and imaging findings are non-specific often hampering the diagnosis.

Imaging findings OR Procedure details

CT findings are non-specific and include consolidation, nodules, cavities, lymphadenopathy, and pleural disease.

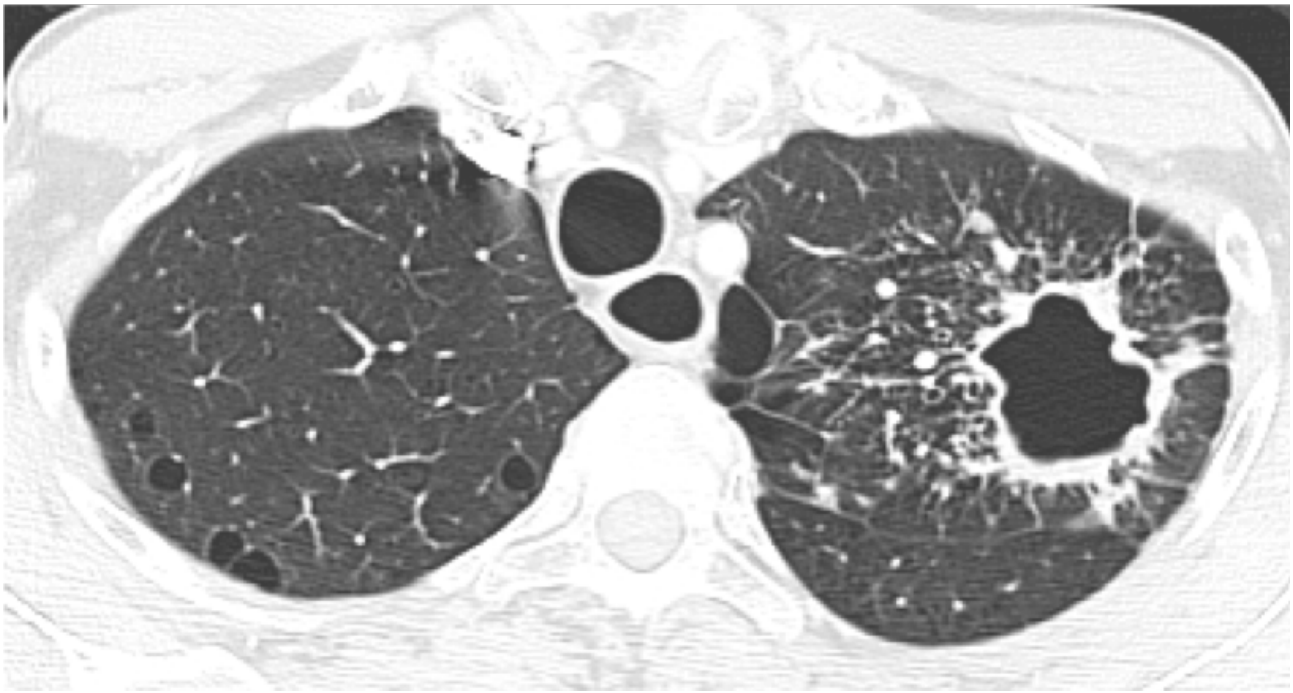

Chronic histoplasmosis infection. CT axial image (lung window) depicts a spiculated cavity with thick walls in the left upper lobe.

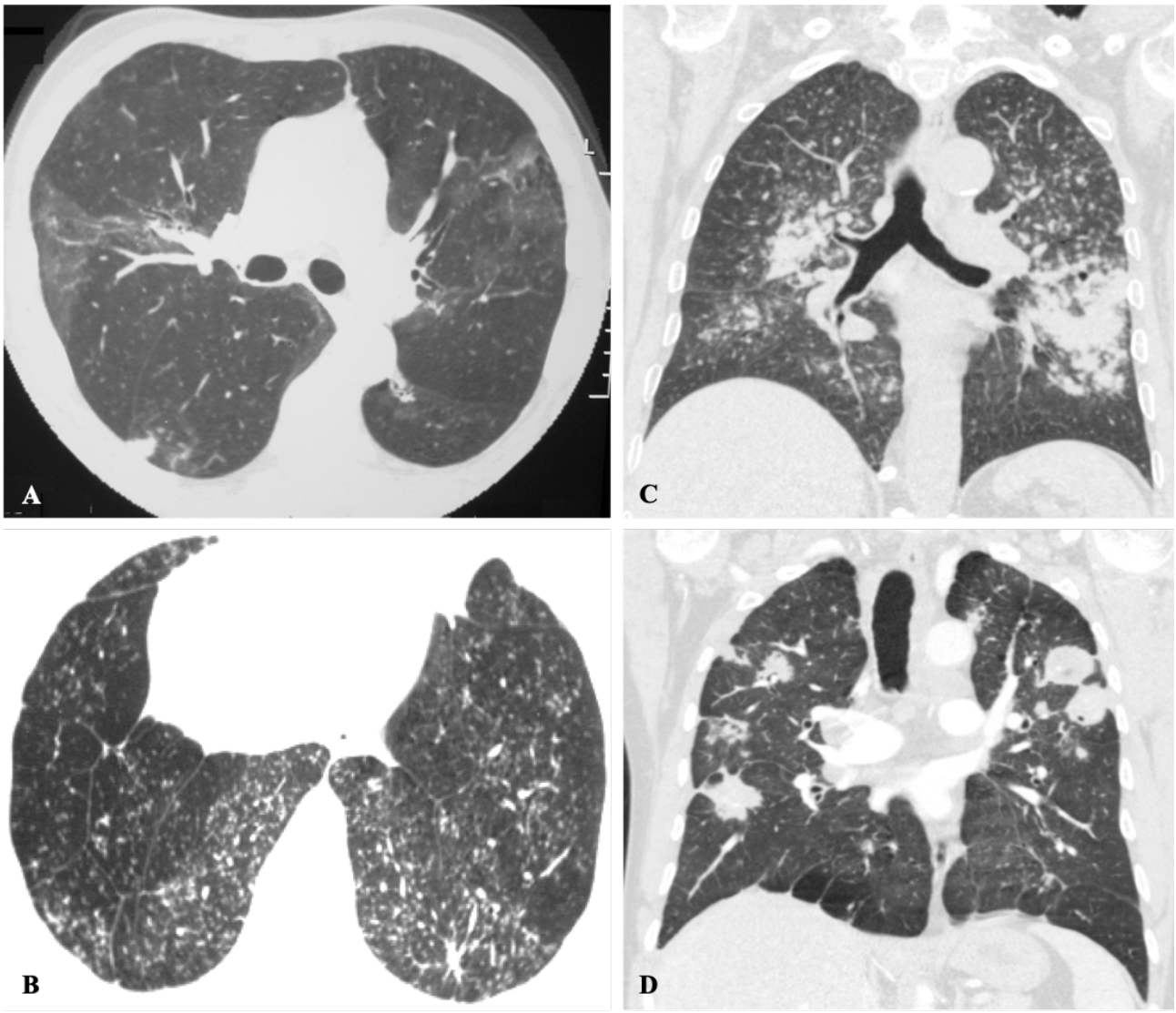

Axial and coronal CT (lung window). Different images findings in different patients with paracoccidioidomycosis

For that reason, the diagnosis can be challenging and can be easily confused with other pathologies, including malignancy, or with other fungal pathogens. In some cases, it may require a lung biopsy to confirm the diagnosis and identify the specific fungal organism causing the infection.

Conclusion

The diagnosis and management of thoracic endemic fungi is difficult and often delayed; therefore, the radiologist should be cognizant of the patient clinical history, demographics and travel history since they are important clues that may lead to a proper diagnosis.

A-725

Thoracic imaging in systemic mastocytosis

A. Knurowska, J. Niemierko
Medical University of Gdańsk, 2nd Department of Radiolog, Gdańsk, Poland

Learning Objectives

This article aims to provide radiologists with an understanding of the imaging findings and patterns of thoracic involvement in systemic mastocytosis.

Background

Systemic mastocytosis (SM) is a rare myeloproliferative disease characterized by uncontrolled proliferation of clonal mast cells. The disease presents with a range of clinical manifestations, with the most common involvement occurring in the hematopoietic system (bone marrow, lymph nodes), gastrointestinal system (liver, spleen, and gastrointestinal tract), and skeletal system. Pulmonary involvement in SM is rare, occurring in less than 20% of patients.[4]

Imaging findings OR Procedure details

Chest radiographs and computed tomography (CT) are the primary imaging methods used to diagnose lung involvement in systemic mastocytosis. Fibrosis is a common finding, as mast cells are significant factors of fibrosis.[4] However, there is no clear pattern of fibrosis specific to SM. Predominantly, perihilar or diffuse interstitial fibrosis has been reported [2]. Centrilobular nodules and round low attenuation cysts that are uniformly distributed throughout the lungs can also be observed in SM patients.[1] Additionally, involvement of mediastinal and hilar lymph nodes is the third most common finding. It is worth mentioning that very few reported cases include histopathologic confirmation of the pulmonary involvement.[3]

Lastly, as SM involve bone marrow in 90% of patients with SM, all skeletal structures should be meticulously check on chest radiographs and CTs in search of diffuse osteosclerosis.

Conclusion

Pulmonary involvement is a rare manifestation of systemic mastocytosis and imaging findings are not specific. Radiologists should be aware of various appearances of this disease to better facilitate diagnosis and patient management. Thoracic CT imaging can help detect changes that occur during disease progression.

References:

[1] Elsaiey A, Mahmoud HS, Jensen CT, et al., Mastocytosis-A Review of Disease Spectrum with Imaging Correlation, Cancers, 13(20), 5102.

[2] M Schmidt, C Dercken, O Loke, S Reimann, S Diederich, S Blasius, S Heidenreich, (2000), Pulmonary manifestation of systemic mast cell disease, European Respiratory Journal , 15: 623-625

[3] Ozturk K, Cayci Z, Gotlib J, Akin C, George TI, Ustun C. , (2021), Non-hematologic diagnosis of systemic mastocytosis: Collaboration of radiology and pathology., Blood Rev. , Jan;45:100693

[4] Leone A, Macagnino S, D'Ambra G, Veltri G, Perla D., Systemic Mastocytosis: Radiological Point of View, Mediterr J Hematol Infect Dis. , 2021;13(1):e2021056

A-458

Thymus or not thymus? An imaging approach in paediatric age group

A. Viegas, C. Mendonça, M. L. Lobo
Centro Hospitalar Universitário Lisboa Norte, EPE, Radiology, Lisboa, Portugal

Learning Objectives

To emphasize the difference between normal and abnormal mediastinal findings in paediatric patients on chest x-ray (CXR).
To discuss how to approach those patients with doubtful or suspicions findings on CXR.
To review and illustrate normal thymus and its differential diagnosis, including common mediastinal masses in children.

Background

The thymus, a normal bilobed organ located in the anterior mediastinal compartment in young children, can be quite prominent with different shapes and variable involution appearances, often resulting in concern and misleading interpretation on CXR.
We present an imaging review of normal thymus and its differentials based on cases collected from our institution.

Imaging findings OR Procedure details

Similarly to adults, the mediastinal masses in children are described according to three compartments based on the CXR: anterior, middle and posterior.
A normal thymus can have a variety of shapes and sizes and can extend superiorly to the thyroid gland, inferiorly towards the diaphragm or have a retrocaval position. Being familiar with these anatomic variants is fundamental to avoid misinterpretations.
Uncertain imaging findings can often be solved by chest ultrasound in young children, thus avoiding unnecessary investigations. A normal thymus has a characteristic ultrasound appearance with scattered hyperechoic foci giving its “starry sky” aspect. Other useful characteristics of the normal thymus are the lack of invasion or compression of the adjacent structures and the typical signs seen on CXR (E.g., thymic sail and wave signs).
In the presence of an anterior mediastinal mass in older children or invasion of the surrounding structures further investigation should be considered.

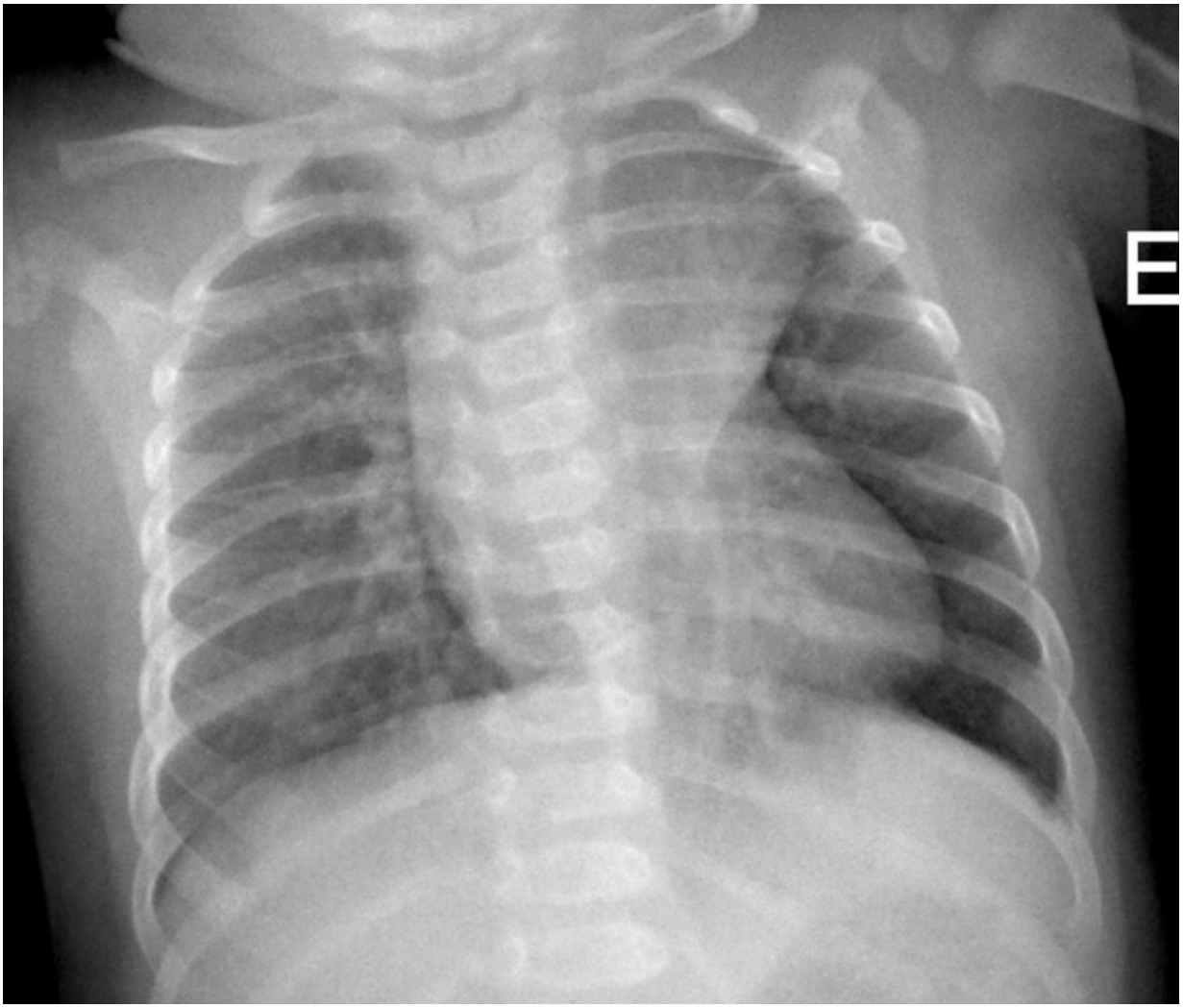

1- CXR of a child showing a prominent but normal thymus with an asymmetric distribution towards the left side. Note that the child is slightly rotated which contributes and exacerbates this finding.

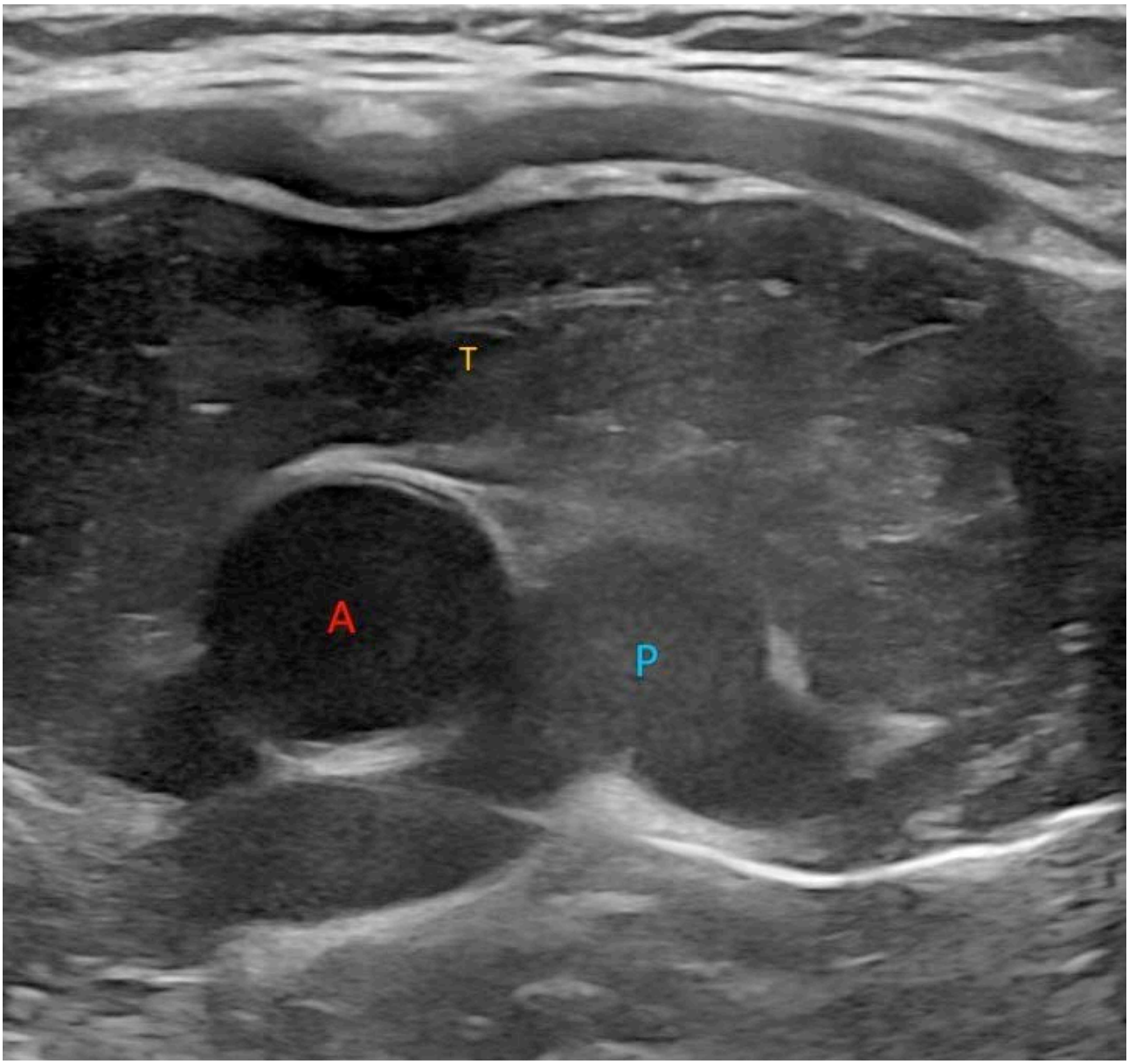

2- Ultrasound image of the same child as shown above (1) confirming the presence of a normal thymus with its typical “starry sky” appearance. There is a slight prominence of the left lobe. A – Aorta; P – Pulmonary artery; T – Thymus.

Conclusion

Radiologists should be aware of the appearance of the normal thymus and its variants, to early recognize signs of abnormal “thymus” that warrant further investigation.

A-362

Tracheobronchopathia osteochondroplastica

F. Ufuk
Pamukkale School of Medicine, Radiology, Denizli, Turkey

Learning Objectives

- To describe the imaging findings of tracheobronchopathia osteochondroplastica.

Background

Tracheobronchopathia osteochondroplastica (TO) is an uncommon and non-neoplastic disorder of the tracheobronchial tree. The estimated prevalence of TA at bronchoscopy is about 0.4% (1). TO is usually seen in males and patients are rarely symptomatic because the severe airway obstruction is unusual (2). On CT, TO is characterized by small calcified (osteocartilaginous) nodules originating from the tracheobronchial cartilage, and these nodules protrude into the lumen of the trachea and proximal bronchi resulting in mild luminal narrowing. The posterior tracheal wall is typically spared, as in the present case (3). It is a benign condition and invasive procedures, such as bronchoscopy and biopsy, are not required (2).

Imaging findings OR Procedure details

A 45-year-old male presented with fatigue and a dry cough for a few months. He has a history of 8 pack-years of smoking and hypertension. Physical examination, including lung auscultation, yielded normal findings, and laboratory test results were within normal limits. Chest x-ray revealed a prominent right hilum and the patient was referred for Chest CT. Chest CT demonstrated multiple calcific nodules along the anterolateral wall of the trachea (Fig. 1).

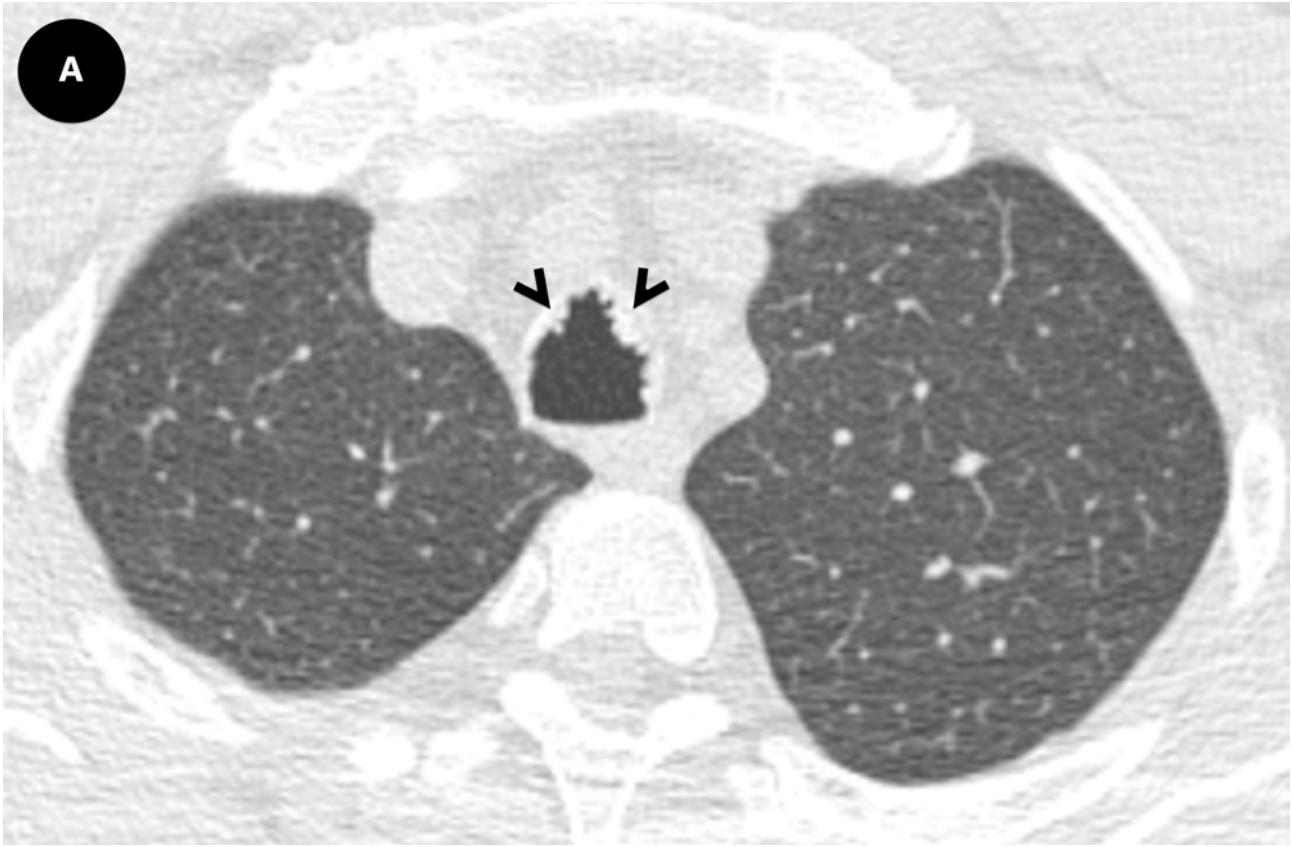

Figure 1

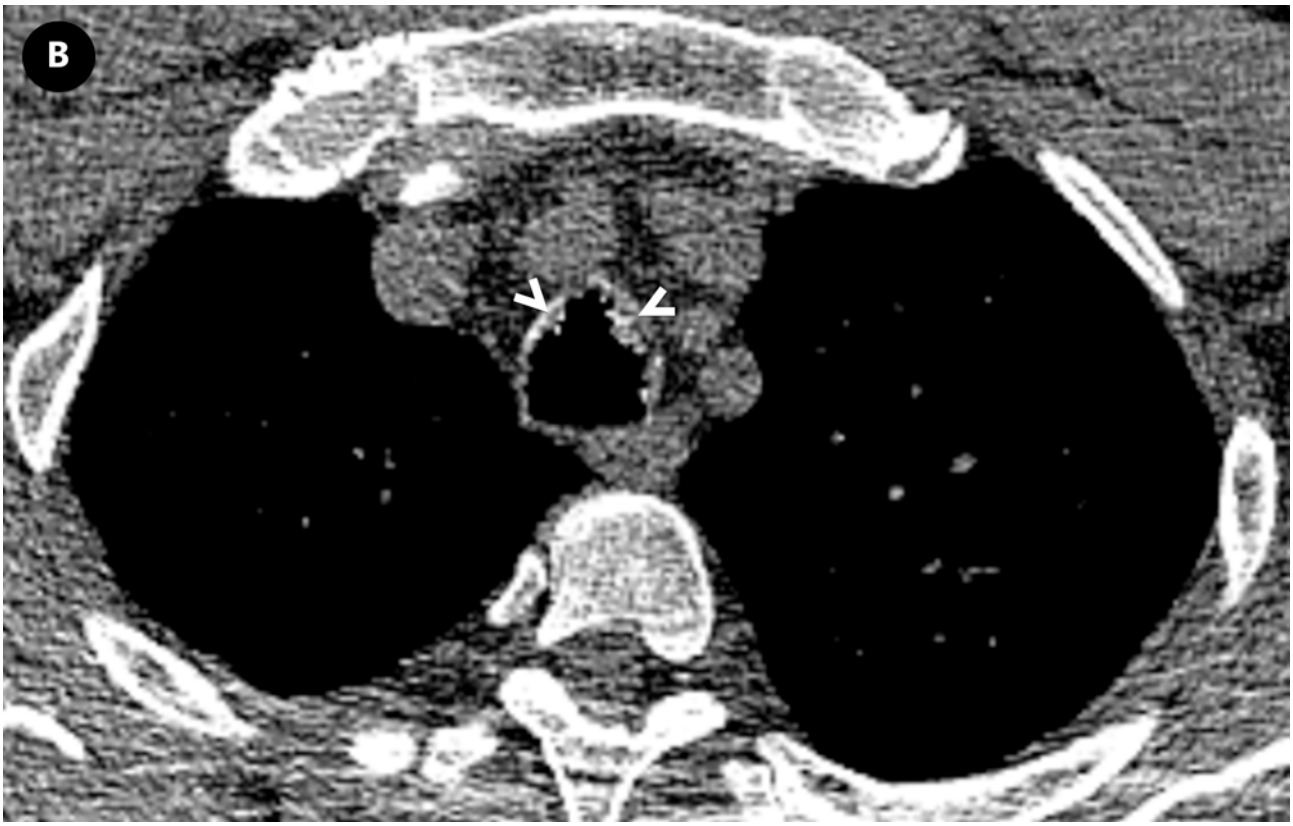

Figure 1B

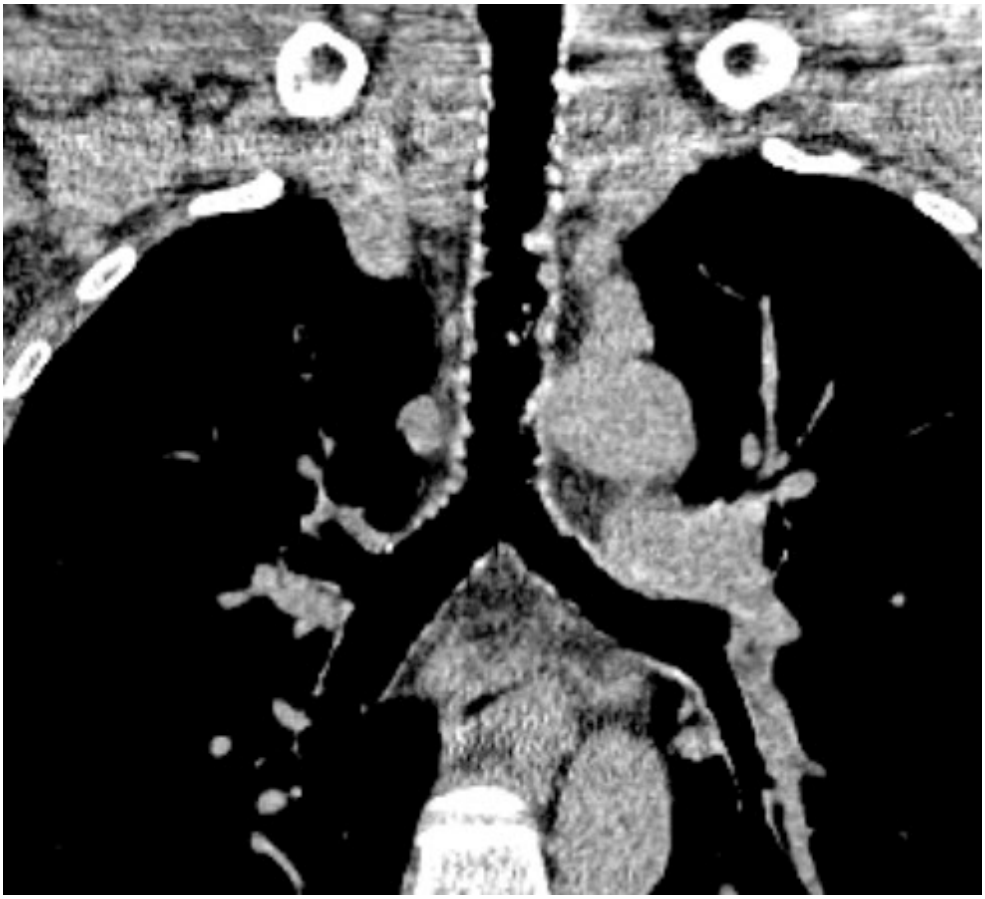

Fig 2

Virtual bronchoscopy revealed extensive tracheal nodular excrescences along the anterior and lateral wall of the trachea sparing the posterior membranous wall.

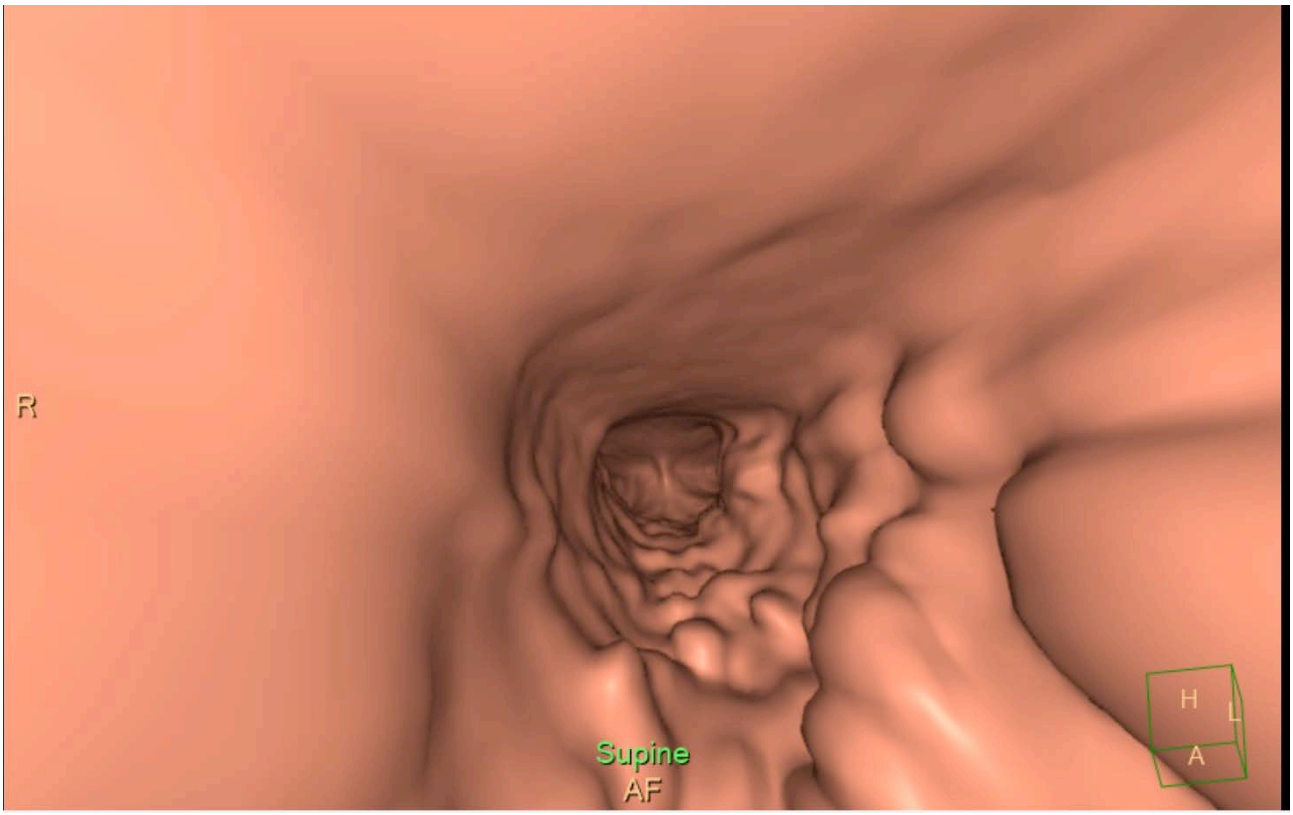

Virtual

Imaging findings were evaluated to be consistent with tracheobroncopathia osteochondroplastica (TO) and no additional invasive procedure was performed. The three-year follow-up of the patient was uneventful.

Conclusion

CT findings of TO are important to avoid unnecessary surgery or invasive procedures. In addition, as a noninvasive examination method, CT virtual bronchoscopy is helpful for the detailed evaluation of airway lumens.

A-445

Unusual nodular lesions in the lung: an iconographic essay.

M. Sbaraini, A. P. Sartori, T. Krieger Bento da Silva, C. Simoes dos Santos, T. Severo Garcia, L. Roses Rizzon, R. Dalla Costa, L. Leimig Telles Parente, J. Meyer Rosa
Pavilhão pereira filho, Radiology, Porto Alegre, Brazil

Learning Objectives
This is an iconographic essay-type study based on illustrative cases that identify the main tomographic findings of pulmonary nodules of unusual causes.
Background
Pulmonary nodules are frequent findings in chest imaging studies, with multiple benign and malignant differential diagnoses. However, several nodules remain with undetermined etiology on computed tomography, and their diagnosis is confirmed only after histopathological analysis.
Imaging findings OR Procedure details
Pulmonary sclerosing hemangioma is a rare benign tumor originating from the pulmonary epithelium, often seen as an intraparenchymal (most commonly juxtapleural) nodule with areas of internal calcification.
Diffuse idiopathic hyperplasia of pulmonary neuroendocrine cells (DIPNECH) is a pathology characterized by diffuse hyperplasia of bronchiolar and bronchial pulmonary neuroendocrine cells. It appears as multiple small solid bronchocentric nodules, usually with inferior and peripheral distribution.
Rendu-Osler-Weber Syndrome is an autosomal dominant disease characterized by the presence of multiple arteriovenous malformations, being observed on imaging as a well-circumscribed vascular mass with enhancement of the dilated feeding artery and draining vein.
Epithelioid hemangioendothelioma is a rare vascular tumor that is usually found incidentally, with multiple nodules in the lungs or pleura of random distribution, with sizes ranging from 0.3 to 2.0 cm.
Diffuse pulmonary meningotheliomatosis is an extremely rare disease characterized by small niches of epithelioid cells in the lung interstitium, identified by the presence of small diffuse bilateral nodules, similar to the miliary pattern, or ground-glass opacities.
Malakoplakia is a granulomatous disease characterized by a chronic inflammatory reaction of undetermined etiology. The most common site of involvement is the urinary tract, but it may have a pulmonary presentation with multiple isolated or confluent nodules. Diagnosis is histological, by visualization of Michaelis-Gutmann bodies and von Hansemann cells.
Conclusion
It is extremely important for radiological practice to recognize unusual causes of pulmonary nodules, in order to perform the adequate characterization of these lesions, determining risk of malignancy and treatment options.

A-493

Variability in congenital thoracic vascular defects: anomalous pulmonary venous return, is it easily recognisable?

S. Giedrys, K. Počepavičiūtė, J. Zaveckienė
Lithuanian University Of Health And Sciences, Radiology, Kaunas, Lithuania

Learning Objectives

To help radiologists understand typical patterns of congenital aberrant thoracic venous connections. To present radiological features of total (TAPVR) and partial (PAPVR) anomalous pulmonary venous return. To highlight diagnostic challenges of PAPVR in adults.

Background

Defects in early embryological development can result in total or partial venous connections that drain into systemic circulation with vast anatomical variability (Fig. 1)[1]. TAPVR is commonly diagnosed in neonates due acute life-threatening symptoms. PAPVR is more often diagnosed later in life, when only some pulmonary veins return directly or indirectly to right atrium leading to onset of latent symptoms [2]. Although rare PAPVR making 0.2-0.7 % of the population, imaging techniques are essential for detecting atypical venous connections, predicting outcomes and patient management[3].

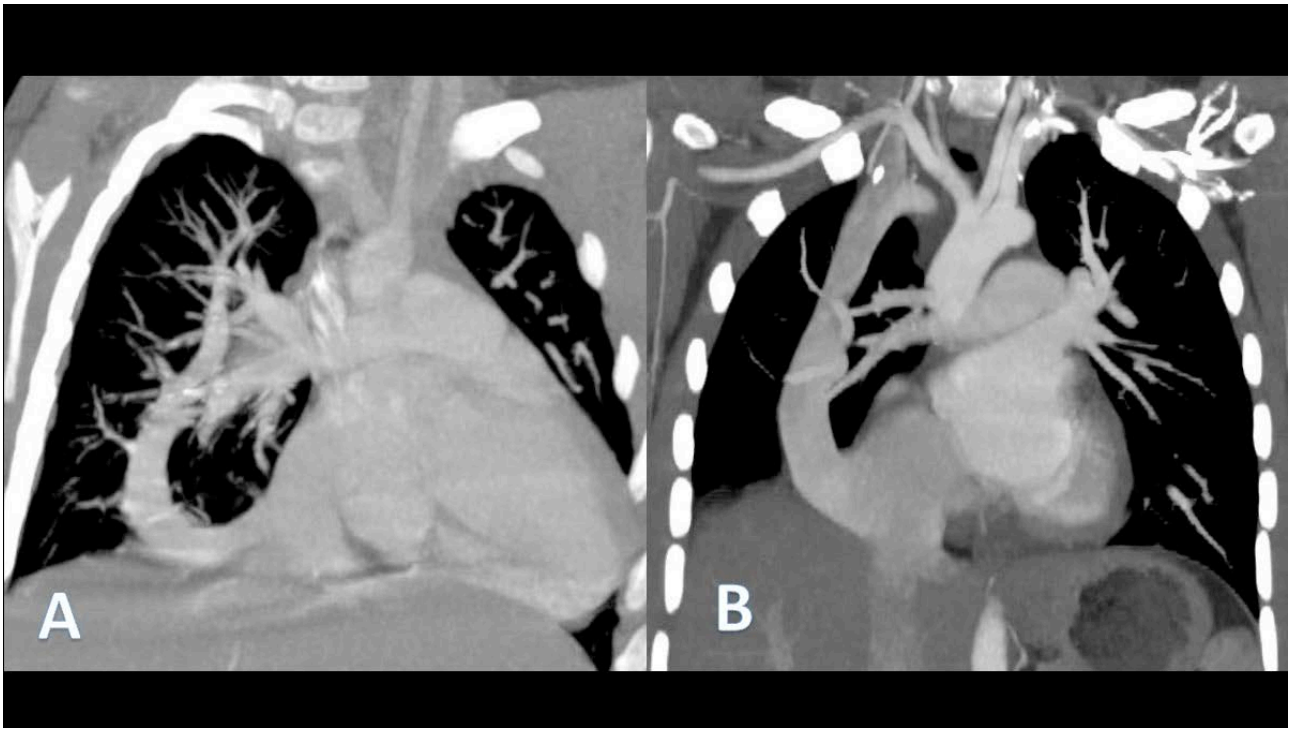

Fig. 1. CTA coronal MIP reconstructions of 2 y/o showing right anomalous pulmonary vein draining into VCI, infracardiac type (A), and 22 y/o woman with aberrant VCS draining right lower lobe veins (not shown) and merging with VCI before connecting to right atrium, supracardiac type (B).

Imaging findings OR Procedure details

Echocardiography is usually first line of imaging of cardiovascular diseases, but it may often be inconclusive[4]. CT angiography with multiplanar reconstructions is increasingly used for identifying abnormal anatomy, while MRI can also provide additional information along with functional assessment.

A common classification describes four types of anomalous connections based on drainage into systemic veins: supracardiac, cardiac, infracardiac and mixed (Fig. 2)[5]. PAPVR may be difficult to diagnose early due to lack of clinical symptoms, but later in life it may show signs of right-sided heart failure, pulmonary hypertension. PAPVR can often be an incidental, but important finding e.g., on x-ray as Scimitar syndrome or suggestive nonspecific findings like cardiomegaly, increased vascular markings or wide mediastinal shadow indicating a need for additional imaging [2].

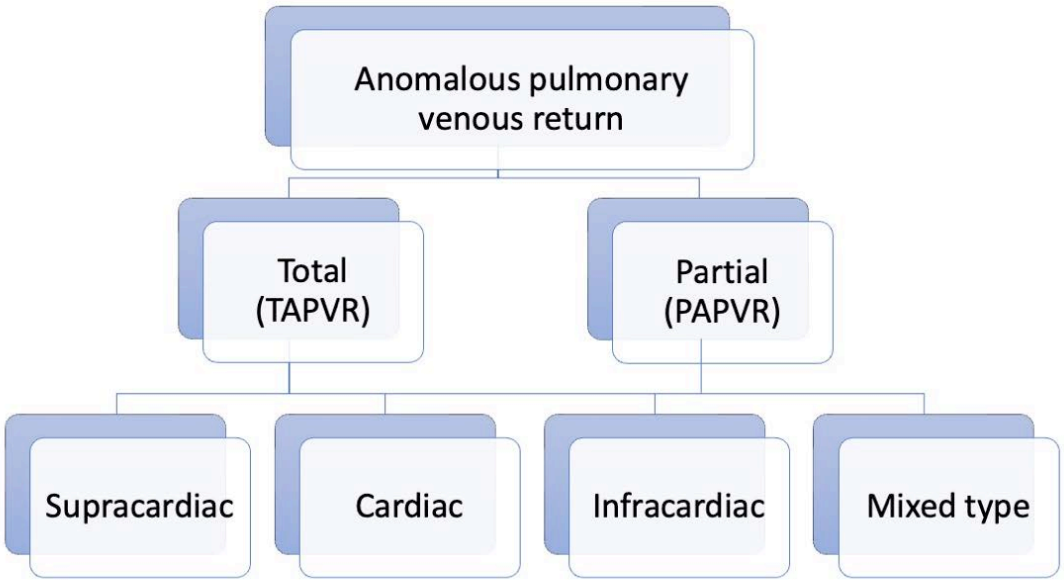

Fig. 2. Classification of anomalous pulmonary venous return suggested by Herlong et. al.

Conclusion

Anomalous pulmonary venous return can be classified into four anatomical groups. PAPVR should not be forgotten as a rare but possible cause of cardiac and respiratory symptoms in adults and imaging techniques are essential for planning optimal patient care.

References:

[1] Marini, T.J., He, K., Hobbs, S.K. et al., (2018), Pictorial review of the pulmonary vasculature: from arteries to veins. , Insights Imaging 9, 971–987
[2] Chao-Chun Chang and Chia-Ying Lin, (2022), Partial Anomalous Pulmonary Venous , Radiology 302:3, 513-513
[3] E. Gözgeç1, M. Kantarci1, F. Guven1, H. Ogul1, N. Ceviz2, S. Eren, (2021), Determination of anomalous pulmonary venous return with high-pitch low-dose computed tomography in paediatric patients. , Folia Morphol, Vol. 80, No. 2, pp. 336–343.
[4] Kao CC, Hsieh CC, Cheng PJ, Chiang CH, Huang SY. J , (2017), Total Anomalous Pulmonary Venous Connection: From Embryology to a Prenatal Ultrasound Diagnostic Update. , Med Ultrasound. Jul-Sep;25(3):130-137.
[5] Ayman Osama, (2013), Role of multi-slice CT angiography in the evaluation of pulmonary venous anomalies., The Egyptian Journal of Radiology and Nuclear Medicine,Volume 44, Issue 2, Pages 193-201.

A-555

Various faces of nonspecific interstitial pneumonia - CT features and clinical scenarios

E. Baltakytė, S. Giedrys, J. Zaveckienė
Lithuanian University of Health Sciences Hospital Kaunas Clinics, Lithuania, Radiology, Kaunas, Lithuania

Learning Objectives

1.To describe computed tomography (CT) features in patients with nonspecific interstitial pneumonia (NSIP) CT pattern.
2.To illustrate a various manifestation of NSIP pattern in distinct clinical scenarios throught CT cases
3.To disscuss possible CT findings based differential diagnosis of NSIP

Background

NSIP is one of the most common pattern associated with interstitial damage observed in connective tissue disease (CTD), as well as in with some drug toxicity, infection or hypersensitivity pneumonitis (HP). NSIP has variable clinical and radiological manifestations, moreover many cases are idiopathic with no known predisposing factor, so diagnostic road can be quite challenging, requiring a multidisciplinary team approach. The goal for radiologist is direct aknowledgement of NSIP CT pattern, identification of pulmonary and extrapulmonary manifestations associated with an underlying conditions.

Imaging findings OR Procedure details

NSIP pattern usually manifests as bilateral, lower-middle lobe predominant diffuse or patchy ground glass opacities (GGO)/consolidations, reticulation with or without traction bronchiectasis and volume loss. Most common demonstrate peripheral predominance, with or without subpleural sparing. Lesions accentuating along bronchovascular bundles. Histologically, these findings correspond to a various degree of uniform fibrosis and interstitial inflammation. However, it can be challenging differentiating overlapping CT features of subpleural fibrotic interstitial lung abnormality, fibrosing NSIP or probable and indeterminate CT usual interstitial pneumonia (UIP) pattern. Although NSIP is not related to smoking, in smokers it must be differencted from desquamative interstitial pneumonia (DIP). As most commonly NSIP are associated with CTD – systemic sclerosis (SS), polymyositis/dermatomyositis, rheumatoid arthitis, Sjogren syndrome - it is beneficial to look for ancillary thoracic and extrathoracic findings that may suggest an underlying CTD's. For example, pulmonary hypertension is a notable feature of SS, airway abnormality in Sjogren, visceral damage of systemic lupus erythematosus. In this review we put emphasis on a possible combinations of a chest CT features, associated thoracic and extrathoracic findings which provides important information in a diagnosis making.

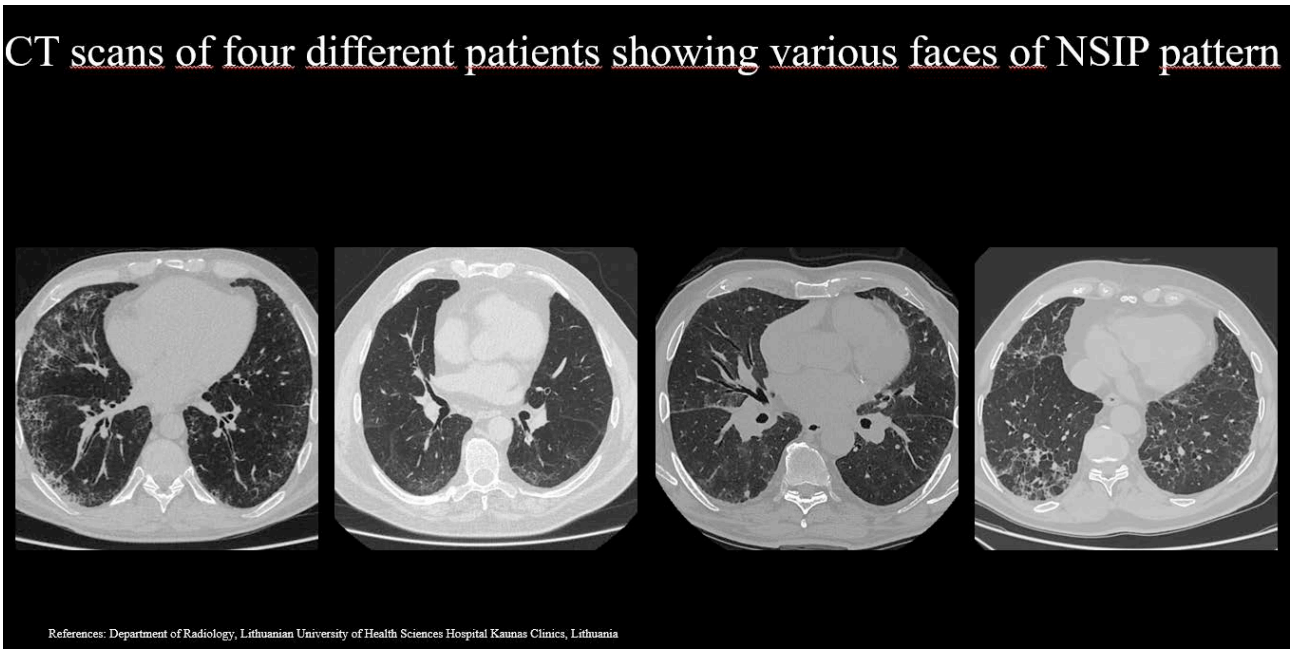

Conclusion

Understanding signs of NSIP pattern in CT, an integration of key imaging findings with patients clinical history helps narrow the differential diagnosis and direct treatment.

A-755

what should we know about pulmonary edema and imaging modalities to diagnose and characterize it properly – Primer for Radiologist

A. Liubauske, Y. Liberman, G. Borisovsky, R. Eisenberg, G. Gittens, D. Litmanovich
Harvard Medical School- Beth Israel Deaconess Medical Center, Radiology, BOSTON, United States of America

Learning Objectives

Fluid accumulation in the lungs, known as pulmonary edema, is a life-threatening condition that urges immediate medical attention. Due to different pathophysiological mechanisms, pulmonary edema is commonly divided into cardiogenic and non-cardiogenic. Distinguishing cardiogenic from non-cardiogenic edema and acute from chronic edema, as well as establishing the etiology are usually the key clinical questions.

Background

All types of pulmonary edema can lead to the same outcome – respiratory failure due to hypoxia.
Imaging plays a crucial part in differentiation between different types of pulmonary edema since various imaging findings closely mirror the pathophysiology of this disease and underlying conditions. Therefore, imaging modalities remain the number one tool in differentiating and diagnosing pulmonary edema and assisting in obtaining prompt clinical decision regarding treatment. Causes of pulmonary edema and their corresponding imaging findings such as acute or chronic heart failure, overhydration caused by renal dysfunction, pregnancy, or systemic disease (e.g., Addison , increased alveolar permeability in the presence of lung injury or,) will be reviewed in this exhibit.

Imaging findings OR Procedure details

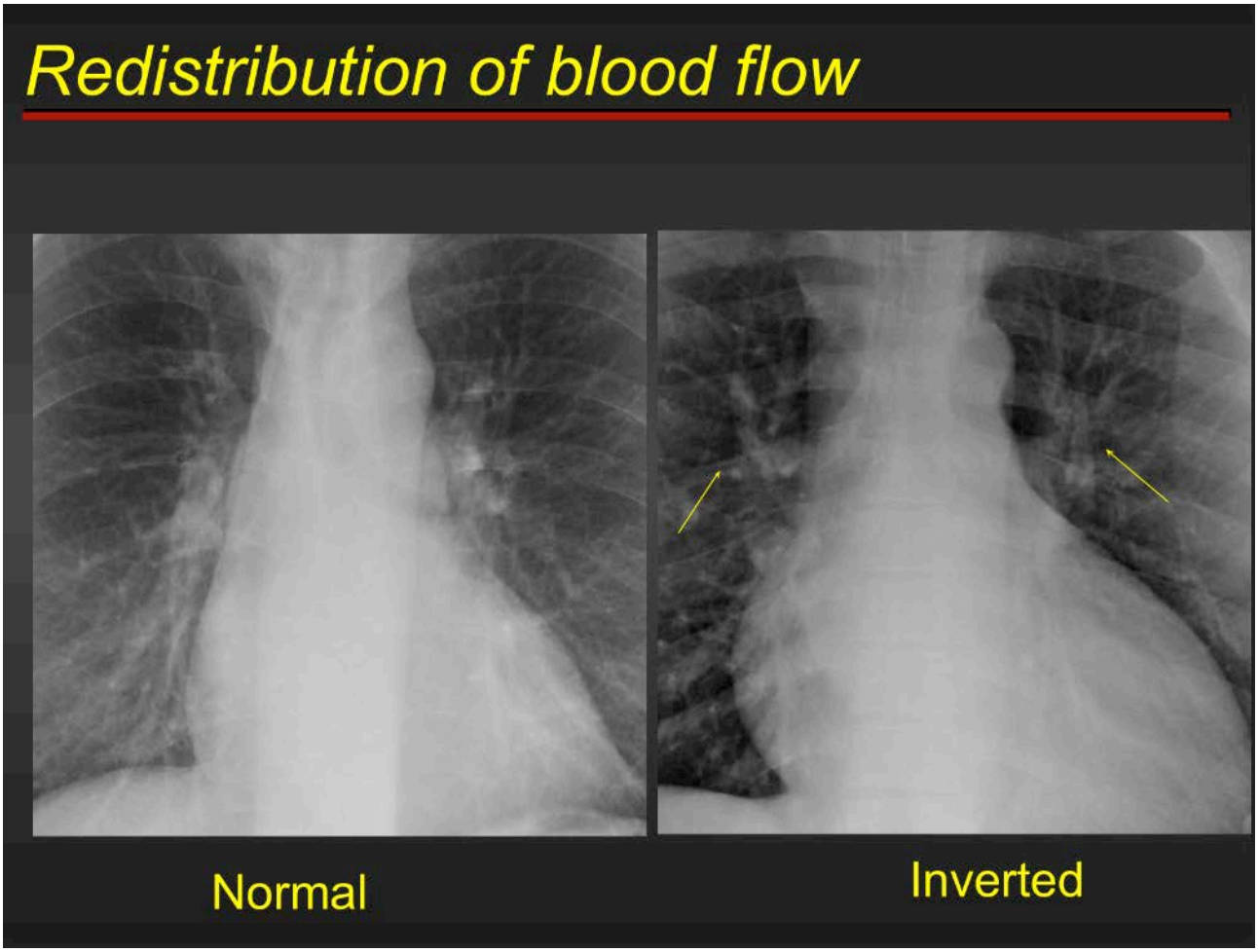

edema1

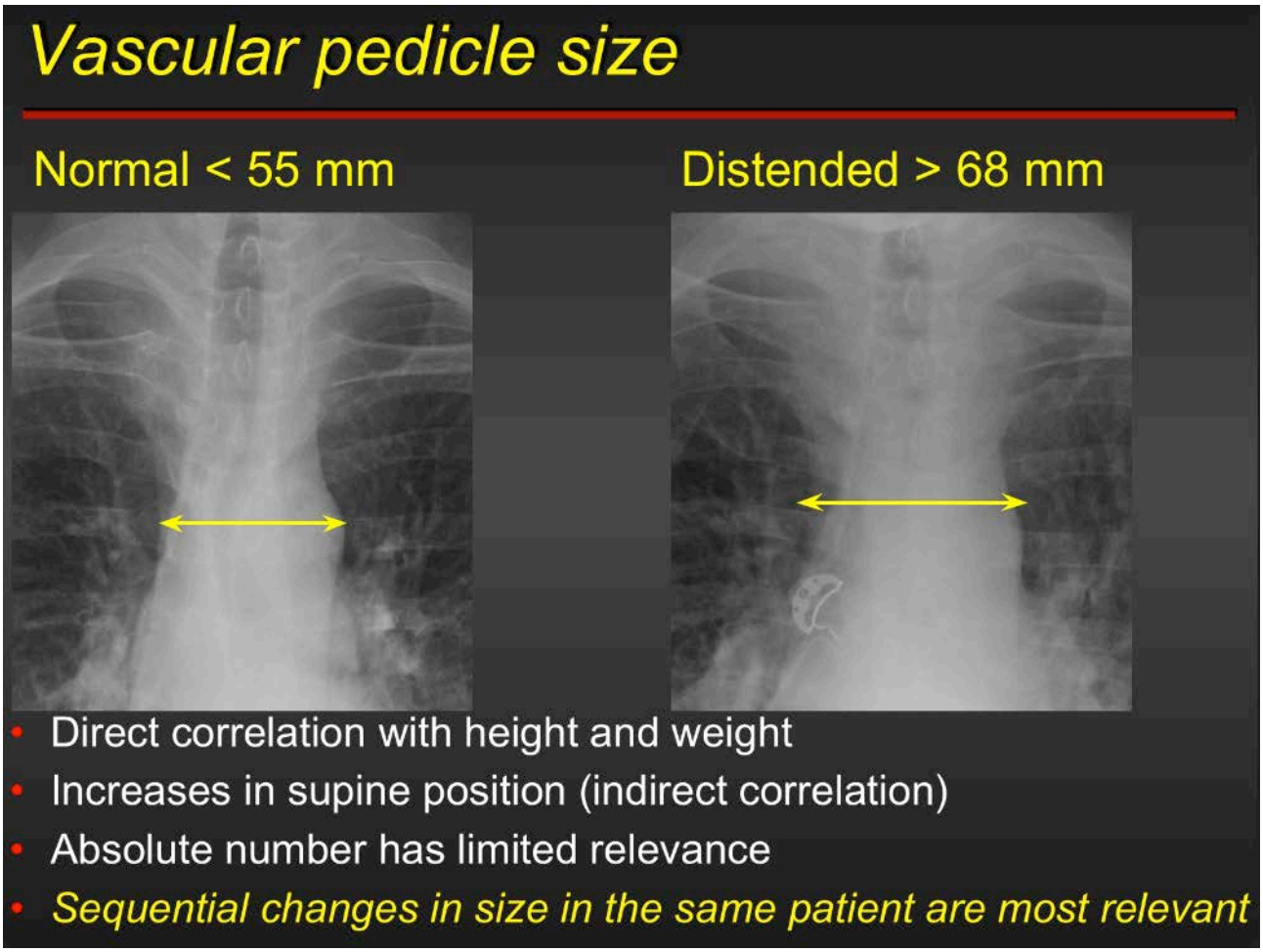

edema2

This exhibit will also focus on both traditional imaging modalities (chest radiographs and CT) as well as ultrasound and MRI and their potential role in diagnosis and risk stratification of pulmonary edema.

Conclusion

In conclusion, this educational exhibit will focus on step by step algorithms that would help residents and practicing radiologists to choose imaging modality to diagnose edema, it's etiology, severity, and potential complications.

A-160

What the radiologists need to know: Updated knowledge on lymphangioleiomyomatosis

H.-J. Lee[1], D. S. Kim[2]
[1]Seoul National University Hospital, Radiology, Seoul, Republic of Korea (South Korea), [2]Inje University Busan Paik Hospital, Radiology, Busan, Republic of Korea (South Korea)

Learning Objectives
1) To understand molecular pathogenesis 2) To introduce the diagnostic criteria 3) To inform the standard treatment guidelines according to the ATS/JRS and ERS guidelines 4) To present representative clinical cases and to compare the radiologic differential findings between LAM and other cystic lung diseases

Background
The knowledge about lymphangioleiomyomatosis (LAM) that is a rare systemic neoplastic disease was recently updated.

Imaging findings OR Procedure details
Genetic studies have revealed that LAM cells have smooth muscle characteristics, circulate in the blood and lymphatic fluid, and have inactivated tuberous sclerosis (TSC) 1 or 2 gene mutations. Loss of TSC gene function activates the mTOR signaling pathway, which regulates cellular growth, motility, and survival. LAM cells also express the lymphangiogenic growth factor and VEGF-D, which promote entry into lymphatic channels and metastatic spread [1]. Definite diagnosis of LAM can be made with the combination of a compatible clinical history (young to middle-aged woman presenting with worsening dyspnea and/or pneumothorax or chylothorax), characteristic HRCT features, and one or more of the following: presence of TSC, angiomyolipomas, chylous effusion, confirmed lymphangioleiomyomas, or elevated serum VEGF-D [2]. For patients with LAM with declining lung function, Sirolimus is recommended rather than observation. For selected patients with LAM with chylous effusion, Sirolimus is suggested before invasive management. In the patients with LAM, ipsilateral pleurodesis after initial pneumothorax is recommended rather than waiting for a recurrent pneumothorax. Pleural procedures including pleurodesis or pleurectomy are known to be associated with increasing bleeding tendency after lung transplantation. However, pleural procedures are not be considered a contraindication to lung transplantation in patients with LAM [2][3][4]. Differential diagnosis between LAM and other cystic lung diseases such as Birt-Hogg-Dube syndrome (BHD) and lymphocytic interstitial pneumonia (LIP) can be challenging. HRCT findings and several clinical features can be overlapped in these diseases. According to recent radiologic studies, diffuse cysts was more likely to be found in patients with LAM than in patients with BHD or LIP, who were more likely to have lower lung predominant cysts. In LAM and LIP, the shape of cysts was usually round. In BHD, the cysts had more irregular shape, more septation, lower and peripheral distribution, larger maximum size, and more attachment to the pleura [5][6]

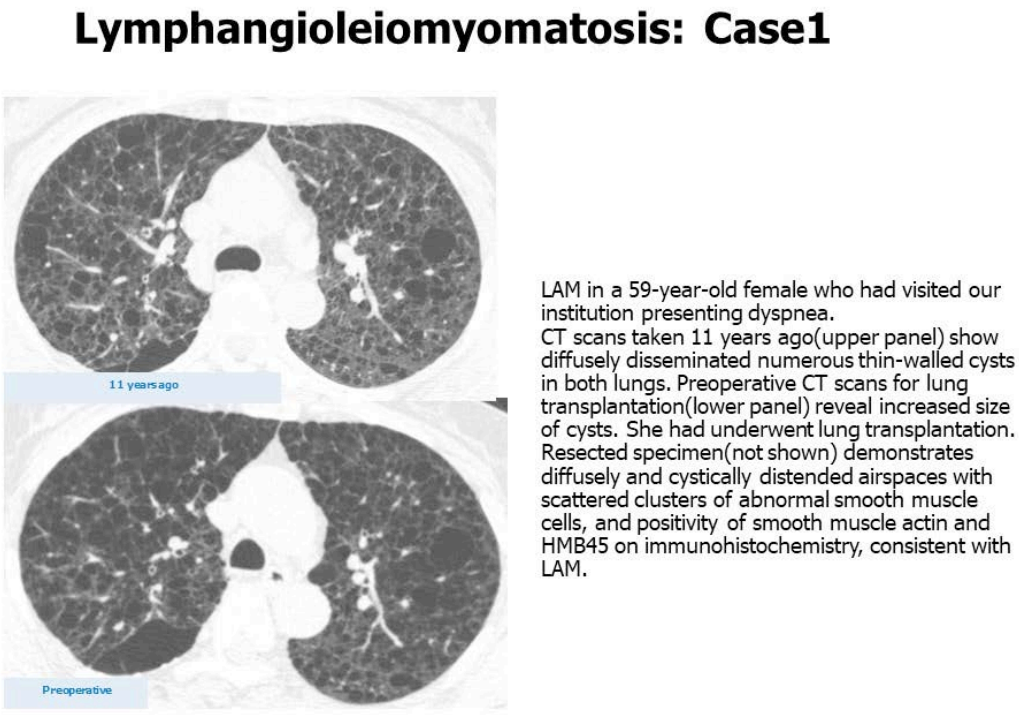

Lymphangioleiomyomatosis: Case1

Lymphangioleiomyomatosis: Case2

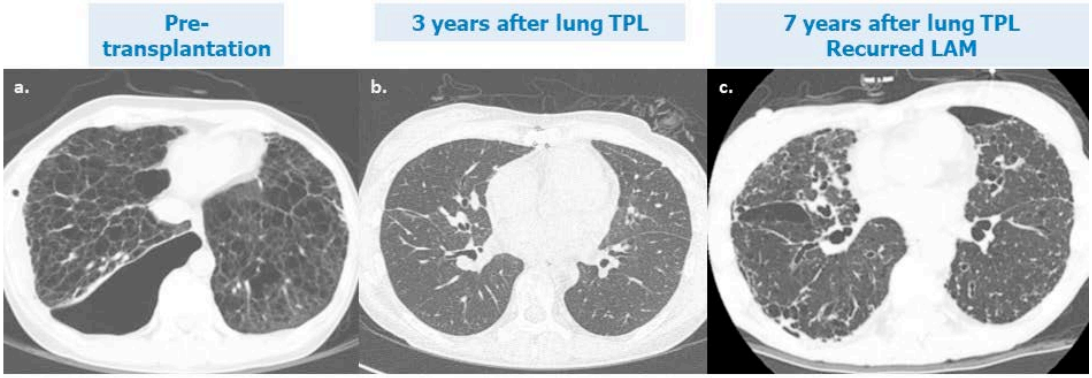

LAM in a 39-year-old female who had visited our institution presenting pneumothorax. (a) CT scan shows diffusely disseminated numerous thin-walled cysts in both lungs and pneumothorax in right lower hemithorax. She had underwent lung transplantation. Resected specimen(not shown) demonstrates multiple cystic lesions lined by cuboidal epithelial cells with smooth muscle proliferation and positivity of smooth muscle actin and HMB45 on immunohistochemistry, consistent with LAM. (b) CT scan after 3 years of operation shows no remarkable complication. (c) CT scan after 7 years of operation shows recurrent LAM with pneumothorax in bilateral thoraces and progression of diffuse fibrosis.

Lymphangioleiomyomatosis: Case2

Lymphocytic Interstitial Pneumonia

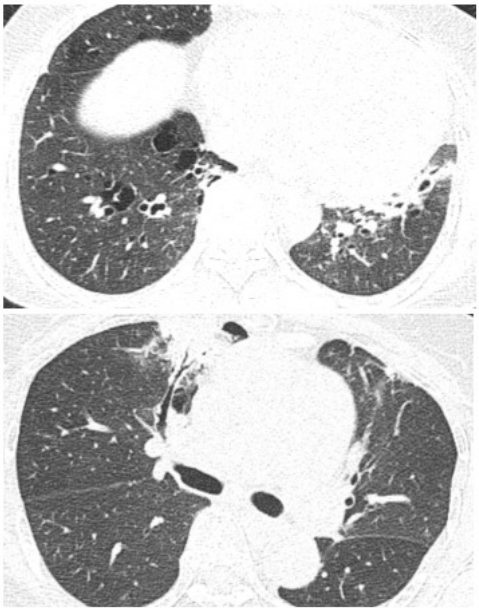

LIP in a patient with Sjogren syndrome (F/68). Several small thin-walled cysts and peribronchovascular thickening in both lower lobes are shown. Patchy consolidation in the RML was proven as lymphoma.

Lymphocytic Interstitial Pneumonia

Birt-Hogg-Dube syndrome

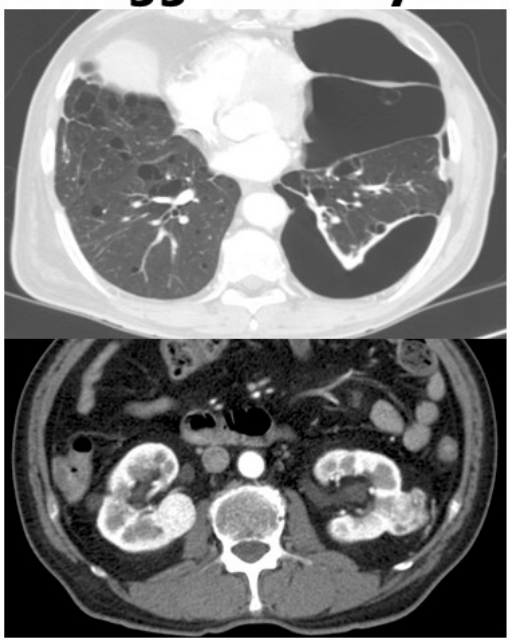

BHD in a 71-year-old male who had visited our institution with recurrent pneumothorax. Multiple thin-walled air cysts in both lungs, and left pneumothorax are shown. Proven RCC, chromopobe type is seen in left kidney. On genetic examination, chromophobe type with folliculin gene mutation was found.

Birt-Hogg-Dube syndrome

.

Conclusion

Understanding of pathogenesis and knowledge of updated diagnostic and treatment methods for LAM are essential for chest radiologists as members of a team that treats patients with this intractable disease.

References:

[1] Juvet SC, McCormack FX, Kwiatkowski DJ, et al. , (2007), Molecular pathogenesis of lymphangioleiomyomatosis: lessons learned from orphans., Am J Respir Cell Mol Biol, 398-408, https://pubmed.ncbi.nlm.nih.gov/17099139/

[2] McCormack FX, Gupta N, Finlay GR, et al., (2016), Official American Thoracic Society/Japanese Respiratory Society Clinical Practice Guidelines: Lymphangioleiomyomatosis Diagnosis and Management., Am J Respir Crit Care Med, 748-761, https://pubmed.ncbi.nlm.nih.gov/27628078/

[3] Gupta N, Finlay GA, Kotloff RM, et al. , (2017), Lymphangioleiomyomatosis Diagnosis and Management: High-Resolution Chest Computed Tomography, Transbronchial Lung Biopsy, and Pleural Disease Management. An Official American Thoracic Society/Japanese Respiratory Society Clinical Practice Guideline. , Am J Respir Crit Care Med, 1337-1348, https://pubmed.ncbi.nlm.nih.gov/29140122/

[4] Johnson SR, (2010), The ERS guidelines for LAM: trying a rationale approach to a rare disease. , Respir Med, S33-41, https://pubmed.ncbi.nlm.nih.gov/20451364/

[5] Escalon JG, Richards JC, Koelsch T, et al. , (2019), Isolated Cystic Lung Disease: An Algorithmic Approach to Distinguishing Birt-Hogg-Dubé Syndrome, Lymphangioleiomyomatosis, and Lymphocytic Interstitial Pneumonia., AJR Am J Roentgenol, 1260-1264, https://pubmed.ncbi.nlm.nih.gov/30888864/

[6] Park HJ, Chae EJ, Do KH, et al. , (2019), Differentiation Between Lymphangioleiomyomatosis and Birt-Hogg-Dubé Syndrome: Analysis of Pulmonary Cysts on CT Images. , AJR Am J Roentgenol, 766-772, https://pubmed.ncbi.nlm.nih.gov/30673341/

A-524

“Not one size fits all”: equivocal appearances of lung cancer on CT imaging

N. Antunes[1], C. A. Ruano[1,2], E. Kucheruk[3], V. B. Carvalho[3]
[1]Hospital de Cascais, Radiology, Lisbon, Portugal, [2]Hospital da Luz, Radiology, Lisbon, Portugal, [3]Centro Hospitalar Universitário de Lisboa Central, Radiology, Lisbon, Portugal

Learning Objectives

- To describe and display atypical and equivocal imaging findings of lung cancer on CT imaging.
- To explain the main histopathologic background for these findings.

Background

Lung cancer remains one of the most frequently diagnosed malignancies and is still the current leading cause of all cancer deaths. Typical radiologic findings include a solid or subsolid pulmonary nodule or mass with or without associated lymphadenopathy. However, lung cancer may present with several under recognized morphologies, which represent potential causes for delayed and/or misdiagnosis.

Imaging findings OR Procedure details

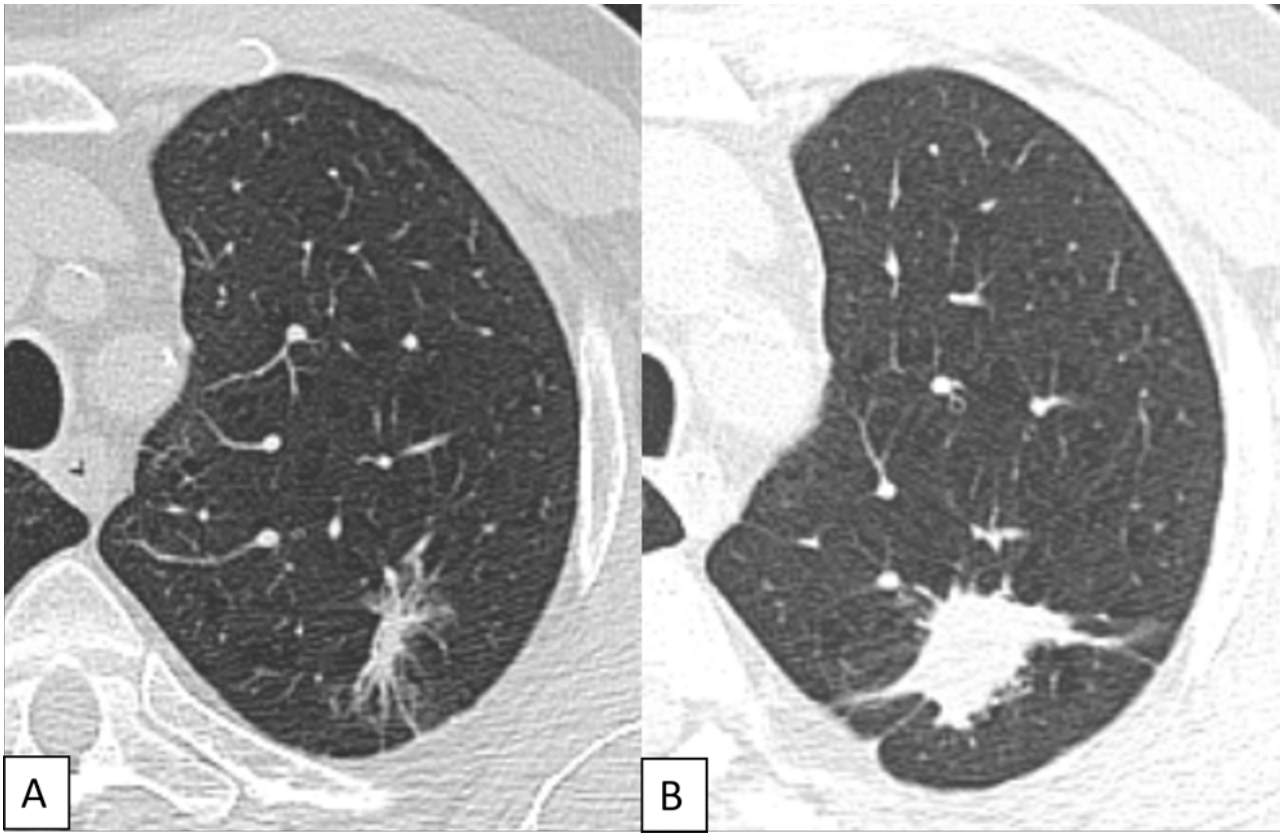

(A) Left upper lobe scar showed progressive enlargement in chest CT performed three years later (B). Lung adenocarcinoma was proved in surgical ressection and histopathologic analysis.

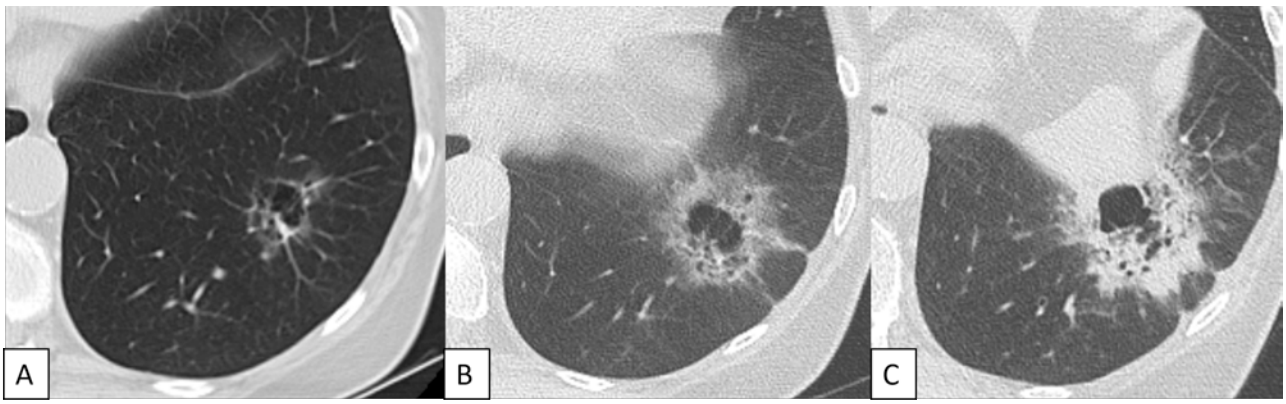

(A) Left lower lobe cystic lesion showed progressive increase of surrounding glound glass component four years later (B) and consolidation five years (C) from initial CT. Surgical ressection and histopathology showed lung adenocarcinoma.

Central lung cancers may produce airway obstruction and present with post-obstructive atelectasis as the dominant finding. Lung scar cancer should be suspected when a new lesion emerges in a known scar or a focal scar shows enlargement in follow-up images. This is

thought to result from a repeated injury and repair process in the scar over a long period of time. The pathogenesis of lung cancer associated with cystic airspaces is still not fully understood but should be suspected in cases where a cystic area is associated with consolidation, enlarging wall thickening and/or ground glass. Primary lung adenocarcinoma may manifest as a focal or diffuse parenchymal consolidation, known as “pneumonic-type lung adenocarcinoma”. It corresponds to adenocarcinoma with a predominant mucinous histology subtype and may be difficult to distinguish from pneumonia. Single or multiple cavitary lesions might also represent lung cancer and most often result from rapid tumor growth that exceeds the blood supply with resultant central necrosis. Multifocal lung cancer is the clinical entity of multiple synchronous or metachronous lesions, usually of the adenocarcinoma subtype, and should be distinguished from pulmonary metastasis. The presence of a miliary pattern may be the initial presentation in patients with lung adenocarcinoma, particularly with EGFR mutation. The halo sign (area of ground glass opacity surrounding a nodule) in an immunocompetent patient should raise the suspicion of lepidic lung adenocarcinoma. Finally, the presence of isolated pleural effusion or lymphadenopathy may represent occult underlying lung malignancy.

Conclusion

A detailed knowledge of the atypical imaging features of lung cancer is key for the correct and early diagnosis of these lesions.